Heart Replacement

Artificial Heart 7

Tetsuzo Akutsu Hitoshi Koyanagi

ISIS
MEDICAL
MEDIA

Heart Replacement

Artificial Heart 7

Tetsuzo Akutsu Hitoshi Koyanagi

ISIS
MEDICAL
MEDIA

Heart Replacement
Artificial Heart 7

The 7th International Symposium on Artificial Hearts and Assist Devices 2000
Tokyo, Japan

Published by Isis Medical Media Limited in collaboration with
Nankodo Company Limited

This edition published in the Taylor & Francis e-Library, 2005.

EDITORS:

Tetuzo Akutsu MD, PhD
Chariman, Terumo Corporation, Shonan Center, 1500 Inokuchi, Nakai-machi, Ashigarakami-gun, Kanagawa 259-01, Japan

Hitoshi Koyanagi MD
Chairman and Professor, Department of Cardiovascular Surgery, The Heart Institute of Japan, Tokyo Women's Medical College, 8-1 Kawada-cho, Shinjuku-ku, Tokyo 162, Japan

This publication was subsidized by the Japan Keirin Association through its promotion funds from KEIRIN RACE

ISBN 0-203-99458-2 Master e-book ISBN

ISBN 1 901865 36 3 Isis Medical Media Limited

Heart Replacement
Artificial Heart 7

Heart Replacement, Artificial Heart 7, is published in conjunction with the *Journal of Congestive Heart Failure & Circulatory Support.* The journal is published quarterly and the subscription rates, including postage, for 2001 are:

Institutional subscription	£180.00/$280.00
Individual subscription	£90.00/$150.00

Subscribers in Canada must add 7% to the value of their order to allow for Canadian GST. Subscribers in Europe must quote their VAT registration number or state that they are not registered. Subscribers in the Netherlands who are not VAT registered must add 6% to the subscription price, to allow for VAT. Orders for subscriptions, back issues and business correspondence should be sent to:

Subscription Manager
Martin Dunitz Limited
The Livery House
7–9 Pratt Street
London, NW1 0AE
Tel: +44 (0)20 7482 2202, Fax: +44 (0)207 267 0159

Dispatch

The journal is dispatched within Europe by surface mail, to other continents by various forms of air-speeded delivery: to the US by air freight for forwarding by second class post, to India by air freight for guaranteed local delivery, and to all other countries by accelerated surface post.

ISSN 1365–5736

Isis Medical Media Staff
Journals' Editor: Harriet Milles
Production Controller: Sarah Sodhi

I S I S
MEDICAL
M E D I A

Heart Replacement
Artificial Heart 7

The 7th International Symposium on Artificial Heart and Assist Devices
Tokyo, Japan
March 10–11, 2000

Organizing Committee

Honorary President Hiromitsu Yoshioka
Chairman, Board of Directors
Tokyo Women's Medical University

President Kintomo Takakura
President, Tokyo Women's Medical University

Vice President Tetsuzo Akutsu
Senior Advisor, Terumo Corporation

Secretary General Hitoshi Koyanagi
Professor and Chairman
Department of Cardiovascular Surgery
The Heart Institute of Japan
Tokyo Women's Medical University

Members

Tetsuzo Akutsu	Senior Advisor, Terumo Corporation
OH Frazier	Chief of Transplant Services, Texas Heart Institute
Kou Imachi	Professor, The University of Tokyo
Kazunori Kataoka	Professor, The University of Tokyo
Akahiko Kawai	Assistant Professor, Tokyo Women's Medical University
Robert L Kormos	Associate Professor, University of Pittsburgh
Hitoshi Koyanagi	Professor, Tokyo Women's Medical University
Hikaru Matsuda	Professor, Osaka University
Hiroshi Nishida	Assistant Professor, Tokyo Women's Medical University
Shinichi Nitta	Professor, Tohoku University
Chisato Nojiri	Research Manger, Terumo Corporation
Yoshiyuki Taenaka	Director, National Cardiovascular Center Research Institute
Setsuo Takatani	Professor, Tokyo Medical and Dental University
Ryohei Yozu	Assistant Professor, Keio University
John T Watson	Active Deputy Director, Lung and Vascular Diseases, NHLBI

ISIS
MEDICAL
MEDIA

Preface

It is a great pleasure for me to offer you here the Proceedings of the 7th International Symposium on Artificial Heart and Assist Devices which was held at Keidanren Kaikan in Tokyo, Japan, March 10–11, 2000. Although some reports of clinical uses of total artificial heart (TAH) and ventricular assist devices (VAD) were presented in the 6th Symposium, the number of presentations has apparently increased in this Symposium. The bridge use of TAH and/or VAD has also increased. In Japan, however, only one bridge use was reported due to the slow acceptance of brain death heart transplantation.

The Proceeding sconsit of ten sessions and 6 invited lectures: they are TAH (2), VAD (4), HT, engineering (2), pathophysiology and biomaterial. The development of hardware in the field of artificial hearts is making excellent progress toward small, implantable, and durable devices.

I hope the Proceedings will be a beneficial asset to both experts and young investigators.

Tetsuzo Akutsu
Vice-President

Past and future perspectives of the Symposium

Sixteen years have passed since the 1st Symposium on Artificial Heart and Assist Devices was held in 1985. Since then, the Symposium has been held in Tokyo, usually biennially, in the midsummers of 1985, 1987, 1990, 1992, 1995, 1996 and 2000. Everyone who has attended the Symposia will remember the weather in downtown Tokyo, which could be described as 'somewhat tropical'!

Dedicated and enthusiastic investigators from the world's major artificial heart laboratories and Institutions, conducting active heart transplantation programs, were invited to all seven Symposia.

By 1985, Japan had finally recovered from difficulties experienced after the Second World War and has since made remarkable advances in all scientific fields, including cardiovascular surgery and cardiology. However, the effective treatment of intractable severe heart failure seemed to be lagging behind compared to other counties.

Therefore, under the direction of Dr. Akutsu, I instigated the 1st Symposium, hoping that it would be an informative, stimulating and encouraging forum. The Symposium has now been an established event for sixteen years, and has involved seven Symposia and six issues of Proceedings. We here present the publication of the 7th Proceedings.

Over recent years, striking changes have occurred in our environment, not only in Japan but also throughout the world. The concepts presented at the Symposia have led to significant advances in medical technology. In the new millennium we hope to benefit still further from the continued development of excellent devices for the treatment of severe heart failure. I propose that the Symposium should be continued for this purpose.

Thank you again for your wonderful support. I am looking forward to seeing all of you here in Tokyo in the new millennium.

Hitoshi Koyanagi, MD
Secretary General

Congratulatory Addresses

Good morning, honorable participants, distinguished guests, ladies and gentlemen.
My name is Kazunari Asanuma, Deputy Director of the Research and Development Division at the Ministry of Health and Welfare.

I apologise that Dr Ito is unable to attend the Symposium, and I am here to read the following statement on his behalf.

It is my great pleasure to be present for this opening ceremony of the 7th International Symposium on Artificial Heart and Assist Devices.

With the rapid progress in science and technology, many medical devices have been developed which have proved enormously beneficial to the advancement of medical procedures. In the 21st century, with an aging population and fewer children, the development of new, effective medical devices becomes increasingly important to improve quality of life. The shortage of heart donors in our country means that Japanese patients with severe heart disease generally have to wait for long periods for heart transplantation

Therefore, the Ministry of Health and Welfare actively promotes research and development in artificial hearts and assist devices by use of health science research funding. I believe that many researchers will continue their contribution to the development of new, effective medical devices as a bridge to heart transplantation.

With this goal in view, I am convinced that the Symposium will be a successful forum for research into the future development of artificial hearts and assist devices.

I hope that this 7th Symposium will prove to be a fruitful event for all of you.

Finally, I extend my sincere thanks to Mr Yoshioka, Dr Takakura, Dr Akutsu and Professor Koyanagi for the organization of this Symposium.

Thank you for listening.

Kazunari Asanuma
Deputy Director, Research and Development Division, Ministry of Health and Welfare, Japan

Ladies and gentlemen

I would like, first of all, to congratulate the Japan Research Promotion Society for Cardiovascular Diseases and all those who have made efforts to convene for this 7th International Symposium on Artificial Heart and Assist Devices. It is a great honor for me to have an opportunity to speak at this important Symposium.

As the Director of the Life Science Division of the Science and Technology Agency, I am in charge of the promotion of life science. Life science aims first at elucidating the complex and sophisticated phenomenon of life and then utilizing its result for health medicine, environmental protection, agriculture, forestry and fisheries, and industry, with the aim of achieving a healthy and productive national life-style. In the budget for this year, a millennium project was advocated by our Prime Minister. Life science is generally held to be the most important aspect of science and technology because it promotes bio-industry, which is a key to the rebirth of our economy, and a happy society that enjoys longevity. Life science includes research on artificial organs, and to finding solutions to various problems in human health.

The research into artificial organs, which we are about to discuss today, is, in my view, of great importance in Japan, where the number of elderly people is rapidly increasing. It goes without saying that research on artificial organs requires extensive cooperation and coordination among research institutions and researchers in such fields as medicine, biology, and engineering. I believe that this Symposium will provide participants with an extremely useful opportunity to exchange the most up-to-date research information, which, I am sure, will greatly contribute to significant progress in this field.

Thank you very much for your attention.

Kimihiko Oda
Director of Life Science Division, Science Technology Agency, Japan

Honorary President Yoshioka, President Takakura, distinguished guests and participants, ladies and gentlemen.

I have a pleasure in extending a message of greeting from Dr. Eitaka Tsuboi, President of the Japan Medical Association.

On behalf of the Japan Medical Association, I would like to offer my congratulations on the occasion of the 7th International Symposium on Artificial Heart and Assist Devices.

Progress in science and technology has been remarkable in Japan over recent years. Developments in the field of health care, research in medical electronics and bioengineering have progressed rapidly, and new treatment methods have been developed. The continuing progress in the development of artificial heart and assist devices has been particularly noteworthy.

Following the enactment of the Organ Transplantation Law in October 1997, Japan's first heart transplantation from a brain dead donor took place in February 1999, exactly one year and four months later. Although a growing number of such operations are anticipated in the future, Japan continues to face a shortage of donors. As a result, the use of the artificial heart as a support for patients during the waiting period has made the development of these assist devices vital as an alternative to heart transplantation.

Entering the year 2000 was a major turning point, and Prime Minister Obuchi has proposed a millennium project which aims to establish the practical application of technology at an early stage, in order to cope with Japan's aging population. As part of this project, the Ministry of Health and Welfare and the Ministry of Trade and Industry have begun the full-scale development of artificial bone and implantable artificial organs, of which the primary focus is the artificial heart. It can be said that the future of health care in the 21th century will address the demand for further development of organ transplantation and the artificial heart.

I hope that this Symposium will greatly contribute to the present and future development of the artificial heart.

Thank you very much for your attention.

Akira Koizumi
Vice-President
Japan Medical Association

I am Chairman of the Board of Directors, Tokyo Women's Medical University. On behalf of the organizing committee, I have the honour of extending a cordial welcome to each of the participants of the 7th International Symposium on Artificial Heart and Assist Devices.

Our ultimate goal is the development of advanced treatment for patients with severe heart failure. I believe this goal can be achieved by organ replacement through heart transplantation or by using an artificial heart. To help accomplish this aim, we held our first Symposium in 1985 and I am very proud that we now have the seventh in the series. As the Japanese proverb says, 'continuation is power'.

We feel that the continued contributions made by the many active researchers at the scientific sessions of this Symposium have been indispensible to this progress.

Thank you.

Hiromitsu Yoshioka
Honorary President

The Yoshioka Memorial Prize, the Akutsu Prize, and the Koyanagi Scientific Exhibition Prize

The Yoshioka Memorial Prize

The International Symposium on Artificial Heart and Assist Devices is a biennial event that has now taken place six times since the 1st Symposium in 1985. The Honorary President of the 7th Symposium, Hiromitsu Yoshioka, is the third generation of the Yoshioka family to hold the position. The late Hiroto Yoshioka was President of the 1st, 2nd, and 3rd Symposia; Hiromitsu Yoshioka, the 4th Symposium; and Morimasa Yoshioka, the 5th. They are the descendents of Professor Yayoi Yoshioka, MD, the founder of Tokyo Women's Medical University, who was especially noted for her accomplishments and her devotion to the education of women in the field of medicine. Tokyo Women's Medical University opened the first heart institute in Japan in 1954 under the auspices of the late Professor Shigeru Sakakibara, an internationally recognized pioneer in cardiovascular surgery in Japan, to conduct comprehensive studies, both in research and in clinical cardiovascular diseases.

During the 46 years since the institution was established, the Yoshioka family have been tireless in their efforts to financially support the development of clinical and research work for patients with heart disease. To promote research in this field, they have also sponsored the International Symposium on Artificial Heart and Assist Devices and assumed responsibility as its President. The Heart Institute of Japan has played a leading role in the field of cardiovascular surgery, cardiology and pediatric cardiology, not only in Japan but also worldwide.

The Yoshioka Memorial Prize was established to honor the contributions of the late Hiroto Yoshioka, who served as President of the International Symposium for the six years following its inception in 1985. The prize is presented to the author of the best clinical paper contributed to the Symposium and includes an award of 500,000 yen.

First Laureate, 1992: Kenji Yamazaki, MD
The Heart Institute of Japan, Tokyo Women's Medical College
Second Laureate, 1995: Ryohei Yozu, MD
Department of Surgery, Keio University
Third Laureate, 1996: Setsuo Takatani, PhD
Faculty of Engineering, Yamagata University
Fourth Laureate, 2000: Timothy B Icenogle, MD
Inland Northwest Thoracic Organ Transplant Program, Sacred Heart Medical Center, Washington

The Akutsu Prize

The Akutsu Artificial Heart Prize was created to honor the significant contributions to the development of the artificial heart and to celebrate the 10th anniversary of the Symposium. The prize carries an award of 300,000 yen. Dr Tetsuzo Akutsu's contribution to development of the artificial heart, together with Dr Kolff, is well known worldwide. From the early stages of the development of the artificial heart up to the present, his tireless efforts manifest his courage and dignity as a researcher. The prize will be awarded for the best paper contributed in the area of basic research of the artificial heart. It is hoped that many young researchers, inspired by the discipline shown by Dr Akutsu, will devote their efforts to development of the artificial heart and that the results they achieve will be for the benefit of mankind.

First Laureate, 1995: Jaromir Vâskû, MD
Vacord Bioengineering Research Company
Second Laureate, 1996: Hiroaki Harasaki, MD
Cleveland Clinic Foundation
Third Laureate, 2000: Eisuke Tatsumi, MD
National Cardiovascular Center, Osaka

Koyanagi Scientific Exhibition Prize

Professor Hitoshi Koyanagi is a cardiovascular surgeon in the Department of Cardiovascular Surgery, the Heart Institute of Japan, Tokyo Women's Medical University, and studied under Professor Shigeru Sakakibara with Professor Soji Konno at the dawn of the era of cardiovascular surgery. Professor Konno, who succeeded to Professor Sakakibara's position, died at the young age of 43 years. However, all cardiovascular surgeons must remember his name in the Konno-Rastan procedure for aortic stenosis with patch grafts and a prosthetic bileaflet valve, and in the Konno-Sakakibara bioptome. The Heart Institute of Japan has contributed greatly to the development of cardiovascular surgery in Japan, and Professor Koyanagi has borne important responsibilities since his appointment to his present position in 1980. He believes his mission is to promote heart replacement treatments such as transplantation and artificial hearts for many patients suffering from severe intractable heart failure since those treatments are performed daily in the western

world. As Secretary General, Professor Koyanagi has served the International Symposium seven times, with Dr. Akutsu acting as Vice-president since 1985, his aim being the realization of treatment by heart replacement. In commemoration of the 10th anniversary of the Symposium and as an expression of their gratitude to Professor Koyanagi for his efforts in handling the Symposium's general affairs, the programme committee members established the Koyanagi Scientific Exhibition Prize. The prize also carries an award of 100,000 yen.

First Laureates 1995: Tokyo University Group,
Tohoku University Group
Second Laureates 1996: Kenji Yamazaki, MD
The Heart Institute of Japan,
Tokyo Women's Medical College
University of Pittsburgh, Waseda University
Sun Medical Technology Research Corporation
Third Laureate 2000: I-ILVAS, Terumo Corporation
(Toyoko Komatsu, Symposium Secretary)

The 7th International Symposium on Artificial Heart and Assist Devices
Tokyo, Japan
March 10–11, 2000

Programme

Friday, March 10, 2000

Session 1 – Total Artificial Heart

Chairpersons: **J Watson and Y Taenaka**

153 **Long-term *in vivo* testing of the National Cardiovascular Center electrohydraulic total artificial heart**

E Tatsumi, Y Taenaka, K Uesho, A Homma, T Nishinaka, Y Kakuta, T Tsukiya, N Katagiri, K Shioya, M Takahashi, H Ohnishi, K Sato, H, Takano, T Masuzawa, M Nakamura, K Tsukahara and K Tsuchimoto

161 **Ultracompact, totally implantable, permanent TAH**

S Takatani, K Ohuchi, M Nakamura and T Sakamoto

167 **Progress in the development of the undulation pump total artificial heart**

Y Abe, T Chinzei, T Isoyama, T Ono, S Mochizuki, I Saito, K Iwasaki, M Ishimaru, A Baba, A Kouno, T Karita, K Baba and K Imachi

Session 2 – Heart Transplantation

Chairpersons: **OH Frazier, H Koyanagi and R Omoto**

173 **Pre- and post-heart transplant management in end-stage cardiac failure patients: Osaka University experience**

N Fukushima, S Ohtake, Y Sawa, M Nishimura, G Matsumiya, S Nakata, S Takashima, M Hori, R Shirakura and H Matsuda

179 **Bridging to heart transplant using paracorporeal and implantable ventricular assist devices**

K Minami, l Arusoglu, A El-Banayosy, A Sezai, D Boethig, M Morshuis, O Fey, P Sarnowski and R Körfer

Invited Lecture

Chairperson: **Y Nosé**

185 **First clinical trials of a totally implantable destination therapy ventricular assist system**

A Snyder, W Pae, J Boehmer, G Rosenberg, W Weiss, W Pierce, J Thompson, J Lewis, D Frank, H Zintak, S Scholl, R Körfer, A El-Banayosy, L Arusoglu, O Fey and M Morshuis

Session 3 – Total Artificial Heart

Chairpersons: **AJ Snyder and K Imachi**

195 **Design of atrial cuff for the undulation pump total artificial heart**

K Imachi, T Chinzei, Y Abe, T Isoyama, T Ono, S Mochizuki, I Saito, M Ishimaru. K Iwasaki, A Baba, T Karita, T Ozeki and A Kouno

201 **Oxygen-demand-based physiological control of the total artificial heart**

M Nakamura, S Takatani, K Ouchi, T Sakamoto, A Homma, E Tatsumi, K Uesho, Y Taenaka and T Masuzawa

Session 4 – Pathophysiology

Chairpersons: J Vâskû and S Nitta

Session 5 – Biomaterial

Chairpersons: K Kataoka and T Okano

Session 6 – Engineering

Chairpersons: T Mussivand and T Yamane

Saturday, March 11, 2000

Session 7 – Engineering

Chairpersons: Y Mitamura, M Umezu and Y Sezai

Session 8 – Ventricular Assist Devices

Chairpersons: S Westaby, S Kitamura and S Takatani

Invited Lecture

Chairperson: K Atsumi

Session 9 – Ventricular Assist Device

Chairpersons: R Yozu, A Kawai, K Affeld and C Nojiri

Invited Lecture

Chairperson: **H Takano**

Session 10 – Ventricular Assist Device

Chairpersons: **T Sakamoto and H Nishida**

Session 1

Total Artificial Heart

Journal of Congestive Heart Failure and Circulatory Support (2001) Vol 1, No 4, 153–160

Long-term *in vivo* testing of the National Cardiovascular Center electrohydraulic total artificial heart

E. Tatsumi MD PhD[1], Y. Taenaka MD PhD[1], K. Uesho MD[1], A. Homma PhD[1], T. Nishinaka MD PhD[1], Y. Kakuta MS[1], T. Tsukiya PhD[1], N. Katagiri MS[1], K. Shioya DVM[1], M. Takahashi PhD[1], H. Ohnishi MD[1], K. Sato MD[1], H. Takano MD PhD[1], T. Masuzawa PhD[2], M. Nakamura MD PhD[3], K. Tsukahara MS[4] and K. Tsuchimoto MS[4]

[1]Department of Artificial Organs, National Cardiovascular Center Research Institute, Osaka, Japan; [2]Ibaraki University, Ibaraki, Japan; [3]Tokyo Medical and Dental University, Tokyo, Japan; and [4]Aisin Cosmos R&D Co., Ltd., Aichi, Japan

Background We have been developing an electrohydraulic total artificial heart (EHTAH) system. The pumping unit comprises diaphragm-type blood pumps and an energy converter consisting of a regenerative pump/brush-less DC motor assembly. The energy converter reciprocates and delivers hydraulic silicone oil to the alternate blood pumps. The left–right output balance is achieved with an interatrial shunt (IAS) made in the composite atrial cuff.

Methods The EHTAH pumping unit with an external controller was evaluated in chronic animal implantation in 16 calves weighing 54–88 kg. The pump rate was manually controlled at an adequate fixed rate (80–90 bpm).

Results and discussion The device demonstrated a good anatomic fit. Five calves survived for more than a week, and the longest surviving animal lived for 86 days until sudden death due to an accidental power-lead disconnection. This animal gained weight from 69 kg to 94 kg during the experiment. Cardiac output ranged between 6–8 L min^{-1}. Power consumption of the device was 13.5 ± 0.9 W, and energy efficiency was estimated to be 9–11%. The left and right atrial pressures were 16 ± 4 and 14 ± 4 mmHg, respectively. The IAS adequately balanced the left–right output difference with 2 ± 3 mmHg of interatrial pressure gradient. Mixed venous oxygen saturation was 65 ± 6% and the serum lactate level was 5 ± 1 mg/dL, representing a favorable oxygen metabolic condition. Temperatures of the energy converter surface and the adjacent pleura were 39.5 ± 0.5 and 38.9 ± 1.5°C, respectively, indicating heat generation/dissipation was acceptable. These results indicate that the EHTAH has the potential to be a totally implantable cardiac replacement.

Keywords total artificial heart (TAH), electrohydraulic TAH (EHTAH), left-right balance, interatrial shunt (IAS), anatomic fit.

Introduction

Development of a fully implantable total artificial heart (TAH) system for long-term cardiac replacement is an important issue given the overwhelming shortage of donor hearts for transplantation[1]. Such a device, without an external tether, can reduce the chance of infection and may provide an acceptable quality of life to the patient with end-stage heart disease. We started development of a fully implantable electrohydraulic TAH (the EHTAH system) in 1987[2,3]. The EHTAH intrathoracic pumping unit, with the core unit composed of blood pumps and an energy converter, has been developed and evaluated in 16 chronic animal implantation trials. This paper describes the results of these trials, together with the detailed experimental course of the longest surviving animal that lived for 86 days postoperatively.

Materials and methods

EHTAH pumping unit

The EHTAH system is comprised of an intrathoracic pumping unit and an electronic unit (Figure 1). The electronic unit is composed of internal and external controller subunits, transcutaneous energy transfer and optical telemetry subunits, and internal and external battery subunits. The present development status and the detailed description of the electronic unit have been published elsewhere[4–6].

The intrathoracic pumping unit consists of a blood pump subunit and an energy converter subunit (Figure 2). The blood pump subunit is composed of diaphragm-type left and right blood pumps, a composite atrial cuff, and aortic and pulmonary artery grafts. Blood pump housings are formed by vacuum injection molding, and are made of polyurethane resin (UP-5170, Kokusai Chemical, Tokyo, Japan). The diaphragms are made of antithrombogenic segmented polycarbonate polyurethane (Miractran E980, Nihon Miractran, Kanagawa, Japan), and the entire blood-contacting surface is coated with the same material. Two Björk-Shiley monostrut tilting disk valves, 23 mm inflow and 21 mm outflow, are mounted in the inlet and outlet ports of each blood pump,

Correspondence to: Eisuke Tatsumi, Department of Artificial Organs, National Cardiovascular Center Research Institute, 5–7–1 Fujishiro-dai, Suita, Osaka 565–8565, Japan.

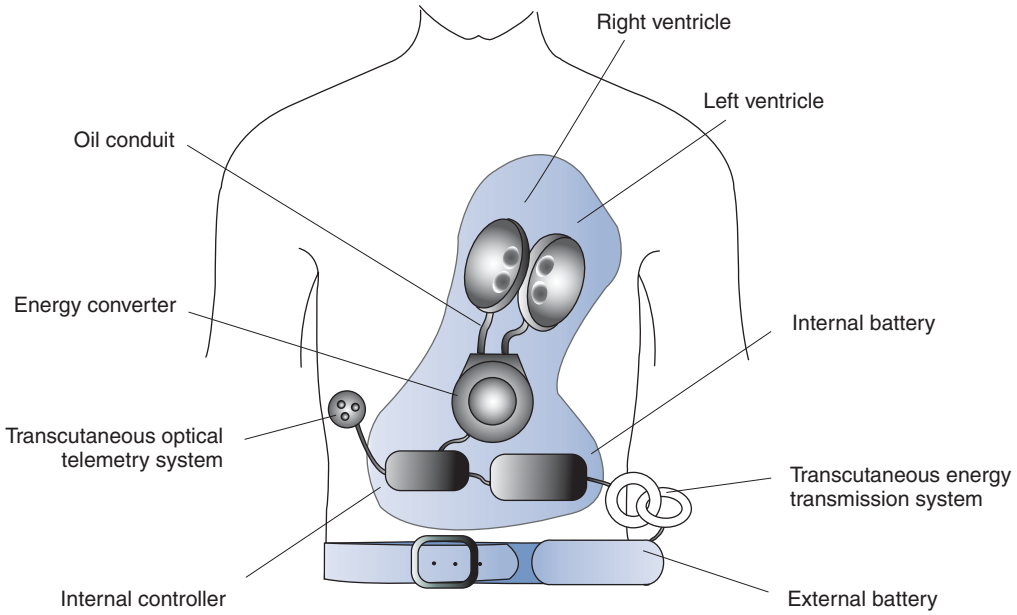

Figure 1. Schematic drawing of the electrohydraulic total artificial heart system. The system is composed of an intrathoracic pumping unit consisting of blood pump and energy converter subunits, and an electronic unit consisting of an internal controller subunit, internal and external batteries, and transcutaneous energy transmission and telemetry subunits.

Figure 2. Intrathoracic pumping unit of the electrohydraulic total artificial heart system. The unit is composed of a blood pump subunit and an energy converter subunit consisting of a brush-less DC motor/regenerative pump assembly.

respectively. The composite atrial cuff is formed by manufacturing left and right cuffs and a common septum in a composite configuration, and is made of another antithrombogenic polyurethane (TM-series, TOYOBO, Osaka Japan) for the blood-contacting surface is reinforced with a velour texture. The aortic and pulmonary artery grafts are made of a woven Dacron graft (Cooley low-porosity, Medox Medical, Oakland, NJ, USA). All the atrial cuffs and grafts are connected to the blood pumps by means of a screw-connecting system in which a freely turning stainless steel screw ring secures a pair of valve holder rings. The polyurethane-made elastic valve-holder ring on the cuff or graft, with its counterpart on the blood pumps, holds the artificial valve tightly, forming virtually seamless joins[3].

The basic shape of the blood pumps was originally designed to be ellipsoidal from the viewpoints of durability and manufacturability, and the optimal dimensions of each pump were determined based on magnetic resonance tomographic images (MRI) of the human chest to fit in the available pericardial space[2]. Consequently, the right blood pump has a flatter configuration than the left, which is in accordance with human anatomy with a considerably shorter distance between the sternum and the right atrioventricular junction. The core dimensions of the current model are $91 \times 64 \times 47$ mm in the left pump, and $100 \times 70 \times 43$ mm in the right pump, respectively. Maximum dynamic stroke volume is approximately 100 mL for both pumps. A good anatomic fit of the blood pumps to the human chest cavity has been confirmed in a three-dimensional thoracic model reconstructed by computer graphics technology[7].

In order to redistribute unequal left and right atrial pressures and volumes due to a left–right output imbalance, which is inherent in the volumetrically coupled EHTAH system, an interatrial shunt (IAS) is employed. In the initial three animal implantations, the IAS was formed by simply punching an orifice at the site of the fossa ovalis in the native atrial septum. However, stenosis of the IAS due to thrombus formation was observed in the third animal, and therefore after the fourth implantation it was made in the artificial atrial septum of the composite atrial cuff. The optimal diameter of the IAS was determined to be 4.0–5.5 mm from our and other groups' previous studies[8–10], and an IAS of 4.5 or 5.0 mm in diameter was used in this study.

The energy converter subunit, designed to be placed outside the pericardial space, consists of a regenerative pump/brush-less DC motor assembly[11]. The brush-less DC motor with three phases and four poles was developed to meet performance demands for both sufficient power and acceptable energy loss in an ordinary-use torque range

(500–1000 g·cm). The regenerative pump reciprocates and delivers silicone hydraulic oil (SH-200, kinematic viscosity: 1.5 cs, specific gravity: 0.853, Toray Silicone, Toray Industries Inc., Tokyo, Japan) to alternate blood pumps through a pair of flexible stainless steel oil conduits (321SS, Cajon, OH, USA) by bi-directional rotation of the impeller. The left and right blood pumps are alternately filled and ejected by displacement of the hydraulic oil and thus create external outputs. The lengths of oil conduits in the animal implantation model are approximately 15 cm for the left pump and 10 cm for the right pump, respectively, and their internal diameter is 10 mm.

Specifications of the current energy converter subunit are approximately 47 mm in thickness, 79 mm in diameter, 280 mL in displacement volume, and 900 g in weight, respectively. *In vitro* testing in a mock circulatory loop (afterloads: 100 mmHg for the left pump and 20 mmHg for the right pump; pre-loads: 10 mmHg for both left and right pumps) demonstrated that the maximum pump output reached over 13 L min^{-1} at 130 bpm, and the maximum efficiency exceeded 14% at 50 bpm when the pump output was approximately 5 L min^{-1} (Figure 3).

Experimental procedure

The EHTAH pumping unit was implanted in 16 Holstein calves weighing from 54–88 kg (mean 66 kg) and was driven by an external controller through a percutaneous lead. The set-up involved induction and maintenance of anesthesia followed by surgical implantation. The surgical procedure is briefly summarized: a right thoracotomy was made through the fifth costal bed, and a cardiopulmonary bypass was instituted using superior and inferior vena caval uptakes and right carotid artery return. The atrial cuffs and outflow grafts were sutured to the respective natural tissues. The blood pumps were orthotopically placed in the pericardial space. In the first nine animals, the energy converter was positioned in the right lower thorax. In the following seven animals, it was positioned in the subcutaneous pocket in the right thoracic region to prevent respiratory failure due to compression and heat accumulation. The atrial and arterial connections to the pump were tightened and de-airing was accomplished through a previously placed catheter. As cardiopulmonary bypass was deliberately withdrawn, the EHTAH was actuated and the pump rate was gradually increased up to approximately 80–90 bpm. After the chest was closed in a standard fashion, the animal was weaned from the respirator, extubated, and transferred back to its living quarters.

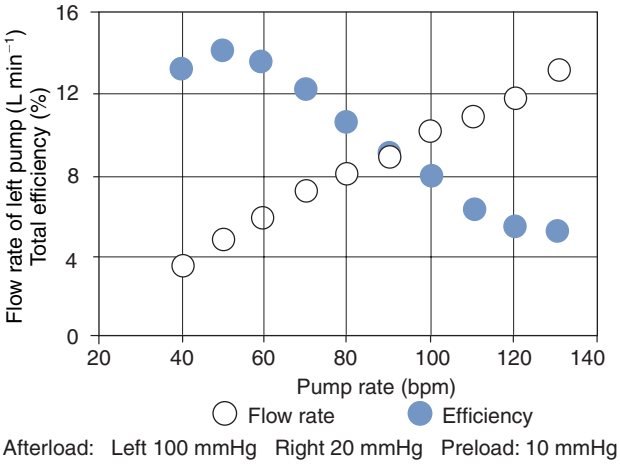

Figure 3. *In vitro* performance of the electrohydraulic total artificial heart pumping unit. Maximum cardiac output reaches 13 L min^{-1} at 130 bpm, while maximum energy efficiency is over 14% at 50 bpm.

Nasal oxygen was routinely supplied postoperatively, and then discontinued as indicated. Intravenous fluid infusion was maintained to remedy circulating blood volume, but no blood transfusion was performed postoperatively except for the return of autologous blood preserved preoperatively or collected from bypass circuit. Furosemide was used as a diuretic to restrict water retention if necessary. Nitroglycerine and isoproterenol were used as the circumstances demanded during the acute postoperative period to reduce systemic or pulmonary vascular resistance. Warfarin sodium (3–5 mg/day) and dipyridamole (400 mg/day) were orally administered after the third postoperative day for anticoagulation.

Hemodynamic and driving parameters were continually registered with a polygraph (NEC San-ei, Tokyo, Japan). Pressures of both atria and the great vessels were monitored with pressure transducers (UK087, Baxter, CA, USA) through fluid-filled catheters placed in the respective vessels. The cardiac output was measured with an ultrasonic flowmeter (Transonic Systems, Ithaca, NY, USA), with a probe positioned on the ascending aorta. In the longest surviving animal, the flowmeter did not work and the cardiac output was estimated based on the known dynamic stroke volume under a full-fill full-eject condition and the pump rate. Arterial and venous blood samples were aspirated from the aortic and pulmonary artery pressure lines and were analyzed with a blood gas analyzer (ABL-500, Radiometer, Copenhagen, Denmark). Input power to the energy converter was continuously monitored with a power meter (AC-DC Digital Power Meter, Model 3192, Hioki, Tokyo, Japan). The condition of heat generation and dissipation from the energy converter was assessed by measuring temperatures of multiple sites on the implanted pumping unit surface with thermocouples (K-type, Okazaki Manufacturing, Kobe, Japan) and a thermometer (Portable Multi Thermometer 2423, Yokogawa M&C, Tokyo, Japan). At the end of the experiment, the animal was given 300 U/kg of heparin and subjected to a postmortem examination.

Results

The overall results are summarized in Table 1. The pumping unit was installed easily in rather small calves as little as 54 kg (Figure 4). Most animals were extubated within

Table 1. Summary of electrohydraulic total artificial heart animal implantation

Experiment No.	Year/month	Body weight (kg)	Surviving time (hours)	Cause of death
1	96/10	62	10	Actuator failure
2	97/11	85	1	Improper operation
3	98/2	72	<1	Interatrial shunt stenosis
4	98/6	88	<1	Power lead breakdown
5	98/8	66	<1	Respiratory failure
6	98/9	60	7	Respiratory failure
7	99/1	73	6	Thromboembolism
8	99/2	66	1	Respiratory failure
9	99/3	61	2	Respiratory failure
10	99/3	69	<1	Convulsion
11	99/4	54	7	Thromboembolism
12	99/5	58	3	Thromboembolism
13	99/6	70	86	Power lead disconnection
14	99/9	58	2	Thromboembolism
15	99/11	55	1	Right outflow valve fall-away
16	00/2	63	42	Oil pressure line breakdown

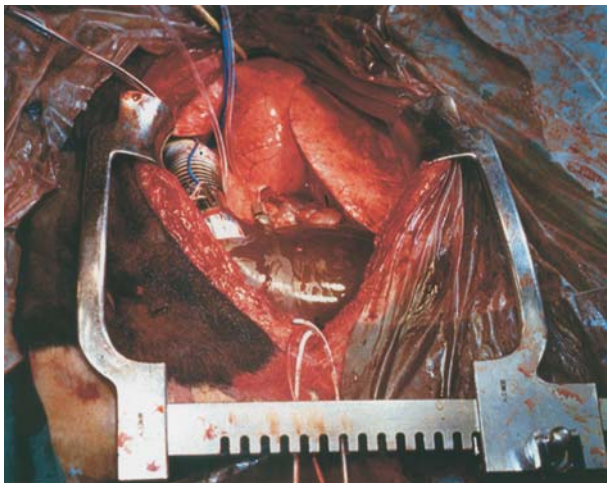

Figure 4. Perioperative view at completion of device installation. The intrathoracic pumping unit was easily implanted through right thoracotomy in calves as small as 54 kg. The right blood pump and the right oil conduit can be seen in this picture.

2 h after surgery, and stood up and started to drink and eat within 4 h. Five out of 16 calves survived for more than 1 week. Major causes of termination were respiratory failure, thromboembolism and device failure, including accident and improper operation. Four out of the first nine animals, in which the energy converter was positioned in the thorax, died of acute respiratory failure, which was probably attributable to compression of the lung by the energy converter in conjunction with heat accumulation. In contrast, there was no occurrence of respiratory failure in the latter seven animals, in which the energy converter was placed in the subcutaneous layer outside the rib cage. Thromboembolism, of which four animals died, was observed more frequently when the animal suffered from infection. Pure mechanical failure occurred in the first case in which bearing breakdown resulted in device malfunction on the 10th day.

One animal survived for over 12 weeks (86 days) until sudden death due to accidental power lead disconnection. This animal underwent the pumping unit implantation without untoward occurrences, exhibited rapid recovery from surgery, and remained in good general condition with almost normal weight gain from 70 kg to 94 kg during the postoperative course (Figure 5). The device was actuated at an adequate fixed rate of 80–85 bpm throughout the experiment. Full-fill full-empty signs were almost always seen in the oil pressure waveforms without accompaniment of a sharp spike wave indicating overfilling or overejecting. The motor revolution speed was manually adjusted to circumvent excessive negative oil pressure in the early diastolic phase, which was a manifestation of inflow obstruction accompanying sucking of the native atrial wall by the active-filling-type EHTAH. The motor revolution numbers were settled at around 1400–1600 rpm for the left systole and 900–1200 rpm for the right systole, respectively, and the resultant left systolic ratio ranged between 40.5–45.3%.

Changes in the mean aortic pressure and the mean pulmonary artery pressure, along with the motor input power, during the experiment of this animal are depicted in Figure 6. Both mean aortic pressure and pulmonary artery pressure stayed rather constant at levels of 87 $\pm$ 8 mmHg and 26 $\pm$ 5 mmHg, respectively, with acceptable motor input power of 13.5 $\pm$ 0.9 W. Cardiac output was estimated to be around 6–8 L min^{-1}, and the energy efficiency from input power to cardiac output was calculated to be approximately 9–11%.

Changes in the left and right atrial pressures and the interatrial pressure gradient during the experiment are

Figure 5. Calf implanted with a pumping unit of the electrohydraulic total artificial heart. The animal exhibited rapid recovery from surgery and survived for more than 12 weeks until sudden death due to accidental power lead disconnection.

illustrated in Figure 7. Average values of the left and right atrial pressures through experimental period were 16 ± 4 and 14 ± 4 mmHg, respectively. The pressure gradient across the IAS was stably maintained at 2 ± 3 mmHg against variations of atrial pressure.

Blood gas data and blood chemistry data are summarized in Tables 2 and 3, respectively. The arterial pH, oxygen and carbon dioxide partial pressures, base excess, and oxygen saturation in the arterial blood were 7.47 ± 0.02, 79 ± 10 mmHg, 42 ± 3 mmHg, 6 ± 2 mEq/L, and 95 ± 1%, respectively. The mixed venous oxygen saturation was 65 ± 4 mmHg. The oxygen metabolic condition was thus maintained favorably during the experiment. In the blood chemistry data, all of the parameters showed almost normal values in the chronic stage of the experiment and there was no evidence of major organ impairment.

Device surface and reference temperatures during the experiment are summarized in Table 4. The temperatures on the energy converter and the oil conduit ranged from 38–40°C, while those of the right parietal pleura and skin were around 39°C and 37°C, respectively.

The device demonstrated good anatomic fit at autopsy, as well as at implantation, without compromising the great vessels and adjacent tissues. The blood pumps were surprisingly clean, and were free from thrombus formation. The IAS was also completely patent and free of thrombus. We found a couple of small chronic infarctions in the kidneys, however we did not see any abnormal findings in the other major organs.

Table 2. Hemoglobin and blood gas data in the longest surviving animal.

Parameter (unit)	Value (mean ± SD)
Blood hemoglobin concentration (g/dL)	10.9 ± 0.9
Arterial blood pH	7.47 ± 0.02
Arterial oxygen partial pressure (mmHg)	79 ± 10
Arterial carbon dioxide partial pressure (mmHg)	42 ± 3
Base excess (mEq/L)	6 ± 2
Arterial oxygen saturation (%)	95 ± 1
Mixed venous oxygen saturation (%)	65 ± 4

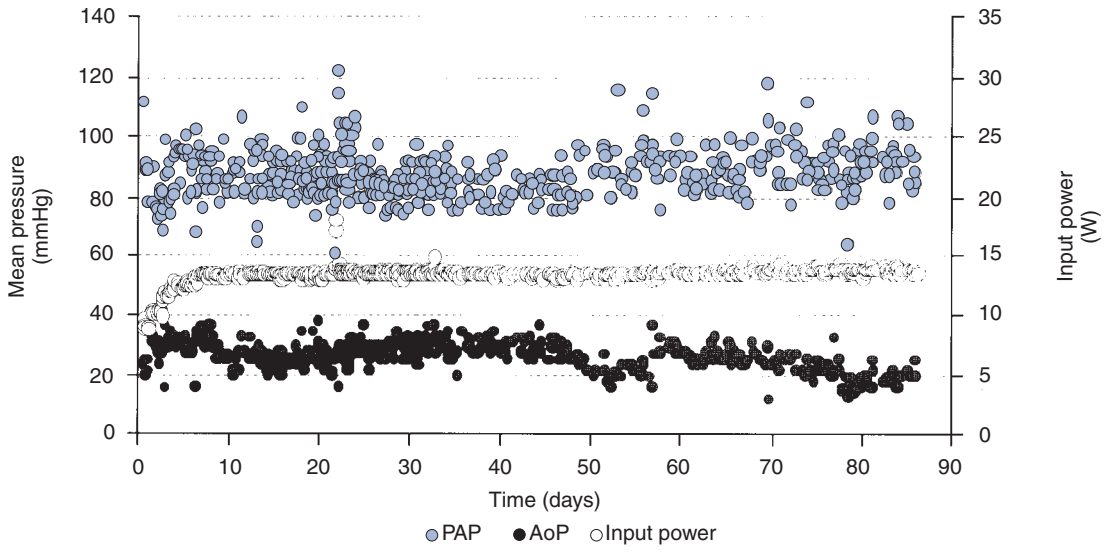

Figure 6. Changes in mean aortic pressure (AoP), mean pulmonary artery pressure (PAP), and motor input power in the longest surviving animal. Both mean aortic pressure and pulmonary artery pressure stayed rather constant, with acceptable motor input power of 13.5 ± 0.9 W. The energy efficiency from input power to cardiac output was calculated to be 9–11%.

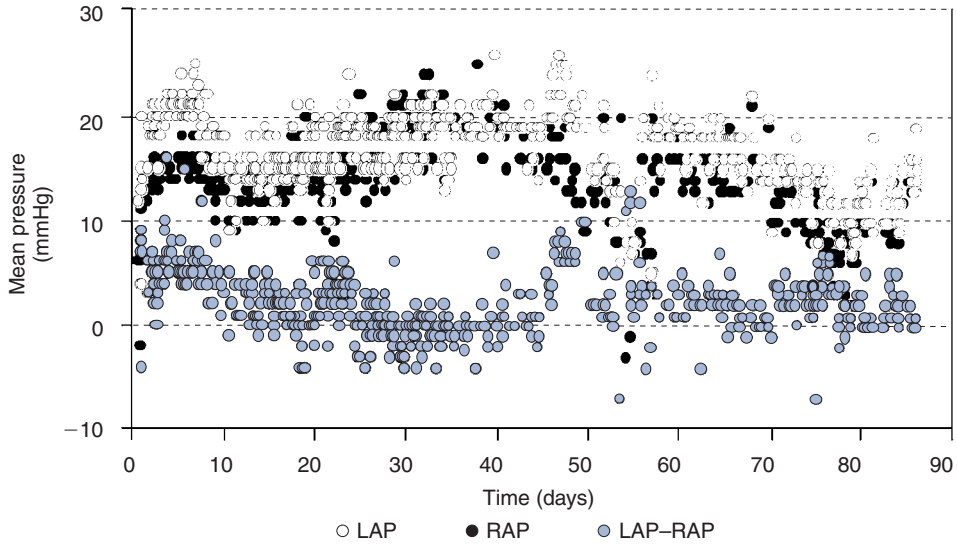

Figure 7. Changes in left and right atrial pressures (LAP and RAP) and interatrial pressure gradient (LAP–RAP) in the longest surviving animal. Average values of the left and right atrial pressures were 16 ± 4 and 14 ± 4 mmHg, respectively, and the pressure gradient across the IAS was stably maintained at 2 ± 3 mmHg.

Table 3. Blood chemical data in the longest surviving animal

Parameter (unit)	4th week	8th week	12th week
Total protein (g/dL)	5.4	6.3	7.2
Albumin (g/dL)	2.2	2.9	2.9
Blood urea nitrogen (mg/dL)	8	13	13
Creatinine (mg/dL)	0.6	0.9	0.4
Glutamic oxaloacetic transaminase (IU/L)	49	40	47
Glutamic pyruvic transaminase (IU/L)	6	9	10
Total bilirubin (mg/dL)	0.7	0.6	0.6
Lactate (mg/dL)	4	7	9

Discussion

After the first clinical application of a pneumatic TAH in 1969, more than 350 patients have been implanted with TAHs, mostly as a bridge to heart transplantation. Pneumatic TAH is not regarded, however, as a practical alternative for permanent cardiac replacement, since previous trial of its permanent use attempted in five patients had to be aborted because of a high incidence of thromboembolism and infection. Recent efforts in TAH development, therefore, have been directed toward a fully implantable system that can reduce the chance of infection and provide an acceptable quality of life for the patient by eliminating an external tether. In the USA, considerable progress has been made in developing fully implantable electric TAH systems during the last decade, being accelerated by NIH-sponsored contracts[12], and the basic feasibility has been demonstrated by the long-term survival of animals of over 5 months[9,13]. Nevertheless, all the systems under development in the USA seem too bulky to be implanted into the pericardial space of standard-sized Asian people. Accordingly, development of a suitable system applicable to smaller recipients is of great necessity in our country.

To meet such anatomic requirements without compromising pumping performance, we contrived in our EHTAH system a unique formation of the components in which the energy converter subunit was located outside the pericardial space, separately from the blood pump subunit. This characteristic feature, derived from the electrohydraulic driving fashion, afforded an excellent anatomic fit, and the pump-

Table 4. Device and body temperature in the longest surviving animal

Site of measurement	Temperature (°C, mean ± SD)
Actuator surface*	39.5 ± 0.5
Oil conduct surface	39.2 ± 0.8
Parietal pleura	38.9 ± 1.5
Reference skin‡	37.1 ± 0.8
Room air	24.4 ± 1.2

*Outside of insulation; ‡in the subcutaneous layer.

ing unit was successfully implanted in calves as small as 54 kg. Separate placement of the blood pump and energy converter subunits also facilitated surgical implantation of the device in terms of enabling surgeons patient-specific installation and relatively free positioning of each blood pump. The implantation procedure for EHTAH was therefore analogous to that for pneumatic TAH, and the cardiopulmonary bypass time was usually less than 3 h.

In the present study, the pumping unit demonstrated a sufficient *in vivo* output of 6–8 L min^{-1} under a fixed driving mode, and sustained the animals' circulation stably for as long as 86 days. It is conceived that a TAH should yield more than 8 L min^{-1} maximum output to provide recipients an acceptable quality of life in terms of capability for moderate exercise[12]. The current EHTAH system with 6–8 L min^{-1} continuous *in vivo* output and up to 13 L min^{-1} *in vitro* maximum output suffices for this performance requirement. To utilize the pumping performance of EHTAH fully, a physiologic control method responsive to output demand is now under development. It is expected to involve in the control algorithm the fill-to-empty variable heart rate control logic which has been well authenticated in *in vitro* and *in vivo* evaluations[9,10]. On this fundamental logic providing a Starling-like response, we contemplate adding an algorithm that transiently augments output increase in response to exercise. A mixed venous oxygen saturation sensor signal is being investigated to be utilized for this purpose[14].

In the development of an electric TAH system, energy efficiency is an important issue both in total energy consumption and in heat generation inside the body. In the longest surviving animal, the input power was 13.5 $\pm$ 0.9 W, and the energy efficiency from input power to cardiac output was estimated to be around 9–11%, which seemed within an acceptable level in terms of energy consumption. The device surface temperatures always remained around 38–40°C, only 1–2°C higher than the body temperature, which seemed compatible with chronic implantation without causing tissue necrosis. We have identified that in our EHTAH system approximately half of the generated heat is dissipated into the blood via the driving fluid and across the diaphragms of the blood pumps[15], which should have resulted in the minute temperature rise in the present study. This advantageous feature was derived from the structure of the electrohydraulic driving system.

In the EHTAH system, an IAS was employed to accommodate the left–right output imbalance that is inherent in a volumetrically coupled TAH system. The IAS has been proven to redistribute unequal left–right atrial pressures and volumes effectively in our and the other groups' previous studies[8–10]. The advantage of an IAS in comparison with the other balancing methods is its simplicity of fabrication and implantation. This approach avoids additional engineering developments, surgical procedures, and space demands. A simple control algorithm based on a passive but dynamic balancing mechanism is another advantage of the IAS. The left–right balancing function of the IAS, therefore, covers a wide range of physiologic conditions.

To determine the optimum diameter of the IAS is of great importance for its practical application, since its diameter influences not only the net forward flow but also the magnitude of reverse flow. In the present study, an IAS with a diameter of 4.5 or 5.0 mm was used based on the results of earlier studies[8–10]. Consequently, adequate left–right balance with an acceptable interatrial pressure difference was obtained against a broad variation of atrial pressures. The blood gas data suggested that mixing of arterial blood with venous blood through the IAS was inconsequential to the systemic oxygenation. Another concern in the use of the IAS is its long-term patency. In the present study, stenosis of the IAS due to thrombus formation was observed in one of the initial three animals in which the IAS was formed by simply punching an orifice in the native atrial septum. Therefore, we made a change so that the IAS was in the artificial atrial septum of the composite atrial cuff, which successfully resulted in perfect patency in the following 13 animals, including one that survived for more than 12 weeks. The University of Utah group, the original proposer of the IAS method, have also reported that an IAS made by the joined left and right free atrial cuff walls was consistently patent in a series of *in vivo* experiments for as long as 5 months[9].

In the present study, four animals died of thromboembolism, and others exhibited small renal infarctions at autopsy. These facts illuminated the still unsatisfactory thrombo-resistant property of the device. To obtain better antithrombogenicity of the blood pumps against its long-term use, the following two approaches have been contemplated. First, optimization of blood pump shapes from a hydrodynamic viewpoint have been implemented according to the results of a newly developed flow visualization technique, which can assess instantaneous wall shear stress inside the diaphragm-type blood pumps[16]. Secondly, a recently developed powerful heparin-coated surface treatment, with which a percutaneous cardiopulmonary bypass circuit could be run continuously for more than 1 month without systemic anticoagulation[17], is planned to be introduced to the entire blood-contacting surface of the EHTAH system.

In summary, with the present study we have demonstrated the basic *in vivo* performance of our EHTAH pumping unit. The pumping unit showed an excellent anatomic fit, and demonstrated 6–8 L min^{-1} of *in vivo* cardiac output with 9–11% energy efficiency. One animal could successfully survive for longer than 12 weeks with a good general condition. These favorable characteristics indicate that the EHTAH has the potential to be a totally implantable cardiac replacement.

Acknowledgements

This work was supported financially, in part, by the Research Grant for Cardiovascular Diseases (10C–2) from the Ministry of Health and Welfare of Japan, a Grant-in-Aid for Scientific Research from the Ministry of Education of Japan (No.10357013), and the New Energy and Industrial Technology Development Organization (NEDO).

References

1. Committee to Evaluate the Artificial Heart Program of the National Heart, Lung, and Blood Institute, Division of Health Care Service, Institute of Medicine. Hogness JR, VanAntwerp M, editors. *The Artificial Heart: Prototypes, Policies, and Patients*. Washington DC: National Academy Press, 1991.
2. Taenaka Y, Takano H, Takatani S *et al.* Design and trial fabrication of a total artificial heart for Japanese. *Jpn J Artif Organs* 1988;17:835–8.
3. Taenaka Y, Sekii H, Tatsumi E *et al.* An electrohydraulic total artificial heart with a separately placed actuator. *Trans Am Soc Artif Intern Organs* 1990;36:M242–5.
4. Tatsumi E, Taenaka Y, Masuzawa T *et al.* Development of an electrohydraulic total artificial heart system. In Akutsu T, Koyanagi H, editors. *Artificial Heart 5. Heart Replacement.* Tokyo: Springer-Verlag, 1996:101–7.
5. Masuzawa T, Taenaka Y, Tatsumi E *et al.* Set-up, improvement, and evaluation of an electrohydraulic total artificial heart with a separately placed energy converter. *ASAIO Journal* 1996; 42: M328–32.
6. Koshiji K, Yazaki T, Nomura T *et al.* Externally-coupled transcutaneous energy transmission system for a totally implantable artificial heart. *Proc 15th Int IEEE Eng Med Biol* 1993;909–10.
7. Zhang B, Masuzawa T, Tatsumi E, *et al*. Three-dimensional thoracic modeling for an anatomical compatibility study of the implantable total artificial heart. *Artif Organs* 1999;23:229–34.
8. Tatsumi E, Nakamura M, Masuzawa T *et al. In vitro* and *in vivo* evaluation of left–right balancing capacity of an interatrial shunt in an electrohydraulic total artificial heart system. *ASAIO Journal* 1997;43:M619–25.
9. Tatsumi E, Khanwilkar PS, Rowles JR *et al. In vivo* long-term evaluation of the Utah electrohydraulic total artificial heart. *ASAIO Journal* 1993;39:M373–80.
10. Tatsumi E, Diegel PD, Holfelt JW, *et al*. A blood pump with an interatrial shunt for use as an electrohydraulic total artificial heart. *ASAIO Journal* 1992;38:M425–30.
11. Masuzawa T, Taenaka Y, Kinoshita M *et al.* An electrohydraulic totally implantable artificial heart with a motor-integrated regenerative pump. In Akutsu T, Koyanagi H, editors. *Artificial Heart 4. Heart Replacement.* Tokyo: Springer-Verlag, 1993:143–6.
12. *Request for Proposal No. NHLBI-HV–92–28*, Bethesda, National Heart, Lung, and Blood Institute, 1992.
13. Snyder AJ, Rosenberg G, Weiss WJ *et al*. *In vivo* testing of a completely implantable total artificial heart system. *ASAIO Journal* 1993;39:M177–84.
14. Nakamura M, Masuzawa T, Tatsumi E *et al.* The development of a control method for a total artificial heart using mixed venous oxygen saturation. *Artif Organs* 1999;23:235–41.
15. Endo S, Masuzawa T, Tatsumi E *et al. In vitro* and *in vivo* heat dissipation of an electrohydraulic totally implantable artificial heart. *ASAIO Journal* 1997;43:M592–7.
16. Nakata M, Masuzawa T, Tatsumi E *et al.* Characterization and optimization of the flow pattern inside a diaphragm blood pump based on flow visualization techniques. *ASAIO Journal* 1998;44:M714–18.
17. Sato M, Kashiwabara S, Tanaka H, Tatsumi E, Taenaka Y, Takano H. *In vitro* antithrombogenic evaluation of newly developed heparinized coating material. *Jpn J Artif Organs* 1999;28:502–8.

Journal of Congestive Heart Failure and Circulatory Support (2001) Vol 1, No 4, 161–166

Ultracompact, totally implantable, permanent TAH

S. Takatani D Med PhD[1], K. Ohuchi MS[1], M. Nakamura MD PhD[1] and T. Sakamoto MD PhD[2]
[1]Department of Artificial Organs, Institute of Biomaterials and Bioengineering; and [2]Department of Replacement Surgery, Tokyo Medical and Dental University, Tokyo, Japan

Abstract An ultracompact, totally implantable, permanent total artificial heart (TAH) has been developed and its performance was tested in a mock circulatory loop. The compact TAH is a one-piece unit that is comprised of a miniature electromechanical actuator consisting of a brush-less DC-motor and a planetary roller-screw, and left and right pusher-plate blood pumps. The left and right pump housings were designed based on data from 26 heart transplant recipients through a computer-aided design and manufacturing (CAD/CAM) process. The pump housings of the prototype model were made of epoxy resin, while the final version will be made of titanium alloy (Ti–6Al–7Nb). The flexing diaphragm is made of polyurethane through a dip-coating technique. The diameter and thickness of the prototype model are 90 mm and 70 mm, yielding an overall volume of 400 cc. The TAH is operated in the left–right alternate-ejecting mode with the device-based information including commutation sensor signals and Hall-effect pusher-plate position signal. Pump rate, stroke volume and pump output can be derived from the Hall-effect sensor signal. An optical reflectance sensor is also mounted on each pump housing to continuously monitor arterial and venous blood hemoglobin content and oxygen saturation. Although the size was reduced, the prototype TAH could provide the maximum flow of 8 L min^{-1}, with a maximum power requirement of approximately 18 W. The maximum electrical-to-hydraulic efficiency was 13.5%. This compact TAH is ready for evaluation in animal experiments.

Keywords total artificial heart (TAH), heart transplantation, bridge to transplantation, mechanical circulatory support (MCS), heart replacement.

Introduction

Mechanical circulatory support devices (MCSDs) such as the total artificial heart (TAH) and ventricular assist device (VAD) have proven their effectiveness in treating patients with end-stage cardiac failure[1–5]. To date, the main usage of MCSDs is as a bridge to heart transplantation. However, because of a donor heart shortage, the waiting time for a heart transplant can be six months or even longer. In addition, because of immunological complications, age limitation and high cost, it is estimated that between 50 000 and 70 000 end-stage cardiac patients die annually without benefiting from heart transplantation[6]. The majority of patients with end-stage heart failure – approximately 75% – can be salvaged with a univentricular support device or VAD, and the remaining 25% with a bi-ventricular support device or replacement-type TAH. Totally implantable, permanent VADs and TAHs are the alternate therapy for patients who cannot receive heart transplantation. For this purpose, totally implantable VADs and TAHs have been under development at various centers around the world[7–10].

This paper addresses the current status of a compact, totally implantable permanent TAH that is under development at our institute[11]. The current model was designed to meet the needs of patients weighing 50–60 kg, including women. The device is one-piece and the design of the left–right pump configuration was based on the anatomical data obtained at Baylor College of Medicine from 26 recipients of heart transplants[12,13].

Materials and methods

Design specifications of the implantable TAH

The design specifications include:

1. The TAH should fit all patients, including women, with a body weight ranging between 50–60 Kg.
2. The TAH should be operated in a passive fill mode with the resting and maximum pump output against 100 mmHg afterload of 4–5 L min^{-1} and 8–9 L min^{-1}, respectively.
3. Power requirements to obtain pump flows as specified in (2) should be 10–15 W with the electrical-to-hydraulic efficiency of 15%.
4. The TAH should be controllable using the device-based information with possible physiological feedback signals.
5. A durability of 2–3 years is desirable.
6. Titanium alloy and polyurethane are the possible candidates for blood-contacting surfaces, including the pump housing, diaphragm and inflow and outflow valves, respectively. Titanium alloy was selected

Correspondence to: Professor Setsuo Takatani MD PhD, Department of Artificial Organs, Institute of Biomaterials and Bioengineering, Tokyo Medical and Dental University, 2-3-10 Surugadai, Kanda, Chiyoda-ku, Tokyo 101-0062, Japan.

because of its inert, stable performance for a prolonged period without exhibiting toxic effects in the biological environment.

Concept of the totally implantable TAH system[14,15]

Figure 1 shows the anatomical configuration of the TAH and its components. The electrical energy will be transmitted inside the body using a transcutaneous energy transmission (TET) concept. The electrical power from the external battery will first be converted to AC power using a switching circuit at around 100–200 KHz and then transmitted inside the body using a coupled coil system. The primary coil will be placed outside the body over the secondary coil implanted in the subcutaneous space. The transmitted electrical energy will then be used to power the implanted blood pump as well as to charge the internal battery. The internal battery can take over the function of powering the TAH for at least 30 min or longer in case the external coil of the TETS is accidentally dislocated or the patient wishes to take a shower or bath. The run time of the external battery should be at least 7–8 h from initiating the re-charging process. A compliance chamber or variable volume device will be implanted inside the chest cavity to compensate for volume changes that occur in the blood side of the pump.

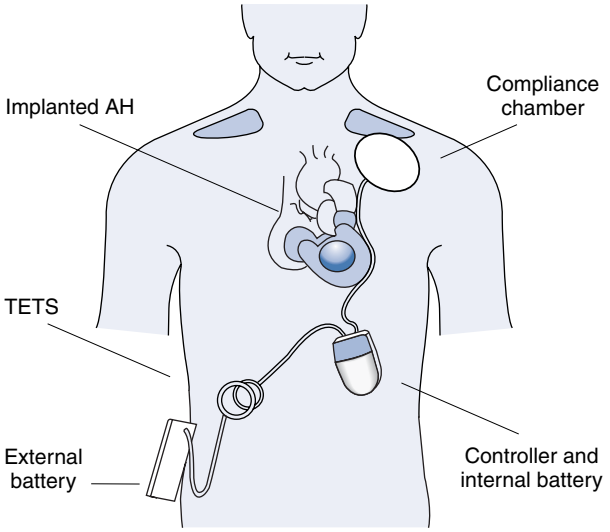

Figure 1. Anatomical placement of totally implantable TAH and its components.

Schematics and components of the TAH

The schematic diagram of the TAH[11] is shown in Figure 2. The TAH is a one-piece unit consisting of the left and right pusher-plate-type blood pumps and a miniaturized actuator sandwiched between the two blood chambers. The actuator comprises a miniature, 14-pole Y-wound brush-less DC-motor (Kollmorgen Inc., USA) and a planetary roller-screw (SKF, France). The rotational motion of the motor is converted to a recti-linear motion of the roller-screw to compress the diaphragm. The motor direction is reversed to alternately eject the left and right blood pumps. The Hall-effect signal of the left pump is used to initiate the

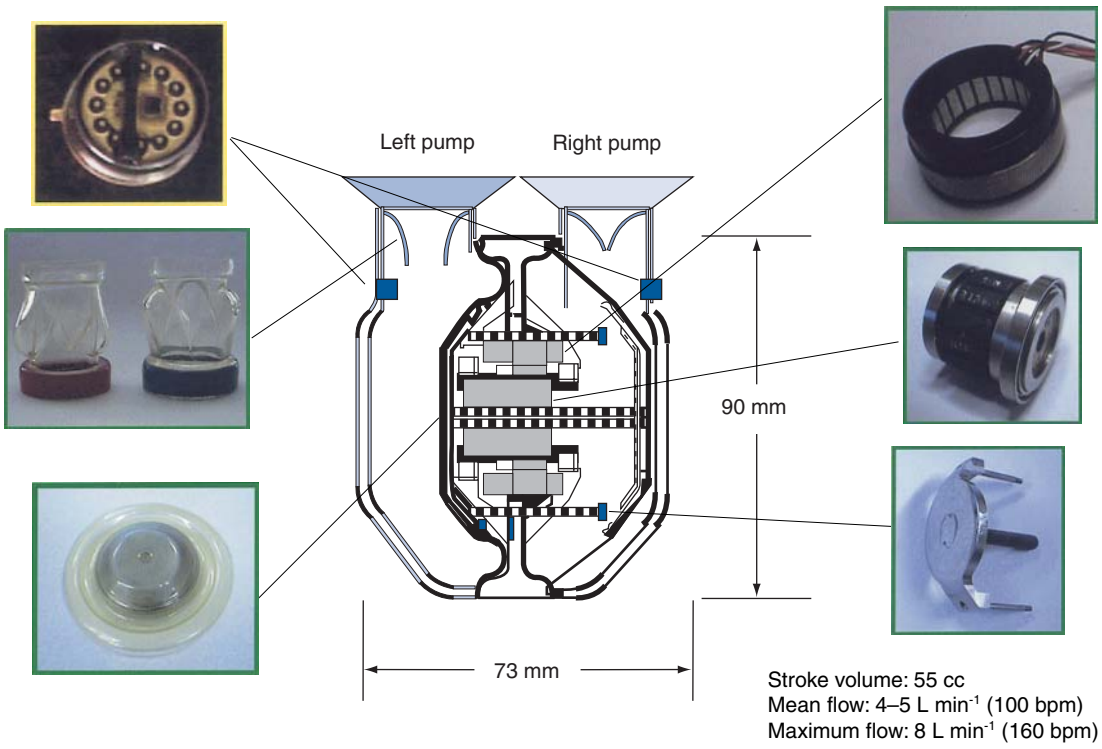

Figure 2. Schematic diagram of totally implantable TAH.

left ejection, followed by the ejection of the right pump. The Hall-effect position signal will also be used to compute the pump rate and stroke volume, and then to derive the minute pump output. The flexing diaphragm is made of polyurethane (Biospan SPU, Polymer Technology Inc., USA) through the dip-coating method. A reflection-type optical sensor will be mounted on each pump housing to monitor arterial and mixed venous hemoglobin content (Hb) as well as hemoglobin oxygen saturation (SaO_2, SvO_2). By combining the information obtained from the optical sensor and Hall-effect displacement sensor, the oxygen consumption of the TAH recipients can be continuously derived. The external diameter of the TAH is 90 mm, allowing an effective inner diameter of 84 mm. The thickness of the TAH is 73 mm and this thickness allows for a stroke length of 12 mm. The designed stroke volume is 55 cc.

Fabrication process of the TAH

The final goal is to fabricate the TAH housing as a one-piece system from a titanium alloy that contains 6% aluminum and 7% niobium (Ti–6Al–7Nb). The fabrication process of the TAH is shown in Figure 3. The computer-assisted design (CAD) system will be utilized to obtain three-dimensional images of the TAH. Based on the CAD data, prototype TAH housings will first be fabricated using the optically curable epoxy resin. By converting the three-dimensional data to computer-assisted machining (CAM) data, titanium alloy pump housings will be fabricated as a one-piece unit.

Pump output control strategy

As for the TAH pump output control, the primary control is the fill/empty control using the Hall-effect pusher-plate position signal. Since the pump operates in a passive fill mode, pump rate and hence pump output will vary in response to venous return or filling pressure. We believe this mode of operation is adequate for the passive fill-type TAH. For monitoring purposes, a reflectance-type optical sensor was installed in the left and right pump housing to continuously monitor the arterial and venous blood hemoglobin (Hb) level and hemoglobin oxygen saturation (SaO_2, SvO_2). By combining this information together with pump output (CO) obtained from the Hall-effect sensor signal, oxygen consumption (VO_2) of the TAH recipients can be estimated using a Fick's equation:

$$VO_2 = 1.34 \times [Hb] \times (SaO_2 - SvO_2) \times CO$$

This information will be useful in understanding the circulatory physiology of artificial heart implanted patients.

Results

Figure 4 shows the CAD TAH images seen from various angles. Adjustments in various pump dimensions were made to improve the appearance of the TAH housings. Figure 5 shows the assembled prototype TAH made of epoxy resin. The inflow and outflow port directions were decided based on the intra-thoracic space, remnant great vessels as well as excised heart data obtained from 26 heart transplantation

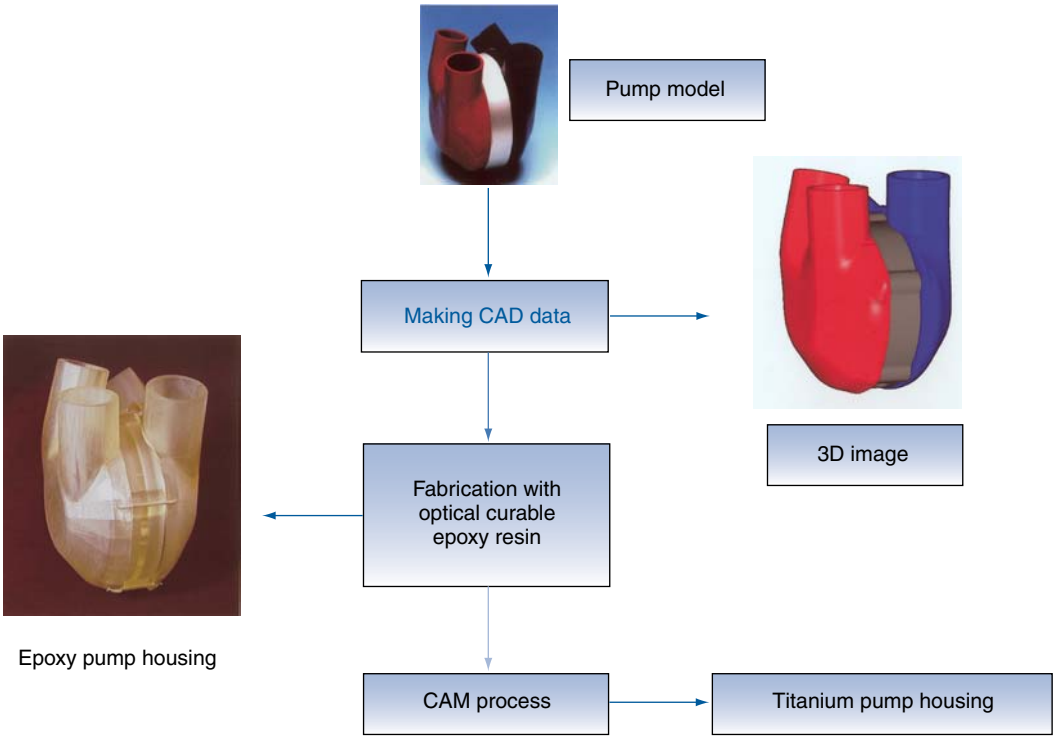

Figure 3. CAD/CAM fabrication process of the TAH.

recipients. The epoxy pump housing models resulted in the volume and weight of 400 cc and 440 g, respectively.

Figure 6 shows the left and right pump flows versus pumping rate. Flows of 4–5 L min^{-1} flows can be obtained at the pump rate of 90 bpm against left and right pump after-loads of 100 mmHg and 25 mmHg, respectively. The maximum flow of 9 L min^{-1} was obtained at the pump rate of 160 bpm. The left pump flow was slightly larger than the right pump flow. Figure 7 shows the left and right pump stroke volume. The average left pump stroke volume was around 54 cc, while that of the right pump was 52 cc. The electrical-to-hydraulic efficiency of the pump system is shown in Figure 8**.** The maximum efficiency of 13.5% was obtained at the pump rate of 120 bpm. The power requirement was 13.3 W and the maximum input power was 18.7 W at 160 bpm. Table 1 summarizes the characteristics of the current model in comparison to the Baylor TAH model. The pump size was considerably reduced, but the maximum pump flow remained approximately the same as with the previous design.

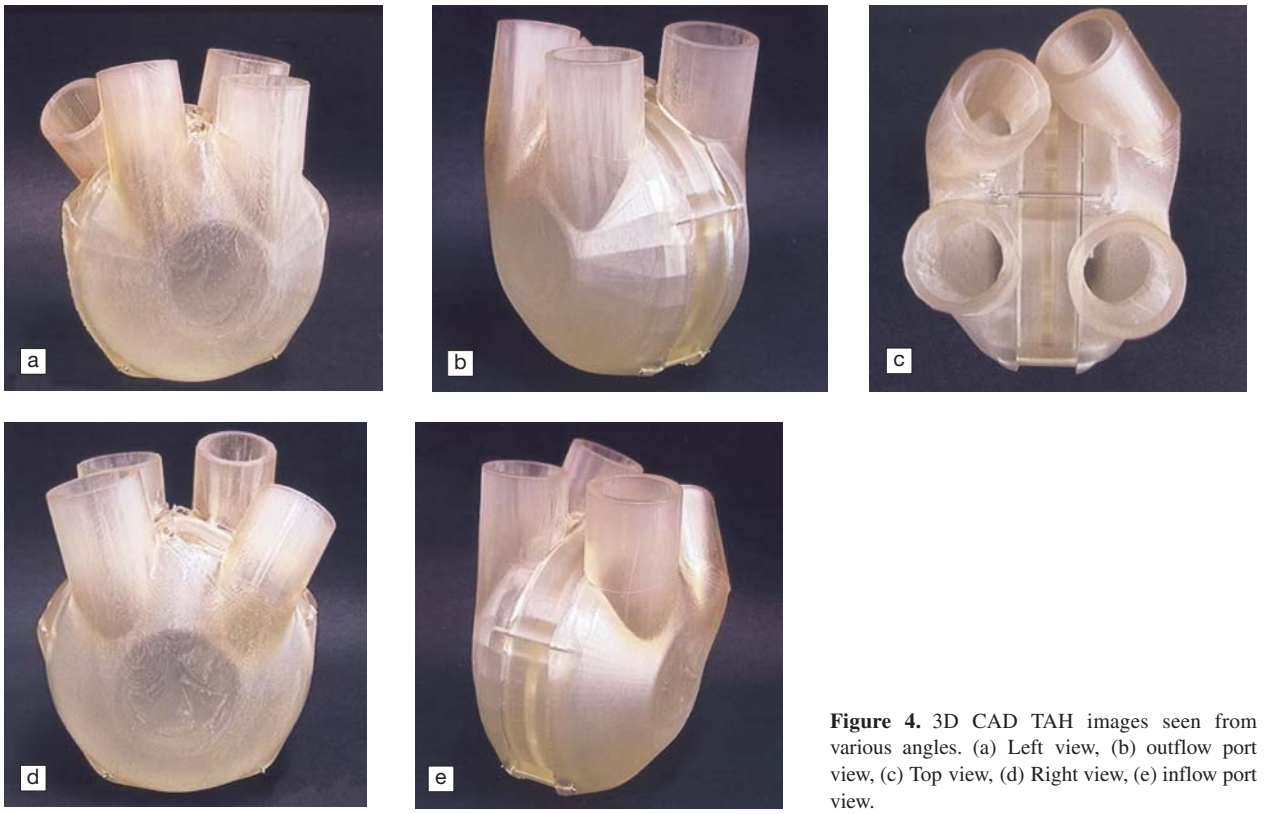

Figure 4. 3D CAD TAH images seen from various angles. (a) Left view, (b) outflow port view, (c) Top view, (d) Right view, (e) inflow port view.

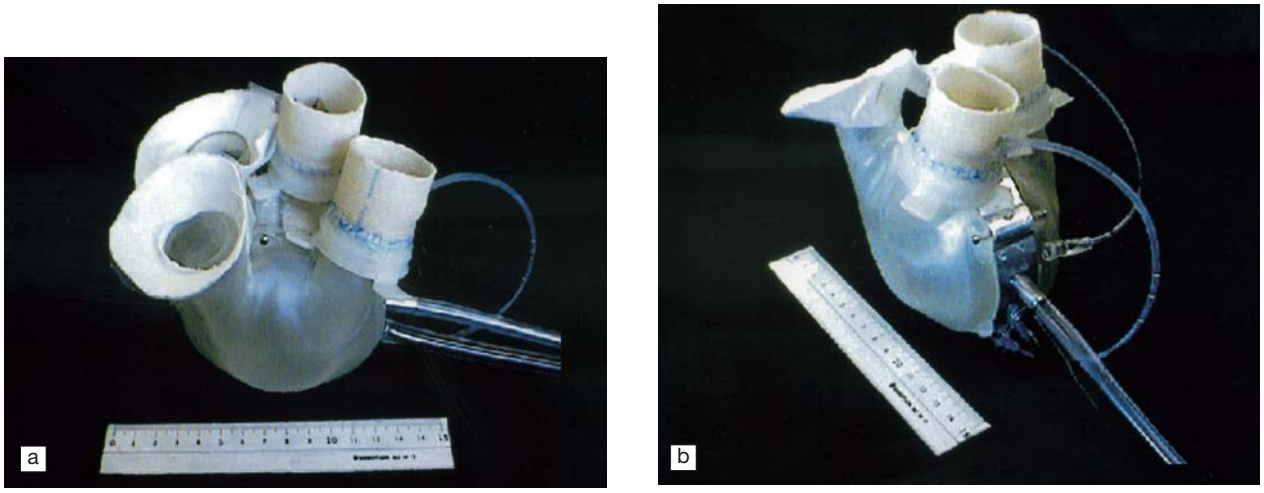

Figure 5. Assembled prototype TAH made of epoxy resin. (a) Right pump front, (b) Side view.

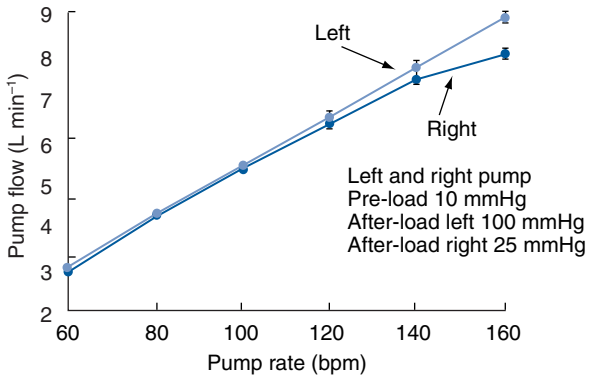

Figure 6. Left and right pump flow versus pump rate.

Discussion

An ultracompact, high-performance, totally implantable TAH intended for use in patients weighing 50–60 kg has been developed based on the anatomical data obtained from 26 heart transplant recipients. The CAD pump data was generated to fabricate the pump housing utilizing a CAM process. The prototype model was fabricated with optically curable epoxy resin to examine its basic performance. Although the size was reduced, the basic performance met the design specifications. The maximum pump output of 9 L min^{-1} was obtained at the pump rate of 160 bpm. This indicates that the net stroke volume is approximately 53 cc. A maximum electrical-to-hydraulic efficiency of 13.5% was obtained at 120 bpm and the required power input was 13.3 W.

The TAH is controlled with the device-based information including motor commutation sensor and Hall-effect pusher-plate position signals. The commutation sensor signals of the brush-less DC-motor are used to control stroke length, motor speed and motor direction. Combining with the Hall-effect pusher-plate position signal, the pump can be operated in the passive fill/full eject mode with the left filling triggering the ejection of the left pump, followed with right ejection. The left pump ejection speed can be varied in response to the left filling speed, which in turn regulates the right filling time, thus regulating the right pump output and consequently left atrial pressure. In this way, the TAH can be controlled with the left fill/full eject primary mode and with the right fill-limited mode. The right pump fill-limited mode allows pump output changes in response to venous return change.

As for left–right flow balance, the right stroke length was made 2 mm shorter than the left. This stroke length difference reduced the right pump stroke volume to approximately 3 cc, which is 5% of the left. If a larger flow differential is required, the screw position can be re-adjusted. Also, a variable volume device or a compliance chamber will be implanted to compensate for the volume differences between the two blood chambers.

If the pump can output at a volume that conforms with Starling's law, no physiological control will be necessary. A passive-fill blood pump, with good fill sensitivity, should fulfil this requirement. Physiological control requires reliable bio-sensors and efficient algorithm control which adds complexity to the system.

For the totally implantable system, we intend to fabricate the pump housing with titanium alloy (Ti–6Al–7Nb) because of its stable, long-term, corrosion-free performance

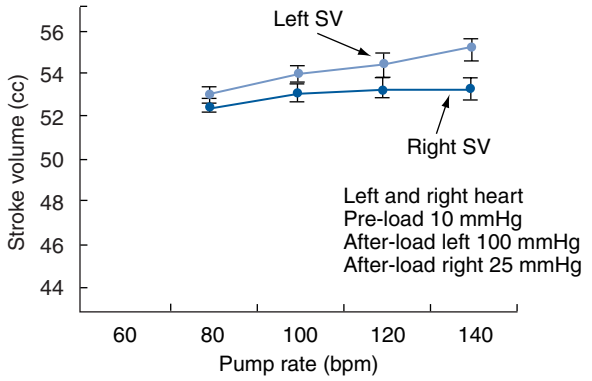

Figure 7. Left and right pump stroke volume.

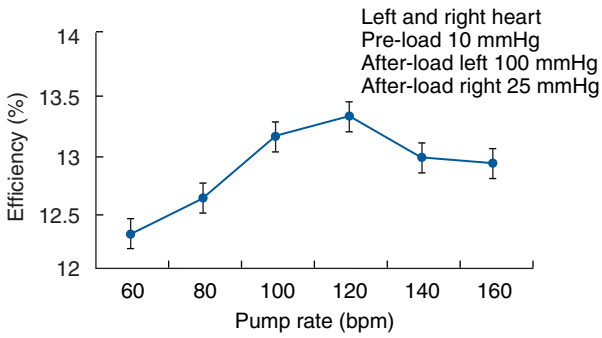

Figure 8. Electrical-to-hydraulic efficiency versus pump rate.

Table 1. Comparison of pump characteristics.

	Diameter	Thickness	Volume	Weight	SV	Maximum flow
TAH	90 mm	73 mm	400 cc	440 g	53 mL	8.5 L min^{-1}
Baylor TAH*	98 mm	82 mm	510 cc	620 g	63 mL	9 L min^{-1}

* Shiono M *et al*. Anatomic constraints for a TAH . . . *J Heart Lung Transplant* 1994;13:250–62.

in the biological environment. Its surface produces a thin oxidized hydrophilic film that may present a long-term, blood-compatible feature. A dedicated microprocessor control system will be built to operate the totally implantable TAH. Initially, we will evaluate the system with the vent port open to the atmosphere, before implanting the compliance chamber inside the chest cavity. A transcutaneous energy transmission system will then be introduced to allow tether-free operation of the system.

Summary

An ultracompact, totally implantable, permanent TAH has been developed for use in patients weighing 50–60 kg. The TAH made of epoxy resin has a volume of 400 cc and a weight of 440 g. It can provide the maximum flow of 9 L min^{-1} at 160 bpm. The maximum electrical-to-hydraulic efficiency was 13.5% at 120 bpm. This TAH is ready for biocompatibility and durability studies in animal experiments.

Acknowledgement

This research was partially supported by grants-in-aid (Nos.11558102, 10044232) from the Ministry of Education in Japan.

References

1. Arabia FA, Copeland JG, Smith RG *et al*. Infections with the Cardiowest Total Artificial Heart. ASAIO J 1998;44(5): M336–9.
2. Arabia FA, Smith RG, Rose DS *et al*. Success rate of long-term circulatory assist device used currently for bridge to heart transplantation. *ASAIO J* 1996;42:M542–6.
3. Loisance D. Mechanical circulatory support toward permanent use. *Artif Organs* 1998;22(1):85–6.
4. Mehta SM, Boehmer JP, Pae WE *et al*. Bridging to transplant: Equal extended survival for patients undergoing LVAD support when compared with long-term medical management. *ASAIO J* 1996; 42:M406–10.
5. Pristas JM, Winowich S, Nastala CJ *et al.* Protocol for releasing Novacor left ventricular assist system patients out-of-hospital. *ASAIO J* 1995;41:M539–43.
6. Hogness JR, VanAntwerp M. *The Artifcial Heart; Prototypes, Policies, and Patients*. Washington, DC: National Academy Press, 1991.
7. Rosenberg G, Snyder AJ, Weiss WJ *et al.* Dynamic *in vitro* and *in vivo* performance of a permanent total artificial heart. *Artif Organs* 1998;22(1):87–94.
8. Kung RTV, Yu LS, Ochs BD *et al*. Progress in the development of the Abiomed total artificial heart. *ASAIO J* 1995;41:M245–8.
9. Abe Y, Chinzei T, Isoyama T *et al.* Present status of the total artificial heart at the University of Tokyo. *Artif Organs* 1999;23(3):221–8.
10. Tatsumi E, Masuzawa T, Nakamura M *et al. In vivo* evaluation of the National Cardiovascular Center electrohydraulic total artificial heart. *Artif Organs* 1999;23(3):242–8.
11. Honda N, Inamoto T, Nogawa M, Takatani S. Ultracompact, completely implantable permanent use electromechanical ventricular assist device and total artificial heart. *Artif Organs* 1999;23(3):253–61.
12. Shiono M, Noon GP, Hess KR *et al.* Anatomic constraints for a total artificial heart in orthotopic heart transplant recipients. *J Heart Lung Transplant* 1994;13:250–62.
13. Takatani S, Shiono M, Sasaki T *et al.* Development of a totally implantable electromechanical total artificial heart. *Artif Organs* 1992;16:398–406.
14. Takatani S, Koyanagi H, Nogawa M, Inamoto T, Nishida H. Ultracompact, high performance, completely implantable permanent electromechanical total artificial heart. *Heart Replacement Artif Heart* 1998;6:8–14.
15. Takatani S, Orime Y, Tasai K *et al.* Totally implantable total artificial heart and ventricular assist device with multipurpose miniature electromechanical energy system. *Artif Organs* 1994;18(1):80–92.

Journal of Congestive Heart Failure and Circulatory Support (2001) Vol 1, No 4, 167–170

Progress in the development of the undulation pump total artificial heart

Y. Abe MD PhD[1], T. Chinzei MD PhD[2], T. Isoyama PhD[2], T. Ono BE[1], S. Mochizucki MD PhD[2], I. Saito PhD[3], K. Iwasaki MS[4], M. Ishimaru MD[1], A. Baba MD[1], A. Kouno BL[1], T. Karita MD[1], K. Baba MD PhD[1] and K. Imachi PhD[1]

[1]Department of Biomedical Engineering, Graduate School of Medicine, The University of Tokyo, Tokyo, Japan; [2]Research Center for Advanced Science and Technology, The University of Tokyo, Tokyo, Japan; [3]Courses of Information and Communication Engineering, Graduate School of Engineering, The University of Tokyo, Tokyo, Japan; and [4]Department of Mechanical Engineering, Waseda University, Tokyo, Japan

Background Based on the experiences of the pneumatically driven total artificial heart (TAH), the development of an implantable TAH using undulation pumps started in 1992.

Methods The undulation pump is a small-sized, continuous flow displacement-type blood pump, and the undulation pump total artificial heart (UPTAH) is a unique implantable TAH using undulation pumps. To date, 25 animal experiments were performed using adult female goats weighing 40.0–79.2 kg. The left pump was driven with completely pulsatile flow mode. The right pump was driven with pulsatile flow on continuous flow mode, in which each pump had systolic high flow and diastolic low flow phases.

Results In spite of the limitation of the chest cavity in goats, the UPTAH could be implanted into the chest in all cases. Using the left atrial pressure control to automatically control the left pump and thereby maintain left atrial pressure below 20 mmHg, ordinarily at around 8 mmHg, 31 days' survival could be obtained in a goat. With the 1/R control, 46 days' survival could be obtained in a goat. In all cases, major thrombus was not found inside the pumps. However, temperature rise in the left motor was a problem.

Discussion More than 1 month's survival could be obtained with UPTAH. How to prevent the temperature rise in motor is the next important subject for future study.

Keywords undulation pump, total artificial heart.

Introduction

At the University of Tokyo, research into an artificial heart started in 1959. Since then, various types of artificial heart have been studied. By using a pneumatically driven paracorporeal total artificial heart (TAH) system, recipient goats survived for 344 days in 1984[1] and for 532 days in 1995[2]. Based on the experiences of pneumatically driven TAH, the development of an implantable TAH using undulation pumps started in 1992[3]. The undulation pump is a small-sized, continuous flow displacement-type blood pump, and the undulation pump total artificial heart (UPTAH) is a unique implantable TAH using undulation pumps. The first animal experiment with UPTAH was performed on a goat in 1996[4]. The goat with TAH survived for a few hours. After this, several improvements and developments were made[5]. In 1999, 46 days' survival was recorded in a goat.

Materials and methods

Undulation pump

The undulation pump is composed of a pump housing with a partition between the inlet and outlet ports, a disc with a slit located in the partition of the housing, an undulation shaft at the center of the pump and seal membranes between the disc and housing (Figure 1). The rotation of the motor is converted to the waving motion of the disc within the undulation shaft. The disc does not rotate, but waves. The blood is transferred from the inlet port to the outlet port according to the undulation of the waving disc. This pump mechanism operates on both sides of the disc with a phase difference of 180°. Thus a continuous output is produced with the addition of both outputs at the outlet port. In the latest model, the angle between the inlet and outlet ports was designed to be 50°.

UPTAH

The UPTAH is composed of two undulation pumps, two undulation shafts and two motors. Each pump has a shaft and a motor. The latest model (UPTAH 3.1) is 76 mm in diameter and 78 mm in length; the weight is 620 g and total volume is 292 ml, which is small enough to be implanted into the chest of small adults. Figure 2 shows UPTAH with outflow cannulae and atrial cuffs. The maximum continuous output is about 11 L min^{-1} against 100 mmHg of pressure load with 1800 rpm limited by the motor performance.

Correspondence to: Yusuke Abe, Associate Professor, Department of Biomedical Engineering, Graduate School of Medicine, The University of Tokyo, 7-3-1 Hongo, Bunkyo-ku, Tokyo, 113-0033, Japan.

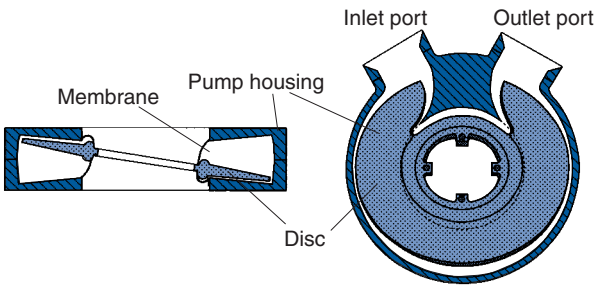

Figure 1. Structure of undulation pump.

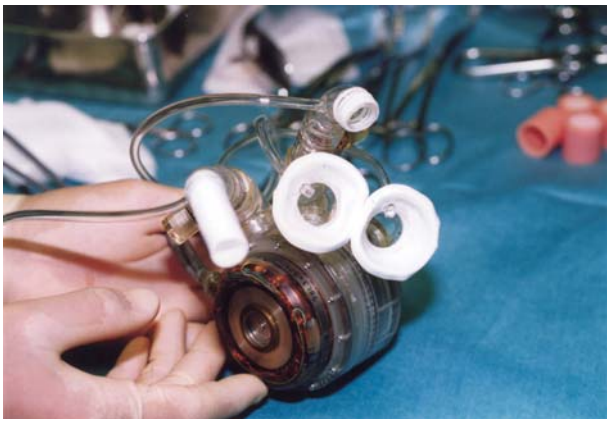

Figure 2. Undulation pump total artificial heart with outflow cannulae and atrial cuffs.

The blood contacting surface of the pump is entirely coated with segmented polyurethane (K-III, Nihon Zeon Co., Ltd., Tokyo, Japan) to prevent thrombus formation. This TAH has one jellyfish valve[6] in the systemic outflow cannula.

Animal experiments

Adult female goats weighing 40.0–79.2 kg were used for implantation. Under general anesthesia with isoflurane, the chest was opened by left thoracotomy with extirpation of the fifth rib. A heparin dose of 100 IU/kg was given. The systemic outflow cannula was anastomosed end-to-side with the descending aorta. Under the extra-corporal circulation, the ascending aorta was clamped using an arterial clamper, and the natural heart was resected at the atrio–ventricular groove. Atrial cuffs were sutured to the remnant atria. The pulmonary outflow cannula was inserted into the pulmonary artery. The UPTAH was set inside the chest, and the cuffs and outflow cannulae were connected to it. A dose of 30 mg of protamine sulfate was given for neutralization of heparin when UPTAH driving started. The drive condition was manually controlled to obtain the cardiac output of 100 ml/kg/min. After the implantation, neither antithrombogenic nor antiplatelet drug were used systemically. Antibiotics (ampicillin sodium 1 g/day and cefotaxime sodium 1 g/day) were given until the termination.

Control method

The undulation pump can produce an arbitrary flow pattern: continuous flow, pulsatile flow on continuous flow and complete pulsatile flow. The left pump was driven in complete pulsatile flow mode. The right pump was driven in pulsatile flow on continuous flow mode, in which each pump had systolic high flow and diastolic low flow phases. The pulse rate was fixed at 60–80 c/min. The same pulse rate was applied to both the left and right sides of the artificial hearts. The ratio of systolic phase to one pulse was controlled depending on the condition.

The cardiac output was maintained at 100 ml/kg/min by controlling the right pump manually. To prevent lung edema, the left pump was controlled automatically to maintain the left atrial pressure below 20 mmHg (the normal pressure is around 8 mmHg). At the same time, another automatic control to detect and release the sucking of atria within one pulse was performed. With this control, when the atrial sucking effect was detected by the quick increase of motor current in the systolic phase, the speed of the relevant motor was decreased immediately to the same level as that in the diastolic phase. In recent cases, 1/R control[7] was applied experimentally.

Results

To date, 25 cases of animal experimentation have been performed. Table 1 shows the results. In spite of the limited size of the chest cavity in goats, the UPTAH could be implanted into the chest in all cases.

In the early cases, the most serious problems were the atrial sucking effect and lung edema. The atrial sucking effect was prevented to some extent mainly by the improvement of atrial cuffs. The lung edema was prevented with the development of the automatic control of left atrial pressure. With these improvements, the animal could survive for 3 days as in case 7.

The next problem was the malfunction of the undulation pump due to a pin-point hole at the membrane. The pin-point hole was created by the rupture of a very small bubble generated in the membrane during production. To prevent the generation of small bubbles in the membrane, several improvements were tried, and finally, a method of manufacturing the membrane with fewer bubbles was established. With this improvement, the animal could survive for 10 days as in case 14.

After that, the mechanical durability was revealed to be too low and the size of the bearings had to be increased. We developed the new model in which the durability was improved. The goat survived for 31 days with the new model as in case 18.

We then tried to install the 1/R control in the control algorithm in cases 19, 22 and 23. In case 19, the 1/R control failed to maintain the cardiac output. After an improvement

Table 1. Results of implantation.

Case	Experiment No.	Body weight (kg)	Survival period	Cause of termination	UPTAH version
1	9604	52.3	3.6 h	Blood pump malfunction	2.1
2	9605	45.7	–	Air embolism	2.2
3	9606	42.5	3 h	Bleeding	2.3
4	9607	55.7	–	Lung edema	2.3
5	9608	42.1	17.3 h	Lung edema	2.3
6	9702	64.4	4.5 h	Lung edema	2.3.1
7	9704	58.5	77.6 h (3.2 days)	Blood pump malfunction	2.3.1
8	9705	42.0	39.5 h (1.6 days)	Blood pump malfunction	2.3.1
9	9706	51.0	42 h (1.8 days)	Drive circuit trouble	2.3.2
10	9708	79.2	6 h	Lung edema	2.3.2
11	9711	44.3	13 h	Bleeding	2.3.3
12	9712	45.0	5.3 h	Brain death	2.3.3
13	9801	49.0	75.3 h (3.1 days)	Bleeding	2.3.3
14	9803	41.3	260 h (10.8 days)	Drive shaft trouble	2.3.3
15	9812	49.1	8 h	Blood pump malfunction	3.0
16	9814	43.5	475.3 h (19.8 days)	Bleeding	3.0.1
17	9901	48.0	8 h	Lung edema	3.0.1
18	9902	45.8	747 h (31.1 days)	Pannus-like thrombus	3.0.1
19	9907	48.2	429.5 h (17.9 days)	Control malfunction	3.1
20	9912	41.7	5.1 h	Cerebral infarction	3.1.1
21	9914	43.0	6.3 h	Lung edema	3.1.1
22	9916	47.7	1119.5 h (46.6 days)	Disconnection of motor cord	3.1.1
23	0001	40.0	188.5 (7.9 days)	Control malfunction	3.1.1
24	0003	48.0	9.5 h	Respiratory failure	3.1.1
25	0004	40.0	5.5 h	Disconnection of motor coil	3.1.1

of the computer program, 46 days' survival could be achieved with the 1/R control, as in case 22 (Figure 3).

Through all the experiments, the temperature rise in the left motor was found to be one of the problems. The coil temperature of the left motor ranged from 42–59°C depending on the sucking of atria, aortic pressure and pump output; a normal body temperature of the goat was around 39°C. The coil temperature of the right motor was from 40–42°C.

Figure 3. The goat that survived for 46 days with the UPTAH (at 31 days).

In several cases hemoglobinuria was found and severe hemolysis occurred. However, in other cases, the hemolysis was not found until the termination of the experiment. In no case was a major thrombus found inside the pumps.

Discussion

To reduce the size of the TAH was thought to be difficult using the conventional blood pumps such as sac-type or diaphragm-type pumps. Therefore, we tried to reduce the size of TAH by using a continuous flow pump. The undulation pump was invented to achieve enhanced performance at a smaller size than that which is achieved with conventional blood pumps, and the UPTAH was designed to be small enough for implantation in a small adult.

The UPTAH has the following advantages:

- it is very compact
- the left and right pumps can be controlled independently
- it can produce an arbitrary flow pattern
- only one valve is necessary
- no compliance chamber is required.

The disadvantage is that the atrial suction effect can easily occur because the undulation pump is basically a

continuous flow pump in which the filling and ejecting are occurring at the same time and at the same speed. Therefore, it was very important to prevent the atrial suction effect in order to maintain cardiac output. Several improvements were made to ensure this, such as the control algorithm, design of atrial cuffs, and so on. As a consequence, the atrial sucking effect could be prevented to some extent. However it still occurred sometimes, especially during the period of postoperative hypovolemia, necessitating careful postoperative treatment with infusion.

The model was redesigned for greater durability after the experiment listed as case 14, where 10 days' survival was achieved; prior to this case, the mechanical durability was found to have a detrimental effect on the long-term survival of the test subject. The redesigning of the model was successful and, as a result, survival times of more than 1 month could be obtained.

We thought that a physiological control such as the the 1/R control was necessary to maintain the good condition of the animal with TAH in the long term. We tried to install the 1/R control in the control algorithm. In the first trial, the 1/R control failed to control the cardiac output as there were faults in the computer program. Ultimately, however, the 1/R control could be run successfully and 46 days' survival was obtained. We are still searching for the suitable parameter for 1/R control on the UPTAH.

The durability and antithrombogenic property of the pumps were demonstrated to be good for more than 1 month. Further observation is required in cases of longer survival. Concerning hemolysis, excessive negative pressure generated by the atrial suction effect has a possible influence on this. However, further study is necessary to clarify the hemolytic factors on the UPTAH. As the temperature rise in the left motor was a problem throughout the experiments, it is essential to prevent this by using a motor with higher efficiency and performance. This is the next important subject for future study.

Acknowledgment

This study was supported in part by the Program for Promotion of Fundamental Studies in Health Science of the Organization for Drug ADR Relief, R&D Promotion and Product Review of Japan.

References

1. Fujimasa I, Imachi K, Nakajima M *et al.* Pathophysiological study of a total artificial heart in a goat that survived for 344 days. In Nose Y, Kjellstrand C, Ivanovich P, editors. *Progress in Artificial Organs-1985*. Cleveland: ISAO Press. 1986:345–53.
2. Abe Y, Chinzei T, Mabuchi K *et al.* Over 500 days survival of a total artificial heart goat with 1/R control. In Akutsu T, Koyanagi H, editors. *Heart Replacement: Artificial Heart 6*, Tokyo: Springer–Verlag, 1998:34–40.
3. Abe Y, Chinzei T, Isoyama T *et al.* Basic study to develop the undulation pump for practical use: antithrombogenicity, hemolysis, and flow patterns inside the pump. *Artif Organs*, 1995;19:691–3.
4. Abe Y, Chinzei T, Isoyama T *et al.* Development of the undulation pump total artificial heart. *Artif Organs* 1997;21:665–9.
5. Abe Y, Chinzei T, Ono T *et al.* Implantation of the undulation pump total artificial heart in the goat *Artif Organs* 1999;23:932–8.
6. Imachi K, Mabuchi K, Chinzei T *et al.* The jellyfish valve: a polymer membrane valve for the artificial heart. In Akutsu T, Koyanagi H, editors. *Heart Replacement: Artif Heart 4*. Tokyo: Springer–Verlag. 1993:41–4.
7. Abe Y, Chinzei T, Mabuchi K *et al.* Physiological control of a total artificial heart: conductance- and arterial pressure-based control. *J Appl Physiol* 1998;84:868–76.

Session 2

Heart Transplantation

Journal of Congestive Heart Failure and Circulatory Support (2001) Vol 1, No 4, 173–177

Pre- and post-heart transplant management in end-stage cardiac failure patients: Osaka University experience

N. Fukushima MD[1], S. Ohtake[1], Y. Sawa[1], M. Nishimura MD PhD[1], G. Matsumiya[1], S. Nakata[1], S. Takashima[2], M. Hori[2], R. Shirakura[3] and H. Matsuda[1]

[1]Department of Surgery, [2]Department of Internal Medicine and Therapeutics, [3]Division of Organ Transplantation, Osaka University Graduate School of Medicine, Suita, Japan

Background Donor shortage is an extremely serious problem in Japan because of very strict organ transplantation laws. We investigated patients registered as heart transplantation candidates to evaluate how to manage them pre- and post-transplant.

Patients A total of 19 patients were registered to the Japan Organ Transplant Network and three to the United Network for Organ Sharing (UNOS). The diagnosis was dilated cardiomyopathy (DCM) in 15, dilated hypertropic cardiomyopathy (dHCM) in five, restrictive cardiomyopathy (RCM) in one and ischemic cardiomyopathy (ICM) in one.

Results Four patients underwent heart transplantation (one in Japan and three in the USA). Ten patients underwent left ventricular assist system (LVAS) implantation (seven extracorporeal Toyobo (T), two Novacor (N) and one TCI) as a bridge to transplant. In seven patients with T-LVAS, five died of multiple organ failure or cerebral disorder, one underwent transplantation in the USA and the other is waiting in hospital for 3 months. In two patients with N-LVAS, one is waiting at home for 740 days and the other underwent transplantation on 125 POD. The latter was the first heart transplantation case in Japan to receive a heart from a legally brain-dead donor. One child died of cardiac failure on percutaneous cardiopulmonary bypass and the other died suddenly at home. Four heart transplantation recipients were treated with a triple immunosuppressive regimen. Two patients had acute rejection treated successfully; none had graft coronary atherosclerosis or a major infection during a mean follow-up of 46 months. Two patients were going to school and the other two were working full-time.

Conclusion In Japan, there is a greater need for bridging options such as LVAS and meticulous medical treatment to manage patients awaiting heart transplantation than in other countries.

Keywords heart transplantation, left ventricular assist device.

Introduction

Unlike the US or European countries, the Japanese system for providing clinical heart transplantation has many problems. One of these problems is the extreme shortage of donors. Nearly two years have passed since the organ donation law was issued in Japan on October 16, 1997. However, only three hearts were obtained from brain-dead donors and transplanted[1], because organ harvesting from brain-dead donors can be carried out only if they have given written informed consent, not only to donate their organs but also to accept brain death. Therefore, this makes the donor shortage in Japan much more serious than in other countries. In these circumstances, options such as the use of left ventricular assist system (LVAS), the Batista operation, and meticulous medical treatment, are required to manage patients awaiting for heart transplantation[2]. One other problem is the extreme limitation of the LVAS.

In Japan, only paracorporeal LVASs, such as the Toyobo-National Cardiovascular Center LVAS (T-LVAS) and the Zeon-Tokyo University LVAS were approved by the government as mechanical circulatory assist devices for profound heart failure[2]. However, implantable LVASs, such as the TCI HeartMate pneumatically and electrically driven LVASs (TCI-IP and -VE) and the Novacor LVAS (N-LVAS) are not approved yet. The TCI-VE and Novacor LVAS are still preparing for clinical trials[3]. In order to utilize TCI-IP LVASs, either the patients or the hospitals have to pay the cost. In such a situation, we have to figure out how we can utilize the currently available devices and decide the best strategy for treating end-stage cardiac disease.

In the present study, we investigated patients registered to the Japan Organ Transplantation Network (JOTNW) or the United Network for Organ Sharing (UNOS) to evaluate how these candidates for heart transplantation in Japan can best be managed.

Patients

From October 1997 to February 2000, 19 patients (17 male, two female) aged 5–55 years (mean 33.4 years) were reg-

Correspondence to: Norihide Fukushima, Department of Surgery, Osaka University Graduate School of Medicine, 2–2 Yamada-oka, Suita, 565-0871 Japan.

istered to JOTNW and from September 1992 to February 2000, three male patients aged 17–46 years were registered to UNOS. The underlying heart disease of 12 patients registered to JOTNW was idiopathic dilated cardiomyopathy (DCM), in five patients it was hypertrophic cardiomyopathy in dilated phase (dHCM), in one restrictive cardiomyopathy (RCM) and in one ischemic cardiomyopathy (ICM). All three patients registered to UNOS were diagnosed as having DCM. The clinical status of eight patients registered to JOTNW was status 1 (four on LVAS and four on catecholamine) and 11 were status 2. Of those registered to UNOS, two were status 1 (on LVAS in one, and one catecholamine) and one was status 2.

Results

Of 11 patients who were initially registered as status 2, the clinical status of four was changed to status 1 (three on LVAS and one on catecholamine). The survival rates in patients registered to JOTNW initially as status 1 and 2 were 48% and 62% at 1 year and 48% and 62% at 2 years, respectively. A total of 11 patients registered to JOTNW and one to UNOS required mechanical circulatory assist devices (10 LVAS and then on percutaneous cardiopulmonary support (PCPS)) during their wait for heart transplantation. The survival rate of patients registered to JOTNW was significantly higher than the freedom rate from death, LVAS or PCPS implantation (log-rank test; $P<0.05$) (Figure 1).

One patient registered to JOTNW and three registered to UNOS underwent heart transplantation, two of them were bridged to transplant. Of eight patients registered to JOTNW, six died of multiple organ failure or cerebral disorder on LVAS, one died of cardiac failure, on PCPS and one died suddenly at home. Four patients have been waiting for transplant as status 1 candidates, two on LVAS and two on catecholamine. The remaining six have been waiting as status 2 candidates (Figure 2).

Pre-transplant management

Ten patients underwent LVAS implantation as a bridge to transplant (Table 1). Of these patients, five underwent LVAS implantation after registration to JOTNW. Seven patients underwent LVAS implantation with Toyobo-LVAS, four using a left atrial inflow cannula (LA-type) and three a left ventricular apical inflow cannula (LV-type) patients. One patient with DCM (LV-type) and one with RCM (LA-type) died of multiple organ failure 37 and 9 days after implantation, respectively. Three patients with Toyobo-LVAS (two with LA-type and one with LV-type) died of

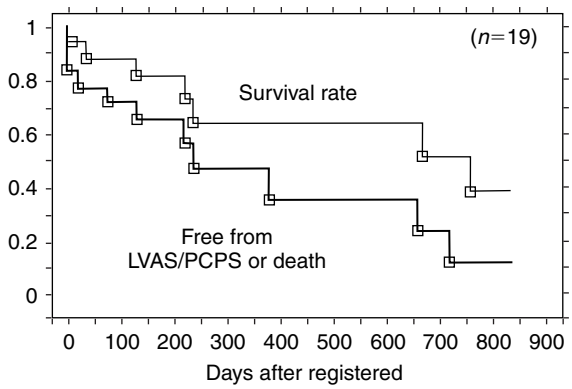

Figure 1. Freedom rate from death and implantation of LVAS or death in patients registered to JOTNW.

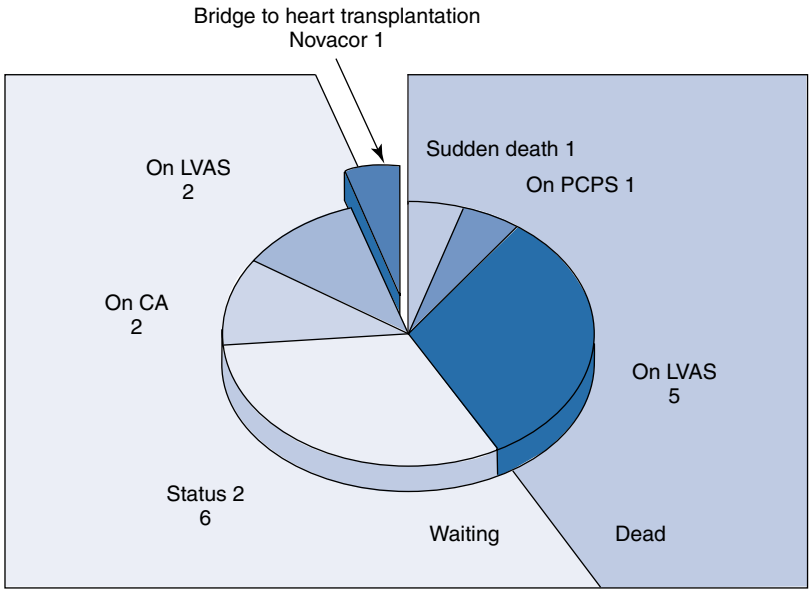

Figure 2. Outcomes of patients registered to JOTNW from Osaka University Hospital.

Table 1. Outcomes of patients who underwent operation with LVAS insertion as a bridge to heart transplantation.

Case	Age	Sex	Diagnosis	Type of LVAS	Support period (days)	Outcome
1	28	M	RCM	Toyobo-LA type	9	Died of MOF
2	35	M	DCM	Toyobo-LA type	40	Died of CVA
3	18	M	DCM	Toyobo-LA type	119	Bridge to HTx in USA
4	50	M	dHCM	Toyobo-LA type	181	Died of CVA
5	51	M	DCM	Toyobo-LV type	37	Died of MOF
6	30	F	DCM	Toyobo-LV type	110*	Waiting in hospital for HTx
7	39	M	ICM	Toyobo-LV type	352	Died of CVA
8	27	M	DCM	TCI-IP LVAS	4	Died of pneumonia
9	46	M	dHCM	Novacor LVAS	125	Bridge to HTx in Japan
10	46	M	dHCM	Novacor LVAS	740*	Waiting for HTx at home

RCM: restrictive cardiomyopathy; DCM: dilated cardiomyopathy; dHCM: dilated phase hypertrophic cardiomyopathy; HTx: heart transplantation; ICM: ischemic cardiomyopathy; LA: left atrial inflow cannula; LV: left ventricular apical inflow cannula; MOF: multiple organ failure; CVA: cerebral vascular accident; * on-going.

cerebral bleeding and/or thrombosis 40, 181 and 352 days after implantation, respectively. One patient moved to the USA by airplane on Toyobo-LVAS[4], was registered to UNOS and underwent heart transplantation in the Texas Heart Institute 119 days after LVAS implantation. The other with postpartum DCM has been waiting for heart transplantation for three months in our hospital after implantation of an LV-type Toyobo-LVAS. One patient with TCI-IP LVAS died of aspiration pneumonia which occurred at cardiopulmonary resuscitation. Two patients who underwent implantation of a Novacor LVAS have been doing well. One has been waiting for heart transplantation at home for 730 days after implantation and the other underwent transplant on 125 POD. The latter patient was the first transplant case to receive a heart from a legally brain-dead donor in Japan[1]. Both patients showed significant increases in peak oxygen consumption and functional status and decreases in serum atrial and B-type natriuretic peptide (ANP and BNP, respectively). These data suggest that the purpose of LVAS was not only to save their lives but also to improve their functional, immunological and nutritional status during their wait for transplantation.

Two patients required PCPS. One patient with life-threatening ventricular arrhythmia experienced a ventricular fibrillation attack in March 1998; this patient was resuscitated using PCPS, an intravenous cardiac defibrillator (ICD) was implanted and the patient is now waiting for a heart transplantation under continuous dopamine and dobutamine intravenous infusion with an effective ICD. The other patient, who was 5 years old, died of severe pulmonary hemorrhage on PCPS.

One patient who had recurrent cardiac failure with a significant increase in left ventricular volume one year after a Batista operation died suddenly at home and was classified as a status 2 candidate. One child with DCM was waiting for a heart transplantation on treatment with dobutamine and milrinone infusion for six months. Another six status-2 patients have been waiting for transplantation under stable conditions, four at home and two in the hospital until now; three of these patients have been waiting away from Osaka.

Post-transplant management (Table 2)

Table 2 shows the outcomes of patients who received heart transplantation. One patient registered to JOTNW and three registered to UNOS underwent transplantation (two in the Texas Heart Institute and one in the Cleveland Clinic Foundation). In four recipients, the immunosuppressive regimen consisted of cyclosporine (CyA), azathioprine (AZA) or mycophenolate mofetil (MMF) and prednisolone (PRD). Two patients were given intravenous anti-CD3 monoclonal antibody (OKT3) because of perioperative renal dysfunction. One patient had three episodes and another had one episode of acute rejection greater than ISHLT grade 3; the first was treated successfully with steroid pulse therapy and the other with an increase in a dose of CyA[5]. Routine intravenous ultrasound revealed no graft coronary atherosclerosis in patients. No patient had experienced a major infectious episode during a mean follow-up of 46 months. Each patient had a New York Heart Association (NYHA) grade of 1. All returned to their school or work place within nine months after heart transplantation; two patients are going to school and the other two are working full-time. Figure 3 shows a patient undergoing an exercise tolerance test after LVAD and transplantation.

Discussion

Unlike some other developed countries, there are problems in the clinical heart transplantation system in Japan, such as

Table 2. Outcomes of patients who underwent heart transplantation

	Transplanted in USA			Transplanted in Japan
	Case 1	**Case 2**	**Case 3**	**Case 4**
Age at HTx (years)	18	46	17	47
Sex	Male	Male	Male	Male
Diagnosis	DCM	DCM	DCM	dHCM
Transplant Center	Texas Heart Institute	Texas Heart Institute	Cleveland Clinic	Osaka University Hospital
Waiting period (days)	63	15	16	502
Status at HTx	Toyobo-LVAS (119 days)	Status 2	On catecholamine	Novacor LVAS (125 days)
Immunosuppressive regimen	CyA, AZA, PRD	CyA, AZA, PRD	CyA, MMF, PRD	CyA, MMF*, PRD
Cytolitic agent	OKT3	None	OKT3	None
Acute rejection greater than ISHLT grade 3	4 Treated with steroid pulse therapy	1 Treated with an increase in a dose of CyA	None	None
Current status	University student	Full-time worker	High school student	Full-time worker
Follow-up period (months)	89	64	16	12

DCM: dilated cardiomyopathy; dHCM: dilated phase hypertrophic cardiomyopathy; LVAS: left ventricular assist support; HTx: heart transplantation; CyA: Cyclosporine; AZA: azathioprine; MMF: mycophenolate mofetil; PRD: prednisilone; *on going.

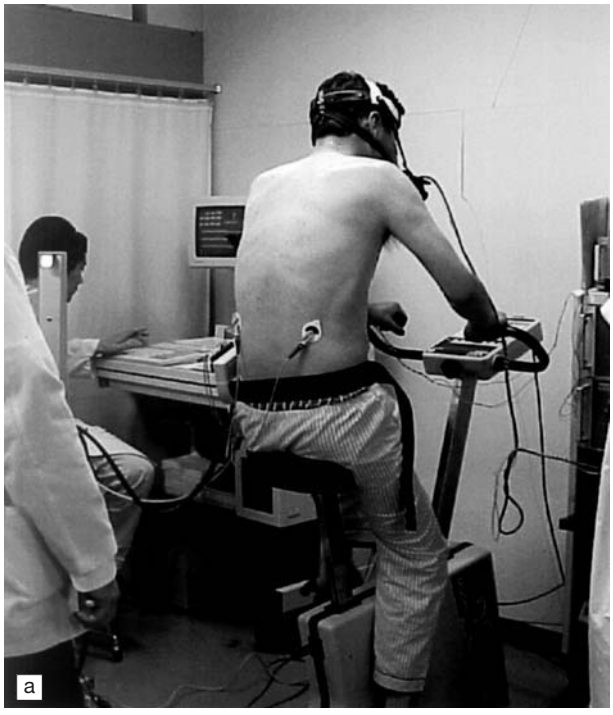

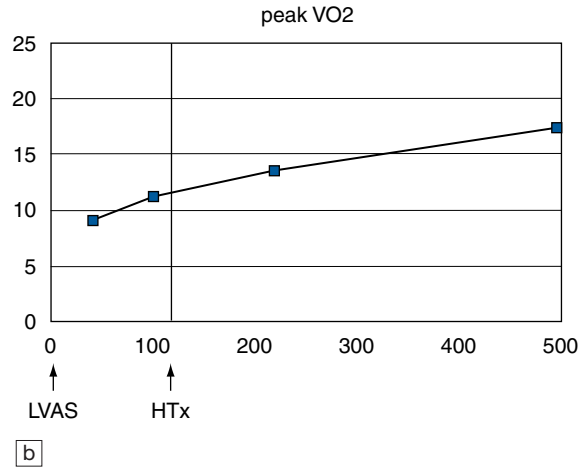

Figure 3. Exercise tolerance of a patient who underwent heart transplantation in out hospital 125 days after Novacor LVAS implantation. (a) Patient doing exercise on ergometer one year after heart transplantation. (b) Change in peak oxygen consumption (peak VO2) after Novacor LVAS implantation and heart transplantation.

the extreme donor shortage and limited availability of LVAS. In these circumstances, options, such as LVAS, PCPS, the Batista operation, and meticulous medical treatment, are required to manage patients awaiting for heart transplantation[2]. In our series, 12 out of 19 patients required mechanical assist devices. Although these devices improved the survival of patients registered to JOTNW, seven patients died during their wait for heart transplantation; only one patient underwent transplant and two are still waiting.

As only paracorporeal LVASs are approved by the Government[2] in Japan, Toyobo-LVASs were implanted in seven patients registered to JOTNW and one to UNOS. Three patients died of multiple organ failure or cerebral disorder within 40 days after LVAS implantation. Although Toyobo-LVASs have supported the circulation of four patients for more than 100 days' implantation, two patients died of cerebral disorders 181 and 352 days after implantation. One patient had several infarction episodes until he

underwent heart transplantation in the USA. As the maximum output of Toyobo-LVAS was 5 L min^{-1}, which was less than that of Novacor or TCI-LVAS, Toyobo-LVAS could not support patients who required a high cardiac output, such as patients with systemic infection or multiple organ failure. Toyobo-LVASs were more susceptible to thromboembolism or infection than implantable LVASs. Therefore, we needed to exchange the Toyobo-LVAS pump at several weekly intervals. Moreover, patients with Toyobo-LVAS had difficulty with movement and rehabilitation and therefore patients using the system should stay in hospital because the LVAS has a large console. These characteristics might limit the support period of this LVAS[2,6]. On the other hand, two patients with Novacor-LVASs have been doing well in our series. One patient underwent heart transplantation in our institute 125 days after LVAS implantation and the other has been waiting for transplantation at home for more than two years. Therefore, if implantable LVASs are approved for use in Japan, we will plan to use extracorporeal LVASs for the patients with a possibility of cardiac recovery for short-term support and implantable LVASs as a bridge to transplantation for long-term support.

With regard to post-transplant management, all four patients have been doing well, although we might owe these results to perioperative management in cardiac centers in the USA. As previously described in several reports[5,7,8], the postoperative courses of Japanese patients who underwent heart transplantation in foreign transplantation centers were as satisfactory as those of cardiac recipients in the USA and European countries[9,10]. Although only three transplants, including our case, have been carried out in Japan, their postoperative courses were also satisfactory with a triple immunosuppressive regimen consisting of CyA, MMF and PRD with a mean follow-up period of 340 days. Only one patient had an episode of acute rejection greater than ISHLT grade 3 and it was successfully treated with steroid pulse therapy. The NYHA grade was 1 for this case. Our patient was working full-time and the others will return to work soon.

Conclusion

Options, such as LVAS and meticulous medical treatment, are urgently required to manage patients awaiting heart transplantation in Japan. Implantable LVASs should be approved for use in Japan in the near future. The post-transplant outcome in Japan was comparable to that in other developed countries.

References

1. Matsuda H, Fukushima N, Sawa Y *et al.* First brain-dead donor heart transplantation under new legislation in Japan. *Jpn J Thorac Cardiovasc Surg* 1999;47:499–505.
2. Fukushima N, Ohtake S, Sawa Y *et al.* Predicting outcomes and management of candidates for heart transplantation. *Transplant Proc* 1999;31(5):1961–2.
3. Nishimura M, Ohtake S, Sawa Y *et al.* Left ventricular assist systems as a bridge to heart transplantation: the role and the strategy in Japan. *Transplant Proc* 1999;31(5):1997–9.
4. Matsuwaka R, Matsuda H, Kaneko M, *et al.* Overseas transport of a patient with an extracorporeal left ventricular assist device. *Ann Thorac Surg* 1995;59(2):522–3.
5. Fukushima N, Ohtake S, Sawa Y *et al.* Use of cyclosporine MEPC (Neoral) in heart transplant recipients. *Transplant Proc* 1998;30(7):3337–8.
6. Takano H, Nakatani T. Ventricular assist systems:experience in Japan with Toyobo pump and Zeon pump. *Ann Thorac Surg* 1996;61(1):317–22.
7. Hachida M, Koyanagi H, Matsuda H *et al.* Assessment of Japanese patients receiving heart transplants overseas. *J Cardiol* 1996;27(1):15–9.
8. Nunoda S, Kurosawa R, Kogashi K, Yamagishi S, Mitsui F, Funabashi W. Points to note from indications for heart transplantation to post-heart transplant care: from the care of patients with refractory heart failure and overseas heart transplantation. *Heart Vessels* 1997;Suppl 12:37–40.
9. Hosenpud JD, Bennett LE, Keck BM, Fiol-B, Boucek-MM, Novick-RJ. The Registry of the International Society for Heart and Lung Transplantation: sixteenth official report–1999. *J Heart Lung Transplant* 1999;18(7):611–26.
10. Keck BM, Bennett LE, Fiol BS, Daily OP, Novick RJ, Hosenpud JD. Worldwide thoracic organ transplantation: a report from the UNOS/ISHLT International Registry for Thoracic Organ Transplantation. *Clin Transpl* 1998:39–52.

Journal of Congestive Heart Failure and Circulatory Support (2001) Vol 1, No 4, 179–184

Bridging to heart transplantation using paracorporeal and implantable ventricular assist devices

K. Minami MD PhD, L. Arusoglu MD, A. El-Banayosy MD, A. Sezai MD, D. Boethig, M. Morshuis MD, O. Fey RN, P. Sanowski MD and R. Körfer MD

Department of Thoracic and Cardiovascular Surgery, Heart Center North-Rhine-Westphalia Bad Oeynhausen, Ruhr-University of Bochum, Germany

Abstract Heart transplantation is an established therapy for end-stage heart disease. However, due to a shortage of donor organs in recent years, the use of mechanical ventricular support has become indispensable.

A total of 1049 heart transplants were performed in our institute from 1989 to 1999, 270 of which (25.7%) were supported by a ventricular assist device (VAD) as a bridge to heart transplant. In this study, we evaluated a paracorporeal (85 Thoratec) and two implantable (61 Novacor and 37 HeartMate) left ventricular assist devices (LVADs), which were used from March 1989 to June 1999. Recently, a totally implantable pulsatile LVAD (Lion Heart VAD) was used in three patients. A nonpulsatile LVAD (DeBakey VAD axial flow pump) was implanted in one patient.

The mean duration of mechanical support was 49 days with Thoratec, 148 days with Novacor and 124 days with HeartMate. The successful transplantation and weaning rates were 64.7% with Thoratec, 59.0% with Novacor and 62.0% with HeartMate. Cerebral embolism, drive-line and pocket infection were major causes of postoperative morbidity and mortality.

The Thoratec device is recommended as a bridge to heart transplantation, especially for patients with biventricular heart failure. Novacor and HeartMate are recommended in case of a long waiting time for heart transplantion. However, thromboembolism, infection and mechanical failure all increase during a prolonged bridging period. Though a further long-term follow-up is mandatory for evaluation of new devices, we believe that the next generation of devices will be effective regarding patient quality of life and we expect good results in the future.

Keywords mechanical ventricular support, bridge to transplantation, Thoratec, Novacor, HeartMate, Lion Heart, DeBakey pump, ventricular assist device (VAD).

Introduction

An estimated two million patients in Europe (0.9% of all Europeans) have severe myocardial insufficiency (NYHA Class III or IV), and it is newly diagnosed in 0.25% of all Europeans (500 000 patients) each year. It is the most frequent reason for hospitalization of patients over 60 years of age. Furthermore, despite improvements in survival with new medical therapies, patients in need of heart transplantation increase year by year. Heart transplantation is performed in more than 700 Eurotransplant cases and more than 500 cases in Germany every year, and it is an established therapy for end-stage heart disease (Figure 1). However, donor shortage has become a serious problem. A total of 1049 heart transplants were performed in our institute from March 1989 to December 1999; 270 of these transplants (25.7%) were supported by a ventricular assist device as a bridge to heart transplantation (Figure 2). Mechanical support as a bridge to heart transplantation has become necessary for many patients on the waiting list for a donor heart. As more patients are using long-term circulatory support, various problems including mechanical failure have gradually been increasing, in addition to complications such as thromboembolism, infection, and bleeding[1,2]. To address these problems, we evaluated the results of implantation in patients supported with paracorporeal or implantable ventricular assist devices (VADs). Two devices were tested (Lion Heart VAD and DeBakey VAD axial flow pump) which incorporate new concepts[3]; the results are reported in this study.

Patients and methods

In our institute, the various mechanical assist devices (BioMedicus BP–80, ABIOMED BVS 5000, Thoratec and Medos as paracorporeal VADs, and Novacor, HeartMate Lion Heart and DeBakey axial flow pump as implantable VADs) have been implanted for end-stage heart disease. The indications for use of the various VADS are listed in Box 1.

Between September 1989 and June 1999, 369 patients were supported with VADs at our institute. The VADs were implanted as a bridge to heart transplantation in 228 of these patients, in 83 patients due to postcardiotomy cardiac failure and in 58 patients due to miscellaneous causes. The various VADs applied in this study are listed in Box 2. They were applied as follows:

Correspondence to: Professor Kazutomo Minami, Georgstr.11, 32545 Bad Oeynhausen, Germany, and Department of Thoracic and Cardiovascular Surgery, Heart Center North-Rhine-Westphalia Bad Oeynhausen, Ruhr-University of Bochum, Germany.

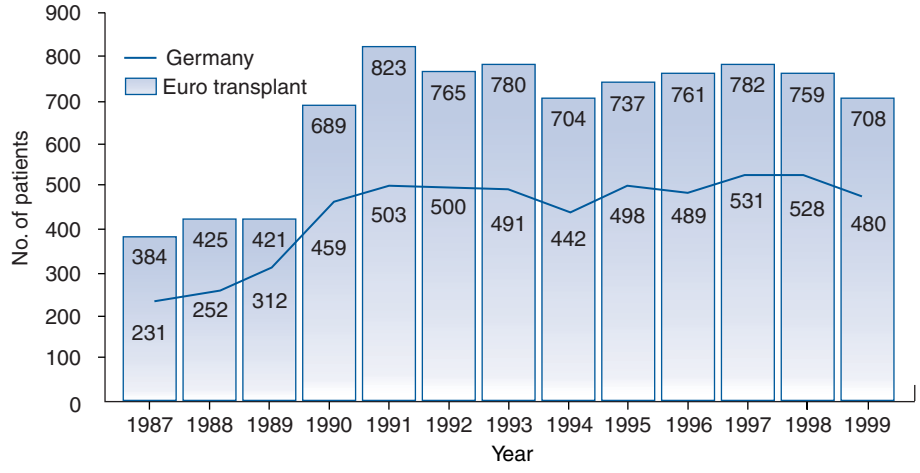

Figure 1. Numbers of heart transplantations within the Eurotransplant region and Germany.

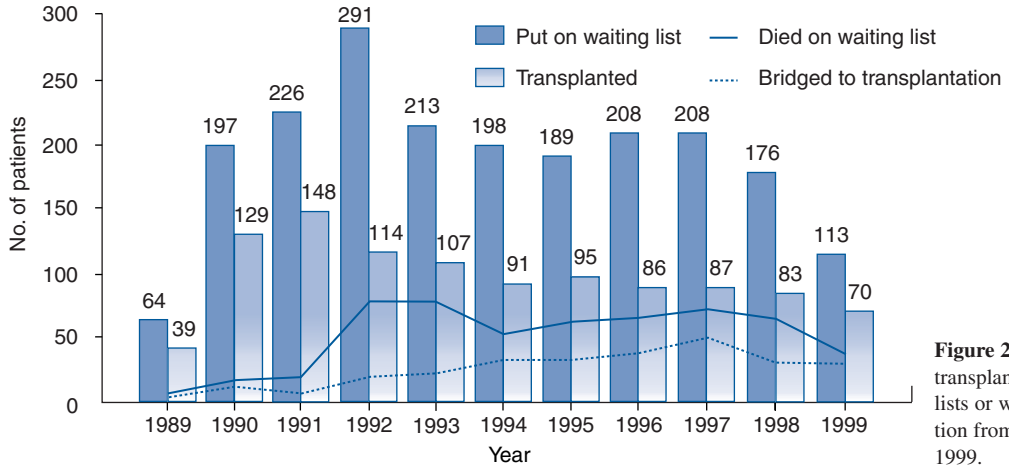

Figure 2. Patients who received transplantations, were on waiting lists or were bridged to transplantation from March 1989 to December 1999.

1. BioMedicus BP–80 for postcardiotomy cardiac failure due to miscellaneous causes.
2. ABIOMED BVS 5000 for postcardiotomy cardiac failure.
3. Thoratec as a LVAD and also a biventricular assist device (BiVAD) as a bridge to heart transplantation.
4. Novacor and HeartMate as LVADs as a bridge to heart transplantation.
5. Medos for an infant.

A total of 183 patients who were supported by a single device were entered in this study of postoperative morbidity and clinical outcome. Of these patients, 85 were supported with a Thoratec system (Thoratec group; 43 of these had a biventricular support), 61 with a Novacor system (Novacor group), and 37 with a HeartMate system (HeartMate group). The mean age at implantation was 48 years (11–67 years) in the Thoratec group, 51 years (16–68 years) in the Novacor group, and 54 years (22–67 years) in the HeartMate group. The Thoratec group consisted of 70 males and 15 females, the Novacor group of 57 males and four females, and the HeartMate group of 35 males and two females. The causative diseases in patients are shown in Box 3. Forty-five patients in the Thoratec group, 61 in the Novacor group and 37 in the HeartMate group received an LVAD; 40 patients in the Thoratec group were supported by a BiVAD.

New devices (the Lion Heart VAD and the DeBakey VAD axial flow pump)

The first human implant of the Lion Heart VAD was performed as an LVAD on October 26, 1999 at our institute; three patients have undergone implantation with these devices to date. The first patient was a 67-year-old male with dilated cardiomyopathy; the second was a 68-year-old male with dilated cardiomyopathy; and the third was a 66-year-old male with ischemic heart disease. The DeBakey VAD axial flow pump (Figure 3) was implanted as a LVAD in a 61-year-old patient with ischemic heart disease.

Results

The mean duration of support was 49 days (maximum 386 days) in the Thoratec group, 148 days (maximum 989 days) in the Novacor group and 124 days (maximum 810 days)

Box 1. Indications for VAD

Paracorporeal VAD
- Short-term bridge to HTx
- Postcardiotomy cardiac failure
- Transport of patients by PCPS
- Temporary RVAD after LVAD

Implantable VAD
- Long-term bridge to HTx (BTT)
- Alternative to HTx (ATT)
- Bridging to recovery (BTR)

Box 2. Application of VADs

Paracorporeal VADs
- Biomedicus BP-80
- ABIOMED BVS 5000
- Thoratec
- Medos

Implantable VADs
- Novacor
- HeartMate
- Lion Heart
- DeBakey axial flow pump

Box 3. Patient characteristics

No. of patients	183
Diagnoses:	
DCM	119
IHD	64
Myocarditis	8
Others	5

in the HeartMate group. This shows that the duration of support with an implantable device (a Novacor or HeartMate system) exceeded 100 days. During the period of support with a ventricular assist device, 30 (35%), 25 (41%), and 14 (38%) patients died in the Thoratec, Novacor and HeartMate groups respectively. Three patients (3.5%) in the Thoratec group, three (4.9%) in the Novacor group and one (2.7%) in the HeartMate group were weaned from a mechanical assist device, although due to pocket infection in one of each of the Novacor and HeartMate groups. Heart transplantation was performed on 52 patients (61%) in the Thoratec group, 33 (54%) in the Novacor group, and 22 (51%) in the HeartMate group.

In 1994, we started a program to allow patients with a VAD to return home. The patients living outside the hospital included 42 patients (69%) in the Novacor group and 18 (49%) in the HeartMate group. Of the 25 patients with an electric console in the HeartMate group, 18 (72%) could return home because HeartMate began to implant with an electric console. In the Thoratec group, one patient with a small-sized console was allowed to return home because this patient's house was located near our institute.

Figure 3. DeBakey axial flow pump.

Complications included:

1. Perioperative bleeding: 35 patients (41%) in the Thoratec group, 27 (45%) in the Novacor group and 17 (46%) in the HeartMate group.
2. Cerebral embolism: 20 patients (24%) in the Thoratec group, 24 (39%) in the Novacor group and seven (16%) in the HeartMate group.
3. Peripheral embolism: two patients (4%) in the Novacor group.

Infections included:

1. Drive-line infection: two patients (2%) in the Thoratec group, 16 (26%) in the Novacor group and eight (18%) in the HeartMate group.
2. Pocket infection: five patients (11%) in the Novacor group and nine patients (24%) in the HeartMate group.
3. Sepsis: 22 patients (26%) in the Thoratec group, 12 (20%) in the Novacor group and five (11%) in the HeartMate group.
4. Conduit endocarditis: three patients (7%) in the Novacor group and one (2%) in the HeartMate group.

Those with pocket infection had particularly poor outcomes, namely four of the seven patients (57%) in the Novacor group and seven of the nine patients (78%) in the HeartMate group died. The time of death was 50–481 days after support in the Novacor group and 48–325 days in the HeartMate group. The majority of the HeartMate group (89%) survived more than 100 days with support. Mechanical failures were observed in three patients (4%) in the Thoratec group. The controller of the newly developed dual-drive console (DDC [TLC II]) was disturbed in all of these patients, and this problem could have been eliminated by changing to the original larger console (DDC). Four patients (9%) experienced the following problems with the HeartMate system:

1. Two patients had a rupture of the polyurethane diaphragm in the pump[6]
2. One had a leakage from the drive-line
3. One had a pump stoppage caused by blood aspiration as a result of drip leakage from the air filter.

In four cases, the LVAD was exchanged due to pump failure; in three patients due to endocarditis in the Novacor group; and in one patient due to membrane perforation in the HeartMate group. Three patients were exchanged under PCPS; two patients died and one patient is waiting for transplantation.

The causes of death whilst using a device included:

1. Multiple organ failure (MOF): 25 patients (29%) in the Thoratec group, eight (13%) in the Novacor group, and four (11%) in the HeartMate group.
2. Sepsis: 18 (12%) in the Thoratec group, six (10%) in the Novacor group and five (14%) in the HeartMate group.
3. Cerebral infarction: seven (8%) in the Thoratec group, 13 (21%) in the Novacor group and seven (19%) in the HeartMate group.
4. Bleeding: one (1%) in the Thoratec group, and seven (11%) in the Novacor group.

MOF was particularly prevalent in the Thoratec group, the reason being that this group had many BiVAD cases. Cerebral infarction and bleeding due to anticoagulation were the major causes of death in the Novacor group.

The three patients with Lion Heart VADs recovered from severe heart failure and were able to walk around in the hospital. However, the first patient suffered a stroke 65 days after implantation; the cause of this stroke was unknown. The patient's condition is currently stable 130 days after support with the new device. The other patients are doing well following their implants 96 and 5 days after support. These three patients have no infection at present. The first patient recovered from severe heart failure while using the DeBakey VAD. Although his pulse pressure was maintained at approximately 5 mmHg and showed nonpulsatile circulation, he was able to walk around in the hospital. However, he died due to inflow thrombosis 38 days after support.

Discussion

The survival rate after severe heart failure has been improved with the development of mechanical assist devices of various types. These devices have also become established as a bridge to heart transplantation[1,2,4,5,7]. Of the 1049 heart transplants performed in our institute from March 1989 to December 1999, 270 (25.7%) were supported by a VAD as a bridge to heart transplantation. The percentage of patients with a VAD has been more than 20% since 1994. Pifarre *et al*[8]. compared the results after heart transplantation in patients who were mechanically supported versus patients who received no mechanical support, and reported that there were no differences found in the 30-day and 1-year survival rates between the two groups. Several VADs are available for clinical use at present and are selected according to the patient's condition[9]. There are two types of device: a paracorporeal and an implantable VAD. The paracorporeal VAD has the advantages of easy implantation and versatility; its disadvantages concern the patient's mobilization and support time. On the other hand, the implantable VAD has the advantages of long-term support, allowing patients to return home, and the fact that complicated anticoagulation therapy is not necessary with HeartMate. Its disadvantages are that it is surgically demanding, not as usable as an RVAD and can give rise to technical problems (Table 1). We take full advantage of these differences and use various mechanical assist devices. However, with more cases using long-term circulatory support, various problems including mechanical failure have gradually been increasing. The incidence of complications such as thromboembolism, infection and bleeding have also increased. Griffith *et al.* reported that the incidence of complications increases when the duration of support exceeds 100 days[10]. At our institute, the mean duration of support has increased year by year; namely, duration was only 32 days in 1994, but exceeded 100 days in 1996 (122 days) and extended to 140 days in 1998. Thromboembolism, infection and bleeding are known to be the major complications after implantation of a VAD, and these complications have not yet decreased to a satisfactory level, although the incidences may differ between devices.

The incidence of thromboembolism has been reported to range from 0–47%. However, this complication occurs at a lower frequency of 0–12.5% with HeartMate systems, for which anticoagulation therapy is performed using aspirin alone or in combination with dipyridamole, without the use of coumadin[2,11–13]. In the present study, thromboembolism occurred in as many as 43% of patients supported with a Novacor system. This indicates the need for re-evaluation of the current anticoagulation therapy and improvement of the device, with a particularly urgent need for an improvement in the quality of inflow prosthesis and appropriate selection of the length of prosthesis suitable to each patient's physique.

The incidence of infection has been reported to be 25–55% and many reports suggest that this complication significantly affects mortality[1,2,11,12,14]. A higher incidence

Table 1. VAD characteristics

	Paracorporeal	Implantable
Advantage	Easy implantation	Long-term support
	Versatile*	Out-of-hospital
		No anticoagulation**
Disadvantage	Patient mobilization	Surgically demanding
	Support time	No RVAD
		Technical problems

*LVAD/RVAD/BiVAD
**HeartMate

has been more frequently observed with HeartMate systems, compared to others, and this incidence is said to increase as the duration of support is prolonged. A report on 100 patients supported with a HeartMate system at the Cleveland Clinic revealed that 59% of these patients had positive blood cultures, and drive-line and pump infection were clinically observed in 28% and 11%, respectively[2]. In the present study, the incidence of infection did not differ between devices. Pocket infection was found to be a particularly serious problem for implantable HeartMate and Novacor systems, which are usually implanted for a long period of time. In order to reduce postoperative effusion in the pocket, which might lead to infection, we covered the upper surface of the blood pump with a coated prosthesis (Hemashield: Meadox Medicals Inc., Oakland, NJ, USA)[15].

The incidence of bleeding has been reported to be 21–60%[1,2,11]. At our institute, this complication occurred at the highest incidence of over 40%, without differences between devices. When the Thoratec and HeartMate devices were implanted, the outflow conduit was wrapped with Hemashield graft to prevent bleeding from the outflow prothesis[16]. Furthermore, in the HeartMate device, the junction of pump and inflow and that of pump and outflow were also wrapped with a Hemashield graft to prevent bleeding from these junctions. This seems to be a reason for the lack of difference between the three types of device.

Mechanical failures have emerged as a new problem related to long duration of support. The report from the Cleveland Clinic revealed that mechanical failures with a HeartMate device occurred in 12% of their patients, and that half of them died[2]. The causes of those deaths were internal tubing in the pneumatic drive-line, bleeding from a broken inflow valved conduit, electric failures, etc. Pennington *et al.*[17] reported that mechanical failures were observed in 17% of their patients supported with a Thoratec system, due to problems in the console or electrical connector. In the present study, mechanical failures occurred in a small number of cases: three (4%) in the Thoratec group and four (9%) in the HeartMate group. The mechanical failures observed in the Thoratec group were equal to those reported by Pennington *et al.* In the HeartMate group, bleeding from a junction in the outflow conduit or inflow cannula was observed as a main symptom of mechanical failure, although two patients developed a rupture of the diaphragm.

These complications should be further studied because the duration of support is likely to be further prolonged due to the shortage of donor hearts.

The Lion Heart VAD was developed as the first fully implantable LVAD, and a clinical trial was started in Europe. The first implantation was performed at our institute. The new fully implantable LVAD eliminates the currently percutaneous drive-line and external tethers by the use of a transcutaneous energy transmission (TET) system. This feature will reduce the risk of infection and improve the patient's quality of life. The TET system and the compliance chamber have performed well in this initial trial. Infection after support was always a serious problem in former VADs. If this feature is effective and can control a patient's condition, this device will be an epoch-making VAD and may replace former VADs. The DeBakey VAD axial flow pump is a nonpulsatile pump designed for long-term support[3]. A clinical trial was started in Europe and the first implantation was performed at the University of Vienna, Austria[18]. Some investigators previously reported that nonpulsatile flow is capable of maintaining circulation without any abnormality in experimental studies[19–21]. In our case, the patient was able to maintain hemodynamics, physical and nervous systems by a nonpulsatile circulation.

Though long-term further observation on thromboembolism, infection and hemolysis is needed for evaluation of a new VAD, we believe that the next generation of devices will be effective in improving patient quality of life. We expect good results and a possibility of wide use of this device in the future. The results of these new devices influence the other totally implantable VADs[22], nonpulsatile axial flow and centrifugal pumps [23–25] and total artificial hearts[26,27], which are being developed at the present time.

Conclusion

VADs are an essential part of heart transplantation because of donor shortage. We recommend that a Thoratec system be employed as a bridge to heart transplantation for patients with biventricular heart failure, and that a Novacor or HeartMate system be implanted into patients requiring long-term circulatory support. However, complications such as thromboembolism and infections (of the drive line and pocket) have increased as the duration of bridge to transplant has increased. Further studies are required on these topics.

References

1. Hunt SA, Frazier OH, Myers TJ. Mechanical circulatory support and cardiac transplantation. *Circulation* 1998;97:2079–90.
2. McCarthy PM, Smedira NO, Vargo RL *et al.* One hundred patients with the HeartMate left ventricular assist device: Evolving concepts and technology. *J Thorac Cardiovasc Surg* 1998;115:904–12.
3. DeBakey M. A miniature implantable axial flow ventricular assist device. *Ann Thorac Surg* 1999;68:637–40.
4. Koerfer R, El-Banayosy A, Posival H *et al.* Mechanical circulatory support: The Bad Oeynhausen experience. *Ann Thorac Surg* 1995;59:S56–63.
5. Minami K, Arusoglu L, El-Banayosy A *et al.* Bridge for heart transplantation by different types of ventricular assist device. In Akutsu T, Koyanagi H editors. *Heart Replacement – Artificial Heart 6*. Tokyo: Springer-Verlag, 1998:81–90.
6. Bonkohara Y, Minami K, Arusoglu L *et al.* A fetal mechanical disorder of the TCI HeartMate left ventricular assist system. *J Thorac Cardiovasc Surg* 1999;118:769–70.

7. Reedy JE, Pennington DG, Miller *et al*. Status I heart transplant patients: conventional versus ventricular assist device support. *J Heart Lung Transplant* 1992;11:246–52.
8. Pifarre R, Sullivan H, Montoya A *et al.* Comparison of results after heart transplantation: mechanically supported versus nonsupported patients. *J Heart Lung Transplant* 1992;11:235–9.
9. Rowles JR, Mortimer BJ, Olsen DB. Ventricular assist and total artificial heart devices for clinical use in 1993. *ASAIO J* 1993;39:840–55.
10. Griffith BP, Kormos RL, Nastala CJ, Winowich S, Pristas JM. Results of extended bridge to transplantation: window into the future of permanent ventricular assist device. *Ann Thorac Surg* 1996;61:396–8.
11. Frazier OH, Rose EA, Macmanus Q *et al.* Multicenter clinical evaluation of the HeartMate 100 IP left ventricular assist device. *Ann Thorac Surg* 1992;53:1080–90.
12. Koul B, Solem J, Steen S, Casimir-Ahn H, Granfeldt H, Lonn UJ. HeartMate left ventricular assist device as bridge to heart transplantation. *Ann Thorac Surg* 1998;65:1625–30.
13. Schmid C, Weyand M, Nabavi DG *et al.* Cerebral and systemic embolization during left ventricular support with the Novacor N100 device. *Ann Thorac Surg* 1998;65:1703–10.
14. McCarthy PM, Schmitt SK, Vargo RL, Gordon S, Keys TF, Hobbs RE. Implantable LVAD infections: Implications for permanent use of the device. *Ann Thorac Surg* 1996;61:359–65.
15. Arusoglu L, Koerfer R, Tenderich G, Alexander WA, El-Banayosy A. A novel method to reduce device-related infections in patients supported with the HeartMate device. *Ann Thorac Surg* 1999;68:1875–7.
16. Minami K, Arusoglu L, Koyanagi T, El-Banayosy A, Koerner MM, Koerfer R. Successful implantation of Thoratec assist device: wrapping of outflow conduit in Hemashield graft. *Ann Thorac Surg* 1997;64:861–2.
17. Pennington DG, McBride LR, Miller LW, Swartz MT. Eleven years' experience with the Pierce-Donachy ventricular assist device. *J Heart Lung Transplant* 1994;13:803–10.
18. Wieselthaler GM, Schima H, Hiesmayr M *et al.* First clinical experience with the DeBakey VAD continuous-axial flow pump for bridge to transplantation. *Circulation* 2000;101:356–59.
19. Nosé Y. Nonpulsatile mode of blood flow required for cardiopulmonary bypass and total body perfusion. *Artif Organs* 1993;17:92–102.
20. Gording LR, Jacobs G, Murakami T *et al.* Chronic nonpulsatile blood flow in an alive, awake animal 34-days survival. *Trans Am Soc Artif Intern Organs* 1980; 8:251–5.
21. Tatsumi E, Toda K, Taenaka Y *et al.* Acute phase responses of vasoactive hormones to nonpulsatile systemic circulation. *ASAIO J* 1995;41:M460–5.
22. Mussivand T, Hendry PJ, Masters RG, King M, Holmes KS, Keon WJ. Progress with the HeartSaver ventricular assist device. *Ann Thorac Surg* 1999;68:785–9.
23. Nosé Y, Nakata K, Yoshikawa M *et al.* Development of a totally implantable biventricular bypass centrifugal blood pump. *Ann Thorac Surg* 1999;68:775–9.
24. Westaby S, Katsumata T, Evans R, Pigott D, Taggart DP, Jarvik RK. The Jarvik 2000 Oxford system: increasing the scope of mechanical circulatory support. *J Thorac Cardiovasc Surg* 1997;116:467–74.
25. Nojiri C, Kijima T, Maekawa J *et al.* Development of Terumo implantable left ventricular assist system (T-ILVAS) with a magnetically suspended centrifugal pump. *J Artif Organs* 1999;2:3–7.
26. Weiss WJ, Rosenberg G, Snyder AJ *et al.* Steady state hemodynamic and energetic characterization of the Penn State/ 3M Health care total artificial heart. *ASAIO J* 1999;45:189–93.
27. Kung RTV. Total artificial heart. In Rose EA, Stevenson LW, editors. *Management of End-Stage Heart Disease*. Philadelphia: Lippincott-Raven 1998:213–20.

Journal of Congestive Heart Failure and Circulatory Support (2001) Vol 1, No 4, 185–192

First clinical trials of a totally implantable destination therapy ventricular assist system

A. Snyder PhD[1], W. Pae MD[1], J. Boehmer MD[1], G. Rosenberg PhD[1], W. Weiss PhD[1], W. Pierce MD[1], J. Thompson BSME[2], J. Lewis MS[2], D. Frank MS[2], H. Zintak PA[2], S. Scholl RN[2], R. Körfer MD[3], A. El-Banayosy MD[3], L. Arusoglu MD[3], O. Fey RN[2] and M. Morshuis MD[3]

[1]The Pennsylvania State University, Hershey, PA, USA; [2]Arrow International, Reading, PA, USA; and [3]Heart Center NRW, Bad Oeynhausen, University of Bochum, Germany

Abstract Our artificial heart research team at the Pennsylvania State University has been engaged since 1971 in the development of mechanical circulatory support systems, including those that provide left ventricular assistance. While for many years these systems were suitable for use only for short-term support, the technology on which they were based was always intended for application to devices and systems for long-term use. We have recently begun the first clinical trials of a left ventricular assist system that operates without percutaneous leads and is intended for application as destination therapy.

The sac-type blood pump uses a smooth segmented polyurethane surface and careful design of transitions to valves and connectors to discourage thrombus formation. The pump is coupled to a roller-screw energy converter. Implanted electronics with a back-up battery, a thoracic compliance chamber, and inductive energy transmission enable the system to operate without percutaneous lines. External subsystems provide the recipient with multiple options for maintaining power to the system and carrying the necessary equipment. The clinician is provided with a simple interface to determine the status of the system and make limited adjustments through a radio frequency telemetry link.

The Clinical Utility Baseline Study (CUBS) is a nonrandomized trial designed to determine the system's utility for treatment of end-stage heart disease patients who are not candidates for heart transplantation. Early experience with the system indicates that the technology necessary to achieve intact-skin operation – the inductive energy transmission and compliance chamber – perform well and will be practical for use in patients, and that the system has considerable potential for treatment of the intended patient population.

System design

The implanted parts of the system are illustrated in Figure 1.

Our experience with pneumatic blood pumps[1–3] taught us important lessons that were carried over to the design of the destination therapy system. Accordingly, the blood pump[4] was designed using a smooth, seamless segmented poly(ether-urethane-urea) blood sac and tilting disc valves, with the chamber shape, port placement and valve orientation selected to encourage diastolic washing of the pump walls. Pump connector and cannula designs are derived from those developed for the Penn State (Pierce–Donachy) ventricular assist device (VAD) and later for our electric motor-driven pumps, with modifications for human fit and manufacturability.

The clinical cannulae use reinforced polyurethane proximal segments. The outlet cannula has a coated, woven polyester, distal segment, while the inlet cannula uses a titanium tip with a sintered outer surface. The sintered surface aids in integration of the cannula with the ventricle, preventing accumulation of loosely adherent thrombus at the cannula–endocardium junction, and aids in physical retention of the cannula. The outlet cannula is constructed of polyurethane and coated polyester graft. Slotted guards on both cannulae prevent kinking of the polyurethane segments near the connectors.

The energy converter (Figure 2) is based upon the roller-screw mechanism first reported in 1982[5]. A compact brushless DC-motor turns the nut of a roller-screw-type anti-friction screw, which in turn causes linear motion of a circular pusher-plate. In systole, the pusher-plate compresses the blood sac to effect pump ejection. In diastole, the motor reverses to withdraw the pusher-plate. An intrathoracic compliance chamber maintains near-thoracic pressure in the energy converter airspace, so that the pump fills passively.

The 13 cm diameter by 1 cm thick compliance chamber is constructed of segmented polyurethane, with an internal tubing skeleton that helps maintain chamber shape when implanted. A polyester velour covering encourages integration with adjacent lung and pleural tissues, and maintenance of flexibility over time. Chambers of this type have functioned without leaks or loss of compliance in over 90 animal

Correspondence to: Alan Snyder, Penn State College of Medicine, The Milton S Hershey Medical Center, Section of Artifical Organs, H151, 500 University Drive, Hershey, PA 17033–2390, USA.

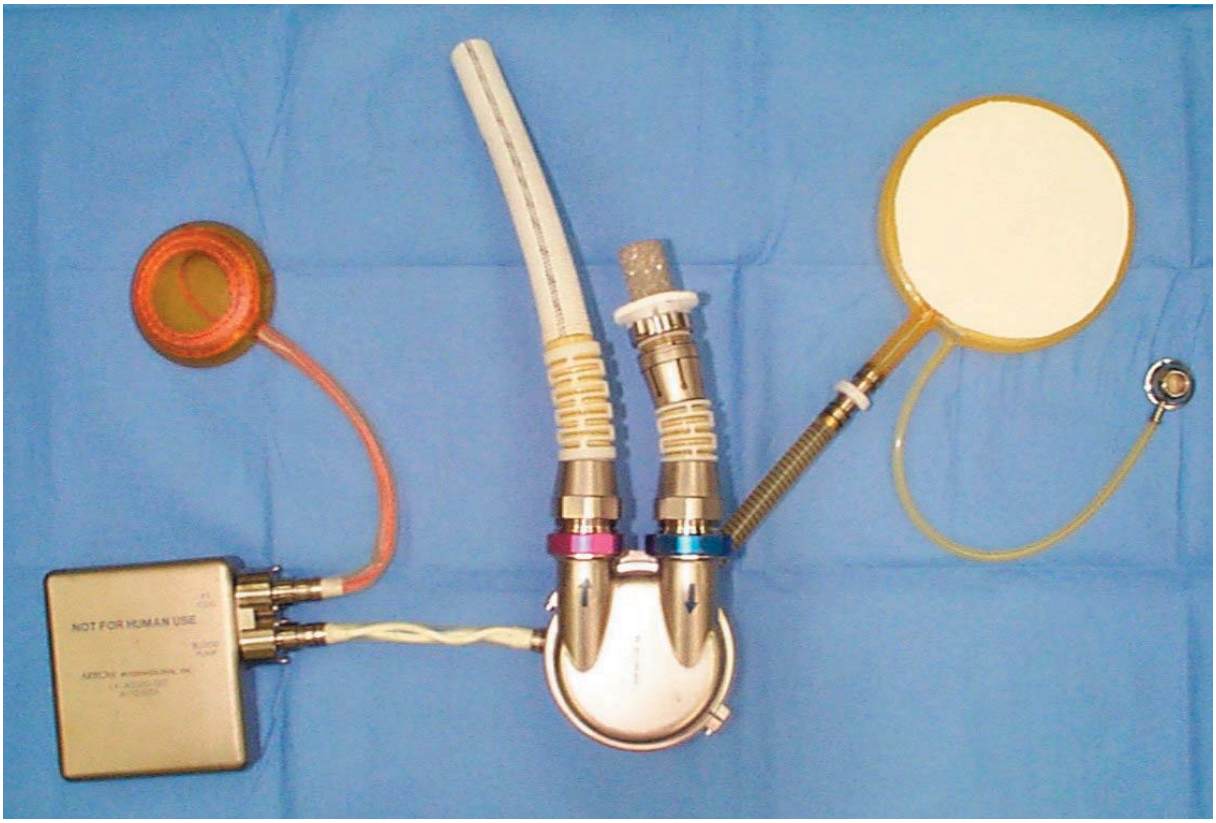

Figure 1. Implanted components of the LionHeart ventricular assist system: pump/energy converter (center), implanted electronics and battery package (lower left), energy transmission secondary coil (upper left), and volume compensation (compliance) chamber (right).

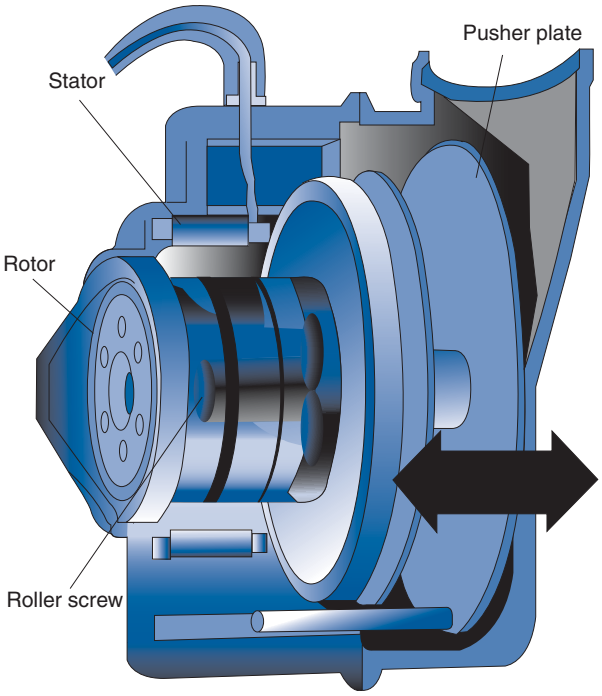

Figure 2. The roller-screw energy converter coupled to the blood pump. Rotation of the electric motor causes motion of the pusher-plate from left to right. The motor reverses to withdraw the plate and allow the pump to fill.

implants. Since gas is continually lost to surrounding tissues by diffusion through the chamber walls, a subcutaneous injection port is used to refill the chamber as necessary.

Passive pump filling permits the pump rate to be controlled according to the speed with which it fills. The control system, described by Snyder *et al.*[6] in the context of a total artificial heart but working according to the same principles for the ventricular assist system, uses no transducers other than the Hall-effect sensors needed to commutate the brush-less motor. By analysis of the motor speed and applied voltage, the controller estimates the load imposed by the pump on the pusher-plate, which varies with the pusher-plate position as it moves from its end-diastolic to its end-systolic position. A precipitous rise in the load indicates the point of contact of the pusher-plate and the blood sac, beyond which pressure is developed in the pump to open the outlet valve. The pusher-plate position at which the point of contact is detected provides an estimate of the pump's end-diastolic volume. This is used for both pump rate control and estimates of pump flow.

An end-diastolic volume greater than 85% of the 70 cc pump capacity is considered acceptable filling. The pump always slows down if filling is below this minimum. Otherwise, the pump seeks an ideal rate as follows: In small increments the rate is increased, and continues to increase as long as the end-diastolic volume is approximately maintained. Once a significant loss of filling is

detected, the pump rate is decreased as long as each drop in rate results in improved filling. At a fixed hemodynamic condition, the rate varies only slightly as the system cycles between trial increases and decreases. With changing conditions, the system will typically go from its minimum rate of approximately 60 bpm to the maximum of 135 bpm in under 1 min.

Inductive coupling[7–9] is used to deliver power to the system. The silicone-coated external coil is kept in approximate alignment with the polyurethane-encapsulated secondary, and alternating current applied to the primary induces a corresponding current in the secondary. The system shuts down safely and triggers a 'check coil' alarm when coil misalignment is excessive or when very close proximity to ferrous materials disrupts the link. Metals more than a few centimeters away typically have no notable effect.

The control electronics, inductive coupling secondary, rechargeable nickel–cadmium battery and a telemetry subsystem are housed in a single thin-walled titanium package. Hermetic electrical connectors permit separate placement of the pump, electronics package and secondary coil and tunneling of the interconnecting leads. The system can run for approximately 40 min on the implanted battery; the instructions to the patient indicate 20 min. Complete recharge of the implanted battery requires approximately 4 h, but 80% of full charge is typically achieved in less than 3 h. The size of the package relates mainly to the battery chemistry used. Substantial reductions in size will follow the transition to lithium-based cells.

The telemetry link permits both monitoring and adjustment of the implant through a radio frequency link, and works in concert with custom software (Figure 3). The telemetry wand is placed on the skin in the area of the implanted electronics. Whenever the wand is within range, the clinician's monitor software maintains a display of device status, including beat rate, percent pump filling, estimated pump flow, and battery status. Additional data that enable detailed diagnosis of system performance are also available, but the clinician is generally not called upon to interpret these data. The software brings attention to any changes in the implant's self-diagnostic results, so that they can be relayed to the manufacturer. A standard set of status data is recorded to a disk file at set intervals. Since the implant identifies itself by serial number through the telemetry link, these data are recorded to patient-specific files, allowing easy retrieval of data when a single Clinician's Monitor is used for multiple patients.

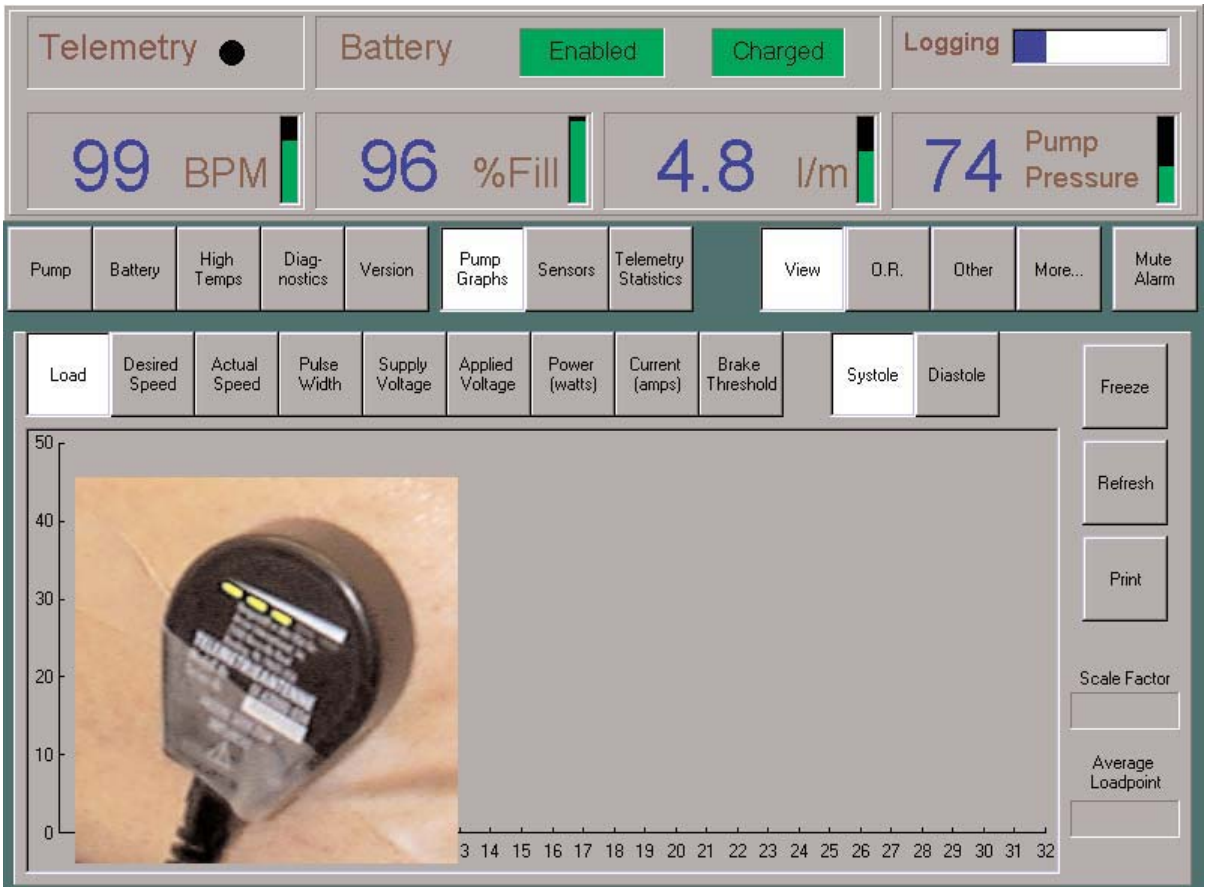

Figure 3. The Clinician's Monitor is used to communicate with the implant via the telemetry link. The telemetry probe (inset) is placed over the implanted electronics. Sufficient adjustments are available for perioperative management, but by design the system requires little intervention.

The system permits the clinician to make limited adjustments to its operation. For preoperative preparation, the system can be set to charge the implanted battery, without attempting to run the pump, by placing a primary coil in a designated position on the intact sterile package. For perioperative management, the system can be stopped and started as required and the maximum beat rate can be limited. Initial start-up can be achieved using very low rates if desired. For the range of beat rates intended for long-term support (over 50 bpm), the system continues to control its rate automatically, up to the maximum set by the physician.

External electronics consist of the energy transmission primary (Power Transmitter), a Power Pack, a battery charger (Figure 4), and portable power supplies. The Power Transmitter provides excitation of the external coil, adjusting as necessary to the power demand of the implant and shutting down as necessary when the link is broken or disturbed. The Power Transmitter also detects a battery status signal that comes through the inductive link from the implant, so that the recipient can be informed when the implanted battery is sufficiently charged to provide the labeled capacity. The unit must be kept close to the patient because efficient power transfer requires that the lead to the primary coil is relatively short. The fabric carrier provided allows the Power Transmitter to be worn in a number of ways (Figure 5).

The Power Pack acts as the primary source of both power and information. It holds identical but independent batteries and also accepts power from an external DC source. In the absence of an external source, one battery is used while the other is held as a back-up. When the first battery is depleted, the system switches to the second and informs the user that the first should be replaced. Thus, the user may rotate batteries indefinitely. Approximately three hours of use are provided from a full charge of the nickel–cadmium packs presently used. Power is preferentially drawn from the external DC source, so that when mobility is not desired, and when the user is sleeping, the two batteries are kept in reserve. A set of indicators (Figure 6) provides the user with needed information:

Figure 4. External electronics. Power Transmitter (lower left), Power Pack (upper left), and battery charger.

Figure 5. Examples of the user's options for carrying external equipment: Power Transmitter case with belt (left) and Power Pack in shoulder bag/waist pack (right). A small cart (not shown) is also provided.

- Status of both batteries
- Need to change a battery
- Need to check the coil alignment
- Whether the implanted battery is ready for full use
- Verification of presence of the external supply
- Failure of the external supply.

Visual indicators are accompanied by audible indicators appropriate to their urgency. When the power transmission coil is intentionally removed, the decoupling alarm can be disabled. The alarm gradually returns to full intensity when the recommended duration of implanted battery usage has expired.

The battery charger can test and recharge two packs simultaneously, and can also provide DC power to the Power Pack for use while sleeping or otherwise not interested in full mobility. Packs are tested using data stored in embedded electronics and by the charger itself. A full battery charge is achieved in approximately 1 hour. Convenience supplies, for both home/workplace and automotive use can be used as more compact sources of DC power.

All electronics comply with relevant international regulations regarding electromagnetic compatibility.

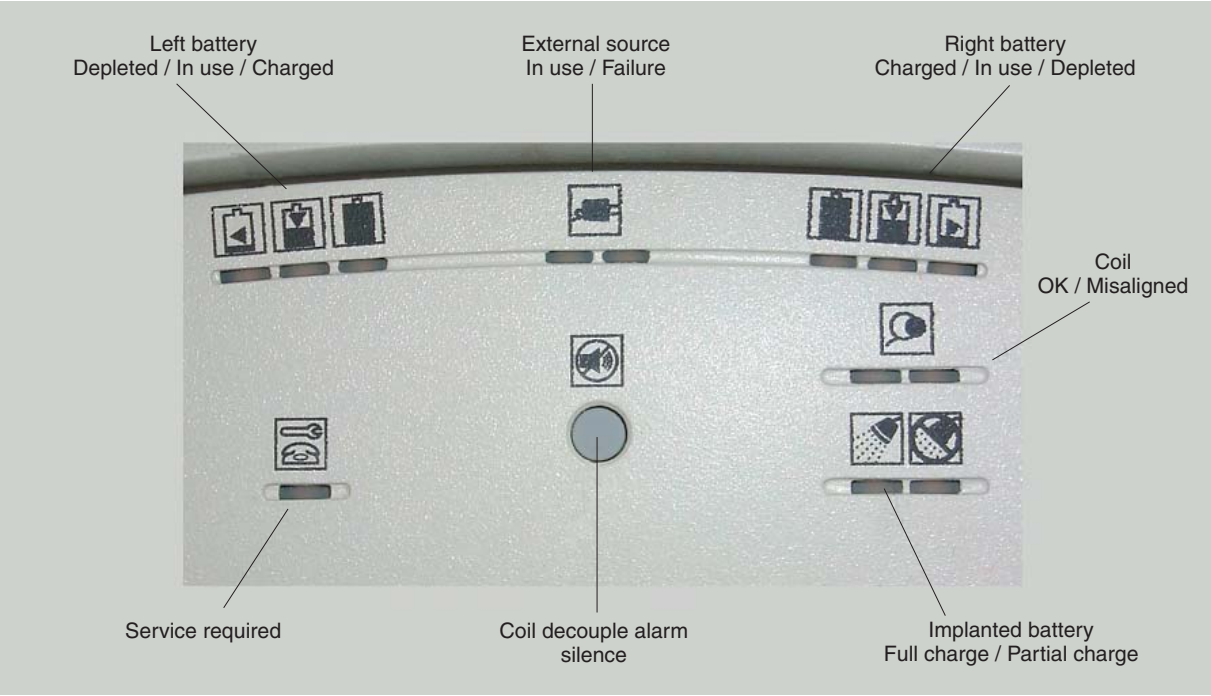

Figure 6. The Power Pack indicator panel. This provides all the status information the user needs to safely use the system.

Implantation

Some variations in the details of implantation will be appropriate to the body habitus of an individual patient and the preferences of the surgeon. Typically, a midline sternotomy is extended to the umbilicus. Once the sternum is divided, the left anterior rectus sheath is opened medially, and a pocket is created behind the rectus muscle to accommodate the assist pump. The pericardium is opened and after institution of normothermic cardiopulmonary bypass, a 3 cm opening is made in the diaphragm to pass the inflow cannula from the pocket to the pericardium. The left ventricular apex is cored with a circular knife, and a felt-covered, reinforced sewing ring is secured to the apex with interrupted pledgeted sutures. The pump is placed in the preperitoneal pocket and the inlet tube of the pump passed through the opening in the diaphragm and placed in the left ventricle. After optimally orienting the small bend in the inlet cannula, it is secured to the previously placed sewing ring using a custom clamp. The outlet graft is anastomosed end-to-side to the ascending thoracic aorta and the proximal end is connected to the pump, which has been primed and de-aired.

Through a right lower quadrant transverse incision a subrectus pocket to accommodate the electronics canister is fashioned and the canister inserted into such. A right sixth intercostal space anterior transverse incision is used to fashion a subcutaneous pocket for the secondary coil and the coil is inserted. The electrical connections from the pump and the secondary coil are tunneled to the electronics package and connected. There are no particular requirements for the sequence in which electrical connections are made. Connectors can safely be removed and re-attached while the system is running.

The pleural space is opened, the variable volume compliance chamber is inserted, and its inlet/outlet tube is tunneled to the pump housing and connected. A 2 cm incision over the lower anterior left chest is used to fashion a subcutaneous tissue pocket for the infusion port. This is inserted and tunneled into the compliance chamber.

The primary coil is applied and the device is activated while cardiopulmonary bypass is gradually discontinued. The system is generally started at 10 bpm so that the surgical connections may be checked for leaks and the outlet graft may be probed for air. Increases in rate are achieved manually, as cardiopulmonary bypass is withdrawn, until the minimum automatic rate of 50 bpm is reached. Thereafter, the pump rate is controlled automatically according to filling, as described above. Clinicians may choose to limit the pumps's maximum rate to limit the abrupt change in the patient's cardiac output and to manage the energy consumption of the right heart.

Trial design

The Clinical Utility Baseline Study (CUBS) trial is a nonrandomized study intended to determine the system's safety utility as destination therapy for end-stage heart disease in nontransplant candidates. We avoid the term 'alternative to transplant,' which would imply that the system presently competes with heart transplantation. Patients to be enrolled in this clinical trial will have advanced (NYHA

Class IV) heart failure with a 1-year survival projected to be on the order of 50%. Specific inclusion criteria for the study are listed in Box 1. Exclusion criteria, given in Box 2, are intended to exclude patients who would not be expected to benefit from the therapy for medical or device-related reasons, such as:

- Co-morbidity that makes the patient's overall prognosis poor or would severely complicate postoperative management
- Cardiac defects that would adversely affect system performance
- Poor prognosis for tolerating the implant procedure
- Patient size.

The study will enroll consecutive eligible patients at the participating institutions, up to a total of 30–40 subjects.

Study end-points, all related to the system's efficacy as a therapy for end-stage heart disease, are: (1) device function, (2) quality of life, (3) exercise capacity, and (4) adverse events. Formal assessment is at three months. Patient follow-up will continue beyond the 3-month assessment period.

Preoperative, postoperative and follow-up evaluation will assess device function, patient functional class, quality of life, hemodynamics, and end-organ function, as outlined in Table 1.

Box 1. CUBS inclusion criteria

Left ventricular ejection fraction <30% within 90 days prior to enrollment

Heart failure of at least 6 weeks' duration

NYHA functional Class IV heart failure

Peak oxygen consumption by cardiopulmonary exercise testing <14 cc kg^{-1} min^{-1} or the patient is unable to exercise due to cardiovascular condition

At least one of the following poor prognostic indicators:

- Serum sodium <135 mEq
- Cardiac arrest within the past year
- Unable to tolerate angiotensin-converting enzyme (ACE) inhibitors or angiotensin II (ANGII) receptor antagonists
- Two or more hospitalizations within the past 6 months or heart failure
- Left ventricular internal diastolic dimension >8.0 cm by echocardiogram (ECHO)
- Resting heart rate ≥90 bpm
- Need for inotropic support within the past 3 months

A cardiac index ≤2.4 L min^{-1} m^{-2} and pulmonary capillary wedge pressure ≥18 mmHg after attempts to tailor optimal medical therapy with oral agents

Patient must be able to communicate effectively with the investigators, provide informed consent and reliably follow a prescribed course of medical therapy

Ineligible for heart transplantation

Early clinical experience

Partial data cannot be reported during the conduct of the study, but we can describe here the early experience with implantation and operation of the system. The first implant was accomplished on October 26, 1999 at the Department of Thoracic and Cardiovascular Surgery, HeartCenter NRW, Bad Oeynhausen, Germany. The patient was a 67-year-old male with a preoperative diagnosis of dilated cardiomyopathy. The patient had a body surface area of 2.0 m^2. The preoperative cardiac index was 2.1 L min^{-1} m^{-2}. The patient's history was notable for atrial fibrillation and significant blockage of the right internal carotid artery with ulcerative plaque.

System implantation was accomplished uneventfully in a 4-hour procedure. Postoperative X-rays are shown in Figure 7. System start-up and weaning from cardiopulmonary bypass were managed as described earlier, using gradual manual increases in pump rate followed quickly by a transition to full automatic control. The power transmission system, the telemetry link and the compliance chamber functioned as intended. There was mild swelling at the coil site and some vigilance in maintaining coil position was initially required; this soon resolved and maintenance of the power link with normal movement and activity was not difficult. Early experience with the compliance chamber indicates that its compliance (change in volume that can occur within a small pressure range) may be larger in humans than

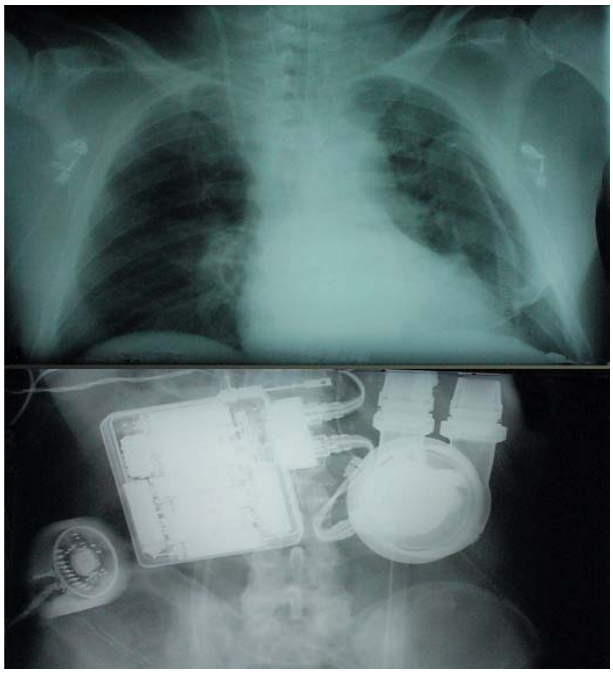

Figure 7. Thoracic and abdominal anterior–posterior X-rays of the first patient immediately after system implantation. The frame of the compliance chamber is visible in the lateral left chest. The abdominal view shows the placement of the pump and electronics package, and the cable to the power transmission secondary coil, which is not visible here. The telemetry wand at the bottom left of the film is lying on the patient's abdomen.

Box 2. CUBS exclusion criteria

Body surface area $<1.5\ m^2$

Severe chronic obstructive pulmonary disease as evidenced by an FEV_1 <1.2 I min^{-1} or $<40\%$ of predicted value or of sufficient severity to preclude cardiothoracic surgery

Acute pulmonary embolus within the past 30 days

Fixed pulmonary hypertension defined as pulmonary vascular resistance >6 Woods units, unresponsive to vasodilator therapy

Presence of a prosthetic heart valve, except for aortic homograft or stentless valves

Heart failure due to:

- Hypertrophic cardiomyopathy
- Constrictive pericarditis
- Restrictive cardiomyopathy including amyloid heart disease
- Clinically significant aortic regurgitation
- Severe mitral stenosis
- Other correctable valvular heart disease
- Uncorrected thyroid disease
- Active myocarditis or
- Correctable coronary artery disease.

Active systemic infection

Severe thrombocytopenia (platelet count $<60\ 000$ or comparable European unit of measurement)

Any contraindication to anticoagulation, including allergy to heparin

Severe renal dysfunction with creatinine $\geq 3.5mg\ dL^{-1}$ or requiring ongoing dialysis

Ongoing drug or alcohol abuse within 6 months of randomization

History of noncompliance or psychiatric disease that may impair compliance

Pregnancy. Women of childbearing age must use adequate contraceptive precautions

Cerebrovascular accident (CVA) within the past 6 months or an impending CVA with uncorrected critical or symptomatic cerebrovascular disease

Impending intra-abdominal surgery or active intra-abdominal inflammatory disease

Ventilatory support greater than 5 days or requiring an FiO_2 >0.70

Documented intracranial bleeding within the past 6 months

Absence of adequate psycho-social support for long-term care

Inability to relocate within 4-hour travel time of the clinical center

Concomitant disease that will limit 2-year prognosis or ability for rehabilitation

Concomitant treatment with another drug or device under investigation

Table 1. Pre- and postoperative evaluation of device recipients

Weeks	Baseline	2	4	8	12	Monthly
Informed consent	X					
Serum pregnancy	X					
Demographics	X					
Physical examination	X	X	X	X	X	X
Neurological examination	X		X		X	
Goldman scale	X		X	X	X	X
NYHA Class	X	X	X	X	X	X
Medical/surgical history	X					X
Ejection fraction	X					
Chest X-ray	X	X	X	X	X	X
12-lead ECG	X	X	X	X	X	X
CPX					X	q 6 months
Hematology and clinical chemistry	X			Days 1,2,3,5,7,q3d		
CT scan of head	X					
Right heart catheterization	X					
LV end-diastolic dimension	X					
Device evaluation						
Quality of life	X		X		X	q 6 months
6-minute walk	X				X	q 3 months
Energy transmission assessment		X	X	X	X	Monthly
Compliance chamber assessment		X	X	X	X	Monthly
ECHO						At discharge

in the calves used for preclinical evaluation. This is not surprising, given the more favorable human thoracic geometry, and may lead to extension of the 4-week interval between compliance chamber checks that is presently prescribed.

The second patient was a 68-year-old male with dilated cardiomyopathy (Figure 8). This patient had a body surface area of 2.0 m^2 and a preoperative cardiac index of 1.8 L min^{-1} m^{-2}. A history of atrial fibrillation was noted, and the patient had an AV-sequential pacemaker. There was significant preoperative renal and hepatic dysfunction secondary to the patient's heart failure. Implantation proceeded uneventfully, with some revision to subsystem placement relative to that used in the first patient.

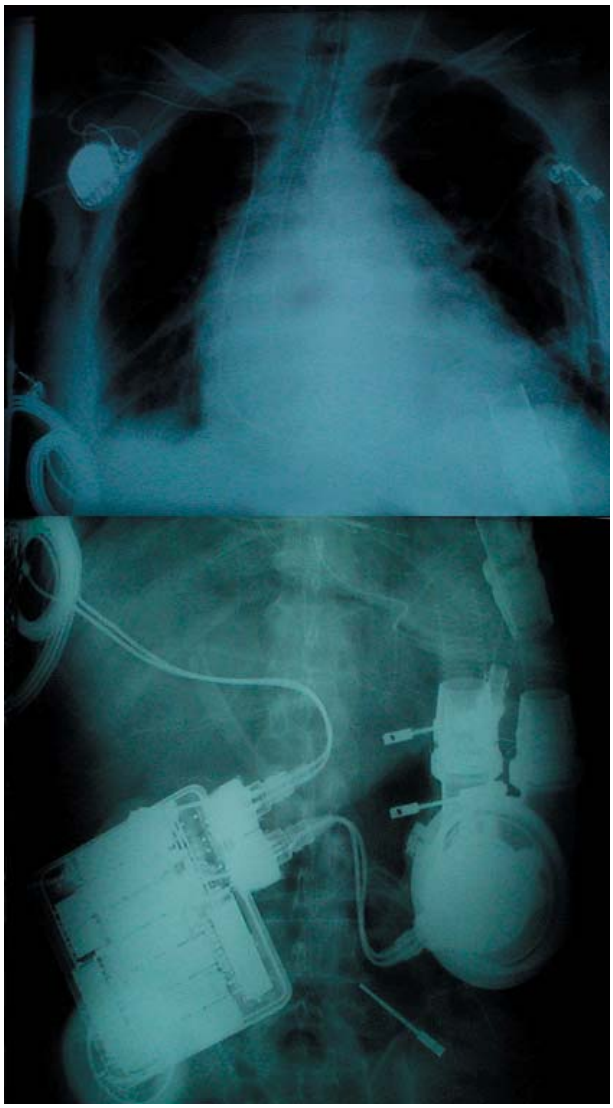

Figure 8. Thoracic and abdominal X-rays from the second patient. Some revision to the placement of the electronics package is evident. The compliance chamber is again visible along the left chest wall. The smaller implanted secondary power transmission coil and larger primary coil are visible on the lateral right chest.

Conclusions

The first clinical applications of a completely implanted, intact-skin, ventricular assist system have been achieved. The system makes use of both transcutaneous inductive energy transmission and an intrathoracic compliance chamber, neither of which had been used clinically before. The early experience indicates that these systems will perform as intended in humans. It does not appear that perioperative management of patients with these systems will be more complex than management of patients with percutaneous lead ventricular assist systems. We are hopeful that the incidence of infection in these patients will be less than that encountered in patients who have percutaneous leads. We are likewise hopeful that we are prepared to meet the inevitable challenges of long-term management of these patients, and that the system will afford our patients a desirable quality of life.

References

1. Pierce WS, Donachy JH, Landis DL *et al.* Prolonged mechanical support of the left ventricle. *Circulation* 1978; 58(1):133–46.
2. Pierce WS, Parr GVS, Myers JL *eta l.* Ventricular assist pumping in patients with cardiogenic shock after cardiac operations. *N Engl J Med* 1981;305(27):1606–10.
3. Pennock JL, Wisman CB, Pierce WS. Mechanical support of circulation prior to cardiac transplantation. *Heart Transplant* 1982;1:299–305.
4. Snyder AJ, Rosenberg G, Weiss W *eta l.* Chronic animal studies with a motor-driven LVAD and an implanted compliance chamber. *Trans Am Soc Artif Intern Organs* 1984;30:92–7.
5. Rosenberg G, Snyder A, Weiss W *eta l.* A rollerscrew drive for implantable blood pumps. *Trans Am Soc Artif Intern Organs* 1982;28:123.
6. Snyder AJ, Rosenberg G, Pierce WS. Non-invasive control of cardiac output for alternately ejecting dual pusherplate pumps. *Artif Organs* 1992;16(2):189–94.
7. Schuder JC, Gold JH, Stephenson HE. An inductively coupled RF system for the transmission of 1 kW of power through the skin. *IEEE Trans Biomed Engr BME* 1971;18(4).
8. Sherman, C, Daly B, Dasse K *et al. Research and Development: Systems for Transmitting Energy Through Intact Skin*. Final Technical Report (N01-HV-0–2903–3), National Heart Lung and Blood Institute, 1983.
9. Weiss WJ, Rosenberg G, Snyder AJ *eta l. In vivo* performance of a transcutaneous energy transmission system with the Penn State motor driven ventricular assist device. *ASAIO Trans* 1989;35(3):285–88.

Session 3

Total Artificial Heart

Journal of Congestive Heart Failure and Circulatory Support (2001) Vol 1, No 4, 195–200

Design of atrial cuff for the undulation pump total artificial heart

K. Imachi PhD[1], T. Chinzei MD, PhD[2], Y. Abe MD, PhD[1], T. Isoyama PhD[2], T. Ono BE[1], S. Mochizuki MD, PhD[2], I. Saito PhD[2], M. Ishimaru MD[1], K. Iwasaki MS[3], A. Baba MD[1], T. Karita MD[1], T. Ozeki MS[2] and A. Kouno BL[1]

[1]Department of Biomedical Engineering, Graduate School of Medicine, University of Tokyo, Tokyo; [2]Research Center for Advanced Science and Technology (RCAST), University of Tokyo, Tokyo; and [3]Department of Mechanical Engineering, Waseda University, Tokyo, Japan

Background The implantable total artificial heart (TAH) is the final goal of artificial heart research. Although various types of implantable TAH are under development in several countries, a more compact TAH is required. In our laboratory, an undulation pump (UP) TAH has been in development for 6 years. The UPTAH is the most compact TAH in the world. It could be implanted into the chest cavity of a goat weighing between 41 and 79 kg.

However, the design of atrial cuff of the UPTAH is very important in order to ensure a good fit, low flow resistance and good blood compatibility in the narrow chest cavity of the goat. The objective of this study is to establish design criteria for the atrial cuff of the UPTAH.

Methods The predominant parameters of the atrial cuff to ensure a good fit, blood compatibility and atrial wall suction protection are: (1) cuff diameter (D), (2) configuration (h) (flat to cone shape), (3) angle to the pump nozzle (α) and (4) angle to the UP (β). In this study, many types of atrial cuff were designed by changing these parameters.

Results Nine types of atrial cuff model were designed and fabricated through animal experiments with goats. The final parameters for optimum design of the atrial cuff were as follows: D = 38 mm, h = 18 mm, α = 40° (R), 30° (L), β = 30°.

Discussion The atrial cuff design is one of the most important key points for good fit, good blood compatibility and good pump performance in the implantable TAH. However, until now few papers have been published concerning the cuff design. As a result of various trials, we were able to finalize the design of the atrial cuff for our UPTAH.

Keywords total artificial heart, implantable total artificial heart, undulation pump, atrial cuff, goat.

Background

The implantable total artificial heart (TAH) is the aim of artificial heart (AH) reseach. At present, various types of TAHs are developing in many laboratories in the world. In the USA, the electromechanical TAH (Hershey Medical Center – 3M Co. Ltd.), and electrohydraulic TAH (Abiomed Co. Ltd. – Texas Heart Institute) are under development in the national project supported by the National Heart, Lung & Blood Institute (NHLBI) of the National Institutes of Health (NIH)[1]. They will be finished with the basic development this year and will proceed to the reliability test aiming at clinical use. Other than the national project, the Milwaukee group is also developing an electromechanical TAH. In Germany, the Helmholtz Institute is developing an electromechanical TAH. In Korea, National Seoul University is also developing an electromechanical TAH called a 'moving actuator TAH'. In Japan, The National Cardiovascular Center is developing an electrohydraulic TAH[2]. However, a more compact TAH without a compliance chamber is required for implantation into people with a small physique, such as Asian people.

In our laboratory, an undulation pump (UP) TAH has been developed over the past six years[3]. The UP is a special pump in which a link mechanism converts the rotational motion of the brush-less DC-motor to the undulation motion of a disc. The nearest line between the disc and housing moves from the inlet to the outlet according to the undulation motion of the disc, which squeezes the blood to the outlet and sucks the blood from the inlet at the same moment. As this phenomenon occurs in both sides of the disc with an 180° phase delay, the pump produces continuous flow when the rotational speed of the motor is constant and an arbitrary flow waveform can be produce by controlling the motor current waveform. The UPTAH is composed of two UPs and two brush-less DC-motors, and is the most compact TAH in the world. This device is 76 mm in diameter and 78 mm in length, and does not need a compliance chamber. This UPTAH could be implanted into the chest cavity of a goat weighing 41–79 kg.

Although the UPTAH is very compact, the design of atrial cuffs is very important in order to ensure a good fit, low flow resistance and good blood compatibility in the narrow chest cavity of the goat. The objective of this study is to establish design criteria for the atrial cuff of the UPTAH.

Correspondence to: Kou Imachi PhD, Department of Biomedical Engineering, Graduate School of Medicine, University of Tokyo, 7–3–1 Hongo, Bunkyo-ku, Tokyo 113-0033, Japan.

Materials and methods

Surgical procedure for implantation of UPTAH

Figure 1 is a schematic illustration of the implantation of the UPTAH into the goat's chest cavity. Under isoflurane anesthesia, the left chest of the goat is opened by 5th rib resection. The aortic cannula is connected to the descending aorta by side-to-end anastomosis. The natural heart is resected at the atrioventricular interface under extracorporeal circulation (ECC). Atrial cuffs are sutured to the left and right atrial wall. The pulmonary artery cannula is inserted into the pulmonary artery and ligated. The UPTAH is connected to two cuffs and two cannulae and driven from the left pump.

Configuration of the inlet and outlet nozzle of UP

The UP is a cylindrical shape with a diameter of 76 mm and a thickness of 18 mm. It has two nozzles with a 20 mm outer diameter for inlet and outlet. The angle between the two nozzles is 60û in the UP model 2 series and 50û in the UP model 3 series. The UPTAH contains two UPs. Figure 2 shows the position of the four nozzles in the UPTAH. As the distance between the four nozzles is so narrow, especially in model 3, the space for the atrial cuffs and cannulae is very restricted.

Design of atrial cuff

Box 1 shows the requirements for the atrial cuff of the implantable TAH. A good fit to the residual atriums is the basic requirement. Low flow resistance is important for good pump performance. Ensuring blood compatibility, so as to prevent thrombus and pannus formation, is an important safety requirement. Atrial suction is a serious problem in this kind of blood pump as the ejection and suction of blood occurs at the same moment. The atrial wall is often sucked into the atrial cuff. This is especially true when the pump output is large at continuous flow or the rise time of flow waveform is steep at pulsatile flow, which disturbs the blood inflow and elevates the left atrial pressure when it occurs on the left side. Easy suturing is also important in order to shorten the operation time. These requirements are

Box 1. Requirements for the atrail cuff

Good fitting
Low flow resistance
Good blood compatibility
Hard to suck the atrium
Easy suturing

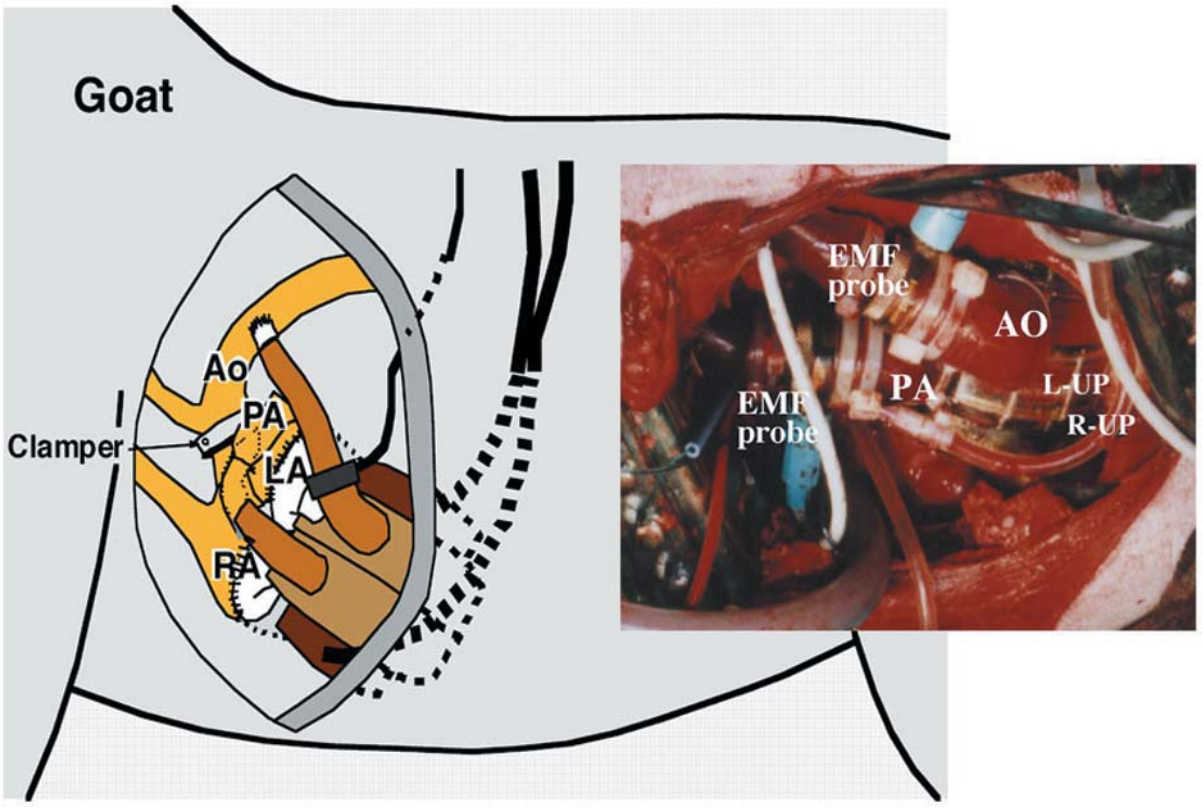

Figure 1. Implantation of the UPTAH in the chest cavity of a goat. Ao: aorta; PA: pulmonary artery; LA: left atrium; RA: right atrium; L-UP: left undulation pump; R-UP: right undulation pump; EMF probe: electromagnetic flow probe.

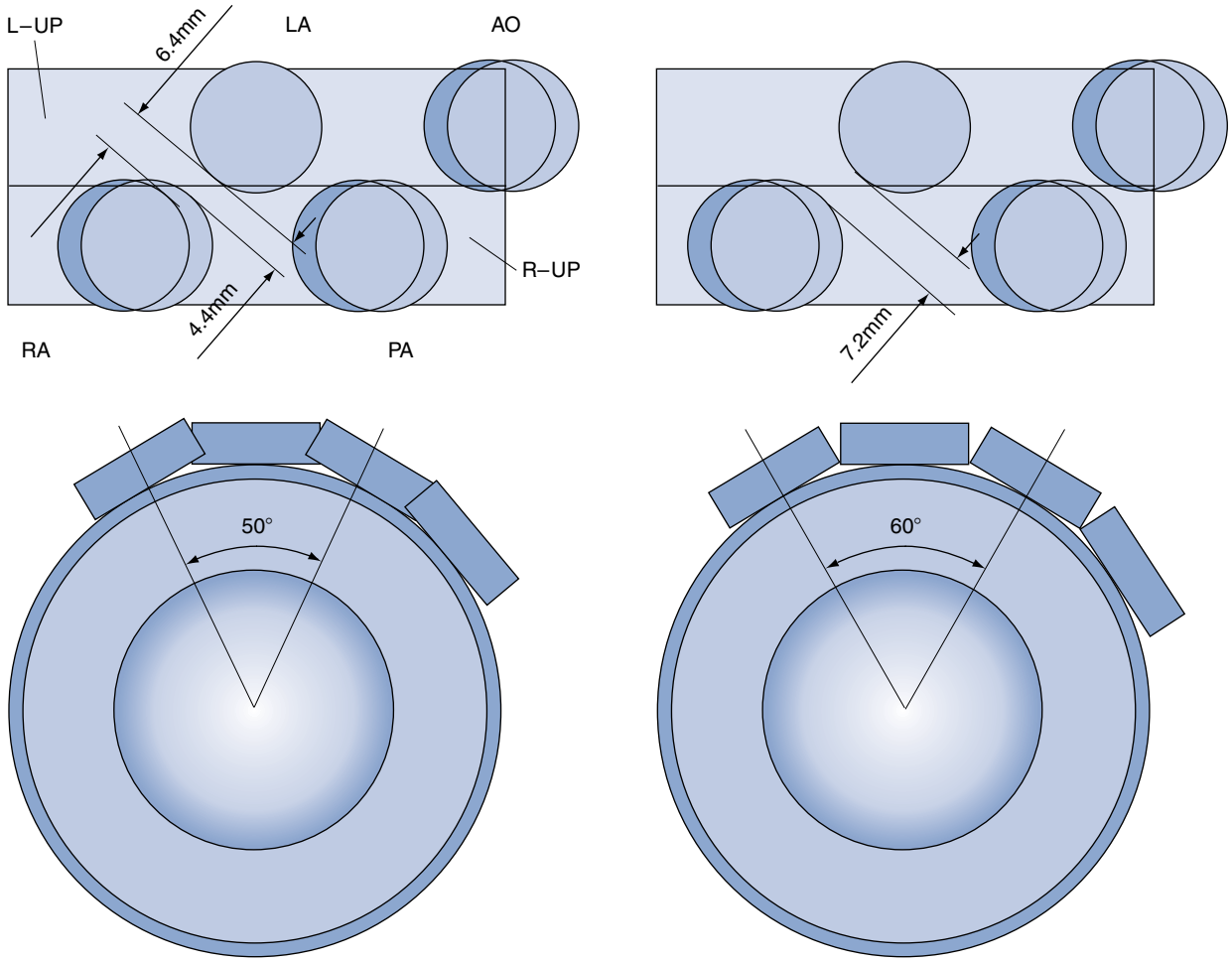

Figure 2. Nozzle angle and distance of UP model 2 (right) and model 3 (left). Ao: aorta; PA: pulmonary artery; LA: left atrium; RA: right atrium; L-UP: left undulation pump; R-UP: right undulation pump.

directly related to the configuration, angle to the blood pump, dimensions and materials as shown in Box 2.

As for the materials of the cuff, an expanded polytetrafluoroethylene (EPTFE, Gore-Tex) sheet has been used in our laboratory. The EPTFE sheet is cut and sutured with Gore-Tex string to form the designed configuration. It is molded into one piece with a connector made of polyvinylchloride (PVC) paste resin, that can fit to the inlet nozzle. The blood-contacting surface is coated with segmented polyurethane (KIII: Nippon Zeon Co. Ltd, Kawaski, Japan)

Box 2. Design criteria for the atrial cuff of implantable TAH

Configuration: flat or streamline shape (h)
Angle to the nozzle (α) and the blood pump (β)
Diameter (D)
Atrial septum: separate or common
Material: rough or smooth

Figure 3 shows the predominant parameters of the atrial cuff needed to ensure a good fit, blood compatibility and atrial wall suction protection. These parameters are: cuff diameter (D), configuration (h) (flat to cone shape), angle to the pump nozzle (α) and angle to the UP (β). In this study, many types of atrial cuff were designed by changing these parameters.

Results

With the parameters mentioned earlier, angle α was fixed 30° from the anatomical position data and D was fixed at 38 mm as in past experiments. Nine models of atrial cuff have been designed and fabricated since the UPTAH animal experiments started in 1996. In models 1 and 2, h was 4 mm and α was 90û (straight), and the PVC connector was molded into one piece in model 2 for easy connection (Figure 4). However, atrial wall suction into the cuff occurred frequently and it was difficult to release quickly by changing the driving condition of the motor; this sometimes induced lung edema when it occurred on the left

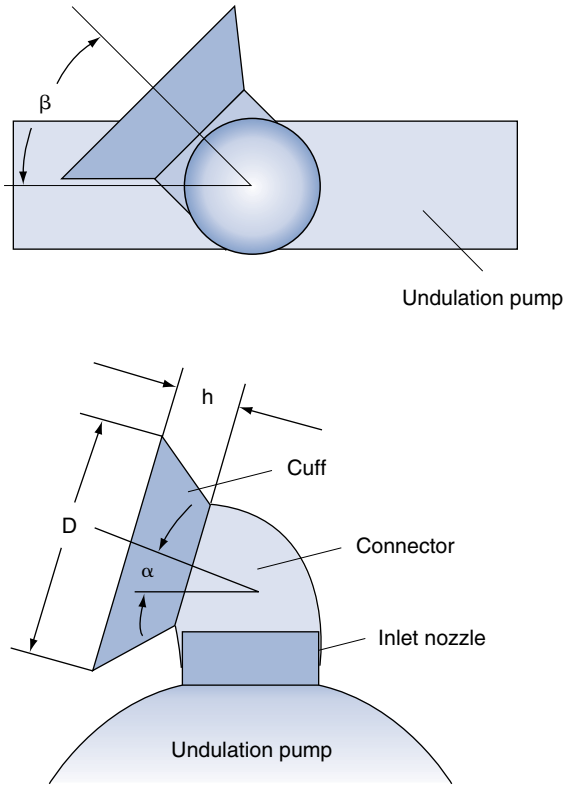

Figure 3. The parameters for atrial cuff design of the UPTAH.

side. Although a cage to prevent the atrial wall from suction into the cuff was mounted in model 3, it was not very effective. We found the atrium sometimes kinked by a malfitting atrial cuff or movement of the UPTAH after chest closure. So, we created an angled connector between the cuff and the inlet nozzle. The angle α was 40û in the right cuff and 0û (right angle) in the left side in model 5 (Figure 5). The left cuff angle was changed to 40û in models 6 and 7. The cuff angle α was finally fixed to 40û in the right cuff and 30û in the left cuff when the UP was changed to model 3. The fitting was greatly improved; however, atrial wall suction was not completely prevented in spite of the introduction of an automatic left atrial pressure control system that was thought to release the suction. We noticed that if a period of time was allowed to elapse before complete suction of the atrial wall into the cuff, the automatic control system could work to release the suction. We then began to change the configuration of the cuff from almost a flat cuff (h=4 mm) to a cone-shaped cuff. A cone height of 12 mm in model 7 was not enough to create the required time delay, and it was finally fixed to 18 mm in models 8 and 9. The left atrial wall suction was almost protected by the combination of cone-shaped and angled atrial cuff and by automatically controlling left atrial pressure.

The next target concerning the atrial cuff design was to change the design for easy suturing. A shortened suturing time of the atrial cuffs can shorten ECC time, and this

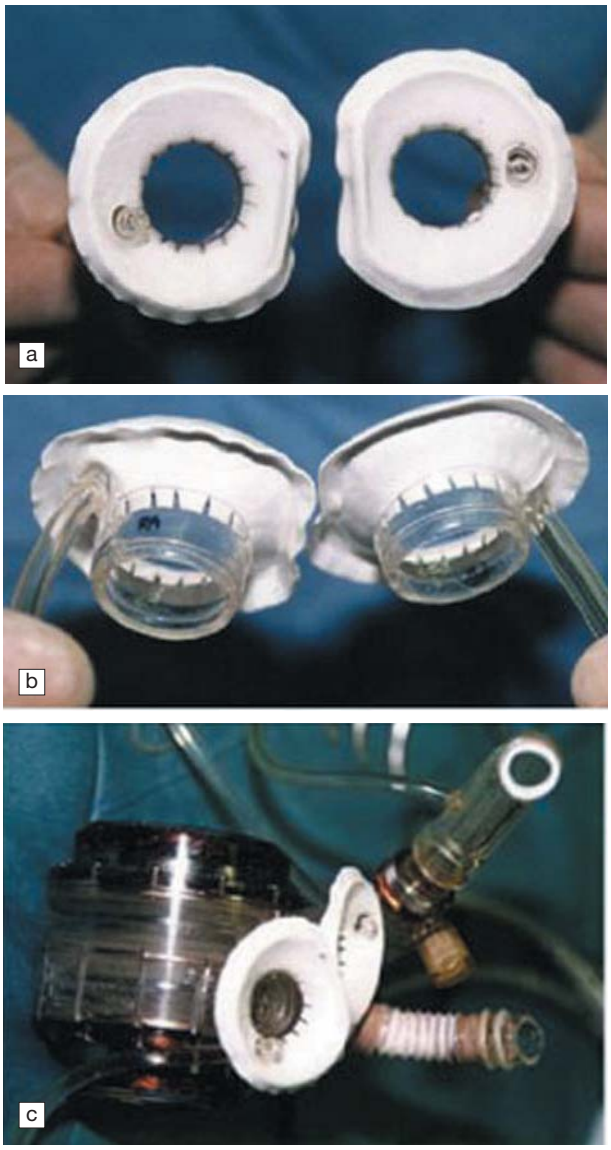

Figure 4. Atrial cuff model 2. D=38mm, h=4 mm, a=90û (straight connector). (a) atrial side view; (b) blood pump side view; (c) fabricated TAH pump.

can improve the recovery of the goat in postoperative care. We developed a newly designed cuff in model 8, in which the septums of the right and left cuff correspond (Figure 6). As shown in Figure 7, the cuff could be sutured to the atrium in the same manner as in heart transplantation and ECC time could be shortened by no more than 2 h. The number of survival days of UPTAH goats was prolonged to 10, 19 and 31 days[4]. However, a pannus-like thrombus formed at the left atrial cuff in a goat that survived 31 days; the thrombus nearly covered the cuff inlet resulting in the cause of death (Figure 8). The pannus-like thrombus formation could arise because the cut end of the natural atrium septum, in which collagen fibers are included, was exposed in the bloodstream after suturing with the septum of atrial cuff. For this reason, the atrial cuff

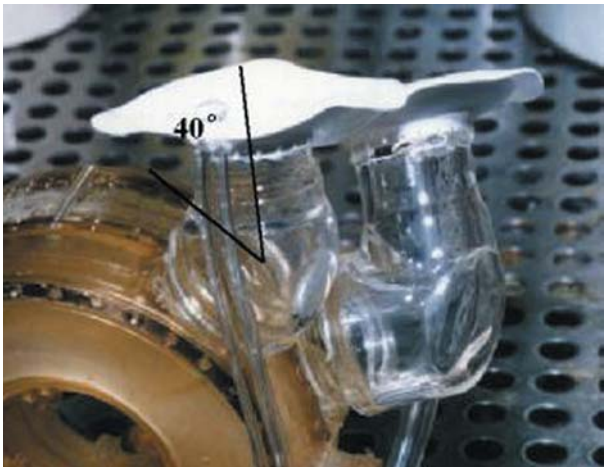

Figure 5. Atrial cuff model 5. D=38mm, h=4 mm, α=0û(L), 40û(R).

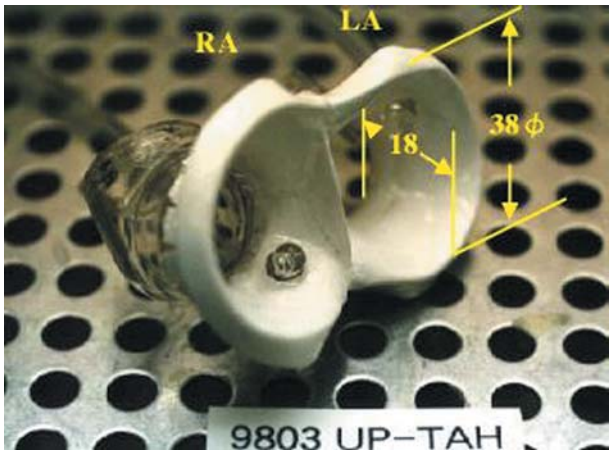

Figure 6. Atrial cuff model 8: common septum, D=38mm, h=18 mm, α=30û(L), 40û(R). LA: left atrium; RA: right atrium.

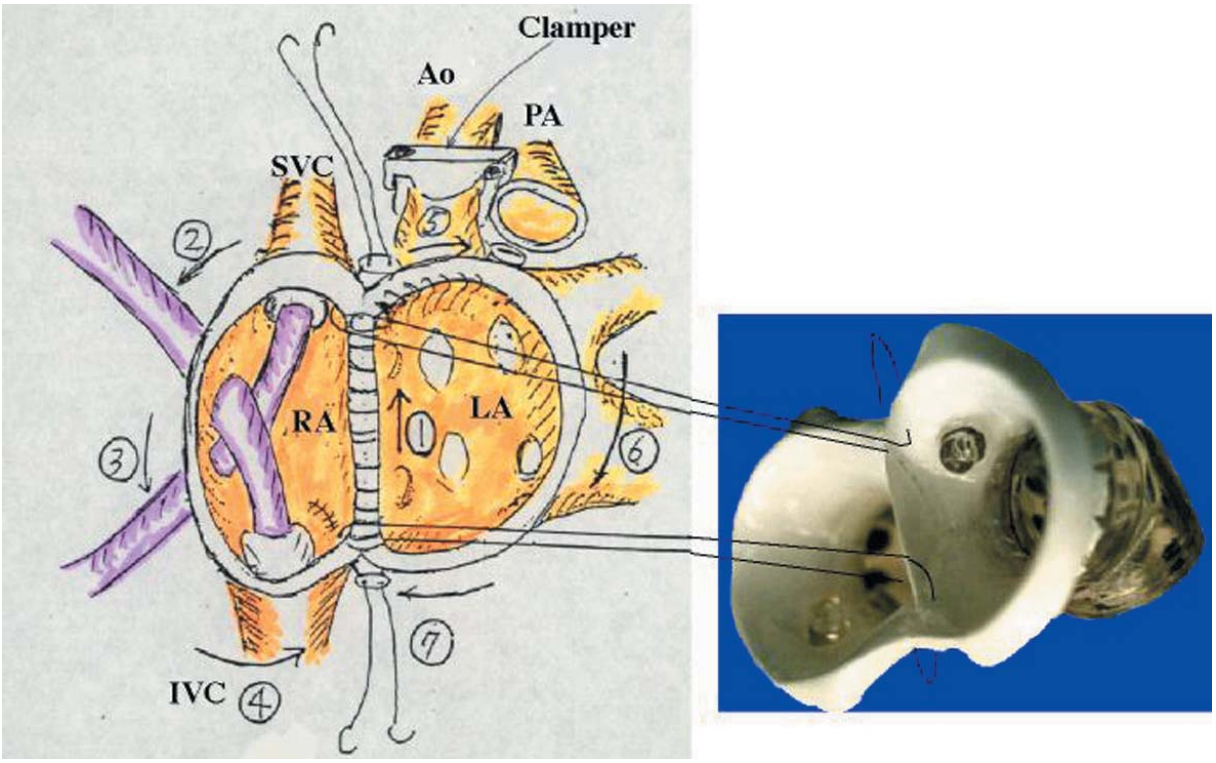

Figure 7. Surgical procedure of the suturing of the atrial cuff in model 8. Ao: aorta; PA: pulmonary artery; LA: left atrium; RA: right atrium; SVC: superior vena cava; IVC: inferior vena cava.

in model 9 was modified to separate the right and left. Figure 9 shows the final cuff model. To date, 46 days' survival of an UPTAH goat has been obtained without pannus formation[5].

Discussion

Atrial cuff design is one of the important key points in ensuring a good fit, blood compatibility and pump performance in the implantable TAH. However, until now few papers have been published concerning cuff design. Jarvik *et al.* reported the importance of a smooth surface and streamline shape of the atrial cuff in preventing pannus formation[6]. Since 1982, in our laboratory, special kinds of TAHs in which the natural heart was resected, but a pneumatically driven TAH was placed on the chest wall, have been studied using the goat[7]. In these experiments, the atrial cuff was made of an EPTFE sheet coated with segmented polyurethane to obtain a smooth surface. Long-term survivors of 340 days (1984), 360 days (1993) and 532 days (1995) were obtained without finding any thrombus and pannus

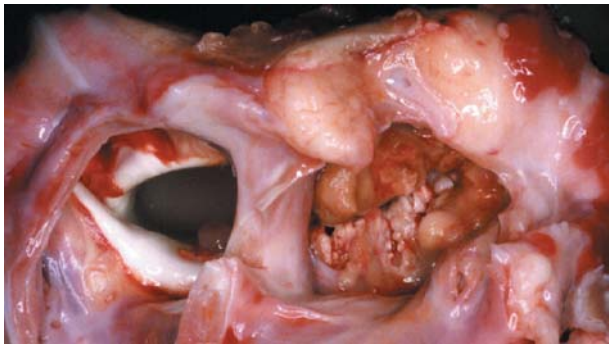

Figure 8. Pannus-like thrombus formation at the left atrium in the atrial cuff of model 8 after 31 days.

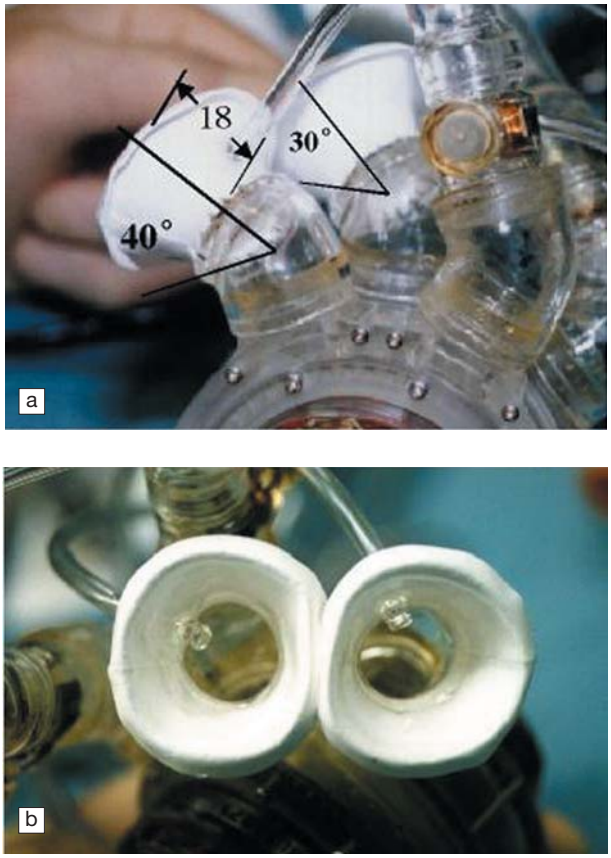

Figure 9. Atrial cuff model 9. L/R separate, D=38mm,h=18 mm, a=30û(L), 40û(R). (a) blood pump side view; (b) atrium side view.

formation at the atrial cuff in spite of no anticoagulant[8]. These results influenced our decision to change our TAH research to the development of an implantable TAH.

The UPTAH is our original TAH and is the most compact TAH in the world at the present time. It can be implanted into the chest cavity of a goat weighing 41–79 kg. However, as the goat's chest cavity is very small, the design of atrial cuff is very important. As shown in this study, the parameters, D, h, α, and β were the most critical in the design of the atrial cuff. The small h and straight connector (α=90°) were advantageous for space reduction. However, these parameters were a problem in ensuring a good fit and atrial wall suction protection. Although the atrial cuff with a common septum was useful for easy suturing, blood compatibility problems discounted this design. After various trials, we were able to finalize the design of the atrial cuff for the UPTAH.

Acknowledgements

Parts of this study were supported by The Program for Promotion of Fundamental Studies in Health Sciences of the Organization for Pharmaceutical Safety and Research (OPSR), Tokyo, Japan.

References

1. Watson J. Prospects for implantable circulatory assist. In: Akutsu T, Koyanagi H, editors. *Heart Replacement – Artificial Heart 6*. Tokyo: Springer-Verlag, 1998:3–7.
2. Tatsumi E, Taenaka Y, Uesho K *et al*. Long-term *in vivo* testing of the National Cardiovascular Center electrohydraulic total artificial heart. *J Congestive Heart Failure and Circulatory Support. Heart Replacement – Artificial Heart 7*. 2001; 1: 153–60.
3. Abe Y, Chinzei T, Ono T *et al*. Implantation of the undulation pump total artificial heart in the goat. *Artif Organs* 1999;23: 932–8.
4. Imachi K, Abe Y, Chinzei T *et al*. One-month survival with an implantable total artificial heart – Undulation pump total artificial heart in a goat. *Artif Organs* 1999;23:619.
5. Abe Y, Chinzei T, Isoyama T *et al*. Progress in the development of the undulation pump total artificial heart. *J Congestive Heart Failure and Circulatory Support. Heart Replacement – Artificial Heart 7*. 2001; 1: 167–70.
6. Jarvik RK, Kessler TR, McGill LD *et al*. Determinants of pannus formation in long-surviving artificial heart calves, and its prevention. *Trans Am Soc Artif Intern Organs* 1981;27:90–6.
7. Atsumi K, Fujimasa I, Imachi K *et al*. Long- term heart substitution with an artificial heart in goats. ASAIO J 1985;8:155–65.
8. Abe Y, Chinzei T, Mabuchi K *et al*. Over 500 days' survival of a goat with a total artificial heart with 1/R control. In: Akutsu T, Koyanagi H, editors. *Heart Replacement–Artificial Heart 6*. Tokyo: Springer-Verlag 1998;34–8.

Journal of Congestive Heart Failure and Circulatory Support (2001) Vol 1, No 4, 201–206

Oxygen-demand-based physiological control of the total artificial heart

M. Nakamura MD PhD[1], S. Takatani DrMed PhD[1], K. Ohuchi MEng[1], T. Sakamoto MD PhD[2], A. Homma DrEng[3], E. Tatsumi MD PhD[3], K. Uesho MD[3], Y. Taenaka MD PhD[3] and T. Masuzawa DrEng[4]

[1]Department of Artificial Organs, Institute of Biomaterials and Bioengineering, Tokyo Medical and Dental University, Tokyo, Japan; [2]Department of Replacement Surgery, Tokyo Medical and Dental Post-Graduate University, Tokyo, Japan; [3]Department of Artificial Organs, National Cardiovascular Center Research Institute, Osaka, Japan; and [4]Department of Mechanical Engineering, Ibaraki University, Ibaraki, Japan

Abstract It is important to establish physiological control of the total artificial heart (TAH) to ensure its effectiveness and reliability. TAH output should be controlled just enough to meet the demand of the recipient. Therefore, we have developed a TAH control method based on oxygen consumption that closely and quickly reflects the oxygen and blood flow demand.

An implantable optical sensor, that uses three LEDs (light-emitting diodes) and one photodiode chip, has been refined specifically for use in TAH systems. Whole blood oxygen saturation and hemoglobin concentration can be measured with this sensor, even through the transparent polyurethane membrane of the TAH pump housing. Combined with pumping rate and stroke volume, oxygen consumption can be continuously calculated by Fick's method.

We also investigated the relationship between oxygen consumption and cardiac output (CO) in three normal calves to establish the TAH control method using monitored oxygen consumption. An approximate linear relationship was found between them with the following regression equation:

$$CO = 9.94 \times x + 51.4$$

where x is monitored oxygen consumption (mL/min/kg) and CO is cardiac output (mL/min/kg).

Currently, we have both the hardware and software necessary to attain oxygen-demand-based physiological control of a TAH, and are now preparing for animal experiments.

Keywords total artificial heart (TAH), physiological control, oxygen consumption, optical sensor, cardiac output (CO).

Introduction

Methods using a total artificial heart (TAH) have been developed as techniques to save patients with end-stage heart disease, for bridging to heart transplantation or permanent replacement. As the shortage of donor hearts is a serious worldwide problem now and for the foreseeable future, alternate methods of heart transplantation are desirable. Pneumatic TAHs have been used successfully in patients with severe bi-ventricular heart failure as a bridge to heart transplantation. It has been reported that more than 100 patients have been saved by them and then discharged safely from the hospital after receiving a heart transplantation[1,2]. As a result, the TAH has proven to be one of the most promising optional methods for heart transplantation, along with bi-ventricular assistance using two ventricular assist devices and xeno-heart-transplantation. However, a pneumatic TAH is not suitable for permanent use, because of the size and portability of its driver as well as the risk of infection from drive lines penetrating the skin. Thus, design and development of a totally implantable electronic TAH system is necessary for long-term or permanent use.

Background

For the advancement of reliable and effective TAH systems, especially with *in vivo* applications, physiological control of the TAH is one of the important issues remaining. When a damaged native heart is replaced with a mechanical TAH system, most of the hemodynamic regulations become dependent on the TAH control. Several pathological findings, such as increasing circulating blood volume and progressive anemia, have been reported in animals with an implanted TAH; some of them are thought to have been due to inadequate output settings and poor response ability to changes in recipient demands[3–5]. Thus, it is important to research and establish effective control methods to maintain good hemodynamic conditions and lessen the likelihood of pathological hazard. Moreover, the activities of the recipients must recover to almost normal levels after TAHs improve their hemodynamics. Therefore, in order to maintain the recipients' quality of life, the TAHs should be controlled effectively, dynamically and automatically according to their activities.

The function of the native heart is controlled by modulating the stroke volume according to Frank–Starling's mechanism, and by regulating heart rate by neural and humoral systems. However, regardless of the control

Correspondence to: Makoto Nakamura, Department of Artificial Organs, Institute of Biomaterials and Bioengineering, Tokyo Medical and Dental University, 2–3–10 Suruga-dai, Kanda, Chiyoda-ku, Tokyo 101-0062, Japan.

pathway, heart functions are ultimately controlled just enough to meet the physiological demands of the whole body. Therefore, TAH output should be appropriately controlled to meet the demands of the recipient. We consider this to be the most essential point of physiologically rational control. For this purpose, however, it is necessary to monitor physiological demands by some established methods.

It is well accepted that oxygen is required for almost all activities of a living body, and that all of the oxygen is delivered and supplied by blood flow. Therefore, oxygen and blood flow demands can be estimated from oxygen (O_2) consumption. Monitoring this parameter seems to be a reasonable approach to finding physiological demands. For this reason, we have been investigating the feasibility of employing O_2 consumption as a monitoring parameter for the control of a TAH.

Methods

Continuous monitoring of oxygen consumption

Oxygen saturation can be measured in a TAH recipient by installing optical sensors in the system. Arterial oxygen saturation (SaO_2) and mixed venous oxygen saturation (SvO_2) can be measured with an optical sensor placed in the left and right heart pumps, respectively. Whole blood total hemoglobin concentration can also be measured at the same time by these optical sensors. Using these measurements together with cardiac output (CO), obtained by multiplying stroke volume by pumping rate, O_2 consumption can be calculated by Fick's method.

In Fick's principle, consumed oxygen is equal to the difference between total oxygen input to the tissue and total oxygen output from the tissue. The oxygen contents of arterial blood and mixed venous blood are calculated as oxygen saturation of each type, multiplied by hemoglobin concentration (Hb) multiplied by 1.34, where 1.34 is mL of oxygen bound with 1 g of hemoglobin. Therefore, O_2 consumption can be obtained by the following equation:

$$O_2\,\text{consumption} = 1.34 \times (SaO_2 - SvO_2) \times Hb \times CO$$

where SaO_2 is arterial oxygen saturation, SvO_2 is mixed venous oxygen saturation, Hb is hemoglobin concentration, and CO is cardiac output. The content of oxygen dissolved in the serum component is ignored, because the concentration is not so significant compared with oxygen carried by hemoglobin. As all of these parameters can be monitored in real time, momentary O_2 consumption can be calculated continuously.

Oxygen-demand-based control of TAH

The concepts and outline of oxygen-demand-based TAH output control are shown in Figure 1. The fundamental concept of our oxygen-demand-based control method is that the targeted TAH output should be controlled according to O_2 consumption, monitored as detailed above. During the actual control procedure, firstly SaO_2, SvO_2, Hb, and CO

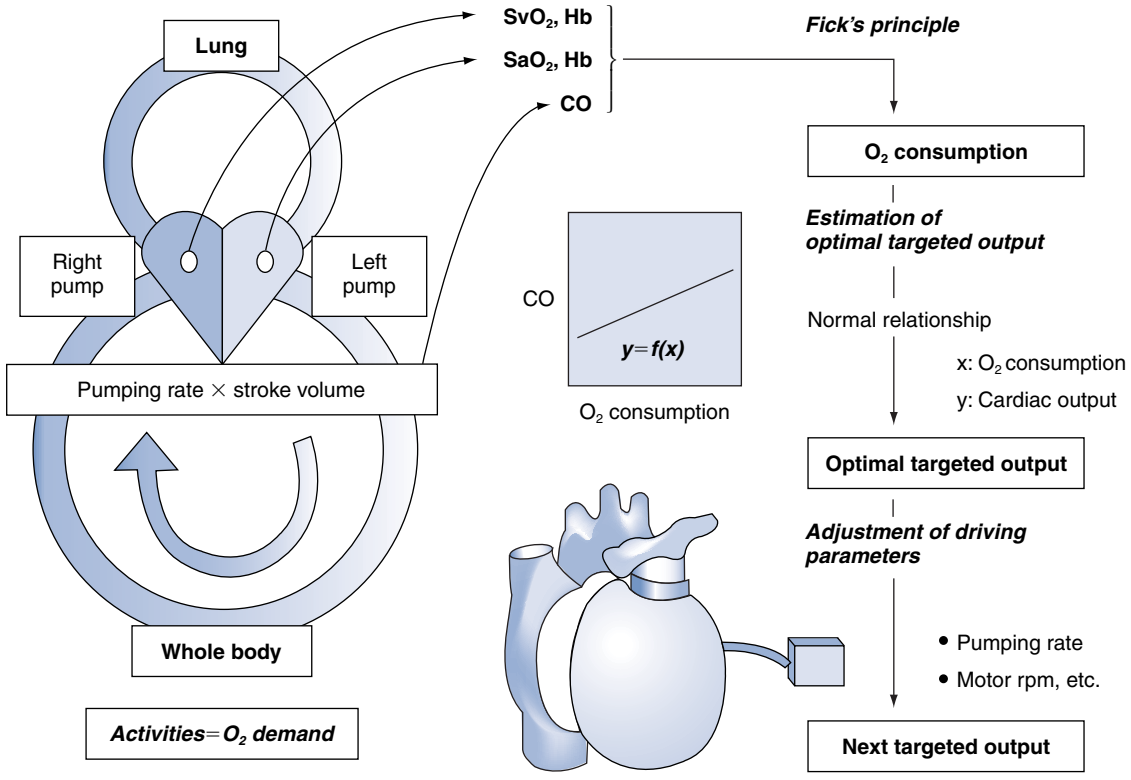

Figure 1. Outline of an oxygen-demand-based control for a total artificial heart.

are measured. Second, O_2 consumption is calculated from these parameters. Third, targeted TAH output can be estimated using the regression equations obtained from a normal reasonable relationship between O_2 consumption and CO in normal subjects. Finally, the drive parameters, such as pumping rate and motor rotation rate, are automatically adjusted to produce the targeted TAH output, based on the properties of the TAH device obtained from *in vitro* experiments in advance. We consider that continuous running of this loop will result in oxygen-demand-based physiological control.

Estimation of optimal targeted TAH output

In order to perform oxygen-demand-based physiological control, the physiologically reasonable relationship between O_2 consumption and CO must be understood in order to obtain optimal targeted TAH output from monitored O_2 consumption. For this purpose, we investigated the normal relationship between O_2 consumption and CO in animal experiments using normal calves.

Three normal Holstein calves, weighing 46 to 72 kg, were implanted with an electromagnetic flowmeter or ultrasound flowmeter probe to the ascending aorta by thoracotomy, and with oximetric catheters to the main pulmonary artery, to measure CO and SvO_2, respectively. Graded treadmill exercise tests were carried out in the chronic phase after surgery.

The standard protocol used was as follows. Six stages were performed, each lasting for 3 min, during which treadmill speed was increased from 1–6 km/h. For some of the tests, we kept the calves running past stage 6, until they collapsed from fatigue. Each measurement was digitally recorded at 100 Hz continuously throughout the test. Data for every 5 s were averaged and used for the evaluation. SaO_2 and Hb were obtained from blood samples taken before the tests, and regarded as constant values during exercise.

The profiles and results of each test are shown in Table 1. Treadmill tests were carried out 6, 3, and 2 times in calf numbers 1, 2, and 3, respectively. A typical time course example is traced in Figure 2. Both CO and O_2 consumption changed in the same manner, according to increases and decreases in exercise intensity.

The relationship between O_2 consumption and CO were plotted, and the results are shown in Figure 3. Figure 4 shows the relationship between O_2 consumption and CO per body weight. A linear-like correlation was observed for all portions of each treadmill test in these relationships. Linear fitting was performed, and the slopes and y-intercepts of the regression lines are also summarized in Table 2. Although the y-intercepts varied for each test, the slopes of the fitting lines are similar, within a range of 6.8–13.1, and the average ± standard deviation is 9.94 ± 2.0. The obtained regression equations are as follows:

$$\text{CO (L/min)} = 9.94 \times 10^{-3} \times O_2 \text{ consumption (mL/min)} + 3.20$$

$$\text{CO (mL/min/kg)} = 9.94 \times O_2 \text{ consumption (mL/min/kg)} + 51.4$$

Discussion

Relationship between CO and O_2 consumption

It is generally known that, in normal human subjects, CO is proportional to O_2 consumption[6–8]. Donald *et al.* reported the following regression equation for normal humans[6]:

$$CI = 5.34 \times x + 3.708$$

CI is cardiac index (mL/min/m^2) and x is oxygen consumption (mL/min/m^2).

Concerning the slope of this increment, Weber *et al.* mentioned that CO increases approximately 600 mL/min/m^2 for every 100 mL/min/m^2 rise in O_2 consumption, even in heart failure patients[7]. This indicates that resemblance in the steepness of the regression lines is one of the important characteristics in physiological response to exercise. Therefore, this slope must be useful in controlling TAH output dynamically.

Table 1. Profile of each treadmill exercise test

No. of calf	No. of exercise test	Postoperative day	Body weight (kg)	Hemoglobin concentration (g/dL)	Exercise time (min:s)
1	1	26	55.0	11.0	18:00
	2	28	55.5	11.4	18:00
	3	31	58.0	10.6	18:00
	4	35	58.0	9.9	18:00
	5	42	60.5	9.7	18:00
	6	44	61.0	9.9	21:00
2	1	23	57.9	10.7	21:00
	2	32	63.7	10.2	18:00
	3	55	77.2	10.8	18:00
3	1	21	77.6	11.5	18:00
	2	22	77.1	11.1	18:00

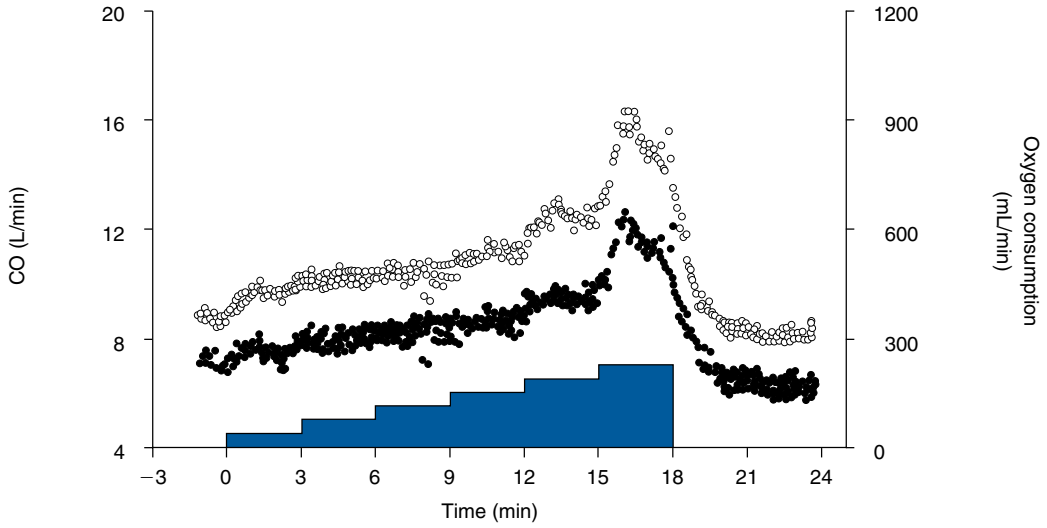

Figure 2. Time course of a representative treadmill exercise test is shown. Open circles (○) represent oxygen consumption and closed circles (●) represent cardiac output (CO). Treadmill speed is expressed by the shaded area.

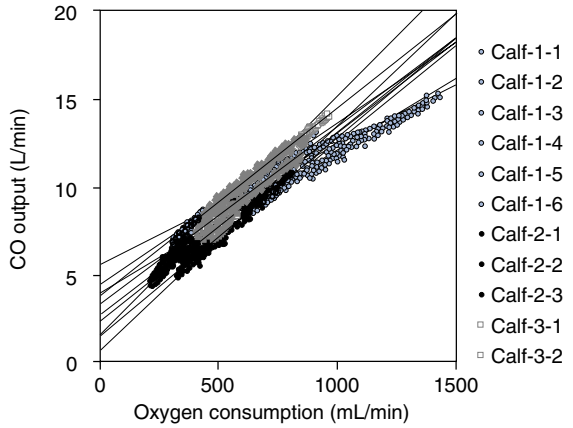

Figure 3. Relationship between oxygen consumption and cardiac output (CO) during treadmill exercise tests in normal calves.

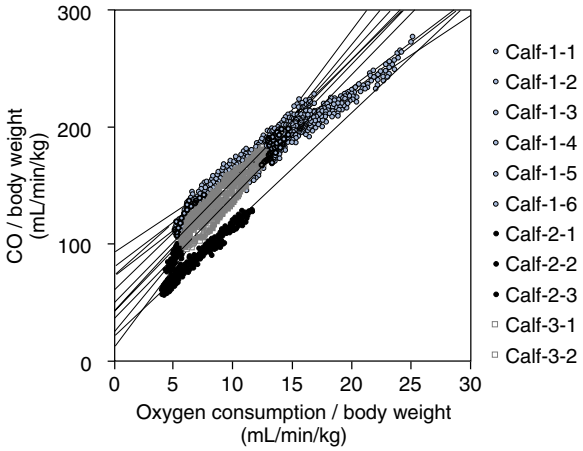

Figure 4. Relationship between oxygen consumption and cardiac output (CO) by body weight during treadmill exercise tests in normal calves.

Table 2. Results of treadmill exercise test. Cardiac output = CO; bodyweight = BW

No. of calf	No. of exercise test	Characteristics of the regression line					
		Relationship between O_2 consumption and CO			Relationship between O_2 consumption/BW and CO/BW		
		Slope (mL/O_2mL)	Intercept (mL/min)	r	Slope (mL/O_2mL)	Intercept (mL/min/kg)	r
1	1	7.942	4000	0.990	7.942	72.738	0.990
	2	9.838	3378	0.991	9.838	60.881	0.991
	3	10.790	2407	0.989	10.790	42.240	0.989
	4	7.736	4677	0.971	7.736	80.642	0.971
	5	9.225	4527	0.986	9.225	74.831	0.986
	6	6.818	5650	0.988	6.818	92.627	0.988
2	1	7.736	4677	0.971	7.736	80.642	0.971
	2	13.061	1548	0.983	13.061	24.875	0.983
	3	9.615	1674	0.988	9.615	21.696	0.988
3	1	10.532	2813	0.994	10.532	36.260	0.994
	2	10.867	3777	0.993	10.867	48.994	0.993
Average		9.469	3557	0.986	9.469	57.857	0.986
standard deviation		1.825	1325	0.008	1.825	24.393	0.008

Because CO cannot be measured directly in humans, these results in humans were all obtained from expired gas analysis, which is noninvasive but slow and dull in the response speed. Strictly speaking, more precise investigation is needed, in which CO and oxygen saturation are measured directly and on time. We have examined only three animals as yet; the number of experiments with direct and real-time measurements should be increased. Although linear fitting was performed in this study according to those previous reports in humans, the most reasonable fitting method should be employed, and TAH output should be controlled based on the relational curve obtained from such precise experiments.

Advantages of the oxygen-demand-based control of TAH

The most significant advantage of using O_2 consumption as a monitoring parameter for TAH output control is that this method is based on a rational physiological background. A well-balanced output to meet O_2 demand is essential for the recipient to maintain a physiologically healthy and active condition. Therefore, this control method can be expected to prevent the recipient from even latent heart failure. In addition, as O_2 consumption reflects metabolic demand due not only to exercise, but also almost all activities such as fever and emotional excitement, this control method is expected to be useful in all of the recipient's activities.

A second advantage is its practicality. Our method has a high potential to be realized in a TAH system because of its technological background. The technologies for measuring oxygen saturation using red and near-infrared rays have already been established, and are used clinically in many kinds of medical instrumentation[9–12]. We have been developing an implantable optical sensor specifically for use in TAH systems[13–15] (Figure 5). It uses three light-emitting diodes (LEDs) and one photodiode, and can measure oxygen saturation and whole blood hemoglobin concentration. The size of the sensor is 8 mm in diameter, which is small enough to be installed in several types of TAH systems. If it is placed on a good wash-out portion of a high-quality antithrombogenic blood pump housing, long-term durability can be expected. We have already confirmed that oxygen saturation can be measured, even through a piece of the transparent polyurethane pump housing, and are now preparing for animal experiments to evaluate this sensor system.

A third advantage of our method is its usefulness as a monitoring system. O_2 consumption, as well as SaO_2, SvO_2, Hb, and CO, are all useful parameters from which valuable diagnostic information can be obtained regarding both the recipient's status and the TAH output[16–20]. The hemodynamics and status of oxygen metabolism in the recipient can be established for many different situations, for example, low CO for the recipient's demands, fever, infection respiratory disorders, and hematological abnormalities including anemia and bleeding. Low CO due to mechanical troubles in the TAH device or in its conduits can also be detected.

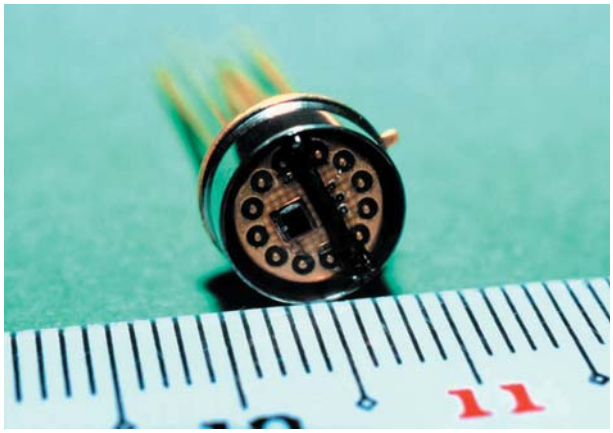

Figure 5. A reflection-type optical sensor for measurement of whole blood oxygen saturation and hemoglobin concentration. Three LEDs (660, 730, 830 nm) and one photodiode chip are arranged and mounted.

Moreover, there is a rapid reaction to the change in O_2 demand. TAH output can be immediately adjusted with our method of control, since O_2 consumption and SvO_2 respond promptly to the start and end of exercise[21,22].

Problems of the oxygen-demand-based control of TAH

Despite the potential advantages, there are still some problems to be solved before practical application of this system. First, the durability and reliability of the sensors (optical sensors and TAH output monitors) must be proven in chronic measurements of O_2 consumption. This is the most important obstacle to be overcome. Next, targeted output derived from O_2 consumption cannot always be realized *in vivo* because of the restriction of venous return and the alterations of pre- and after-load of the TAH. In such disordered cases, abnormal levels are predicted in aortic pressure or left and right atrial pressures. Since the monitoring system for O_2 consumption cannot detect either these abnormal pressures or the mechanical operation of the device by themselves, other sensors are required. By combining these monitors together, this control method can contribute effectively to a safe, reliable and truly physiological application of a TAH.

Conclusion

TAH development must not remain in the realm of theory only. With whatever technologies are available, TAH systems should be developed and become more reliable and practical devices. Oxygen-demand-based control of a TAH has many important advantages, in both physiological and practical areas. Though several basic evaluation studies must be carried out in both *in vitro* and *in vivo* tests, we consider this method to be a feasible means of realizing physiological control. Further, since the monitoring systems for this control method provide useful and important information, we propose that they should be installed in TAH systems, even if their measurements are not used for

control. The information obtained from this monitoring system would allow for a safer and more reliable TAH system. After long-term durability and reliability can be proven satisfactorily, they could then be used for control of a TAH.

Acknowledgment

This work was supported by the Research Grant for Cardiovascular Diseases (10C–2) from the Ministry of Health and Welfare of Japan and a Grant-in-Aid for Scientific Research from the Ministry of Education of Japan (Nos. 10357013, 10680813 and 08408038) and the New Energy and Industrial Technology Development Organization (NEDO).

References

1. Copeland JG. Current status and future directions for a total artificial heart with a past. *Artif Organs* 1998; 22:998–1001.
2. Arabia FA, Copeland JG, Smith RG *et al*. CardioWest total artificial heart: a retrospective controlled study. *Artif Organs* 1999;23:204–7.
3. Harasaki H, Takatani S, Suwa S *et al*. Hemodynamic regulation in total artificial heart recipients. *Artif Organs* 1981;55:38–45.
4. Deleuze PH, Riebman JB, Paulis RD, Olsen DB, Loisans DY. regulation of pneumatic total artificial heart function: a review. *Int J Artif Organs* 1988;11:147–52.
5. Nakamura M, Tatsumi E, Taenaka Y *et al*. Early changes in circulating blood volume and volume-regulating humoral factors after implantation of an electrohydraulic total artificial heart. *ASAIO J* 1997;43:M663–8.
6. Donald KW, Bishop JM, Cumming G, Wade OL. The effect of exercise on the cardiac output and circulatory dynamics of normal subjects. *Clin Sci* 1954;14:37–73.
7. Weber KT, McElroy PA. Systemic hypertension. In Weber KT, Janicki JS. Dreibelbis D, editor. *Cardio Pulmonary Exercise Testing: Physiologic Principles and Clinical Applications.* Philadelphia: W.B. Saunders Company, 1986:239.
8. Guyton AC, Hall JE, editors. *Textbook of Medical Physiology. 9th Ed.* Philadelphia: W.B. Saunders, 1996:240–41.
9. Wirtzfeld A, Heinze R, Liess HD, Stangl K, Alt E. An active optical sensor for monitoring mixed venous oxygen-saturation for an implantable rate-regulating pacing system. *Pace* 1983;6Part-II:494–7.
10. Takatani S, Tanaka T, Nakatani T *et al*. Development of hemoglobin oxygen optical sensors for automatic control of artificial heart output. *Trans Am Soc Artif Intern Organs* 1985; 31:45–9.
11. Stangl K, Wirtzfeld A, Heinze R, Laule M. First clinical experience with an oxygen saturation controlled pacemaker in man. *Pace* 1988;11Part-II:1882–7.
12. Rouby JJ, Poete P, Bodin L, Bougeois JL, Athaud M, Viars P. Three mixed venous saturation catheters in patients with circulatory shock and respiratory failure. *Chest* 1990;98:954–8.
13. Bartminn J. *Design and Evaluation of a Hybrid Optical Reflectance Oxygen Saturation and Haemoglobin Content Sensor for Mechanical Total Artificial Heart Control*. Yamagata University Faculty of Engineering/University of Technology Aachen, Helmholtz Institute for Biomedical Engineering, Germany. Diploma-thesis, October 30, 1998.
14. Kaiwa T, Frankort A, Bartminn J, Nogawa M, Takatani S. Development of a hybrid optical reflectance oxygen saturation and hematocrit sensor. *JJME* 1999;37(Suppl 2): 274.
15. Kaiwa T, Mori T, Nogawa M, Kijima T, Nojiri C, Takatani S. Measurement of blood hematocrit inside a magnetically suspended centrifugal pump using an optical technique. *Jpn J Artif Organs* 1999;28:173–7.
16. Jamieson WR, Turnbull KW, Larrieu AJ, Dodds WA, Allison JC, Tyers GF. Continuous monitoring of mixed venous oxygen saturation in cardiac surgery. *Can J Surg* 1982;25:538–43.
17. Birman H, Haq A, Hew E, Aberman A. Continuous monitoring of mixed venous oxygen saturation in hemodynamically unstable patients. *Chest* 1984; 86:753–6.
18. Norfleet EA, Watson CB. Continuous mixed venous oxygen saturation measurement: a significant advance in hemodynamic monitoring? *J Clin Monit* 1985;1:245–58.
19. Kupeli IA, Satwicz PR. Mixed venous oximetry. *Int Anesthesiol Clin* 1989;27:176–83.
20. Takatani S, Noda H, Takano H, Akutsu T. Continuous in-line monitoring of oxygen delivery to control artificial heart output. *Artific Organs* 1990;14:458–65.
21. Casaburi R, Daly J, Hansen JE, Effros RM. Abrupt changes in mixed venous gas composition after the onset of exercise. *J Appl Physiol* 1989;67:1106–12.
22. Nakamura M, Masuzawa T, Tatsumi E *et al.* Mixed venous oxygen saturation as a promising parameter for control of total artificial heart. *ASAIO J* 2000(in press).

Journal of Congestive Heart Failure and Circulatory Support (2001) Vol 1, No 4, 207–212

Vagal nerve activity suggests a new control method of an artificial heart

S. Nanka[1], T. Yambe MD[1], S. Nitta MD[1], S. Kobayashi MD PhD[1], M. Yoshizawa[2] and A. Tanaka[1]
[1]Department of Medical Engineering and Cardiology, Institute of Development, Aging and Cancer, Tohoku University, Sendai, Japan; and [2]Graduate School of Engineering, Tohoku University, Sendai, Japan

Background In order to develop the autonomic control algorithm for the total artificial heart (TAH) from a physiological viewpoint, the neural interface is thought to be useful.

Method Seven healthy adult goats were used in this study. Under general anesthesia, fifth-rib resection was performed. The electrocardiogram (ECG), aortic pressure (AoP), and other hemodynamic parameters were continuously measured. The vagal nerve was exposed at the left neck, and bipolar electrodes attached. After the anesthesia was terminated, hemodynamic time series data and vagal nerve activity were recorded. The goats were then anesthetized again, and the vagal nerves were cut at the distal point of the electrode. After the anesthesia was terminated, the time series data were recorded again.

Results Before the vagus was cut, vagal nerve activity did not significantly correlate with AoP. However, after the distal end of the vagal nerve was cut, the activity correlated with the alteration of AoP and increased before the animals began standing up.

Discussion Results of this study suggest that body motion and AoP are affected by vagal nerve activity. Monitoring of vagal nerve activity may be useful for the physiological autonomic control algorithm of the TAH.

Keywords vagal nerve activity, awake, artificial heart.

Introduction

Today there are many artificial heart pumps, but few control methods to drive them. These control methods work well in hospitals[1,2] for short periods of time. Assist devices have saved many patients' lives. Many investigators controlled their artificial hearts according to Starling's law[3,4], and others controlled their pumps to maintain aortic pressure (AoP)[4,5], but these control methods were not based on the autonomic nervous system or cardiac hormones. These investigators found their devices worked well initially, but a few months after implantation, problems arose (for example, central venous pressure increased, thyroid dysfunction occurred etc.)[6,7]. These problems were solved by 1/R control according to Abe[8], but the control brake by only one trouble in the pressure transducer.

In order to develop the autonomic control algorithm for the total artificial heart (TAH) from a physiological viewpoint, the neural interface is thought to be useful. Vagal nerve activity was measured and analyzed to develop the new control method for the TAH.

Method

Seven healthy adult goats weighing 50–70 kg were used in this study. They were fasted for 2 days before the experiments.

On the first day, the animals were anesthetized in a normal fashion with a tracheotomy and halothane inhalation on a respirator. Atropine sulfate was not used. Electrocardiogram (ECG) electrodes were attached to the body and legs. Under general anesthesia, fifth-rib resection was performed and the left pleural cavity was opened. Then the cardiac sensors were implanted, and AoPs, right atrium pressure (by the pressure transducer), aortic flow (by the electromagnetic flowmeter), and other hemodynamic parameters were continuously measured. A 10-cm segment of the vagal nerve was exposed along the left side of the neck and bipolar electrodes were attached. The stainless steel electrodes were 0.2 mm in diameter and coated with enamel for insulation, except at the needle cusp. The vagal nerve and electrodes were covered by a tube of polyvinyl chloride to avoid detection of superfluous noise. The vagal nerve and electrodes were embedded in the tube with resin (Semicosil No. 932, Wacker Chemie Co., Munich, Germany).

The AoP was measured by a pressure transducer fixed onto the cage. The neurogram was amplified by the preamp and amp, then integrated at the time constant 0.1 s. A high pass filter (300 Hz) and a low pass filter (0.03 Hz) were used. These parameters were recorded on digital audio tape and analyzed by personal computer.

On the second day, after the anesthesia was terminated, hemodynamic time series data and vagal nerve activity were recorded. Methoxamine and nitroglycerine were injected intravenously. The volume of drug injection was adjusted to achieve an AoP range of ±30~50 mmHg. Each drug

Correspondence to: Shunsuke Nanka, Department of Medical Engineering and Cardiology, Institute of Development, Aging and Cancer, Tohoku University 4–1 Seiryo-machi, Aoba-ku, Sendai 980–8575, Japan.

was injected in 2–5 mg doses. Drug administration was performed while the subject was in the sitting position, and each drug dose was injected at intervals greater than 30 minutes.

Next, a neurogram and hemodynamic parameters were recorded while the subject was standing up and sitting down. We waited until the goats could stand up by themselves before they were anesthetized again, and the vagal nerves were cut at the distal point of the electrode.

On the third day and after (once the anesthesia was terminated) the time series data were recorded again. Following this, drug injection was performed again in the same dose and the neurogram was recorded when the goats were standing.

In another two goats, ECG, carotid artery pressure and neurogram were measured at the left neck, and an endurance test of the electrodes was performed.

Analysis

The neurogram, which recorded the respiratory frequency, was analyzed. A spectral analysis was performed. The time series data of about 300 beats were analyzed with the use of Fast Fourier Transform.

An average of six beats for the mean AoP and the integrated neurogram were calculated before and after drug administration. The time series data of about six beats was analyzed. The data just before the drug injection and just after the AoP peak were selected for the analysis.

Moving averages of 2 s for the integrated neurogram and hemodynamic parameters were calculated to show when they began to increase or decrease. The time series data during drug administration and standing up motion were analyzed. AoP, integrated neurogram, right atrium pressure, and peripheral resistance which was calculated from aortic flow and AoP, were calculated.

The change ratio of the integrated neurogram and AoP during drug administration were calculated. An average of six beats for before and after injection were analyzed.

Result

A neurogram recorded the respiratory frequency of five goats. After the vagus cut, the data from only three goats could be recorded. A neurogram could not be recorded in two goats because of the failure of electrodes. The neurogram recorded respiratory information on only one goat while it was in the process of standing up.

The electrodes worked for more than 3 weeks. One goat was lost after loss of appetite 21 days after the operation, and another was lost 14 days after the operation. In each goat, some electrodes worked well on the last day (Figure 1) but other electrodes were detached from the vagal nerve probably because of body motion.

Spectral analysis

In the spectral analysis, the integrated neurogram and AoP had a peak of around 0.3 Hz (Figure 2).

Drug administration

Before the vagus was cut, vagal nerve activity did not correlate significantly with AoP. However, after the vagal nerve was cut at the distal point of the electrode, vagal nerve activity correlated with the alteration of AoP. The change ratio of the integrated neurogram correlated with the change ratio of AoP (Figure 3).

Before the vagus was cut, mean AoP was 112.4 mmHg (±27.5). The integrated neurogram was 21.1 μV•s (±28.1) in the sitting position; mean AoP was 124.7 mmHg (±22.2), and the integrated neurogram was 65.3 μV•s (±65.8) in the standing position.

Mean AoP always increased in all goats after the methoxamine injection. But vagal nerve activity and mean right atrium pressure did not change before the vagus was cut, nor did heart rate change. AoP increased from 113.4 mmHg (±24.5) to 147.5 mmHg (±42.3) and the integrated neurogram increased from 36.1 μV•s (±74.0) to 60.1 μV•s (±77.5).

Mean AoP always decreased in all goats after the nitroglycerine injection, but vagal nerve activity, mean right atrium pressure, and heart rate did not change so significantly before the vagus was cut. AoP was decreased from 116.9 mmHg (±34.2) to 81.4 mmHg (±22.1) and the integrated neurogram decreased from 45.8 μV•s (±51.3) to 43.1 μV•s (±55.7).

After the vagus was cut, vagal nerve activity increased significantly along with mean AoP after the methoxamine injection, but heart rate and right atrium pressure did not change so significantly. AoP increased from 117.3 mmHg (±8.3) to 165.6 mmHg (±13.7) and the integrated neurogram increased from 17.5 μV•s (±29.2) to 83.4 μV•s (±81.5).

After the vagus was cut, vagal nerve activity and mean AoP decreased after the nitroglycerine injection. Heart rate and right atrium pressure did not change so significantly. AoP decreased from 115.0 mmHg (±11.8) to 71.0 mmHg (±5.3). The integrated neurogram decreased from 86.2 μV•s (±58.4) to 33.1μV•s (±34.5).

These data are summarized in Table 1.

Change ratio

The change ratio of the AoP and vagal nerve activity during drug administration was calculated. Vagal nerve activity appeared to be changed and was correlated with the change in AoP.

The methoxiamine injection group and the nitroglycerine injection group were significantly different ($P < 0.05$) (Figure 3).

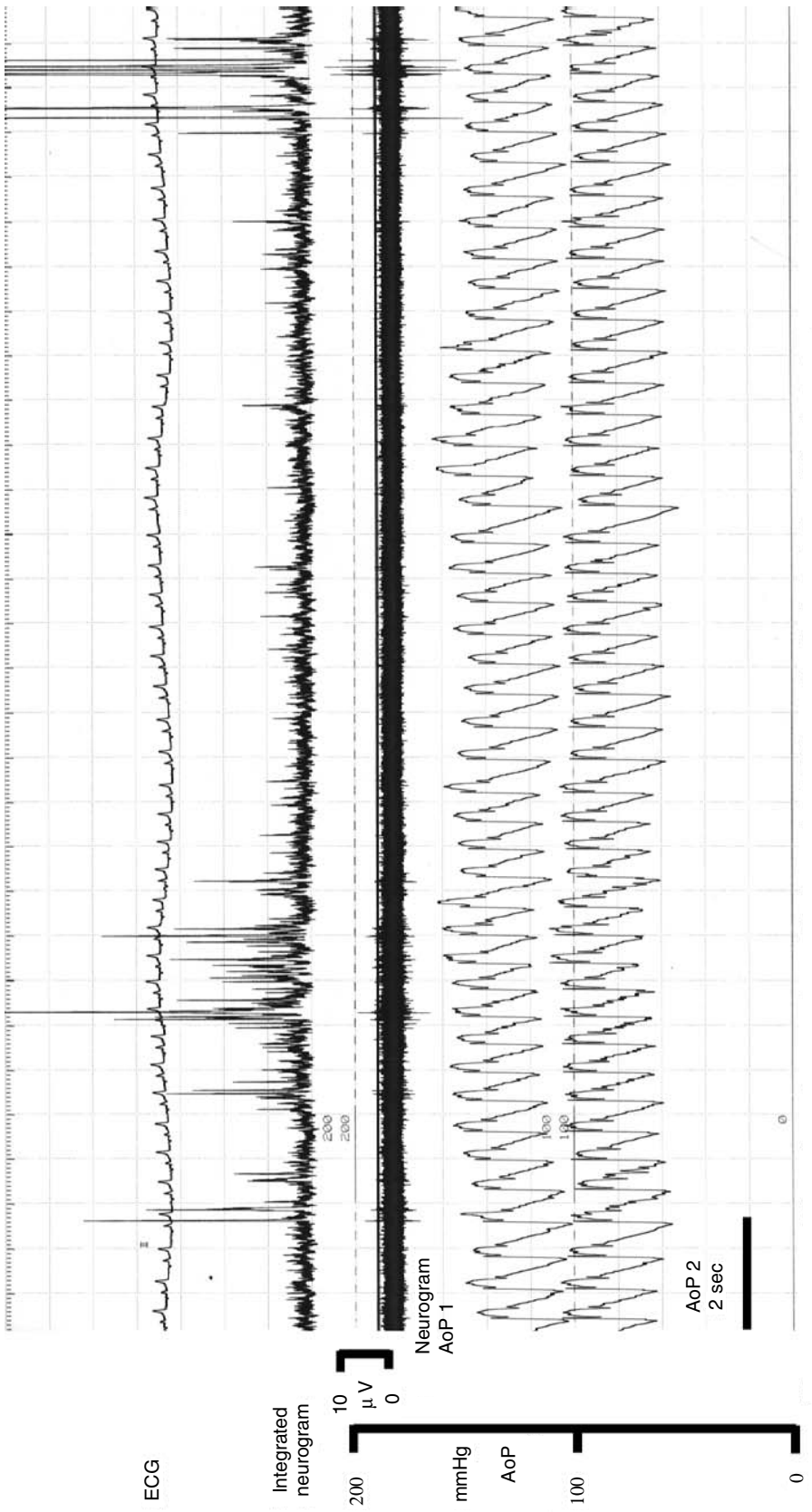

Figure 1. Hemodynamic parameters and vagal nerve activity (18 days after nerve electrode implantation). Aortic pressure 1 is measured at the pressure transducer fixed on a pole outside the cage. Aortic pressure 2 is measured at the pressure transducer fixed on the goat's body. The goat was sitting down. The neurogram monitored respiratory frequency 18 days after the operation. AoP = aortic pressure, ECG = electrocardiogram.

Table 1 The average (± standard deviation) of the aortic pressure and integrated neurogram

	Status	Aortic pressure (mmHg)	Integrated neurogram (μ V • s)
Before vagus cut	Sitting position	112.4 (± 27.5)	21.1 (±28.1)
	Standing position	124.7 (± 22.2)	65.3 (± 65.8)
	Pre-methoxamine injection	113.4 (±24.5)	36.1 (±74.0)
	Post-methoxamine injection	147.5 (±42.3)	60.1 (±77.5)
	Pre-nitroglycerin injection	116.9 (±34.2)	45.8 (±51.3)
	Post-nitroglycerin injection	81.4 (±22.1)	43.1 (±55.7)
After vagus cut	Pre-methoxamine injection	117.3 (±8.3)	17.5 (±29.2)
	Post-methoxamine injection	165.6 (±13.7)	83.4 (±81.5)
	Pre-nitroglycerin injection	115.0 (±11.8)	86.2 (±58.4)
	Post-nitroglycerin injection	71.0 (±5.3)	33.1 (±34.5)

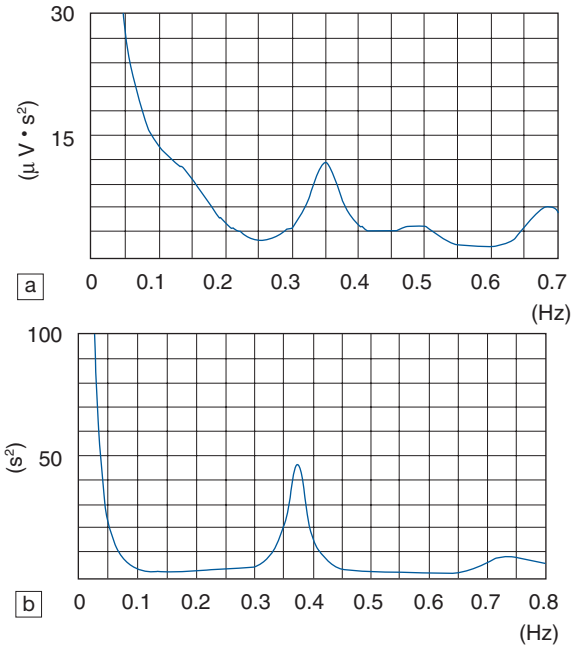

Figure 2. The spectral analysis of the integrated neurogram (a) and the heart rate variability (b).

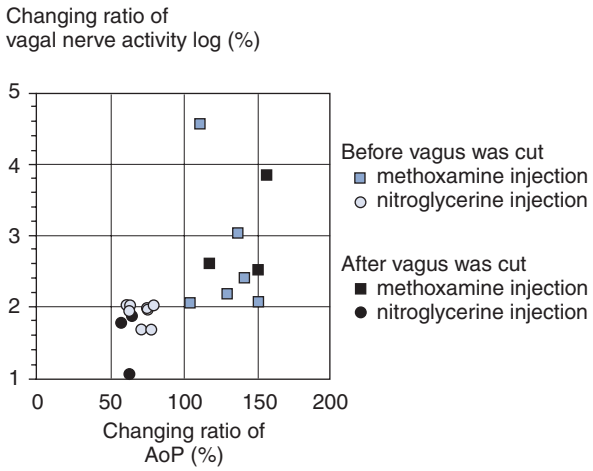

Figure 3. Changing ratio of vagal nerve activity after drug administration. AOP = aortic pressure.

2-second moving average

In this study, pressure transducers were fixed onto a pole outside of the subject's cage. AoP and atrium pressure seemed to increase when the subject stood up. We also analyzed the standing-up motion by changes in blood pressure and observation of the goats.

Vagal nerve activity, AoP and peripheral resistance started to increase about 2.5 s before the subject stood up. This result suggests that body motion could be anticipated by vagal nerve activity (Figure 4).

During drug administration, the moving average of vagal nerve activity was significantly changed. When AoP increased after by the methoxamine injection, the moving average of vagal nerve activity increased and continued to increase until AoP began to decrease. When AoP decreased after the nitroglycerine injection, the moving average of vagal nerve activity increased for a short period of time and then decreased to nearly 0 (Figure 5).

Discussion

Spectral analysis

Spectral analysis is very useful to evaluate the autonomic nervous system. ECG and other cardiac parameters were analyzed by spectral analysis. Heart rate variability is said

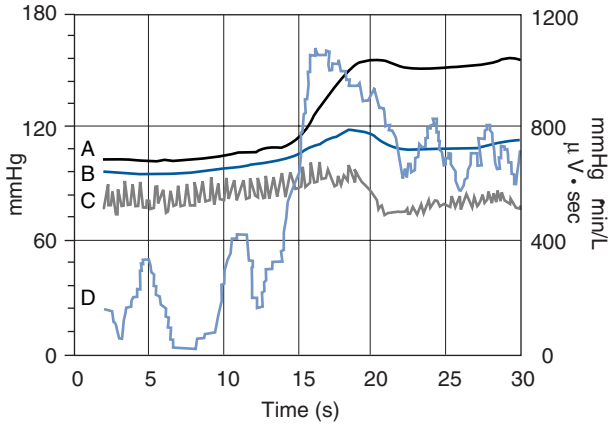

Figure 4. 2-second moving average of hemodynamic parameters and integrated neurogram during standing up motion. (A) aortic pressure, (B) aortic pressure/right atrium pressure, (C) peripheral resistance, (D) integrated neurogram.

to show autonomic nerve activity[9–11], and it can be calculated using a noninvasive test. But the spectral analysis needs long-term data; this method of analysis is not useful in estimating the fast change of AoP. We have previously reported that vagal nerve activity does not correlate with the high frequency peak of heart rate variability[12].

Drug administration and changing ratio

We measured vagal nerve activity while the subject was concious. Because vagal nerve activity changed in correlation with AoP, this may indicate the possibility of estimating changes in AoP by vagal nerve activity.

Before the vagus was cut, vagal nerve activity did not correlate so significantly with changes in AoP, but after it was cut, its efferent fiber activity did correlate with AoP changes. After the vagus was cut, no cases suggested that AoP and vagal nerve activity changed in divergent ways. It is possible to recognize changes in AoP over time by monitoring vagal nerve activity.

2-second moving average

When the goat wanted to stand up (but before standing was initiated), the 2-second moving average of the AoP, integrated neurogram and peripheral resistance increased. These indicators began to increase about 2.5 s before standing was initiated. Vagal nerve activity increased before standing was initiated, and rapidly decreased after standing was initiated. An increase in peripheral resistance was induced by changes in respiration and muscle blood flow. Because vagal nerve activity and peripheral resistance did not change until AoP was increased by the methoxamine injection, swallowing and nodding movements did not appear to significantly change vagal nerve activity.

When the goat wanted to stand up, the sympathetic nervous system would be activated, but until the initiation of

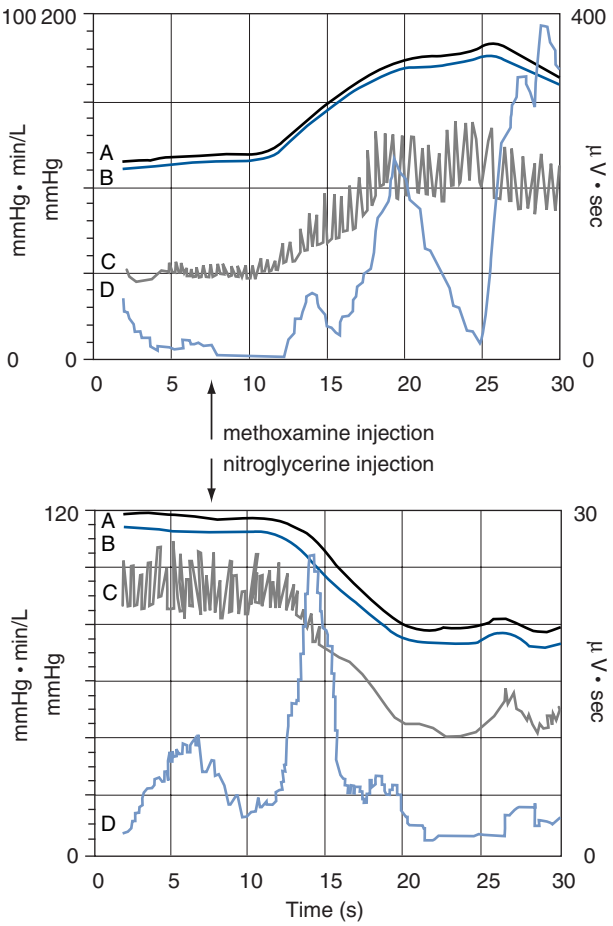

Figure 5. 2-second moving average of the hemodynamic parameters and integrated neurogram drug administration. (A) Aortic pressure, (B) aortic pressure/right atrium pressure, (C) peripheral resistance, (D) integrated neurogram.

standing, the parasympathetic nerve system would be activated to antagonize the sympathetic nerve system.

Vagal cut

In this study, we cut the left vagal nerve in the left neck. We could not find a report of the goat's vagal nerve anatomy, but a human's and a dog's vagal nerve anatomy were reported. It was found that the left vagal nerve mainly controls the atrioventricular node and the left ventricle. In this study, none of the goats showed signs of having an atrioventricular block after the vagal cut. After drug administration, no significant difference was observed in AoP before the vagus was cut.

Electrodes

We currently use a substantial number of neural electrodes, such as those used for microneurograms and functional electric stimulates. In future, we want to be able to control the TAH permanently using the neurogram. In that case

electrodes that are easily dislodged or polarized would not be useful. Instead, we would use a new electrode, made of stainless steel and 0.2 mm in diameter. This needle electrode has a hook, so it is hard to remove from the nerve, and is thick enough to sample nerve activity while maintaining stability.

In future, it will be possible to control a TAH using vagal nerve activity. The neural interface has some advantages:

1. The vagal nerve is activated before standing is initiated as there is an increase in AoP. We can predict when goats will stand up by monitoring vagal nerve activity.
2. The vagal nerve heart branch is cut in TAH implantation. It is possible to use the branch to control the artificial heart and no further surgical intervention is needed.

Conclusion

1. Electrodes work for more than 3 weeks.
2. Vagal nerve activity correlates with alterations in AoP.
3. Vagal nerve activity increases 2 or 3 s before body motion.
4. These results suggest that vagal nerve activity may be useful when calculating changes in hemodynamic parameters.

Acknowledgements

This study was supported by the Program for Promotion of Fundamental Studies in Health Sciences of the Organization for Drug ADR Relief, R&D Promotion and Product Review of Japan.

References

1. Mehta SM, Aufiero TX, Pae WE Jr, Miller CA, Pierce WS. Combined registry for the clinical use of mechanical ventricular assist pumps and total artificial heart in conjuction with heart transplantation. Sixth official report 1994. *J Heart Lung Transplant* 1995;14:585–93.
2. Mehta SM, Aufiero TX, Pae WE Jr, Miller CA, Pierce WS. Results of mechanical ventricular assistance for the treatment of post cardiotomy cardiogenic shock. *ASAIO Journal* 1996;42:211–8.
3. Hiller KW, Serigel W, Kolff WJ. A servomechanism to drive an artificial heart inside the chest. *ASAIO Trans* 1962;8:125–30.
4. Snyder AJ, Rosemberg G, Reibson J, *et al*. An electrically powered total artificial heart: over 1 year survival in the calf. *ASAIO J* 1992; M707–12.
5. Yambe T, Abe Y, Yoshizawa M *et al*. Strange hemodynamic attractor with 1/R total artificial heart automatic control algorithm. *Int J Artif Organs* 1996;19:302–6.
6. Aufiero TX, Magovern JA, Rosenberg G, Pae WE, Donachy JH, Pierce WS. Long-term survival with a pneumatic artificial heart. *Trans Am Soc Artif Intern Organs* 1987;33:157–61.
7. Vasku J. Perspectives of total artificial heart research as a valuable modelling system for general physiology and pathophysiology. In Akutsu T, Koyanagi H, editors. *Artificial Heart 4. Heart Replacement*. Tokyo: Springer-Verlag, 1992:161–71.
8. Abe Y, Chinzei T, Isoyama T *et al*. Long-term hemodynamics and pathophisiology in a total artificial heart goat survived for 532 days with 1/R control. *Jpn J Artif Organs* 1997;26:21–26.
9. Yambe T, Nitta S, Sonobe T. Origin of the rhythmical fluctuations in the animal without a natural heartbeat. *Artif Organs* 1993;17:1021–71.
10. Akselrod S, Gordon D, Madwed JB, Snidman NC, Shannon DC, Cohen RJ. Hemodynamic regulation: investigation by spectral analysis. *Am J Physiol* 1985;249:H867–75.
11. Nishinaka T, Eisuke T, Nishimura T, Taenak Y, Takano H. Analysis of an autonomic nervous system during long-term nonpulsatile left ventricular assistance. *Jpn J Artif Organs* 1998;27(Suppl): S144.
12. Yambe T, Nanka S, Kobayashi S *et al*. Vagal nerve activity and the high frequency peak of the heart rate variability. *Int J Artif Organs* 1999;22:324–8.

Journal of Congestive Heart Failure and Circulatory Support (2001) Vol 1, No 4, 213–217

Development of the implantable centrifugal right ventricular assist device: combined use with LVAD as an alternative to the total artificial heart

H. Nishida[1], K. Yamazaki[1], M. Endo[1], H. Koyanaghi[1], K. Tajima[2], K. Higuchi[2] and T. Mori[2]

[1]Department of Cardiovascular Surgery, The Heart Institute of Japan, Tokyo Women's Medical Univeristy; and [2]Sun Medical Technology Research Corporation, Tokyo, Japan

Background Pulsatile left ventricular assist devices (LVADs) have been widely used clinically as either a bridge to heart transplantation or definitive treatment for end-stage heart failure. Recently, the clinical usage of nonpulsatile LVADs has also been initiated. Although biventricular support is necessary in 15% of patients with end-stage heart failure, development of a total artificial heart (TAH) still has a long way to go. Donors for heart transplantation are also very limited. To save patients with end-stage biventricular failure under such circumstances, the most realistic strategy may be to develop an implantable right ventricular assist device (RVAD) that can be used with an implantable LVAD.

Methods Based on the design of a prototype of an implantable centrifugal LVAD currently under development (Sun Medical Technology Research Corporation, Suwa, Japan), we have developed a RVAD with a similar design. The targeted flow performance was 6 L min^{-1} against a 50 mmHg after-load at 2000 rpm.

Results The outer diameter of the fin is 36 mm, which is 90% of that of the LVAD. The calculated mean electric power requirement is 4.5 W, which is 60% of that of the LVAD. The calculated efficiency of the pump is 45%.

Discussion We believe this RVAD can be implanted into the right upper quadrant of the abdominal wall and be powered from a common battery source with an LVAD.

Keywords centrifugal pump, right ventricular assist device (RVAD), implantable pump, total artificial heart (TAH).

Introduction

Pulsatile left ventricular assist devices (LVADs), such as Novacor and TCI, have been widely used clinically as either a bridge to heart transplantation or definitive treatment for end-stage heart failure[1]. Recently, the clinical usage of a completely implantable pulsatile LVAD, LionHeart, and nonpulsatile LVADs such as the Micromed DeBakey pump and Jarvik 2000 pump has also initiated. Although LVADs have established their status as effective and realistic devices, 15–20% of patients with end-stage heart failure require biventricular support. This fact, coupled with the severe donor shortage for heart transplantation, emphasizes the need for establishment of a biventricular support strategy. Because we believe the combined use of LVADs and right ventricular assist devices (RVADs) is more realistic than developing a total artificial heart (TAH) at present, we have started to develop a nonpulsatile RVAD that can be used with either a pulsatile or nonpulsatile LVAD.

Materials and methods

Pump concept

First, we compared the efficiency and size of two approaches for implantable nonpulsatile RVADs, through mathematical and theoretical analysis:

1. Diversion of a currently developing LVAD[2] under the right heart condition by simply driving it with a lower rotational speed.
2. Development of a similar design of VAD exclusively for the right heart.

The target flow performance required for the implantable RVAD was set at 6 L min^{-1} against a 50 mmHg after-load at a rotational speed of 2000 rpm. As summarized in Table 1, we found the size could be reduced to 90% of that of the LVAD when we developed a similar design to the LVAD for exclusive use as a RVAD, and total pump

Table 1. Comparison of 'diversion of LVAD' and 'exclusive RVAD'

	Diversion of LVAD	Exclusive RVAD
Outer diameter of FIN	40.0 mm	36.8 mm
Motor power (W)	7.41	4.47
Total pump efficiency	9%	14.9%

Correspondence to: Hiroshi Nishida MD, Department of Cardiovascular Surgery, The Heart Institute of Japan, Tokyo Women's Medical University, 8-1 Kawadacho, Shinjuku-ku, Tokyo 162-8666, Japan.

efficiency could be improved by 50%. Therefore, we decided to make a prototype of an implantable nonpulsatile pump for exclusive use as a RVAD.

Experimental study

We evaluated the hydraulic pump performance, using the experimental circuit shown in Figure 1, by circulating water at room temperature. Flow rate was recorded within the range of 0–15 L min^{-1} with simultaneous recording of total pump head pressure; alteration of the rotational speed was within the range of 1300–2200 rpm at 100 rpm intervals.

Results

Figure 2 shows the appearance of the outer housing; the diameter is 46 mm. Figure 3 shows the appearance of the rotational fin; the outer diameter is 30 mm and very compact – 75% of that of the LVAD.

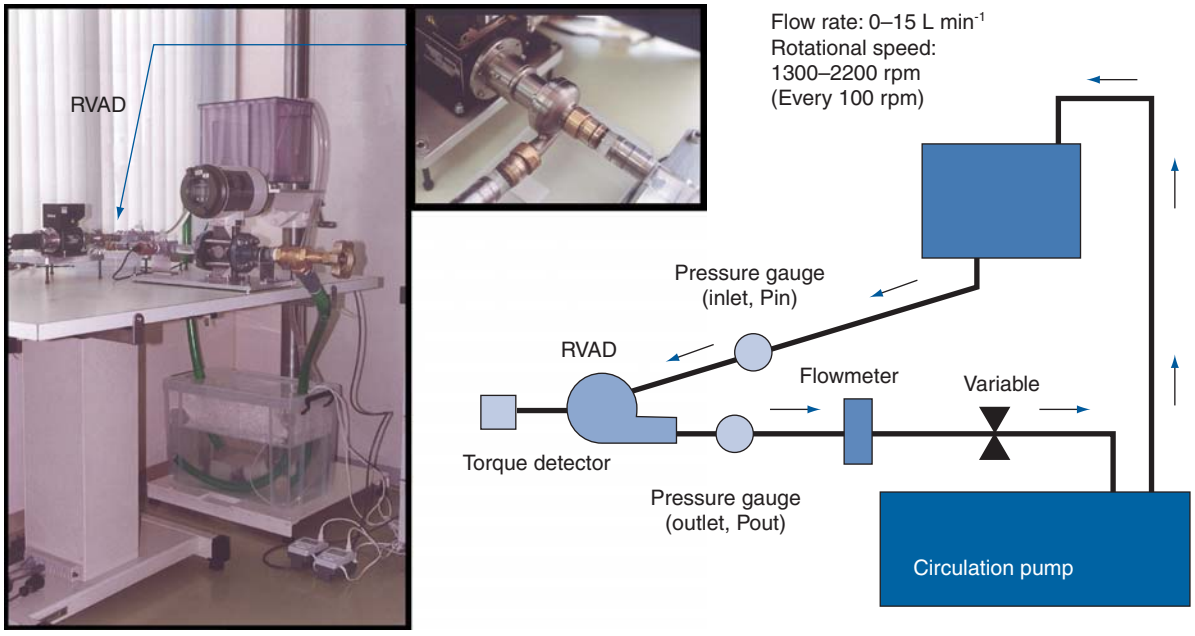

Figure 1. Experimental circuit.

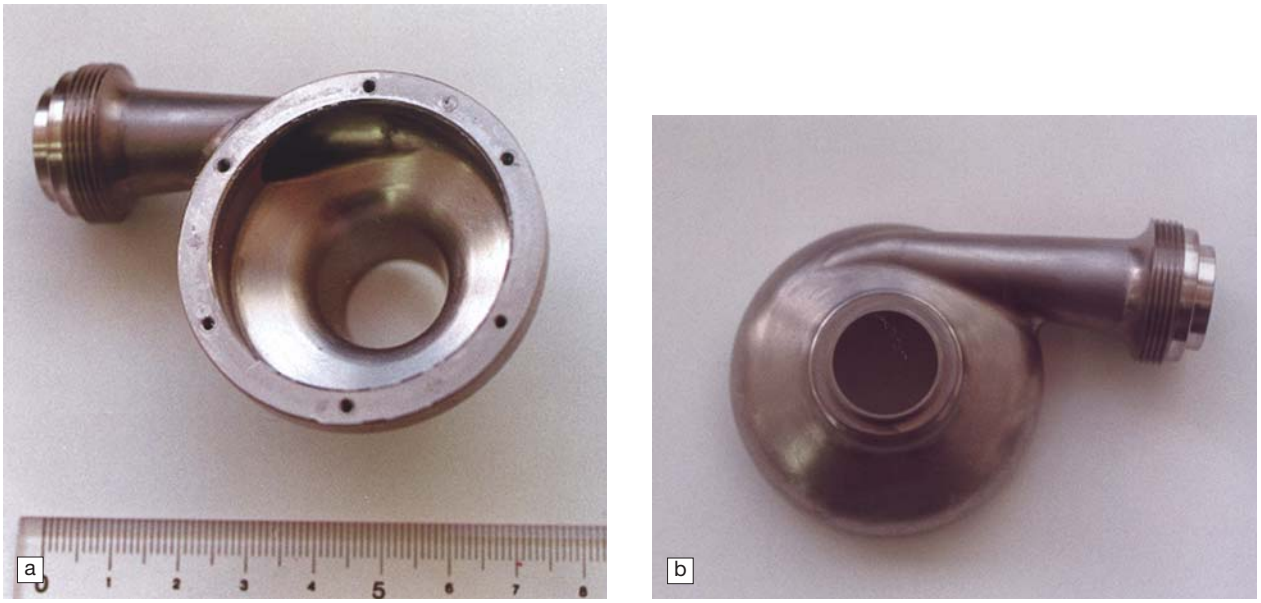

Figure 2. The diameter (a) and appearance (b) of the outer housing.

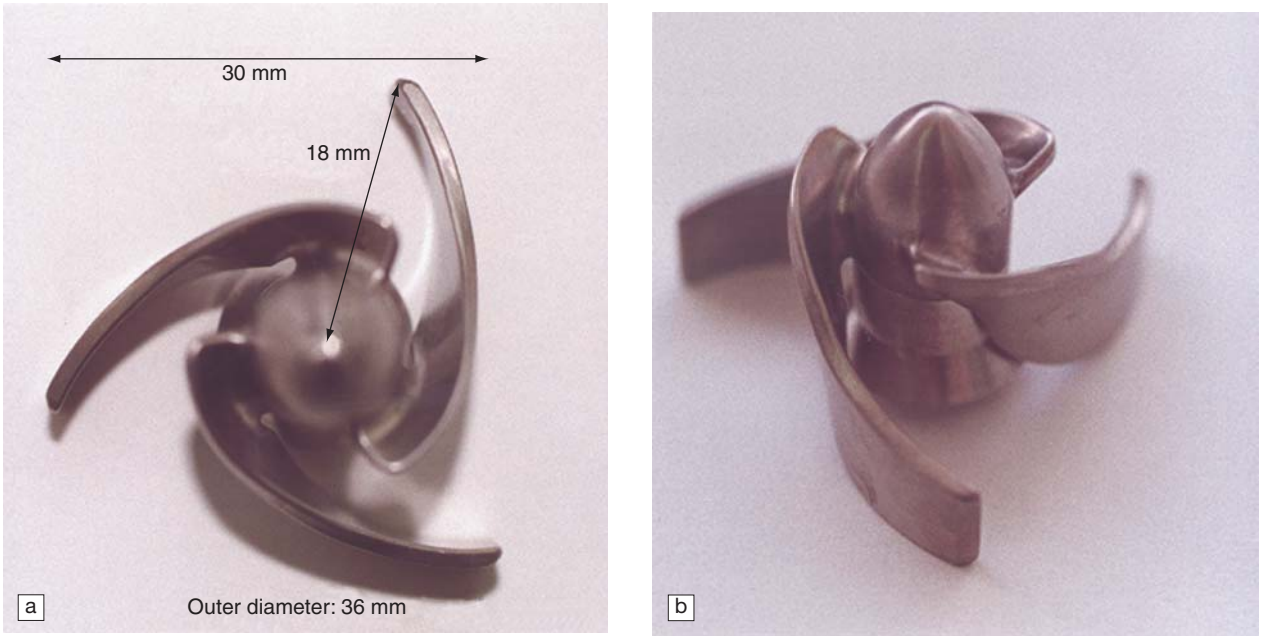

Figure 3. The diameter (a) and appearance (b) of the rotational fin.

Hydraulic pump performances

Figure 4 shows the relationship between pump flow rate and total pressure head (delta pressure). The design point of the pump is a flow rate of 6 L min^{-1} against a total pressure head of 50 mmHg. Under these conditions, the rotational speed was 2100 rpm. The pump flow was 5 L min^{-1} at a rotational speed of 2000 rpm and a total pressure head of 50 mmHg.

Figure 5 shows pump efficiency at various pump flow rates and rotational speeds. A high pump efficiency of approximately 45% was obtained at a flow rate of around 5 L min^{-1}.

Figure 6 shows the relationship between torque and pump flow rate under various rotational speeds.

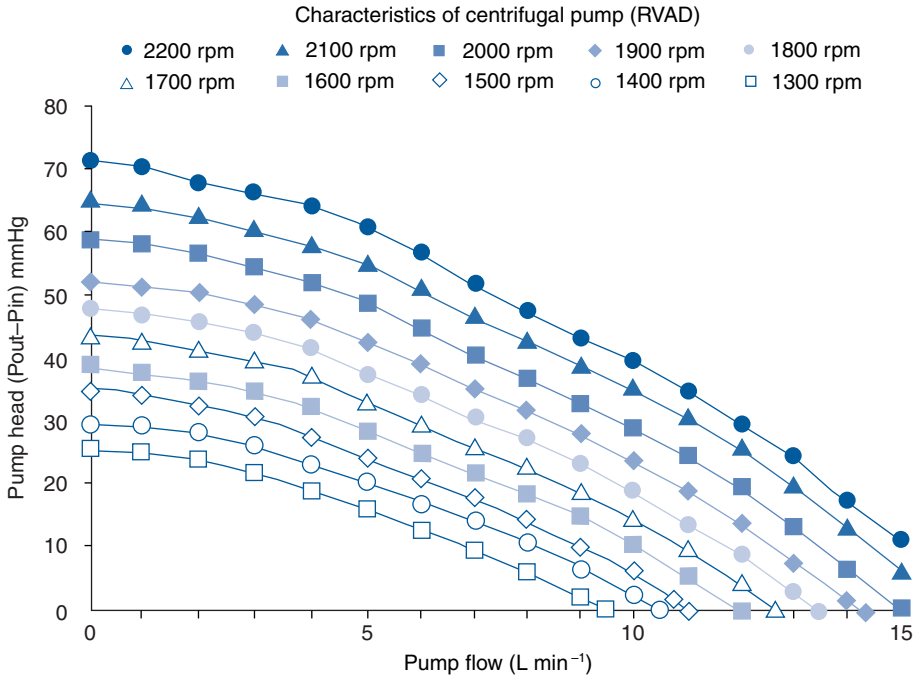

Figure 4. Relationship between pump flow rate and total pressure head.

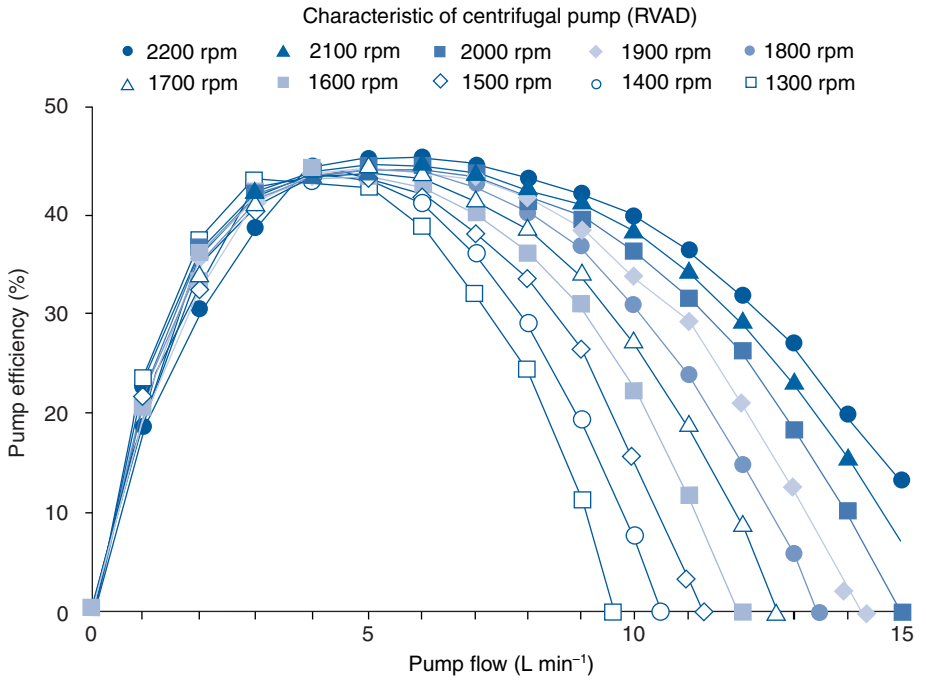

Figure 5. Pump efficiency at various pump flow rates and rotational speeds.

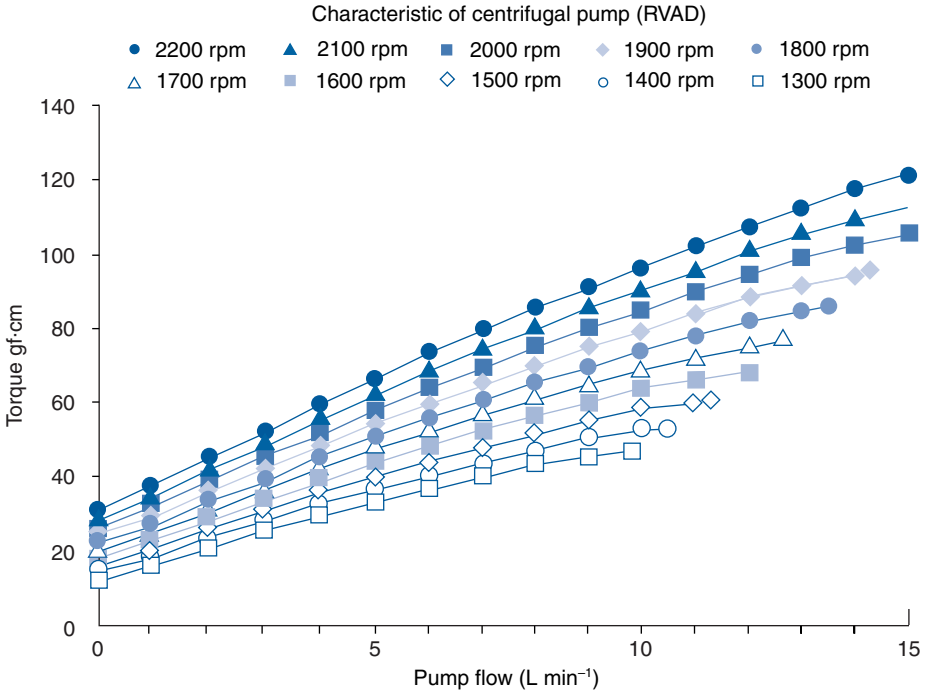

Figure 6. Relationship between torque and pump flow rate.

Discussion

TAH or BiVAD (LVAD + RVAD) for biventricular failure

For biventricular failure (Table 2), which approach – total artificial heart or combined use of left and right ventricular assist devices – is more realistic at present? The development of a TAH requires greater developmental cost and time; the device cost will also be higher. Recently, the lasting recovery of end-stage dilated cardiomyopathy with ventricular unloading using an LVAD has been demonstrated [1]. We believe that the need for permanent or long-lasting mechanical assist for circulation is less for the right ventricle than the left ventricle. A number of patients can be weaned from RVAD and require only LVAD support for a

Table 2. Reasons for biventricular failure

	TAH	LVAD + RVAD
Developmental cost	High	Low
Duration	Long	Short
Device cost	High	Low
Weaning	Impossible	Possible
Liability	High	Low
Malfunction	Instantaneous catastrophe	Room for treatment

long period of time. In such patients, the RVAD can be removed. The option of weaning from the device is not available with the TAH. Therefore, biventricular support with a VAD for each ventricle should be undertaken at an early stage rather than directly implanting a TAH into patients with end-stage biventricular failure. Furthermore, malfunction of the TAH leads to an instantaneous catastrophe, while malfunction of a VAD leaves room for treatment because the patient's own heart can maintain the circulation for a while. These aspects of the TAH will present a hurdle of extremely high product liability compared with the other option: combined use of left and right VADs.

Optimal combination in LVAD/RVAD strategy

There are four possible combinations for combined use of left and right VADs as shown in Table 3. The combination of pulsatile LVAD and pulsatile RVAD is bulky and too expensive. The combination of nonpulsatile LVAD and pulsatile RVAD seems unrealistic, and the combination of nonpulsatile LVAD and nonpulsatile RVAD has problems in terms of difficult regulation due to mutual interference. Therefore, we believe the combination of pulsatile LVAD and nonpulsatile RVAD may be the most realistic approach, and thus decided to develop an implantable, compact nonpulsatile RVAD.

Requirement for RVAD

The targeted pump performance was a pump flow rate of 6.0 L min^{-1} against a total pressure head of 50 mmHg at a rotational speed of around 2000 rpm. We believe that this basic goal *per se* has been achieved.

Table 3. Four possible combinations for LVAD + RVAD strategy

LVAD	RVAD	Comments
Pulsatile	Pulsatile	Bulky and expensive
Pulsatile	Nonpulsatile	Most realistic?
Nonpulsatile	Pulsatile	Unrealistic?
Nonpulsatile	Nonpulsatile	Difficult regulation?

When important requirements for clinical use of RVADs are considered, it should be noted that excessive flow, which leads to pulmonary edema, is worse than inadequate flow. Therefore, actual regulation of the RVAD uses a fixed rotational speed to obtain a lower flow than the targeted flow rate used in usual situations. At lower rotational speeds, the flow rate at which maximum efficiency was obtained moves toward 3–4 L min^{-1} (Figure 5), which is favorable when considering the safety net in RVADs. From this standpoint, the pump performance of this RVAD prototype is reasonable but may still be excessive.

Future investigation and perspectives

We plan to perform an experiment to obtain hemolysis data and evaluate pump performance in a circulation simulator under various conditions that mimic concomitant use with either a pulsatile or nonpulsatile LVAD. The following points will be investigated:

1. How pulsatility is maintained when flow from this pump and ejection from the patient's own right ventricle overlap.
2. Effect of long-term nonpulsatile flow on the lung.
3. Flow fluctuation when intrathoracic pressure rises momentarily under circumstances such as coughing and the Valsalva maneuver (strained breath).

Through these analyses, we aim to determine the optimal performance and regulation of the RVAD as an adjunct to the LVAD.

Conclusion

The development of an implantable centrifugal RVAD, which is used together with a pulsatile LVAD as an alternative to the total artificial heart, seems a feasible and realistic approach. We believe this RVAD can be implanted into the right upper quadrant of the abdominal wall and be powered from a common battery source with an LVAD.

Acknowledgement

This work was supported by the Research Grant for Cardiovascular Diseases (10C–2) from the Ministry of Health and Welfare in Japan.

References

1. Hetzer R, Muller J, Weng Y, Wallukat G, Spiegelsberger S, Loebe M. Cardiac recovery in dilated cardiomyopathy by unloading with a left ventricular assist device. *Ann Thorac Surg* 1999;68:742–9.
2. Yamazaki K, Litwak P, Tagusari O *et al.* An implantable centrifugal blood pump with a recirculating purge system (CoolSeal system). *Artif Organs* 1998;22:466–74.

Journal of Congestive Heart Failure and Circulatory Support (2001) Vol 1, No 4, 219–226

Eccentric roller type total artificial heart

M. Watari MD[1], H. Wada MD[1], S. Fukunaga PhD[2], H. Sakai MD[1], K. Orihashi MD[1], T. Sueda MD[1] and Y. Matsuura MD[1]

[1]*First Department of Surgery, Hiroshima University School of Medicine, Hiroshima Japan; and*
[2]*Department of Clinical Engineering, Hiroshima International University, Hiroshima, Japan*

Abstract We have produced an eccentric roller-type total artificial heart (ERTAH). As the first step in the development of this ERTAH, we conducted simulations such as a numerical simulation, a mock test, and an acute animal experiment using DeBakey roller pumps. The aim was to analyze the left–right balance and discover the appropriate inter atrial resistance for its operation. The next step was to redesign the blood chambers to improve energy efficiency and implant the ERTAH with an interatrial shunt into an animal to evaluate the *in vivo* performance of this device. In the simulations, shunt flow through the bronchial arteries was approximately 500–600 mL min^{-1}, and the inter atrial resistance varied from 2.9–7.7 mmHg·L min^{-1}. The redesigning of the blood chambers in the mock test resulted in a 20% increase in energy efficiency, approximately a two-fold increase in cardiac output and an improved durability compared to the previous type in the mock test. In the animal experiment, the ERTAH operated with a left flow rate of 6.0 L min^{-1} and a right flow rate of 5.4 L min^{-1}. The interatrial shunt flow rate was 250–400 mL min^{-1}. Hemodynamic parameters of LAP, RAP, PAP and (AoP) were kept within an acceptable physiological range. The equiping of an interatrial shunt is a useful method for balancing the blood flow between the left and right heart of the ERTAH. A decrease in friction resistance and prevention of backward flow resulted in an increase in energy efficiency, cardiac output, and improved durability, in spite of a downsizing of the blood chambers.

Keywords total artificial heart (TAH), roller pump, interatrial shunt, left–right balance.

Abbreviations

AP: aortic pressure; CAO: compliance of aorta; CLA: compliance of left atrium; CO: output of the ERTAH; CPA: compliance of pulmonary artery; CRA: compliance of right atrium; ECG: electrocardiogram; ERTAH: eccentric roller-type total artificial heart; FL: flow rate of LAH; FR: flow rate of RAH; LAH: left artificial heart; LAP: left atrial pressure; LL shunting: left-to-left shunting; PAP: pulmonary artery pressure; QALR: interatrial (left to right) shunt flow; QLL: LL shunt flow; QP: pulmonary flow; QS: systemic flow; RAA: interatrial resistance; RAH: right artificial heart; RAP: right atrial pressure; RLL: LL shunt resistance; RP: pulmonary resistance; RS: systemic resistance; SV: stroke volume of ERTAH; TAH: total artificial heart.

Introduction

We have developed various prototypes of a totally implantable total artificial heart (TAH) at the Hiroshima University School of Medicine[1–6], and our efforts to improve the TAH are continuing for the following reasons: (1) a satisfactory cardiac output has not yet been obtained; (2) the energy efficiency was low; and (3) the problem of antithrombogenicity remains. Among recent prototypes of electric motor-driven TAH studies, the latest to be developed is an ERTAH in which right and left silicone blood chambers output blood alternately, being compressed by alternate rotations of eccentric rollers[3,7,8].

The advantages of this artificial heart are that no valves are mounted and that it is one of the most compact devices in the world (8 × 10 cm). The disadvantages are that the left–right output balance of the device is fixed, its output volume is relatively low and its energy efficiency and durability are unsatisfactory.

Like the DeBakey roller pump, its right and left output volumes are determined to be constant by the chamber volumes and rolling rates of the rollers because of an active filling mechanism. Under physiological conditions, however, the volume of circulating blood in the left side is larger than in the right side; this is due to blood circulation through the bronchial artery (left to left [LL] shunting). Furthermore, the left pump after-load and workload are larger than those of the right pump. In the current ERTAH, the left–right balance of the artificial heart is maintained by differences in the size of the left and right chambers[7,8].

This technology was thought to have a limitation in that it could not accommodate physiological fluctuations because the left–right output ratios were constant. For these reasons we conducted simulations for LL shunting under the ERTAH operation, and redesigned the blood chambers to improve its basic performance.

Correspondence to: Dr. Masanobu Watari, First Department of Surgery, Hiroshima University School of Medicine, 1-2-3 Kasumi, Minamiku, Hiroshima, 734-8551, Japan.

Materials and methods

Through all of the animal experiments, an i.v. line was established in the marginal ear vein. General anesthesia was induced by thiopental sodium (5 mg kg $^{-1}$) administered intravenously. Tracheal intubation was performed. Anesthesia was maintained with isoflurane inhalation after connecting a tracheal cannula with an anesthetic device (AM 210, Aika Co., Ltd., Tokyo, Japan). Blood flows were measured using electromagnetic flowmeters (MFV2210, Nihon Koden Co., Ltd.). Electrocardiagram (ECG), blood flows and blood pressures were recorded on a polygraph (361, NEC Medical Systems, Ltd., Tokyo, Japan). The animals received humane care in compliance with the *Principles of Laboratory Animal Care* formulated by the National Society for Medical Research and the *Guide for the Care and Use of Laboratory Animals* prepared by the Institute of Laboratory Animal Resources and published by the National Institutes of Health (NIH publication No. 86–23, revised 1985).

Simulations of left–right balance of blood flow in the ERTAH

Numerical simulation

Figure 1 and Box 1 show the simulation circuit and basic equations for vascular resistance, vascular compliance, and artificial heart, replaced by resistance, capacitance, and current sources, respectively. The vascular system is reconstructed as a lumped element network, as depicted in Figure 1. We chose the resistance of the interatrial shunt (RAA)

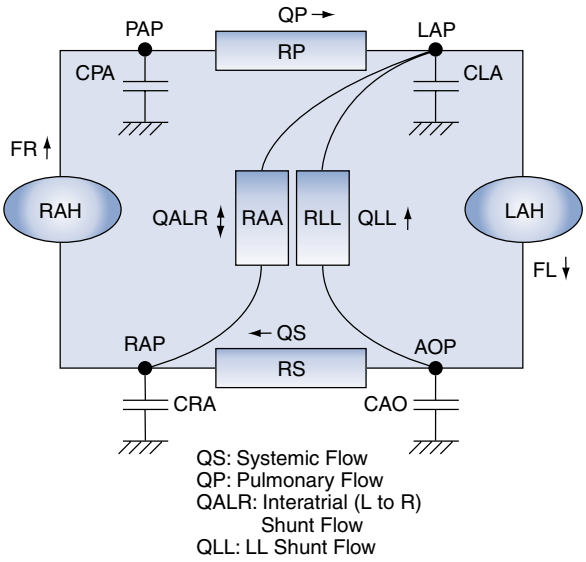

Figure 1. Numerical simulation circuit.

Box 1. Basic equations, constants and variables

Basic equations	$AoP \times CAO + RAP \times CRA + PAP \times CPA + LAP \times CLA = V0$	(1)
	$AoP - RAP = RS \times QS$	(2)
	$PAP - LAP = RLL \times QP$	(3)
	$AoP - LAP = RLL \times QLL$	(4)
	$LAP - RAP = RAA \times QALR$	
	$FL = QS + QLL$	(5)
	$FR = QS + QALR$	(6)
	$FR = QP$	(7)
	$QP + QLL = FL + QALR$	(9)
Constants	$FL = 6$ (L min^{-1})	
	$CLA = 5$ (L mmHg^{-1}) at 4 mmHg	
	$CAO = 1$ (L mmHg^{-1}) at 100 mmHg	
	$CRA = 10$ (L mmHg^{-1}) at 0 mmHg	
	$CPA = 1$ (L mmHg^{-1}) at 15 mmHg	
	$RS = 16$ (L mmHg^{-1})	
	$RP = 2.5$ (mmHg·L min^{-1})	
	$RLL = 160$ (mmHg·L min^{-1})	
	VO = 135 (mL), total blood volume in compliance (CAO, CRA, CPA, CLA)	
Variables	$FR = 5 - 6$ (L min^{-1})	
	$RAA = 0n\ 500$ (mmHg·L min^{-1})	

and right artificial heart flow rate (FR) as independent variables, and the other parameters are fixed at appropriate values. The right-to-left and left-to-right shunt flows (QALR) are presented as positive and negative blood flows, respectively.

Mock test using DeBakey roller pumps for simulation of left–right balance of ERTAH

Two DeBakey roller pumps were connected to the right and left sides of a Donovan mock circulatory system and an interatrial shunt was created between the inlet ports of the left and right roller pumps. An electromagnetic flowmeter was used to measure interatrial shunt flow rate, and catheter lines were connected to the aorta to determine pressures of the pulmonary artery, and right and left atria. Cardiac output and blood pressures were measured at a fixed pump speed of 60 rpm on the left side for making a constant FL (4.8 L min^{-1}); the pump speed on the right side varied from 45 to 75 rpm and consequently FR varied from 3.6 L min^{-1}. The following three sizes of interatrial shunts were prepared and compared: 6, 8, and 10 mm.

Acute animal experiment using DeBakey pumps for simulation of left–right balance under ERTAH operation

As in the mock test, two roller pumps were used to bypass the right and left hearts of a goat weighing 60 kg. An interatrial shunt 10 cm in length and 10 mm in inner diameter was set between the left and right inlet ports. The blood flow from the two rotary pumps and in the interatrial shunt were measured using an electromagnetic flowmeter at a fixed pump speed of 60 rpm for the left side, and a varying pump speed for the right side. Vascular grafts were sutured to the left atrium, the pulmonary artery, and the descending aorta (inner diameters 19, 12, and 12 mm, respectively). An exsanguination catheter (inner diameter 12 mm) was inserted into the inferior vena cava through the jugular vein. With three grafts and a line connected, extra-corporeal circulation was established using a roller pump; the roller pump was driven and the hemodynamic parameters were measured.

Improvement of ERTAH performance

Redesign of blood chambers

The pump system basically has the same configuration as that previously reported, in which right and left silicone blood chambers output blood alternatively by compressing them with alternate rotations of eccentric rollers (Figure 2). The newer system has smaller blood chambers (right side volume 35 mL; left side volume 40 mL) than those of the previous ERTAH (right side volume 53 mL; left side volume 60 mL). These chambers were designed to have as large a stroke volume as possible (Figure 3). In addition, the designs of the inlet and outlet ports were modified to prevent backward flow. It is expected that these modifications will improve energy efficiency and durability, and increase output volume through a possible reduction of the friction resistance generated between the blood chambers and casing, although the previous pulsatile-like waveform will not be obtained.

Figure 2. Principle and structure of the eccentric roller2type total artificial heart. The whole view (upper right), and cross-sectional view (upper left).

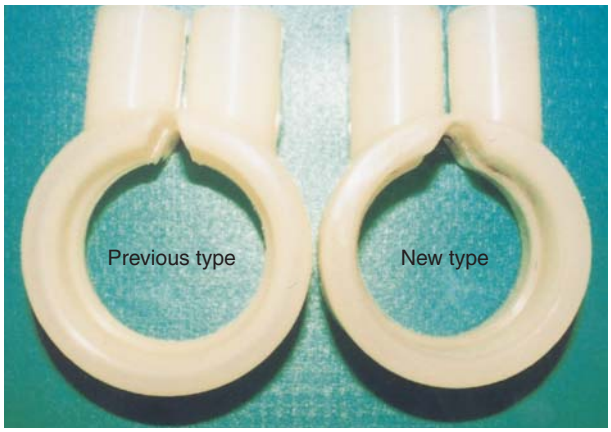

Figure 3. Left blood chambers. (Left) Previous type, (Right) new Type. The size and shape of the chambers are different; the left blood chamber volume has been changed from 60 ml to 40 mL and the right from 53 ml to 35 mL. The form between the inlet and outlet ports were modified to prevent backward flow.

Mock test for evaluation of basic ERTAH performance

A mock test was performed using a Donovan-type mock circulatory system. In the test the newer ERTAH without an interatrial shunt was connected to a mock circulatory system and the basic performance of the device as a blood pump system was evaluated.

Animal experiment for implantation

An animal experiment involving an adult goat weighing 40 kg was performed under general anesthesia with a cardiopulmonary bypass. A 24–Fr exsanguination catheter (FEM II–0142V, Baxter Corporation, Utah, USA) was inserted into the inferior vena cava through the jugular vein. After

placement of a tube for the blood supply into the descending aorta, a cardiopulmonary bypass (CPB) was established. After induction of ventricular fibrillation using a fibrillator in the cardiopulmonary bypass condition, inflow cannulas for the TAH with an inner diameter of 12 mm were inserted into the left and right atriums via the left and right apexes of the heart, respectively. A blood supply tube with an inner diameter of 8 mm was inserted into the aorta and the pulmonary artery, respectively. The central side of the aorta and the pulmonary artery were ligated after vascular cannulations were completed. The blood flow into the CPB was gradually reduced and the blood flow into the TAH was increased correspondingly. Finally, a transition from CPB to TAH was achieved after weaning from CPB. A shunt circuit with an inner diameter of 10 mm and a length of 5 cm was created between the left and right exsanguination tubes (Figure 4). Blood flows at the outlet ports of the right and left sides of the TAH and that in the interatrial shunt were measured using electromagnetic flowmeters.

Results

Simulations of left–right balance of ERTAH

Numerical simulation

Numerical simulation was performed under conditions where the flow of the FL was fixed at 6 L min^{-1}, the flow of the FR was varied from 4.8 L min^{-1} to 6 L min^{-1}, and the RAA was 0 and 20 mmHg. L min^{-1}. The relationship between QALR and output of the left and right artificial hearts was balanced when the FR was 5.45 L min^{-1} (FR–FL = 0.55 L min^{-1}). Regarding the relationships between the pressure data (RAP, LAP, PAP, and AoP) and the interatrial shunt, there were no changes in RAP, LAP, PAP, and AoP when the RAA was zero. LAP and PAP increased and RAP and AoP decreased as RAA increased (Box 2).

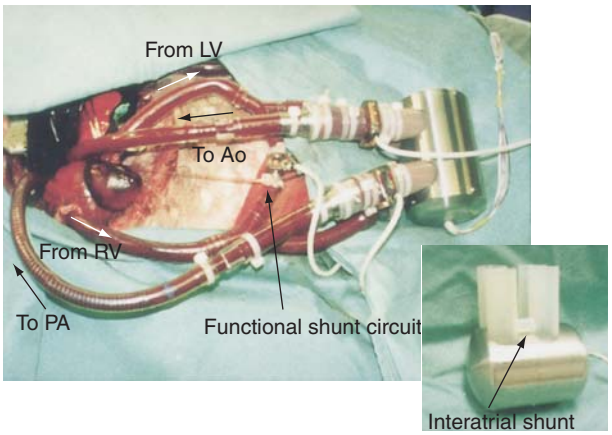

Figure 4. Acute animal experiment involving an adult goat. (Left) Functional shunt circuit with inner diameter of 10 mm. A length of 5 cm was crated between the left and right exsanguination tubes. (Right) ERTAH equipping internal shunt.

Mock test using DeBakey pumps for simulation of left–right balance of ERTAH

In the mock test, LAP increased and RAP decreased with the increase in left-to-right shunting, as shown in the numrical simulation (Box 2). Furthermore, when the diameter of the interatrial shunt became smaller and shunt resistance was increased, the absolute left-to-right atrial pressure difference was increased. When the interatrial shunt flow rate was zero, the pressure difference was also zero. Because there was no LL shunt in this mock system, the flow difference between left and right roller pumps (FR–FL) was 0 when the QALR was 0. The RAA of the mock system was varied from 7.1–8.3 (mean 7.7) mmHg · L min^{-1}, 3.5–4.6 (mean 4.3) mmHg · L min^{-1} and 2.6–3.8 (mean 2.9) mmHg . L min^{-1} when the inner diameter of the interatrial shunt was 6 mm, 8 mm, and 10 mm, respectively (Table 1).

Acute animal experiment using DeBakey pumps for simulation of left–right balance under ERTAH operation

The outputs of both roller pumps (FR and FL), the interatrial shunt flow rate (QALR), AoP, PAP, RAP, and LAP were measured under conditions where the speed of the roller pump used for the left side bypass was fixed at 60 rpm and that for right side bypass was varied. The right-to-left and left-to-right shunt flows were presented as negative and positive blood flows, respectively. The flow of the left pump was almost constant (4.7 L min^{-1}). The FR was approximately 4.1 L min^{-1} when the QALR was 0, allowing that the LL shunt flow in this goat's heart was approximately 0.6 L min^{-1} (Figure 5). Regarding the relationships between pressure data (RAP, LAP, PAP, and AoP) and QALR, an increase in left-to-right shunting was associated with increases in LAP, PAP, and AP, and a decrease in RAP (Figure 6).

Table 1. Result of the mock test for simulation to left–right balance of the ERTAH

Shunt size inner diameter (mm)	Interatrial shunt flow rate (min^{-1})	Interatrial pressure gradient (mmHg)	Resistance of interatrial shunt (mmHg · L min^{-1})
6	−1.2–1.2	−10–9.1	7.1–8.3 (mean 7.7)
8	−1.2–1.2	−5.5–5.4	3.5–4.6 (mean 4.3)
10	−1.2–1.2	−3.3–2.8	2.6–3.8 (mean 2.9)

Box 2. Result of numerical simulation

(A) RAA = 0 mmHg · L min^{-1}

FR	L min^{-1}	5.00	5.10	5.20	5.30	5.40	5.50	5.60	5.70	5.80	5.90	6.00
AoP	mmHg	89.34	89.33	39.32	89.30	89.29	89.27	89.26	89.24	89.23	89.21	89.20
RAP	mmHg	2.07	2.06	2.04	2.03	2.01	2.00	1.98	1.97	1.95	1.94	1.93
PAP	mmHg	14.57	14.81	15.04	15.28	15.51	15.75	15.98	16.22	16.45	16.69	16.93
LAP	mmHg	2.07	2.06	2.04	2.03	2.01	2.00	1.98	1.97	1.95	1.94	1.93
QS	L min^{-1}	5.45	5.45	5.45	5.45	5.45	5.45	5.45	5.45	5.45	5.45	5.45
QP	L min^{-1}	5.00	5.10	5.20	5.30	5.40	5.50	5.60	5.70	5.80	5.90	6.00
QLL	L min^{-1}	0.55	0.55	0.55	0.55	0.55	0.55	0.55	0.55	0.55	0.55	0.55
QALR	L min^{-1}	−0.45	−0.35	−0.25	−0.15	−0.05	0.05	0.15	0.25	0.35	0.45	0.55

(B) RAA = 20 mmHg · L min^{-1}

FR	L min^{-1}	5.00	5.10	5.20	5.30	5.40	5.50	5.60	5.70	5.80	5.89	6.00
AoP	mmHg	91.53	91.03	90.54	90.04	89.55	89.05	88.56	88.06	87.57	87.07	86.58
RAP	mmHg	5.00	4.34	3.68	3.02	2.36	1.71	1.05	0.39	20.27	20.93	21.58
PAP	mmHg	9.33	10.72	12.11	13.50	14.88	16.27	17.66	19.05	20.44	21.82	23.21
LAP	mmHg	23.17	22.03	20.89	0.25	1.38	2.52	3.66	4.80	5.94	7.07	8.21
QS	L min^{-1}	5.41	5.42	5.43	5.44	5.45	5.46	5.47	5.48	5.49	5.50	5.51
QP	L min^{-1}	5.00	5.10	5.20	5.30	5.40	5.50	5.60	5.70	5.80	5.90	6.00
QLL	L min^{-1}	0.59	0.58	0.57	0.56	0.55	0.54	0.53	0.52	0.51	0.50	0.49
QALR	L min^{-1}	20.41	20.32	20.23	20.14	20.05	0.04	0.13	0.22	0.31	0.40	0.49

Improvement of ERTAH performance

Redesign of blood chambers and mock test for evaluation of basic performance of ERTAH

The results of the mock test using a Donovan-type mock circulatory system are shown in Box 3. When the pump speed increased, the AoP and pump output increased. The ERTAH operated at a driving rate of 68–166 rpm with a left cardiac output ranging from 2.5–6.3 L min^{-1} and a right cardiac output ranging from 2.4 to 5.8 L min^{-1}. Input power ranged from 19 to 36 W and output power ranged from 0.5 to 2.3 W, which varied according to the driving rate. The overall efficiency of the ERTAH was 2.6–6.4%. Cardiac output increased to about twice as much as in the old-type blood chambers, in spite of the smaller blood chambers. The overall efficiency of the ERTAH was improved by about 20% in comparison with the old-type blood chambers[7]. We deduced that the improvement was mainly dependent on the prevention of backward flow by modification of the form between the inlet and outlet ports. Moreover, its flow pattern changed from a pulsatile-like flow to an entirely nonpulsatile flow.

Box 3. Mock test for evaluation of basic performance of ERTAH

Driving rate (rpm)	68	88	141	166
AoP (mmHg)	82	107	112	138
PAP (mmHg)	17	18	21	25
Left CO (L min^{-1})	2.5	3.4	5.7	6.3
Right CO (L min^{-1})	2.4	3.0	5.0	5.8
Input power (W)	19	24	34	36
Output power (W)	0.5	0.9	1.7	2.3
Overall efficiency (%)	2.6	3.8	5.0	6.4
Left SV (mL)	37	39	40	38
Right SV (mL)	35	34	35	35

AoP: aortic pressure; PAP: pulmonary arterial pressure,
CO: output of the ERTAH, SV: stroke volume of the ERTAH.

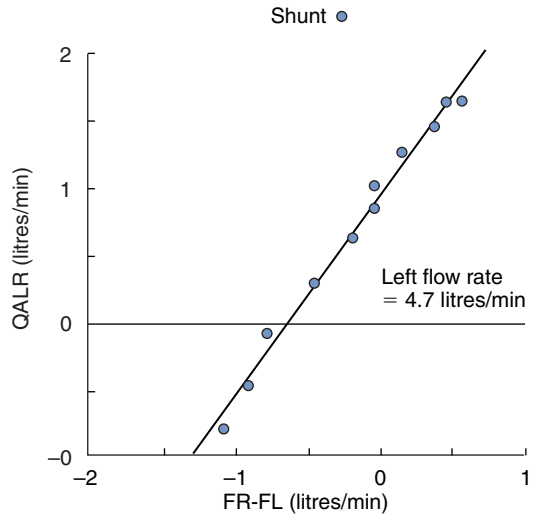

Figure 5. Interatrial shunt flow rate (QALR) versus right-to-left balance (FR–FL) in acute animal experiment. DeBakey roller pumps were used for simulation of the left–right balance of ERTAH. The flow of the left pump was almost constant (4.7 L min^{-1}). The flow of the right pump (FR) was approximately 4.1 L min^{-1} when the QALR was 0, allowing consideration that the LL shunt flow in the goat's heart was about 0.6 L min^{-1}.

In the durability test performed simultaneously, no problems were detected in the body of the ERTAH or in the blood chambers at 18 h. The results demonstrated an improvement in durability since a breakage of the sac had been detected at approximately 8 h in the previous blood chambers[7].

Animal experiment for implantation

The ERTAH operated at a driving rate of 160 rpm with a left cardiac output of 6.0 L min^{-1} and a right cardiac output of 5.4 L min^{-1}. The interatrial shunt flow rate was 250–400 mL min^{-1}. Hemodynamic parameters of LAP, RAP, PAP and AoP were kept within an acceptable physiological range (Figure 7). The animal experiment was terminated after 12 h of ERTAH operation.

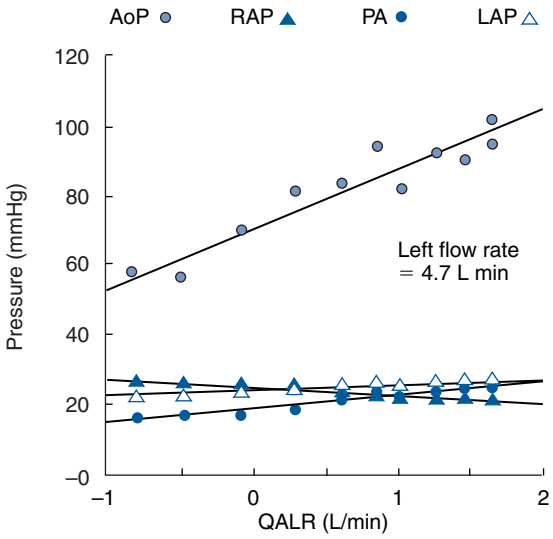

Figure 6. Pressure data (AoP, PAP, LAP, RAP) and interatrial shunt flow rate (QALR) in the acute animal experiment. An increase in the left-to-right shunting was associated with LAP, PAP, and AoP and a decrease in RAP

Discussion

Although there are many problems to be solved in developing the ERTAH, the advantages of this system are that it is simple and one of the most compact devices in the world (8 × 10 cm). The major problems encountered in developing the ERTAH were mechanical problems including its low performance as a blood pump, and a fixed flow balance between the left and right side that was controlled by the principle of a roller pump. In the current version of the ERTAH, the left–right flow balance is maintained by controlling differences in the volumes between the left and right chambers, and the device was operated for several hours in acute experiments. However, it may be limited to balancing with this method alone when working toward a completely implantable TAH[7–9]. An interatrial shunt was designed for balancing the left and right sides of the electrohydraulic TAH by the University of Utah[10–14]. Therefore, our attention focused on a method whereby an interatrial shunt could be set at the inlet side to achieve a left–right balance. Prior to trial manufacture of an ERTAH with an interatrial shunt, the actual LL shunt flow and effectiveness of the interatrial shunt on left–right balance, when this artificial heart was operated in nonpulsatile and at regular flow, was evaluated by means of a numerical simulation test. This was a mock test using DeBakey roller pumps and an acute animal experiment. In these series of simulations, the shunt flow through the bronchial arteries was approximately 500–600 mL min^{-1}, and positioning an interatrial shunt between the inlet ports seems useful for balancing.

Regarding the basic performance of the pump, the two modifications – downsizing of the blood chambers (although the basic configuration of the pump was not

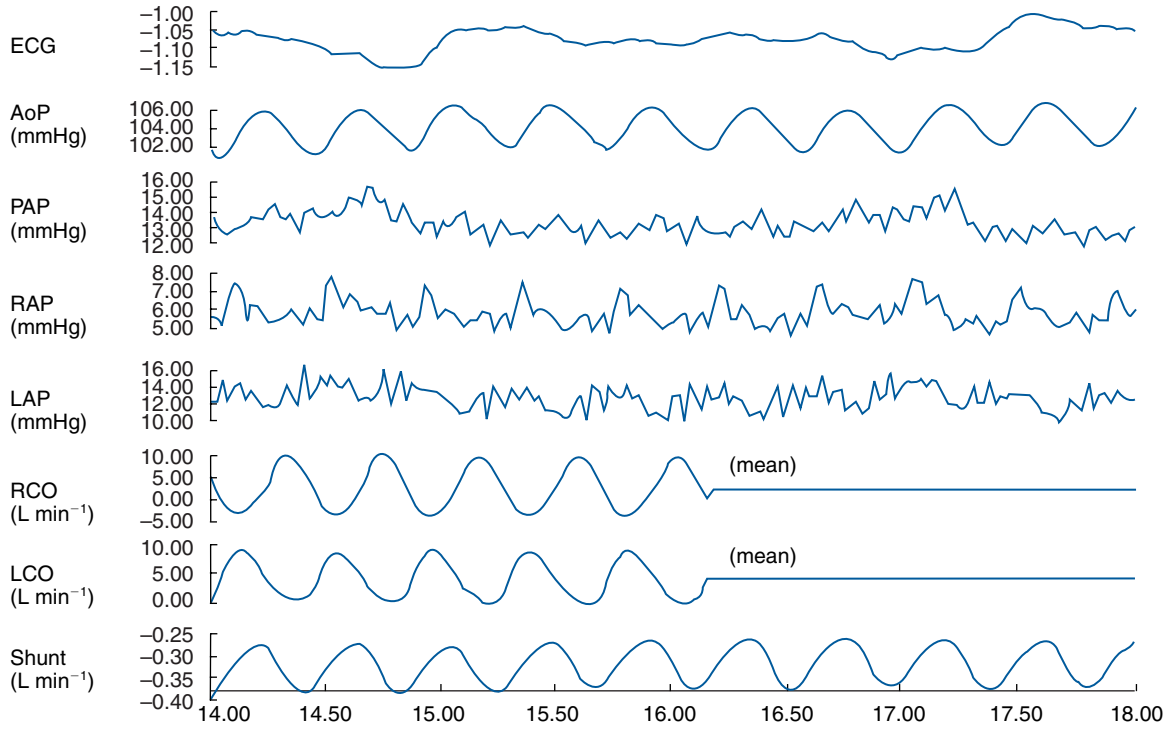

Figure 7. Hemodynamic parameters in acute animal experiment of the ERTAH. The ERTAH operated at a driving rate of 160 rpm with a left cardiac output of 5.4 L min^{-1} and the interatrial shunt flow rate was 250–400 mL min^{-1}.

modified), and redesigning the inlet and outlet ports to prevent regurgitation – resulted in the following:

1. A 20% increase of energy efficiency
2. About a two-fold increase in cardiac output
3. Improved durability compared with the previous type.

It is thought that the decrease of regurgitation primarily contributes to the improved basic performance. Although a maximal increase of energy efficiency of 6.4% was achieved, the possibilities are endless. To achieve this goal, it is necessary to incorporate seven features into the system:

1. Small size
2. Atraumatic features
3. Antithrombogenic features
4. Anti-infection features
5. A simple and durable design
6. Low energy requirement with easy controllability.

In a discussion, the following may be analyzed:

- Size
- Design
- Energy requirement
- Durability.

In other respects, this device leaves some problems to be resolved. Especially in the atraumatic features, the increase of serum potassium level due to hemolysis, which is characteristic of roller pumps, has not been assessed and is not satisfactory at this stage.

We are planning further improvements, including employment of a different material for the sac, such as polyurethane, and a more effective motor. Furthermore, waterproofing of the system needs to be realized for a totally implantable artificial heart.

Acknowledgements

The authors are indebted to Mr Shinsaku Koguchi (President of Eba Machinery Works Co., Ltd., Hiroshima, Japan) for fabrication of the device. This work was supported in part by a Research Grant for Cardiovascular Disease 10C-2 from the Ministry of Health and Welfare in Japan.

References

1. Fukunaga S, Hamanaka Y. Implantable motor-driven artificial heart. In: Akutsu T, editor. *Artif Heart* 2. Tokyo: Springer-Verlag, 1998:343–349.
2. Fukunaga S, Hamanaka Y. An artificial heart using an ultrasonic motor. *Artif Organs Today* 1999;1:237–43.
3. Koura Y. Study of a pendulum swing type total artificial heart. *Artif Organs Today* 1995;5:65–77.
4. Matsuura Y, Fukunaga S. Past, present, and future of total artificial heart developments at Research Institute of Replacement Medicine. Hiroshima University School of Medicine. *Artif Organs* 1996;20:1073–92.

5. Matsuura Y, Tamura M. On our total artificial heart. *Jpn J Surg* 1972;34:1055–62.
6. Sueshiro M, Fukunaga S. Study of electromagnetic total artificial heart. Papers of Technical Meeting on Linear Drive, Institute of Electrical Engineers, Japan 1995;LD–95–68:29–35.
7. Sueshiro M, Fukunaga S. Eccentric roller type total artificial heart designed for implantation. *Artif Organs* 1998;22:451–7.
8. Sueshiro M, Fukunaga S. Trial manufacture of eccentric roller type total artificial heart. *Artif Organs* 1997;21:735–8.
9. Wada H, Fukunaga S. Flow balance between the left and right cardiac output of an eccentric roller type total artificial heart. *Artif Organs* 1999;23:741–6.
10. Crump KR, Khanwilkar PS. *In vitro* analysis of an atrial shunt in balancing an electrohydraulic total artificial heart. *Trans Am Soc Artif Intern Organs* 1990;36:254–7.
11. Kinoshita M, Hansen CA. Determination of atrial shunt size needed to balance an electrohydraulic total artificial heart. *Trans Am Soc Artif Intern Organs* 1991;37:264–5.
12. Long JW, Khanwilkar PS. Right left ventricular balance in implanted electrically powered artificial hearts. *Trans Am Soc Artif Intern Organs* 1990;36:287–90.
13. Olsen DB, Long JW. Simplified right-left balance for the implanted artificial heart. In: Akutsu T, Koyanagi H, editors. *Heart Replacement – Artificial Heart* 3. Tokyo: Springer-Verlag. 1990:235–243.
14. Tatsumi E, Diegel PD. A blood pump with an interatrial shunt for use as an electrohydraulic artificial heart. *Trans Am Soc Artif Intern Organs* 1992;38:425–30.

Session 4
Pathophysiology

Journal of Congestive Heart Failure and Circulatory Support (2001) Vol 1, No 4, 229–233

Changes in heart rate variability during long-term left ventricular assist in normal goats

T. Nishinaka MD[1], E. Tatsumi[1], Y. Taenaka[1], T. Nishimura[1], K. Shioya[1], H. Takano[1] and H. Koyanagi[2]
[1]Department of Artificial Organs, National Cardiovascular Center, Osaka, Japan; and [2]Department of Cardiovascular Surgery, Tokyo Women's Medical University, Tokyo, Japan

Background Implantation of a left ventricular assist device (LVAD) in patients with severe heart failure has been reported to improve their heart rate variability (HRV). However, the pure effect of an LVAD on HRV has not been clarified. The purpose of this study is to elucidate the effects of LVAD on HRV in a chronic animal study using normal goats.

Method A pulsatile LVAD was implanted in five healthy goats and driven for 6 weeks. Three-minute data of R-R intervals were acquired on the day before, and then at 2, 4, and 6 weeks after implantation. Data were analyzed by maximum entropy spectral analysis and the least squares method, and then used to evaluate the following: mean R-R intervals, power of the low-frequency band (0.04–0.15 Hz; LF), power of the high-frequency band (0.15–0.40 Hz; HF), normalized units of LF and HF (indicators of relative power of LF and HF; LFnorm and HFnorm) and LF/HF.

Results and discussion Bypass flow and mean aortic pressure results were consistent. The mean R-R intervals showed a slight tendency to increase after LVAD implantation, though recovery to preoperative levels was seen 6 weeks after implantation. LF and LF in a normalized unit both showed a tendency to decrease. HF and HF in a normalized unit also showed a decreasing tendency, while LF/HF showed an increasing tendency. In summary, long-term LVAD applied to normal goat hearts was found to exert suppression of HRV. Interpretation of changes in HRV during LVAD support requires great caution.

Keywords nonpulsatile circulation, left heart bypass, autonomic nervous function, heart rate variability (HRV).

Introduction

Spectral analysis of heart rate variability (HRV) is a widely used noninvasive technique for assessing autonomic nervous indices of neural cardiac control[1–5]. The power of low-frequency (LF) and high-frequency (HF) bands are two major parameters of HRV. LF, with a frequency band of 0.04–0.15 Hz, reflects sympathetic and parasympathetic nervous influence, though their balance is dependent on other conditions as well. HF, with a frequency band of 0.15–0.40 Hz, reflects parasympathetic nervous influence[1]. HRV is currently widely used in clinical medicine. For example, depressed HRV is a powerful predictor of mortality in a patient after acute myocardial infarction[6–8] and is observed in congestive heart failure patients[9–11]. It can also be used to explore the influences of various agents on the cardiac autonomic nervous activity. Improvement of HRV is observed with effective ß-blocker and/or angiotensin-converting enzyme inhibitor treatment in congestive heart failure patients[12–14]. Implantation of a left ventricular assist device (LVAD) in patients with severe heart failure improves their neurohormonal and cardiac autonomic nervous condition by alleviating hemodynamic disturbance, therefore it is also expected to improve their HRV results[15,16]. However, the effect of long-term LVAD usage on the HRV and its mechanism in patients with severe heart failure remains poorly understood. Even the pure effect of long-term LVAD usage on the HRV has not been clarified, though the mechanical properties of interposed cardiopulmonary structures such as LVAD might exert some influence on HRV through blood pressure wave modulation[17]. The purpose of this study is to elucidate the effects of LVAD on HRV in a chronic animal study using normal goats.

Materials and methods

Five healthy goats weighing 44–61 kg were used. Under general anesthesia with isoflurane and nitrous oxide, the chest was opened at the fifth costal bed. A left heart bypass was instituted between the left atrium and the aorta with uptake and return cannulae, and a pulsatile ventricular assist device (VAD) (Toyobo, Osaka, Japan)[18] was implanted and then driven for six weeks at 60 bpm. Electrocardiogram (ECG) results were continuously recorded. Between 11:00 a.m. and 3:00 p.m., 3-minute data of the R-R intervals were acquired the day before, and at two, four, and six weeks after LVAD implantation (Before, 2W, 4W, and 6W, respectively). All animals were cared for by a veterinarian, in accordance with the National Academy of Sciences' *Principles of Laboratory Animal Care and Use of*

Correspondence to: Tomohiro Nishinaka, Department of Artificial Organs, National Cardiovascular Center Research Institute, 5–7–1 Fujishirodai, Suita, Osaka 565–8565, Japan.

Laboratory Animals, published by the US National Institutes of Health (NIH).

Maximum entropy spectral analysis and the least squares method (MemCalc)[19] were then employed to obtain the following parameters representing cardiac autonomic nervous function:

1. Mean R-R intervals
2. Power of low frequency band between 0.04 and 0.15 Hz (LF)
3. LF power in normalized unit (LFnorm: LF/total power – very low frequency band under 0.15 Hz power)
4. Power of high frequency band between 0.15 and 0.40 Hz (HF)
5. HF power in normalized unit (HFnorm: HF/total power – very low frequency band under 0.15 Hz power)
6. Ratio of LF to HF (LF/HF).

LF and LFnorm reflect sympathetic and parasympathetic nervous influence, while HF and HFnorm reflect parasympathetic nervous influence. LF/HF generally indicates the balance of the two branches of the cardiac autonomic nervous systems[1]. We also measured mean aortic pressure (mAoP), along with plasma levels of norepinephrine (NE), vasopressin (VP), renin activity (RA), endothelin-I (ET-I), and hemoglobin (Hb). Plasma NE levels were measured by high-pressure liquid chromatography, while VP, RA, and ET-I levels were measured by a radioimmunoassay method. Bypass flow (BF) was measured with electromagnetic flowmeters (MF-2100, Nihon-Koden, Tokyo, Japan). The pump flow was regulated to maintain a consistent mAoP and BF. To obtain normal controls (Control), same parameters were measured in 20 normal healthy goats. The average values were then compared between Control, Before, 2W, 4W, and 6W. Comparisons of the measured parameters were made using analyses of variance. Values of $P<0.05$ were considered statistically significant.

Results

The experiments were carried out under the conditions shown in Table 1. mAoP could be maintained from 98 to 113 mmHg, and there were no significant differences between Control, Before, 2W, 4W, and 6W. Bypass flow during LVAD support was from 75 to 80 mL/min 1kg, and there were no significant differences between 2W, 4W, and 6W. Hemoglobin levels were from 8.8 to 11.0 g/dL, and no anemia was observed. Vasoactive hormone levels are shown in Table 2; no significant differences were observed between Control, Before, 2W, 4W, and 6W for NE, VP, and ET-I. However, RA had a tendency to increase at 6W.

The mean R-R intervals showed a slight increasing tendency after LVAD implantation; however, they recovered to preoperative levels at 6W (Figure 1). LF had an increasing tendency at 4W, but decreased remarkably at 6W (Figure 2). LFnorm showed a slight decreasing tendency (Figure 3), while HF decreased remarkably at 6W. The HF levels at 6W were lower than those of Control ($P<0.05$) (Figure 4). HFnorm also showed a tendency to decrease during LVAD support (Figure 5), while LF/HF showed an increasing tendency (Figure 6).

Discussion

The findings of our study revealed that LF, HF, and their normalized units had a tendency to decrease, while LF/HF had a tendency to increase during LVAD support. These results might indicate a suppression of cardiac parasympathetic nervous influence, and a relative domination of cardiac sympathetic elements over parasympathetic nervous elements. In the present study, both LF and HF were depressed at 6W. However, other previous reports concerning implantation of an LVAD in congestive heart failure patients

Table 1. Hemodynamic conditions of the experiment

	Control	Before	2W	4W	6W
Mean aortic pressure (mmHg)	97±4	98±7	101±11	100±8	113±6
Bypass flow (mL/min/kg)	–	–	75±7	77±6	80±6
Hemoglobin (g/dL)	9.6±0.3	8.8±0.3	9.4±0.6	10.8±0.3	11.0±0.5

Values are means ± standard error (SE). Control, normal controls; Before, before implantation of LVAD; 2W, 4W and 6W, at the end of 2, 4, and 6 weeks after LVAD implantation, respectively.

Table 2. Vasoactive hormone levels

	Control	Before	2W	4W	6W
Norepinephrine (ng/mL)	0.2±0.1	0.1±0	0.2±0	0.3±0.1	0.2±0.1
Vasopressin (pg/mL)	0.9±0.1	0.9±0.1	0.6±0.1	0.9±0.1	0.6±0.1
Endothelin (pg/mL)	2.4±0.2	1.9±0.2	2.1±0.5	2.9±0.3	2.6±0.6
Renin activity (ng/mL/h)	0.8±0.3	0.4±0.1	0.5±0.1	1.1±0.5	1.5±0.4

Values are means ± standard error (SE). Control, normal controls; Before, before implantation of LVAD; 2W, 4W and 6W, at the end of 2, 4, and 6 weeks after LVAD implantation, respectively.

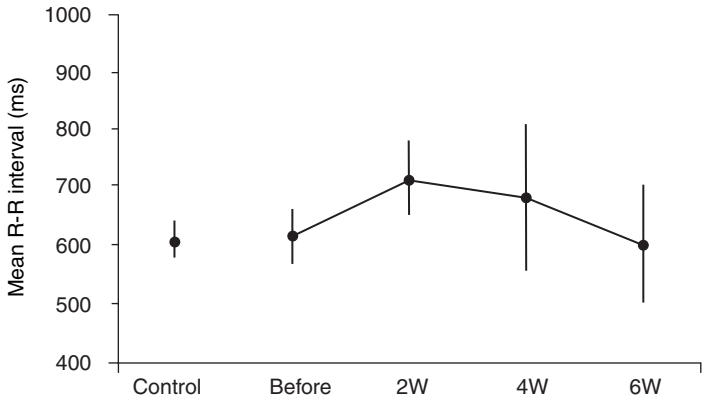

Figure 1. Changes in mean R-R intervals. Mean R-R intervals showing a slight increasing tendency after LVAD implantation and then recovering to preoperative levels at 6W. Bars indicate means ± SE. Control, normal controls; Before, before implantation of LVAD; 2W, 4W, and 6W, at the end of 2, 4, and 6 weeks after LVAD implantation, respectively.

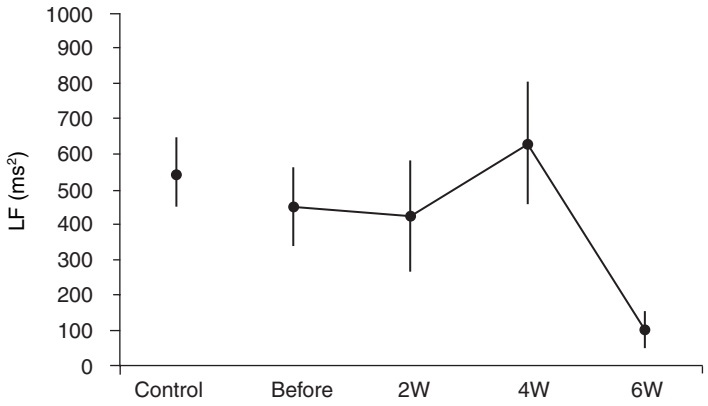

Figure 2. Changes in LF. LF with an increasing tendency at 4W, and then decreasing remarkably at 6W. Bars indicate means ± SE. Control, normal controls; Before, before implantation of LVAD; 2W, 4W, and 6W, at the end of 2, 4, and 6 weeks after LVAD implantation, respectively.

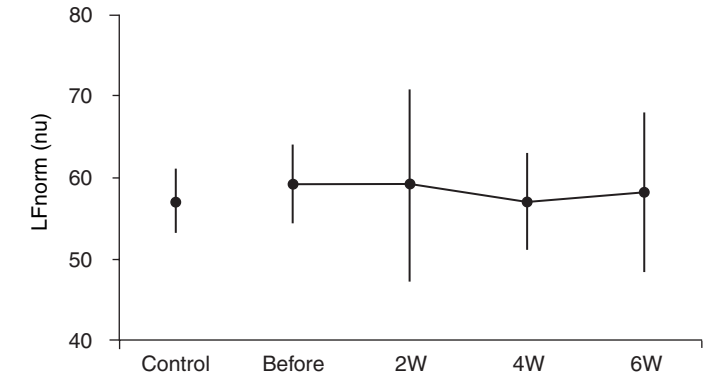

Figure 3. Changes in LFnorm. LF in normalized unit showing a slight decreasing tendency. Bars indicate means ± SE. Control, normal controls; Before, before implantation of LVAD; 2W, 4W, and 6W, at the end of 2, 4, and 6 weeks after LVAD implantation, respectively.

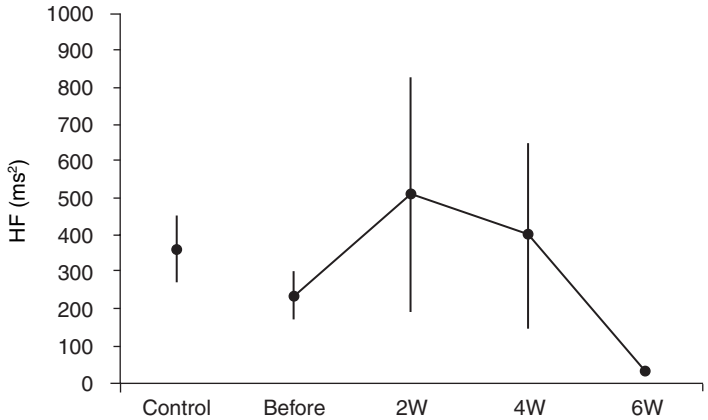

Figure 4. Changes in HF. HF is shown decreasing remarkably at 6W. HF levels at 6W were less than the normal controls (P<0.05). Bars indicate means ± SE. Control, normal controls; Before, before implantation of LVAD; 2W, 4W and 6W, at the end of 2, 4 and 6 weeks after LVAD implantation, respectively.

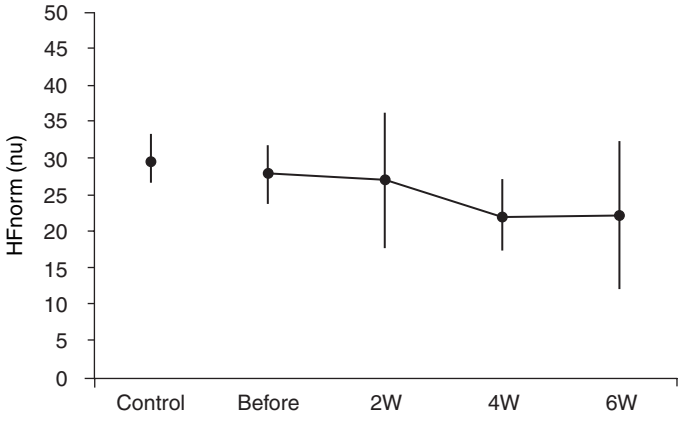

Figure 5. Changes in HFnorm. HF in normalized unit showing a decreased tendency during LVAD support. Bars indicate means ± SE. Control, normal controls; Before, before implantation of LVAD; 2W, 4W and 6W, at the end of 2, 4 and 6 weeks after LVAD implantation, respectively.

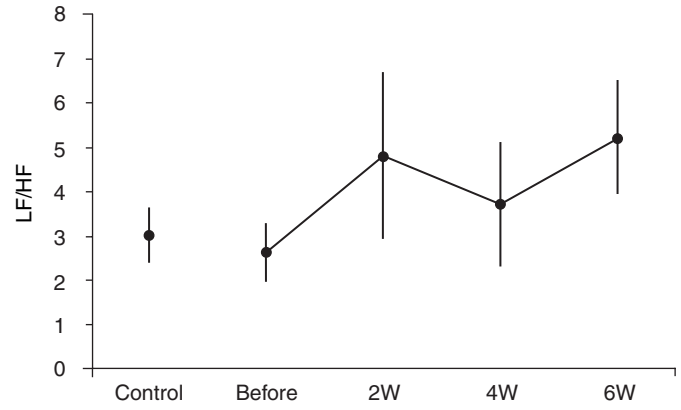

Figure 6. Changes in LF/HF. LF/HF showing an increasing tendency. Bars indicate means ± SE. Control, normal controls; Before, before implantation of LVAD; 2W, 4W and 6W, at the end of 2, 4 and 6 weeks after LVAD implantation, respectively.

noted an improvement of LF, though the HF results did not correspond[15,16]. Long-term LVAD in goats with normal hearts exerted a different influence on HRV from that seen in severely affected heart failure patients. Considering the results of the present study, we speculated on whether a long-term LVAD implant in an animal with a normal heart would have a negative effect on hemodynamics. Then it is possible that LVAD support has a negative effect in well-recovered heart patients during the time of LVAD support. Furthermore, HRV might contribute to determining the optimal amount of device control. However, this interpretation includes some doubts. Heart failure patients have a large amount of hormonal derangement and it is supposed that they have depressed HRV. However, in our results, there was no remarkable hormonal derangement found, except for renin, and no low systemic perfusion.

We further speculated as to why depressed HRV was observed. The genesis of LF oscillation in HRV has two constructs: one is the baroreflex response to Mayer waves and buffering of HF oscillation, and the other is central rhythmic modulation of neural activity[20–23]. In heart failure patients, depressed LF oscillation is thought to be caused by depressed central nervous rhythmic modulation owing to activated neurohormonal factors. For this reason, the results of the present study require another mechanism for the depressed LF oscillation of HRV seen in heart failure patients. It is assumed that the HF oscillations are caused by respiratory blood pressure waves[24–28]. It has also been reported that respiration-induced changes in blood pressure are reduced as a result of mechanical properties of interposed cardiopulmonary structures such as an LVAD[17]. The depressed HF oscillation of HRV in the present study does not necessarily signal a suppression of parasympathetic influence, but might reflect a reduction of respiratory blood pressure waves caused by the LVAD. Interpretation of changes in HRV during LVAD support requires great caution and further study will be needed, especially concerning the relationship between HRV and blood pressure variability. However, LVAD-supported circulation provides a unique opportunity to investigate the mechanisms of HRV neural regulation.

Conclusion

1. Long-term LVAD implantation in goats with normal hearts exerted suppression of HRV.
2. Interpretation of changes in HRV during LVAD support requires great caution and further study will be needed.

Acknowledgments

This work was financially supported, in part, by a Research Grant for Cardiovascular Diseases (10C–2) from the

Ministry of Health and Welfare of Japan, by Grants-in Aid for Scientific Research from the Ministry of Education of Japan (No. 10470280 and No. 11470279), and by Japan Science and Technology Corporation.

References

1. Task force of the European Society of Cardiology and the North American Society of Pacing and Electrophysiology. Heart rate variability. Standards of measurements, physiological interpretation, and clinical use. *Circulation* 1996;93:1043–65.
2. Hayano J, Sakakibara Y, Yamada A *et al*. Accuracy of assessment of cardiac vagal tone by heart rate variability in normal subjects. *Am J Cardiol* 1991;67:199–204.
3. Pomeranz B, Macaulay RJB, Caudill MA *et al*. Assessment of autonomic function in humans by heart rate spectral analysis. *Am J Physiol* 1985;248:H151–3.
4. Malliani A, Pagani M, Lambarni F, Cerutti S. Cardiovascular neural regulation explored in the frequency domain. *Circulation* 1991;84:482–92.
5. Malliani A, Lombardi F, Pagani M. Power spectrum analysis of heart rate variability: a tool to explore neural regulatory mechanisms. *Br Heart J* 1994;71:1–2.
6. Kleiger RE, Miller JP, Bigger JT, Mossv AJ, and the Multicenter Post-Infarction Research Group. Decreased heart rate variability and its association with increased mortality after acute myocardial infarction. *Am J Cardiol* 1987;59:256–62.
7. Bigger JT Jr, Fleiss JL, Steinman RC, Rolnnitzky LM, Kleiger RE, Rottman JN. Frequency domain measures of heart period variability and mortality after myocardial infarction. *Circulation* 1992;85:164–71.
8. Odemuyiwa O, Malik M, Farrell T, Bashir Y, Poloniecki J, Camm J. Comparison of the predictive characteristics of heart rate variability index and left ventricular ejection fraction for all-cause mortality, arrhythmic events and sudden death after acute myocardial infarction. *Am J Cardiol* 1991;68:434–9.
9. Saul JP, Arai Y, Berger RD, Lilly LS, Colucci WS, Cohen RJ. Assessment of autonomic regulation in chronic congestive heart failure by heart rate spectral analysis. *Am J Cardiol* 1988;61:1292–9.
10. Binkley RF, Nunziata E, Haas GJ, Nelson SD, Cody RJ. Parasympathetic withdrawal is an integral component of autonomic imbalance in congestive heart failure: demonstration in human subjects and verification in a paced canine model of ventricular failure. *J Am Coll Cardiol* 1991;18:464–72.
11. Kienzle MG, Ferguson DW, Birkett CL, Myers GA, Berg WJ, Mariano DJ. Clinical hemodynamic and sympathetic neural correlates of heart rate variability in congestive heart failure. *Am J Cardiol* 1992;69:482–5.
12. Townend JN, West JN, Davies MK, Littler WA. Effect of quinapril on blood pressure and heart rate in congestive heart failure. *Am J Cardiol* 1992;69:1587–90.
13. Binkley PF, Haas GJ, Starling RC *et al*. Sustained augmentation of parasympathetic tone with angiotensin converting enzyme inhibition in patients with congestive heart failure. *J Am Coll Cardiol* 1993;21:655–61.
14. Goldsmith RL, Bigger JT, Bloomfield DM *et al*. Long-term carvedilol therapy increases parasympathetic nervous system activity in chronic congestive heart failure. *Am J Cardiol* 1997;80:1101–4.
15. Kim SY, Montoya A, Zbilut JP *et al*. Effect of HeartMate left ventricular assist device on cardiac autonomic nervous activity. *Ann Thorac Surg* 1996;61:591–3.
16. Cooley RL, Montano N, Cogliati C *et al*. Evidence for a central origin of the low-frequency oscillation in RR-interval variability. *Circulation* 1998;98:556–61.
17. Triedman JK, Saul JP. Blood pressure modulation by central venous pressure and respiration. Buffering effects of the heart rate reflexes. *Circulation* 1994;89:169–79.
18. Takano H, Nakatani T, Taenaka Y, Umezu M. Development of the ventricular assist pump system. Experimental and clinical studies. In: Akutsu T, Koyanagi H, editors. *Heart Replacement: Artificial Heart 1*. Tokyo:Springer-Verlag, 1986:141–50.
19. Ohtomo N, TanakaY. New method of time series analysis and MemCalc. In: Saitoh K, Koyama A, Yoneyama K, Sawada Y, Ohtomo N, editors. *A Recent Advance in Time Series Analysis by Maximum Entropy Method*. Sapporo:Hokkaido University Press, 1994:11–29.
20. DeBoer RW, Karemaker JM, Strackee J. Hemodynamic fluctuations and baroreflex sensitivity in humans: a beat-to-beat model. *Am J Physiol* 1987;253:H680–9.
21. Saul JP, Berger RD, Chen MH, Cohen RJ. Transfer function analysis of autonomic regulation. II. Respiratory sinus arrhythmia. *Am J Physiol* 1989;256:H153–61.
22. Sleight P, La Rovere MT, Mortara A *et al*. Physiology and pathophysiology of heart rate and blood pressure variability in humans: is power spectral analysis largely an index of baroreflex gain? *Clin Sci* 1995;88:103–9.
23. Preiss G, Polosa C. Patterns of sympathetic neuron activity associated with Mayer waves. *Am J Physiol* 1974;226: 724–30.
24. Akselrod S, Gordon D, Madwed JB, Snidman NC, Shannon DC, Cohen RJ. Hemodynamic regulation: investigation by spectral analysis. *Am J Physiol* 1985;249:H867–75.
25. Toska K, Eriksen M. Respiration-synchronous fluctuations in stroke volume, heart rate and arterial pressure in humans. *J Physiol* 1993;472:501–12.
26. Scheffer GJ, TenVoorde BJ, Karemaker JM, Ros HH. Effects of epidural analgesia and atropine on heart rate and blood pressure variability: implications for the interpretation beat-to-beat fluctuations. *Eur J Anaesthesiol* 1994;11:75–80.
27. Bernardi L, Leuzzi S, Radaelli A, Passino C, Johnston JA, Sleight P. Low-frequency spontaneous fluctuations of R-R interval and blood pressure in conscious humans: a baroreceptor or central phenomenon? *Clin Sci* 1994;87:649–54.
28. Piepoli M, Sleight P, Leuzzi S *et al*. Origin of respiratory sinus arrhythmia in conscious humans. An important role for arterial carotid baroreceptors. *Circulation* 1997;95:1813–21.

Journal of Congestive Heart Failure and Circulatory Support (2001) Vol 1, No 4, 235–248

Pathophysiological study of the heterotopic experimental cervical allotransplantation of the canine heart

J. Vaŝkû MD DSC[1] and P. Dobŷák MD PhD[2]
[1]VACORD Bioengineering Research Co., BRNO-Husovice, Cacovická, Czech Republic; and [2]CFDR, St. Anna Faculty Hospital and Masaryk University, BRNO-Husovice, Cacovická, Czech Republic

Abstract Heterotopic cervical heart allotransplantions were carried out in 35 dogs. The authors studied the response of the recipient and the function of the transplant without any immunosuppressive therapy.

The donor's heart was taken in the form of an isolated heart–lung preparation being maintained during the transplantation by its own circulatory system.

The recipient's response to the transplant was clinically markedly expressed. In the allotransplant, the first signs of rejection appeared from the second postoperative day. The transplanted heart and recipient's heart displayed different degrees of metabolic damage. Morphologically, edema, hemorrhage, fragmentation of the tissue fibers and the changes of stainability were observed both in the graft and in the recipient. The mononuclear mixed infiltration was conspicuous.

The occurrence of the Anitschkow's caterpillar cells in the heart of the recipient proved the presence of the myocardial immunologic lesion; this was an outstanding finding.

Keywords heterotopic allotransplantation, rejection, autoimmune reaction of the recipient.

Introduction

From the beginning, our work on mechanical heart assist devices and the total artificial heart was accompanied by basic research dedicated to heart transplantation[1–5]. We have dealt with problems related to experimental isotopic, and auto- and allotransplantation of the heart[6–8]. Our first experiments with isotopic allotransplantation exhibited a remarkable percentage of early death after surgery due to failure of the graft for various reasons. A very unfavourable factor influencing the results of the isotopic transplantation in dogs was the need for a long-term bypass, which these animals endured with great difficulty. We found cerebral lesions, disturbances of hemocoagulation leading to diffuse hemorrhages after the surgery, and other complications. Rejection is a complex problem and our goal was to define it by its clinical course, electrocardiogram (ECG) and laboratory examinations, and further by postmortem biochemical analysis of the heart graft. Finally its histopathological evaluation and more developed steps of rejection, without the influence of immunosuppression therapy, were taken into account. For this reason we chose the study of the heterotopically localized heart allotransplant connected to the cervical vessels of the recipient. Thus, we availed ourselves of a method that permits maintenance of the transplant in its full functional state, enabling us to study all parameters of interest. Simultaneously, great attention was given to the reaction of the recipient with its own intact heart to the presence and function of another foreign heart that was connected to its vasculatory system [9–11]. Some authors studied this problem years ago in similar ways [12,13]. Thus, the main focus of our study was the behavior of the allotransplant and, simultaneously, the recipient's reaction to it, which is an absolutely unusual situation for the recipient. Attempts were made to use the biological heart allotransplant as an auxiliary organ, leaving the sick heart *in situ* in the chest cavity. Also for this reason the elaboration of such experiments and their pathophysiological evaluation can bring more clarification to the remarkable reactions of the recipient, which are partially reflected in the function and pathological changes of its own heart.

Materials and methods

The experiments were performed on 35 dogs as recipients; 35 other dogs served as donors. The body weight of donors varied between 8 and 12 kg, while that of the recipients was 18–20 kg. In 18 animals the heart was transplanted directly; in 17 animals after conservation for 3 h in the physiological solution at 32ºC. From 18 allografts that were directly transplanted, 15 were functional; from 17 allografts that were transplanted after the conservation, the same number, i.e. 15 grafts, showed a sufficient function. Altogether 30 transplants were functional from 1–13 days. Three allografts in the group of directly transplanted hearts and two grafts after conservation did not start their pumping function, either due to bleeding from the anastomoses or due to obturation of the vessels after the surgery. In total, 30

Correspondence to: Professor Jaromír Vaŝkû, VACORD Bioengineering Research Co., 614 00 BRNO-Husovice, Cacovická 53, Czech Republic.

grafts were evaluated. The function of the transplant was followed by the ECG recording, the recording of pressure in the left ventricle and the general clinical reaction of the recipient to the transplanted heart. When the transplanted heart ceased its function, the experiment was terminated by sacrificing the recipient. Figure 1 shows the explanted heart–lung preparate.

Surgical procedure

The animals were anesthetized with 5% thiopental and after intubation kept anesthetized with a mixture of oxygen and ether. A polyethylene tube was introduced into the femoral artery of all animals to register the systemic blood pressure. Another tube was introduced into the femoral vein for taking samples for hematological and biochemical examinations, for supplying blood and fluids, and for the administration of medication. Figure 2 shows the isolated heart–lung preparate after it was removed from the donor's chest.

We took the hearts of the donors in the form of an isolated heart–lung preparation[9–11]. Thereafter, bilateral thoracotomy was performed through the fourth intercostal space whereupon the heart of the donor was gradually isolated and the brachiocephalic truncus, the left subclavian artery, the inferior vena cava, the descending aorta below the origo of the subclavian artery and finally the superior vena cava were ligated and transsected. This done, the left lung was removed and a polyethylene tube was introduced into the descending stump of the aortic arch. This tube was connected with the stabilizing reservoir and with a pressure chamber with the aid of a two-way cock for the registration of blood pressure in the preparate. After transsection of the trachea the polyethylene tube was introduced into the distal stump of the trachea to be connected with the respirator and the heart–lung preparate was withdrawn from the thorax *en bloc*. This preparate was either transferred directly to another surgical table, where the recipient was ready, or into the reservoir with physiological (saline) solution at the temperature of 32ºC, where it was stored for 3 h. During suturing, the lung preparate was ventilated with the aid of a respirator; the preparate was kept up with its own blood circulatory system. The graft was fixed using the modified Lillehei technique described previously by Mann *et al*[14, 15].

In the left side of the recipient's neck, a wide subcutaneous pocket was formed; the left external jugular vein was prepared and arteria carotis communis was isolated. After the transsection of the recipient's arteria carotis communis, the anastomosis between the proximal stump of the recipient's arteria carotis communis and the donor's brachiocephalic trunc was performed (Figure 3). Further, the anastomosis between the distal stump of arteria carotis

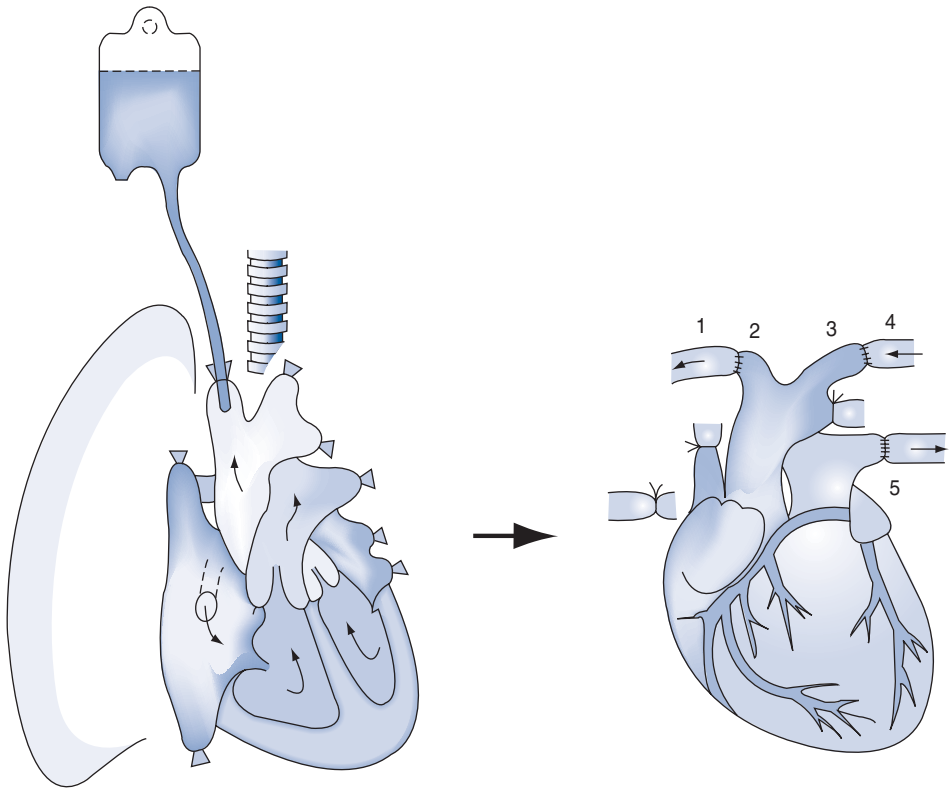

Figure 1. (Left) Schematic drawing of the explanted heart–lung preparate. (Right) the schematic drawing of the suturing of the transplant to the recipient's neck is shown. 1, 2: anastomosis between recipient's proximal stump of arteria carotis communis and donor's truncus brachiocephalicus. 3, 4: anastomosis between recipient's distal stump of arteria carotis communis and donor's arteria subclavia. 5: anastomosis between vena jugularis externa and the donor's right branch of the pulmonary artery.

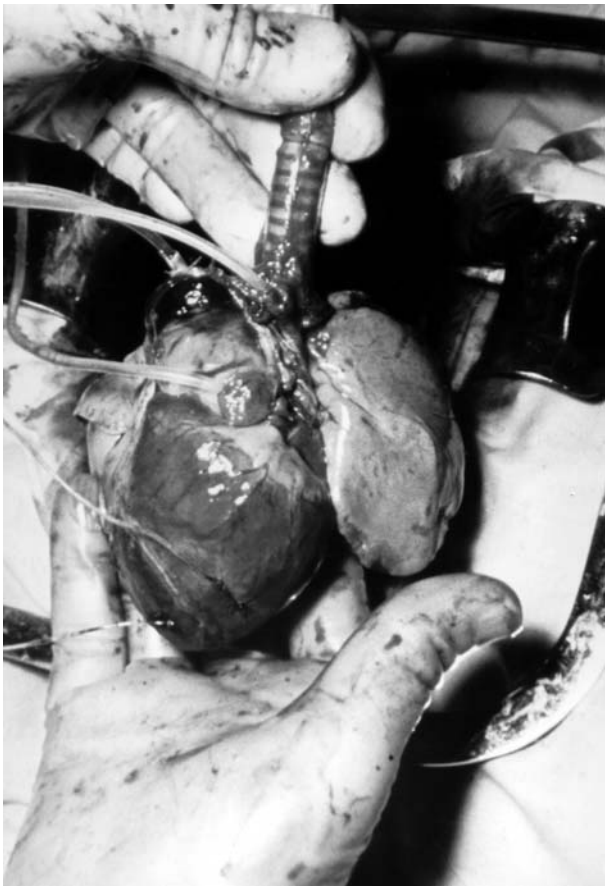

Figure 2. Isolated heart–lung preparate after withdrawal from the chest of the donor.

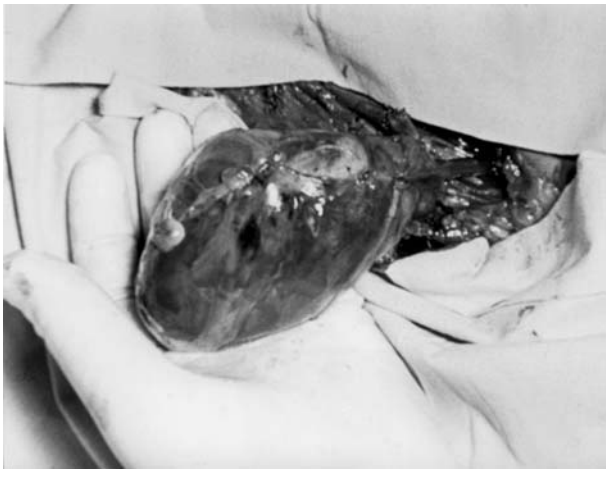

Figure 3. Anastomosis between the proximal stump of the recipient's arteria carotis communis and the donor's truncus brachiocephalicus. An anastomosis between the distal stump of the recipient's arteria carotis communis and the arteria subclavia of the allograft is shown. Finally, the anastomosis between the recipient's external jugular vein and the right branch of the donor's pulmonary artery is shown.

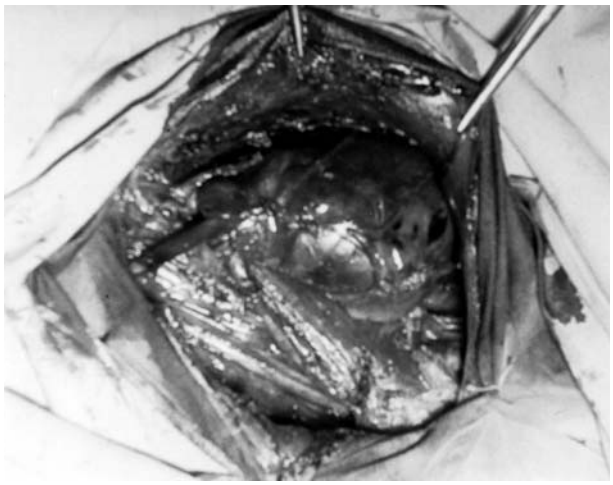

Figure 4. Cervical pocket in the left side of the recipient's neck with the heart allograft *in situ*.

Figure 5. The heart allotransplant situated on the neck of the recipient after the surgery has been finished.

communis of the recipient and subclavian artery of the transplant was performed. Finally, the anastomosis between the recipient's left external jugular vein and the donor's right branch of the pulmonary artery was performed.

This done, the cervical pocket in the left side of the neck of the recipient was closed (Figure 4). Figure 5 shows the postoperative state of the recipient with heart allotransplant situated on the neck. In the postoperative course, we followed the pressure in the left ventricle and in the right atrium of the graft, and these values together with ECG recording by means of a four-channel mingograph were registered. Blood samples were taken every day from the recipient's vein for biochemical and hematological examinations after the surgery. The animals were given only conventional medication after every major surgery, and no measures were taken to prolong the life of the graft through intensive postoperative care, nor were immunosuppressive substances administered. The transplant function was studied

until its activity was terminated, and after its withdrawal, the tissue samples were taken for biochemical and histological analyses. Simultaneously, the recipient was sacrificed by deep anesthesia and its organ samples were taken for biochemical and histological examination. Special attention was paid to the electrolyte composition and histopathological state of the heart tissue of both the graft and the recipient's heart.

Results

Survival time of the graft and complications

Out of a total of 35 dogs, 30 were evaluated. A comparative evaluation was performed of the group with the fresh, directly transplanted hearts and the group with the hearts after conservation. The graft survival time in both groups was conjointly evaluated.

In four dogs the transplant survived for 1 day, in one dog it survived 2 days, in three dogs it survived 3 days, in six dogs the graft ceased to function on the fourth day after surgery, in eight dogs the transplant was functional up to 5 days, and in six dogs the transplant was fully functional up to 6 days. One graft was active up until 10 postoperative days, while one ceased to function on the thirteenth postoperative day. Thus, the majority of graft rejection was situated between the fourth and sixth days after surgery in both groups. The longest survival of the directly implanted heart was 13 days, whereas the longest survival of the previously conserved allotransplant was 6 days.

In three cases of the experiments on the 35 dogs a technical failure was involved (bleeeding from the anastomoses), and two recipient dogs died immediately after surgery. Therefore, these animals were excluded from the evaluation. In the majority of dogs, the implanted heart continued its normal function in sinus rhythm after loosening of the vessel clamps. It was rarely necessary to restore the graft function through defibrillation.

Function of the allograft

The function of the transplanted heart was tested preponderantly through palpation in the cervical region of the recipient by ECG recording and by measuring the pressure in the left ventricle. As a rule, the significant finding in the subcutaneous pocket, which was aspirated by punction, was a hemorrhagic exudate from the second day after transplantation. Postoperatively, the transplant increased in volume as a result of fluid accumulation in the pericardial sac and the heart contractility gradually diminished.

The mean pressure in the left ventricle of the graft after the withdrawal of the preparate from the thorax of the donor and during suturing was about 55 mmHg. After fixation, the mean pressure in the left ventricle varied from 80 to 118 mmHg. From the second day after surgery, the pressure in the left ventricle of the transplant gradually decreased, and in the grafts that functioned for more than 6 days, the left ventricular pressure varied between 35 and 50 mmHg. The pressure in the right atrium did not show any essential changes during the time period from the surgery to the termination of the experiment.

After the withdrawal of the allograft from the thorax of the donor, the heart rhythm of the allograft during transfer and implantation showed a mean rate of 68–70 bpm. After loosening the vessel clamps, the action of the allotransplant quickly accelerated within a very short time and was stabilized on the first day after surgery to a mean value of 130 bpm. From the second day, the heart rate of the graft gradually and regularly decreased. Thus, the difference between the recipient's heart rate and that of the transplant gradually increased. While a recipient's heart maintained an almost constant rate of about 120 bpm, with a slight tendency to accelerate from the fifth day after surgery, the heart rate of the allotransplant dropped from 80–118 bpm on the second day after surgery to an average of 40 bpm on the sixth day after surgery.

Clinical course of the experiment in the recipient

The recipient responded to the presence of the transplant with a progressive apathy, lack of apetite, leukocytosis, and increased sedimentation and body temperature. The recipient's leukocytes varied from the day of surgery at about 8.280. They increased to the average number of 14.170 as early as on the first day after implantation and increased during the following days. After a slight remission between the fourth and fifth days after surgery, they were stabilized from the sixth day to around 16.000. The red blood cell sedimentation increased in the postoperative period after the transplantation. On the day of the surgery, it averaged 6/8 (1h/2h), during the following day it increased to 12/22, and on the sixth day it averaged 70/110. The body temperature measured rectally increased in the recipient during the postoperative period from the average of 37.2ºC to 39ºC, which was still within physiological variations (Table 1 and Figure 6).

Electrocardiographic findings in the allograft and recipient

For the ECG recording, three standard leads were used in the recipient and unipolar electrodes placed over the allograft. The ECG recording followed immediately after the transplantation, 6 and 12 h after the surgery and from the first postoperative day the ECG was taken every day until termination of the experiment. ECG changes were regularly found both in the allotransplant and in the recipient.

The changes in the allograft can be characterized by signs of ischemia (Figure 7) and electrolyte changes in myocardial fibers, and by the changes in the pericardial sac with growing edema and development of fresh necrosis of heart tissue. A progressive voltage decrease and arrhythmia were observed. Reduced voltage and diminution of the electric cardiac vector (Figure 8), mostly accompanied by changes in the electric heart axis, were very typical findings that depended on the time period from transplantation in the

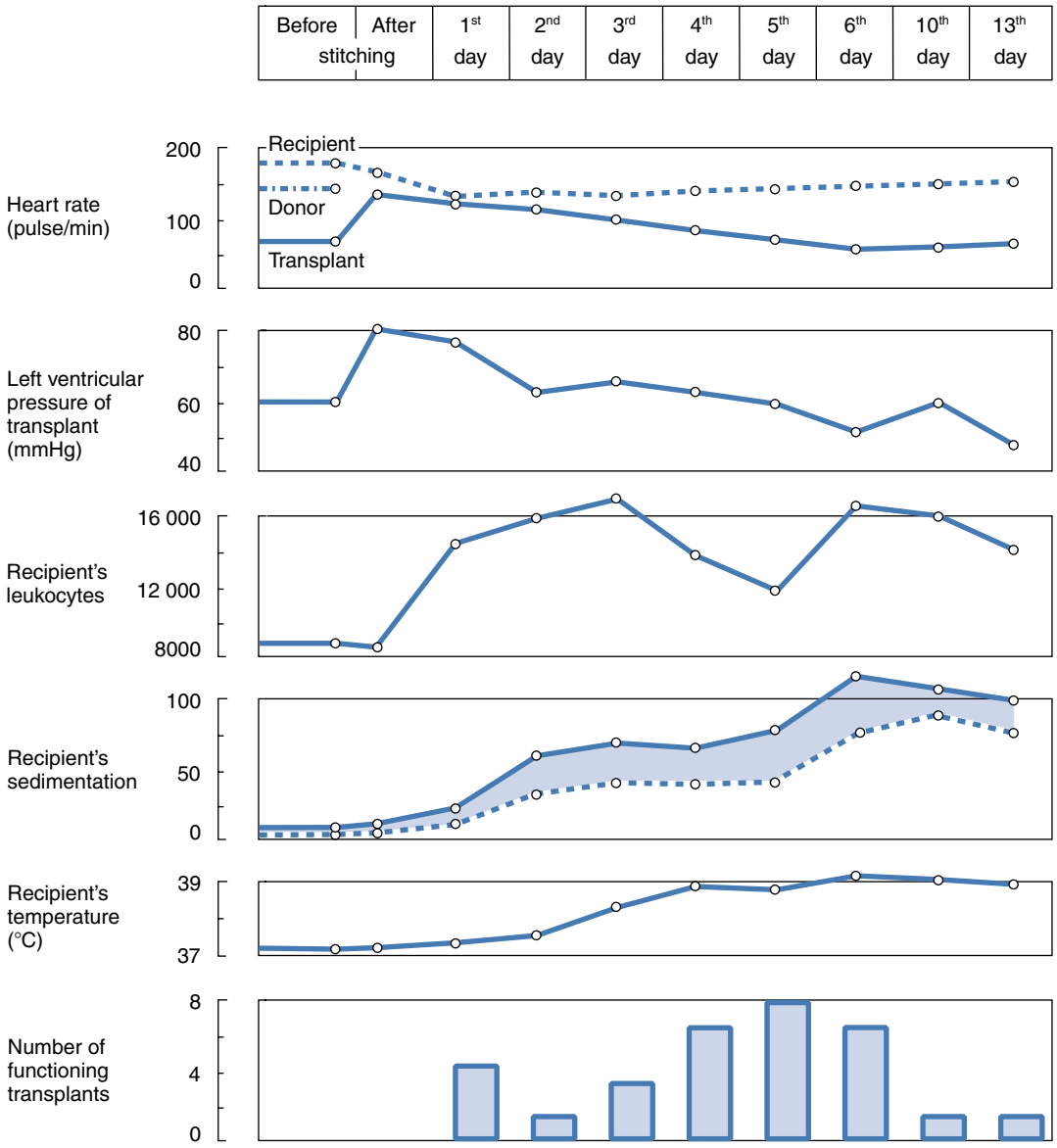

Figure 6. Heart rate and the left ventricular pressure of the transplant, and the general pathophysiological response of the recipient. The number of functioning transplants in the consecutive days after surgery is included. Data represent average values in the decreasing number of survivors in the days after surgery.

Table 1. Clinical data for the donor, recipient and transplant during the postoperative period

Clinical data	Before stitching	After stitching	1st day	2nd day	3rd day	4th day	5th day	6th day	10th day	13th day
Heart rate (pulse/min)										
Donor	140									
Recipient	176	160	120	125	120	125	130	135	130	135
Transplant	68	130	118	100	88	72	56	40	40	48
Left ventricular pressure of transplant (mmHg)	55	80	75	56	60	55	50	40	50	35
Recipient's leukocytes	8600	8280	14 170	15 625	16 500	13 150	11 100	15 950	15 300	13 100
Recipient's sedimentation	5/6	6/8	12/22	32/59	41/66	36/61	37/73	70/110	80/100	65/90
Recipient's temperature (°C)	37.2	37.2	37.3	37.5	38.3	38.8	38.7	39.0	38.8	38.0
No. of functioning transplants	–	–	4	1	3	6	8	6	1	1

Data represent average values in the deceasing number of survivors in the days after surgery.

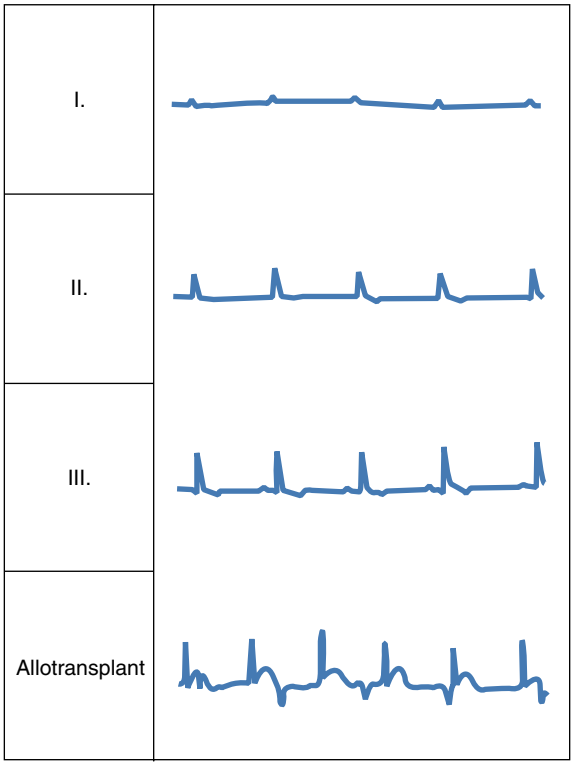

Figure 7. The ECG of the recipient (dog no. 15) and the Pardee's wave over the allograft on the fourth day after surgery.

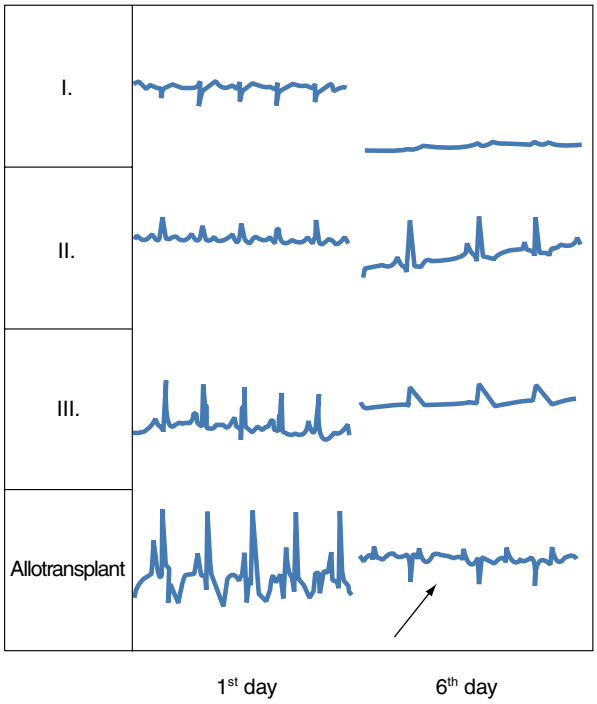

Figure 8. The ECG recording in the recipient (dog no. 11) and allograft on the first and sixth days after surgery. The allotransplant was previously conserved for 3 h. Note the decreased voltage on the sixth day in both hearts.

majority of the experimental dogs. Among other ECG changes, supraventricular arrhythmia, disturbances in the heart transmission system and sometimes the blockade of the right Tawara's branch were observed. Also in the recipient's ECG, the functional heart changes were recorded. They occurred in some dogs only, approximately in one-third of the recipients, and predominantly from the third day after the surgery. These changes were represented by a decrease of voltage, changes in the electric heart axis and supraventricular changes in the heart rhythm (Figures 9 and 10).

Electrolyte changes in heart tissue

The survey of the biochemical changes in the myocardial tissue of the left ventricle of the allograft and of the recipient are presented in Figure 11.

The transplanted heart displayed various degrees of disturbance of electrolyte composition in the heart fibers. The increase of calcium and sodium on the sixth day was very conspicuous and a decrease in potassium and magnesium also occurred on this day. The sixth day is the mean of the maximal intensity of rejection. At the same time, some correlation was observed between electrolyte metabolic changes of the recipient's heart and the allograph. The electrolyte composition in the heart of the recipient varied over normal values in all cases. Elevated potassium and magnesium levels were a frequent finding in the tissue of the left ventricle of the recipient, especially on the first day in the recipient with a direct, nonconserved graft, and on the third and sixth days in the recipient with a previously conserved graft.

Pathohistological changes in myocardial tissue of the graft and heart of the recipient

The myocardium of the donor and recipient were histologically examined. Extensive edema with hemorrhage was observed in the transplant and the recipient's heart tissue, which was significant, especially in the graft (Figure 12). In both organs the fragmentation of the fibers and a change in the stainability of the tissue were found. The mononuclear infiltration in the tissue of the graft attained a considerable intensity. The infiltrates were mostly of a mixed type; in the main, they were composed of lymphocytes, plasma cells and monocytes (Figure 13). The infiltrates in the transplant were localized preponderantly in the perivascular region and subendothelial zone; moreover they penetrated diffusely into the myocardial tissue (Figure 14). The spreading of the mononuclear infiltration was accompanied by a large myocardial edema and myolysis of the heart fibers (Figure 13). In the pericardium of the allograft, marked hemorrhages, edema and mixed mononuclear and polymorphonuclear infiltrates were observed. In the allograft, neutrophilic infiltrates also occurred more extensively than in the recipient's myocardium.

In the recipient's heart tissue, mononuclear and polymorphonuclear infiltrates were observed to a far lesser

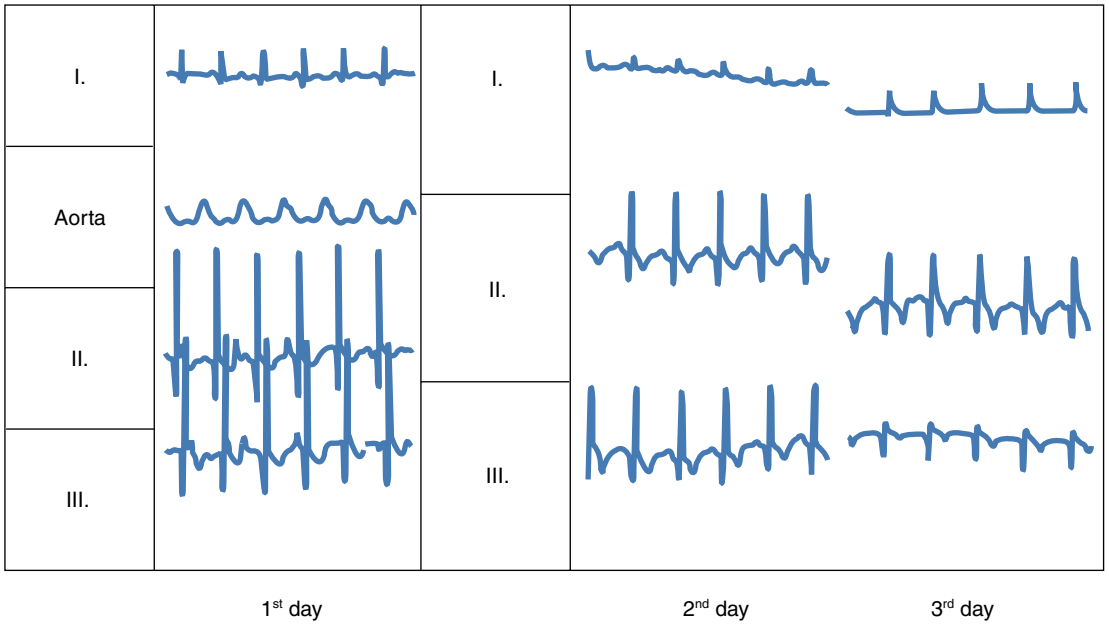

Figure 9. The gradual voltage reduction and change of the electric axis of the recipient's ECG (dog no. 14).

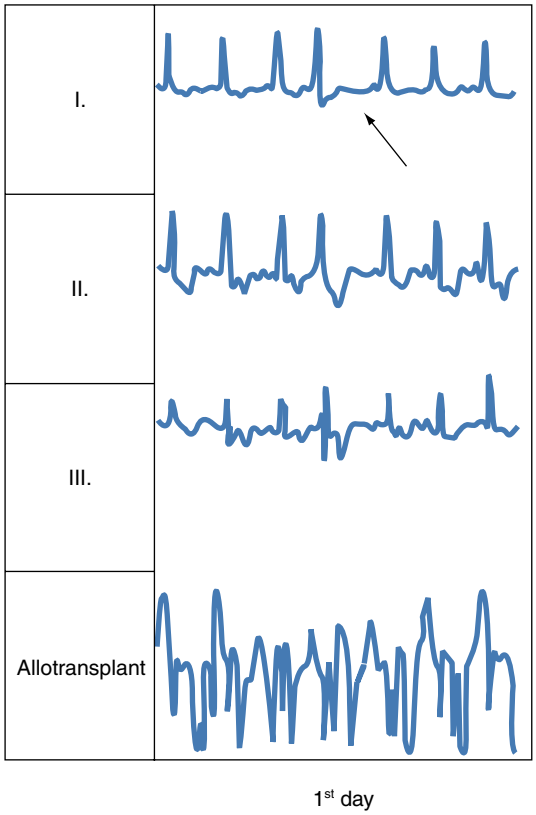

Figure 10. The extrasystole in the recipient (dog no. 8) on the first day after surgery.

degree than in the graft. A marked change in both the graft and the recipient's myocardium was the fuchsinophilic degeneration which was accompanied by a relatively considerable occurrence of necrosis (especially in the allotransplant).

In the recipient, a very significant finding was the occurrence of the so-called Anitschkow's caterpillar cells. These cells are also known from rheumatic hearts and are assumed to be signs of an exaggerated histiocytic reaction based on autoimmune stimulation (Figures 15–17).

In the suprarenal glands of the recipient, a decrease of the lipids in the fascicular zone and lymphatic organs – thymus, spleen and lymph nodes – a major desintegration of the lymphoid elements, was observed. Periodic acid-Schiff (PAS)-positive material was found in the renal glomeruli (Figure 18).

Discussion

The idea of the heterotopically implanted heart seems feasible to some authors as a useful method for the study of different problems concerning the transplant's functional connection with the recipient's organ and the mechanisms of its rejection [16–32]. Some authors have studied the transplant's capability of maintaining the systemic and pulmonary circulation of the recipient[16,17]. Some have used the heterotopic cardiac allotransplantation as a tool for diagnosis of rejection[18]. One very interesting study of heterotopic heart transplantation aimed to analyze the participation of nitric oxide (NO) in the acute rejection of the heart graft. The role of NO seems to be very controversial. NO may accelerate the process of rejection and, conversely, NO generated in the allografts may prolong survival[24]. Another interesting

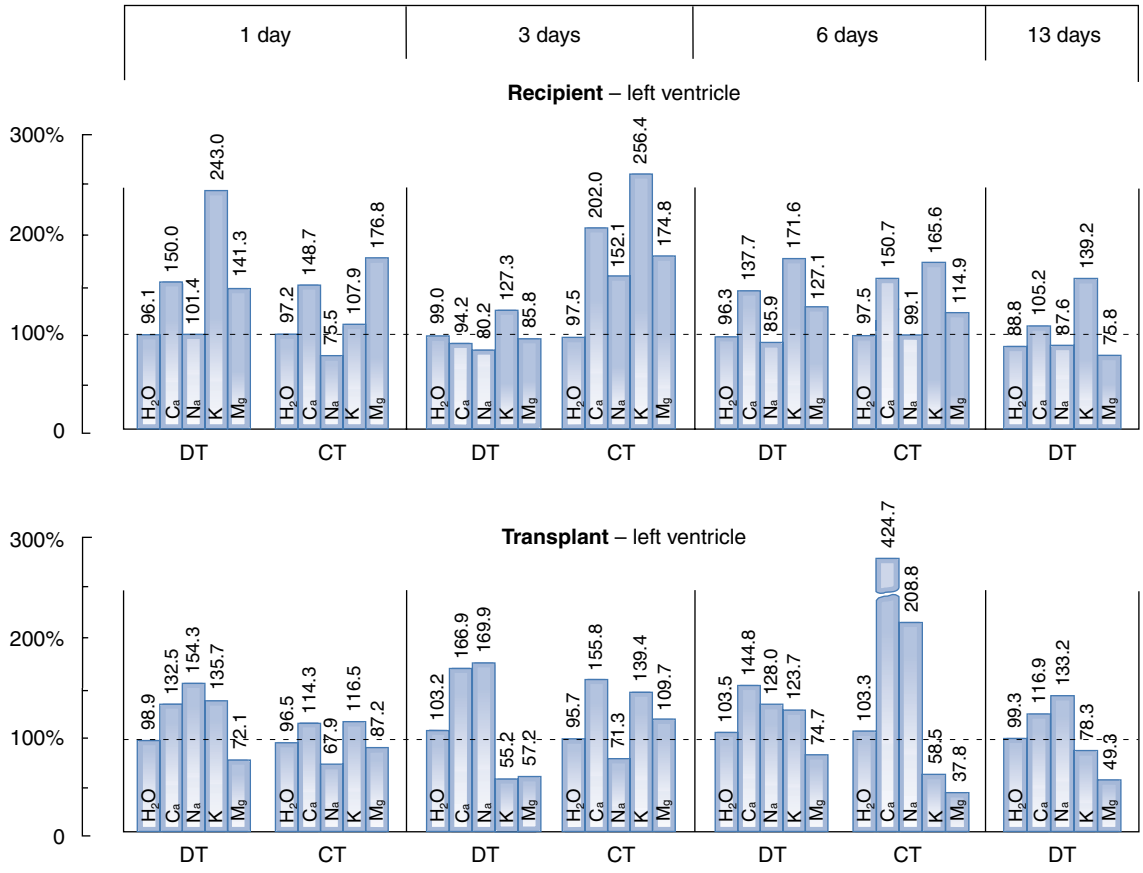

Figure 11. The electrolyte changes in the tissue of the left ventricle of the recipient and of the allograft. DT: direct transplantation, CT: transplantation of the previously conserved transplant. The variations from the average normal value (100%) are significant in both hearts. The absolute values were transferred into the percentual expression, where 100% represents the normal values. Thus the pathological variations are more evident. Data represent average values in the decreasing number of survivors in the days after surgery.

Figure 12. The allotransplant after 10 days of implantation. The pericardial sac of the explanted graft is markedly thickened (right), with extensive hemorrhage and cellular infiltration.

study proved that coronary blood flow does not decrease during the period of allograft rejection in heterotopic heart grafts[20]. Similar results were obtained by Pirolo *et al*.[22]. Another group of authors has studied the usefulness of quantitative ultrasound analysis as an important tool for the noninvasive evaluation of acute cardiac allograft rejection[23], whereas another group preferred to develop noninvasive methods for the rejection in orthotopic experimental canine model[25]. Capuano *et al.* accentuate the importance of heterotopic heart transplantation as a useful model for various complex studies of allograft rejection[26].

The authors placed the allotransplant either into the thorax[16,18,22], into the abdomen[24,26,27,29,30] or in the cervical region[17,19,20,23]. For the method of heterotopic allotransplantation, mainly rats[19,24 26–30] or dogs[16,18,20,22,23] were used. Studies of heterotopic cardiac xenotransplantation were also performed[21,31].

Yu and Wright[31] used the xenotransplant from a fish (*Tilapia*), which was placed on the venous side of a rat's circulation between the left kidney and the inferior vena cava by end-to-side anastomosis of the donor's aorta to the recipient's inferior vena cava and by end-to-end anastomosis of the donor's sinus venosus to the recipient's left renal vein. The rejection was hyperacute, evaluated by histopathological examination and immunofluorescent

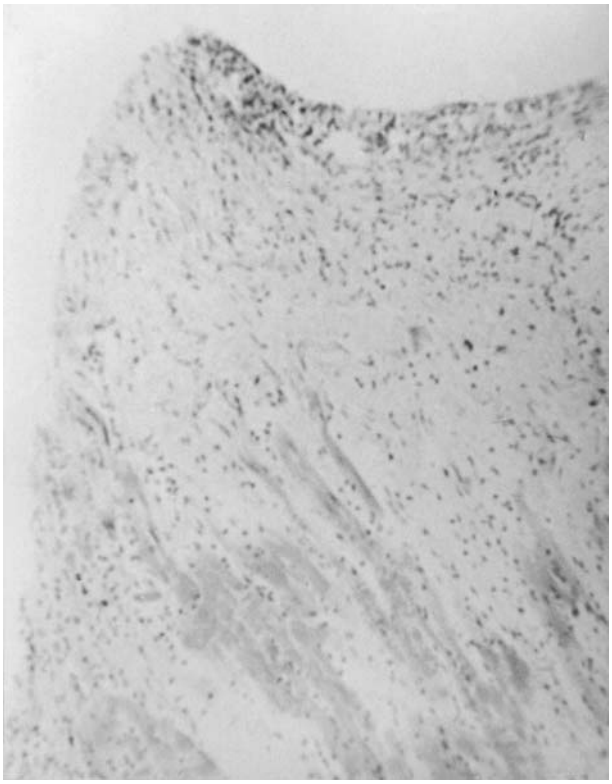

Figure 13. The histologic picture of the posterior papillary muscle of the left ventricle of allotransplant without previous conservation is shown. Edema, round cell infiltration and marked myolysis with the vanishing heart muscle fibers are visible. Raab called such a picture in case of metabolic cardiomyopathy a 'Matterhorn necrosis'. HE stain. Original magnification 210×.

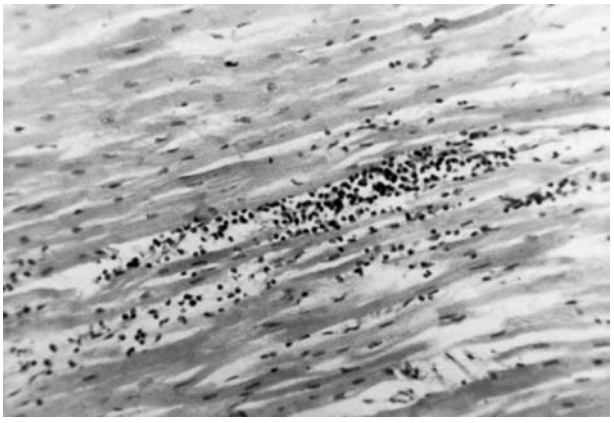

Figure 14. Lymphocytic infiltration of the papillary muscle of the left ventricle of the conserved allotransplant. HE stain. Original magnification 420×.

staining for immunoglobulin and complement, but the rejection occurred in hours rather than in minutes. Such experiments and intensive genetic studies are very valuable, but we can expect it to take a long time to overcome the phylogenetic obstacles thrown up by hundreds of millions of years of animal evolution[31].

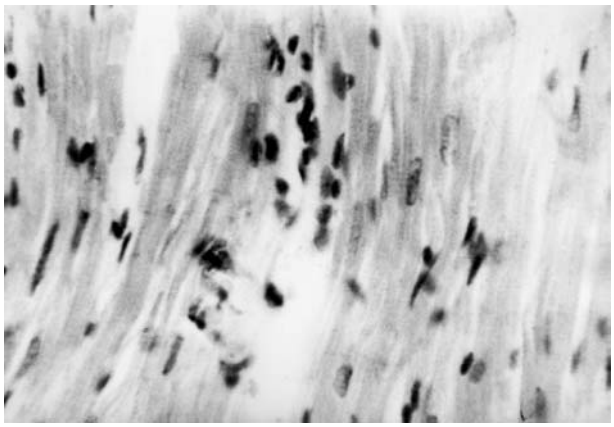

Figure 15. The tissue of the right ventricle of the recipient with the nonconserved allograft. Note the exaggerated histiocytic reaction with the occurrence of Anitschkow's caterpillar cells. HE stain. Original magnification 850×.

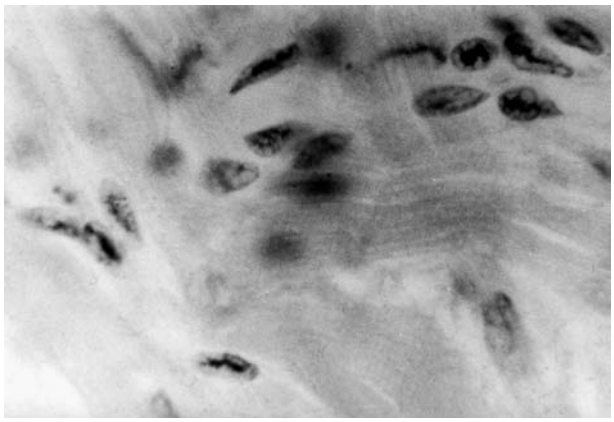

Figure 16. Higher magnification of the Anitschkow's caterpillar myocytes in the right ventricle of the recipient with the previously nonconserved allograft. HE stain. Original magnification 1600. Oil immersion.

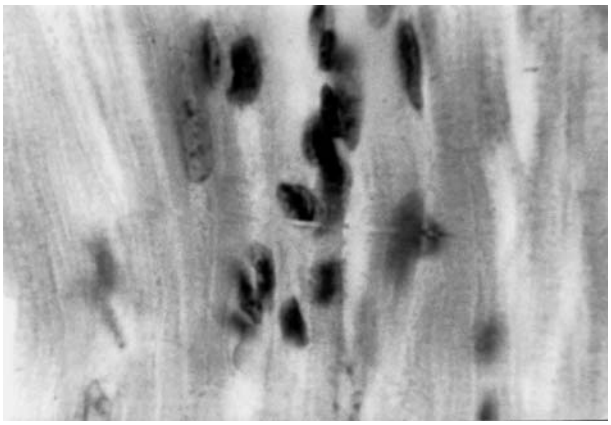

Figure 17. Anitschkow's caterpillar myocytes in the left ventricle of the recipient, bearing the previously conserved heart allograft. HE stain. Original magnification 1600×. Oil immersion.

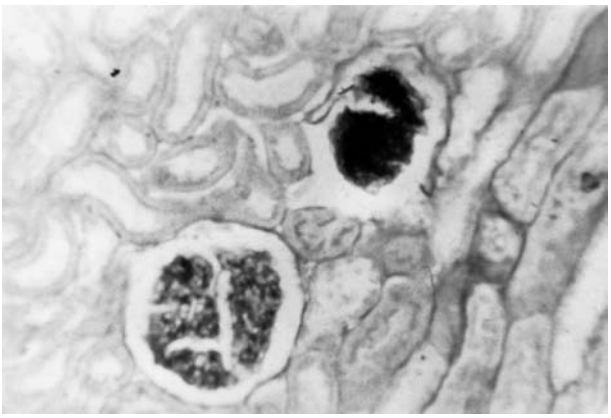

Figure 18. Renal glomeruli of the recipient with the conserved allograft. The renal glomeruli of the recipient show the accumulation of PAS-positive material, indicating an excretion of immunoglobulins. PAS stain. Original magnification 670×.

The heterotopic allograft method was also used in an interesting study by Sihvola *et al.* aimed at preventing the cardiac allograft arteriosclerosis[28]. They succeeded in the prevention of platelet-derived growth factor (PDGF-AA-R alpha and R-beta) produced in the intimal cells, which correlates with the development of cardiac allograft arteriosclerosis by the protein-tyrosin-kinase inhibitor[28].

In our experiments immunosuppresive therapy was avoided because the goal was to study the rate of rejection, its evaluation by ECG and blood pressure recording in the left ventricle of the allograft, and also by the blood pressure in the right atrium. Furthermore, analysis was made by laboratory, biochemical and hematological analyses in the recipient and finally, by histopathological examination. A very important goal of our study was the reaction of the recipient to the heart allograft.

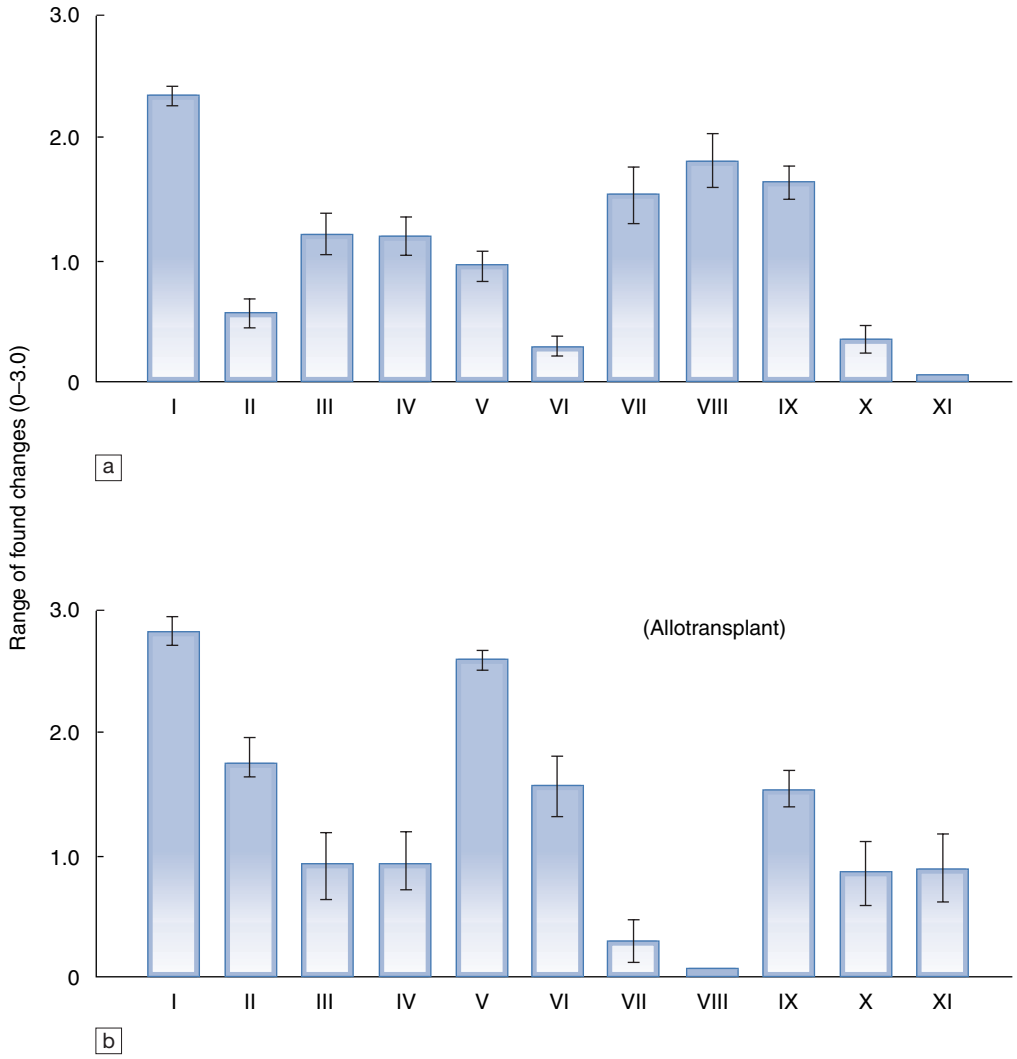

Figure 19. An evaluation of pathologic and histopathologic changes on the base of an arbitrary scale 0–3 in the myocardial tissue of the recipient (a) and myocardial tissue of the allograft (b). I: Edema; II: hemorrhage; III: fragmentation; IV: change of stainability; V: mononuclear infiltration; VI: polymorphonuclear infiltration; VII: histiocytic activation; VIII: occurrence of Anitschkow's cells; IX: fuchsinophilia; X: necroses; XI: myolysis.

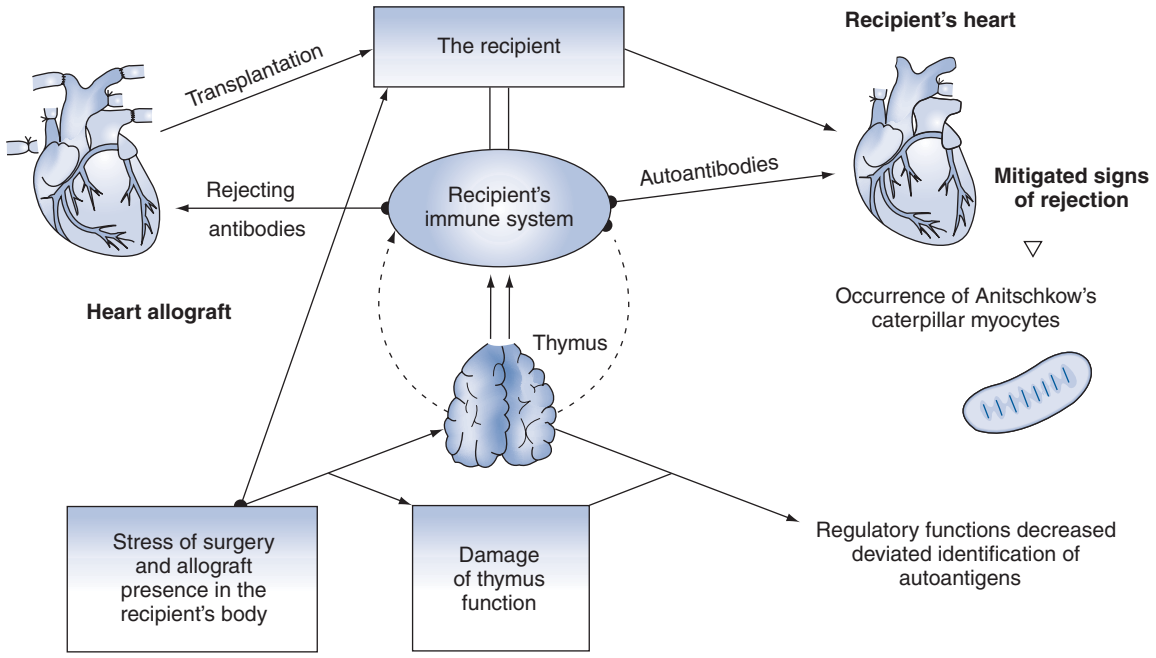

Figure 20. An explanation of the signs of occurence of autoantibodies in heart tissue of the recipient with the implanted heart allograft.

The first signs of rejection were observed from the second day after surgery. The highest rejection crisis started between the fourth and sixth days after transplantation. The first signs of rejection were manifested by the accumulation of exudate in the pericardial sac, which was easily palpable on the neck of the animal, and further by the diminution of the blood pressure in the left ventricle of the allograft and decrease in heart rate.

The recipient responded to the presence of the allotransplant with marked leukocytosis, elevated sedimentation and elevated body temperature as early as from the second day. The ECG of the graft showed significantly expressed changes characterized by rejection. These changes were represented first of all by a marked voltage reduction, arrhythmia, signs of heart ischemia and finally by pericardial changes.

ECG changes were also observed in the recipients, i.e. voltage reduction, arrhythmia and pericardial changes. These changes were less expressed than in the allograft. Such changes are, in certain respects, in agreement with the disturbances of the electrolyte metabolism, i.e. prevailingly by the deviation of the whole picture of normal electrolyte pattern of the heart fibers. A very conspicuous finding was the increased levels of potassium and magnesium in the heart fibers of the recipient, whereas in the allograft myocardial fibers, a marked increase of sodium and calcium occurred.

The pumping function of the allograft is perceived by the vasomotoric regulations of the recipient as a foreign functional element in the body. Therefore, the deviations in the electrolyte composition in the recipient's heart may occur due to a deviated neurohormonal stimulation of heart activity. We can say that the effect of the heart transplant on the activity of the recipient's heart is mediated through an abnormal neurohormonal stimulation, and is also expressed by the pathological changes in the ECG and pathological shifts in the electrolyte pattern of the heart fibers.

Concerning the histopathological examination, in the allograft, a classical rejection reaction setting in between the second and sixth day was observed. Besides the current mononuclear and polymorphonuclear infiltrates in the transplant, and to a far lesser degree also in the recipient, we could observe a change of stainability of heart fibers, fragmentation and myolysis with signs of tissue necrosis in the allograft and in a moderate form in the recipient's heart (Figure 19).

A very frequent finding was a fuchsinophilic degeneration of the heart fibers that preceded the development of necrosis. The changes in the electrolyte metabolism of the heart tissue undoubtedly participate in this metabolic disturbance. The immunologic factors bringing about the rejection also participate in these fuchsinophilic changes.

A very conspicuous and interesting finding in the recipient's heart was the occurence of the so-called Anitschkow's caterpillar myocytes, which indicate the lesion of the myocardium immunologically. These histopathological findings show that against the antigens of heterotopic allograft aggressive immunoglobulins in the immunological system of the recipient are formed. These attack not only the heart tissue of the allotransplant but may also react cross-wise with recipient's myocardial tissue and, in this way, act as a certain form of autoantibodies. This is also documented by the cellular reactions with typical mononuclear infiltrates, which occur in the allograft and in moderate form also in the recipient's heart. Moreover, the tissue heart changes in the case of rheumatism are known. These changes are assumed to be the exaggerated histiocytic

reactions of the autoallergic type. They are also expressed by the occurrence of the peculiar form of monocytes called Anitschkow's caterpillar cells[32,33]. These cells correspond to some extent with the Aschoff bodies[34]. The Anitschkow's caterpillar cells were observed in the heart tissue of the recipient bearing both the fresh, directly implanted allograft, and also in the previously conserved heterotopic allograft. The occurrence of Anitschkow's cells only in the recipient testifies to the fact that only the natural heart of the recipient bears the functional basis for a histiocytic activity of this type because these cells are assumed to be a certain cellular indicator of an attack of autoantibodies against the recipient's own heart tissue. Therefore, they were observed only in the heart tissue of the recipient and not in the tissue of the graft (Figure 19).

The possibility of autoaggression against the recipient's own cardiac cells has been observed by some authors. They proved that binding of the rabbit antidog sarcolemmal immunoglobulin conjugated with fluorescein to the heart cells in almost all donor hearts. A conspicuous histological demonstration of rejection of the graft was proved. At the same time, however, in many cases they also found sarcolemmal immunoglobulin in the recipient's heart[35]. Thus, it has been clearly proven that the antibodies produced by the immunological system of the recipient and detected against the donor's heart tissue may also react cross-wise with the antigens on the surface of the recipient's heart cells[35] that produce such antibodies. The concomitant reaction of the recipient's heart tissue is an immediate histiocytic stimulation that produces the peculiar Anitschkow's caterpillar myocytes (Figure 20).

The finding in the adrenal glands and lymphocytic stress organs speak in favour of a marked increase of 17-OH corticosteroid secretion. The surgical intervention and the following condition during the survival and the function of the allograft call forth a marked stress reaction in experimental animals. In fact, the increased l7-OH cortico-steroid secretion acts as an endogenous immunosuppression, but only to a certain degree and only for a limited period of time. The rejection of the graft is only partly postponed and ultimately the process of rejection sets in with full intensity. Since the stressed state of the experimental animal also attacks an important regulator of immunologic mechanisms, namely the thymus, it can be assumed that regular activities of the thymus may be altered. As a consequence the immunologlobulins produced by the recipient's immune system cease to differentiate between foreign and native antigens, and the antibodies also attack the recipient's heart. Thus, our morphological findings of thymic destruction testify to the importance of thymic integrity to prevent an immunologic autoaggressive reaction of this kind.

The integrity of T-lymphocytes is important from the point of view of general pathology. Some observations concerning the pathogenesis of the cutaneous T-lymphomas accentuate the necessity of uninterrupted development of T-lymphocytes for their normal function. If the development of T-lymphocytes is stopped in the stage of the medullar precursor to the functional helper cell, the malignant expanse of the T-lymphocytic clones starts. It is interesting that extracorporeal photochemotherapy, primarily indicated for the therapy of cutaneous T-lymphomas, can be used for the therapy of the graft-versus-host disease[36–38].

The rejection of the allograft, which was transplanted directly without a previous conservation, is more expressed in comparison to the transplant previously conserved in saline solution. This fact proves that the conservation of the allograft decreases its antigenic capabilities but the rejection starts and takes place with a sufficient intensity to reject the foreign heart tissue. Nevertheless, the survival of directly implanted heart grafts is longer (13 days in the longest survivor) than in the heart that had been previously conserved in saline solution (6 days' survival).

The findings described in the recipient during heterotopic allotransplantation are also of importance, mainly from the viewpoint of providing a more exact understanding of the questions that may be connected with the mechanisms of rejection in paired organs after transplantation.

Summary

A heterotopic cervical allotransplantation was carried out in 35 dogs. The function of the transplant and the response of the recipient not receiving immunosuppressive therapy was studied. The donor's heart was taken in the form of isolated heart–lung preparate, the allograft being maintained during transplantation by its own circulatory system.

The allograft was connected to the recipient's circulatory system either directly, or after a previous conservation in the physiological solution for 3 h at a temperature of 32ºC. The signs of rejection appeared as early as the second day after surgery, and were expressed by changes in ECG, a decrease of the blood pressure in the left ventricle of the allograft, fluid accumulation in the pericardial sac and diminished cardiac contractility. The process of the transplant's rejection was more intense in the allograft directly transplanted in comparison to a previously conserved graft, apparently due to a slightly decreased antigenicity of the conserved allograft. In spite of this, a directly transplanted allograft survived longer.

The recipient's response to the transplant was expressed by a lack of appetite, general apathy, leukocytosis, an increased sedimentation rate and a slightly increased body temperature. ECG changes were also recorded.

The transplanted heart displayed a certain degree of metabolic damage of the myocardium, expressed mainly by an increase in sodium and calcium in the heart tissue. Conversely, the recipient's myocardium exhibited an increase of potassium and magnesium.

Histopathological findings showed signs of edema, hemorrhage, changes in tissue stainability, fragmentation of heart fibers, fuchsinophilic degeneration and necrosis, myolysis and typical mononuclear mixed infiltrations in the

allograft. These effects also occurred in the recipient's heart but to a lesser degree.

A very important and outstanding finding in the recipient's heart tissue was an exaggerated histiocytic reaction with occurence of Anitschkow's caterpillar myocytes, which are assumed to be a morphological sign of an autoaggressive immunological reaction in the heart tissue. The significant problem of the genesis and the immunologic importance of Anitschkow's cells in the myocardium is still being discussed[39–43].

Acknowledgments

The authors express their gratitude to Miss Viola Krejčí and Mr Ivo Filip for their excellent technical cooperation, Professor František Aujeský for the proof-reading and Mrs Hana Dvořáková for typing the manuscript.

References

1. Vašků J. Artificial heart: Pathophysiology of the total artificial heart and of cardiac assist devices. *Acta Facultatis Medicae Universitatis Brunensis J.E. Purkyně Brno* 1982:397.
2. Vašků J. Brno experiments in long-term survivals with total artificial heart. *Acta Facultatis Medicae Universitatis Brunensis J.E. Purkyně Brno* 1984:662.
3. Vašků J. Changes in total artificial heart driving diaphragms after long-term TAH pumping. In: Akutsu T, Koyanagi H, editors. *Heart Replacement: Artificial Heart 5*. Tokyo: Springer-Verlag 1996:53–64.
4. Dobšák P, Dostál M, Nečas J, Sehnalová O, Vašků J, Kuchtíčková Š. Microcirculation of a bulbar conjunctiva in calves with the total artificial heart: Results of a long-term study. *Pathophysiology* 1996;3:213–7.
5. Vašků J. Actual pathophysiological problems in the contemporary research on the TAH. *Ann Thor Cardiovasc Surg* 1996;2:315–30.
6. Bednařík B, Navrátil J, Tomeček J, Pešťový S, Hoffmann K, Olejník O. Transplantace srdce u psa (Heart transplantation in the dog). *Rozhl Chir* 1967;46:363–72 (in Czech with English summary).
7. Bednařík B, Pešťový S, Tomeček J, Vašků J, Bednář O, Hoffmann K. Unsere Erfahrungen mit der Herztransplantation beim Hunde. *Wiederbeleb u Organers* 1968;6:45–53.
8. Bednařík B, Nevrtal M, Vašků J *et al.* Funkční stav srdce dva roky po izotopické transplantaci (Functional state of the heart two years after isotopic transplantation). *Rozhl Chir* 1970;49:27–36 (in Czech with English summary).
9. Bednařík B, Vašků J, Urbánek M, Pešťový S, Štěpánek V. Preservation of the heart for transplantation in the form of a surviving heart–lung transplant. Proc VIIth Cardiosurg Conference Bratislava-Smolenice 1971; May 17–19:105–8.
10. Bednařík B, Vašků J, Pešťový S *et al*. Herzkonservierung und Transplantation. *Wiederbeleb u Organers* 1971;8:80–9.
11. Vašků J, Bednařík B, Urbánek E, Štěpánek V, Pešťový S, Vítek J. Experimental heterotopic allotransplantation of the heart. *Scripta Medica Facultatis Medicae Universitatis Brunensis* 1971;44:359–71.
12. Robicsek F, Sanger PW, Taylor FH. Simple methods of keeping the heart 'alive' and functioning outside of the body for prolonged periods. *Surgery* 1963;53:525–34.
13. Robicsek F, Lesage A, Sanger PW, Dougherty HK, Galucci V. Transplantation of 'live' hearts. *Am J Cardiol* 1967;20: 803–11.
14. Lillehei RC. Transplantation of the heart. *Int Coll Chest Physicians Meeting Copenhagen* 1966: August 25–28.
15. Mann FC, Priestley JT, Markowitz J, Yater WM. Transplantation of the intact mammalian heart. *AMA Arch Surg* 1963;20:219–28.
16. Sueda T, Matsuura Y, Matsushima T, Mukai S, Ishihara H, Kajihara H. A functional new experimental biventricular model of heterotopic cardiac transplantation. *Hiroshima J Med Sci* 1989;38:23–6.
17. Hirooka Y, Kazui M, Hosoda Y. Experimental study of cervical heterotopic cardiac transplantation as a temporary left ventricular assisst device. *Transplant Proc* 1989;21:2563–6.
18. Sueda T, Matsuura H, Matsushima T, Mukai S, Kajihara H. A heterotopic cardiac transplantation model for evaluation of rejection using transvenous endomyocardial biopsy. *Hiroshima J Med Sci* 1990; 39:15–18.
19. Okouchi Y, Shimizu K, Yamaguchi A, Kamada N. Effectiveness of University of Wisconsin solution for heart preservation as assessed in heterotopic rat heart transplant model. *J Thorac Cardiovasc Surg* 1990;99:1104–8.
20. Bando K, Fraser CD Jr, Chacko VP *et al.* Coronary blood flow does not decrease during allograft rejection in heterotopic heart transplants. *J Heart Lung Transplant* 1991;10:251; discussion, 6:256–7.
21. Rodeheffer RJ, McGregor CG. The development of cardiac transplantation. *Mayo Clinic Proc* 1992;67:480–4.
22. Pirolo JS, Liptay MJ, Brunt EM, Shuman TA, Cox JL, Fergusson TB Jr. Early cardiac allograft rejection is independent of regional myocardial blood flow. *Ann Thorac Surg* 1993;55:441–9.
23. Stempfle HU, Angermann CE, Kraml P, Schutz A, Kemkes BM, Theissen K. Serial changes during acute myocardial allograft rejection: quantitative ultrasound tissue analysis versus myocardial histologic findings. *J Am Coll Cardiol* 1993; 22:310–17.
24. Tanaka S, Kamiike W, Ito T *et al.* Evaluation of nitric oxide during acute rejection of heart transplantation in rats. *Transplant Proc* 1995;27:576–7.
25. Everett JE, Palmer MN, Jessurun J, Shumway SJ. Non-invasive diagnosis of cardiac allograft rejection in an orthotopic canine model. *Ann Thorac Surg* 1966;62:1337–40; discussion 1340–1.
26. Capuano LG, Velluci R, Toppi L *et al.* Heterotopic heart transplantation in the rat: a preliminary study. *Ann Ital Chir* 1998;69:351–6.
27. Baxter K, Hao PM, Howden BO, Saunder A, Jablonski P. Modified technique of abdominal transplantation in the rat. *J Heart Lung Transplant* 1998;17:1057–64.
28. Sihvola R, Koskinen P, Myllarniemi M *et al*. Prevention of cardiac allograft arteriosclerosis by protein tyrosine kinase inhibitor selective for platelet-derived growth factor receptor. *Circulation* 1999;99:2295–301.
29. Dambrin C, El Feghaly M, Abhal M *et al.* A new rejection criteria in the heterotopically placed rat heart by non-invasive measurement of Dp/Dt max. *J Heart Lung Transplant* 1999;18:524–31.

30. Wada T, Ono K, Hadama T, Uchida Y, Shimada T, Arita M. Detection of acute cardiac rejection by analysis of heart rate variability in heterotopically transplanted rats. *J Heart Lung Transplant* 1999;18:499–509.
31. Yu W, Wright JR jr. Heterotopic cardiac xenotransplantation: fish to rat. *Xenotransplantation* 1999;6:213–19.
32. Selye H. The chemical prevention of cardiac necrosis. New York: The Ronald Press Company 1958:104.
33. Selye H. *Pluricausal Cardiopathies*. Springfield, Illinois: Charles C. Thomas, 1961:9:237.
34. Murphy GM. Nature of rheumatic heart disease. *Medicine* 1960;39:289–384.
35. Shumak KH, Goldman BS, Silver JB, Bigelow WG, Grookston JH. Pathogenesis of rejection of canine cardiac allografts. *Circulation* 1970;12–13 (Suppl II):98–103.
36. Edelson RL. Cutaneous T-cell lymphoma: A model for selective immunotherapy. *Cancer J Sci Am* 1998;4:62–71.
37. Vašků J. Současné možnosti léčby T-lymfomů (Contemporary possibilities of the therapy of cutaneous T-lymphomas). *Scripta Medica Facultatis Medicae Universitatis Brunensis* 1997;70:453–4 (in Czech with English summary).
38. Sniecinski I. Photochemotherapy for GvHD. *Int J Artif Organs* 2000;23:1–10.
39. Mikat KW. Anitschkow cell development in rat myocardium. *Arch Pathol* 1964;77:47–52.
40. Beranek JT. Anitschkow cells in experimental autoimmune myocarditis. *Circulation* 1992;86:1659–60.
41. Fraser WJ, Haffejee Z, Cooper K. Rheumetic Aschoff nodules revisited: an immunohistologic reappraisal of the cellular component. *Histopathology* 1995;27:457–61.
42. Satoh F, Tsutsumi Y. Anitschkow cells in the human heart. *Path Int* 1999;49:85–7.
43. Stehbens WE, Zuccollo JM. Anitschkow myocytes or cardiac histiocytes in human hearts. *Pathology* 1999;31:98–101.

Journal of Congestive Heart Failure and Circulatory Support (2001) Vol 1, No 4, 249–257

Quantification of pulsatility of the arterial blood pressure waveform during left ventricular nonpulsatile assistance: a brief review and a recent study series

S. Kawahito[1], T. Takano[1], K-I. Nakata[2], T. Maeda[1], K. Nonaka[1], J. Linneweber[1], S. Schulte-Eistrup[1], T. Sato[1], M. Mikami[1], J. Glueck[1] and Y. Nosé[1]

[1]Department of Surgery, Baylor College of Medicine, Houston, Texas, USA; and [2]The Second Department of Surgery, Nihon University School of Medicine, Tokyo, Japan

Background When using a rotary blood pump for a left ventricular assist device (LVAD), the arterial blood pressure waveform changes with the LVAD condition because the rotary blood pump produces a nonpulsatile flow while the native heart produces a pulsatile flow. The aim of this study is to examine the correlation between the LVAD condition and the arterial blood pressure waveform.

Methods The mock circulation loop was composed of an aortic compliance chamber, a left atrial compliance chamber, a pneumatic pulsatile pump as a native heart, and a rotary blood pump representing the LVAD with left atrial drainage. The Fast Fourier Transform (FFT) technique was utilized to analyze the arterial blood pressure waveform and calculate the pulsatility index (PI) and the pulse power index (PPI). The correlation between the LVAD condition and the arterial blood pressure waveform in a fixed cardiac output condition, and the correlation between the cardiac output and the arterial blood pressure waveform in a fixed LVAD condition were examined. In addition, these relationships were confirmed using animal models.

Results In a fixed cardiac output condition, the PI and PPI decreased with the increase of the LVAD rotational speed, flow rate, and assist ratio. In a fixed LVAD condition, the PI and PPI increased with the increase of the cardiac output, and decreased with the increase of the assist ratio, exponentially. In animal models, the PI and PPI also decreased with the increase of the assist ratio, exponentially. A close relation between the measured assist ratio with flowmeters and the assist ratio calculated from regression equations was observed.

Conclusion From this viewpoint, an ideal LVAD condition may be estimated from the pulsatility change of the arterial blood pressure waveform.

Keywords left ventricular assist device (LVAD), rotary blood pump, arterial blood pressure waveform, pulsatility, Fast Fourier Transform (FFT), pulsatility index (PI), pulse power index (PPI), quantification.

A brief review

Analysis of the pulsatility of the arterial blood pressure waveform

Recent developments in arterial hemodynamics have indicated that the arterial blood pressure waveform contains more information than is available from conventional sphygmomanometry. A lot of investigators have attempted to quantify the pulsatility of the arterial blood pressure waveform[1–9]. The arterial blood pressure waveform is derived from the complex interaction of the left ventricular stroke volume and the physical properties of the arterial circulation. That shape is a nonlinear function of stroke volume, heart rate, and many other cardiovascular parameters. There are many reports about estimation of cardiac function[1–6], intravascular volume[7,8], and systemic vascular resistance[9] from analysis of the arterial blood pressure waveform. Among them, the biggest factor that influences the pulsatility of the arterial blood pressure waveform may be cardiac output.

Cardiac output (CO) is used clinically to evaluate cardiac function in critically ill patients, aid in the diagnosis of cardiovascular disease and guide therapeutic decisions in complex clinical situations. Thermodilution, the current gold standard, provides relatively accurate estimates of CO, however, now less invasive monitoring is required. It is well known that in various clinical situations the arterial blood pressure waveform is variable following CO. Especially under the very low CO state, the pulsatility of the arterial blood pressure waveform disappears. From this aspect, the analysis of the pulsatility change of the arterial blood pressure waveform may be useful in assessing changes in CO. Some investigators have attempted to estimate CO from the arterial blood pressure waveform clinically[3–6]. These 'pulse-contour' techniques employ simple linear Windkessel models of the arterial system. Furthermore, these methods can also be applied to the

Correspondence to: Shinji Kawahito, Department of Surgery, Baylor College of Medicine, One Baylor Plaza, Houston, Texas, 77030, USA.

estimation of the suitable left ventricular assist device (LVAD) condition.

Fast Fourier Transform (FFT) technique

There are many methods used to quantify the pulsatility of the complex waveform. In 1957 Womersley[10] applied the Fast Fourier Transform (FFT) technique to perform analysis of pulsatile flow by transforming the complex waveform into a series of simple sinusoidal waves, each of which has a different amplitude and is an integer multiple of the original frequency. The FFT of the arterial blood pressure waveform is performed with a digitizing oscilloscope.

Pulsatility index (PI) and pulse power index (PPI)

Many parameters obtained from the FFT analysis were reported[11].We quantified the pulsatility of the arterial blood pressure waveform in terms of the pulsatility index (PI) and the pulse power index (PPI) proposed by Grossi *et al.*[12]. These equations are as follows:

$$PI = \sum_{i=0}^{n} Ai^2/A0^2$$

$$PPI = \sum_{i=0}^{n} Ai^2\omega_i{}^2/A0^2$$

where Ai = amplitude of i'th harmonic of flow, A0 = amplitude of mean flow, andω = frequency of flow (cycles/s)

The PI and PPI are based on transforming the pulsatile flow wave using the FFT technique[13–16]. Thus a key first step in analyzing a complex waveform is to separate the two independent variables of pulse shape and pulse rate. Gosling *et al.*[13,14] proposed a unit-less PI based on this harmonic analysis of a pulsatile waveform. The PI is the sum of the square of its harmonics components divided by the square of the mean flow. This PI reflected the relative 'sharpness' of a given waveform with respect to its mean flow and was independent of its frequency. By redefining this index, and not normalizing for frequency, one can measure as proposed here, a PPI (cycles/s)^2, which quantifies the relative power of a pulsatile waveform with respect to a nonpulsatile equivalent flow. The two components of a pulsatile waveform, shape (quantified by PI) and rate, can be measured independently and can be combined to yield a measurement of PPI. With these methods it is possible to develop standard criteria for measurement of pulsatile flow.

Recent progress of nonpulsatile left ventricular assist device (LVAD)

According to the technology assessment conducted by the Institute of Medicine, 60 000 patients in the USA may be saved annually either by heart transplantation or cardiac prostheses[17–19]. Unfortunately, available donor hearts in the USA remain in the range of 2000 per year[20]. Thus, an implantable ventricular assist device can salvage patients with end-stage cardiac disease who cannot undergo heart transplantation owing to age limitations, lack of a donor heart, or complications in using immunosuppressive drugs. With the development of the rotary blood pump, remarkable progress has been made, and this device is anticipated to be the next generation of implantable cardiac assist devices[21–24].

The rotary blood pump has been effectively used for cardiopulmonary bypass and short-term circulatory assistance. The nonpulsatile rotary blood pump demonstrates efficient and reliable performance in various clinical situations. The nonpulsatile blood pump has a simple and reliable design that is easily manufactured and has several desirable features. There is no need to incorporate heart valves, which can be thrombogenic and cause blood trauma. A continuous flow pump does not require a large orifice inflow conduit and proves to be easier to implant into patients with minimal damage to the myocardium. There is no need to incorporate a compliance volume-shifting device, which is essential for a pulsatile blood pump[24]. The utility of the rotary blood pump is widely recognized. Recently, LVADs have been used not only as a bridge to transplant, but also in the treatment of dilated cardiomyopathy[25]. When the rotary blood pump is used as an LVAD, the arterial blood pressure waveform changes with the LVAD condition because the rotary blood pump produces a nonpulsatile flow and the native heart produces a pulsatile flow. Also, it is well known clinically that the arterial blood pressure waveform is variable following LVAD implantation. However, the link between the rotary blood pump's condition and the arterial blood pressure waveform was unclear. From this viewpoint, an estimation of the pulsatility change of the arterial blood pressure waveform may indicate a suitable LVAD condition.

A recent study series

Preliminary study: estimation of cardiac output from analysis of the arterial blood pressure waveform

Prior to LVAD study, the mock circulation loop was utilized to examine the correlation between the CO and the arterial blood pressure waveform. It was composed of an aortic compliance chamber, a left atrial compliance chamber, and a pneumatic pulsatile pump as a native heart (Figure 1). This mock circulation loop was filled with 37% glycerin water. The outlet pressure (the arterial blood pressure) was measured, and the CO was measured with an ultrasound tubing flowmeter (Transonic System, Inc., Ithaca, NY, USA). The FFT of the arterial blood pressure waveform was performed with a digitizing oscilloscope (TDS 420, Tektronix, Inc., Pittsfield, MA, USA) and pulsatility was examined with the PI and PPI. The pneumatic pulsatile pump, simulating the natural heart, produced 1.00–3.86 L min^{-1} flow (stroke volume 11.70–65.20 ml; heart rate 50–100 bpm). In this study, changing the stroke volume and the heart rate changed the CO. The PI and PPI of the artrial blood pressure waveform were measured at 36 different points of the CO.

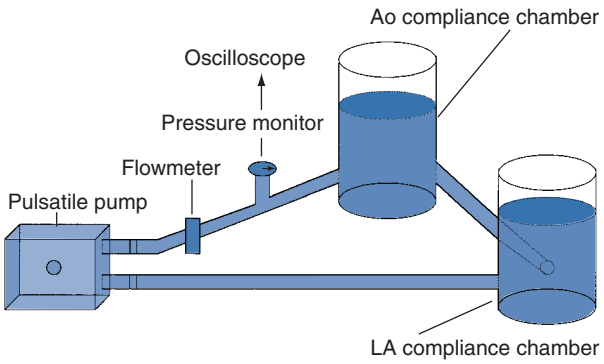

Figure 1. Schematic drawing of a mock circulation loop. The pneumatic pulsatile pump was used as a natural heart. Ao=aorta, LA=left atrium.

Figure 2 shows the arterial blood pressure waveforms and the FFT waveforms under the 1, 2.4 and 3.5 L min^{-1} CO. In relationship to the arterial blood pressure waveforms, when the CO was increased, then systolic arterial blood pressure was increased, while diastolic arterial blood pressure was decreased, and the pressure gradient was increased. In relationship to the FFT waveforms, when the CO was increased, then the amplitude of mean flow (A0) was decreased, and the amplitude of all other waves was increased. There was a positive significant correlation between the CO and the PI and PPI. The PI and PPI increased exponentially with the increase of the CO, (Figure 3). These results indicate that it may be possible to estimate CO from the analysis of the pulsatility of the arterial blood pressure waveform using FFT technique.

In vitro study: analysis of the arterial blood pressure waveform during LVAD

Fixed cardiac output condition

A change in pulsatility of the arterial blood pressure waveform was utilized to examine the correlation between the LVAD assist ratio and the arterial blood pressure waveform. For this study, a mock circulation loop was modified and a centrifugal pump was included as an LVAD with left atrial drainage (Figure 4). The Gyro C1E3 pump (Kyocera Corporation, Kyoto, Japan) was utilized as the LVAD. The outlet pressure (arterial blood pressure) was measured, and the LVAD flow and pulsatile pump flow were measured with ultrasound flowmeters. This centrifugal pump (C1E3) was developed as a cardiopulmonary bypass pump and a short-term LVAD[26–28]. The pneumatic pulsatile pump simulating the natural heart produced 3.5 L min^{-1} flow (stroke volume 50 ml, heart rate 70 bpm). In this study, the LVAD rotational speed was increased at 50 rpm increments under a fixed condition of the pulsatile pump. The LVAD rotational speed

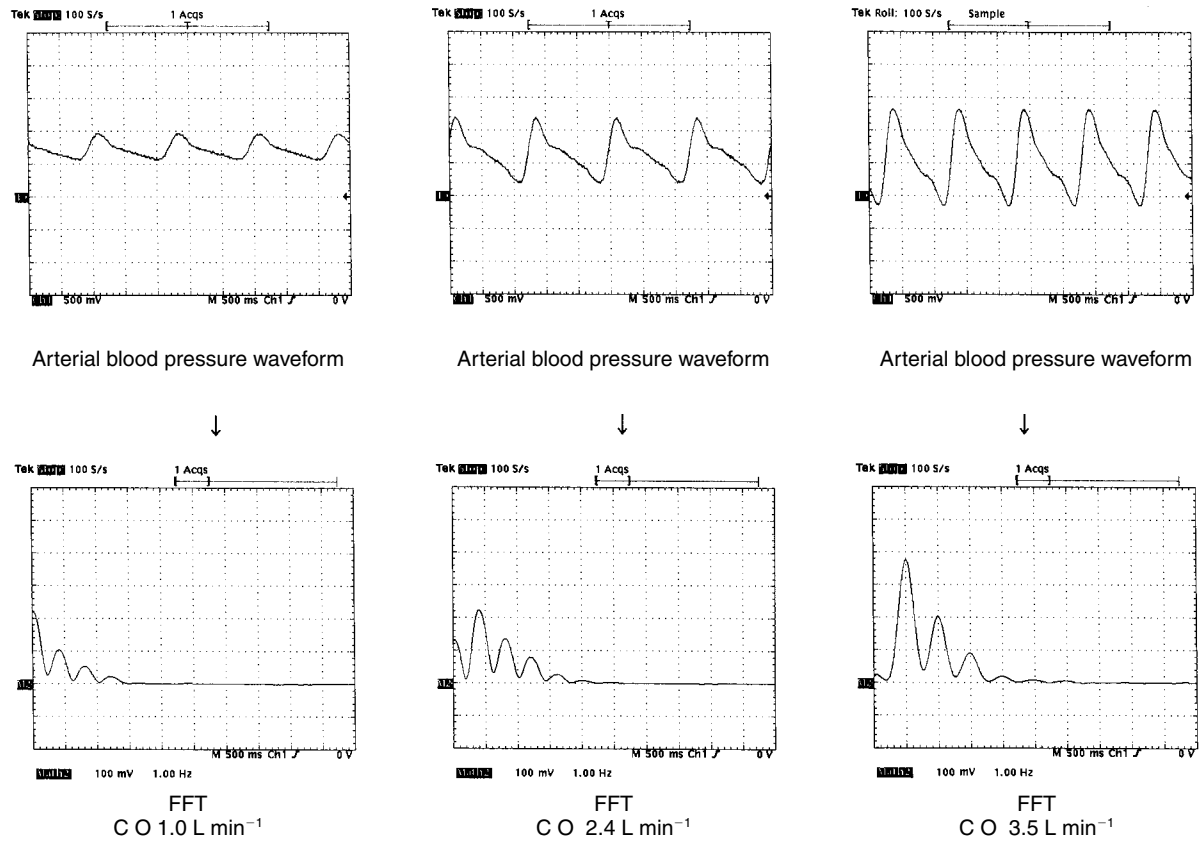

Figure 2. Actual flow waveforms and Fast Fourier Transform waveforms. (Left) Cardiac output 1.0 L min^{-1}; (middle) cardiac output 2.4 L min^{-1}; (Right) Cardiac output 3.5 L min^{-1}. FFT=Fast Fourier Transform, CO=cardiac output.

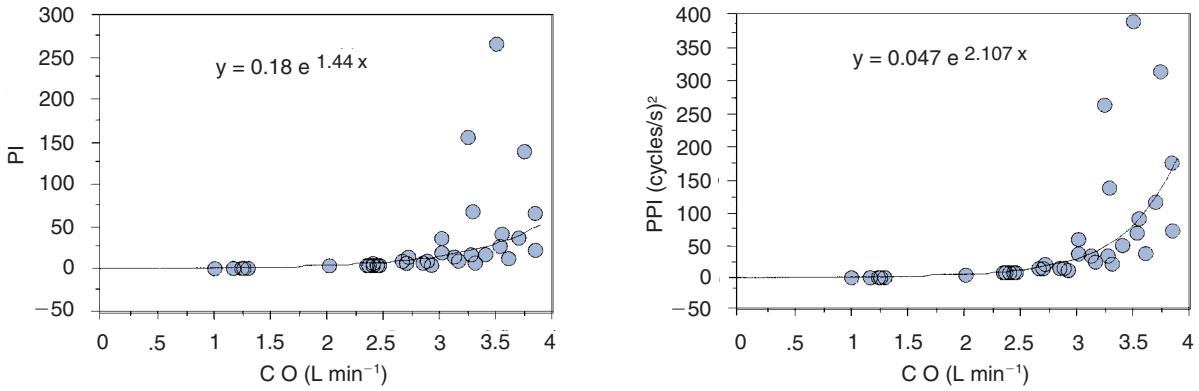

Figure 3. Correlation of the cardiac output and PI, and PPI. (Left) Correlation of the cardiac output and PI; (Right) Correlation of the cardiac output and PPI. PI=pulsatility index, PPI=pulse power index, CO=cardiac output.

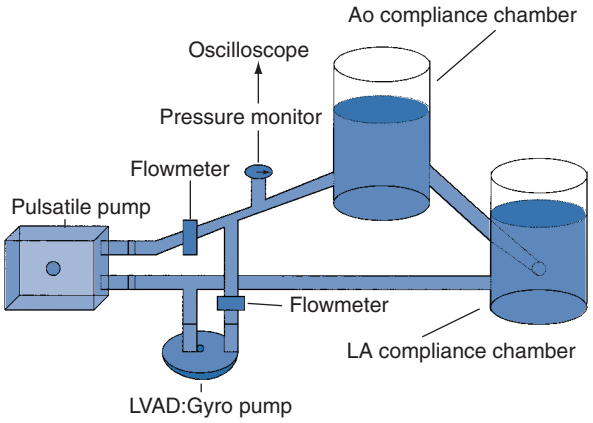

Figure 4. Schematic drawing of a mock circulation loop with LVAD. The centrifugal pump was employed as a LVAD, and the pneumatic pulsatile pump was used as a natural heart. Ao = aorta, LA = left atrium, LVAD = left ventricular assist device.

changed from 300 to 2200 rpm. During this time, the LVAD pump flow changed from 0 to 10 L min^{-1}. According to this flow rate change, the assist ratio (AR) (AR = LVAD flow rate/pulsatile blood pump rate + LVAD flow rate) was changed from 0 to 99%. The PI and PPI of the arterial blood pressure waveform were measured at 39 different points of the LVAD rotational speed.

There was a significant negative correlation between the LVAD's rotational speed, flow rate, AR and the PI, and PPI. The PI and PPI decreased with the increase of the LVAD's rotational speed, flow rate and AR, exponentially (Figure 5). It was also possible to analyze the relationship of the PPI and AR using a simple linear regression.

Various cardiac output conditions in a fixed LVAD rotational speed

Next, the correlation between the LVAD AR and the arterial blood pressure waveform was examined under various CO conditions. The LVAD rotational speed was maintained at 700 rpm. The pneumatic pulsatile pump produced 0.24–2.96 L min^{-1} flow (stroke volume 4.8–46.8 ml; heart rate 50–100 bpm). According to this change in the CO, the LVAD pump flow changed from 2.03 to 3.26 L min^{-1} and the AR was changed from 41 to 93%. The PI and PPI of the arterial blood pressure waveform were measured at 36 different points in various CO conditions. In a fixed LVAD rotational speed, the PI and PPI increased with the increase of the CO, and decreased with the increase of AR, exponentially (Figure 6a).

Various cardiac output conditions in a fixed LVAD flow rate

The LVAD flow rate was maintained at 3.3 L min^{-1}. The pneumatic pulsatile pump produced 0.21–2.70 L min^{-1} flow (stroke volume 4.2–45.0 ml, heart rate 50–100 bpm). According to this change of CO, the LVAD rotational speed changed from 700 to 930 rpm and the AR was changed from 55 to 94%. The PI and PPI of the arterial blood pressure waveform were measured at 36 different points in various CO conditions. Likewise in a fixed LVAD flow rate, the PI and PPI increased with the increase of the CO, and decreased with the increase of AR, exponentially (Figure 6b).

In vivo study: analysis of the arterial blood pressure waveform during LVAD in animal models

Based on evidence of the *in vitro* study, the change of the arterial blood pressure waveform during left ventricular assistance was evaluated using animal models. All animals involved in this study received humane care in compliance with the *Guiding Principles in the Care and Use of Animals* approved by the Council of the American Physiological Society (revised 1980) and the *Guide for the Care and Use of Laboratory Animals* published by the National Institutes of Health (NIH Publication No. 85–23, revised 1985). After the left pleural cavity was opened through the fifth intercostal space under general anesthesia, a prototype implantable rotary blood pump was implanted as an LVAD into six healthy calves. The direct left carotid arterial blood pressure waveform was measured and recorded by an oscilloscope. Implantable ultrasonic flow probes were attached to the outlet graft and main pulmonary artery. After completing the surgical procedure, measurements were taken

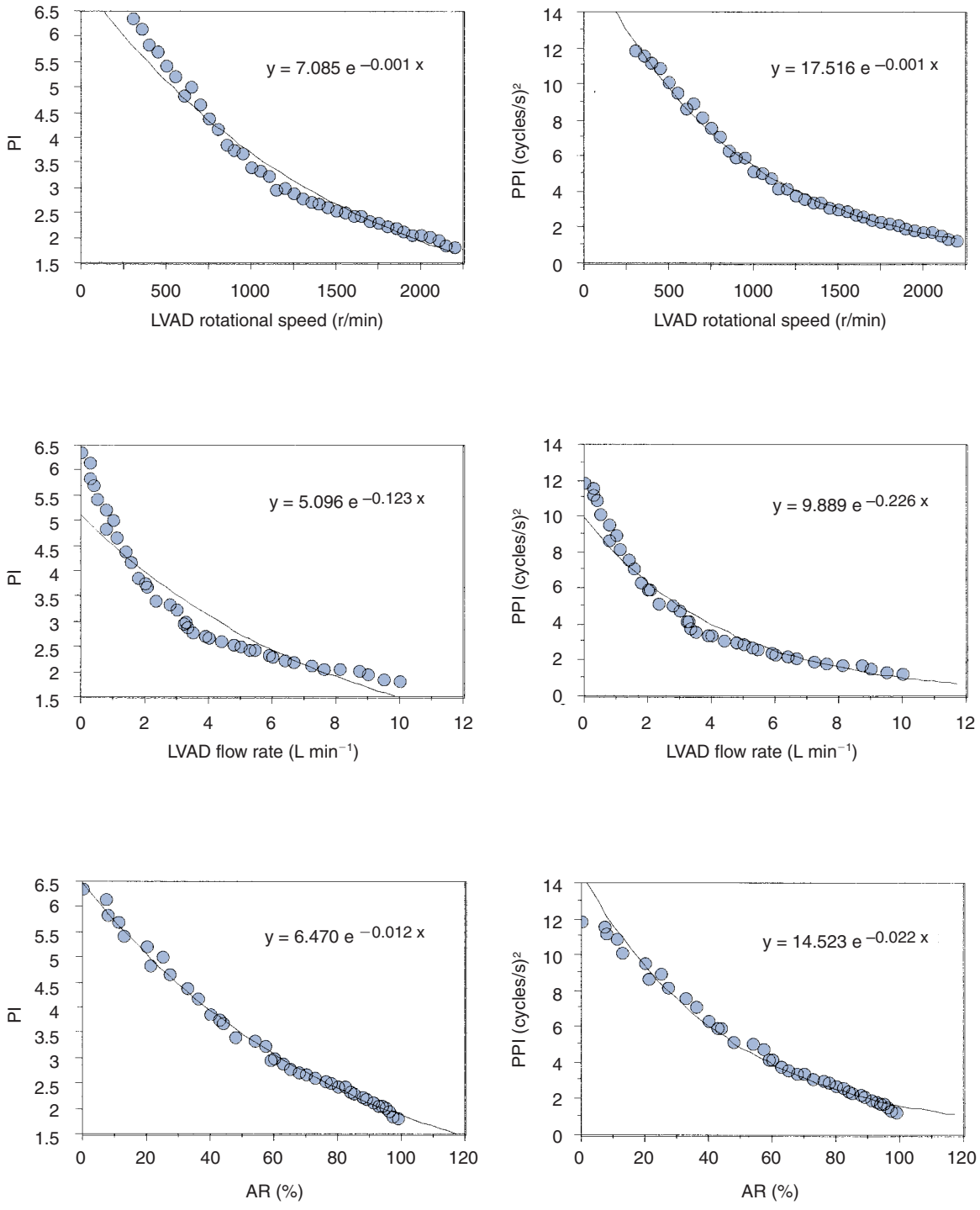

Figure 5. Correlation of the LVAD rotational speed, flow rate, assist ratio and PI, PPI. LVAD = left ventricular assist device, PI = pulsatility index, PPI = pulse power index, AR = assist ratio.

under a stable hemodynamic condition. The LVAD rotational speed was adjusted to 1440–2929 rpm. According to this rotational speed, the LVAD flow rate changed at 3.92–8.91 L min^{-1}. The pulmonary artery flow (CO) was 6.77–19.40 L min^{-1}. According to the change in the LVAD flow rate and pulmonary artery flow rate, the assist ratio (AR) was changed from 29.7 to 92.8%. The PI and PPI of the arterial blood pressure waveform were measured at

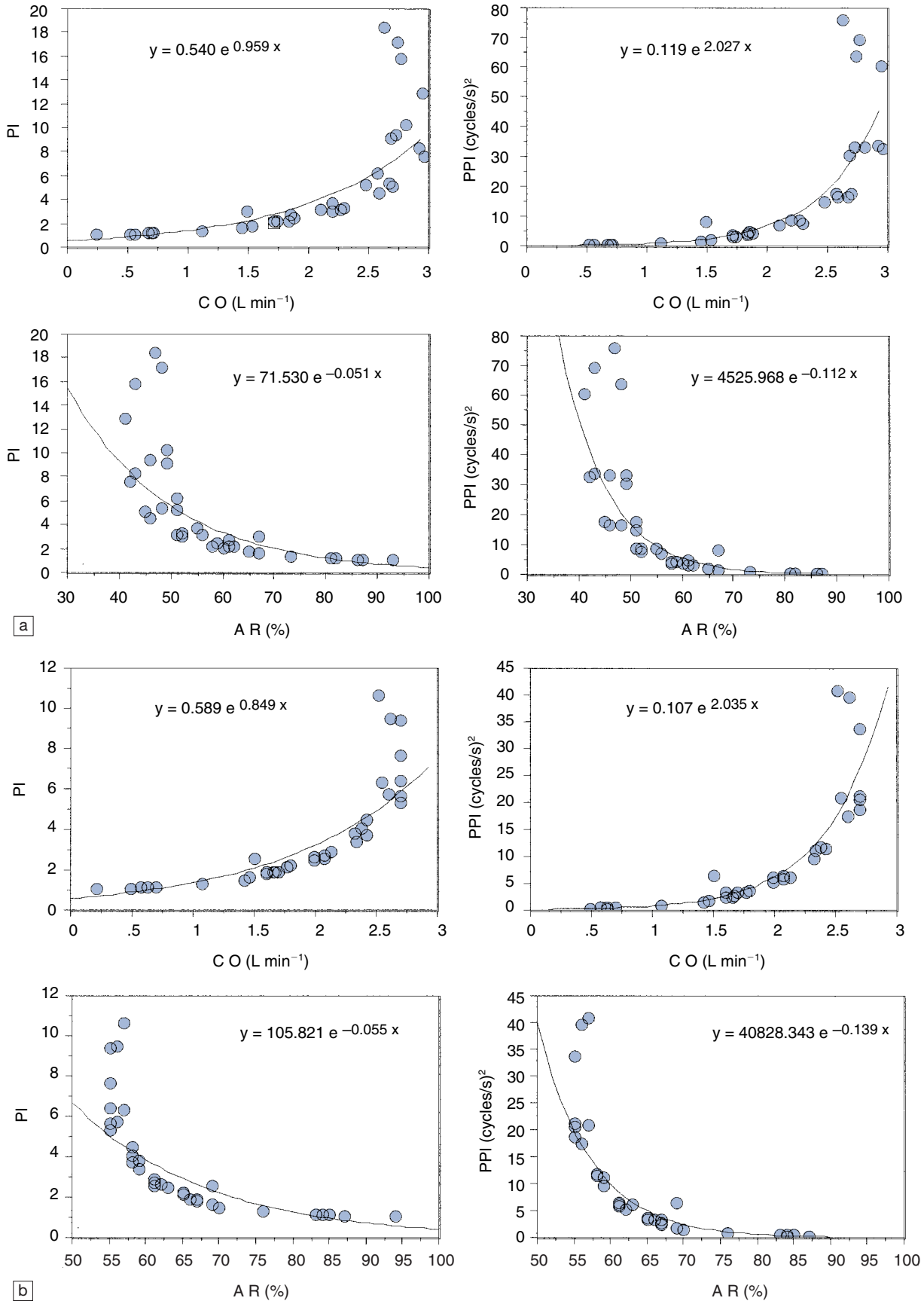

Figure 6. (a) Correlation of the cardiac output, assist ratio and PI, PPI in a fixed LVAD rotational speed; (b) Correlation of the cardiac output, assist ratio and PI, PPI in a fixed LVAD flow rate. LVAD=left ventricular assist device, PI=pulsatility index, PPI=pulse power index, CO=cardiac output, AR=assist ratio.

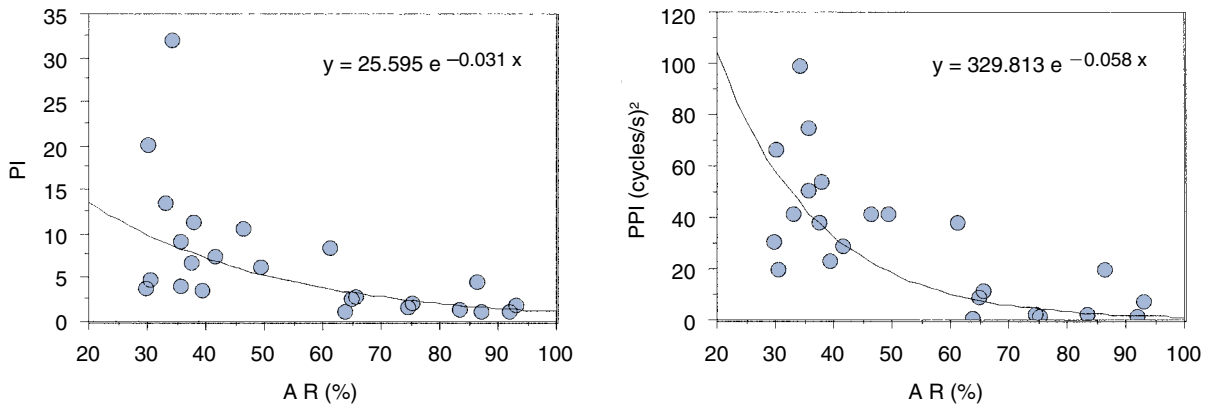

Figure 7. Correlation of the LVAD assist ratio and PI (left), PPI (right) in animal models. LVAD=left ventricular assist device, PI=pulsatility index, PPI=pulse power index, AR=assist ratio.

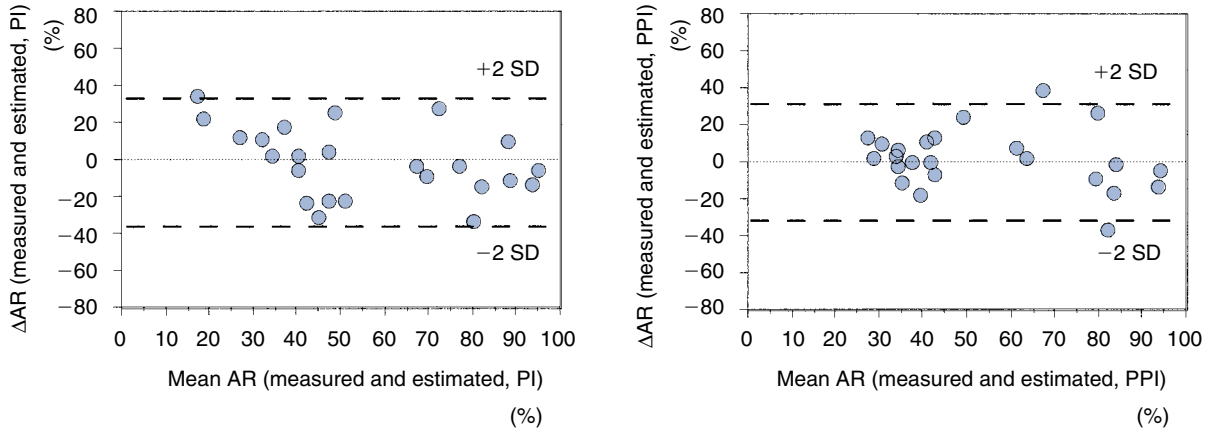

Figure 8. Differences between the two measurements against their means. (Left) Bland–Altman plot of measured AR and estimated AR from PI; (Right) Bland–Altman plot of measured AR and estimated AR from PPI. AR = assist ratio, PI = pulsatility index, PPI = pulse power index.

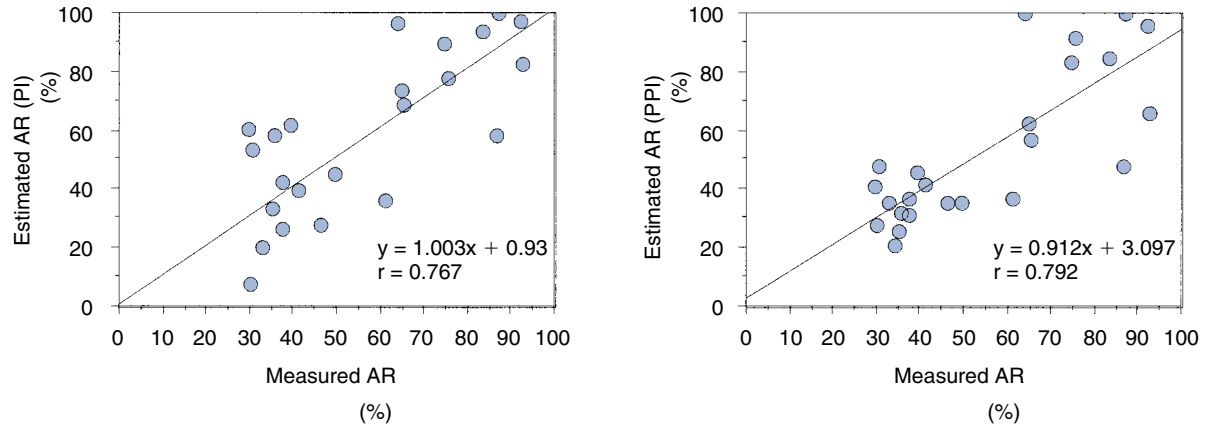

Figure 9. Correlation of the measured AR and estimated AR from PI and PPI. (Left) Correlation of measured AR and estimated AR from PI; (Right) Correlation of measured AR and estimated AR from PPI. AR=assist ratio, PI=pulsatility index, PPI=pulse power index.

24 different points during various conditions (four times per calf).

There was no significant correlation between the LVAD's rotational speed, flow rate, CO and the PI and PPI. However, there was a significant negative correlation between AR and the PI and PPI. Similar to the *in vitro* study, the PI and PPI decreased exponentially with the increase of the AR during left heart bypass with the rotary blood pump. Regression

equations were as follows: $y = 25.595\, e^{-0.031\, x}$, $y = 329.813\, e^{-0.058\, x}$, respectively (Figure 7). Therefore, the PI and PPI can be used as a reverse estimate of the AR.

Next, the accuracy of the AR calculated from the regression equation (estimated AR), in comparison to AR measured with a flowmeter (measured AR), was tested by the method according to Bland and Altman[29]. Bias between methods was determined as the mean difference between estimated AR and measured AR. The precision of AR measurements was given by the limits of agreement (2 SD of the mean difference between methods). Additionally, correlation analysis was performed between methods. Wilcoxon signed-ranks test was used to compare the mean difference with zero, and a probability value of < 0.05 was considered to be significant.

Differences between methods and correlation analysis are shown in Figures 8 and 9. The mean difference of measured AR and estimated AR from PI was 1.07% (2 SD of differences between methods = 37.44%). The mean difference of measured AR and estimated AR from PPI was 1.78% (2 SD of differences between methods = 31.6%) (Figure 8). Correlation analysis between estimated AR from PI and measured AR showed a close linear relationship between both measurement techniques ($r = 0.767$). The coefficient of correlation for the comparison of estimated from PPI and estimated AR was 0.792 (Figure 9). There were no significant differences between estimated AR from PI, PPI and measured AR. An improved fit was observed between the estimated AR from PPI and the measured AR.

Discussion

The rotary blood pump will be an implantable LVAD in the near future. However, the best control method and the interrelationship between the rotary blood pump and native heart function are unclear. Thus it is necessary to obtain the optimum LVAD assist ratio by estimating the native heart function. The FFT technique was used to quantify the pulsatility of the arterial blood pressure waveform. The present experimental series had two goals: to quantify the pulsatility of the arterial blood pressure waveform during left ventricular nonpulsatile assistance in terms of PI and PPI, and to examine the correlation between the LVAD condition and PI, and PPI both *in vitro* and *in vivo* study.

These results indicate that PI and PPI were good indicators of the arterial blood pressure waveform changes depending on changes in the pulsatility. When the LVAD's AR was increased, the amplitude of A0 was increased and the amplitude of the other waves were decreased. A0 is the component of direct current, and the other waves are the components of alternating currents. In other words, the component of direct current increased, and the components of alternating currents decreased following the increase of the LVAD's AR. These findings were confirmed with the change of the PI and PPI. In consequence, there was a significant negative correlation between the PI, PPI and the AR. Similar to the *in vitro* study, the PI and PPI *in vivo* study also decreased exponentially with the increase of the assist ratio. These indices could be used as a reverse estimate of the AR. In addition, a significant agreement between the AR calculated from the regression equation and the AR measured with a flowmeter was observed by plotting the difference against the mean value of the two measurements (Bland–Altman plot) [29].

The analysis of the pulsatility of the arterial blood pressure waveform using the FFT technique may be useful in estimating an ideal LVAD condition. However, these results have important limitations. The principal limitation is that the influences of the peripheral vascular factors were not taken completely into account. The arterial blood pressure waveform is influenced by the systemic vascular resistance[9]. Thus, the arterial blood pressure waveform contains information regarding both the functions of the left ventricle and the arterial system. Another limitation is that this method requires accuracy and a noise-free pressure signal. Even minimal noise will produce major distortion. This is not always possible in the clinical environment. Therefore, our measurements show considerable scatter around the regression line. In addition, it should be noted that patients with arrhythmia would probably give erratic or erroneous results.

Conclusion

The analysis of the arterial blood pressure waveform using the FFT technique may be useful in assessing the LVAD condition under fixed and various CO conditions. These results of *in vitro* study were confirmed using animal models. By using this analysis methodology, a physiologically effective ventricular assistance may be achieved.

References

1. Martin JF, Volfson LB, Kirzon-Zolin VV, Schukin VG. Application of pattern recognition and image classification techniques to determine continuous cardiac output from the arterial pressure waveform. *IEEE Trans Biomed Eng* 1994;41:913–20.
2. Guarini M, Urzua J, Cipriano A, Gonzalez W. Estimation of cardiac function from computer analysis of the arterial pressure waveform. *IEEE Trans Biomed Eng* 1998;45:1420–8.
3. Weissman C, Ornstein EJ, Young WL. Arterial pulse contour analysis trending of cardiac output: Hemodynamic manipulations during cerebral arteriovenous malformation resection. *J Clin Monit* 1993;9:347–53.
4. Tannenbaum GA, Mathews D, Weissman C. Pulse contour cardiac output in surgical intensive care unit patients. *J Clin Anesth* 1993;5:471–8.
5. Irlbeck M, Forst H, Briegel J, Haller M, Peter K. Continuous measurement of cardiac output with pulse contour analysis. *Anaesthesist* 1995;44:493–500.
6. Buhre W, Weyland A, Kazmaier S *et al.* Comparison of

cardiac output assessed by pulse contour analysis and thermodilution in patients undergoing minimally invasive direct coronary artery bypass grafting. *J Cardiothorac Vasc Anesth* 1999;13:437–40.
7. Preisman S, Pfeiffer U, Lieberman N, Perel A. New monitors of intravascular volume: a comparison of arterial pressure waveform analysis and the intrathoracic blood volume. *Intensive Care Med* 1997;23:651–7.
8. Urtua J, Salinas C, Cipriano A, Guarini M, Lema G, Canessa R. Estimation of ventricular volume and elastance from the arterial pressure waveform. *J Clin Monit Comput* 1998;14:177–81.
9. Mohr R, Meir O, Smolinsky A, Goor DA. A method for continuous on-line monitoring of systemic vascular resistance (COMS) after open heart procedures. *J Cardiovasc Surg* 1987;28:558–65.
10. Womersley JR. An elastic tube theory of pulse transmission and oscillatory flow in mammalian arteries. *WADC Technical Report* TR 56–614. Dayton: Wright Air Development Center, 1957.
11. Contant CF Jr, Robertson CS, Crouch J, Gopinath SP, Narayan RK, Grossman RG. Intracranial pressure waveform indices in transient and refractory intracranial hypertension. *J Neurosci Methods* 1995;57:15–25.
12. Grossi EA, Connolly MW, Krieger KH *et al*. Quantification of pulsatile flow during cardiopulmonary bypass to permit direct comparison of the effectiveness of various type of 'pulsatile' and 'nonpulsatile' flow. *Surgery* 1985;98:547–54.
13. Gosling RG, Dunbar G, King DH *et al*. The quantitative analysis of occlusive peripheral arterial disease by a non-intrusive ultrasonic technique. *Angiology* 1971;22:52–5.
14. Gosling RG, King D, Woodcock JP. Blood-velocity waveforms in the evaluation of atheromatous changes. In Roberts C, editor. *Blood Flow Measurement*. Baltimore: Williams & Wilkins Co., 1972:33–6.
15. Souma A. The effect of 'pulsation' on resistance during extracorporeal circulation experimental study based on the quantification of pulsatile flow curve. *J Jpn Assoc Thorac Surg* 1988;36:102–11.
16. Nakata K, Ohashi Y, Tayama E *et al.* Estimation of the native cardiac output from a rotary blood pump flow: *In vitro* study. *Artif Organs* 1998;22:411–13.
17. Hogness JR, VanAntwerp M. Executive summary. In Hogness JR, VanAntwerp M, editors. *The artificial heart: prototypes, policies, and patients*. Committee to evaluate the artificial heart program of the National Heart, Lung, and Blood Institute. Washington, DC: National Academy Press, 1991:1–13.
18. Funk D. Epidemiology of end-stage heart disease. In Hogness JR, VanAntwerp M, editors. *The artificial heart: prototypes, policies, and patients*. Committee to evaluate the artificial heart program of the National Heart, Lung, and Blood Institute. Washington, DC: National Academy Press, 1991: 251–61.
19. Oz MC, Rose EA, Levin HR. Selection criteria for placement of left ventricular assist devices. *Am Heart J* 1995;129:173–7.
20. Hunt SA. Current status of cardiac transplantation. *JAMA* 1998;280:1692–8.
21. Noon GP. Clinical use of cardiac assist devices. In: Akutsu T, Koyanagi H, editors. *Artificial Heart 4. Heart Replacement*. Tokyo: Springer–Verlag, 1993:195–205.
22. Curtis JJ. Centrifugal mechanical assist for postcardiotomy ventricular failure. *Semin Thorac Cardiovasc Surg* 1994; 6:140–6.
23. Körfer R, el-Banayosy A, Posival H *et al.* Mechanical circulatory support: the Bad Oeynhausen experience. *Ann Thorac Surg* 1995;59(2 Suppl):S56–63.
24. Nosé Y, Kawahito K, Nakazawa T. Can we develop a nonpulsatile permanent rotary blood pump? Yes, we can. *Artif Organs* 1996;20:467–74.
25. Tayama E, Nosé Y. Can we treat dilated cardiomyopathy using a left ventricular assist device? *Artif Organs* 1996;20:197–201.
26. Nakazawa T, Makinouchi K, Takami Y, Glueck J, Takatani S, Nosé Y. The effect of the impeller-driver magnetic coupling distance on hemolysis in a compact centrifugal pump. *Artif Organs* 1996;20:252–7.
27. Nakazawa T, Makinouchi K, Takami Y, Glueck J, Takatani S, Nosé Y. Modification of a pivot bearing system on a compact centrifugal pump. *Artif Organs* 1996;20:258–63.
28. Makinouchi K, Nakazawa Y, Takami Y, Takatani S, Nosé Y. Evaluation of the wear of the pivot bearing in the Gyro C1E3 pump. *Artif Organs* 1996;20:523–8.
29. Bland JM, Altman DG. Statistical methods for assessing agreement between two methods of clinical measurement. *Lancet* 1986;1:307–10.

Journal of Congestive Heart Failure and Circulatory Support (2001) Vol 1, No 4, 259–262

Pathophysiological aspect of an implantable ventricular assist device with short stroke and high frequency

T. Yambe[1], N. Owada[1], S.-I. Kobayashi[1], A. Tanaka[1], M. Yoshizawa[2], K.-I. Abe[2], K. Tabayashi[3], H. Takeda[4], H. Hashimoto[5] and S.-I. Nitta[1]

[1]Department of Medical Engineering and Cardiology, Institute of Development, Aging and Cancer, Tohoku University; [2]Graduate School of Engineering, Tohoku University; [3]Department of Thoracic and Cardiovascular Surgery, Tohoku University School of Medicine; [4]Faculty of Engineering, Tohoku-gakuin University; and [5]Institute of Fluid Sciences, Tohoku University, Sendai, Japan

Abstract The design concept of short stroke volume and high frequency was adopted for the development of a totally implantable ventricular assist device (VAD). The transcutaneous energy transmission system (TETS) using amorphous fiber was developed to constitute the totally implantable VAD. The vibrating flow pump (VFP), which was developed with short stroke volume in mind, works with a high frequency of 10–50 Hz compared with the natural heart of a biological system. In this research, acute and chronic animal experiments were carried out on healthy adult goats. All hemodynamic data was stored on magnetic tape and analyzed in the computer system through an AD converter. Adequate pump flow was provided by the left ventricular cannulation. A 100% left heart bypass was confirmed by measuring aortic and left ventricular pressures. Peripheral vascular resistance was compared during total left heart bypass with a VFP and a rotary pump (RP). Resistance during VFP assist was significantly higher compared with that during RP assist, suggesting that the effect of a left heart bypass with the VFP upon vascular resistance was lower. During left heart bypass with VFP, blood flow distribution was measured using various pumping frequencies. The results, according to an alteration of the drive frequency, showed that blood flow distribution was significantly changed even during the same total blood flow with 100% left heart bypass. The TETS with amorphous fibers performed well enough in chronic animal experiments and the temperature rise was not significant. It may be possible to control the blood flow distribution during left ventricular assistance with our newly developed VFP system. We are anxious to continue our development of a totally implantable VAD.

Keywords ventricular assist device (VAD), vibrating flow pump (VFP), rotary pump (RP), totally implantable VAD.

Introduction

The artificial heart is an important alternative to transplantation in the treatment of profound heart failure[1–10]. Recently, there has been a resurgence in the clinical application of heart transplantation in Japan. However, patients with severe heart failure cannot afford to wait too long for a donor. A ventricular assist device (VAD) is used as a bridge to transplantation[11–14] and the waiting time may be prolonged in many cases. The patient's quality of life (QOL) during their wait for a donor heart is an important consideration. The clinical application of the totally implantable VAD is of great importance in such cases. However, the VADs developed in Europe and the USA are too large to be implanted into oriental people. A VAD designed for a smaller body is required and, for that purpose, development has been carried out in many institutions[5–11]. The rotary pump was an important development; however, there is some doubt concerning the influence of nonpulsatile flow. For that reason, we have been developing a new, small artificial heart. In this system, the driving rate is increased and the stroke volume decreased, so the flow becomes an oscillated flow of high frequency (10–50 Hz). The influence of oscillated blood flow is evaluated in this study.

Vascular resistance

Before the clinical application of the vibrating flow pump (VFP) is considered, the influence of vibration must be examined. First, a 100% total left heart bypass with an oscillated blood flow controlled by a VFP was compared with a continuous flow bypass controlled with a rotary pump (RP).

Time-series data of the hemodynamic parameters is shown in Figure 1. The 100% total left heart bypass is apparent, because left ventricular pressure was lower compared with aortic pressure. In this study, peripheral vascular resistance was compared (Figure 2). There were a few influences on the living body as a result. The figure shows that resistance was not significantly decreased compared with that during RP total left heart bypass. This data may be favorable in maintaining resistance when considering the clinical application.

Correspondence to: Tomoyuki Yambe MD PhD, Department of Medical Engineering and Cardiology, Institute of Development, Aging and Cancer, Tohoku University, 4–1 Seiryo-machi, Aoba-ku, Sendai 980–8575, Japan.

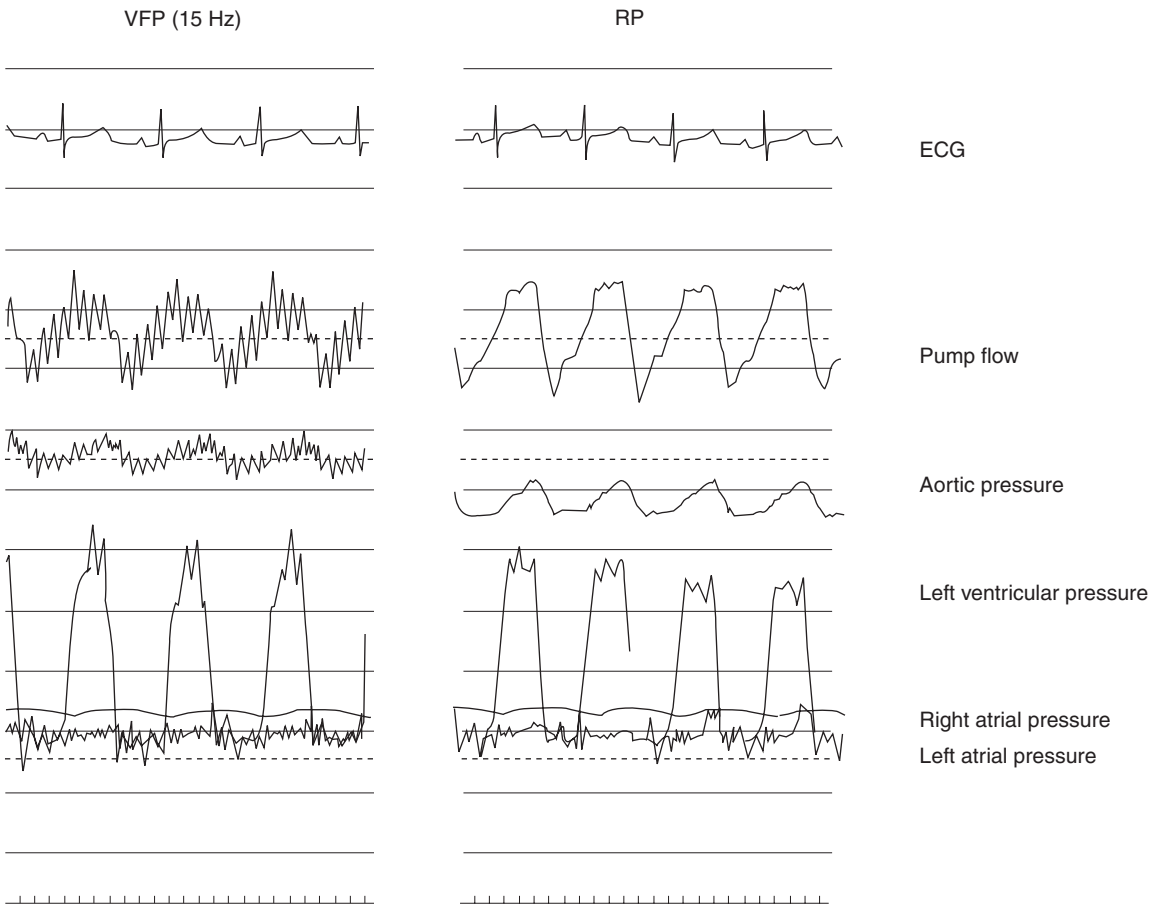

Figure 1. Time-series data of the hemodynamic parameters during total left heart bypass with a vibrating flow pump (VFP) and rotary pump (RP).

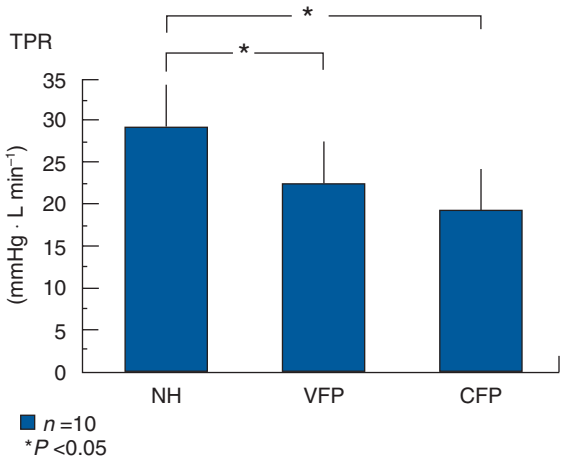

Figure 2. Peripheral vascular resistance during total left heart bypass with a vibrating flow pump (VFP) and rotary pump. NH: native heart; VFP: vibrating flow pump; CFP: continuous flow pump.

Blood flow distribution

The effect of the alteration in drive frequency was compared with the same amount of total blood flow in 100% left heart bypass. In this study, we paid attention to the distribution of the blood flow; the result is shown in Figure 3. This figure shows the time-series data of the hemodynamic derivatives with various drive frequencies of the VFP. 100% left heart bypass was achieved in each drive frequency.

As shown in the Figure 4, the blood to the lower half of the body increases according to the alteration of the oscillated frequency. This result shows the feasibility of controlling blood flow distribution with the VFP.

These data show that the frequency of blood flow influences the circulatory regulatory system. This phenomenon was compared with aortic input impedance patterns evaluated from the flow and pressure waveform. The results are presented in Figure 5. The impedance pattern was examined by electrical circuit simulation[15]. The influence of the frequency was analyzed.

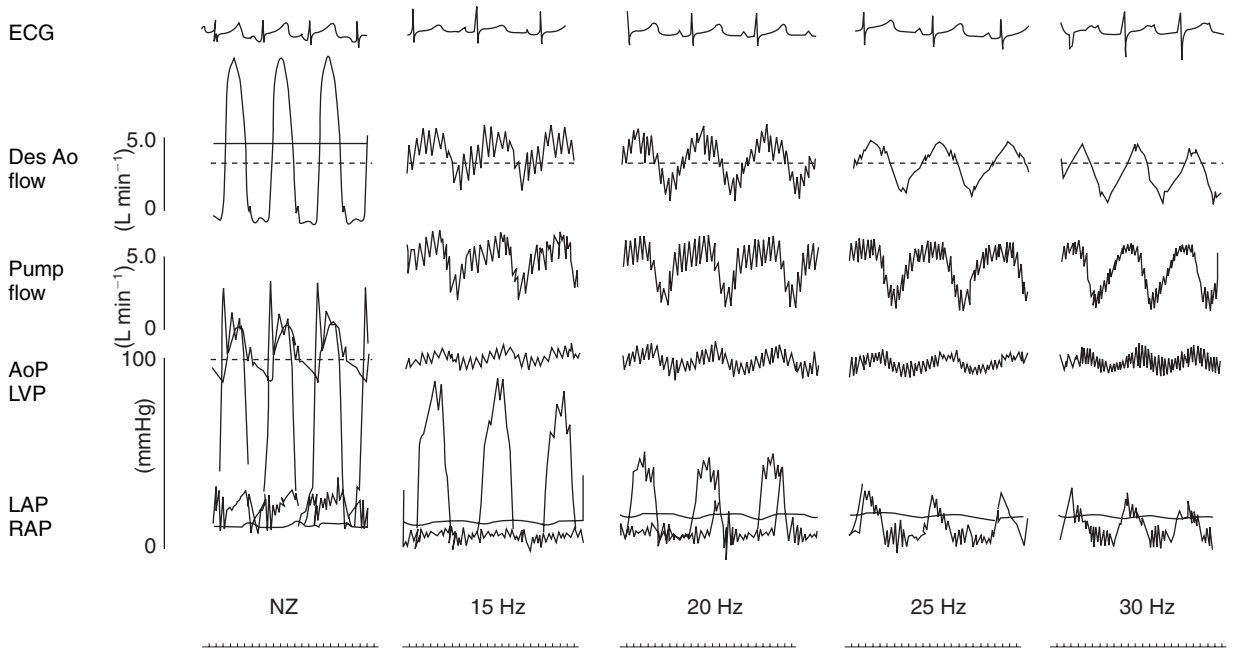

Figure 3. Time-series data of the hemodynamic parameters during total left heart bypass with a vibrating flow pump with various drive frequencies.

Discussion

As our results show, vibration of blood flow influences the body in various ways. However, there were fewer influences than when an RP was used. Some interesting results were observed; for example, the blood flow distribution appeared to be altered during the same amount of total flow. This phenomenon suggests the influence of blood flow on the characteristics of the blood vessels.

Blood vessel characteristics were examined further by the use of input impedance patterns. This suggested that the frequency of blood flow had an influence on blood vessel characteristics. Therefore, the influence of vibration on the cardiovascular system could not be ignored. This becomes apparent when we consider the application of these characteristics. For example, when circulation is assisted, its effect on the function of other internal organs is significant. The vibration of the blood flow can influence this; thus, a new dimension is added to assisted circulation when the results are considered. This study will continue with the next candidate for the VAD.

Acknowledgements

The authors thank Mr Kimio Kikuchi for his experimental preparation and kind cooperation; Miss Rie Sakurai,

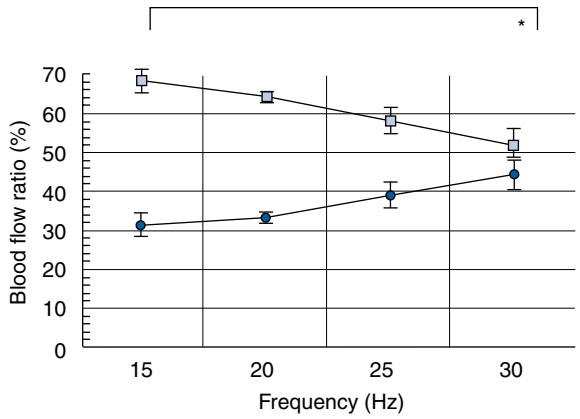

Figure 4. Blood flow distribution during total left heart bypass with a vibrating flow pump with various drive frequencies.

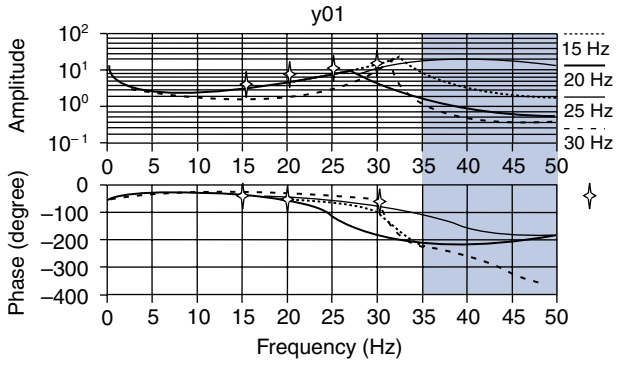

Figure 5. Impedance patterns calclated from an electrical circuit model (Ruchti *et al.*)

Miss Takako Iijima, and Mrs Hisako Iijima for their excellent technical assistance and kind cooperation.

This work was partly supported by a Grant-in-aid for Scientific Research (No. 11480253), Research Grant for Cardiovascular Diseases from the Ministry of Health and Welfare and Program for Promotion of Fundamental Studies in Health Science of Organizing for Drug ADR Relief, R&D Promotion and Product Review of Japan.

References

1. Snyder AJ, Rosenberg G, Reibson J *et al.* An electrically powered total artificial heart: Over 1 year survival in the calf. *ASAIO J* 1992;38:M707–12.
2. Yambe T, Abe Y, Yoshizawa M *et al.* Strange hemodynamic attractor parameter with 1/R total artificial heart automatic control algorithm. *Int J Artif Organs* 1996;19:302–6.
3. Hiller KW, Seigel W, Kolff WJ. A servomechanism to drive an artificial heart inside the chest. *ASAIO Trans* 1962;8:25–30.
4. Yambe T, Nitta S, Sonobe T *et al*. Development of total artificial heart having advantages in economy and durability. *Int J Artif Organs* 1998;21:279–84.
5. Tatsumi E, Nakamura M, Masuzawa T, *et al*. *In vitro* and *in vivo* evaluation of a left–right balancing capacity of an interatrial shunt in an electrohydraulic total artificial heart system. *ASAIO J* 1997;43: M619–5.
6. Kung RTV, Yu RS, Ochs BD *et al*. Progress in the development of the ABIOMED total artificial heart. *ASAIO J* 1995;41:M245–8.
7. Yambe T, Nitta S, Sonobe T *et al.* Chaotic hemodynamics during oscillated blood flow. *Artif Organs* 1994;18:633–7.
8. Yambe T, Nitta S, Sonobe T *et al.* Effect of left ventricular assistance on sympathetic tone. *Int J Artif Organs* 1990;13:681–6.
9. Yambe T, Nitta S, Katahira Y *et al.* Fundamental rhythm of the sympathetic nerve discharges in animals with total artificial hearts. *ASAIO J* 1992;39:91–5.
10. Nojiri C, Kijima T, Maekawa J *et al.* More than 1 year continuous operation of a centrifugal pump with a magnetically suspended impeller. *ASAIO J* 1997;43:M548–52.
11. Yambe T, Nitta S, Sonobe T *et al.* Deterministic chaos in the hemodynamics of an artificial heart. *ASAIO J* 1995;41:84–8.
12. Yambe T, Nitta S, Sonobe T *et al.* Origin of the rhythmical fluctuations in hemodynamic parameters in animals without natural heartbeat. *Artif Organs* 1993;17:1071–21.
13. Yambe T, Nitta S, Sonobe T *et al.* Chaotic behavior of the hemodynamics with ventricular assist device. *Int J Artif Organs* 1995;18:17–21.
14. Yambe T, Owada N, Kobayashi S *et al.* Left heart bypass using the oscillated blood flow with totally implantable vibrating flow pump. *Artif Organs* 1998;22:426–9.
15. Ruchti T, Brown R, Cjeutter D, Feng X. Identification algorithm for systemic arterial parameters with application to total artificial heart control. *Ann Biomed Eng* 1993;24:221–6.

Session 5
Biomaterial

Journal of Congestive Heart Failure and Circulatory Support (2001) Vol 1, No 4, 265–270

Phospholipid polymer biomaterials for making ventricular assist devices

K. Ishihara PhD[1], Y. Iwasaki PhD[2] and C. Nojiri MD PhD[3]

[1]Department of Materials Science, Graduate School of Engineering, The University of Tokyo, Hongo, Bunkyo-ku, Tokyo, Japan; [2]Division of Organic Materials, Institute of Biomaterials and Bioengineering, Tokyo Medical and Dental University, Kanda-surugadai, Chiyoda-ku, Tokyo, Japan; and [3]R&D Center, Terumo Co., Inokuchi, Nakai, Ashigarakami-gun, Kanagawa, Japan

Abstract Elastic polymeric biomaterials that are highly non-thrombogenic and stable under biological conditions are necessary for successful implantation of the artificial heart. We designed a new polymer biomaterial, which was inspired from cell membrane structure; that is, the synthesis of a 2-methacryloyloxyethyl phosphorylcholine (MPC) polymer that has typical phospholipid polar group in the side chains. The elastic segmented polyurethane (SPU) was modified with the MPC polymer and the bioresponse of the material was evaluated *in vitro* and *ex vitro*. When the surface of the SPU was coated with the MPC polymer, plasma protein adsorption and following platelet adhesion and activation after contact with blood were significantly suppressed. The MPC polymer was coated on the inner surface of the pulsatile pump in a ventricular assist device (VAD) made of SPU, and the pump was applied to sheep. Very few thrombi were observed on the MPC polymer-coated pump after 27 days' application; however, the original SPU pump induced strong thrombus formation, even after only 4 days' application. The amount of plasma protein adsorbed on the surface of the MPC polymer-coated pump was very small compared with that on the SPU pump. From these results, we concluded that the MPC polymer is a useful tool that can be used to control the bioresponse on VAD.

Keywords blood compatible material, 2-methacryloyloxyethyl phosphorylcholine (MPC) polymer, surface modification, non-thrombogenicity, pulsatile pump, ventricular assist device (VAD).

Background

Many polymeric materials have been used for the fabrication of biomedical devices that come into contact with blood, body fluids and tissues[1]. Upon contact with blood, biocomponents in blood such as lipids and proteins interact with these surfaces and are adsorbed on them. Well-designed polymers are required to regulate their interactions. The adsorption state of these biocomponents strongly affects blood cell adhesion and activation, which induces thrombus formation. The final goal of this study is the control of protein adsorption and conformational change of the protein by regulation of the structure of the material surface. This is because protein adsorption is the first significant event when blood contacts with material and it induces a subsequent bioreaction towards clot formation[2].

New concepts for making a biocompatible polymer surface have been proposed and focus on the outer surface of the cell membrane, the biomembrane, which is mainly constructed of natural phospholipid molecules. Thus, we designed the molecular structure and synthesized a methacrylate monomer with a phospholipid polar group, 2-methacryloyloxyethyl phosphorylcholine (MPC)[3]. Polymers from the MPC group and other various alkyl methacrylates or styrene were prepared and their biocompatibility was carefully evaluated with attention to the blood–material interactions[4–7]. Blood cell adhesion and activation were suppressed on the surface of the MPC polymers when the MPC composition was above 25 mol%. Small plasma proteins were adsorbed on the MPC polymer surface compared with that on hydrophobic poly(*n*-butyl methacrylate)[poly(BMA)] and hydrophilic poly(2-hydroxyethyl methacrylate) surfaces. Many groups have been inspired by our research, and have recently recognized the superior resistance of protein adsorption and cell response on the surface of various phospholipid polymers[8–11].

In this article, biomedical segmented polyurethane (SPU) was modified with the MPC polymer by adding a coating to make novel medical polymers. The SPUs are widely used as biomedical materials because of their excellent mechanical properties[12]. However, the biocompatibility of the SPUs is not satisfactory for long-term implantation as an artificial blood vessel of artificial heart including a valve. We designed the molecular structure of MPC polymers as a coating material that is synthesized from MPC, hydrophobic alkyl methacrylate and methacrylate

Correspondence to: Kazuhiko Ishihara, Department of Materials Science, Graduate School of Engineering, The University of Tokyo, 7–3–1 Hongo, Bunkyo-ku, Tokyo 113–86956, Japan.

having urethane bond in the side chain. The MPC polymer-coated SPU membrane is characterized according to its surface property, mechanical property and biocompatibility. Finally, *ex vivo* evaluation of blood compatibility was carried out by coating the MPC polymer on the blood-contacting surface of the pulsatile pump in the ventricular assist device (VAD), and applying it to sheep.

Materials and methods

Preparation of materials

MPC and 2-methacryloyloxyethyl butylurethane (MEBU) were synthesized by a method reported previously[3,13]. *n*-Butyl methacrylate (BMA) was reagent grade and purified by vacuum distillation. Poly(etherurethane), Pellethane (PT) 2363–90 (Upjohn Co., USA) was kindly supplied from Terumo Co. Ltd. Other reagents were commercially available in extra-pure grade and were used without further purification.

The MPC, BMA and MEBU were copolymerized in ethanol using 2,2′-azobisisobutyronitrile (AIBN) as an initiator. The MPC polymer formed was purified by precipitation method. The structure of the ternary copolymer composed of MPC, BMA and MEBU (PMBBU) was confirmed by ^{1}H-NMR (nuclear magnetic resonance) spectroscopy, infrared spectroscopy (IR), and elemental analysis. The mole fraction of each component in the polymer was determined from the results of phosphorus analysis for the MPC units and nitrogen analysis for both the MPC and MEBU units. The chemical structure of the PMBBU is shown in Figure 1.

Preparation of polymer membrane and coating of the MPC copolymer

The PT membrane was prepared by a solvent evaporation technique. The thickness of the membrane obtained was 300 mm. The PMBBU was dissolved in ethanol to make a 0.3 wt% solution. The PT membrane was immersed in the solution containing the PMBBU for 1 min and dried at room temperature overnight to evaporate the solvent. After this procedure was repeated twice, the membrane was dried in vacuo at room temperature. The surface of the membrane coated with the PMBBU was analyzed using an X-ray photoelectron spectroscope (XPS) (ESCA–200, Uppsala, Sweden).

The pulsatile pump in the VAD was prepared with the PT by the thermal molding method. The inner side of the pump was coated with PMBBU from an ethanol solution using a similar procedure mentioned earlier.

Blood contacting test

The disk-shaped PT membranes and those coated with the PMBBU (15 mm in diameter) were placed into a 24-well cell culture plate and fixed with a silicone ring. The membrane surface was equilibrated with phosphate-buffered solution (PBS pH 7.4; ionic strength 0.15 M). After removing the PBS, 1 mL of platelet-rich plasma (PRP) prepared from human citrated blood was poured onto the membrane and allowed to remain at 37°C for 3 h. The PRP was removed and the membrane was rinsed three times with PBS. To fix the blood components that adhered to the surface, glutaraldehyde in PBS was applied. After rinsing sufficiently with distilled water, the membrane was freeze-dried. The surface of the membrane was observed with a scanning electron microscope (SEM, JEOL JSM–5400, Tokyo, Japan).

Animal experiment

The pulsatile pumps, either original PT or coated with PMBBU in a VAD, were applied to sheep by normal surgery. After a given period, the inner surface of the pump was observed optically. The surface was also observed with SEM after the usual treatment. Figure 2 demonstrates the animal experiment.

Results

Surface characterization of PT membrane coated with PMBBU

The synthesis of the MPC polymer, PMBBU was successful and a good yield was achieved. The synthetic results are shown in Table 1. The chemical structure of the PMBBU was confirmed by spectroscopy and elemental analysis. The unit mole fraction of the PMBBU used in this study was MPC/BMA/MEBU = 0.36/0.53/0.11. It was dissolved in ethanol, N,N-dimethylformamide, N,N-dimethylacetoamide, but insoluble in water. The coating of the PMBBU on the PT membrane was confirmed by XPS. The representative XPS chart of PT and that coated with PMBBU is shown in Figure 3. The carbon (C_{1s}) peaks attributed to the C=O bond at 287 eV and the C=O group at 288 eV showed clearly, and the new peaks of nitrogen (N_{1s}) at 403 eV and phosphorus at

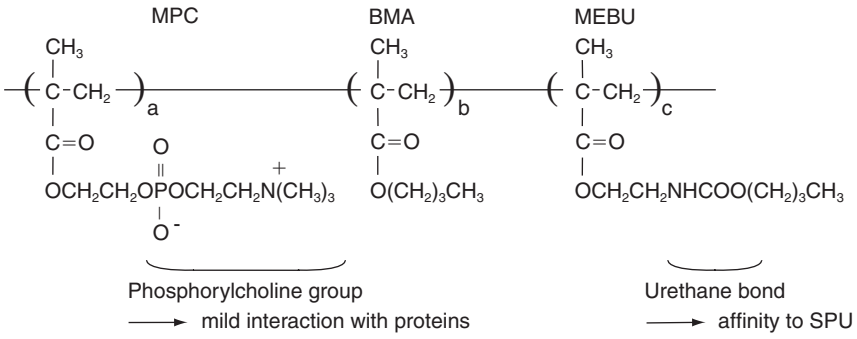

Figure 1. Chemical structure of the MPC polymer used in this study (PMBBU).

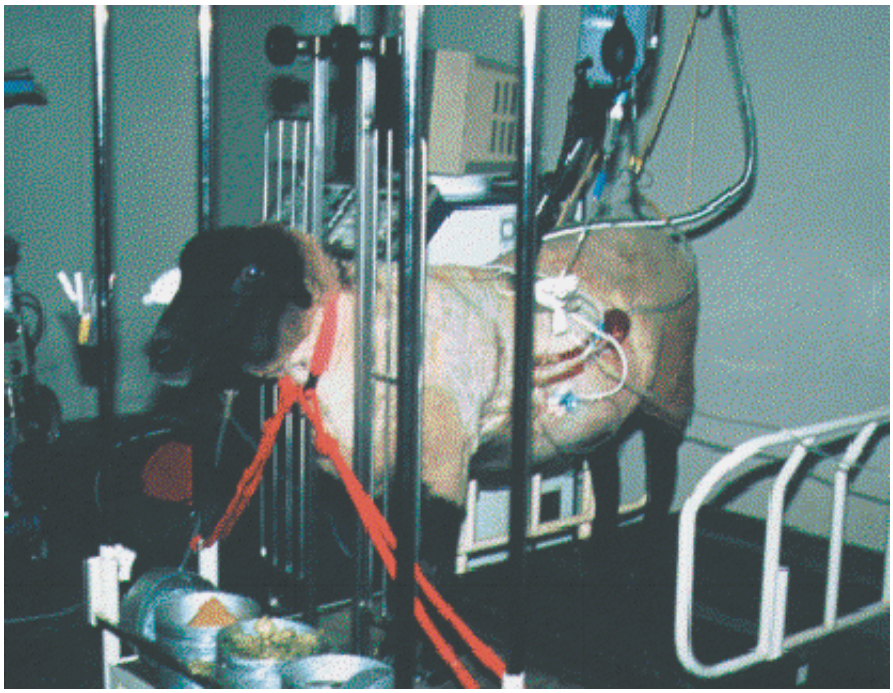

Figure 2. *Ex vivo* evaluation system of blood compatibility of the polymer using sheep.

Table 1. Synthetic results of the MPC polymer

Abb.	Mole fraction (MPC/BMA/MEBU)		Time[1] (h)	Yield (%)	MW[2] 10^5
	in feed	in copoloymer			
PMBBU	0.30/0.60/0.10	0.36/0.53/0.11	4	40.8	3.8

[1] [Monomer] = 1.0 mol L^{-1} and [AIBN] = 1.0 mmol L^{-1} in ethanol. Polymerization temperature = 60°C.
[2] Weight averaged molecular weight (MW) was determined by gel-permeation chromatography with polystyrene standard (eluent = N,N-dimethylformamide).

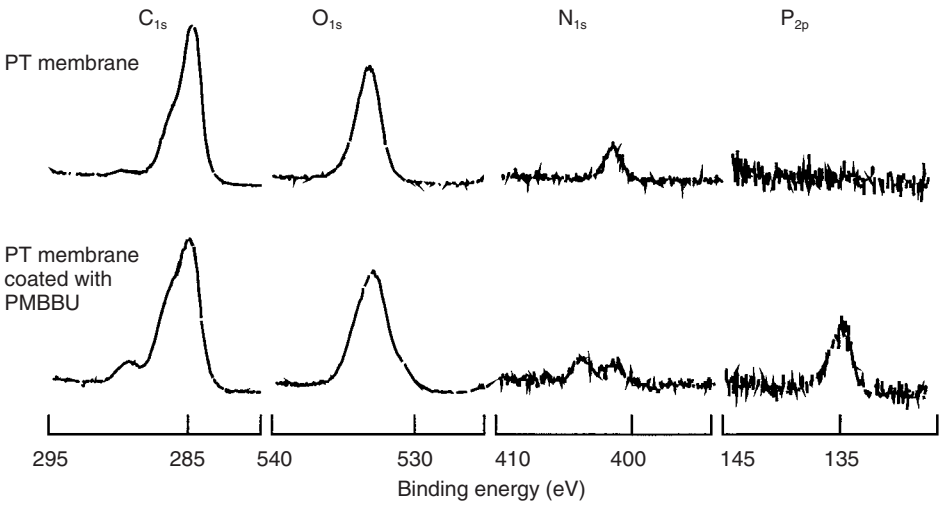

Figure 3. XPS chart of PT and that coated with the PMBBU.

134 eV were observed after the PMBBU coating. The ratio of the peak area of phosphorus (P_{2p}) to that of carbon (P/C) after immersion in water did not change significantly ($P>0.01$) from the original value for the PT-coated membrane with PMBBU. The amounts of the PMBBU eluted from the surface in an elution test in water and 40% aqueous ethanol solution were not detected quantitatively because the amounts were too small.

Effects of PMBBU coating on platelet adhesion

Figure 4 shows the SEM pictures of the surface of the original PT membrane and those coated with the MPC copolymers after contact with PRP for 3 h. A significant number of platelets adhered to the orignal PT membrane. However, the coating of the PMBBU effectively reduced the number of adherent platelets. Moreover, the shape change in the adherent platelets was also suppressed by the PMBBU coating.

***Ex vivo* evaluation of the clot formation on the PT membrane coated with PMBBU**

Figure 5 demonstrates the picture of the original pulsatile PT pump in a VAD and that coated with the PMBBU after an *ex vivo* experiment. The clot formation at the surface of the VAD pump coated with the PMBBU could not be observed, even after 27 days' application. On the other hand, the original VAD pump induced clot formation considerably, in particular near the heart valve area, within only 4 days. The SEM picture indicates much more clearly the differences between the original pump and the PMBBU-coated pump. As shown in Figure 6, the surface of both the housing part and diaphragm part of the VAD pumps coated with the PMBBU maintained clear but serious cell adhesion and activation, and fibrin net formation was observed on the original VAD pump. Though the amount of protein adsorbed onto the surface of the original pump during the experiment was 16.3 μg/cm^2 4 days after application, it was less than 13% on the PMBBU-coated pump, even when the application period was as long as 27 days.

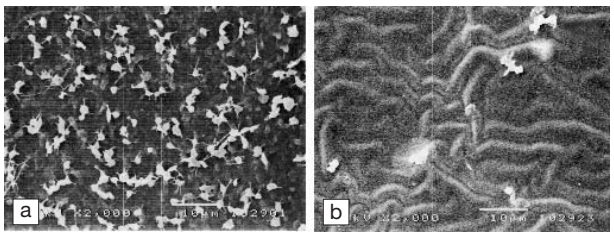

Figure 4. SEM picture of (a) the PT membrane and (b) that coated with PMBBU after contact with PRP for 3 h.

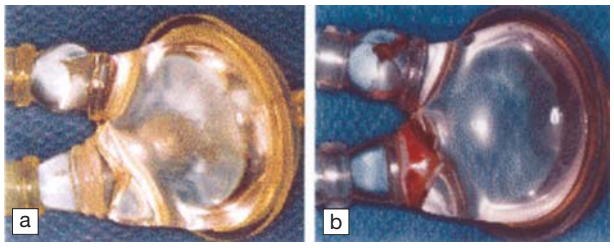

Figure 5. Picture of pulsatile pump in VAD after application to sheep. (a) PT pump coated with PMBBU after 27 days' application; (b) original PT pump after 4 days application.

Discussion

In the biomedical field, SPUs have been used widely because of their excellent mechanical properties[12]. The SPUs assume a so-called 'microdomain structure', that is, hard segments interact through hydrogen bonds and aggregate in the domains of the soft segments. However, the amount of protein adsorbed on the SPU surface is extremely large and cells were adhered to the surface. Our previous articles reported the syntheses of biomedical polymers having phospholipid polar groups, MPC copolymers, and evaluation of the blood compatibility focusing on cell adhesion and protein adsorption *in vitro*[4–7]. That is, the MPC polymer composed of MPC and BMA (PMB) could suppress platelet adhesion and their activation, even in contact with human whole blood in the absence of an anticoagulant[7]. The results could be explained by a reduction of the amount of protein adsorbed on the PMB. We have suggested that the PMB is used as a coating material. The SPUs are generally used under loading of continuous stress and deformation. Therefore, it is necessary to immobilize the coating polymer tightly on the surface to prevent detachment. We considered that if a urethane bond is introduced into the polymer, especially in the side chain, the polymer will have affinity for the SPU through hydrogen bonds[13]. Therefore, the PMBBU was synthesized with MPC, BMA and MEBU. The copolymerization of these monomers in ethanol proceeded well, and the mole fraction of each monomer unit in the copolymer obtained almost corresponded to that in the feed. Thus, it is very easy to obtain a suitable MPC polymer having a urethane bond in the side chain.

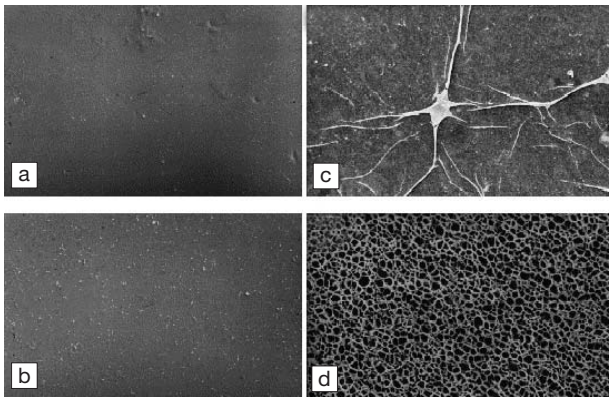

Figure 6. SEM pictures of inside of PT pump and that coated with PMBBU. (a, c) Housing part; (b, d) Diaphragm part. (a, b) PT pump coated with PMBBU after 27 days' application; (c, d) original PT pump after four days' application.

Previous reports on the blood compatibility of the MPC polymer indicated that more than 25 mol% in the polymer was necessary to obtain satisfactory platelet adhesion- and protein adsorption-resistant properties[4,5]. The MPC polymers became hydrated when they were immersed in water but did not dissolve in water. The MEBU units were expected to act as an anchor to the hard segment located at the surface of the SPU membrane. It is considered that the immobilization of hydrated MPC polymer can be achieved with a simple coating. In fact, an elution test revealed the effectiveness of the urethane bond in the side chain. The elution of the PMB occurred easily when the SPU membrane coated with PMB was immersed in a solvent containing ethanol, whereas the PMBBU hardly detached, even when the SPU membrane coated with the PMBBU was immersed in ethanol, which is a good solvent for MPC polymers.

The platelet adhesion of the PT was effectively suppressed after coating with the PMBBU and did not depend on the contact periods of up to 3 h. This finding indicated that the MEBU residues did not show any adverse effects on the platelet adhesion-resistant property of the PMB. Based on these observations, it is concluded that the MPC polymer with MEBU units is a useful material to improve surface blood compatibility of the PT by a simple coating method using their ethanol solution.

Ex vitro evaluation strongly demonstrated the effectiveness of the coating with the PMBBU on prevention of clot formation. We could observe that the clot did not form, even at the diaphragm and the valve parts. This fact is very important in that the coating did not peel off during 27 days' application. Elastic biomaterials are necessary for the construction of medical devices in the field of cardiovascular medicine. Normally, silicone rubber and SPU are applied. However, these materials did not have good blood compatibility and biocompatibility. The modification of these surfaces with the MPC polymer is an effective method to obtain blood compatibility.

The application of the MPC polymer to create a small-diameter vascular prosthesis by blending it with SPU has also been attempted[14]. Polyester prostheses were used as a substrate and served as a mechanical vehicle to support and retain the polymer. The polymer blend composed of SPU and MPC polymers (SPU/MPC polymer) could be easily coated on the polyester prosthesis, and the micropores of the prosthesis were filled with the SPU/MPC polymer. The SPU/MPC polymer vascular prosthesis is flexible enough for easy handling during an operation. The SPU/MRC polymer prosthesis showed significant non-thrombogenicity compared with the SPU prosthesis when these prostheses were implanted into a rabbit. The longest period for implantation of the SPU/MPC polymer vascular prosthesis without clot formation and occlusion is more than 8 months.

From these observations, it is concluded that one of the phospholipid polymers, the MPC polymer, which constructs the biomembrane-like surface showed excellent blood compatibility, that is reduction of protein adsorption and prevention of cell adhesion. Thus, these polymers are applicable for the modification of medical devices that come into contact with blood.

Acknowledgements

This study was supported in part by a Grant-in-Aid for Scientific Research (B) from the Ministry of Education, Science, Sports and Culture, Japan (09480250); one of the authors (KI) would like to express his appreciation for this support.

References

1. Tsuruta T, Hayashi T, Kataoka K, Ishihara K, Kimura Y, editors. *Biomedical Applications of Polymeric Materials*. Boca Raton, FL: CRC Press, 1993.
2. Brash JL, Horbett T, editors. *Proteins at Interfaces: Physiochemical and Biochemical Studies.* Washington, DC: American Chemcial Society, 1987.
3. Ishihara K, Ueda T, Nakabayashi N. Preparation of phospholipid polymers and their properties as polymer hydrogel membranes. *Polym J* 1990;22:355–60.
4. Ishihara K, Aragaki R, Ueda T, Watanabe A, Nakabayashi N. Reduced thrombogenicity of polymers having phospholipid polar groups. *J Biomed Mater Res* 1990;24: 1069–77.
5. Ishihara K, Ziats NP, Tierney BP, Nakabayashi N, Anderson JM. Protein adsorption from human plasma is reduced on phospholipid polymer. *J Biomed Mater Res* 1991;25:1397–407.
6. Kojima M, Ishihara K, Watanabe A, Nakabayashi N. Interaction between phospholipids and biocompatible polymers containing a phosphorylcholine moiety. *Biomaterials* 1991;12:121–4.
7. Ishihara K, Oshida H, Ueda, Endo Y, Watanabe A, Nakabayashi N. Hemocompatibility of human whole blood on polymers with a phospholipid polar group and its mechanism. *J Biomed Mater Res* 1992;26:1543–52.
8. Campbell E, O'Bryne V, Statford P *et al*. Biocompatible surface using methacryloyloxyethyl phosphorylcholine lauryl methacrylate copolymer. *ASAIO J* 1994:4(3):853–7.
9. Marra KG, Winger TTM, Hanson SR, Chaikof EL. Cytomimetic biomaterials. 1. In-situ polymerization of phospholipids on an alkylated surface. *Macromolecules* 1997; 30:6483–9.
10. Kohler AS, Parks PJ, Mooradian DL, Rao GH, Furcht LT. Platelet adhesion to novel phospholipid materials: modified phosphatidylcholine covalently immobilized to silica, polypropylene, and PTFE materials. *J Biomed Mater Res* 1996;32:237–42.
11. van der Heiden AP, Goebbels D, Pijpers AP, Koole LH. A photochemical method for the surface modification of poly(etherurethanes) with phosphorylcholine- containing compounds to improve hemocompatibility. *J Biomed Mater Res* 1997;37:282–90.
12. Lamba NMK, Woodhouse KA, Cooper SL, editors. *Polyurethanes in Biomedical Applications*. Boca Raton, FL: CRC Press, 1998.

13. Ishihara K, Hanyuda H, Nakabayashi N. Synthesis of phospholipid polymers having a urethane bond in the side chain as coating material on segmented polyurethane and their platelet adhesion-resistant properties. *Biomaterials* 1995;16; 873–9.

14. Yoneyama T, Ito M, Sugihara K, Ishihara K, Nakabayashi N. Small-diameter vascular prosthesis with a nonthrombogenic phospholipid polymer surface: preliminary study of a new concept for functioning in the absence of pseudo- or neointima formation. *Artif Organs* 2000;24:23–8.

Journal of Congestive Heart Failure and Circulatory Support (2001) Vol 1, No 4, 271–275

Surface modification with polymeric micelle and its characterizations

K. Emoto[1,2], M. Iijima[1], Y. Nagasaki[1] and K. Kataoka[2]

[1]Department of Materials Science and Technology, Science University of Tokyo, Noda, Chiba, Japan; and [2]Department of Materials Science, Graduate School of Engineering, University of Tokyo, Hongo, Bunkyo-ku, Tokyo, Japan

Abstract The stabilized aldehyde-bearing micelle from an end-derivatized block copolymer, acetal-poly(ethylene glycol)-poly(DL-lactic acid)-methacrylate (PEG–PLA) with a diameter of ca 35 nm was coated on a variety of aminated substrates including glass and poly(dimethylsiloxane) (PDMS) in the monolayer and laminated forms. The multilayer coating of micelle was carried out by coating the substrates with the micelles and poly(allylamine) alternately. The ζ-potential measurement revealed that the micelle coating was applicable to more surfaces than the grafting of linear PEG, while grafting aminated PDMS with PEG resulted in a low surface coverage, even under an optimal condition. The micelle coating under moderate conditions reduced ζ-potential to an extremely small variation indicative of high surface coverage. The multilayered micelle also showed small variation of ζ-potential as long as the micelle was at the top layer, and surfaces with poly(allylamine) exhibited ζ-potential corresponding to the protonation of the polymer. The surface topography significantly changed with lamination; while the monolayer on the substrate exhibited granules with the same size order as the micelle, lamination resulted in pronounced undulation of layers due to the low surface coverage and the conformation of poly(allylamine) on the micelle layer. Such micelle coating, despite its preparation under a moderate condition, reduced protein adsorption as effectively as the high-density PEG grafting under a harsh condition. The micelle coating exhibited a property as a reservoir for hydrophobic drugs; the number of coatings controlled layer and release rate. The micelle coatings are expected to be useful for biomedical and bioanalytical applications.

Keywords polymeric micelle, poly(ethylene glycol) (PEG), poly(DL-lactic acid) (PLA), poly(dimethysiloxane) (PDMS).

Background

Modification of surfaces with hydrophilic polymers has been investigated to alter the surface property without changing the bulk property. These coatings prevent nonspecific interaction with biopolymers such as plasma proteins and nucleic acids, which results in the fouling of materials and reduction of the resolution analysis[1,2]. Coating hydrophilic polymers such as poly(ethylene glycol) (PEG) can minimize these effects. PEG coatings reduced protein adsorption a great deal, resulting from an increased hydrophilic capacity, masked surface charge, and increased osmotic effect by the coated polymer[1–4].

We are interested in coating polymeric micelles prepared from block copolymers containing PEG. A block copolymer consisting of both hydrophilic and hydrophobic segments can form a micelle with hydrophobic core and hydrophilic corona in an aqueous solution. We have synthesized a block copolymer of PEG (molecular weight [mw] ~5000) and poly(DL-lactic acid) (PLA; mw ~5000) baring acetal group at PEG-end and methacryloyl at the PLA-end. The resultant micelle of ca 30 nm in diameter was reactive and stable by the hydrolytic conversion of an acetal into an aldehyde and polymerization, respectively[5–9]. The stabilized micelle maintains its structure, even after the attachment to the surface. The density is high enough to prevent the adsorption of proteins and adhesion of cells. The surface-attached micelle is also expected to hold drugs. The drug on the surface of the micelle may be released in a controlled manner, and can be used as a micro-reservoir for sustained release systems. On the latter application, the amount of micelles should be high in order to control the loading and releasing of drugs. In this regard the micelle was coated on a surface in the form of multilayers by alternately coating aldehyde-bearing micelles and poly(allylamine) (PA1Am).

This report discusses surface characterization of the micelle coatings and its eligibility for biomedical applications.

Methods and materials

All the reagents used for the synthesis were purified by distillation before use. The 2 mmol of 3-diethoxypropanol, 2 mmol of potassium naphthalene and subsequently 227 mmol of chilled ethylene oxide were mixed in a dry tetrahydrofuran (THF) in a round-bottomed flask. The solution was stirred at 22°C for two days to polymerize the

Correspondence to: Kazunori Kataoka, Department of Materials Science, Graduate School of Engineering, University of Tokyo, 7-3-1 Hongo, Bukyo-ku, Tokyo, Japan

ethylene oxide. Following the PEG polymerization, DL-lactide was polymerized. After the addition of some potassium naphthalene, 83 mmol of DL-lactide was added and stirred for 2 h at 22°C. The living polymerization was terminated by the addition of 30 mmol of methacrylic anhydride stirring for three days. The block copolymer was purified by precipitation in chilled isopropanol and freeze-dried with benzene. The mw of the polymer was ca 5000 for PEG and 4500 for PLA. The peak integration of NMR revealed the same amount of an acetal group in the synthesized polymer as a methacryloyl group indicative of the presence of both groups at each of the polymer ends.

Micelles were prepared by the dialysis of the PEG–PLA block copolymer in dimethylacetamide (DMAc) against Mili-Q grade water. The 280 mg of block copolymer was dissolved in 40 mL of DMAc and the solution was dialyzed against distilled water with a membrane tube with a cut-off mw of 12 000–14 000 (Spectra/Pro) for 24 h. The pH of the solution was adjusted from 5.8 to 2 with HCl and stirred for 2 h to hydrolyze the acetal group at the PEG end to an aldehyde group. The pH was then re-adjusted to ~6 and dialyzed against water for 24 h to remove salts from the solution. The diameter of the micelle at this state was ca 30 nm from the dynamic light scattering (DLS)[6–9]. After the second dialysis, the core of the micelle was stabilized with the polymerization of the methacryloyl group at the end of the PLA segment. The 0.3% (w/w) of $K_2S_2O_8$ was added to the micelle solution as an initiator and purged of air with Ar. The solution was stirred for 24 h at 50–55°C. The DLS indicated that the size of the core-polymerized micelle was about 30 nm, which is comparable to the micelle without core-polymerization.

Prior to the micelle coating, the substrates were aminated. Dry glass and Si wafers cleaned by Piranah method[10] were aminated by immersing into a 1% (v/v) solution of 3-aminopropyltriethoxysilane (APTS) (Aldrich, Milwaukee, WI, USA) in toluene for 4 h. After rinsing in toluene to remove excess APTS, the APTS-coated substrates were cured at 160°C in the vacuum for 20 h. The commercial poly(dimethylsiloxane) (PDMS) and polypropylene (PP) samples dried under vacuum were treated with RF-plasma composed of N_2 and H_2 in a plasma chamber (Samco, Tokyo, Japan). The pressure of the chamber was reduced to below 3 mTorr before the treatment. The pressure was adjusted to 1.5 Torr by flowing N_2 and H_2 (20 and 40 mL min^{-1}, respectively) and then a 95 W-RF electric field was applied. These plasma-treated films were stored in water; however, the coating of micelle was performed within 2 h.

The aminated substrates were coated with micelle and aldehyde-derivatized PEG (mw 5000) as a comparison. Monomethoxy-PEG-aldehyde was coated under an optimal condition[1,4,11]. The aminated substrates were immersed in a 5% (w/v) solution of PEG-aldehyde in 0.5 M Na_2SO_4 containing 0.25% (w/v) $NaCNBH_3$ and 0.01 M NaH_2PO_4, pH 5.5. After the substrate in the PEG solution was heated to 80°C for 2 h, it was rinsed with water repeatedly and stored in deionized water until use. For the monolayer coating of the reactive micelle, the aminated substrates were immersed in approximately 1 mg/mL micelle solution in 0.01 M NaH_2PO_4 containing 0.25% (w/v) $NaCNBH_3$ at 25°C. After coating micelles, the samples were rinsed with Mili-Q grade water repeatedly and stored in water until characterization. The samples were characterized within 2 days after the preparation. For the coating of multilayered micelle, the substrate was immersed in ~1.2 mg/mL micelle solution in 0.04 M HEPES (pH 6.7) containing 3.2×10^{-3}% (w/v) $NaCNBH_3$ at 22°C for 2 h. After the light rinsing with Mili-Q water, the micelle-coated substrate was immersed into a solution of 0.6% (w/v) PAlAm in 0.04 M HEPES (pH 6.7) containing 0.25% (w/v) $NaCNBH_3$ at 22°C for 2 h. This procedure was repeated until the desired number of coatings was obtained. The final micelle coating was carried out in the same manner but with a higher concentration of $NaCNBH_3$ (0.25%) in order to reduce unreacted aldehyde groups on the micelle surface into the hydroxyl group.

Results and discussion

Figure 1 shows the alteration of ζ-potential versus pH profile of APTS glass coated with PEG-aldehyde and micelle. The ζ-potential was measured with the laser Doppler electrophoresis analyzer (LESA–600, Otsuka Electronics Co., Osaka, Japan). When the APTS glass was coated with PEG and micelle, ζ-potential over the pH range of 2–11 was significantly reduced due to the surface charge masking by the PEG or the micelles attached to the surface. When the PAlAm was coated on the micelle layer, the ζ-potential was

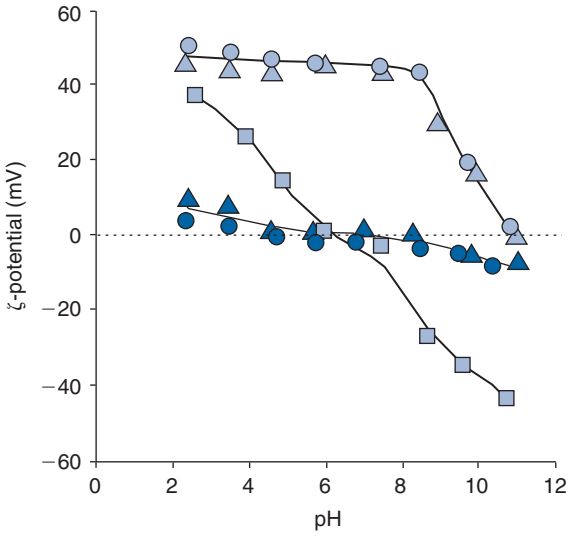

Figure 1. Profile of ζ-potential versus pH of APTS-glass surface (■) coated with single, double and triple layer of micelles (●,▲) and poly(allylamine) (●,▲).

highly positive in the whole pH range. Since the ζ-potential is little varied below pH 8 and no negative potential was observed at higher pH, the effect of the silanol group on the substrate was fully masked. Furthermore, the profile only reflected the protonation and deprotonation of the amino group of PAlAm on top of the micelle layer. Further coatings of PAlAm and subsequent micelles also showed identical ζ-potential profiles to the previous coatings of PAlAm and micelle, respectively.

Note that while the grafting of PEG-aldehyde densely on rigid glass reduced ζ-potential variance versus pH as significantly as the micelle coating, the ζ-potenital of grafting on soft aminated PDMS exhibited less reduction than the micelle coating. Since the polymer chain of PDMS is flexible, the flip-flop prevented an attachment of the PEG end group, and resulted in low density despite grafting under an optimal condition. On the other hand a micelle with hundreds of reactive aldehydes on its surface seemed to have successfully covered the PDMS surface.

The scanning probe microscope (SPM) height images of aminated Si wafers coated with multilayers of micelles were obtained by Bioscope (Olympus Co., Tokyo, Japan) equipped with a Nanoscope IIIa controller (Digital Instruments, Santa Barbara, CA, USA) as in Figure 2. Single micelle coating resulted in surfaces covered with granules of approximately 30–50 nm in diameter. As the micelle coating was multiplied, the undulated structure was pronounced. The nodular size was more than 50 nm and varied. The PAlAm did not seem to be abundant enough to cover fully the micelle-coated surface. The polymer molecule attached on the surface preferentially takes a coiled structure rather than a completely flattened structure. When the micelle is attached to the PAlAm, the loop structure of the PAlAm is more pronounced and leads to the undulation of the surface.

The thickness of the layer was also measured by scanning the scraped area using the same cantilever. The area of 1×1 μm^2 scraped by strong force was scanned by the tapping mode. The height of the single micelle layer is ca 25 nm. This is somewhat smaller than the size determined by DLS. It is either due to the artifact by the SPM imaging or the flattening of the particle upon attachment to the surface. After the second coating of micelles, the thickness of the layer was increased to about 45 nm. The cross-section shows serrated nodes, and the size of the serrated grain seemed to be comparable to the micelle size. For the triple coating of micelle, the thickness increased to over 80 nm, but the nodes are larger than the single and double coating of micelles as in Figure 2. Although the increase in thickness was not proportional to the number of coatings probably due to the conformation of the PAlAm between the micelle layers, the increase was stepwise with the number of coatings.

Such monolayer and multilayer micellar coatings for biomedical applications should have a minimal nonspecific interaction with biological systems, induce no immunogenic reactions, and immobilize biologically active molecules such as proteins in their native form[1–3,12,13]. In this regard, the interaction of the coated surface with a plasma protein, bovine serum albumin (BSA), was investigated. Aminated PP films coated with the micelles and PAlAm alternately were exposed to 45 μg/mL of BSA solution in phosphate-buffered saline (PBS) at pH 7.4 and 22°C for 60 min. After rinsing, the adsorbed BSA was eluted with sodium dodecylsulfate and the Cu^{2+} reduced into Cu^{+} by BSA was complexed with bicinchoninic acid[14]. The amount of adsorbed BSA was determined by the UV absorbance of the complex, and is presented in Figure 3. Obviously, the gel surface with micelle at the top layer significantly reduced the protein adsorption. This is comparable to a surface coated with a high density of PEG[15]. On the other hand, BSA adsorbed appreciably when the PAlAm was exposed on the layer surface. The amount of BSA adsorbed on the micelle-coated PP is comparable to that grafted with a high density of PEG grafted from a high concentration solution in K_2SO_4 at high temperature[15]. Since a high density of PEG grafting exhibited reduced adsorption of

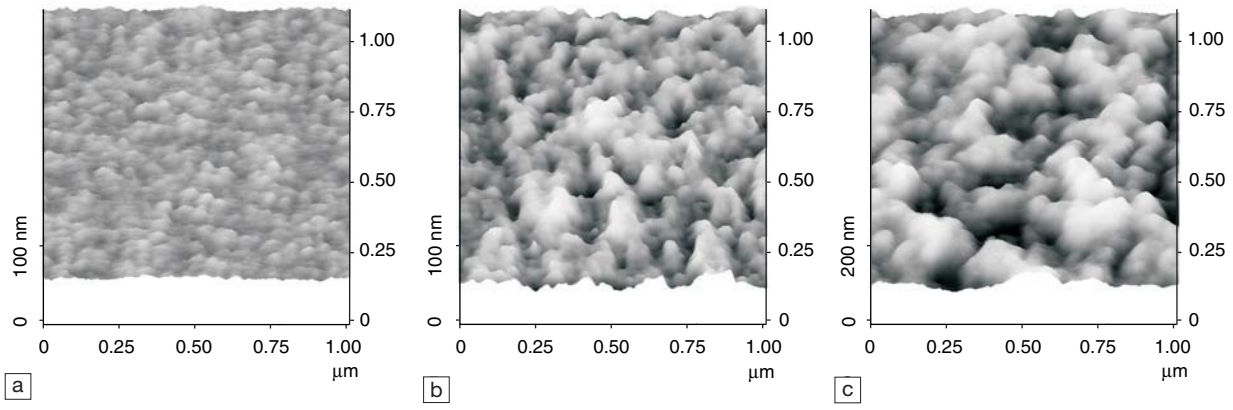

Figure 2. Scanning force images of APTS-Si wafers coated with (a) single (b) double, and (c) triple layers of micelle.

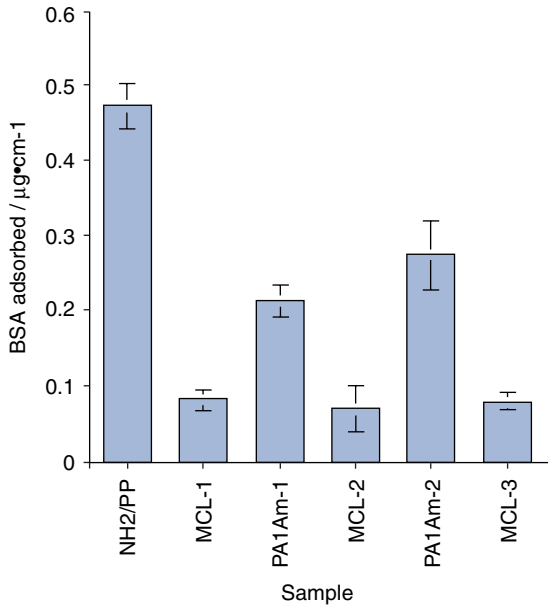

Figure 3. The adsorption of BSA to the coatings of micelle (MCL) and poly(allylamine) (PAlAm) to aminated polypropylene (NH2/PP). The number following the denotation indicates the cycle of coatings of MCL or PAlAm.

plasma proteins[16], this result indicates that the micelle coatings under a moderate condition also reduce many plasma proteins.

Adsorption of plasma proteins such as BSA correlates with the electrokinetic properties of the surface[17]. When the micellar layer was at the top, the surface exhibited a small ζ-potential indicative of the masking of surface charge as in Figure 1. It should be noted that the micellar coating showed a small receding contact angle indicative of its low tendency to dehydrate[18], which resulted in an increased hydrophilic capacity by the micellar coating and therefore reduction of protein adsorption. When the PAlAm covers the outermost layer, the surface has a positive charge as demonstrated by the ζ-potential, and possibly becomes less hydrophilic than the surface with the micellar top layer[18,19]. Consequently, due to the hydrophobic and electrostatic effects, negatively charged BSA is appreciably adsorbed to the PAlAm surface.

The micellar coating has another unique property that is not typical of conventional coatings. Each micelle in the layer possesses a hydrophobic core with a narrow size distribution in the range of ~10 nm. Apparently the micellar core can hold hydrophobic reagents[20–23], and therefore is expected to encapsulate and release hydrophobic drugs in a controlled manner. As a model drug, pyrene was incorporated into the micelle by mixing pyrene with the micellar solution at 60°C for 4 h following the procedure by Kwon *et al*[23]. The pyrene-incorporated micelles were coated on an aminated glass slide in the aforementioned manner. The sample was then exposed to an excess amount of Mili-Q water. By measuring the fluorescence at λ_{ex} = 336 nm, release of pyrene from the micelle-coated surface was monitored. The peak intensity ratio of I ([0,0] band) to III ([0,2] band) of the emission spectrum obtained for the pyrene/micelle solution and the glass slides coated with the pyrene-loaded micelles was about 1.4, indicating that pyrene was localized in the hydrophobic core of the micelle[23]. The plot of the fluorescence intensity at λ_{em} = 363 nm of the micelle-coated glass slide with exposure time to water is presented in Figure 4. It should be noted that the fluorescence from the glass slide itself at this wavelength was negligible compared with the sample. The initial amount of pyrene as well as the rate of release were dependent on the number of micelle coatings; as the number of coatings increased, the initial fluorescence was higher and release rate evaluated from the decline in the fluorescence intensity was slower. The formation of a multilayered structure with thickness increased by the alternate coating process resulted in an increased retention capacity of pyrene in the gel layer and consequently lowered the release rate.

Repetitive loading and release of pyrene were also successfully accomplished with the micellar coatings. After the hexapoid coatings of pyrene-free micelle, the samples were exposed to the micelle solution containing pyrene for 12 h to transfer pyrene from solution to the gel phase. The initial fluorescent intensity of the pyrene-loaded micellar layer coincides with that of the layer coated with pyrene-preloaded micelles. Pyrene was also released from the coatings in the same manner as the coatings of pyrene-preloaded micelles. The loading and release of pyrene can be reproduced repeatedly.

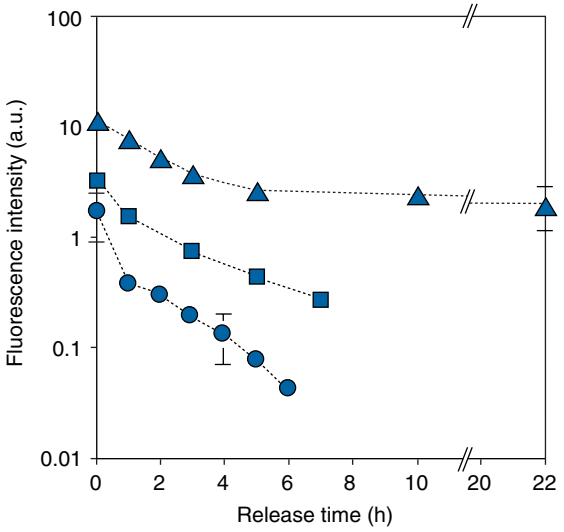

Figure 4. The relationship between the number of coatings of micelle and a decrease in fluorecsent intensity of APTS glass coated with (●) single, (■) triple and (▲) hexapoid layer of micelle with exposure to water.

The thin hydrogel layer made by alternate coating of micelles and PAlAm exhibited nonfouling properties and worked as the reservoir for hydrophobic reagents. The loading capacity and release rate of a drug can be controlled by the number of coatings. The thickness of the gel layer is easy to control; each increase in the number of coatings resulted in an increase in the thickness by 30–40 nm. Diffusion and permeation of solute molecules should be regulated with this thin layer of laminated micelles. In the present investigation, the thin micelle layer was prepared on flat surfaces. However, the coating can be applied to a variety of surfaces with different shapes and curvatures, including microparticles. These surfaces covered with micelles should have a nonfouling property and may exhibit few adverse effects on the biological environment; they can be used in diverse fields of medicine and biology to construct high-performance medical devices and drug delivery systems.

References

1. Gölander CG, Herron J, Lim K, Claesson P, Stenius P, Andrade JD. Properties of immobilized PEG films and the interaction with proteins: experiments and modeling. In: Harris JM, editor. *Poly(ethylene glycol) Chemistry: Biotechnical and Biomedical Applications*. New York: Plenum Press, 1992:221.
2. Österberg E, Bergström K, Holmberg K *et al*. Protein-rejecting ability of surface-bound dextran in end-on and side-on configurations: comparison to PEG. *J Biomed Materials Res* 1995;29:741.
3. Herron BJ, Shafer SG, van Alstine JM, Harris JM, Snyder RS. Control of electroosmosis in coated quartz capillaries. *J Colloid Interface Sci* 1988;115:46.
4. Emoto K, Harris JM, van Alstine JM. Grafting poly(ethylene glycol) epoxide to amin-derivatized quartz: effect of temperature and pH on grafting density. *Anal Chem* 1996; 68:3751.
5. Scholtz C, Iijima M, Nagasaki Y, Kataoka K. A novel reactive polymeric mecelles-Polymeric micelle with aldehyde groups on its surface. *Macromolecules* 1995;28:7295.
6. Nagasaki Y, Okada T, Scholz C, Iijima M, Kato M, Kataoka K. The reactive polymeric micelle based on an aldehyde-ended poly(ethylene glycol)/poly(lactide) block copolymer. *Macromolecules* 1998;31:1473.
7. Nagasaki Y, Kataoka K. The reactive polymeric micelle, convenient tool for targeting drug delivery system. In McCullough I, Shalaby S, editors. *Materials for Controlled Release Applications*. Washington DC: ACS Symposium Series, American Chemical Society, 1998;105.
8. Iijima M, Okada T, Nagasaki Y, Kato M, Kataoka K. Core-polymerized reactive micelles from heterotelechelic amphiliphilic block copolymers. *Macromolecules* 1999; 32:1140.
9. Kim JH, Emoto K, Iijima M *et al.* Core stabilized polymeric micelle as potential drug carrier—increased solubilization of taxol. *Polym Adv Technol* 1999; 10:647.
10. Bearinger JP, Castner DG, Golledge SL, Rezania A, Hubchak S, Healy KE. P(AAm-co-EG) interpenetrating polymer networks grafted to oxide surfaces: surface characterization, protein adsorption, and cell detachment studies. *Langmuir* 1997;13:5175.
11. Emoto K. Thesis, Huntsville, AL: University of Alabama, 1997.
12. Sigal GB, Bandad C, Barberis A, Strominger J, Whitesides GM. A self-assembled monolayer for the binding and study of histidine-tagged proteins by surface plasmon resonance. *Anal Chem* 1996;68:490.
13. Holmberg K, Bergström K, Stark M. Immobilization of proteins via PEG chains. In: Harris JM, editor. *Poly(ethylene glycol) Chemistry: Biotechnical and Biomedical Applications*. New York: Plenum, 1992:303.
14. Smith PK, Krohn RI, Hermanson GT *et al.* Measurement of protein using bicinchonic acid. *Anal Biochem* 1985;150:76.
15. Emoto K, Iijima M, Nagasaki Y, Kato M, Kataoka K. Preparation of nonfouling surface through the coating with core-polymerized block copolymer micelles having aldehyde-ended PEG shell. *Colloid Surface B* 2000 (in press).
16. Malmsten M, Emoto K, van Alstine JM. Effect of chain density on inhibition of protein adsorption by poly(ethylene glycol) based coatings. *J Colloid Interface Sci* 1998;202:507.
17. Norde W, Lyklema J. The adsorpton of human plasma albumin and bovine pancreas ribonuclease at negatively charged polystyrene surfaces III. Electrophoresis. *J Colloid Interface Sci* 1978;64:277.
18. Emoto K, Nagasaki Y, Kataoka K. Coating of surfaces with stabilized micelles from poly(ethylene glycol)-poly(DL-lactic acid) block copolymer. *Langmuir* 1999;15: 5212.
19. Elbert DL, Herbert CB, Hubbell JA. Thin polymer layers formed by polyelectrolyte multilayer techniques on biological surfaces. *Langmuir* 1999;15: 5355.
20. Yokoyama M, Miyauchi M, Yamada N *et al.* Adriamycin-conjugated poly(ethylene glycol)-poly(aspartic acid) block copolymer. *J Controlled Release* 1990;11:269.
21. Yokoyama M, Miyauchi M, Yamada N *et al.* Characterization and anticancer activity of the micelle-forming polymeric anticancer drug adriamycin-conjugated poly(ethylene glycol)-poly(aspartic acid) block copolymer. *Cancer Res* 1990; 50:1693.
22. Yokoyama M, Okano T, Sakurai Y, Kataoka K. Improved synthesis of adriamycin-conjugated poly(ethylene oxide)-poly(aspartic acid) block copolymer and formation of unimodal micellar structure with controlled amount of physically entrapped adriamycin. *J Controlled Release* 1994;32:269.
23. Kwon GS, Suwa S, Yokoyama M, Okano T, Sakurai Y, Kataoka K. Enhanced tumor accumulation and prolonged circulation times of micelle-forming poly(ethylene oxide-aspartate) block copolymer-adriamycin conjugates. *J Controlled Release* 1994;29:17.

Journal of Congestive Heart Failure and Circulatory Support (2001) Vol 1, No 4, 277–283

Closure of the pericardium using synthetic bioabsorbable polymers

K. Sakuma MD[1], Y. Tanaka MD[1], S. Watanabe MD[1], H. Yokoyama MD[1], A. Iguti MD[1], Y. Ikada MD, PhD[2] and K. Tabayashi MD[1]

[1]*Department of Cardiovascular Surgery, Graduate School of Medicine, Tohoku University, Sendai, Japan; and* [2]*Department of Medical Electronics, Suzuka University of Medical Science, Suzuka, Japan.*

Background Pericardial substitutes secure safer re-sternotomy at re-operation. The synthetic sheet made from expanded polytetrafluoroethylene (e-PTFE) was most commonly used as a pericardial substitute. The e-PTFE sheet, however, brought on severe inflammatory reaction and diffuse fibrosis.

Objective This study was designed to investigate the absorbable rate and tissue reaction to the following absorbable pericardial substitutes: gelatin sheet and L-lactic acid$_{\varepsilon}$ -caprolactone copolymer (L-C copolymer). In addition, the e-PTFE sheet and autologous pericardium were used as control.

Methods A total of 48 dogs were divided into the following four groups:

1. Group A ($n = 12$): a 3×3 cm segment of pericardium was excised and the autologous pericardium was resutured.
2. Group B ($n = 12$): the pericardial defect was replaced with gelatin sheet.
3. Group C ($n = 12$): the defect was replaced by L-C copolymer sheet.
4. Group D ($n = 12$): the defect was replaced with an e-PTFE sheet. The implanted membranes were retrieved at two weeks ($n = 1$), four weeks ($n = 3$), 12 weeks ($n = 5$), and 24 weeks ($n = 3$) after implantation.

Results The e-PTFE sheet produced a more notable inflammatory reaction and severe adhesion to the heart and pleura when compared with the gelatin sheet. The absorbable pericardial substitutes were completely absorbed 24 weeks after implantation, and were replaced with fibrous membrane.

Conclusions Absorbable pericardial substitutes may cause less adhesion and fewer inflammatory reactions than e-PTFE.

Keywords pericardium, L-lactic acid$_{\varepsilon}$ -caprolactone, gelatin, expanded polytetrafluoroethylene.

Background

Primary closure of the pericardium is recommended to reduce the formation between the heart and chest wall. In some patients, autologous pericardium cannot be used for various reasons, and pericardial substitutes secure safer re-sternotomy at re-operation in these patients. Several materials can be used as pericardial substitutes, including silicone rubber[1], polyurethane[2], fascia lata[3,4], expanded-polytetrafluoroethylene (e-PTFE) sheet[2,5,6], heterologous porcine, equine and bovine pericardium[7–10], Dacron[11,12], and dura mater[13].

However, several side-effects were reported, such as dense adhesions and severe inflammatory reactions. Recently, many authors have described materials that reduce adhesion formation in the retrosternal space. These materials, however, are not yet widely used because of possible side effects. The purpose of this study is to evaluate the absorbable pericardial substitutes (gelatin sheet and L-lactic acid$_{\varepsilon}$ -caprolactone copolymer [L-C copolymer]) (Figure 1) by comparing the most commonly used e-PTFE sheet, and autologous pericardium.

Methods

A total of 48 dogs weighing 8–27 kg (mean 12 kg) were used as a pericardial reconstraction model. Animal care was in compliance with *The Principles of Animal Use* formulated by the Animal Use Committee at Tohoku University, Sendai, Japan.

Experimental groups and pericardial substitutes

The animals were divided into four groups of 12 dogs each:

1. Group A (n=12): control (a segment of pericardium was excised, and the autologous pericardium was resutured)
2. Group B (n=12): the pericardial defect was replaced with an 0.1 mm gelatin sheet (Gunze, Kyoto, Japan)
3. Group C (n=12): the pericardial defect was replaced with an 0.4 mm L-lactic acid$_{\varepsilon}$ -caprolactone (50:50) copolymer sheet (Gunze, Kyoto, Japan)

Correspondence to: Kei Sukuma, Department of Cardiovascular Surgery, Graduate School of Medicine, Tohoku University , 1-1 Seiryomati Aoba-ku, Sendai 980–8574, Japan.

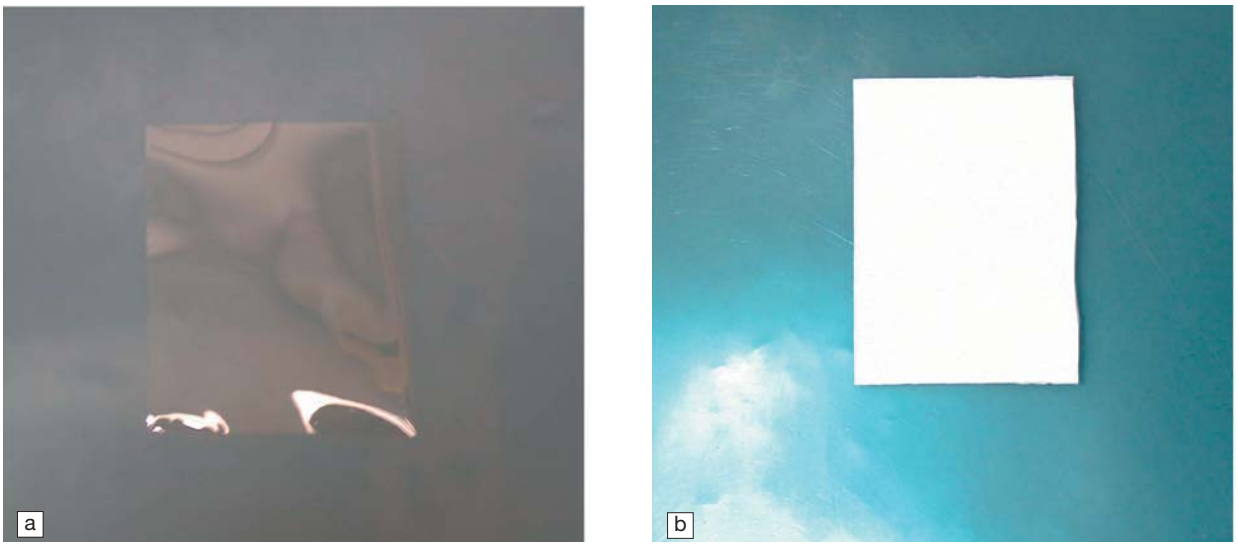

Figure 1. Synthetic bioabsorbable polymers. (a) Gelatin sheet; (b) L-C copolymer sheet.

4. Group D (n=12): the defect was replaced with an 0.1 mm expanded-polytetrafluoroethylene (e-PTFE) sheet (W.L. Gore & Associates, Inc. Elkton, MD, USA)

The fabrication process of the gelatin sheet and L-C (50:50) copolymer sheet is as follows.

Gelatin, extracted with the alkaline method from bovine bone (type I collagen), was donated by Nitta Gelatin Co. Ltd., Osaka, Japan. To prepare gelatin films, gelatin powder was dissolved in distilled water to a concentration of 10 % wt. The solution was cast on glass plates and air dried to obtain gelatin films of 0.1 mm thickness. Cross-linking was introduced by exposing both the sides of gelatin films to UV light for 10 h and air dried at 60 cm apart from a UV lamp (Toshiba GL–15 [15 W]).

L-C (50:50) copolymer sheet 50:50 sponge sheet L-lactide and ε -caprolactone copolymer (50:50 mol%, mw = 220 000) was dissolved in 1,4-dioxane to a concentration of 6 % wt. This solution was poured into a mold and frozen at −135°C. The frozen content was then freeze-dried to yield a porous sponge sheet of 0.5 mm thickness. This sponge sheet was completely dried at 70°C *in vacuo* for 12 h.

The sheet was used as a pericardial substitute after sterilization with ethylene oxide gas.

Surgical procedure

An intravenous line and an electrocardiographic monitor were established. Anesthesia was induced with 2.5% thiamylal sodium at a dose of 25 mg kg^{-1}. Anesthesia was maintained with halothane in oxygen. Mechanical ventilation was instituted with an approximate tidal volume set at 10 mL kg^{-1} body weight with 100% oxygen at a rate of 8–14 cycles per minute. Under sterile conditions a left lateral thoracotomy incision through the fourth or fifth intercostal space was performed and a 3 × 3 cm segment of pericardium about 1 cm anterior to the phrenic nerve was excised. After scattering 5 mL of autologous blood into the pericardial defect, a sheet was anchored to the surrounding pericardium with 5–0 Prolene (Ethicon Inc., Somerville, NJ, USA) mattress sutures as shown in Figure 2.

Care was taken to avoid contact with the epicardial surface of the heart. Prophylactic antibiotics were given intravenously just after the operation.

At 2–24 weeks after the operation, dogs were sacrified and the *en bloc* heart, including pericardium and left lung, was removed through a left-sided thoracotomy. The implant tissue sites were then examined and photographed.

Evaluations

Adhesion formation was evaluated by the macroscopic findings, particularly in the pleura or lung-to-pericardium and pericardium-to-epicardium regions. The degree of adhesion was quantitatively classified as shown in Table 1.

In each animal, specimens of myocardium, epicardium and pericardium were taken for light microscopic studies.

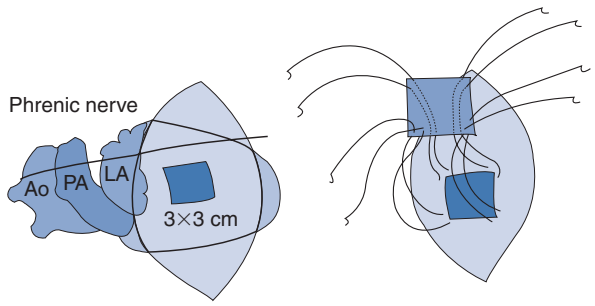

Figure 2. Surgical procedure. Ao: aorta; PA: pulmonary artery; LA: left atrium.

Table 1. Classification of adhesion degree

Score	Characteristics
0	None
1	Adhesion could be readily separated by finger dissection
2	A combination of 1 and 3
3	Adhesion necessitating sharp dissection

The sections were fixed in 10% phosphate-buffered formalin for at least three days and were embedded in paraffin and sectioned at 5 μm. The sections were then stained with hematoxylin eosin and elastica-Masson stain to assess inflammatory reaction as well as changes in the pericardial substitutes.

The severity of the inflammatory reaction is histopathologically defined by increasing numbers of infiltrating inflammatory cells inflammatory foci. The inflammatory reaction of each sheet was quantitatively classified as shown in Table 2.

Statistical methods

ANOVA (Scheffe) was used to evaluate differences of adhesion formation. A *P*-value of less than 0.05 was considered significant.

Table 2. Classification of inflammatory reactions

Score	Characteristics
0	No cell infiltration
1	Sparse focal neutrophils, lymphocytes and plasma cell infiltration
2	Focal infiltration of neurophiles, plasma cells and lymphocytes
3	Diffuse infiltration of neutrophiles, plasma cells and lymphocytes

Results

All animals survived implantation and were evaluated as scheduled. There was no differentiation after two weeks among the dogs in the four groups .

In Group A, the adhesion of the autologous pericardium four weeks after implantation was minimal and the adhesions of both pleura-to-pericardium and pericardium-to-epicardium could be separated by finger in the dog in Figure 3a. However, this was not a consistent finding. In another two animals, autologous pericardium had moderately or completely adhered to the underlying epicardium. Conversely, in Group B at four weeks a thin membrane had replaced the gelatin sheet with no adhesions within the pericardium in all

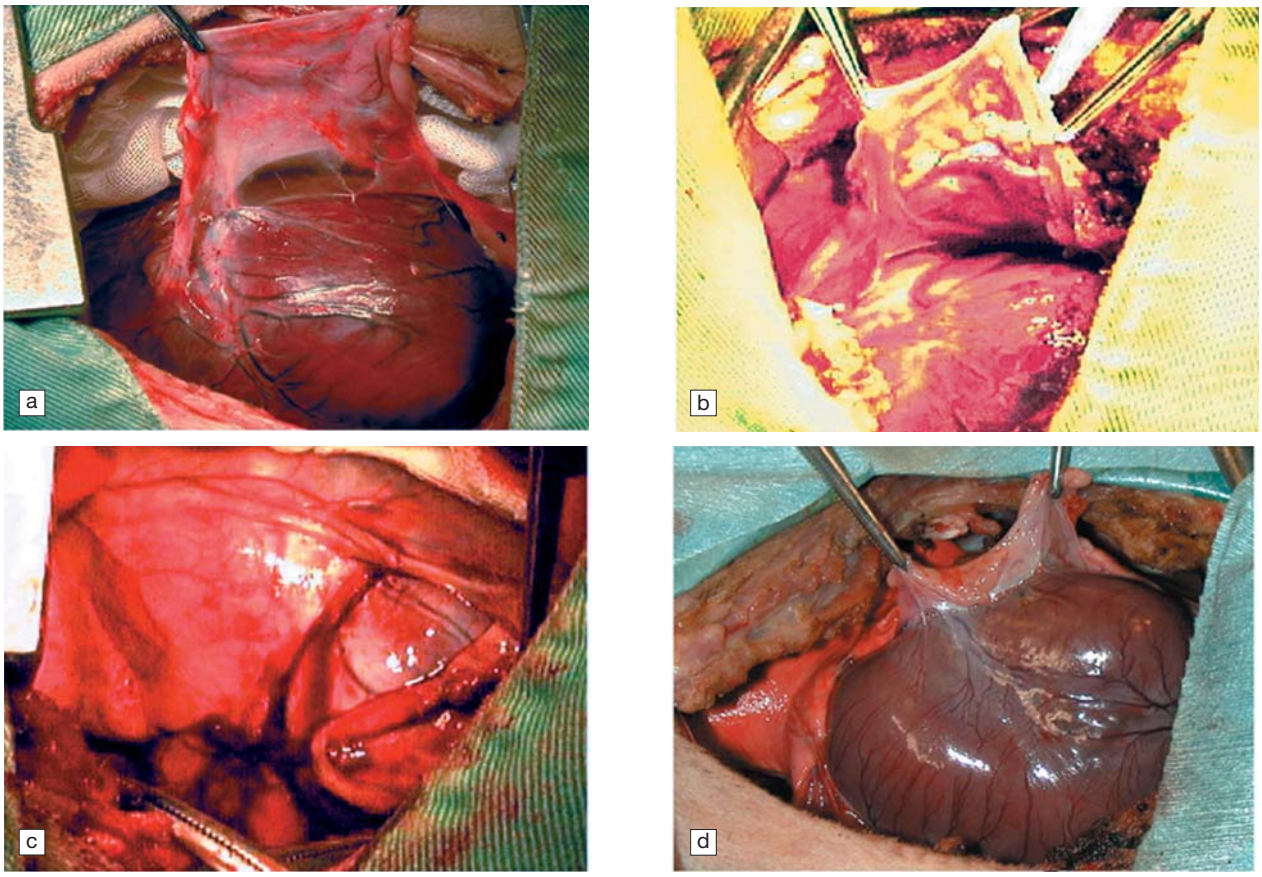

Figure 3. Macroscopic findings after 4 weeks. (a) Group A: autologous pericardium 4 weeks after implantation; (b) Group B: gelatin sheet 4 weeks after implantation; (c) Group C: L-C copolymer 4 weeks after implantation; (d) Group D: e-PTFE sheet 4 weeks after implantation.

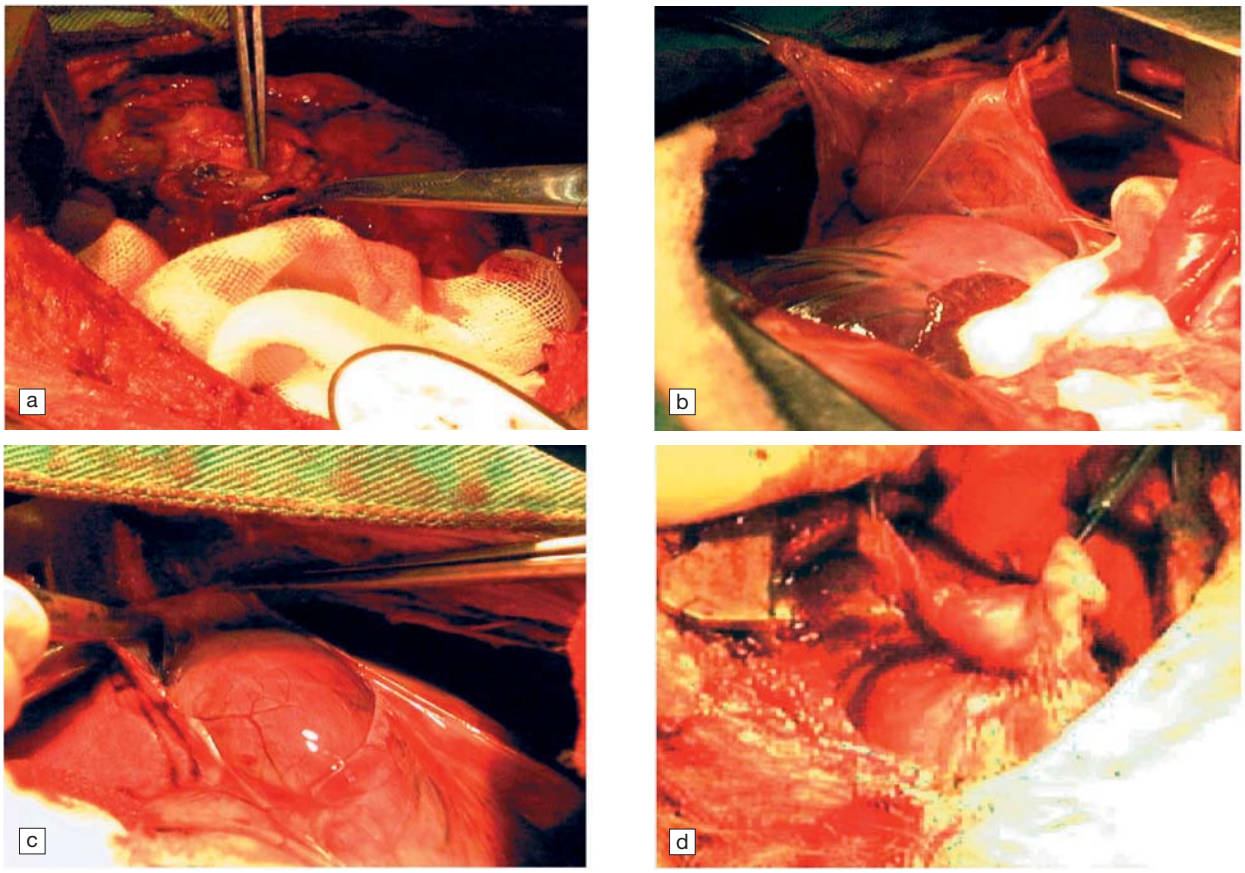

Figure 4. Macroscopic findings after 24 weeks. (a) Group A: autologous pericardium 24 weeks after implantation; (b) Group B: gelatin sheet 24 weeks after implantation; (c) Group C: L-C copolymer 24 weeks after implantation; (d) Group D: e-PTFE sheet 24 weeks after implantation.

animals; this membrane was covered with autologous tissue and lung (Figure 3b).

In Group C, a membrane had incompletely replaced an original caprolactone sheet; the degree of epicardial adhesion in this dog was nil (Figure 3c) and in two other dogs in Group C was minimal to moderate. No adhesions of both pleura-to-e-PTFE sheet and e-PTFE sheet-to-epicardium could be seen in two dogs, but dense adhesions were observed in one dog in Group D (Figure 3b).

The adhesion of autologous pericardium 24 weeks after implantation was absent or minimal in pericardium-to-epicardium and adhesion to the pleura was absent to moderate (Figure 4a). The pericardial space was free of adhesions in two out of three dogs in Group B and there were no adhesions in pleura or pericardium in all three dogs (Figure 4b). In Group C, a thin membrane had completely replaced the original caprolactone sheet and the degree of epicardial adhesion was nil to minimal (Figure 4c).

In Group D, dense adhesions were seen between the e-PTFE sheet and epicardium in one dog (Figure 4d) but there was no adhesion of the e-PTFE sheet to epicardium in the other two dogs.

The macroscopic results of this test are summarized in Figure 5. The figures represent an average of the adhesion scores. The adhesion formation of the gelatin sheet, both the pleural and pericardial sides, was significantly less than that of the e-PTFE sheet 24 weeks after the operation.

Microscopic evaluation

After four weeks in Group B, a considerable amount of gelatin was absorbed. At the site of the remaining gelatin sheet, a slight inflammatory reaction was observed (Figure 6b). In Group C, only a part of the L-C copolymer sheet was absorbed and a piece of the L-C copolymer formed granulation tissue (Figure 6c). In Group D, neutrophil infiltration was extensive around the e-PTFE sheet (Figure 6d).

After 24 weeks in Group B, the gelatin sheet was completely absorbed and replaced by autologous membrane with sparse fibrous tissue. No inflammatory reaction was observed (Figure 7b). In Group C, the L-C copolymer sheet was almost completely replaced by a thin layer of fibrous connective tissue, with some degree of granulation tissue (Figure 7c).

The microscopic results of this test are summarized in Figure 8. The figures represent average of the inflammation scores. There was no significant difference among the subjects in the four groups.

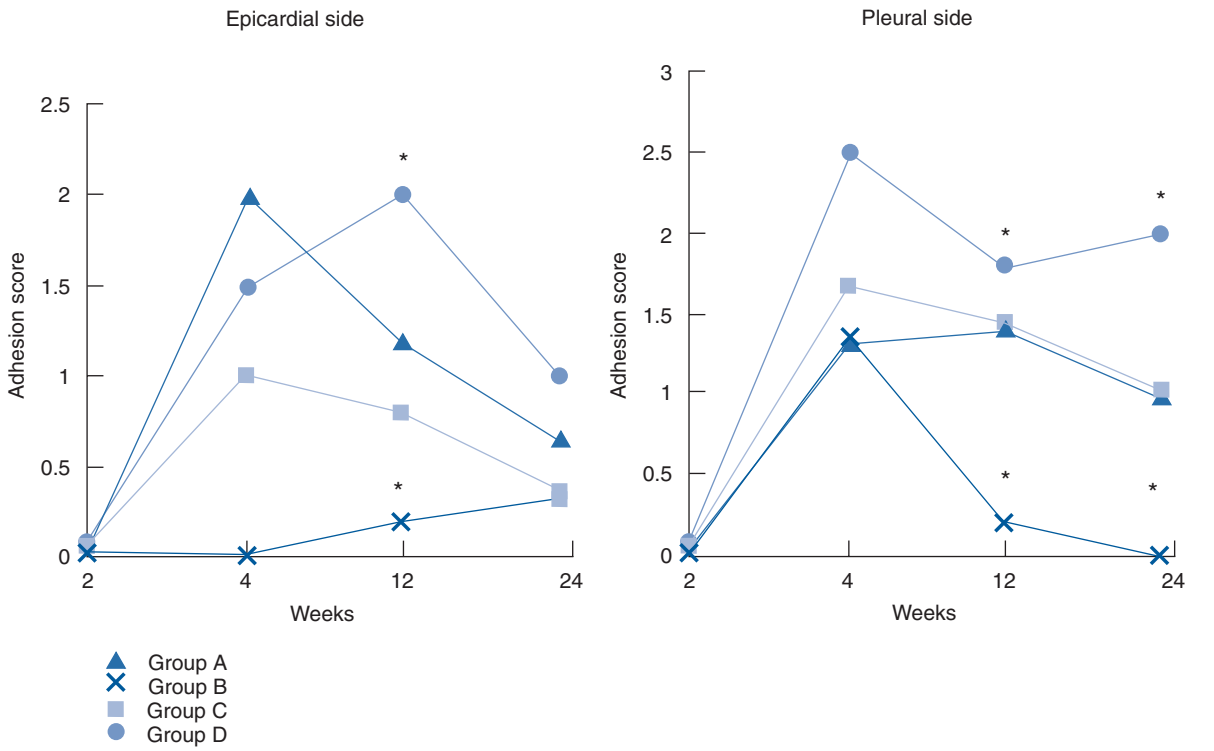

Figure 5. Adhesion score. *$P<0.05$ Group B versus Group C.

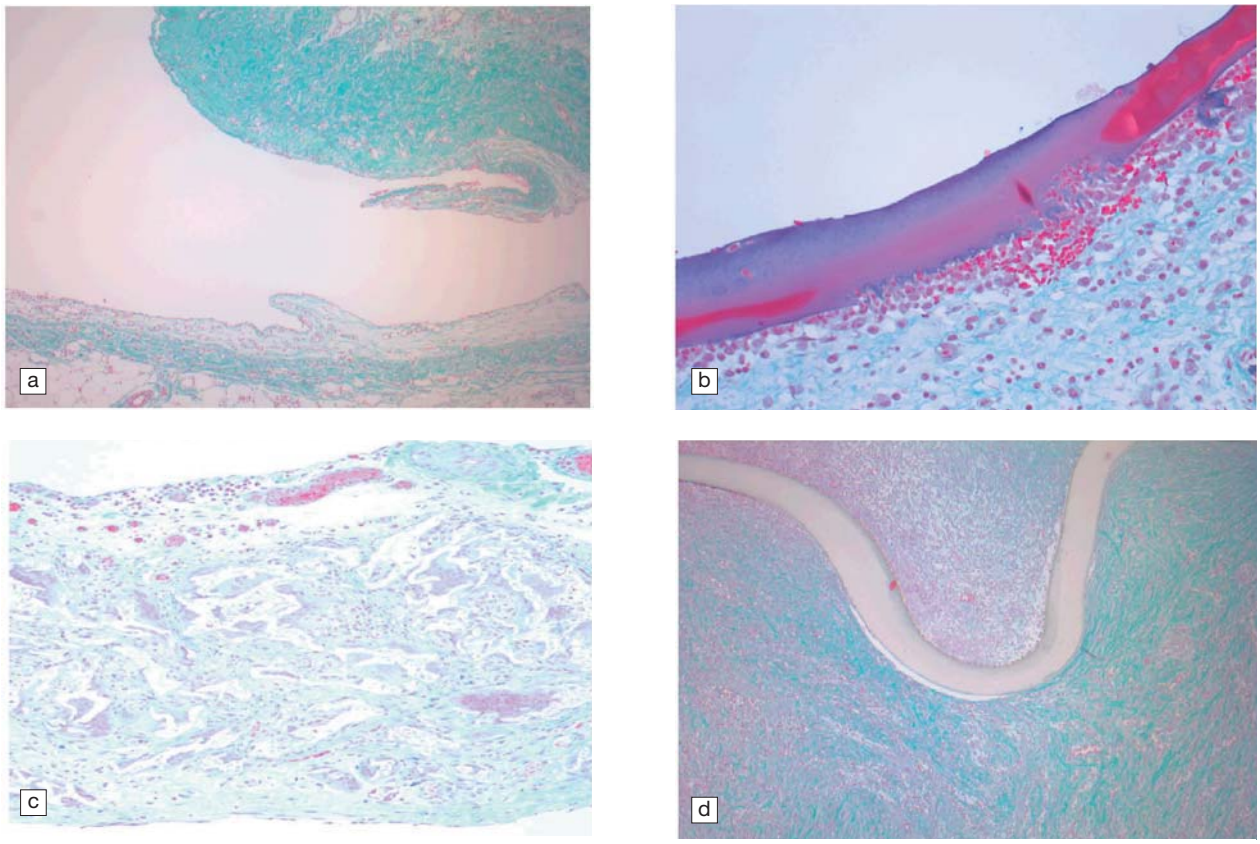

Figure 6. (a) Group A: autologous pericardium 4 weeks after implantation; (b) Group B: gelatin sheet 4 weeks after implantation; no inflammatory reaction was observed; (c) Group C: L-C copolymer 4 weeks after implantation. Piece of the L-C copolymer formed granulation tissue; (d) Group D: e-PTFE sheet 4 weeks after implantation. Neutrophil infiltration is extensive around the e-PTFE sheet.

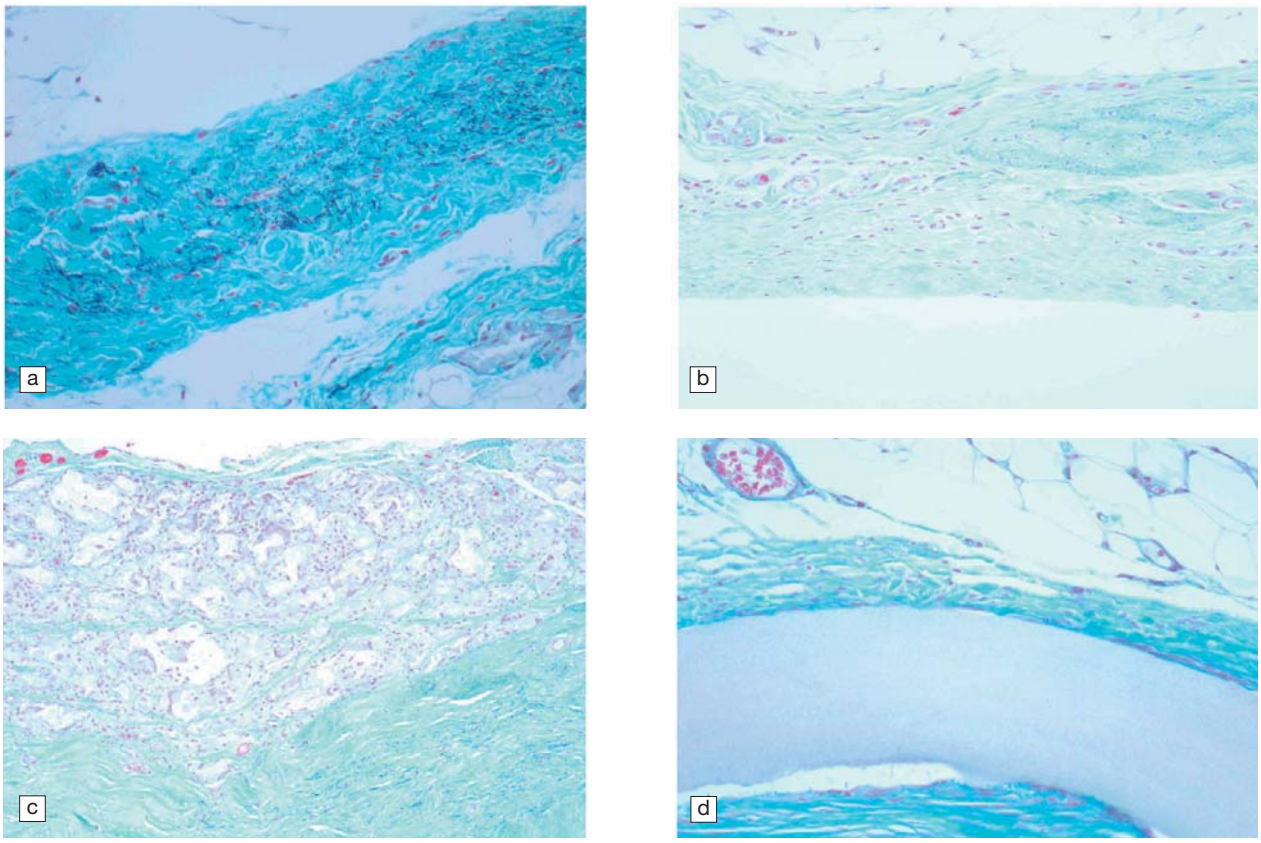

Figure 7. (a) Group A: autologous pericardium 24 weeks after implantation; (b) Group B: gelatin sheet 24 weeks after implantation. At the site of the remaining gelatin sheet, a light inflammatory reaction is apparent; (c) Group C: L-C copolymer 24 weeks after implantation. The copolymer sheet was almost completely replaced by a thin layer of fibrous connective tissue with a degree of granulation tissue; (d) Group D: e-PTFE sheet 24 weeks after implantation. The e-PTFE sheet consisted of dense connective tissue.

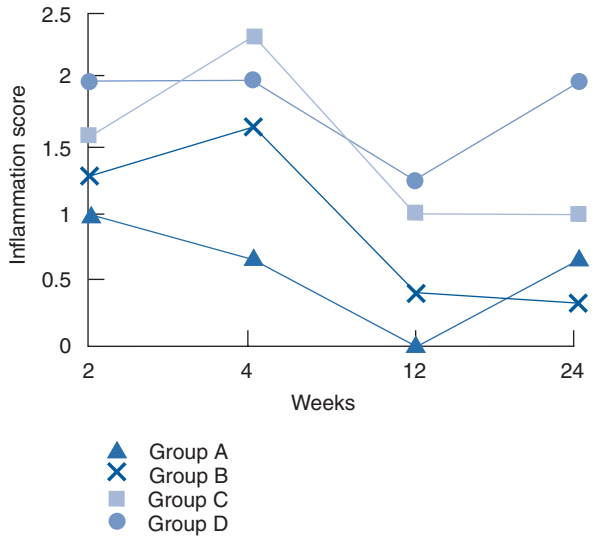

Figure 8. Inflammation score.

Discussion

Many experimental and clinical attempts have been made to solve the problem of adhesions after open-heart operations by using different types of pericardial substitutes. The materials used include silicone rubber[1], polyurethane[2], fascia lata[3,4], e-PTFE sheet[2,5,6], heterologous porcine, equine and bovine pericardium[7–10], Dacron[11,12], and dura mater[13].

Experimental results using animals have been far superior to the results of human clinical trials, which have demonstrated varying degrees of success.

Gabbay *et al.*[14] pointed out that blood clotting after cardiopulmonary bypass might be the reason for such clear differences between results seen in animal experiments and clinical cases. The synthetic sheets made from e-PTFE are widely used as pericardial substitutes. The e-PTFE sheet has, however, a number of significant disadvantages: (1) it remains a permanent foreign body and causes an extensive inflammatory reaction, and (2) the sheet might increase the incidence of mediastinitis. Therefore, the host reaction of the absorbable pericardial substitutes (gelatin sheet and L-C copolymer) were evaluated in this study.

Although not statistically significant, both absorbable

pericardial substitutes caused less adhesion than the autologous pericardium and e-PTFE sheet; this finding corresponds to the report by Okuyama *et al.*[15].

Moderate adhesion was observed between the pleura and bioabsorbable materials four weeks after implantation of the absorbable pericardial substitutes; the newly formed membranous tissue, however, could be easily removed in the same groups at 12 and 24 weeks after the operation. Once bioabsorbable materials were totally absorbed, no host reactions were induced afterward. Microscopic examinations also revealed that whereas a strong foreign body reaction was present four weeks after the implantation, the number of infiltrating inflammatory cells was substantially reduced at 12 and 24 weeks after the operation.

The gelatin sheet seemed to prevent adhesion formation better than L-C copolymer sheet; again the difference was not significant. The extent of adhesion formation can be, at least in part, explained by the difference in the absorption rate. While the gelatin sheet is totally absorbed in four weeks, the L-C copolymer sheet takes 12 weeks. It is speculated that there is some relation between the absorption rate and the degree of adhesion formation, but adhesion formation may be more closely related to the characteristics and properties of the bioabsorbable materials.

There are several reports that the L-C copolymer sheet has been used to repair a defect in the dura mater in experimental models. Among these reports, Yamada *et al.* have described that the L-C copolymer sheet must be gradually absorbed and replaced by a dura-like connective tissue[16].

In our study, bioabsorbable sheets were completely absorbed and replaced by fibrous membranous tissue. The gelatin sheet causes a less fibrous reaction than the L-C copolymer sheet. The fibrous membrane tissue that is replaced by the L-C copolymer sheet has sufficient strength, while a very thin membrane was formed after gelatin sheet was absorbed. Complete closure of the pericardial defect with membranous tissue formed after the absorbable pericardial substitutes may adequately protect the heart from injury at the time of resternotomy, but avoidance of adhesion formation is a far more important component for the pericardial substitutes. The gelatin sheet is, therefore, promising for the clinical application as a pericardial substitute.

Conclusions

1. Both the gelatin sheet and L-C copolymer sheet were completely absorbed by 24 weeks after implantation.
2. The gelatin sheet reduced the formation of pleural adhesions compared with the e-PTFE sheet 24 weeks after implantation.
3. It might be useful for the reconstruction using the absorbable substitutes.

References

1. Laks H, Hammond G, Ceha AS. Use of silicone rubber as a pericardial substitute to facilitate reoperation in cardiac surgery. *J Thorac Cardiovasc Surg* 1981;82:88–92.
2. Mester CA, Comas JV, Ninot S *et al*. The use of polyetherurethane urea (Mitrathane) and polytetrafluoroethylene (Gore-Tex) membrane for pericardial closure; initial clinical results. *Thai J Surg* 1986;125–8.
3. Kohanna FH, Adams PX, Cunningham JN *et al*. Use of autologous fascia lata as a pericardial substitute following open-heart surgery. *J Thorac Cardiovase Surg* 1977;74:14–9.
4. Yu-Chin K. The repair of operative pericardial defect with fascia lata for the prevention and treatment of herniation of the heart. *Chin Med J* 1959;78:210–3.
5. Revuelta JM, Gracia-Rinaldi P, Val F *et al.* Expanded polytetrafluoroethylene surgical membrane for pericardial closure. *J Thorac Cardiovasc Surg* 1985;89:451–5.
6. Minale C, Hollweg G, Nicol S *et al.* Closure of the pericardium using expanded polytetrafluoroethylene (Gore-Tex) surgical membrane: clinical experience. *J Thorac Cardiovasc Surg* 1987;35:312–5.
7. Gallo JI, Pomer JL, Artinano E *et al.* Heterologous pericardium for the closure of pericardial defects. *Ann Thorac Surg* 1987;26:149–54.
8. Gallo Jl, Artinano E, Duran CG. Late clinical result with the use of heterologous pericardium for the cardial cavity. *J Thorac Cardiovasc Surg* 1985;89:709–12.
9. Dietzman RH, Hotler AR, Lynch MF *et al.* Protection of the heart during reoperation using a bovine pericardial shield; clinical experience. *Contemp Surg* 1984;24:35–9.
10. Yakirevich VS, Abdulati SA, Abbott CR *et al.* Reconstruction of the pericardial sac with glutaraidehyde preserved vobine pericardium. *Tex Heart Inst J* 1984;11:238–42.
11. Youmans CR, White J, Derrick JR. The prevention of pleural and pericardial adhesions with Silastic. *J Thorac Cardiovasc Surg* 1968;55:383–8.
12. Mazuji MK, Lett JC. Siliconized Dacron as a pericardial patch. *Arch Surg* 1963;87:104–7.
13. Bonnabeau RC, Armanious AW, Tarnay TJ. Partial replacement of pericardium with dura substitute. *J Thorac Cardiovasc Surg* 1973;66:196–201.
14. Gabbay S, Guindy AM, Andrews JF *et al.* New outlook on pericardial subsutitution after open heart operations. *Ann Thorac Surg* 1989;48:803–12.
15. Okuyama N, Inui I, deZerega GS, Shimazaki Y. Development of bioabsorbable films for prevention of retrosternal adhesions. *Jpn J Artif Organs* 1999;28(1):200–4.
16. Yamada K, Miyamoto S, Nagata I *et al*. Development of a dural substitute from synthetic bioabsorbable polymers. *J Neurosurg* 1997;86:1012–17.

Journal of Congestive Heart Failure and Circulatory Support (2001) Vol 1, No 4, 285–289

Fate of latissimus dorsi muscle flap in cardiomyoplasty and availability of omental flap

M. Okada, T. Tsukube, T. Hariu, Y. Ootaki and Y. Okita
Kobe University School of Medicine, Department of Surgery, Division II, Kobe, Japan

Abstract Background Much attention has been paid to the application of dynamic cardiomyoplasty (DCMP) to patients with end-stage coronary artery disease. However, there are very few reports concerning the fate of the latissimus dorsi muscle flap (LDMF) in DCMP. This study evaluates the fate of the LDMF in the long-term and the effect of the omental flap (OMF) to modulate atrophy of the LDMF.

Methods Mongrel dogs weighing 10–18 kg were used in this study. From 6 weeks to 12 months after DCMP operation, the LDMF was stimulated by a cardiomyostimulator. The heart with the LDMF was sliced vertically to a long axis of the left ventricle at the level of the papillary muscle, and the cover ratio of the LDMF and histological examination were analyzed. The application of the OMF to the LDMF was performed in the other group.

Results The cover ratio equals the external circumference of both ventricles covered with the LDMF divided by the total external circumference of both ventricles. This decreased to less than 20% eight months after DCMP, and DCMP did not augment the left ventricular systolic function. The histological study disclosed atrophic and fibrous changes from the distal portion of the LDMF. However, application of the OMF induced angiogenesis of the distal LDMF and ameliorated muscular atrophy. The mechanism of action was due to enhanced expression of vascular endothelial growth factor (VEGF) by OMF.

Conclusions In DCMP, the LDMF demonstrated more atrophic alteration as the duration after the DCMP procedure became longer, especially longer than eight months. Application of the omental flap to the LDMF seemed to prevent muscular atrophy.

Background

Dynamic cardiomyoplasty (DCMP), direct assistance by simultaneous contraction with the heart, has been applied in clinical cases around the world, and over 700 DCMP operations have been performed to date[1]. Clinical investigation of long-term survivors that received DCMP has shown recovery of symptom and exercise. However, these clinical studies reported that left ventricular functions such as cardiac output and ejection fraction deteriorated and returned to preoperative levels in the chronic phase[2].

This decrease in DCMP performance may be attributed to muscular atrophy of the latissimus dorsi muscular flap (LDMF). The cause of muscle atrophy is known to be multifactorial, however, ischemia of the muscle flap has been proven to induce peripheral muscular atrophy of the flap and preservation of the blood flow is important in preventing muscular atrophy. The blood flow of the latissimus dorsi muscle flap is constituted from the thoracodorsal artery, intercostal arteries and lumbar arteries; the dominant area of the thoracodorsal artery is about 50% the muscle. In the preparation of the LDMF, all of the collateral circulation was ligated and only the thoracodorsal artery was preserved. Therefore, the peripheral blood flow of the LDMF would decrease and peripheral LDMF would become ischemic by the chronic state, resulting in about 25–50% of LDMFs becoming atrophic and fibrotic.

We postulated that application of an angiogenetic factor would improve vascularity and perfusion of the latissimus dorsi muscle and would prevent peripheral muscle atrophy. An omental flap was selected in this study for application of an angiogenetic factor, as the efficacy of an omental flap (omentopexy) against refractory broncho-pleural fistula or perforation of duodenal ulcer is widely known; the omental flap has also been proven to be effective in experiments of healing ischemic tissue. The mechanism of omentopexy has recently clarified that angiogenic factors are upregulated in the omentum and increased in ischemic tissue attached to the omentum. Vascular endothelial growth factor (VEGF) is one of the specific angiogenic factors that the omentum secretes at the highest level of proteins of all tissues. It has also been proven that hypoxia upregulates the expression of VEGF and augmentation of expression of VEGF may be responsible for enhancing the angiogenic activity in the setting of ischemia[3].

Therefore, we investigated the fate of the LDMF in the chronic phase after the DCMP procedure and whether a decrease in systolic performance was correlated with muscular atrophy of the LDMF. We then examined whether the application of the omental flap, as a possible biological carrier of the angiogenetic factor to the LDMF might modulate muscular atrophy of the LDMF.

Correspondence to: Masayoshi Okada MD PhD, 1–1–39–103 Sumiyoshihonmachi, Higashinada-ku, Kobe 658-0051, Japan.

Materials and methods

A total of 29 adult mongrel dogs weighing 10–18 kg were used in this study. All animals received humane care in compliance with the *Principles of Laboratory Animal Care* formulated by the National Society for Medical Research, and the *Guide for the Care and Use of Laboratory Animals* prepared by the National Institutes of Health (NIH Publication No. 86–23, revised 1985).

Study–1

Experimental preparation

Nine adult mongrel dogs weighing 10–15 kg were used in this study. Dogs were anesthetized and prepared for the following sterile surgical procedures. General anesthesia was induced with ketamine hydrochloride (5 mg kg^{-1}) and thiamylal sodium (30 mg kg^{-1}) and was maintained with a dose of sodium pentobarbital given intravenously as needed. Endotracheal intubation and positive-pressure mechanical ventilation were performed. Then 1.5–2.5% of sevoflurane was introduced to maintain anesthesia. The dogs were placed in a right decubitus position, and a longitudinal skin incision was made from the left axilla toward the costovertebral angle. The left lattissimus dorsi muscle was dissected free from all attachments, except for the neurovascular pedicle, which was carefully preserved for good circulation and nerve response. A 3 cm portion of the lateral aspect of the second rib was resected to permit passage of the dissected muscle flap into the thoracic cavity. The proximal tendinous humeral insertion of the LDMF was secured to the second rib to prevent tension on the neurovascular bundle. A left anterolateral thoracotomy was performed in the fifth intercostal space and the pericardium opened. The LDMF was then passed into the left chest cavity and wrapped around both ventricles in a clockwise fashion. The muscle was sutured to the myocardium with six to eight horizontal mattress sutures of 3-0 polypropylene, tied over teflon pledgets. The operative pneumothorax was evacuated with a chest tube and all incisions were closed in layers. A 6-week recovery period was allowed for adhesion formation between the LDMF and the myocardium. The effects of DCMP were then studied in these nine dogs.

Hemodynamic evaluation

Left ventricular heart catheterization was performed 6 weeks to 12 months after the DCMP procedure. For each hemodynamic measurement, the dogs were anesthetized with sodium pentobarbital (30 mg kg^{-1}, intravenously) and permitted to breathe spontaneously with diminished eyelash reflex. Each study took place after the dogs had rested supine in a quiet laboratory for a minimum of 20 min at room temperature. Under sterile conditions, a 5 F pigtail catheter was advanced from the femoral vein to the left ventricle under fluoroscopic guidance. Left ventricular pressure was monitored continuously on an oscillograph (model 363, NEC San-ei Instruments Ltd., Tokyo, Japan) and continuously recorded (model 8M14; NEC San-ei Instruments Ltd., Tokyo, Japan). Left ventricular pressure under the LDMF stimulated by the cardiomyostimulator was compared to the pressure without stimulation and expressed as a percentage change in left ventricular pressure.

Evaluation of the LDMF wrapping

At the end of the study, the dogs were sacrificed and their hearts were excised with the LDMF. The degree of LDMF wrapped around the heart was expressed by cover ratio, which is the ratio of a length of the external circumference of both ventricles covered with LDMF on a length of the total external circumference of both ventricles.

Study 2

Experimental preparation

A total of 20 adult mongrel dogs weighing 10–18 kg were used in this study. Each animal was anesthetized and prepared for the following sterile surgical procedures. General anesthesia with endotracheal intubation and positive-pressure mechanical ventilation was performed. First, with the dog in the left lateral decubitus position, the right latissimus dorsi muscle was dissected free from all attachments, except for its thoracodorsal pedicles. The origin of the latissimus dorsi muscle was reattached to the ribs to maintain a resting tension of the muscle, and then the wound was closed. Second, with the dog in the right lateral decubitus position, the left latissimus dorsi muscle was dissected free from all attachments, except for its thoracodorsal pedicles. The origin of the latissimus dorsi muscle was reattached to ribs to maintain resting tension of the muscle, and then under a midline incision of the abdomen, the omentum was dissected free except for the right gastroepiploic artery. The omental flap was brought to the outside of the left chest wall through a subcutaneous tunnel, and wrapped around the peripheral part of the left LDMF. At 12 weeks after the first operation, the animals were anesthetized and prepared for the following sterile surgical procedures. General anesthesia was maintained with a dose of sodium pentobarbital given intravenously as needed without endotracheal intubation. Tissue blood flow, maximal muscle isotonic strength, morphological features, and tissue VEGF were examined in the left LDMF with the omental flap (OM group) and the right LDMF served as the control (control group).

Tissue blood flow

The blood flow of the LDMF was measured by the laser tissue blood flow system. The tissue blood flow was measured in three parts, including proximal (one-third of the muscular flap), middle (middle of the muscular flap), and the distal part. Tissue blood flow was measured 10 times in each part and averaged values were used.

Maximal muscle isotonic tension

Unipolar electrodes (model 6500, Medtronic Corp., Minneapolis, MN, USA) were woven around the thoracodorsal nerve into the midportion of the LDMF. The stimulating leads were connected to an external R-wave synchronous stimulator (cardiac stimulator model BC-03, Fukuda Densi Inc., Tokyo, Japan), which was programmed to deliver burst stimuli synchronously with cardiac systole. The pacemaker was set to the following parameters: DDD mode, atrioventricular interval 20 ms, cardiac sensitivity 0.5 mV, muscular burst duration 200 ms, muscular frequency 20 Hz, pulse amplitude 2.5–7.5 V. Stimulation was limited to brief periods because the muscle flap was not transformed before the experiment. The maximal isotonic tension was measured during burst stimulation and expressed as Newton (N: kilogram-gravity).

General latissimus morphologic features

The right and left LDMF were evaluated subjectively from hematoxylin and eosin (H&E)-stained and silver-stained sections. Biopsy specimens were taken from the proximal, middle, and distal part of the LDMF and placed in 20% neutral formalin (4°C). The samples were embedded in Paraplast medium and 7 μm sections were prepared. Each slide was reviewed at ×100 magnification. The percentage of muscle fibers replaced by fat and fibrous tissue was estimated to evaluate change of general latissimus morphologic features. Fatty areas were unstained and had a size similar to that of the muscle fiber they replaced.

Vascular endothelial growth factor (VEGF)

Biopsies were taken of proximal, middle, and distal parts of the LDMF. The biopsies were extensively washed with saline and then electrically homogenized in protein extraction buffer (10 mM Tris, pH 8.0, 0.14 M NaCl, 0.025% sodium azide, 2% Triton X-100, 1 mM phenylmethylsulfonyl fluoride (PMSF), and 1 μM leupeptin). Homogenates were subsequently centrifuged for 10 min (13 500 rpm at 4°C). Total protein was quantified using the bicinchroninic acid (BCA) protein assay kit (Pierce Chemicals, Rockford, IL, USA). Equal amounts of total proteins (100 μg) from each specimen were incubated with pre-equilibrated heparin at 4°C for 2 h. A competitive VEGF enzyme immunoassay kit (Quantikine, Human VEGF Immunoassay, R&D Systems, Minneapolis, MN, USA) was used to quantify the level of VEGF in each specimen. A standard curve was included every time and triplicate wells were conducted for each specimen

Statistical analysis

Statistical analyses were performed with a statistical program (Statview 4.0, Cricket Software, Inc. Philadelphia, PA, USA). All values were expressed as the mean ± SD. Analysis of variance for repeated measures was performed to determine the significance of changes of hemodynamic, humoral variables. A paired *t*-test was used to assess the differences in hemodynamics. An unpaired *t*-test was used to assess differences in tissue blood flow, muscle strength, morphologic features, and tissue VEGF. Differences were considered significant when $P < 0.05$.

Results

Hemodynamic parameters

Left ventricular pressure was significantly augmented and then percent change in left ventricular pressure was greater than 110% if DCMP was performed within 6 months. However, in 8 and 12 months after the DCMP procedure, left ventricular pressure could not be elevated significantly.

Cover ratio

The cover ratio of each animal is summarized in Figure 1. The cover ratio was maintained at greater than 58% during the 6 months after the DCMP procedure. The cover ratio at 8 month was 20% and at 12 months, it decreased to 5%. These results correlated with a decrease in augmentation of the left ventricular function, in which (after 8 months) no significant augmentation of the pressure was obtained.

Tissue blood flow

As proximal blood flow of the LDMF varied significantly in each dog, even with controlled hemodynamics, the tissue blood flow of the middle and distal part of the LDMF was expressed by percent change from proximal tissue blood flow. In the middle part, tissue blood flow was 60.5±4.8% in the OM group and 50.7±6.8% in the control group. There was no statistically significant difference between the two groups. However, in the distal part, tissue blood flow of the OM group was significantly higher than in the control group (86.4±6.5% in the OM group and 33.6±3.4% in the control group, $P<0.05$). These results showed that the omental flap significantly increased blood flow of the LDMF.

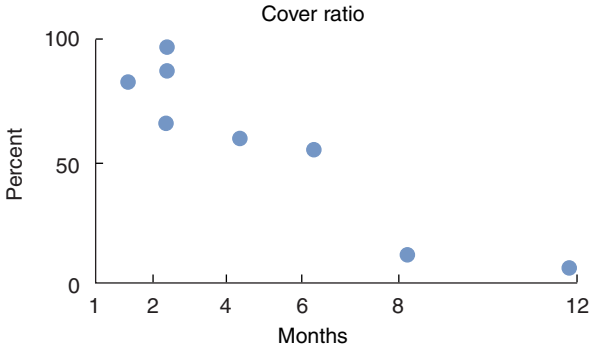

Figure 1. Relationship between time after dynamic cardiomyoplasty procedure and cover ratio of the latissimus dorsi muscle flap to the heart.

Maximal isotonic tension

The maximal isotonic tension under a 2.5 V electric stimulation was 3.2±0.2 N in the OM group and 2.1±0.4 N in the control group, and there was a statistical significance between the two groups. With 5.0 V, the maximal isotonic tension was significantly higher in the OM group as compared to the control group ($P<0.05$). This significant difference was also observed with 7.5 V stimulation. This improved maximal isotonic tension was well correlated with the increase in tissue blood flow of the LDMF (Figure 2).

Histological features of the right and left latissimus dorsi

Fatty and fibrous changes were significantly higher in the control group as compared to the OM group. Microscopic findings of H&E-stained specimen from the distal part of the LDMF showed that the fatty and fibrotic changes were increased in the control group, and muscle fibers were well preserved in the OM group.

Vascular endothelial growth factor (VEGF)

Tissue VEGF expression of the proximal part of the LDMF was 44.0±4.8 pg/100 µg protein in OM, and 37.8±5.0 pg/100 µg protein in the control group. In the middle part, tissue VEGFs were 31.7±3.3 pg/100 µg protein in the OM group and 36.3±4.3 pg/100 µg protein in the control group. There was no significant difference in VEGF expression between the OM group and the control group in both the proximal and middle parts. However, in the distal part, VEGF expression of the OM was 49.6±7.9 pg/100 µg protein and significantly higher than that of the control group. The increase of VEGF expression in distal LDMF was consistent with an increase in blood flow of the distal LDMF (Figure 3).

Discussion

In 1985, Carpentier and Chachques first succeeded in using the latissimus dorsi muscle flap for a clinical case of a left ventricular defect[4]. Since then DCMP has emerged as a promising surgical treatment for patients with end-stage heart disease who may not be candidates for heart transplantation. DCMP has been performed in more than 700 patients worldwide[1]. Despite symptomatic improvement, objective beneficial hemodynamic effects or improved rates of survival have not been demonstrated consistently[2]. The efficacy of DCMP is mainly considered to protect further dilatation of the left ventricle (so-called 'girdling effect') rather than direct cardiac assistance.

The decrease of direct cardiac assistance of DCMP might be related with deteriorated performance of the LDMF. Moeira *et al.* reported that despite preferable clinical outcomes, left ventricular function up to 5 years after DCMP tended to decrease and returned to preoperative levels at 5 years[2]. They also reported that two important factors were the possibility of ischemic compromise of the muscle flap and the fact that the distal part of the latissimus dorsi muscle may eventually become fibrotic and atrophic.

In the present study, we analyzed a cover ratio of length of the external circumference of both ventricles covered with LDMF to the length of the total external circumference of both ventricles, as an index of the degree of atrophy of the LDMF[5]. This ratio (cover ratio) was well correlated with direct cardiac assistance of the DCMP in the chronic state. If the cover ratio decreased less than 20%, DCMP did

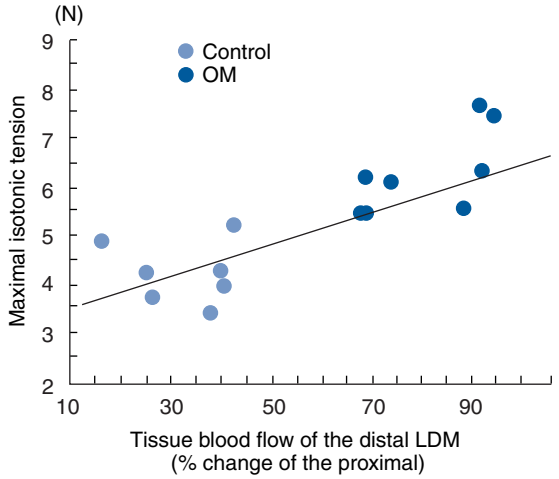

Figure 2. Relationship between tissue blood flow of the distal one-third of the LDMF and the maximal isotonic tension of the LDMF. There was a linear correlation between tissue blood flow and muscle strength of the LDMF (r=0.864). Y=3.255+0.032X. OM: left LDMF with omental flap; Control: right latissimus dorsi muscle flap.

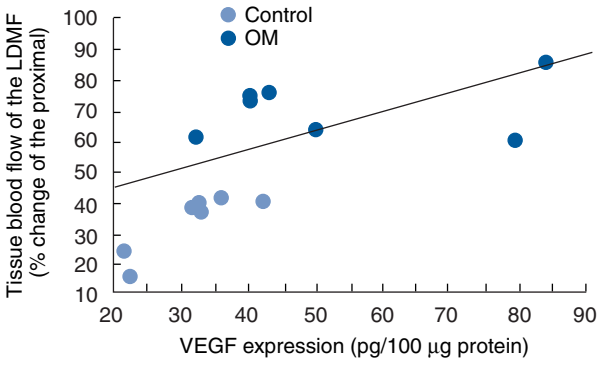

Figure 3. Relationship between VEGF expression and tissue blood flow of the distal one-third part of the LDMF. There was a linear correlation between VEGF and tissue blood flow (r=0.593). Y=28.226+0.77XOM: left LDMF with omental flap; Control: right latissimus dorsi muscle flap.

not augment the left ventricular function, and that histological examination revealed atrophy and fibrosis beginning from the distal part of the LDMF.

Mannion and other investigators reported that an improved morphologic appearance of the latissimus dorsi muscle was associated with improved blood perfusion, and they emphasized that preservation of blood perfusion was an important factor in the prevention of muscular degeneration[6]. Furthermore they reported that preserved morphology was associated with muscle strength[5]. These results are consistent with the fact that improved muscle strength is well correlated with an increase in tissue blood flow of LDMF in the present study[7,8].

Induction of the neoangiogenesis may be one of the therapeutic options in the preservation of blood perfusion of the LDMF. The omentum flap has been widely used for the refractory bronchopleural fistula and perforation of the duodenal ulcer, and has shown its efficacy in promoting wound healing and to stimulating the revascularization of ischemic tissues. The mechanism of the omental flap was recently proved in that VEGF expression of the omentum is greatest in the body, and moreover ischemia upregulated VEGF expression of the omentum. Therefore, we chose the omental flap for application of an endogenous angiogenic factor to the LDMF, and postulated that the omentum would improve vascularity and perfusion of the latissimus dorsi and prevent peripheral muscle atrophy. In the present study, application of the omental flap to the LDMF ameliorates atrophy of the LDMF and muscle strength of the LDMF is well preserved. These changes correspond to the expression of the endogenous VEGF by the omental flap.

VEGF is one of the special angiogenic factors and a heparin-binding, endothelial cell-specific mitogen. Zhang *et al.* reported that the omentum demonstrated the highest VEGF secretion rate as well as the highest concentration of VEGF protein of various rat tissues and organs examined. In addition, it was reported that hypoxia upregulated the expression of VEGF, and augmented expression of VEGF may be responsible for enhancing the angiogenic activity in the setting of ischemia[2]. This result is consistent with the present study, in which VEGF expressed at a higher level on the distal part of the LDMF wrapped with the omental flap as compared with distal parts of the LDMF without treatment.

Dynamic cardiomyoplasty remains an experimental operation. The clinical experience with cardiomyoplasty showed that the symptoms of the patients continued to improve, however, systolic augmentation disappeared in the chronic state. In the present study, we first applied an omental flap to the LDMF to prevent muscular degeneration overall, and found that induced endogenous VEGF expression preserved blood perfusion and muscular strength. The results suggest that dynamic cardiomyoplasty may not lose long-term direct cardiac assistance when an omental flap was applied to LDMF.

Conclusion

Our result proved that muscular atrophy of the LDMF appeared in the chronic state after the DCMP procedure. An omental flap induced angiogenesis of the distal LDMF and ameliorated muscular atrophy. Clinical application of this modification during the DCMP procedure promises swifter long-term direct cardiac assistance and improved patient performance.

References

1. El Oakley RME, Jarvis JC. Cardiomyoplasty: A critical review of experimental and clinical results. *Circulation* 1994;90: 2085–90.
2. Moeira LFP, Noedir A, Stolf NAG *et al*. Clinical and left ventricular function outcomes up to five years after dynamic cardiomyoplasty. *J Thorac Cardiovasc Surg* 1995;109: 353–63.
3. Zhang Q-X, Magovern CJ, Mack CA *et al*. Vascular endothelial growth factor is the major angiogenetic factor in omentum: Mechanism of the omentum-mediated angiogenesis. *J Surg Res* 1997;67:147–54.
4. Carpentier A, Chachques JC. Myocardial substitution with a stimulated skeletal muscle: first successful clinical case. *Lancet* 1985;1:1267.
5. Hariu T, Okada M, Tsukube T, Ootaki T. Availability of omental flap on prevention against muscular atrophy of a latissimus dorsi cardiomyoplasty. *Kobe J Med Sci* 1999;45:51–72.
6. Mannion JD, Velchik M, Hammond R *et al.* Effects of collateral blood ligation and electrical conditioning on blood flow in dog latissimus dorsi muscle. *J Surg Res* 1989;47:332–40.
7. Kartz JM, Johnson WS, Mukherjee LVTR *et al*. The relation between latissimus dorsi skeletal muscle structure and contractile function after cardiomyoplasty. *J Thorac Cardiovasc Surg* 1994;107:868–78.
8. Okada M, Toyoda T, Mukai T, Kashem MA, Tsukube T. The Effect of Cardiomyoplasty on Coronary Blood Flow and Diastolic Dimension of the left Ventricle. *Heart Replacement – Artificial Heart 6*, 1998; pp 243–47.

Session 6
Engineering

Journal of Congestive Heart Failure and Circulatory Support (2001) Vol 1, No 4, 293–297

Extension of durability of jellyfish valve for long-term use in artificial hearts

K. Iwasaki MS[1], M. Umezu PhD[1], K. Imachi PhD[2], Y. Abe MD PhD[2], T. Chinzei MD PhD[3], T. Isoyama PhD[3], I. Saito PhD[3] and T. Fujimoto MD[4]

[1]Department of Mechanical Engineering, Waseda University; [2]Department of Biomedical Engineering, Graduate School of Medicine, The University of Tokyo; [3]Research Center for Advanced Science and Technology, The University of Tokyo; and [4]Institute for Science and Engineering, Waseda University, Tokyo, Japan

Background A chronic animal experiment of over 300 days in which jellyfish valves were incorporated into conventional sac-type blood pumps revealed fracture and calcification on the thin flexible leaflet. The aim of the present study was to make clear the cause of these problems from an engineering point of view, with the goal of facilitating longer durability (a guarantee of approximately 1 year) of the jellyfish valve.

Design improvement of jellyfish valve Finite element analysis of the closed phase of the jellyfish valve indicated that the mechanical strain generated on the leaflet was a prominent cause of fracture and calcification, as found in the animal experiment. Moreover, further analysis suggested that incorporation of an additional concentric ring into the valve seat would be effective in reducing strain concentration. *In vitro* steady and pulsatile flow tests demonstrated that a modified valve with a 0.5 mm-wide ring located at a radius of 7.0 mm had a comparable hydrodynamic performance to the original jellyfish valve.

Durability tests A commercially available accelerated fatigue tester was employed; tests revealed that the durability of the modified valve had been extended beyond that of the original jellyfish valve by 10 times.

Animal experiment By means of conventional sac-type blood pumps and undulation pump total artificial hearts, 13 animal experiments have been performed. The modified jellyfish valve showed excellent blood compatibility after a minor modification of the configuration of the valve seat at the attachment of the leaflet.

Conclusion The modification of this polymer valve shows great promise for clinical artificial heart application.

Keywords jellyfish valve, calcification, fracture, durability, mechanical strain, finite element analysis, accelerated fatigue test, artificial heart.

Introduction

In vitro mock circulation studies of the jellyfish valve, plus animal trials of up to four months' duration, in which the valve was incorporated into conventional sac-type blood pumps[1], have revealed that this valve has:

1. excellent antithrombogenicity (no need for systemic anticoagulant and antiplatelet therapy)
2. excellent hydrodynamic performance
3. little noise at the instant of valve closure.

However, throughout a chronic animal experiment, in which jellyfish valves were used in blood pumps for over 300 days[2], a fracture was observed in the thin (approximately 50–70 μm) flexible leaflet of the left side of the valve after 312 days. In addition, calcification was observed on leaflets of valves from both the left and the right sides of the blood pumps (the right side of the pump was exchanged after 414 days due to thrombus formation inside the blood pump). As revealed in this case, poor durability and calcification still remain serious problems, limiting the long-term application of polymer valves in artificial hearts. The aim of this study was, therefore, to make clear the cause of leaflet fracture and calcification in the jellyfish valve, from an engineering point of view, and to improve the valve's durability until it can be relied upon to function for approximately 1 year with a generous safety factor.

Finite element analysis

In the animal experiment, a leaflet fracture was observed in the center of the area between two spokes, as shown in Figure 1. In addition, calcification was also observed on the surface of the flexible leaflet, which is made of a segmented polyurethane (K-III, Nippon Zeon Co. Ltd. Tokyo, Japan), as shown in Figure 2. A circumspect survey of the leaflet surfaces by scanning electron microscope (SEM) and energy dispersive X-ray analyzer (EDX) indicated that calcification was deposited in two specific regions of the leaflet: (1) above the spoke edge, on the downstream side of the leaflet, and (2) in the center of the area between adjacent spokes, in the upstream side of the leaflet. Calcification is one of the most troublesome problems in the long-term use of polymer components such as moving diaphragms in artificial hearts, limiting functional capacity and durability, and tending to induce

Correspondence to: Kiyotaka Iwasaki, 3-4-1 58-322 Ohkubo, Shinjuku-ku, Tokyo 169–8555, Japan.

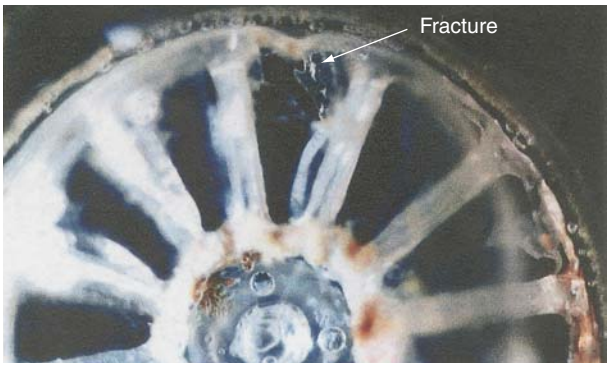

Figure 1. Leaflet fracture of a jellyfish valve after 312 days' use in a conventional sac-type blood pump.

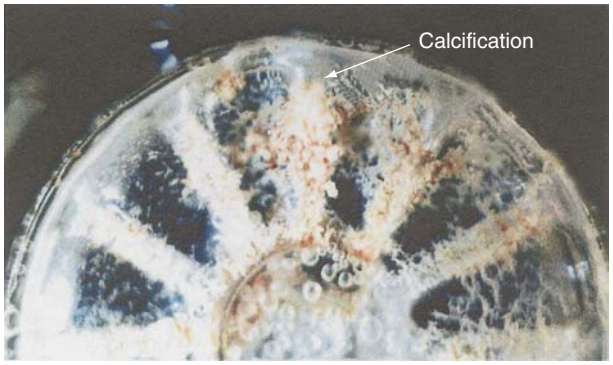

Figure 2. Calcification on the leaflet surface of a jellyfish valve after 414 days' use. Front view of the figure shows the downstream side of the leaflet.

thromboembolic complications[2–7]. Some researchers have empirically pointed out that mechanical stress and physicochemical changes of the material would have an important role in the calcification of polymer surfaces[2–8]. However, the mechanism of this process has not yet been clarified. As for the jellyfish valve, movement of the leaflet is not restrained during the opening and open phases except for a central attachment to the valve seat. Thus, the mechanical restraint of the leaflet by the valve seat during the closed phase was assumed to be the major contributor to leaflet fracture as well as calcification. Therefore, in order to investigate the cause of these two problems, equivalent elastic strain, equivalent Von Mises stress, and deflection during the closed phase under a pressure load of 90 mmHg were modeled by means of the finite element method (FEM). The analysis was performed on only one of the 12 radial segments of the jellyfish valve, taking the symmetric shape into consideration. The results showed that strain concentrations occurred in the center of the area between two spokes, and above the spoke edge, while the stress concentration and the maximum deflection were respectively observed above the spoke edge and in the center of the area between two spokes. In addition, a further FEM analysis on the thickness-wise direction of the leaflet clarified that tensile strain was concentrated in the center of the area of two spokes in the upstream side and also concentrated above the spoke edge in the downstream side as shown in Figure 3. Then, a comparison between these analysis results and the animal experimental results indicated that the strain-concentrated area by FEM analysis was consistent with the fracture location of the leaflet. Even more demonstrably, the area of concentration of tensile strain was coincident with the area of calcific deposition. Therefore, it was confirmed that the strain concentration during the closed phase would be the prime factor in inducing leaflet fracture and calcification.

Design improvement of jellyfish valve

Reduction of strain concentration during the closed phase was considered to be the most effective way to extend the durability of the jellyfish valve. Therefore, further theoretical analysis was performed to explore an ideal design that

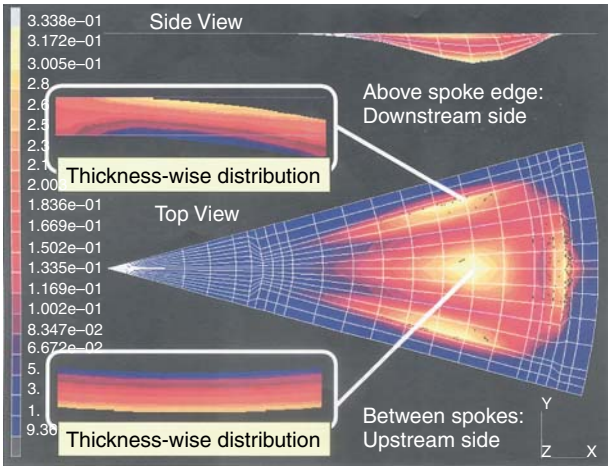

Figure 3. Strain map on the leaflet of a jellyfish valve during the closed phase under a pressure load of 90 mmHg.

could minimize strain concentration. Calculations resulting from a theoretical analysis suggested that incorporation of an additional concentric ring into the valve seat would be highly effective in reducing the strain concentration[9]. Moreover, the result of FEM analysis also indicated that the optimal location of the additional ring would be at a radius of 7 mm, corresponding to the location of maximum strain. Then, based on these findings, a new valve seat was designed as shown in Figure 4. A tapered configuration was applied to the additional ring. The width of the concentric ring surface contacting the leaflet during the closed phase was determined as 0.5 mm, whereas the width of the inflow side was determined as 0.1 mm, to minimize inflow obstruction. The new valve seat was essentially fabricated in six stages:

1. A computer code was written.
2. A computer-controlled machine fabricated a wax male mold for the proposed valve seat.
3. A female mold was cast by insertion of RTV silicone into the wax mold.
4. A polyurethane valve seat was cast from the silicone mold.

5. A NC lathe was cut on the outflow side of the valve seat to make an attachment to the leaflet.
6. The valve seat was coated with K-III polyurethane in a clean-air room, to achieve excellent blood compatibility (coating of the valve seat was performed twice, for safety to prevent peeling of the coating when assembling the valve into the blood pump).

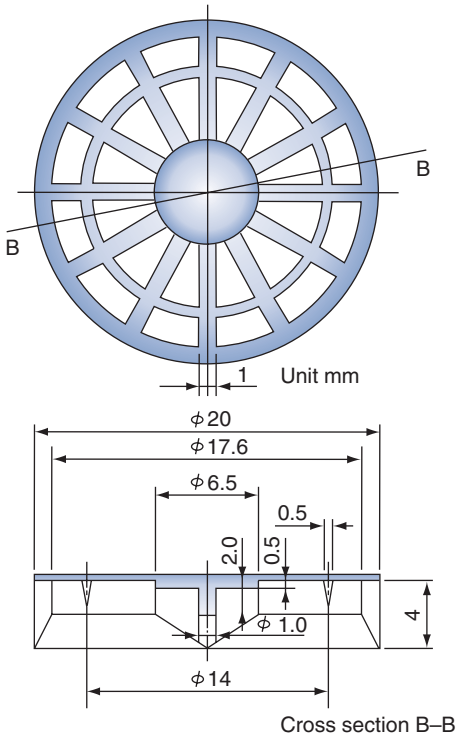

Figure 4. Configuration of the newly designed valve seat.

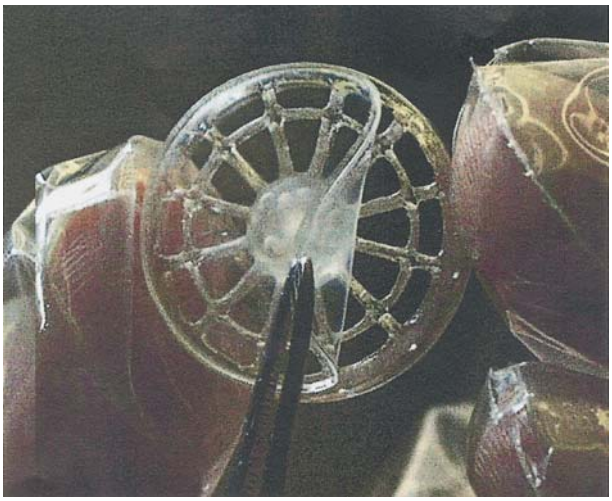

Figure 5. Modified jellyfish valve designed with the expectation of longer durability.

The leaflet was fabricated by casting technique. The blood-compatible segmented polyurethane, named K-III, was used for the leaflet material. Then the valve seat and the leaflet were jointed at the central position with K-III. Therefore all the surfaces of the valve are of a blood-compatible uni-material.

Figure 5 shows the new valve seat finally fabricated.

In vitro steady and pulsatile flow tests

Both steady and pulsatile flow tests assessed the hydrodynamic performance of the modified jellyfish valve. In the steady flow test, pressure drop across the valve seat was compared between the modified valve and the original valve. The results showed that the increase in pressure drop of the modified valve was just 1 mmHg as compared with that of the original valve, under a mean flow rate of 10 L min^{-1}.

In the pulsatile flow test of the modified jellyfish valve, a pneumatically driven pulse duplicator as shown in Figure 6 was employed. The original jellyfish valve and a Bjork–Shiley mechanical heart valve with the same orifice diameter were used for a comparative study. These three valves were tested in the mitral position, and the original jellyfish valve was installed in the aortic position. A unique feature of this tester is that a load cell is mounted in the

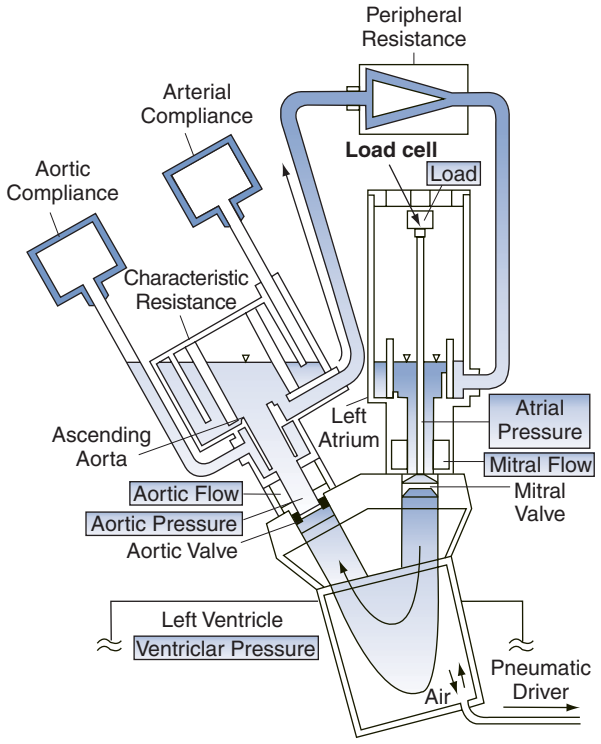

Figure 6. Schematic drawing of test apparatus for the comparative study of hydrodynamic performance among the modified jellyfish valve, the original jellyfish valve, and the Bjork–Shiley mechanical heart valve.

mitral position, to measure the impact load at valve closure. Each valve was tested at three typical conditions, in which mean aortic flow rate was adjusted to 4.7 L min^{-1} (90 bpm), 5.5 L min^{-1} (105 bpm), and 6.3 L min^{-1} (120 bpm), under an aortic pressure of 110 (130/90) mmHg. The transvalvular flow rate and the impact load at valve closure were specifically examined in this study. Figures 7 and 8 show comparison between the three valves. Figure 7 suggested that in terms of pump output the modified jellyfish valve had comparable performance to the original valve and surpassed the Bjork–Shiley valve. Moreover, the impact load at valve closure (Figure 8) was apparently decreased in the modified jellyfish valve, as compared to the original valve.

Durability test

An accelerated fatigue tester, which was originally designed by Professor H. Reul (at Helmholtz Institute, Germany), was employed to assess the durability of the modified jellyfish valve. The maximum pressure gradient at valve closure was adjusted to 120 mmHg in 37ûC water as recommended by ISO 5840[10]. In addition, mean outlet pressure of the valve and mean transvalvular flow rate were adjusted to 115 mmHg and 5.0 L min^{-1}, respectively. Three modified jellyfish valves and three original jellyfish valves were tested in turn. Accelerated fatigue tests were conducted at the frequency of 10 Hz (600 bpm). The results showed that the repetition number to fracture was 7.29×10^6 cycles as to the three original jellyfish valves. On the other hand, the repetition number for the modified jellyfish valve was 7.54×10^7 cycles. Therefore, it was successfully revealed that the durability of the modified jellyfish valve was extended by 10 times as compared with the original valve. If the cycles-to-fracture in the accelerated fatigue tests are simply commuted to the durability under a physiological pump rate of 70 bpm, the commuted durability of the modified valve is 24.9 months, whereas that of the original valve is 2.4 months. According to the result of the animal experiment at a mean pump rate of 105 bpm, the durability of the jellyfish valve was 10.4 months. As shown in this case, the severe conditions in the accelerated fatigue tests generally reduce the durability in comparison with that in the physiological range of pump rate. These data suggested that the durability of the modified jellyfish valve would be extended beyond two years. The accelerated fatigue test successfully demonstrated that the durability of the modified valve was longer than that of the original valve by a factor of 10.

Animal experiments

Achieving long-term blood compatibility of an implanted material is one of the most important themes of this study. One animal experiment, in which the modified jellyfish valve was incorporated into conventional sac-type blood pumps, and 12 animal experiments in which the valve was incorporated into an implantable total artificial heart (the undulation pump total artificial heart [UPTAH]) have been performed. In the sac-type blood pumps, an original jelly-

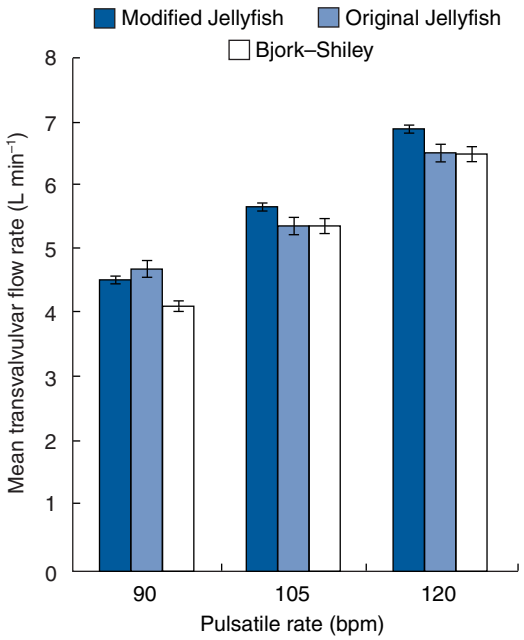

Figure 7. Comparison of the mean transvalvular flow rate among the modified valve, the original, and the Bjork–Shiley valve under three typical conditions.

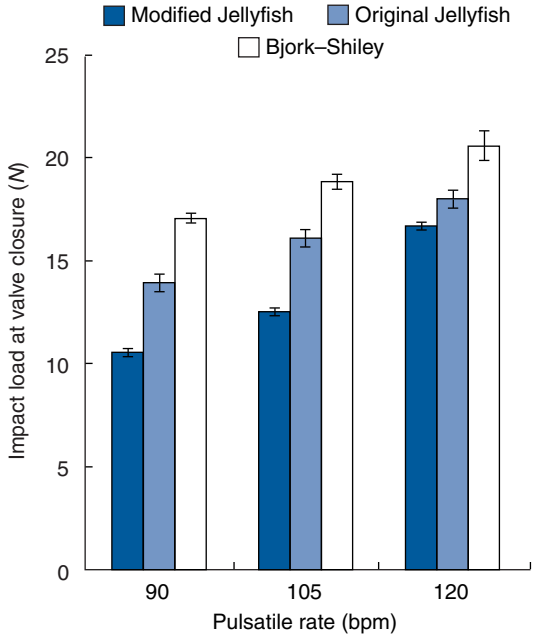

Figure 8. Comparison of the impact load at the instance of valve closure among the modified valve, the original, and the Bjork–Shiley valve under three typical conditions.

fish valve was incorporated into the inlet side of the left blood pump, and three modified valves were incorporated into the outlet side of the left blood pump and into the right blood pump. In this case, thrombus formation was observed around the attachment of the leaflet and the valve seat, forcing exchange of the right side of the blood pump after 91 days, and of the left side of the blood pump after 113 days. The cause of the thrombus formation was found to be a misfabrication of the valve seat at the location of the leaflet attachment. The side face of the attachment area was penetrated, and micro gaps were detected around the joint between the leaflet and the valve seat. This allowed invasion of blood elements and induced thrombus formation. The phenomenon was also observed in the first six animal experiments of the modified jellyfish valves using undulation pumps. Therefore, the diameter to drill 0.5 mm in depth for the attachment of the leaflet was changed from 6.5 mm to 6 mm to eliminate invasion of blood from the side face there (see Figure 4). After this modification, five animal experiments were performed using the undulation pumps, with survival times ranging from 5 h to 46 days; in all cases, no thrombus formation on the modified jellyfish valves was detected at autopsy. Further long-term animal experiments of the modified jellyfish valve are expected to reveal its long-term blood compatibility and calcification tendency, for comparison with the results for the original jellyfish valve.

Conclusion

With the aid of finite element analysis, the jellyfish valve was improved with the expectation of longer durability. The accelerated fatigue tests successfully demonstrated that the repetition number to fracture of the modified jellyfish valve was extended in comparison with that of the original jellyfish valve by 10 times, corresponding to over two years *in vivo*. Moreover, animal experiments revealed that the modified valve had excellent blood compatibility after a minor modification of the leaflet attachment. These data indicate that the modified valve has great promise for clinical application in artificial hearts.

Acknowledgements

This investigation was performed with the aid of the following research funds: The program for promotion of fundamental studies in health science of the organization for drug ADR relief, R&D Promotion and Product Review of Japan (No. 96–12), and a Grant-in-aid for Scientific Research of Japan (Nos. 09557112 and 09470288).

References

1. Imachi K, Mabuchi K, Chinzei T *et al*. Fabrication of a jellyfish valve for use in an artificial heart. *Trans Am Soc Artif Intern Organs* 1992;38:237–42.
2. Imachi K, Abe Y, Chinzei T *et al*. Calcification and thrombus formation on polymer surface of an artificial heart. Akutsu T, Koyanagi H, editors. *Artificial Heart 6* Tokyo: Springer-Verlag 1996:110–5.
3. Imachi K, Matsuura H, Karita T *et al*. Mechanism of calcification on the jellyfish valve and its protection. *Proc Third World Congress of Biomechanics*, Sapporo 1998:199.
4. Harasaki H, Gerrity R, Kiraly R, Jacobs G, Nosé Y. Calcification in blood pumps. *Trans Am Soc Artif Intern Organs* 1979;14:305–10.
5. Whalen RL, Snow JL, Hrasaki H, Nosé Y. Mechanical strain and calcification in blood pumps. *Trans Am Soc Artif Intern Organs* 1980;16:487–92.
6. Nosé Y, Harasaki H, Murray J. Mineralization of artificial surfaces that contact blood. *Trans Am Soc Artif Intern Organs* 1981;17:714–19.
7. Vašku J. Changes in total artificial heart driving diaphragms after long-term pumping. Akutsu T, Koyanagi H, editors. *Artificial Heart 5*. Tokyo: Springer-Verlag 1995:53–64.
8. Vašku J, Urbanek P. Electron microscopic study of driving diaphragms in long-term survival with a total artificial heart. *Artif Organs* 1995;19(4):344–54.
9. Iwasaki K, Umezu M, Kobayashi Y, Imachi K, Fujimoto T. Development of a durable polymer valve based on finite element analysis. *Proc of the 4th Asia-Pacific Conference on Medical & Biological Engineering*, Seoul 1999:252.
10. ISO: ISO5840 Cardiovascular implants–Cardiac valve prosthesis. Committee draft. 1994:18–24.

Journal of Congestive Heart Failure and Circulatory Support (2001) Vol 1, No 4, 299–303

Sensorless estimation of pressure head and flow of a continuous-flow artificial heart

M. Yoshizawa PhD[1], T. Sato MS[2], A. Tanaka PhD[1], K. Abe PhD[1], H. Takeda PhD[3], T. Yambe MD[4], S. Nitta MD[4] and Y. Nosé MD[5]

[1]Department of Electrical and Communication Engineering, Graduate School of Engineering, Tohoku University, Sendai, Japan; [2]Institute of Engineering Mechanics and Systems, University of Tsukuba, Tsukuba, Japan; [3]Department of Electrical Engineering, Tohoku Gakuin University, Tagajo, Japan; [4]Institute of Development, Aging and Cancer, Tohuku University, Sendai, Japan; and [5]Department of Surgery, Baylor College of Medicine, Houston, TX, USA

Abstract The present study has proposed a new method for estimating the pressure head ($P(t)$[mmHg]) and flow ($Q(t)$[L min^{-1}]) of a centrifugal pump by using voltage ($V(t)$[V]), current ($I(t)$[A]) and rotational speed ($N(t)$ [k(rpm)]) of the DC motor for the pump without any additional sensors. Two auto-regressive exogeneous (ARX) models are employed in the proposed estimation method. One ARX model has one output: $P(t)$ or $Q(t)$, and three inputs: $VI(t) = V(t)I(t)$, $N(t)$ and the gain constant (K) of the system from $VI(t)$ to $N(t)$. It can be regarded that K may include the information on viscosity of blood. The coefficient parameters of this ARX model are identified in an off-line fashion before implantation of the pump. After implantation, $P(t)$ or $Q(t)$ is estimated by the same ARX model with the pre-identified parameters. The other ARX model is used to identify K on the basis of $VI(t)$ and $N(t)$ in an on-line fashion every time the viscosity of blood may change. In the experiment, a mock circulatory system consisting of a centrifugal pump and a reservoir with glycerin 37% or water was employed. The root mean square error between measured Q and its estimate obtained from the proposed method was 1.82 L min^{-1}. On the other hand, the different method based on a single ARX model with inputs of $VI(t)$ and $N(t)$ but without the additional input of K yielded the corresponding estimation error of 2.38 L min^{-1}. This means that the proposed method can reduce its estimation error in comparison with the method that cannot cope with the change in blood viscosity.

Keywords sensorless estimation, flow, pressure, continuous-flow blood pump, ARX model, viscosity.

Introduction

For the development of implantable artificial hearts, a method must be found for estimating the recipient's blood pressure and flow without using pressure sensors and flowmeters that have to be implanted inside the body. In the case of electric motor-driven artificial hearts, the voltage, current and rotational speed of the motor can be measured easily and accurately. Hence, it is desirable to estimate pressure and flow by processing these three signals. Such an approach has already succeeded to some extent in the case of centrifugal blood pumps in other studies[1,2]. These estimation methods must include a compensation procedure for the change in blood viscosity. However, conventional compensation procedures are not suitable for automatic and on-line estimation. For example, hematocrit value may be useful in compensating for the change in blood viscosity[2] but direct measurement of this value should be avoided.

The present study proposes a new method for estimating instantaneous values of pressure head ($P(t)$[mmHg]) and flow ($Q(t)$[L min^{-1}]) on the basis of voltage ($V(t)$[V]), current ($I(t)$[A]) and rotational speed ($N(t)$[k<rpm>]) in a DC-motor-driven centrifugal pump used as a ventricular assist device (VAD). The proposed estimator can automatically compensate for the effect of the change in viscosity of blood on the accuracy of estimation by employing two kinds of auto-regressive exogeneous (ARX) models.

Methods

Steady state model

For general expression, let $y(t)$ denote either $P(t)$ or $Q(t)$. Define electrical power ($VI(t)$) supplied to the motor as $VI(t) = V(t) \cdot I(t)$. In the steady state or the static situation where the notation of time (t) of every variable is omitted, the previous preliminary experiments revealed that y (pressure head or flow) can be approximated by:

$$y = b_1 \cdot N^2 \cdot VI + b_2 \cdot N \cdot VI + b_3 \cdot VI + b_4 \cdot N^2 + b_5 \cdot N + b_6 \quad (1)$$

where b_j; $j = 1,2, ..., 6$ are constant coefficients.

Correspondence to: Makoto Yoshizawa, Department of Electrical and Communication Engineering, Graduate School of Engineering, Tohoku University, Aoba-yama 05, Aoba-ku, Sendai 980–8579, Japan.

ARX model I for output estimation without additional input

The static system (1) can be extended to the following ARX model (ARX model 1) as a dynamic time series model.

$$y(k) + \sum_{i=1}^{n} a_i y(k-i) = \sum_{i=1}^{m_j} \sum_{j=1}^{6} b_{ij} u_j(k-i+1) + w(k) \quad (2)$$

where k is discrete time satisfying $t = k\Delta t$, Δt is sampling period, $w(k)$ is residue assumed to be a white noise, n is order of output, m_j is order of input, $u_j(k)$ is six kinds of exogenous input as follows:

$$u_1(k) = N^2(k) \cdot VI(k) \quad (3)$$
$$u_2(k) = N(k) \cdot VI(k) \quad (4)$$
$$u_3(k) = VI\,(k) \quad (5)$$
$$u_4(k) = N^2(k) \quad (6)$$
$$u_5(k) = N\,(k) \quad (7)$$
$$u_6(k) = 1 \text{ (Dummy data for estimating bias)} \quad (8)$$

Let $m_6 = 1$ and $m_1 = m_2 = \cdots = m_5 = m$ for simplicity.

After off-line identification of a_i and b_{ij} based on measured data $y(k)$ and $u_j(k)$, the ARX model I given by (2) can generate an estimate ($\hat{y}(k)$) of $y(k)$. The number n and m can be chosen so as to minimize the root mean square value (ε) of the error between $y(k)$ and $\hat{y}(k)$ defined as:

$$\varepsilon = \sqrt{\frac{1}{D} \sum_{k=1}^{D} \{y(k) - \hat{y}(k)\}^2} \quad (9)$$

where D is data size.

ARX model II for output estimation with additional input

If viscosity of blood changes considerably, the ARX model I given by equation (2) will not be able to estimate $y(t)$ because the true coefficients a_i and b_{ij} will also change. Thus, let us consider a new ARX model (ARX model II) as follows:

$$y(k) + \sum_{i=1}^{n} a_i y(k-i) = \sum_{i=1}^{m_j} \sum_{j=1}^{7} b_{ij} u_j(k-i+1) + w(k) \quad (10)$$

where the first six inputs are the same as equations (3) to (8), respectively, and the seventh input, i.e. a new additional input is:

$$u_7(k) = K \quad (11)$$

where K is the gain constant obtained from the ARX model III shown in equation (12). Let $m_6 = m_7 = 1$, and $m_1 = m_2 = \cdots = m_5 = m$. The method of determining m is the same as that of ARX model I.

ARX model III for estimation of gain constant

The change in viscosity of blood must affect ease of rotation of the motor. Hence, a parameter depending on ease of rotation may include information on viscosity. One of the candidates for such a parameter is the gain constant K of the system from the supplied power $VI(t)$ to the rotational speed $N(t)$. Assume that the system can be approximated by another very simple ARX model (ARX model III):

$$N(k) + a_1 N(k-1) + a_2 N(k-2) = b_{11} VI(k) + b_{21} VI(k-1) + b_{12} + w(k) \quad (12)$$

and then, the gain constant K can be identified by using the above coefficients as:

$$K = \frac{b_{11} + b_{21}}{1 + a_1 + a_2} \quad (13)$$

This identification process can be carried out every time when the viscosity may change because both $VI(k)$ and $N(k)$ are always measurable.

In this study, a function *arx* in the System Identification Toolbox of Matlab (Mathworks, Inc., Natrick, MA, USA) was used to identify the coefficients of ARX models, I, II and III.

Experiment

An *in vitro* experiment was carried out in a mock circulatory system consisting of a centrifugal pump (Kyocera C1E3) driven by a brush-less DC motor, tubes, a reservoir, and a clamp. To compare the different effects of change in viscosity on an estimation of accuracy, two components of the mock system (glycerin 37% and water) were employed. An electromagnetic flowmeter was used to measure the outflow of the pump. Two pressure sensors at the inlet and the outlet ports of the pump were used to measure the pressure head. Sampling period Δt was 10 ms. To maintain the persistent excitation condition for accurate identification, the driving voltage $V(t)$ was changed randomly between 5 V and 9 V. The gap of the clamp was also randomly changed manually to simulate the effect of transient change in cardiac load made by the natural heart connected in parallel with the blood pump as the VAD.

Results

Figure 1 shows time trajectories of $V(t)$, $I(t)$, $N(t)$, $P(t)$ and $Q(t)$. The left and the right parts of the figure correspond to glycerin 37% (interval A) with high viscosity and water (interval B) with low viscosity, respectively. The data file of Figure 1 was made by simply connecting two data files corresponding to intervals A and B, which were independently measured at different times.

Figure 2 shows the result of estimation of outflow $Q(k)$ using the ARX model I ($n = 2$, $m = 10$) whose coefficients were identified on the basis of the data obtained from both intervals A and B. The estimation error$_\varepsilon$ defined by calculation (9) was 2.38 L min^{-1}. The correlation coefficient (r) between $Q(k)$ and its estimate was $r = 0.619$. It can be seen that the amplitude of the estimate is narrower than that of the measured value.

Figure 3 shows the result of estimation of outflow $Q(k)$ using the combination of ARX models II ($n = 2$, $m = 10$)

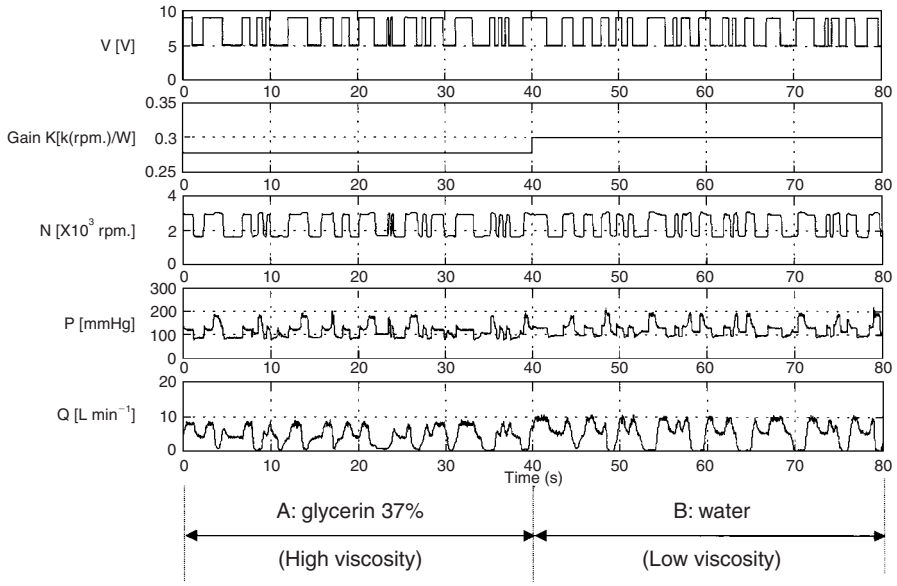

Figure 1. Time trajectories of measurements when the motor was driven by random voltage and the outlet tube was randomly clamped.

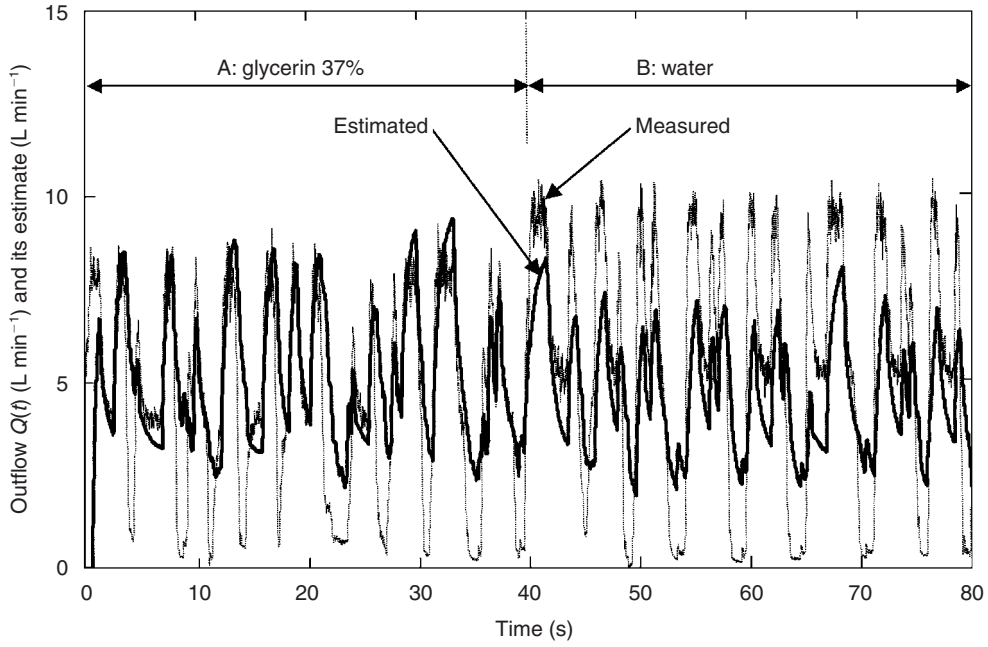

Figure 2. Flow estimation using the ARX model I ($n = 2$, $m = 11$) whose coefficients were identified during both Intervals A and B. Root mean square error:$_{\varepsilon}$ = 2.38 L min^{-1}. Correlation coefficient: $r = 0.619$.

and III ($n = 2$, $m = 1$) whose coefficients were identified on the basis of the data obtained from both intervals A and B. The error$_{\varepsilon}$ and correlation coefficient r were 1.82 L min^{-1} and 0.801 L min^{-1}, respectively. This means that the estimation accuracy of Figure 3 was considerably improved in comparison with that of Figure 2.

In the case of pressure estimation as well as flow estimation,$_{\varepsilon}$ and r obtained from the same data as flow estimation are shown in Table 1. The table indicates that pressure estimation yielded significantly fewer differences between ARX model I and the combination of ARX models II and III than flow estimation. This means that pressure estimation was not affected significantly by the change in fluid viscosity, at least in the centrifugal pump used in the present study.

Discussion

Of course, the estimation error will be more reduced if identification is carried out only in either interval within which the viscosity does not change. However, this situation is impossible because the viscosity is not always constant. In

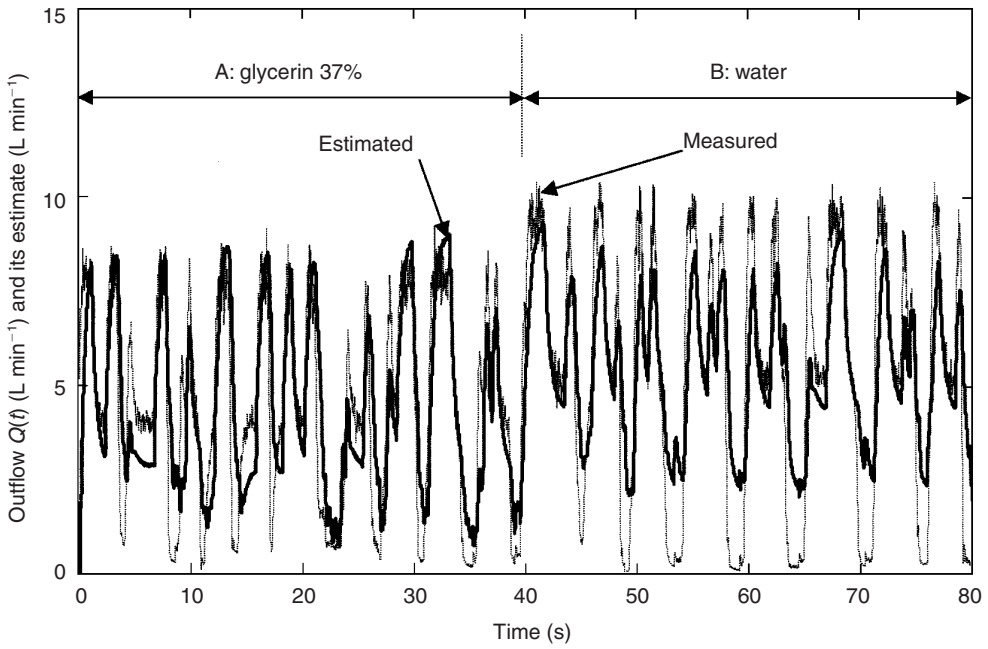

Figure 3. Flow estimation using the combination of ARX models II ($n = 2, m = 10$) and III ($n = 2, m = 2$) whose coefficients were identified during both Intervals A and B. Root mean square error:$\varepsilon = 1.82$ L min^{-1}. Correlation coefficient : $r = 0.801$.

Table 1. Estimation error$_\varepsilon$ and correlation coefficient r

	Flow estimation		Pressure estimation	
	ARX model I	**Combination of ARX models II and III**	**ARX model I**	**Combination of ARX models II and III**
Estimation error$_\varepsilon$	2.38 L min^{-1}	1.82 L min^{-1}	16.8 mmHg	16.6 mmHg
Correlation coefficient r	0.619	0.801	0.826	0.831

general, a recipient to be estimated is different from an animal used for identification; even if identification is carried out in the same recipient, the viscosity must change according to the change in the recipient's hemodynamic state.

Tsukiya *et al.*[1] proposed an indirect measurement method for flow and pressure difference in a magnetically suspended centrifugal pump. To overcome the effect of the change in fluid viscosity, their method needs a calibration procedure. However, it is necessary to clamp an outflow tube of the pump and shut down blood flow in the calibration procedure, which should be avoided because of inducing thrombosis formation. On the other hand, in our method, ARX model III for obtaining the gain constant K can be identified without clamping the outlet tube, always after implantation of the pump. The random clamping of the outlet tube is needed only before implantation.

Wakisaka *et al.*[2] proposed another method of estimating flow and pressure head, which includes a compensation process for the change in viscosity. Because their method utilizes hematocrit value of blood, which needs an off-line measurement procedure, it is difficult to extend their method to a fully automatic estimation system. On the other hand, the gain constant K reflecting fluid viscosity can be identified on the basis of voltage, current and rotational speed. Because these measurements can be derived directly from the motor, the estimation process of our method can be carried out in a fully automatic and on-line fashion.

As shown in Table 1, the estimation accuracy of our method was not high in comparison with other estimation methods. This may be because the test data used in the present experiment were produced under random change in voltage and random outlet clamping in order to ascertain the estimation ability in the transient state. On the other hand, other estimation methods were evaluated only in the steady state or near steady state condition, and thus, our method cannot directly be compared in estimation accuracy with other methods.

Conclusions

The present study has proposed a new method for estimating the pressure head and flow of a centrifugal pump by using voltage, current and rotational speed of the motor for the pump without any additional sensors. The proposed estimator consists of two ARX models. One ARX model has one output (pressure head or flow) and three inputs (supplied power, i.e. product of voltage and current rotational speed, and the gain constant of the system from supplied power to rotational speed). The gain constant is regarded to reflect viscosity of blood and is identified by means of the other ARX model. The proposed method has attained about 20% improvement in estimation accuracy compared with another different ARX model without the gain constant as an input. On the other hand, it has been shown that there was little effect of additional input with respect to the gain constant on the estimation accuracy in the case of pressure estimation.

To improve the estimation accuracy, it can be considered that artificial neural networks[3,4] should in future studies be introduced to the estimator to compensate for the nonlinear part of the residue, which cannot be expressed by linear models such as ARX models.

References

1. Tsukiya T, Akamatsu T, Nishimura K. Flow rate measurement for magnetically suspended centrifugal blood pump. *Jpn J Artif Organs* 1997;26:98–102 (in Japanese).
2. Wakisaka Y, Okuzono Y, Taenaka Y *et al*. Development and evaluation of a flow rate estimation of a centrifugal blood pump for circulatory support. *Jpn J Artif Organs* 1997; 26:103–6 (in Japanese).
3. Kisanuki M, Yoshizawa M, Abe K *et al*. Parameter estimation of cardiovascular dynamics for artificial heart control. *Jpn J Artif Organs* 1995; 24:1099–106 (in Japanese)
4. Yoshizawa M, Kisanuki M, Abe K, Yambe T, Nitta S. Hemodynamic waveform estimation of artificial hearts using artificial neural networks. *Biomed Eng – Application, Basis & Communications* 1996;8:76–85.

Journal of Congestive Heart Failure and Circulatory Support (2001) Vol 1, No 4, 305–308

Development of an implantable centrifugal blood pump

T. Tsukiya[1], Y. Taenaka[1], E. Tatsumi[1], H. Takano[1], T. Sawairi[2], Y. Konishi[2], T. Masuzawa[3] and Y. Okada[3]
[1]Department of Artificial Organs, National Cardiovascular Center, Japan, [2]Nikkiso Co., Ltd.; and [3]Department of Mechanical Engineering, Ibaraki University, Japan

Abstract The National Cardiovascular Center (Nikkiso Co., Ltd.) and Ibaraki University have been collaborating to develop an implantable ventricular assist device that utilizes a centrifugal blood pump. The development of an integral motor has significantly reduced the size of the pump unit. The impeller containing permanent magnets works as the rotor of a brushless DC-motor. The size of the blood pump is 50 × ϕ58 mm, and the weight is 300 g. The impeller geometry was designed to maximize the washing out flow throughout the pump and thus improve antithrombogenicity. The pump has hydraulic characteristics and mechanical hemolysis tests were carried out. The pump can be operated at the standard working point (5 L min^{-1} against a pressure head of 120 mmHg). As a left ventricular assist system (LVAS), it can be operated at a rotational speed of 2500 rpm with the input power of approximately 5 W. The tested performance of the pump seemed to be sufficient as a LVAS.

Keywords left ventricular assist system, centrifugal blood pump.

Introduction

Our research group has been developing an implantable ventricular assist system (VAS) that uses a centrifugal blood pump. This system carries a high potential for an implantable device for the long term. Implantable ventricular assist devices are in great need to provide long-term support for patients with end-stage heart disease, because they cause fewer infections through the skin-penetrating cannulae and enhance the patient's quality of life.

Rotary blood pumps have several advantages over the existing pulsatile devices being used for this purpose. A rotary pump basically has a single moving part, called an impeller, which rotates at a constant speed. These pumps do not occupy a large amount of space. The total size of the whole system including the controller and the internal battery can be quite small from anatomical point of view. Moreover, the power consumption is relatively low due to the continuous rotation in a single direction, as opposed to the alternate one used in some pulsatile devices. This enables pump operation for several hours without a power supply, much longer than for other such devices. The use of such a low energy-consuming structure and the fact that no valves are needed will reduce the cost of the system.

We have been developing a seal-less centrifugal blood pump that utilizes a coupling of permanent magnets[1]. The biocompatibility of the pump system including the magnitude of hemolysis and anticoagulation has been proven acceptable in long-term chronic animal studies using the pump as a left ventricular assist device (LVAD). A period of more than 1-years' survival without pump exchange was achieved in the longest record. Implantation of the pump into the thoracic cavity of a goat was tried in a previous study[2]. The anatomical fitting of the pump was reported to be within an acceptable range, but further miniaturization of the pumping unit was considered necessary for enhanced reliability in clinical use.

This study discusses the development of the implantable centrifugal blood pump, which was improved to significantly reduce the size by aiming to build a versatile VAS system including a LVAS with an internal secondary battery or a biventricular assistance system (BVAS) with two implantable blood pumps. The hydraulic performance and system efficiency were evaluated as well as mechanical damage to blood caused by the pump in an *in vitro* hemolysis test.

Blood pump design

Our former prototype utilized a coupling of permanent magnets. The magnets were embedded in the hub of the impeller, and the counterpart was attached to a commercially available brushless DC-motor. The total length of the core part of the pump was 115 mm and the weight of the pump reached 720 g. We integrated the impeller and the motor so the permanent magnet in the impeller might work as a rotor of a brush-less DC-motor. The total length of the pump was reduced to 50 mm and the weight to 300 g. The priming volume of the pump, however, remained 20 ml. Figure 1 shows the appearance of the newly developed pump compared with our former model. The pump housing including the inlet and the outlet port is made of titanium.

Correspondence to: Tomonori Tsukiya, Department of Artificial Organs, National Cardiovascular Center, Research Institute, 5-7-1 Fujishiro-dai, Suita, Osaka, 565-8565, Japan.

Figure 1. The newly developed centrifugal pump (left) and the former model (right). The length of the core part was decreased from 115 mm to 50 mm. The weight of the pump was 300 g.

The cross-sectional view of the newly developed pump is shown in Figure 2. The impeller contains six polar permanent magnets in the hub, facing against the surrounding stator. The gap size of the passage between the magnets was 0.5 mm. This integral motor significantly contributed to the size reduction of the pump.

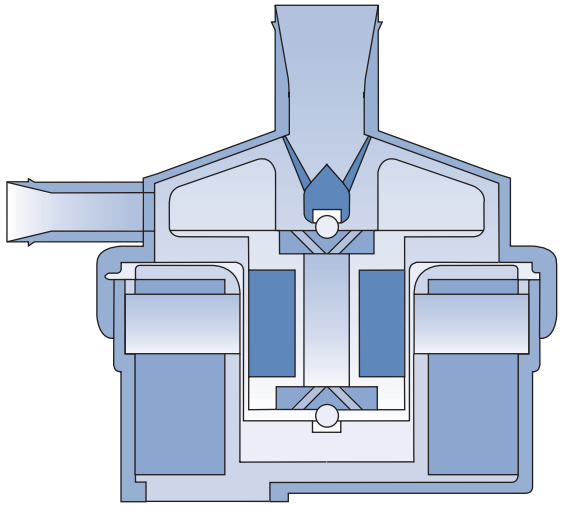

Figure 2. Cross-sectional view of the centrifugal blood pump. The permanent magnets are embedded in the impeller hub to work as a rotor of the integral motor. The impeller is suspended by ball-pivot bearings located at both ends.

Another problem with the former model was the suspension system of the impeller. From a mechanical engineering point of view, the sealing mechanism of the pump is one of the crucial factors that dominate the pump's durability. Some groups have tried to solve this problem by using sophisticated magnetic bearings, which eliminate mechanical contacting parts inside the pump[3,4]. The feasibility of this mechanism has proved effective, especially for antithrombogenicity. It has, however, drawbacks of excessive power consumption and mass for the magnetic bearing. The former model had no sealing part but had a sliding thrust bearing, which worked as a guide to prevent the impeller from shifting toward the inlet port due to the fluid force, which varied with the change of working conditions. The freedoms of motion except for the rotation along the impeller axis were completely uncontrolled. The stability of the impeller was largely dependent on the damping force of the fluid between the impeller and the casing. As use of an integral motor required stronger magnets, we needed to develop a rigid suspension system in order to suspend the impeller against the radial load that was inherently unstable. We employed ball-pivot bearings that comprised an alumina ceramic (Al_2O_3) ball, which is 3 mm in diameter. Female pivots, made of ultra high molecular weight

polyethylene, were embedded at the top of the impeller and in the cap attached to the pump inlet port. The pivot bearing of the same structure was also located at the bottom of the impeller hub.

Obtaining sufficient washing out flow around the bearing part, especially at the bottom of the impeller, is one of the crucial design points that enables better antithrombogenicity. The impeller plate, called the 'shroud', was attached to the blade in order to maximize the pressure difference across the backflow region including the central hole of the impeller. A photograph of the impeller is shown in Figure 3. The straight vanes were employed in order to generate a higher pressure difference at the same rotational speed than by the curved profile of the former model.

Hydraulic performance test

Hydraulic performance was tested in a closed loop at various motor speeds. Flow rate was adjusted by a resistor, and was measured by an electromagnetic flowmeter. Pressure difference through the pump was measured by pressure gauges. Sampling ports for measuring pressure were located 15 cm upstream and downstream of the pump. The input power was calculated from the measured current and voltage of the motor controller. System efficiency was defined as the hydraulic work of the pump divided by the input power. The rotational speed was adjusted from 2000 to 4000 rpm. Figure 4 shows the hydraulic performance of the pump. It could pump out 5 L min^{-1} of water against the pressure head of 120 mmHg at 2500 rpm. It could also generate pressure difference higher than 300 mmHg when operated at 4000 rpm. Figures 5 and 6 show the input power and system efficiency of the pump plotted against the flow rate, respectively. The input

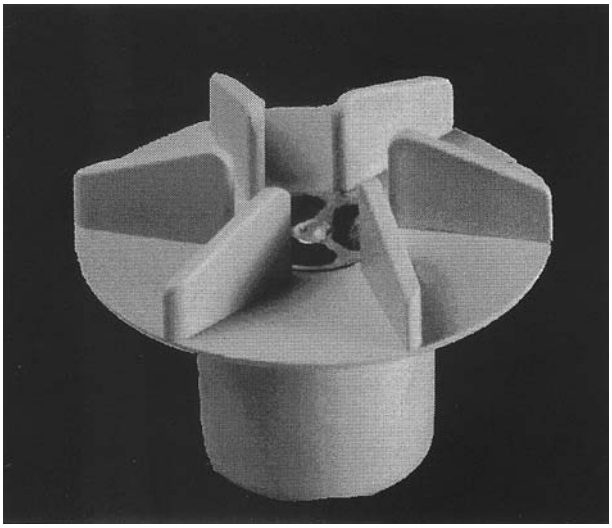

Figure 3. The impeller of the blood pump. The shroud was attached to the impeller to increase wash-out flow at the bottom. Straight vanes were also employed.

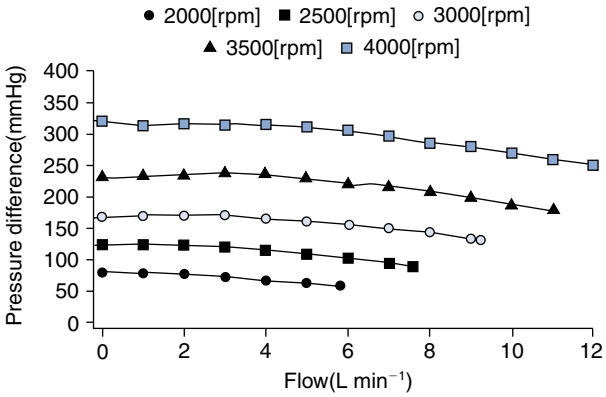

Figure 4. The relationship between pressure difference and flow rate at various rotational speeds. A working condition of 5 L min^{-1} against 120 mmHg required 2500 rpm.

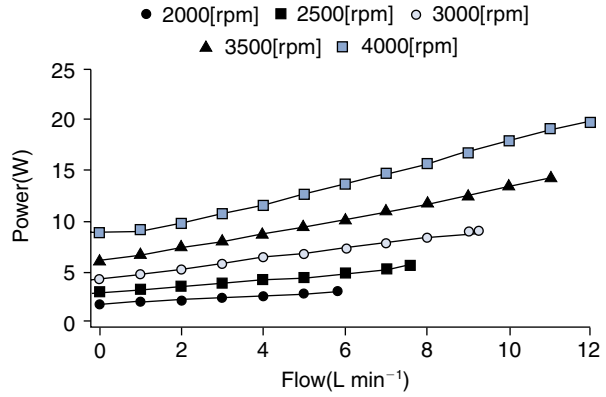

Figure 5. The relationship between input power and flow rate at various rotational speeds. Power of 5 W was required to drive the pump at the working condition of 5 L min^{-1} at 2500 rpm.

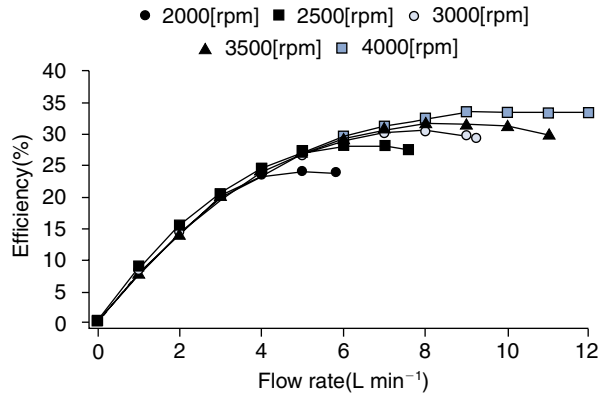

Figure 6. The relationship between efficiency and flow rate.

power at the standard working point mentioned earlier is approximately 5 W, which seemed sufficient for an implanted device in terms of heat generation. A longer period of continuous operation of several hours driven by an implanted secondary battery could be realized by using this pump and implanted secondary battery. The performance of the developed pump was considered to be sufficient as a LVAD.

Hemolysis test

The mechanical damage caused by the blood pump was assessed by *in vitro* hemolysis test using fresh goat blood. The blood was circulated in a closed loop containing a reservoir, an electromagnetic flowmeter, transducers for pressure measuring, and the pump. The pump was operated for 4 h at the working point that flow rate was 5 L min^{-1} and pressure difference was 100 mmHg. The temperature of the circuit was not controlled. Blood was sampled from the measuring port, and then it was centrifuged to separate plasma, of which free hemoglobin concentration was measured. The extent of hemolysis was compared in the form of normalized index of hemolysis (NIH), which was calculated with the following formula:

$$NIH = \Delta FreeHb \times V \times (100–Hct) / (100 \times Q \times T)$$

where V was the blood volume in a circuit, Q was flow rate, T was operation period, Hct was hematocrit, and ΔFreeHb was change in concentration of plasma free hemoglobin. The index of the developed pump was higher than that of the control, BP–80 blood pump. The value itself was within an acceptable range for chronic study, but further design modification to reduce hemolysis was considered necessary (Figure 7).

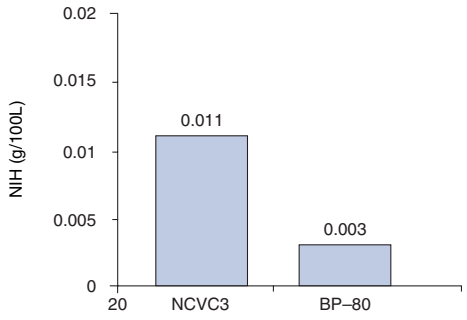

Figure 7. The damage to blood caused by the blood pump in NIH. The hemolysis level was within an acceptable range, though the index was higher than that of BP–80.

Conclusion

The centrifugal blood pump that has achieved considerable size reduction was developed as an implantable LVAD. The tested performance of the pump *in vitro* was considered sufficient for the chronic study, though further design improvement in terms of hemolysis and system efficiency would be necessary to improve reliability. An estimation of the durability of the pump including wear at the pivot bearing and antithrombogenicity is planned through chronic animal experiments in the near future.

Acknowledgement

The authors are grateful to the Japanese Ministry of Health and Welfare for supporting this study with Health Science Research Grants.

References

1. Wakisaka Y, Taenaka Y, Chikanari K *et al.* Long-term evaluation of a nonpulsatile mechanical circulatory support system. *Artif Organs* 1997;21(7):639–44.
2. Wakisaka Y, Taenaka Y, Chikanari K *et al.* Intrathoracic and intraabdominal wall implantation of a centrifugal blood pump for circulatory support. *Artif Organs* 1998;22(6):493–7.
3. Akamatsu T, Nakazeki T, Itoh H. Centrifugal blood pump with a magnetically suspended impeller. *Artif Organs* 1992,16: 305–8.
4. Allaire PE, Kim KC, Maslen EH *et al.* Prototype continuous flow ventricular assist device supported on magnetic bearings.

Session 7
Engineering

Journal of Congestive Heart Failure and Circulatory Support (2001) Vol 1, No 4, 311–315

Flow visualization study to obtain suitable design criteria of a centrifugal blood pump

M. Nishida[1], T. Yamane[1], T. Masuzawa[2], T. Tsukiya[3], Y. Taenaka[3], Y. Tsukamoto[4], K. Ito[4] and Y. Konishi[4].

[1] Mechanical Engineering Laboratory AIST, MITI, Ibaraki, Japan; [2]Ibraki University, Ibaraki, Japan and [3]National Cardivascular Center and [4]Nikkiso Co. Ltd

Abstract Quantitative flow visualization was performed to investigate the cause of hemolysis and thrombogenesis in a centrifugal blood pump and to obtain suitable design criteria. Particular attention was paid to the high shear in the impeller–casing gap on hemolysis, and to the effect of the washout hole geometry in preventing thrombus formation, which may be caused by stagnation. Experiments were conducted with 2.5 times scale-up models based on the Nikkiso HPM-15 with 64 wt% sodium iodide solution as working fluid and 150 μm silicon dioxide particles as tracer. A 7 W Ar-ion laser light sheet and a 4500 frame s^{-1}, 256 × 256 pixel high-speed video camera were used for lighting and photography respectively, and image analysis was made by particle-tracking velocimetry. All driving conditions were set for a flow rate of 5 L min^{-1} and a head of 300 mmHg representing an extracorporeal assist condition.

Results were as follows:

1. In comparing the standard model, the small radial gap model and the small radial gap with relocated outlet, it was found that the small radial gap causes high shear and consequently high hemolysis regardless of outlet flow behavior.
2. In comparing various diameters and radial positions of washout holes, it was found that the optimal washout hole geometry minimizes the flow-stagnant area in the gap behind the impeller.

Both the small and large holes decrease the washout effect because too large a hole causes reversal flow. The best washout was achieved with the standard-hole model.

Keywords flow visualization analysis, centrifugal blood pump, high shear, stagnation, bio-fluid engineering.

Introduction

Flow visualization analysis is one of the best techniques used to optimize the geometry of the blood pump because it can quantify blood flow behavior in detail. Since blood trauma such as hemolysis and thrombogenesis is closely correlated to the unique flow behavior such as high shear and flow stagnation, the pump geometry can be optimized for blood compatibility by evaluating the flow and removing high shear and stagnation. This process will be able to substitute a lot of blood test from the geometry optimization.

There have been a number of simplified studies in the past[1, 2] that have investigated the relationship between hemolysis and high shear, and that between thrombogenesis and stagnation. Shear stress and blood exposure time are the dominant index factors for both hemolysis and thrombogenesis from the fluid mechanical point of view. These factors have been quantified already in some shear stressors with simple geometry, and the index has been established. However, the geometry of artificial hearts is complicated. Certain numbers of flow visualization works and computational fluid dynamics works clarified the geometry effects on the flow behavior in pumps qualitatively; however, the criteria from flow quantification seemed to be unclear.

In this study, in order to eliminate the hemolysis and thrombogenesis of a centrifugal blood pump, we quantified high shear and stagnation in pumps with varying geometry. We focused especially on the effect of a radial gap between the impeller and casing on hemolysis, and of the geometry of the washout hole on stagnation in the gap behind the impeller.

Methods

Figure 1 shows a schematic diagram of the experimental apparatus. We used:

1. a 250% scale model as test pumps.
2. 64 wt% sodium iodide solution as working fluid, which has a refractive index of ~1.5 – the same as that of an acrylic material.
3. 150 μm SiO2 particles as tracer, which has a density the same as the sodium iodide solution[3].

The dimensional analysis was utilized for the experiments using scale models and the working fluid. Since the 250% scale model and the 64 wt% NaI solution that has a kinematic viscosity (1.8 × 10^{-6} m^2 s^{-1} at 20ûC) is 3/5 that of human blood (~3.0 × 10^{-6} m^2 s^{-1} at 37ûC) were used in our experiment, the ratio of the rotational speed and flow

Correspondence to: Masahiro Nishida, Biomimetics Division, Mechanical Engineering Laboratory, AIST, MITI, Namiki 1-2, Tsukuba, Ibaraki, 305-8554 Japan.

rate were set at 0.096 and 1.5, respectively. A 7 W laser Ar-ion light sheet and 256 × 256 pixel × 4500 frame high-speed video camera were used for lighting and photography, and images were analyzed by particle-tracking velocimetry. Particle-tracking velocimetry was performed using two methods. One method is the 4-time particle tracking method[4], which is superior for grasping the straight flow field and the other is the spring method[5], which is superior for grasping the altering flow field.

Figures 2 and 3 show the geometry of the tested pump. We used a Nikkiso HPM-15 as a model. We focused on two regions: the volute (radial gap region between the impeller tip and the casing wall), which is likely to cause the hemolysis; and the gap behind the impeller, which is likely to cause stagnation that may cause the thrombogenesis.

First, we compared three casings (Models 1, 2 and 3 in Figure 2A–C), where Model 1 has a 3 mm radial gap between the impeller and the casing, and Models 2 and 3

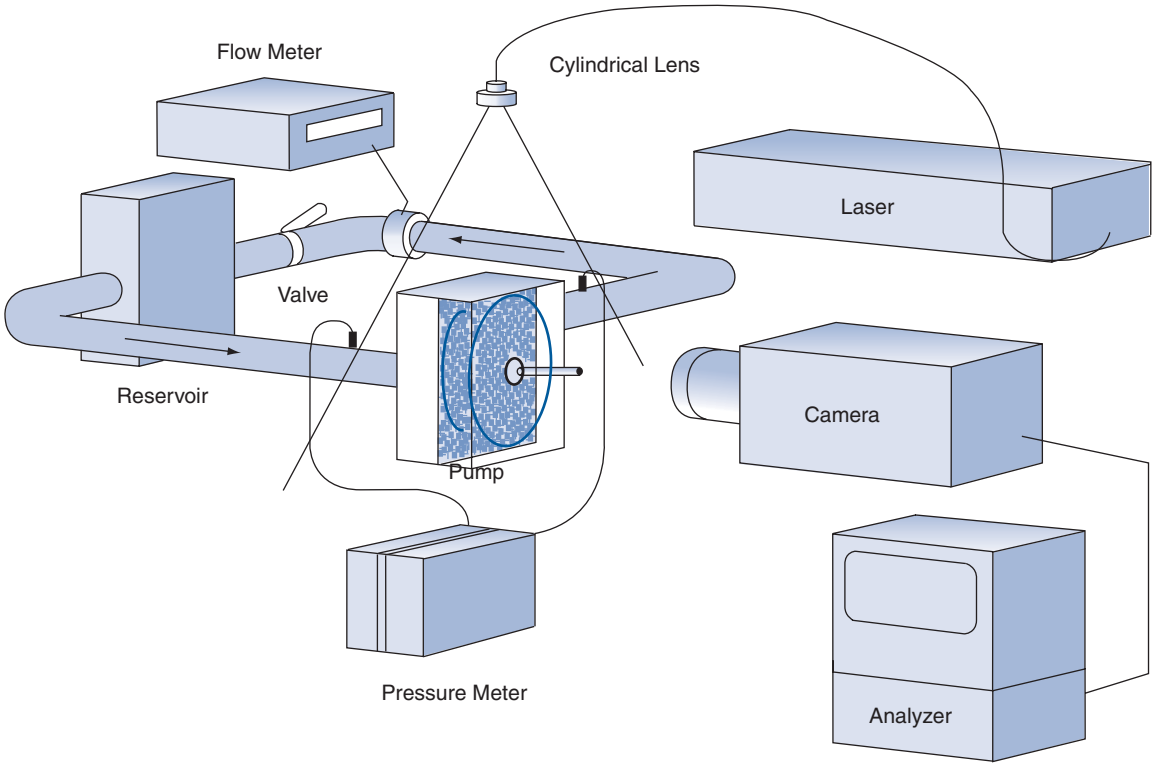

Figure 1. Experimental apparatus.

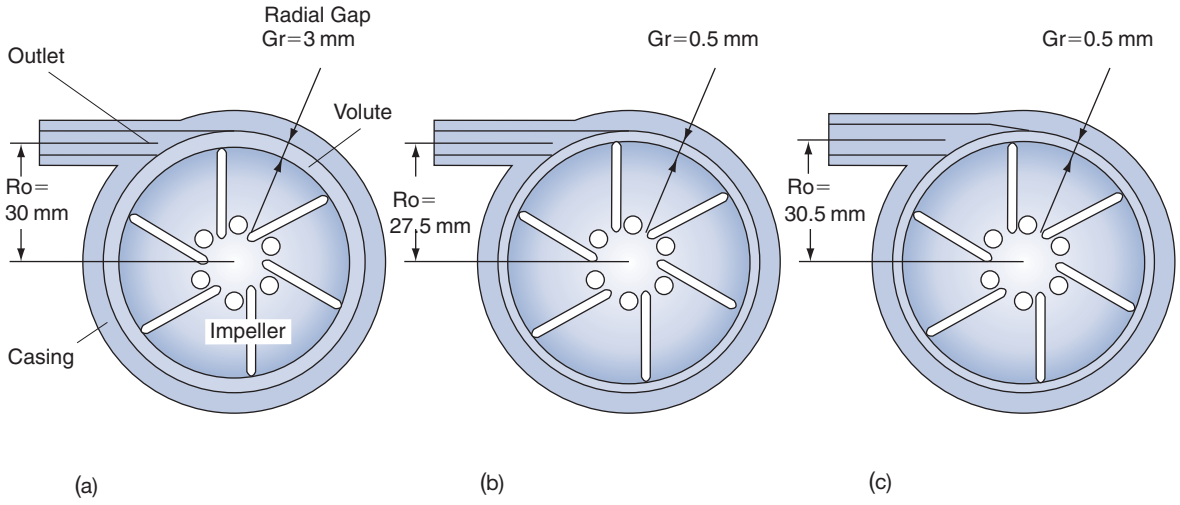

Figure 2. Geometry of various test pumps used to clarify the high shear effect.

have a 0.5 mm radial gap, to investigate the effect of the gap on the shear and hemolysis. Model 3 has a relocated outlet positioned in order to obtain a smooth outlet flow. The high shear region is usually located near the wall, therefore, we visualized the flow near the casing wall with the use of a long-focus microscopic lens. Second, we compared six impellers (Models 4–9 in Figure 3A–F) to investigate the effect of the geometry of washout holes on the flow stagnation behind the impeller. These were found to have the following characteristics:

- Model 4 has holes with a diameter of 3.5 mm and a radial position of 8.5 mm
- Model 5 has no hole
- Model 6 has holes with a diameter of 2 mm
- Model 7 has holes with a diameter of 4.5 mm
- Model 8 has holes with a radial position of 7.5 mm
- Model 9 has holes with a radial position of 12.5 mm.

All experiments were carried out under the conditions of a pressure of 300 mmHg and a flow rate of 5 L min^{-1}. These conditions were decided upon because clear differences of hemolysis were confirmed.

Results

Figure 4 shows the velocity distribution near the volute casing wall: high shear with high velocity graduate was located in quite a narrow area near the wall, whereas the low shear occupied almost all regions in the volute. A region of high shear was located within 0.2 mm of the wall in Model 1, whereas it was located within 0.1 mm of the wall in Models 2 and 3. Maximum shear velocities are 60000 s^{-1} in Model 1 whereas they are 110000 s^{-1} in Models 2 and 3. Therefore, a one-sixth decrease of the radial gap causes almost twice the increase in maximum shear velocity. Hemolysis results corresponded well with these flow results. The hemolysis level in Models 2 and 3 were 1.5 times higher than that in Model 1 as shown in Table 1[6]. Here, there seems to be little effect of the relocated outlet on hemolysis. These flow results also corresponded well with the computational fluid dynamic results[7]. Therefore, it was clearly confirmed that high shears near the casing wall in the pump directly correlate with the hemolysis level.

Table 1. Total evaluation for high shear.

Model	**1**	**2**	**3**
Radial gap (mm)	**3**	**0.5**	**0.5**
Outlet position (mm)	**30**	**27.5**	**30.5**
Impeller rotational Speed (rpm)	3100	3500	3100
Outlet flow	Smooth	Smooth	Separation
Maximum shear stress (Pa) (visualization result)	180	330	300
Maximum shear stress (pa) (CFD result)	215	1158	903
Hemolysis (mg dl^{-1} 4 h^{-1})	20.2	31.5	31.6

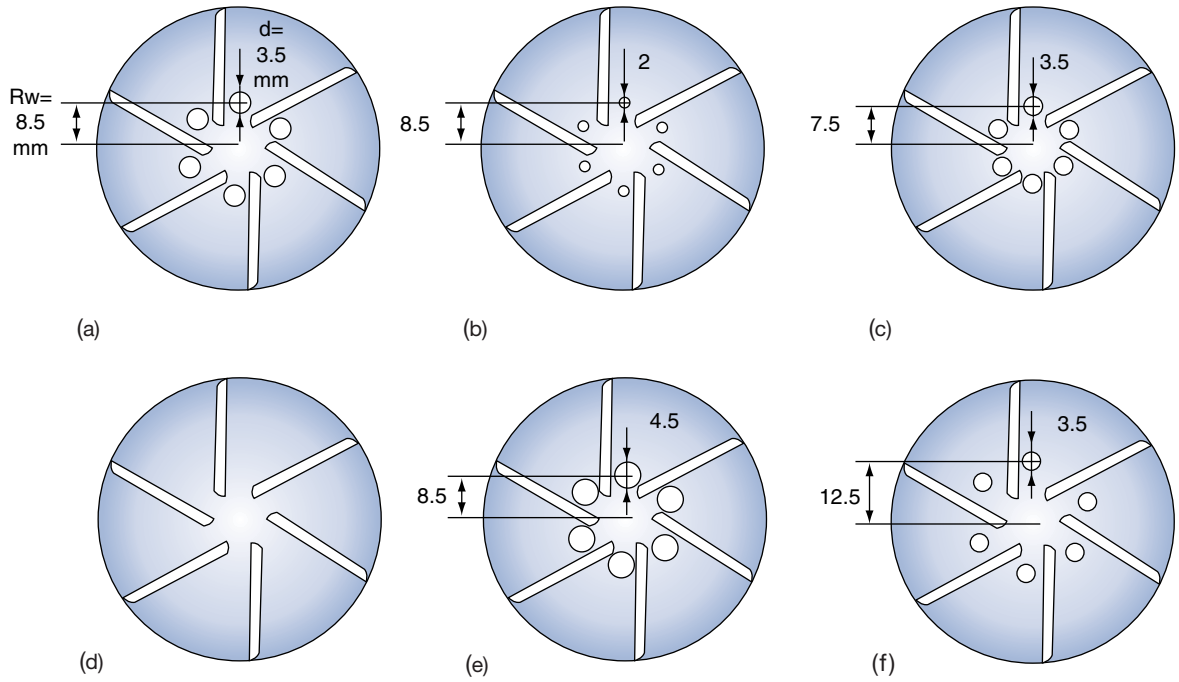

Figure 3. Geometry of various test pumps used to clarify the stagnation effect.

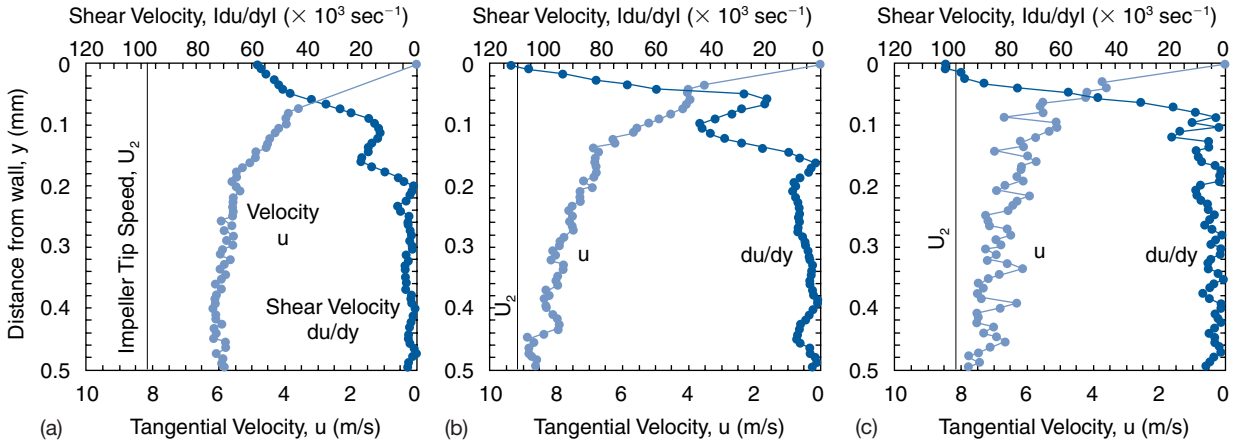

Figure 4. Shear and velocity distribution near the volute wall. (a) Model 1, (b) Model 2 and (c) Model 3.

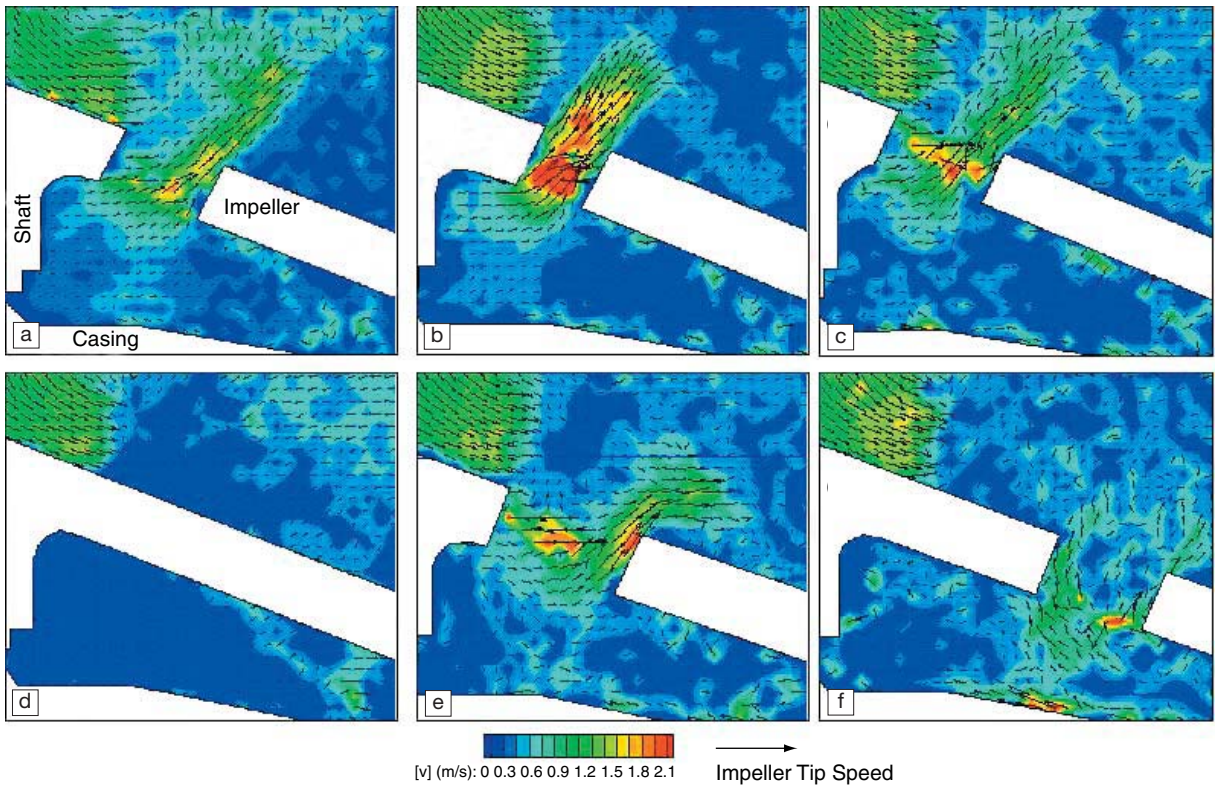

Figure 5. Flow vector map and velocity contour of the secondary flow behind the impeller. (a) Model 4, (b) Model 5, (c) Model 6, (d) Model 7, (e) Model 8 and (f) Model 9.

Figure 5 shows the secondary flow vector map behind the impeller. This flow vector quantifies the radial and axial circulatory flow, which corresponds to the washout effect. We can easily find that the flow through the washout hole causes the secondary flow behind the impeller. In comparison of all models, it was found that Models 4, 6, and 8 had an adequate secondary flow of material that washed around the shaft behind the impeller, whereas in Model 5 the material hardly washed around the shaft at all because there is no washout hole flow. Model 7 had a reverse flow through the washout hole because too large a washout hole decreased the pressure difference between flow of material in and out of the washout hole, and in Model 9, there was little wash of material around the shaft because the hole position was too outward.

Figure 6 shows the flow rate through the washout hole in

pumps with varying washout hole geometry. The flow rate was calculated by an approximate integration of the velocity inside the washout hole[8]. It can be clearly found that the flow rate through the inward-positioned washout hole was faster. The flow rate through the outward-positioned washout hole was slower, and the velocity profile in the washout hole skews inward so that it hardly seemed to be effective for centrifugal force. On the other hand, the flow rate through both the small and large washout holes was almost the same as that through the standard hole. Despite the large hole generally decreasing the flow resistance, Model 7 with its large washout holes caused a large reverse flow in the washout hole, which set off the resistance decrease effect. Therefore, it was found that the hole size does not significantly affect the flow rate through the washout holes; as shown in Table 2, Models 4, 6, and 8 seem to cause good washout effect.

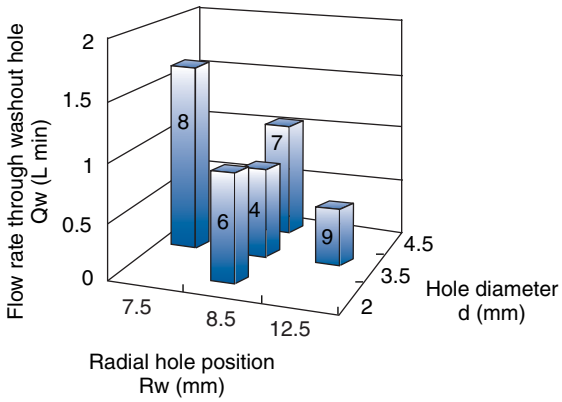

Figure 6. Flow rate through the washout hole in pumps with various washout hole geometry.

Table 1. Pre- and postoperative evaluation of device recipients.

Weeks	Baseline	2	4	8	12	Monthly
Diameter of washout hole (mm)	**3.5**	**0**	**2**	**4.5**	**3.5**	**3.5**
Radial position of washout hole	**8.5**	**–**	**8.5**	**8.5**	**7.5**	**12.5**
Wash around shaft	Good	Bad	Good	Good	Good	Bad
Hole flow (l min^{-1})	0.8	–	0.9	1.0	1.6	0.5
Reverse washout hole flow	No	–	No	Yes	No	Yes
Total evaluation	Good	Bad	Good	Bad	Good	Bad

Conclusion

1. Hemolysis closely correlates with high shear generated near the casing wall, and the gap reduction between the impeller and casing increases the maximum shear velocity near the wall, which causes a high rate of hemolysis.
2. A high shear layer is located within a layer about 0.1 mm of the casing wall.
3. Washout holes cause the secondary flow behind the impeller that eliminates stagnation behind the impeller.
4. Too large a hole and an outward-positioned hole barely improves the wash of material around the shaft.

References

1. Hellums JD, Brown CH. Blood cell damage by mechanical forces, In: Hwang NHC, Normann NA, editors. *Cardiovascular Flow Dynamics and Measurements*. Baltimore: University Park Press, 1977:800–23.
2. Hanson SR. Device thrombosis and thromboembolism. *Cardiovasc Pathol* 1993;2:157S–65S.
3. Nishida M, Yamane T, Orita T *et al.* Quantitative visualization of flow through a centrifugal blood pump: Effect of washout holes. *Artif Organs* 1997;21:132–8.
4. Kobayashi T, Saga T, Haeno T, Tsuda N. Development of a real-time velocity measurement system for high Reynolds fluid flow using a digital image processing design. *Experimental and Numerical Flow Visualization ASME* 1991; FED 128:9–14.
5. Okamoto K, Hassan YA, Schmidl WD. New tracking algorithm for particle image velocimetry. *Experiments in Fluids* 1995;19:342–7.
6. Masuzawa T, Tsukiya T, Endo S *et al*. Development of design methods for a centrifugal blood pump with a fluid dynamic approach: Results of hemolysis tests. *Artif Organs* 1999;23:757–61.
7. Miyazoe Y, Sawairi T, Ito K *et al*. CFD analyses to establish design process of centrifugal blood pump–second report. *Artif Organs* 1999;23:762–8.
8. Nishida M, Yamane T, Asztalos B. Washout hole flow measurement for the development of a centrifugal blood pump. *Artif Organs* 1998;22:386–92.
9. Nishida M, Asztalos B, Yamane T *et al*. Flow visualization study to improve hemocompatibility of a centrifugal blood pump. *Artif Organs*. 1999;23:697–703.

Journal of Congestive Heart Failure and Circulatory Support (2001) Vol 1, No 4, 317–320

Durability enhancement of monopivot magnetic suspension blood pump

T. Yamane PhD[1], O. Maruyama PhD[1], K. Mizuhara PhD[1], M. Nishida PhD[1], K. Nonaka[1] and T. Tateishi PhD[2]

[1]Department of Material Science & Bioengineering, Mechanical Engineering Laboratory, MITI; and [2]National Institute for Advanced Interdisciplinary Research, MITI, Tsukuba, Japan

Background A monopivot magnetic suspension blood pump is an energy-saving centrifugal pump that uses a passive magnetic bearing, is small in size and uses a direct drive mechanism. It is important for the system to enhance the durability of the pivot for the implantable artificial heart.

Methods A suitable combination of pivot materials was selected through rotational wear tests. Subsequently, a durability test for a new pump system using the pivot was conducted and pivot wear was measured with a high-speed video camera.

Results It was found that the combination of ceramics/ultra high molecular weight polyethylene (UHMWPE) can reduce the wear in saline solution significantly compared to the combination of ceramics/ceramics. Furthermore, the diameter of the pivot ball seems to be optimum at 3 mm to keep wear to a minimum. A 3-month pump durability test was then safely completed.

Discussion The lifetime of material can be extended by magnetic and geometric design improvements. Hemolysis tests with animal blood verified that the monopivot pump showed a sufficiently low level of hemolysis.

Keywords monopivot, pivot bearing, centrifugal pump, durability test, rotational wear test.

Background

The Mechanical Engineering Laboratory is developing a monopivot magnetic suspension blood pump for an implantable artificial heart[1] (Figure 1), with its impeller supported by a single pivot bearing and a magnetic bearing with permanent magnets. Its features include its high efficiency and simplicity of the system components. The size of 160 mL volume, is smaller than a fist and the hemolytic property is lower than a commercial centrifugal pump. However in order to satisfy a durability requirement for long-term use, pivot wear should be suppressed below an allowable level[2], which might be related to the capacity of macrophage that eats the wear particles in the biological body. The pivot in our system should sustain a rotation speed of 1900 rpm and an axial load of 1.2 kg for more than 1 year. Therefore, rotational wear tests have been conducted to select a suitable material combination for the pivot; subsequently, a durability test with a new pump has been conducted to evaluate the pivot wear with a high-speed video camera.

Methods

Pivot wear evaluation

The pivot was modeled as a ball and plate for simplicity, though the plate actually has a small dimple. The ball was attached to a rotating shaft through a Teflon socket and a cubic plate was put into a square pit. The rotational wear test machine (FALEX–6, Falex Corporation, Aurora, IL, USA) was used. The ball and the plate were dipped in saline solution of which the temperature was kept at 37°C (Figure 2). Saline solution was used to ensure reproducibility of the test results. To prevent splash, a cover plate and several fins were provided in the vessel. Specimens, dipped in saline solution were dried in vacuum for 30 min and were left to air dry for 20 min to achieve a reproducible moisture distribution in the material and on the surface. The weights of a plate and a ball socket were then measured using a precise balance (M3, Mettler, Greitensee, Switzerland), of which the accuracy was ±1μg. Each rotational wear test was conducted for 16 h at a rotational speed of 2000 rpm and with an axial load of 1 or 2 kg. After the experiment, the dry weights of each component were measured again and the weight losses were evaluated.

Pump durability and fundamental hemolytic property

Using one of the best combinations for pivot material, a new pump system, DD3, was composed. The test circuit was filled with 33% glycerol solution, of which the viscosity at around 20°C is similar to human blood. The room temperature was kept between 22 and 24°C during this period. The pivot wear was evaluated by measuring the impeller/casing gap around the pivot with a high-speed video camera (Fastcam Ultima-UV, Photron, Tokyo, Japan). Moreover, to ensure that the fundamental hemolytic property did not

Correspondence to: Takashi Yamane PhD, Department of Material Science & Bioengineering, Mechanical Engineering Laboratory, Namiki 1–2, Tsukuba, Ibaraki 305–8564, Japan.

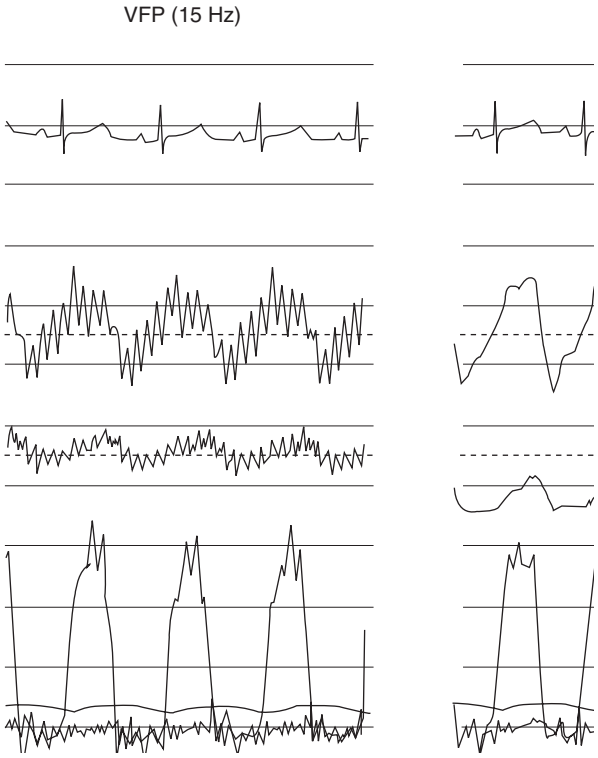

Figure 1. Monopivot magnetic suspension blood pump (DD3).

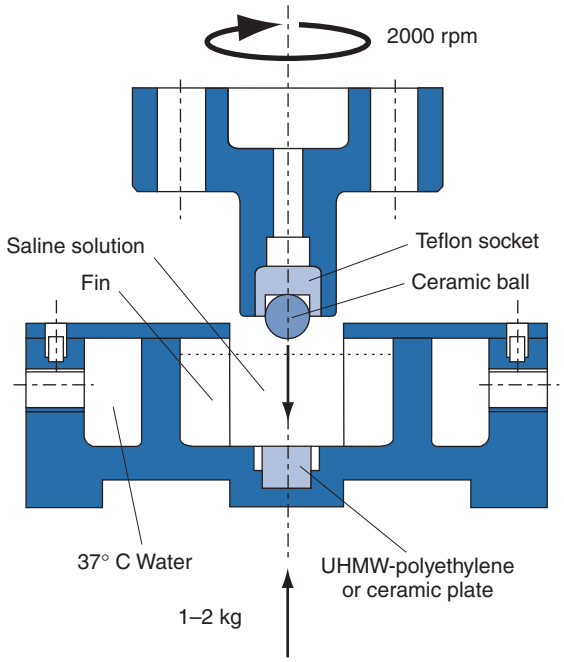

Figure 2. Test module of rotational wear test apparatus.

deteriorate in the new pump, a hemolysis test was conducted in comparison with a commercial centrifugal pump (BP–80, Medtronic BioMedicus, Eden Prairie, MN, USA) using bovine blood in which heparin was added.

Results and discussion

Pivot wear test

A number of ceramics types (Si_3N_4, SiC, Al_2O_3 and ZrO_2; diameters: 1/16 in = 1.59 mm, 1/8 in = 3.18 mm, 5/32 in = 3.97 mm) were used for pivot balls and two materials (Si_3N_4 and UHMWPE size 6 × 6 × 4.9 mm), for pivot plates (Table 1).

First, wear over time was checked by stopping the apparatus at sampling times. It was found that the amount of wear increased linearly with respect to time (Figure 3).

Eight kinds of material combinations were tested using balls of 3.97 mm in diameter. It was found that the application of a UHMWPE plate can reduce the total wear amount by 70–90% compared to a Si_3N_4 plate against different ceramic balls (Figure 4). Secondly, the diameter of the pivot ball and the axial load were varied and the minimum wear was obtained at a ball diameter of 3 mm in the case of Si_3N_4/UHMWPE. However, the effect of the axial load was not so clear in the range of 1–2 kg (Figure 5). These results are similar to those in the case of artificial hip joints. While observing the surfaces of the ball and plate with a video microscope, coaxial scratch marks were found for a combination of Al_2O_3/Si_3N_4, though the surface of a ball is so smooth for a combination of Al_2O_3/UHMWPE (Figure 6). During an examination of the maximum Hertz pressure on a 3 mm Al_2O_3 ball at 1 kg axial load, a large difference (1890 MPa for an Si_3N_4 plate and 45 MPa for an UHMWPE plate) was estimated. When the latter set of pivot was applied to a new centrifugal blood pump with a 0.6 mm impeller/casing gap, the durability was estimated to be several months if the pivot geometry is not changed.

Pump durability and hemolysis tests

A durability test of a new pump model, DD3, was conducted for 3 months with a 3 mm Al_2O_3 ball and UHMWPE plate. The size of the impeller/casing back gap changed

Table 1. Characteristics of pivot materials

Material	Al_2O_3	SiC	Si_3N_4	$ZrO_2(Y_2O_3)$	UHMWPE*
Density (g cm^{-3})	3.8	3.13	3.2	6.05	0.93
Young's modulus (GPa)	363	402	314	205	0.588
Poisson's ratio	0.23	0.14	0.26	0.31	
Hardness, Hv (GPa)	18	25	18	12	

* Molecular weight: 6×10^6.

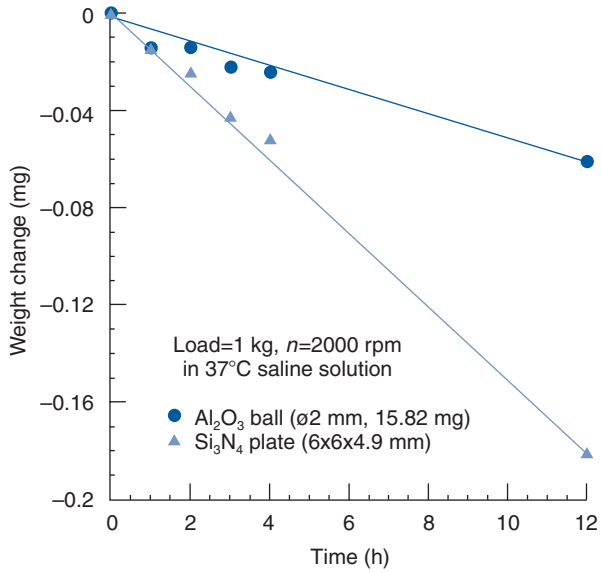

Figure 3. Pivot wear over time.

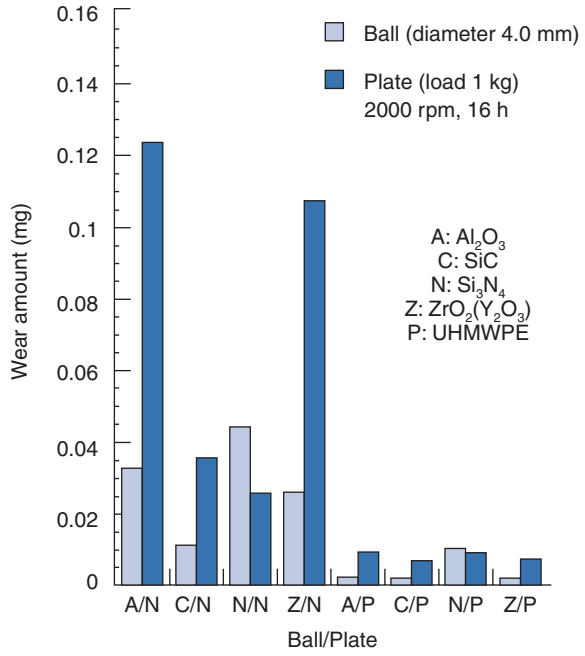

Figure 4. Wear amounts for different combinations of materials.

from 0.8 mm to 0.5 mm over 3 months (Figure 7). No change in gap size for the first 3 weeks was caused by the climbing of a pivot ball along a dimple on UHMWPE plate due to a hydrodynamic side force or by some hydrodynamic lubrication effect. The gap size seems to change along a hyperbolic curve with respect to time, since the wear degree of linearly decreases as was suggested by rotational wear tests. The test was completed without any problem.

A lower level of hemolysis was found for DD3 than for a commercial centrifugal pump (Table 2). Therefore, the fundamental hemolytic property has been verifiied for the new model.

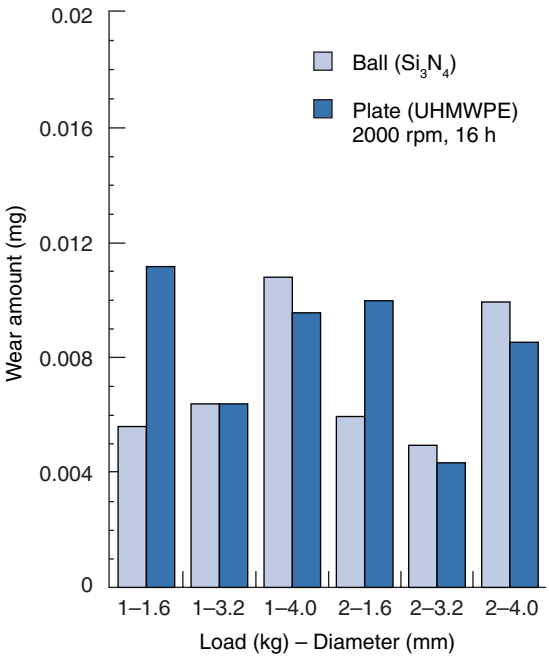

Figure 5. Wear amounts for different ball diameters and axial loads.

Table 2. Hemolytic property of DD3
(TMB: 3,3′,5,5′-tetramethylbenzidine)

Conditions	
Hematocrit & blood	30% bovine blood
Blood volume & temperature	0.5 L, 21°C
Flow & pressure	5 L min^{-1}, 100 mmHg
Evaluation method	TMB method
Increase of plasma-free haemoglobin and NIH:	
Control	−3.6 mg dL 4 h^{-1}
BP-80	6.9 mg dL 4 h^{-1}, NIH = 0.0020
DD3	2.2 mg dL 4 h^{-1}, NIH = 0.0006

Conclusions

Rotational wear tests have been conducted to find a suitable material combination and pivot size for long-term use of centrifugal blood pumps. It was found that the combination of UHMWPE plate/ceramic ball can reduce the amount of wear significantly in saline solution compared to the combination of ceramic plate/ceramic ball, and that the minimum wear can be obtained at a ball diameter of 3 mm. A new pump system, DD3, was composed with the best pivot combination and this test has been completed without any problem. Moreover, a hemolysis test has verified that the fundamental hemolytic property has not deteriorated in this new pump.

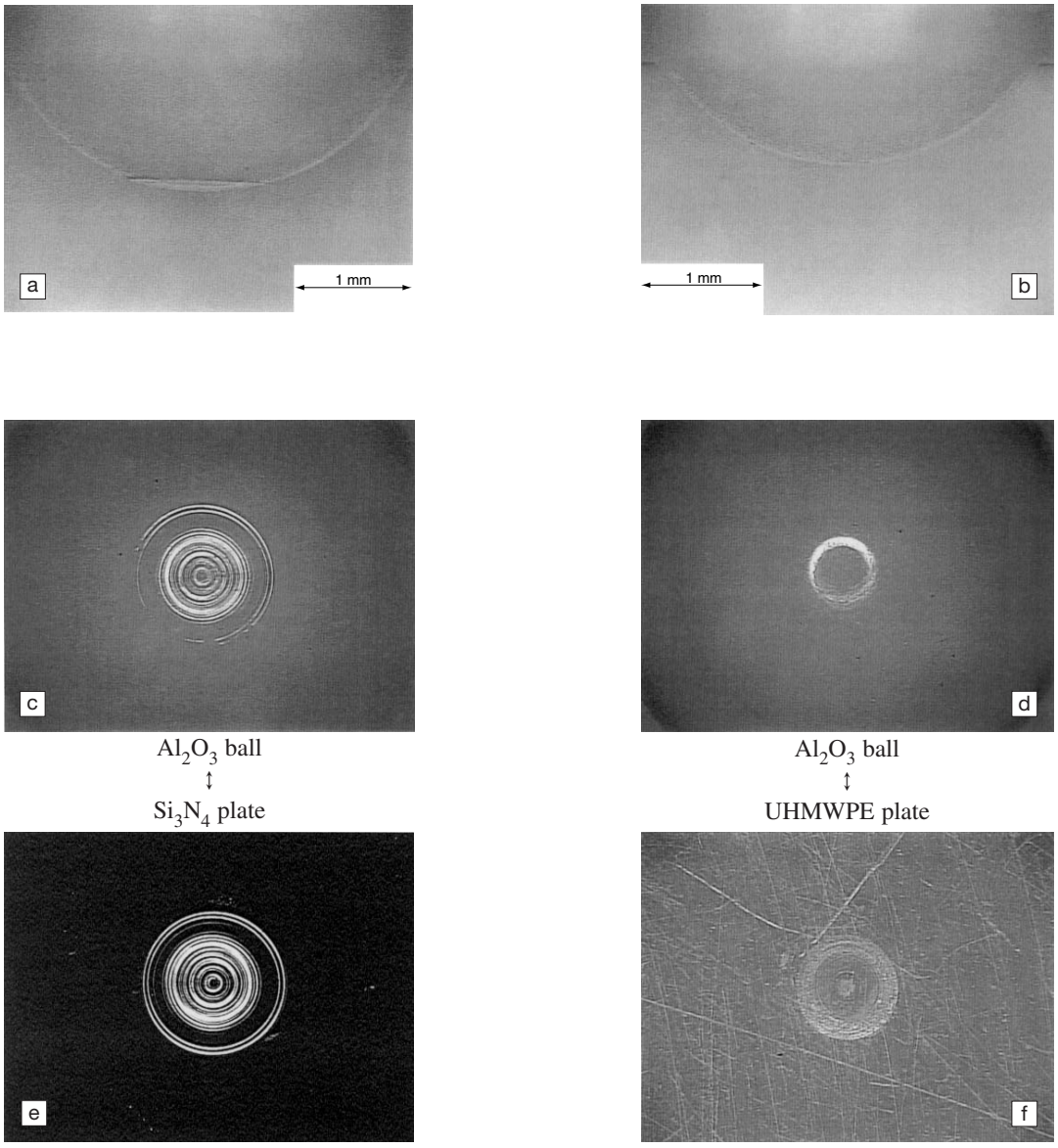

Figure 6. Micrograph of wear scars on pivots.

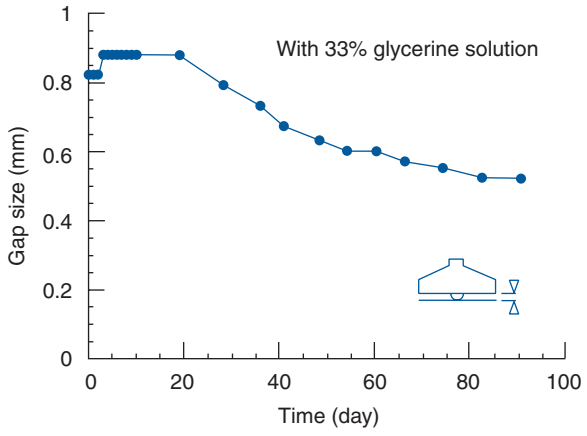

Figure 7. Pivot wear in pump durability test of DD3 for 3 months.

Acknowledgements

The authors express thanks to Koyo Seiko Co., Ltd. and Kyocera Corporation for offering the materials for this study.

References

1. Yamane T, Nishida M, Kijima T, Maekawa J. New mechanism to reduce the size of the Monopivot Magnetic Suspension Blood Pump: Direct drive mechanism. *Artif Organs* 1997;21:620–4.
2. Makinouchi K, Nakazawa T, Takami Y, Takatani S, Nosé Y. Evaluation of the wear of the pivot bearing in the Gyro C1E3 pump. *Artif Organs* 1996;20:523–8.

Journal of Congestive Heart Failure and Circulatory Support (2001) Vol 1, No 4, 321–325

Miniature undulation pump for the study of renal circulation

I. Saito PhD[1], Y. Abe MD PhD[2], T. Chinzei MD PhD[3], T. Ono BE[2], T. Isoyama MD PhD[3], S. Mochizuki MD PhD[3], K. Iwasaki MS[4], A. Kouno[2], T. Karita MD[2], M. Ishimaru MD[2], A. Baba MD[2] and K. Imachi MD PhD[1]

[1]Courses of Information and Communication Engineering, Graduate School of Engineering; [2]Department of Biomedical Engineering, Graduate School of Medicine; [3]Artificial Biomechanism, Research Center for Advanced Science and Technology, The University of Tokyo, Japan; and [4]Department of Mechanical Engineering, Waseda University, Tokyo, Japan

Background In order to investigate the concept of the distributed artificial heart (D-AH), the undulation pump with one-half scale model was designed for use as a renal artificial heart.

Method This pump can generate arbitrary flow pattern: continuous flow, pulsatile on continuous flow and complete pulsatile flow. The outer diameter, thickness and priming volume of the pump were 38 mm, 11 mm and 3.2 mL, respectively. The total size and weight of the constructed miniature undulation pump with motor was 38 mm in diameter, 32 mm in length and 67.5 g, respectively. The maximum output was 5 L min^{-1} against 100 mmHg of pressure load in a mock circulation loop, using water as a fluid at 3600 rpm of the motor speed. We performed animal experiments with goats. The pump was connected between the left atrium and the left renal artery.

Results It was confirmed that the pump performed well enough as a renal artificial heart and could generate an arbitrary flow pattern and a blood flow rate greater than control flow.

Discussion The miniature undulation pump is suitable for studying the renal circulatory physiology. The most difficult task in the animal experiment was connecting the pump output cannula to the renal artery. We are planning to develop a new cannula and to perform a chronic animal experiment on kidney perfusion in the goat.

Keywords undulation pump, miniature pump, renal artificial heart, distributed artificial heart (D-AH), flow pattern.

Introduction

Imachi *et al.* proposed a new concept of 'distributed artificial heart (D-AH)' in 1993 as a next generation artificial heart[1]. Figure 1 shows the concept of the D-AH. The D-AH is composed of a right heart and many small pumps that are distributed to tissues and organs. The D-AH has the following advantages:

1. It can control the blood flow rate of tissues and organs.
2. It is useful to investigate the circulatory physiology of organs.
3. It can treat some specific diseases of organs such as ischemia.

As the first step of investigation of the D-AH, we tried to develop a renal artificial heart and performed acute animal experiments with goats.

Materials and methods

The undulation pump is composed of a pump housing, inlet and outlet ports, a separator, a disc, a pair of seal membranes and an undulation shaft. The housing is the shape of a thin, hollow cylinder. The inlet and outlet ports are located on the circumference of the housing at an angle of 50°. The separator is located in the housing between the inlet and outlet ports. The disc is the shape of a ring with a slit corresponding to the separator and it is located in the center of housing. The seal membrane between the housing and disc seals the pump room. The undulation shaft is located in the center of the pump housing and disc; it converts the rotary motion of the motor to the wavy motion of the disc.

Figure 2 shows the pumping mechanism of the undulation pump. The disc does not rotate, but undulates. During the disc undulation, the closed line between the disc and housing (indicated by a pale blue line in Figure 2) moves from the inlet to the outlet. The closed line pushes the blood to the outlet and at the same time sucks the blood from the inlet. As this pumping action occurs in both sides of the disc with an 180° phase delay, continuous flow is generated when the motor's revolutional speed is constant. The undulation pump can generate arbitrary flow patterns and complete pulsatile, pulsatile on continuous and continuous flow by controlling the current waveform of the motor.

Correspondence to Itsuro Saito, Artificial Biomechanism, Research Center for Advanced Science and Technology, The University of Tokyo 4-6-1 Komaba, Meguro-ku, Tokyo 153–8904, Japan.

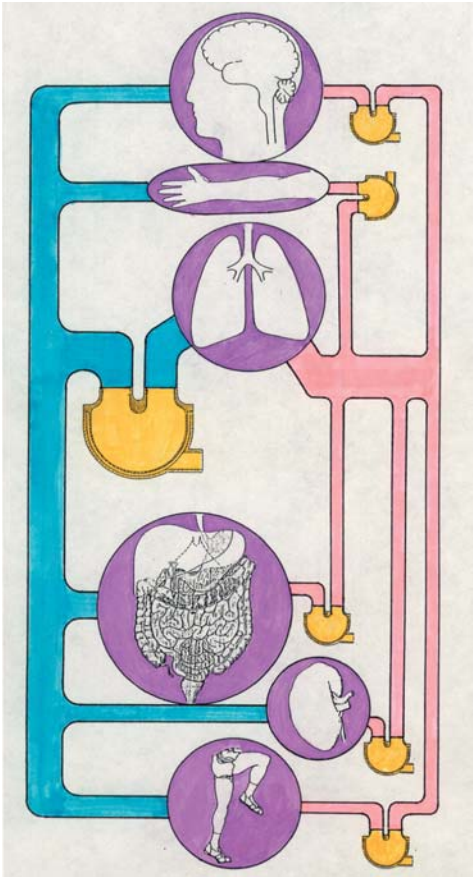

Figure 1. Concept of the distributed artificial heart.

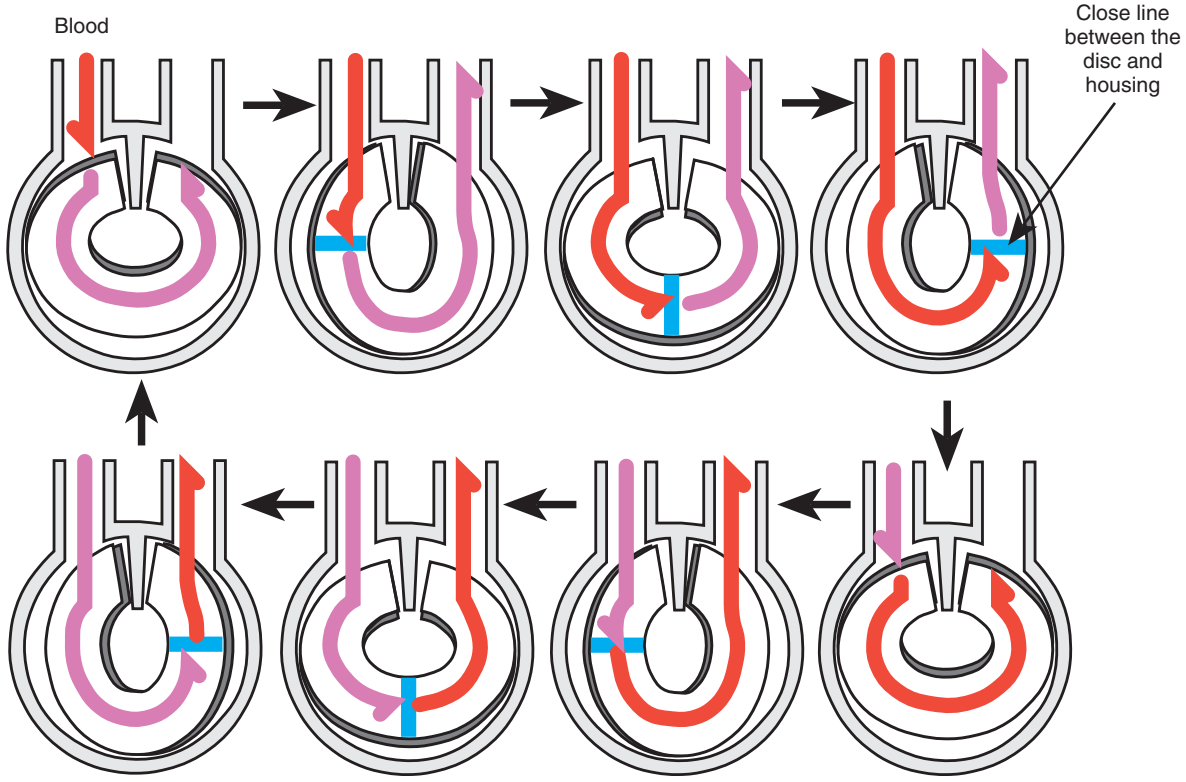

Figure 2. Pumping mechanism of the undulation pump.

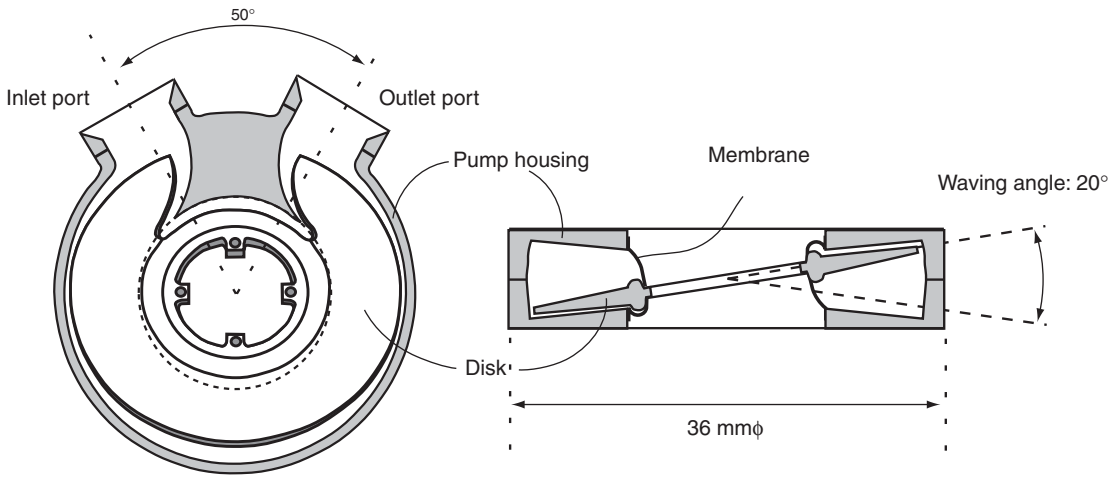

Figure 3. Design of the miniature undulation pump.

The miniature undulation pump is half the size of the original undulation pump used in the total artificial heart[2,3]. Figure 3 shows the design of the miniature undulation pump. The disc and pump housing were made from urethane resin and the membrane was made from polyurethane (Cardiomat 610, Nihon Zeon Co. Ltd., Tokyo, Japan). The inner surface of the pump room was wholly coated with segmented polyurethane (K-III, Nihon Zeon). The diameter and waving angle of the disc are 33 mm and 20°, respectively. The clearance of the closed line between housing and disc is 0.4 mm. The outer diameter, thickness and priming volume of the pump are 38 mm, 11 mm and 3.2 mL, respectively.

Acute animal experiments using goats were performed. Figure 4 shows the result of surgical implantation of the renal artificial heart in a goat. The miniature undulation pump (UPmini) is connected between the left atrial and left renal arteries using cannulae. The pump output is measured with an electromagnetic flow probe (Nihon Koden, Tokyo, Japan) mounted at the outlet port of the pump. The pump outlet and inlet pressures are measured with pressure transducers (Nihon Koden). The right renal artery blood flow is measured with an electromagnetic flow probe (Nihon Koden) attached to the right renal artery. The urine output per minute is measured. The measuring procedure is as follows:

1. Set the pump output and flow pattern.
2. Leave the pump for 5 min to stabilize.
3. Gather the urine output for 1 min and measure the pump output and pump outlet and inlet pressure.

The measuring pump output and flow pattern is a combination of low, normal and high pump output compared with control flow and complete pulsatile, pulsatile on continuous and continuous flow.

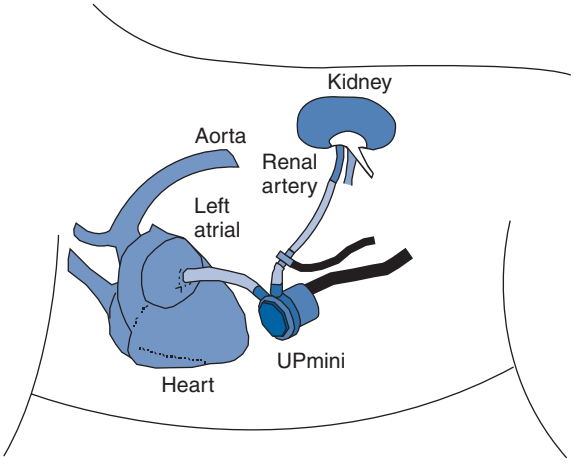

Figure 4. Schematic drawing of surgical outcome of the renal artificial heart implantation in a goat. UPmini: miniature undulation pump.

Results

Figure 5 shows the assembled the UPmini. A miniature brush-less DC-motor (Inland Motor, Radford, VA, USA) was used, with the stator molded with epoxy resin. The total size of the assembled miniature undulation pump with motor is 38 mm in diameter and 32 mm long. The total weight is 67.5 g and the total volume is 27.5 mL.

The revolutional speed of the motor is controlled with pulse width modulation (PWM) by using a motor controller, therefore the pump output can be controlled by the PWM output of the motor controller. Figure 6 shows the performance of the UPmini in a mock circulation loop with water as the test fluid. The maximum output was 5 L min^{-1} against 100 mmHg pressure load at the motor speed of 3600 rpm.

Figure 7 is a photograph of the animal experiment. Figure 8 shows the pump flow rate (QLK), pump outlet pressure (POP) and pump inlet pressure (PIP) of complete pulsatile, pulsatile on continuous and continuous flow. The

Figure 5. Assembled UPmini.

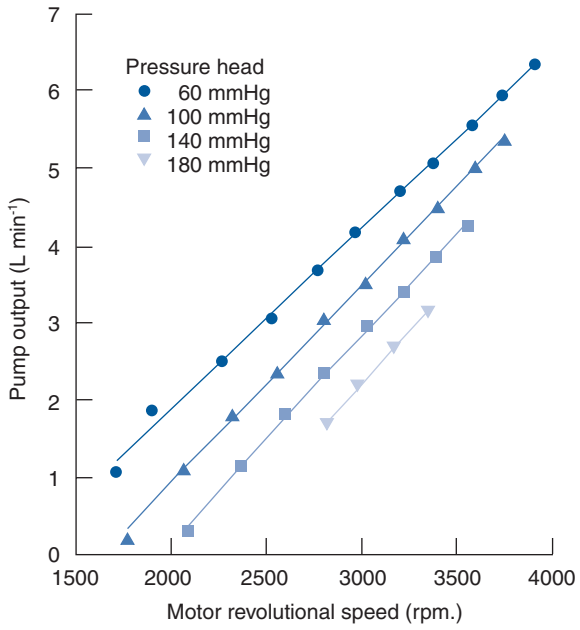

Figure 6. UPmini performance in a mock circulation loop with water as test fluid.

control renal blood flow in this experiment was 0.2 L min^{-1}. Figure 9 shows the urine output data per hour by changing the pump output and flow pattern in another animal experiment. The control renal blood flow in this experiment is 0.1 L min^{-1}.

Discussion

Physiologists and artificial heart (AH) researchers have been interested in the kinds of flow patterns that influence organ functions. However until now, there have been no

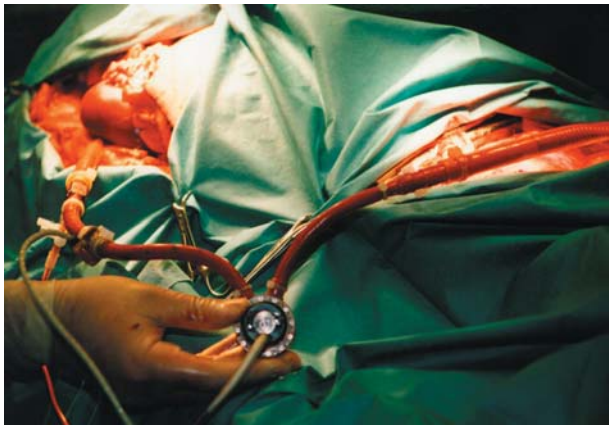

Figure 7. Photograph of the animal experiment.

effective methods of generating various kinds of flow patterns. It was reported that an extraordinarily high pulse rate spoils the microcirculation[4]. As the undulation pump can generate various kinds of blood flow patterns including complete pulsatile, pulsatile on continuous and continuous flow, it would be a useful tool in the investigation of the circulatory physiology of many organs.

The UPmini developed in this study performed well enough for a renal artificial heart. It was confirmed in acute animal experiments that the UPmini could generate arbitrary pump output flow patterns. In this study, urine output was increased in proportion to the pump output. Although the urine output did not change in various flow patterns, it can be assumed that a longer period of observation in chronic animal experiments is required. These results indicate that the UPmini is suitable for studying the renal circulation physiology.

The most difficult task in the animal experiment is connecting the pump output cannula to the renal artery. Although the kidney requires a substantial blood flow, the renal artery is thin; therefore, the optimum cannula design is required. It is difficult to set the kidney in a natural position using a long cannula, because the kidney is located near the backbone; this causes blood flow obstruction of the renal artery and vein. The pump output pressure is higher than normal aortic pressure in this experiment, because a thin, long cannula is used. We are planning to develop a new cannula in the shape of a 'J' which can set the Kidney in a natural position without blood flow obstruction.

Blood compatibility, durability, efficiency, heat generation in the motor, control etc. are the next important problems to be solved. We are planning an animal experiment into chronic kidney perfusion using this pump system on the goat.

Acknowledgement

This study was supported in part by a Grant for 'Research for the Future Program No.97I00401' from the Japan Society for the Promotion of Science.

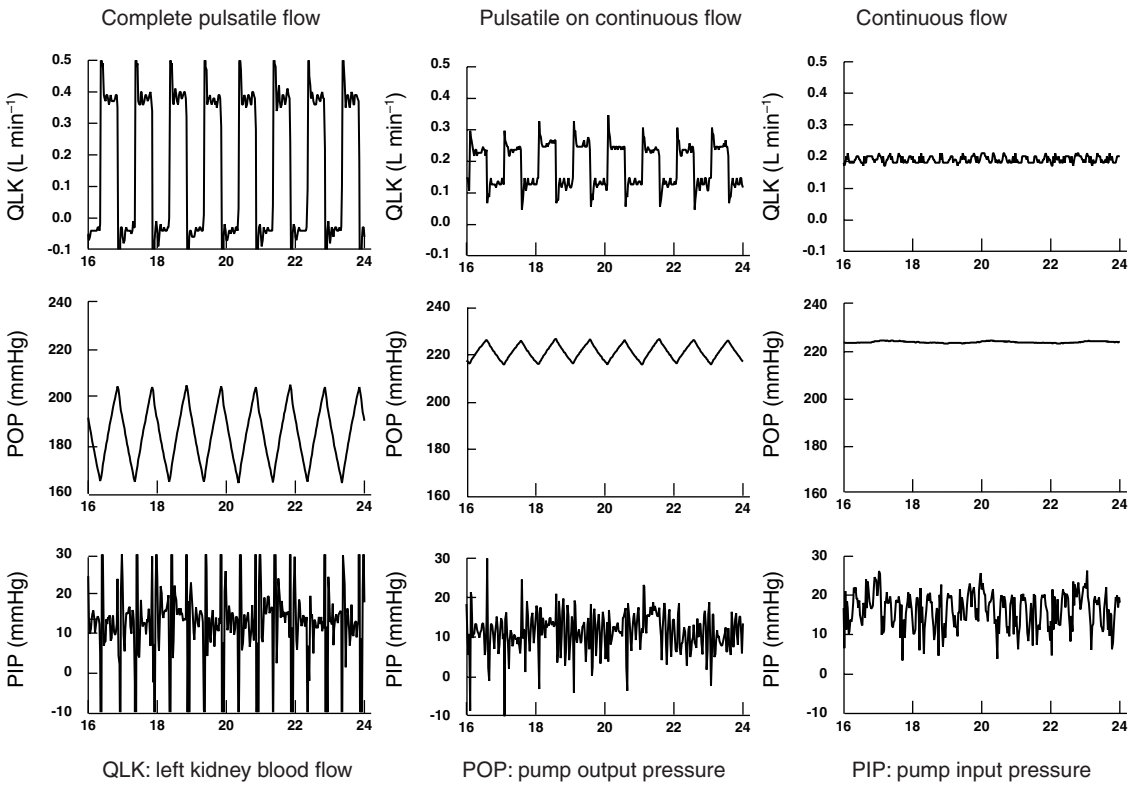

Figure 8. Pump flow rate, and pump outlet and inlet pressures in an animal experiment.

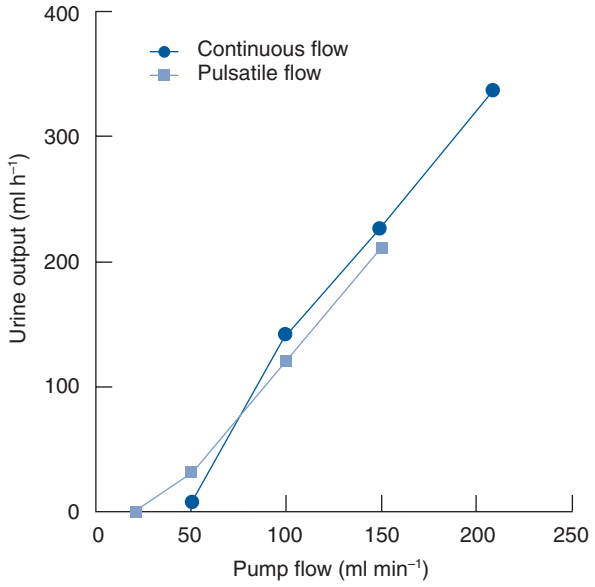

Figure 9. Urine output per an hour by changing pump output and flow pattern in an animal experiment.

References

1. Imachi K, Chinzei T, Abe Y *et al.* The distributed artificial heart: An artificial heart in the next generation. *ASAIO Abst* 1993;10.
2. Abe Y, Chinzei T, Isoyama T *et al.* Development of the undulation pump total artificial heart. *Artif Organs* 1997;21(7):665–9.
3. Abe Y, Chinzei T, Ono T *et al.* Implantation of the undulation pump total artificial heart in the goat. *Artif Organs* 1999;23(10):932–8.
4. Imachi K, Chinzei T, Abe Y *et al.* A new method for the chronic evaluation of the microcirculation during artificial heart pumping. In Akutsu T, Koyanagi H, editors. *Heart Replacement – Artificial Heart 5*. Tokyo: Springer-Verlag. 1996:281–8.

Journal of Congestive Heart Failure and Circulatory Support (2001) Vol 1, No 4, 327–330

Flow-transformed pulsatile total artificial heart using axial flow blood pump

T. Isoyama PhD[1], T. Chinzei MD PhD[1], Y. Abe MD PhD[2], T. Ono BE[2], S. Mochizuki MD PhD[1], I. Saito PhD[1], M. Ishimaru MD[2], K. Iwasaki MS[3], A. Baba MD[2], T. Karita MD[2], T. Ozeki[1], A. Kouno[2] and K. Imachi PhD[2]

[1]*Artificial Biomechanism, Research Center for Advanced Science and Technology, The University of Tokyo, Tokyo, Japan;* [2]*Department of Biomedical Engineering, Graduate School of Medicine, The University of Tokyo, Tokyo, Japan; and* [3]*Department of Mechanical Engineering, Waseda University, Tokyo, Japan*

Background The flow-transformed pulsatile total artificial heart (TAH) has been designed as a pulsatile TAH that consists of a single rotary blood pump and blood flow switching valves. It can perfuse the pulmonary and systemic circulations alternately with pulsatile flow.

Methods A small axial flow pump is employed as a rotary blood pump. Four jellyfish valves with a polyurethane soft valve leaflet are used as a passively operated one-way valve. Two jellyfish valves are located at one port of the axial flow pump, and the other two are located at the other port of the pump. The valves are connected to the aorta, left atrium, pulmonary artery, and right atrium respectively. The axial flow pump turns reversibly at the phase of pulmonary circulation. Pivots at both ends of the impeller suspend the impeller. The rotating force of the motor is driven to the impeller by a magnet coupling.

Results The priming volume of the axial flow pump is 18 ml, which is small enough to reduce the mixture of arterial and venous blood. The total volume of each component such as the axial flow pump, jellyfish valves and conduits is 150 ml.

Discussion Because of the small volume of this TAH, in future we plan to implant it in the right ventricle and apply less invasive surgery using a transxyphoid approach.

Keywords total artificial heart (TAH), rotary pump, pulsatile flow.

Introduction

The concept of the flow-transformed pulsatile total artificial heart (FTPTAH) is to perfuse the pulmonary and systemic circulation alternately with pulsatile flow using a single continuous-flow blood pump and blood flow switching valves. This mechanism is expected to make the whole system compact enough to be implanted in the human chest cavity. In former studies we developed several types of FTPTAH using the combination of centrifugal pump and electrical switching valves[1], and used the combination of undulation pump and jellyfish valves[2,3].

In this study, we employed an axial-flow blood pump. The aims of this study are to reduce the volume of the total artificial heart (TAH) system, perfuse the pulsatile flow with no compliance chamber, facilitate implantation without removal of the natural heart and apply minimally invasive surgery.

Methods

The axial-flow blood pump is designed as a reversible rotary pump. The configuration is almost similar to the DeBakey VAD[4]. Pivots at the inducer and diffuser suspend the impeller. There are eight small neodymium-iron-boron magnets in the blades of the impeller and two magnets connected to the motor rotor outside of the pump. Magnetic coupling using these magnets transmits the rotating force of the motor.

The jellyfish valves are used to select the direction of blood flow. Its valve leaf is a thin polymer membrane and its valve seat is made of polyurethane. In our laboratory, jellyfish valves are normally involved in the sac-type artificial heart pumps and are tested in chronic animal experiments over 300 days. In this TAH, there are two jellyfish valves located in a row and in opposite directions at one of the ports of the axial flow pump. There are also two valves located at the other port in the same manner. These four valves are connected to the pulmonary artery (PA), left atrium (LA), right atrium (RA) and aorta (Ao) respectively. Switching the direction of motor rotation causes flow transformation, so no electrical flow-switching valve is required.

The mechanism of the FTPTAH is shown in Figure 1. The normal direction of rotation of the impeller opens the LA jellyfish valve and Ao valve, and perfuses the systemic circulation; furthermore, the reverse rotation of the impeller opens the RA and PA valves, and performs the pulmonary circulation.

Results

Figure 2 shows the actual model of the FTPTAH using an axial flow pump. The pump and motor housing are made of acrylic resins, and the conduits involving jellyfish valves are made of polyvinyl chloride. The components of the FTPTAH are shown in Figure 3. The impeller is made of

Correspondence to: Takashi Isoyama, Artificial Biomechanism, Research Center for Advanced Science and Technology, The University of Tokyo, 4–6–1 Komaba, Meguro-ku, Tokyo 153–8904, Japan.

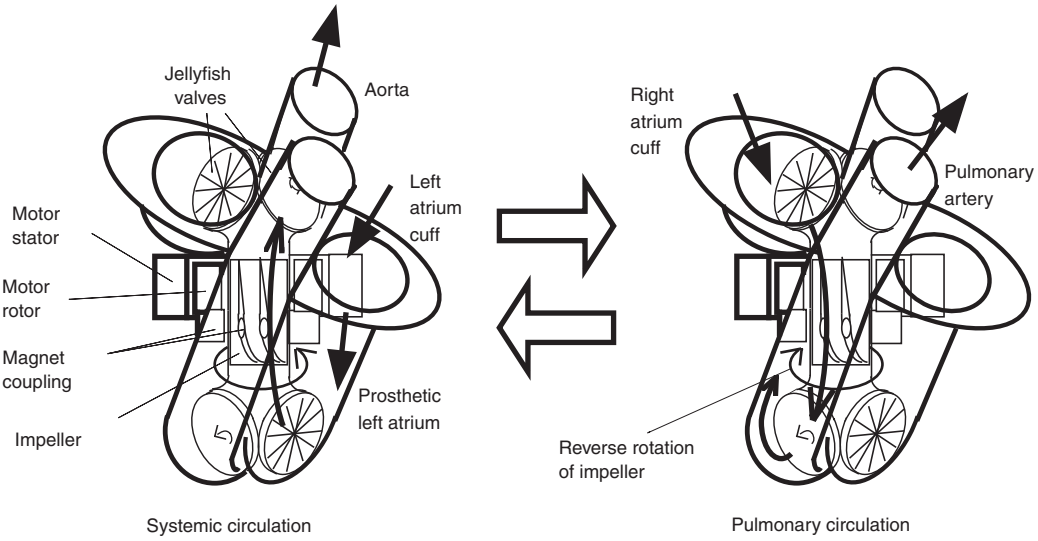

Figure 1. Mechanism of flow transformation.

polyurethane and its diameter is 12 mm. The whole length of the pump is about 80 mm. The total volume of the FTPTAH is 150 ml and the priming volume is 18 ml. The direct current brushless motor is made by Kollmorgen Inland Motor (Radford, VA, USA).

Figure 4 shows the implantation of the FTPTAH in the right ventricle. The left atrium and left ventricle of the natural heart are used as a big inflow blood reservoir for systemic circulation. On the other hand Figure 1 shows the total replacement application of the FTPTAH; this involves right and left atrium cuffs and a prosthetic left atrium.

Discussion

The flow-transformation mechanism has been proposed in order to reduce the volume of the TAH. The advantages of this mechanism are that it has one pump, one motor, pulsatile flow and no compliance chamber. Unfortunately the hydraulic pump performance is not satisfactory at this stage, so we could not report the data on the mock circulatory system. The shape of the blades and the clearance between impeller and housing are important to ensure good pump performance.

The disadvantages of the FTPTAH using an axial-flow pump are hemolysis and blood mixture. Because the rotation direction must be reversed, the shear stress at the transient stage is estimated to be quite high. The blood mixture between oxygenated and unoxygenated blood occurs in the axial flow pump at the phase of flow transformation. We will be able to minimize the blood mixture because we employ an axial flow pump with a small priming volume.

Recently, minimally invasive cardiac surgery (MICS) has been popular, for example for a left anterior small thoracotomy. Its application via the xiphoid process is not popular yet, but the advantages are that it protects the pleura and simplifies the approach to the bottom of the right ventricle. Figure 5 shows a future plan to implant the FTPTAH via the xiphoid process using MICS with percutaneous cardio-pulmonary support. This will prevent harm to the pleura or diaphragm.

Figure 2. Actual model of the flow-transformed pulsatile total artificial heart.

Figure 3. Components of the flow-transformed pulsatile total artificial heart.

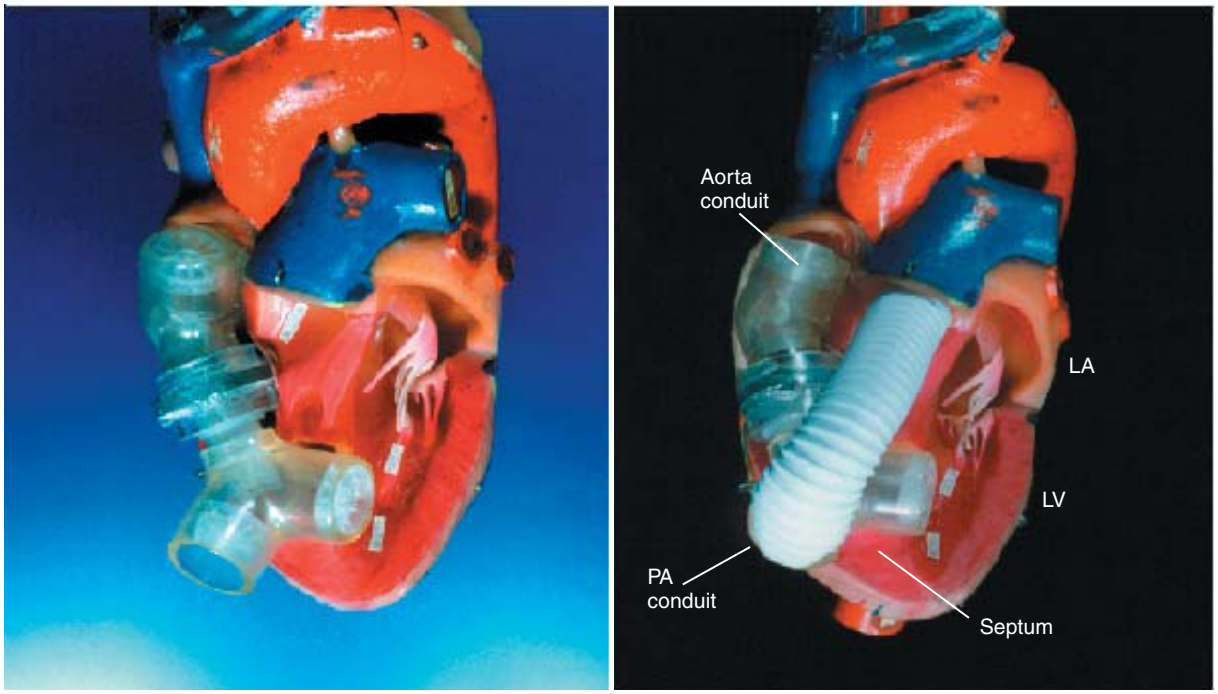

Figure 4. Anatomical layout implanted in right ventricle. LA = left atrium, LV = left ventricle, PA = pulmonary artery.

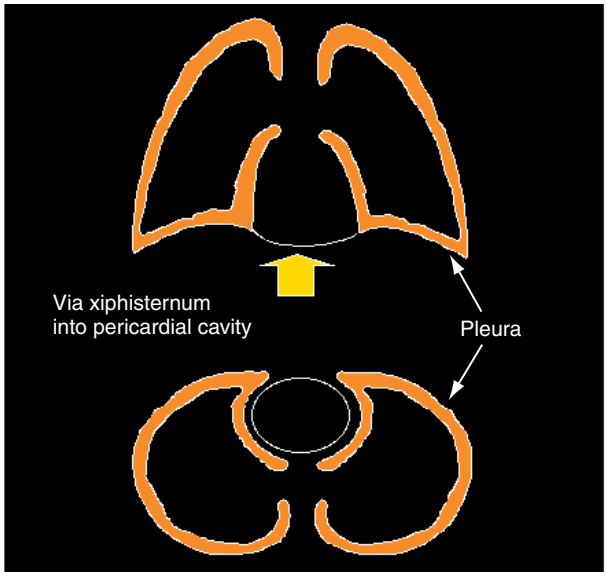

Figure 5. Minimally invasive approach.

References

1. Isoyama T, Imachi K, Chinzei T *et al.* Development of a pulsatile total artificial heart using a single continuous flow pump – the development of the third model. *Artificial Heart 4. Heart Replacement*. Tokyo: Springer–Verlag, 1993:287–90.
2. Isoyama T, Imachi K, *et al.* New version of flow transformed pulsatile total artificial heart having no electrical switching valve. *Artif Organs* 1995;19,694–6.
3. Isoyama T, Imachi K, Chinzei T *et al.* Flow-transformed pulsatile total artificial heart (FTPTAH) with no electrical switching valve. *Artificial Heart* 4. *Heart Replacement*. Tokyo: Springer–Verlag, 1996:125–27.
4. Nakazawa T, Makinouchi K, Ohara Y*et al.* Development of a pivot bearing supported sealless centrifugal pump for ventricular assist. *Artif Organs* 1996;20:485–90.

Journal of Congestive Heart Failure and Circulatory Support (2001) Vol 1, No 4, 331–336

Prediction of hemolysis in rotary blood pumps with computational fluid dynamics analysis

Y. Mitamura PhD[1], H. Nakamura MS[2], K. Sekine BS[1], D.W. Kim PhD[3], R. Yozu MD[4], S. Kawada MD[4] and E. Okamoto PhD[2]

[1]Department of Biomedical Systems Engineering, Division of Systems and Information Engineering, Graduate School of Engineering, Hokkaido University, Japan; [2]Department of Electronic and Information Engineering, School of Engineering, Hokkaido Tokai University, Japan; [3]Division of Information Technology Engineering, Soonchunhyang University, Korea; and [4]Department of Surgery, School of Medicine, Keio University, Japan

Background Low hemolysis is one of the key factors in the production of successful rotary blood pumps. It is, however, difficult to identify the areas where hemolysis occurs. Computational fluid dynamic (CFD) analysis enables the engineer to predict hemolysis on a computer.

Methods Fluid dynamics in five different axial flow pumps was analyzed three-dimensionally using CFD software. The impeller was rotated at a speed which supplied a flow of 5 L min^{-1} at a pressure difference of 100 mmHg. Changes in the turbulent kinetic energy along streamlines through the pumps were computed. Reynolds' shear stress (τ) was calculated using the turbulent kinetic energy. Hemolysis was evaluated based on Reynolds' shear stress and its exposure time (t): $dHb/Hb = 3.62 \times 10^{-5}\tau^{2.416}t^{0.785}$ Hemolysis of the pumps was measured *in vitro* using fresh bovine blood to which citrate phosphate dextrose was added to prevent clotting. A pump flow of 5 L min^{-1} was maintained at a pressure difference of 100 mmHg for 3 h. The normalized index of hemolysis (NIH) was measured.

Results Reynolds' shear stress was high behind the impellers. The measured NIH and the calculated hemolysis (dHb/Hb) showed a good correlation; NIH = 0.00015 (dHb/Hb) (r = 0.87, n = 5) in the range of NIH between 0.003 and 0.3.

Discussion CFD analysis can predict the *in vitro* results of hemolysis as well as the areas where hemolysis occurs.

Keywords computational fluid dynamics (CFD), hemolysis, turbulent kinetic energy.

Introduction

Implantable cardiovascular assist devices have been clinically used as a means of maintaining the cardiac output of a failing natural heart. This has led to the development of many blood pumps of various designs, both pulsatile and nonpulsatile. Currently available pulsatile flow assist devices, however, are too large and expensive to be used for the general population. Continuous flow devices such as axial and centrifugal blood pumps are small and inexpensive. However, present continuous flow pumps generally provide only short-term cardiac support because of problems such as hemolysis and thrombus formation.

The fluid dynamics in a continuous flow pump play an important role in reducing the problems of hemolysis and thrombus formation. Areas of flow separation, recirculation, and flow stagnation, which can lead to thrombus formation, are undesirable. The pump should not generate high fluid shear rates, thus minimizing damage to red cells. One of the primary requirements for a pump is that it should be able to generate blood flow an approximate of 5 L min^{-1} at a pressure difference of 100 mmHg. A blood pump should be designed so that the fluid dynamics satisfy all the requirements.

Experimental flow visualization techniques have been used to evaluate pump flow dynamics. These techniques, however, enable only a two-dimensional evaluation of flow in the plane of the laser sheet. Also, experimental techniques take a long time to set up, measure, and process data.

The use of advanced numerical techniques for characterizing the performance of a blood pump is cost-effective and alternative to experimental evaluation. A numerical model of the pump geometry can be created using computer-aided design (CAD) software. With the help of computational fluid dynamics (CFDs), the entire flow field in the pump can be simulated and analyzed. Based on the results of the analysis, different design modifications can be implemented on the numerical prototype. The effect of these modifications on the fluid dynamics can be studied further with the CFD model.

Several investigators[1–9] have designed rotary blood pumps, either axial or centrifugal, based on CFD analysis. The main objective of these studies was to reduce both high shear stress and stagnation areas in a pump. To characterize fluid dynamics in a pump, several parameters were used. They were velocity[4–8], shear stress[1,2,5,7–9], and

Correspondence to: Yoshinori Mitamura, Department of Biomedical Systems Engineering, Division of Systems and Information Engineering, Graduate School of Engineering, Hokkaido University, Kita 13 Nishi 8, Kita-ku, Sapporo 060-8628, Japan.

streamlines[1,3,9]. In several studies the relationship between fluid dynamic parameters and hemolysis was studied. However, the CFD results were not compared with experimental results[1] or were compared only qualitatively with measured hemolysis[6,7].

The purpose of this study is to develop a quantitative method to predict hemolysis based on CFD analysis and also to demonstrate the usefulness of CFD analysis in developing a blood-compatible rotary blood pump.

Materials and methods

The fluid dynamics of five different axial flow pumps were analyzed three-dimensionally using CFD software (ANSYS/FLOTRAN ver 5.5, ANSYS, Inc., Canonsburg, PA, USA). The structure of the axial flow pump with a four-vane impeller is shown in Figure 1[10]. The axial flow pump consists of a direct current brushless motor, an impeller, and a guide vane. The motor and impeller assembly is fixed to a stainless steel casing via the guide vane. The casing is a 40-mm cylinder with a 25 mm diameter inlet and a 38 mm diameter outlet. The motor casing is equipped with a semi-spherical cap to prevent swirling. A spacer is fixed to the motor housing between the impeller and the motor housing to reduce stagnation of flow. The motor is housed in a stainless steel cylindrical casing of 22 mm in outer diameter and 30 mm in length.

Five different impellers were used. The structure of a four-vane impeller is shown in Figure 2. The impeller has four vanes with an outer discharge angle of 19.2°. The outer diameter of the impeller is 22 mm, and the hub diameter is 13 mm. Radial clearance between the impeller and the housing is 0.5 mm. A four-vane two-stage impeller was also used. Two four-vane impellers with the same design as the above four-vane impeller were connected in series. The structure of a six-vane impeller is shown in Figure 3. The impeller has six vanes with an outer discharge angle of 23.6°. The outer diameter of the impeller is 22 mm, and the hub diameter is 13 mm. The radial clearance between the impeller and the housing is 0.5 mm.

Analysis of fluid dynamics in pumps

A k-ε turbulent flow model was used to analyze the fluid dynamics. Models of the impeller and the pump were generated on a computer using CAD software (Pro/Engineer Release 20.0, Parametric Technology Corp., Waltham, MA, USA). A schematic drawing of the grid of the four-vane impeller pump is shown in Figure 4. The model was divided into about 150 000 elements. Boundary conditions were given as follows: an inflow of 5 L min^{-1} and an outlet pressure of 100 mmHg. The rotational speed of the impeller was given for each pump to satisfy the above boundary conditions. In computation the models of the impeller and the housing were fixed and rotational speed was given to the fluid elements. Fluid was assumed to be Newtonian fluid having a density of 1.06×10^3 (kg/m^3) and a viscosity of 6×10^{-3} (Pa/s).

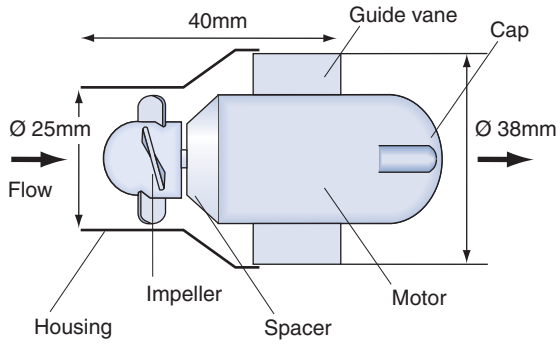

Figure 1. Structure of an axial flow blood pump. Ø = diameter.

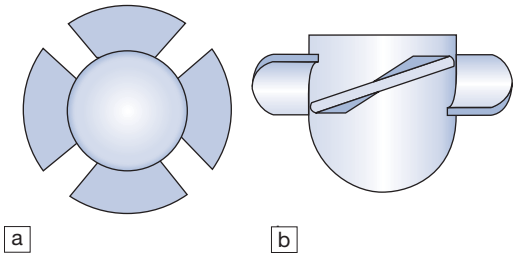

Figure 2. Design of four-vane impeller. (a) Top view, (b) side view.

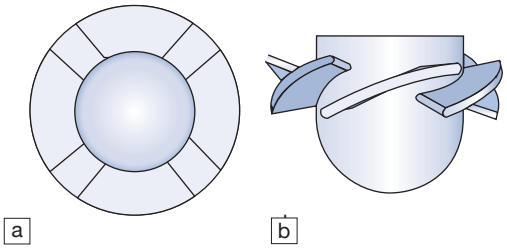

Figure 3. Design of six-vane impeller. (a) Top view, (b) side view.

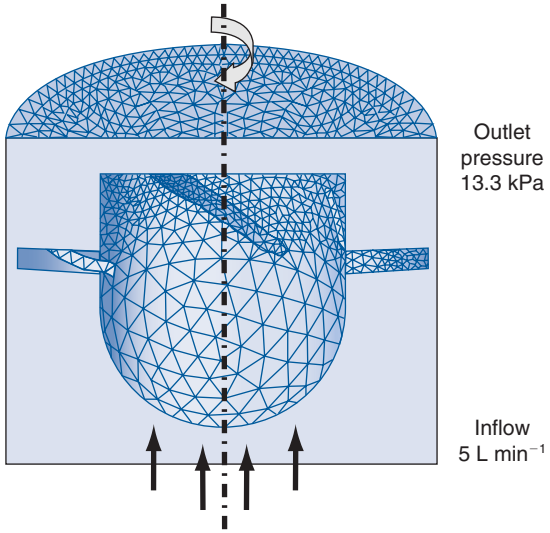

Figure 4. Schematic drawing of the grid for the four-vane impeller pump.

Measurements of hemolysis

The pump was connected to a reservoir bag (volume: 1000 mL) with silicone tubes (inflow side: 10 mm inner diameter and 141 cm long; outflow side: 10 mm inner diameter and 142 cm long) (Figure 5). In the test of the four-vane impeller pump at rest, the Bio-Pump (BP–80, Medtronic Bio-Medicus, Inc., Eden Prairie, MN, USA) was connected to the axial flow pump in series. The pump was placed 90 cm below the reservoir bag. A quantity of 1000 mL of fresh bovine blood to which citrate phosphate dextrose was added to prevent clotting was used. The reservoir bag was immersed in a water bath with a maintained temperature of 39°C. Outflow resistance was changed by compressing the outflow tube with a clamp. The flow was monitored with an electromagnetic flowmeter using a 10 mm probe, and the inlet and outlet pressures were measured with pressure transducers (Model P23XL, Spectramed, Statham, Singapore). A flow of 5 L min^{-1} was maintained for 3 h while keeping the differential pressure at 100 mmHg. The flow rate, differential pressure, inlet pressure, outlet pressure, and motor speed were recorded on a pen-recorder. A quantity of 2 mL of blood was sampled from the circulating blood and the control blood every 30 min. The control blood was also kept in the waterbath maintained at 39°C. Free plasma hemoglobin was measured by the tetramethylbenzene method (527-A, SIGMA, St. Louis, MO, USA). The normalized index of hemolysis (NIH) was calculated as follows:

$$NIH[g/100L] = \Delta freeHb \times V \times (100–Hct)/100 \times 100/(flow\ rate \times time)$$

where ΔfreeHb is the increase in plasma-free hemoglobin (g/L), V is the blood volume (L), Hct is the hematocrit (%), flow rate is the pump flow rate (L min^{-1}), and time is the sampling interval [min]. Tests were conducted using axial flow pumps with different impellers. Also the four-vane impeller pump at rest was tested. Blood was supplied from the Bio-Pump (Figure 5).

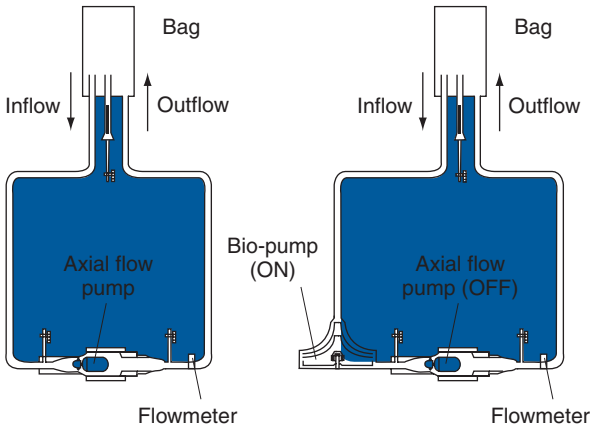

Figure 5. Set-up for the hemolysis test.

Results

Analysis of fluid dynamics in pumps

Turbulent kinetic energy in the four-vane and six-vane impeller pumps is shown in Figure 6. A color scale indicates turbulent kinetic energy. Red colors indicate high turbulent kinetic energy and blue colors low turbulent kinetic energy. Higher turbulent kinetic energy was observed behind the impeller. There were more high turbulent kinetic energy areas in the six-vane impeller pump than in the four-vane impeller pump.

Changes in the turbulent kinetic energy along streamlines are shown in Figure 7. This figure shows 30 streamlines originating from a quarter region of the circular flow channel. Markers indicate a time interval of 1 ms.

Figure 8 shows the turbulent kinetic energy in the four-vane impeller pump at rest. Higher turbulent kinetic energy was found near the impeller, but the absolute value was much lower than that in the pump in motion.

Hemolysis was predicted based on the level of shear stress and the exposure time of the cell membrane to these forces. Turbulent kinetic energy k is defined by the following equation:

$$k = \overline{u_i^2} / 2 \quad (1)$$

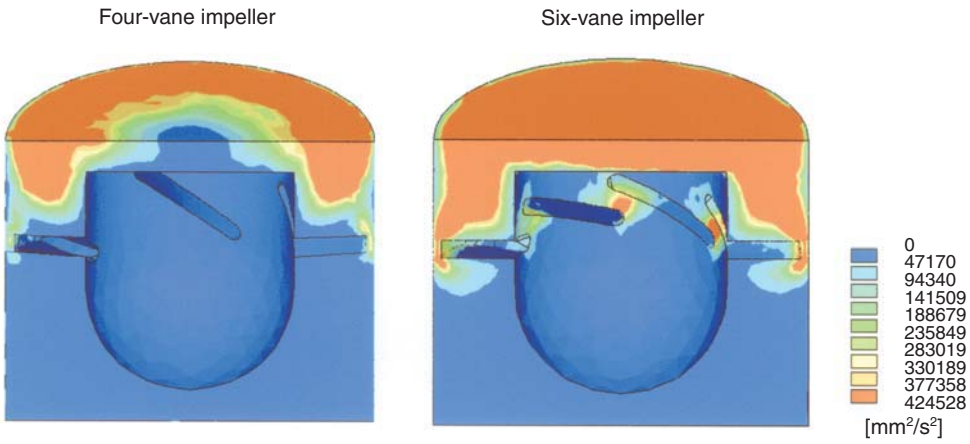

Figure 6. Turbulent kinetic energy in four-vane and six-vane impeller pumps.

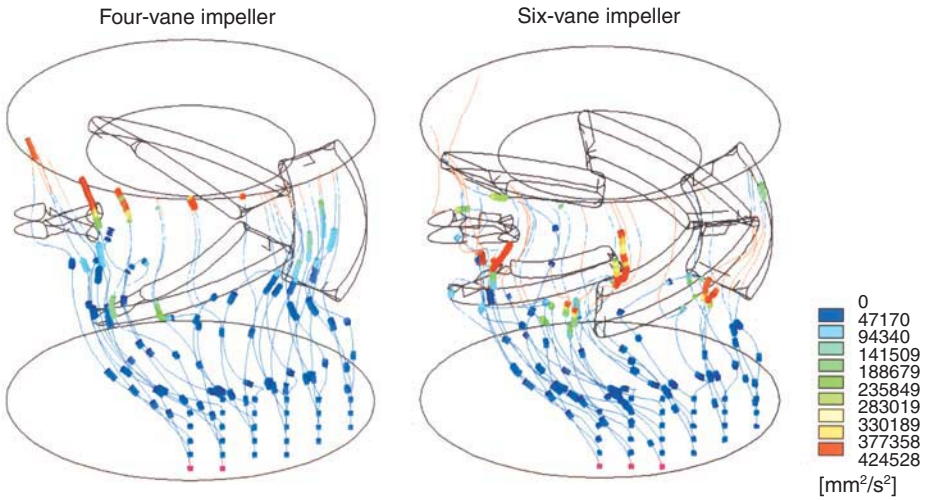

Figure 7. Changes in turbulent kinetic energy along streamlines in four-vane and six-vane impeller pumps.

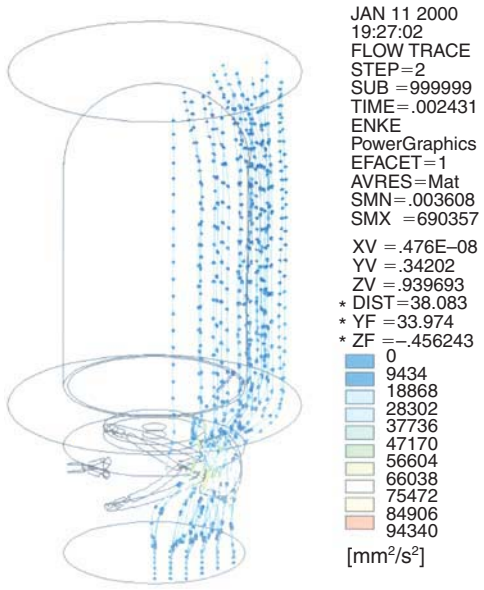

Figure 8. Changes in turbulent kinetic energy along streamlines in four-vane impeller pump at rest.

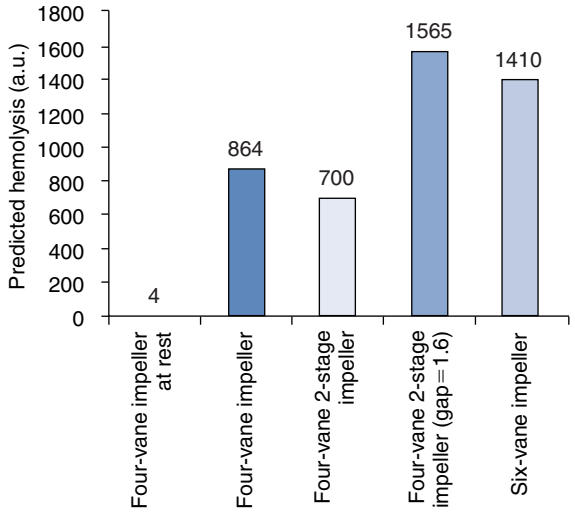

Figure 9. Predicted hemolysis for various axial flow pumps.

where u_i indicates a fluctuating component of velocity and $\overline{\ }$ a time average. Reynolds' shear stress is defined by the following equation:

$$\tau = -\rho\ \overline{u_i v_j} \quad (2)$$

where ρ is density, u_i is the fluctuating component of velocity in a certain direction, and v_j is the fluctuating component of velocity in the direction perpendicular to u_i. From the equations 1 and 2 the shear stress was approximated by the following equation based on the turbulent kinetic energy:

$$\tau = -2\rho k \quad (3)$$

The mechanisms of damage and the effects of shear stresses on blood corpuscles were investigated by Wurzinger and co-workers[11–13]. A basic model for the estimation of blood damage was proposed as follows:

$$dHb/Hb = 3.62 \times 10^{-5} \times t^{0.785} \times \tau^{2.416} \quad (4)$$

where Hb is hemoglobin content, dHb is damaged hemoglobin content, ρ is shear stress, and t is exposure time. According to this equation an index of hemolysis was predicted. Considering axis symmetry, equation 4 was calculated for 30 streamlines originated from a quarter area of the total flow channel.

Figure 9 shows the calculated values of hemolysis for various impeller pumps. The calculated value was higher with the six-vane impeller than the four-vane impeller.

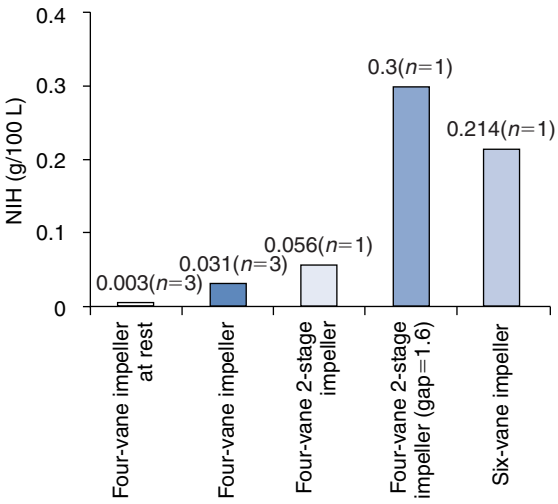

Figure 10. Measured normalized index of hemolysis (NIH) of various axial flow pumps.

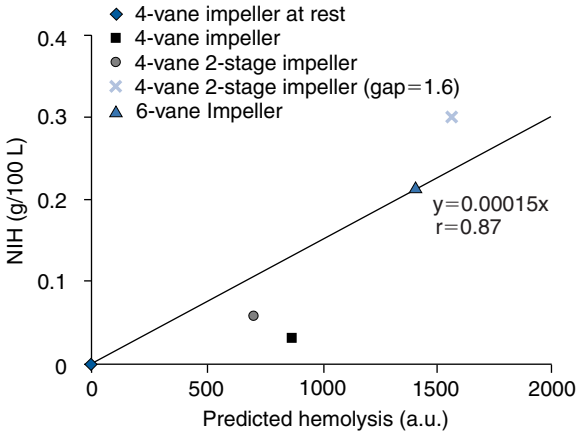

Figure 11. Comparison between predicted and measured hemolysis. NIH = normalized index of hemolysis.

Measurements of hemolysis

Measured NIH is shown in Figure 10. The measured NIH was higher with the six-vane impeller than the four-vane impeller. Comparison between the measurements of hemolysis and the calculated values is shown in Figure 11. The calculated hemolysis showed a good correlation with the measured values (correlation coefficient 0.87).

Discussion

During the last 50 years, many investigators have tried to develop an atraumatic blood pump. Hemolysis is one of the most important performance parameters of blood pumps. Hemolysis produces the release of hemoglobin into the plasma, the change in red blood cell morphology, and the shortening of its life span *in vivo*. Generally a rotary blood pump induces more hemolysis than a pulsatile blood pump, because a rotating impeller at a high speed induces higher shear stress. Since CFD analysis enables the engineer to predict hemolysis on a computer, the technique enables faster evaluation of the performance of various candidate designs and avoids the need to actually fabricate and test each design.

It has been experimentally observed that red blood cell damage in a shear flow is due to two factors acting at the same time: the level of shear stress and the exposure time of the cell membrane to these forces. Hence, a low level of hemolysis can be expected in flows with high shear stress if the exposure time is short enough. Conversely, a high level of hemolysis can be expected in flows with low shear stress if the exposure time is long enough.

A quantitative model of blood traumatization, with potential use to predict hemolysis, was developed by Wurzinger and co-workers[11–13]. Empirical correlation formulas based on experimental data of blood damage using a couette-type viscometer were proposed. The percentage of hemoglobin factor release can be calculated as a function of the exposure time and of the shear stress exerted on blood cell membranes as shown in equation 4. The major contribution of Wurzinger's experiments is to predict data from uniform shear stress distribution (up to 255 Pa) and from very short exposure times (order of magnitude of ms; up to 1000 ms) in a range of values representing the hydrodynamic situation found in heart valve prostheses and blood pumps.

Recently at the Helmholtz Institute, a high shear couette system was designed for the quantification of blood damage under controlled loading conditions[14]. The results showed that blood damage under laminar flow conditions at shear stresses up to approximately 500 Pa for exposure times up to 1 s is overestimated by earlier investigations (equation 4), in some cases by about one order of magnitude.

Schima *et al*. found discrepancies between experimental and predicted values (equation 4)[15]. Such differences were observed in high but short-lasting shear stress in a throttle (136 Pa; 3.23 ms) and in low but long-lasting shear stress in tubing (4.5 Pa; 3.5 s). The values of hemoglobin release in such cases were much smaller than those predicted by Wurzinger's formulas (two and three orders of magnitude smaller in tubing and in throttle, respectively).

In this study, Wurzinger's empirical formula was used to predict hemolysis in the axial flow pump, because equation 4 is the most accurate among those available in the literature and is suitable for numerical simulations. In the analysis of the four-vane impeller pump, the exposure time of a particle to shear stresses was in the range of 30–60 ms in flow regions with a mean shear stress of 165 Pa (median 6.2 Pa). Most of the shear stresses and exposure times were in the range of the Wurzinger equation. Therefore errors related to the nonlinearity of equation 4 were minimized.

In turbulence models, shear stress is obtained from the summation of the components of the molecule viscosity stress and Reynolds' stress:

$$\tau = \mu\ (\Delta V / \Delta y) + (-\rho\overline{u_i v_j})$$

Molecule viscosity stress derives from the multiplication of viscosity (μ) and the mean velocity gradients ($\Delta V / \Delta y$). Reynolds' shear stress is composed of nine components ($-\rho\overline{u_i v_j}$). Since Reynolds' shear stress is much greater than molecule viscosity shear stress, shear stress is obtained from Reynolds' shear stress. Total shear stress is defined as:

$$\tau = \sqrt{\tau_{xy}^2 + \tau_{yz}^2 + \tau_{zx}^2}$$

$$= \rho \sqrt{\overline{uv}^2 + \overline{vw}^2 + \overline{wu}^2}$$

Turbulent kinetic energy (k) was calculated based on the following equation:

$$k = (u^2 + v^2 + w^2) / 2$$

Turbulent kinetic energy corresponds to diagonal components of the Reynolds' stress tensor. Therefore turbulent kinetic energy was used in this study to approximate total shear stress. In the simulation of a backward-facing step flow, Reynolds' shear stress and turbulent kinetic energy showed almost the same profile[16]. The peak turbulent kinetic energy appeared at the same region where the Reynolds' shear stress reached its maximum level. Higher turbulence intensity generates higher shear stress, thus damaging red cells.

Good correlation was found between the predicted and measured hemolysis in an axial flow blood pump (Figure 11). CFD analysis can predict the *in vitro* results of hemolysis as well as the areas where hemolysis occurs (Figure 6). In conclusion, CFD analysis is useful for developing an atraumatic rotary blood pump and can replace the current 'trial and error' approach.

Acknowledgment

This study was supported in part by the Program for Promotion of Fundamental Studies in Health Sciences of the Organization for Drug ADR Relief, R&D Promotion and Products Review of Japan.

References

1. Pinotti M, Rosa ES. Computational prediction of hemolysis in a centrifugal ventricular assist device. *Artif Organs* 1995;19:267–73.
2. Bludszuweit C. Three-dimensional numerical prediction of stress loading of blood particles in a centrifugal pump. *Artif Organs* 1995;19:590–6.
3. Antaki JF, Ghattas O, Burgreen GW, He B. Computational flow optimization of rotary blood pump components. *Artif Organs* 1995;19:608–15.
4. Sukumar R, Athavale MM, Makhijani VB, Przekwas AJ. Application of computational fluid dynamics techniques to blood pumps. *Artif Organs* 1996; 20:529–33.
5. Miyazoe Y, Sawairi T, Ito K *et al.* Computational fluid dynamic analyses to establish design process of centrifugal blood pumps. *Artif Organs* 1998;22:381–5.
6. Miyazoe Y, Sawairi T, Ito K, Yana J. Development of the small caliber centrifugal blood pump. *Artif Organs* 1998;22: 461–5.
7. Masuzawa T, Tsukiya T, Endo S *et al.* Development of design methods for a centrifugal blood pump with a fluid dynamic approach: results in hemolysis tests. *Artif Organs* 1999;23:757–61.
8. Miyazoe Y, Sawairi T, Ito K *et al.* Computational fluid dynamics analysis to establish the design process of a centrifugal blood pump. Second report. *Artif Organs* 1999;23:762–8.
9. Nakamura S, Ding W, Smith WA, Golding LAR. Numeric flow simulation for an innovative ventricular assist system secondary impeller. *ASAIO J* 1999;45:74–8.
10. Mitamura Y, Nakamura H, Okamoto E, Yozu R, Kawada S, Kim DW. Development of the Valvo pump: an axial flow pump implanted at the heart valve position. *Artif Organs* 1999;23:566–71.
11. Wurzinger LJ, Opitz R, Eckstein H. Mechanical blood trauma. In Affeld K, Schichl K, Yoganathan A. *Nonpulsatile Blood Pumps: Summary of the ESAO Workshop on Rotary Blood Pumps*. Axam 1985, Berlin: Hermann-Foettinger Institut der Technischen Universität Berlin, 1986:30–44.
12. Wurzinger LJ, Opitz R. Hematological principles of hemolysis and thrombosis with special reference to rotary blood pumps. *Proceeding of International Workshop on Rotary Blood Pumps* 1991:19–25.
13. Giersiepen M, Wurzinger LJ, Opitz R, Reul H. Estimation of shear stress-related blood damage in heart valve prostheses – *in vitro* comparison of 25 aortic valves. *Int J Artif Organs* 1990;13:300–6.
14. Paul R, Schugner F, Reul H, Rau G. Recent findings on flow induced blood damage: critical shear stress and exposure times obtained with a high shear couette-system. *Artif Organs* 1999;23:680.
15. Schima H, Muller MR, Tsangaris S *et al.* Mechanical blood traumatization by tubing and throttles in *in vitro* tests: experimental results and implications for hemolysis theory. *Artif Organs* 1993;17:164–70.
16. Miyata H. *Analysis of Turbulent Flows*. Tokyo: University of Tokyo Press, 1995.

Journal of Congestive Heart Failure and Circulatory Support (2001) Vol 1, No 4, 337–343

Computational fluid dynamics analysis for centrifugal blood pumps

Y. Tsukamoto[1], K. Ito[1], Y. Konishi[1], T. Masuzawa[2], T. Yamane[3], M. Nishida[3], A. Aouidef[3], T. Tsukiya[4] and Y. Taenaka[4]

[1]Nikkiso Co., Ltd., Shizuoka, Japan; [2]Ibaraki University, Ibaraki, Japan; [3]Mechanical Engineering Laboratory, MITI, Tsukuba, Japan; and [4]National Cardiovascular Center, Osaka, Japan

Background The authors' aim is to establish a design theory of rotary blood pumps, which would be effective in developing rotary blood pumps, in combination with a computational fluid dynamics (CFD) analysis, flow visualization study, and hemolysis test. This paper focuses on two main issues: hemolytic performance and flow stagnation, in conjunction with thrombus formation.

Methods After changing radial gaps and outlet diffuser locations from the standard model, CFD analysis and hemolysis tests were conducted. Fluid dynamical indices were obtained with CFD. In order to observe the flow stagnation, we conducted another comparative study to clarify the effectiveness of wash-out holes and the influence of the hole diameter and location change.

Results The smaller the radial gaps, the larger the area of high shear stress became. It was not clear whether the outlet location changes affected the hemolysis. CFD indicated that the fluid in the model with the wash-out holes behind the impeller around the shaft rotated faster than the model without wash-out holes. Therefore, the wash-out holes were effective in reducing the flow stagnation. The flow visualization study showed a similar tendency to the CFD results.

Discussion High shear stress was observed close to the outlet diffuser. If the shear stress in the fluid is largely influential for hemolysis, the configuration of the pump around the outlet diffuser should be designed very carefully. The model with wash-out holes in the outer position of the radius might not cause a significant wash-out effect around the shaft, as with the model with small wash-out holes. The optimal configuration of the wash-out holes would exist.

Keywords computational fluid dynamics (CFD), hemolysis, shear stress, flow stagnation, thrombus formation, wash-out holes.

Introduction

Recently, turbo pumps have been widely applied in extracorporeal circulation. Many studies have been carried out by a number of cardiologists[1–5]. Turbo pumps for blood circulation have been developed by trial and error; it has taken a long time to accomplish such development, so it has been necessary to establish a design theory that would ensure efficient development. We have been comparing flow visualization studies and hemolysis *in vitro* studies, and studying the results of computational fluid dynamics (CFD) analyses carried out to date[6–10].

This report focuses on two topics: (1) hemolysis, and (2) flow stagnation considered to be related to thrombus formation. Specifically, we investigated the correlation between pump configuration and hemolysis using fluid dynamic indices obtained by CFD and hemolysis results, and then found indices relating to hemolysis. We paid attention to the flow pattern at the area around the shaft behind the impeller, where the fluid is considered relatively stagnant, and examined pump configuration presenting fluent flow. We tried to clarify the differences in flow between the models with and without wash-out holes through both CFD and flow visualization studies. Furthermore, in order to find out how the location and diameters of the wash-out holes affected the flow pattern, four comparative models were prepared.

Following the previous studies, this study was conducted to focus on the influence of the radial gaps, and the flow difference behind the impeller between the models with and without wash-out holes. In this paper, we focus on CFD analysis. In order to study the role of the wash-out holes, a comparative study was conducted using CFD analysis.

Materials and methods

Numerical method and CFD model

Figure 1 shows an outline of the numerical model for use of CFD. The numerical analysis is applied to the standard k-epsilon method, which is widely used on turbulence models. The commercial CFD software, CFX-TASCflow (AEA Technology), was chosen. The computational grid is composed of four blocks: pump part, volute, inlet passage, and outlet diffuser, adding up to 113 896 nodes.

In order to find the relationship of hemolysis, pump dimensions and fluid dynamical indices, we prepared three models. Figure 2 and Table 1 show pump configuration.

Correspondence to: Yuuki Tsukamoto, R & D Center, Shizuoka Plant, Nikkiso Co., Ltd., 498–1, Shizutani, Haibara-cho, Haibara-gun, Shizuoka, 421-0496, Japan.

Figure 3 shows the symbols of Table 1. In Model 2, the radial gap between the impeller and the casing issmaller than that of Model 1. In Model 3, the outlet diffuser is in a more outward position than in Model 2 in order to make the tangential flow from the volute. Numerical conditions are set to simulate hemolysis tests as much as possible, and a flow rate of 5 L min^{-1} and a differential pressure of 300 mmHg.

In order to study the stagnation, which is considered to be correlated with thrombus formation, we first studied the influence of the presence or absence of wash-out holes. Then we studied the way in which the flow pattern is affected by changing hole location and diameter and then prepared four comparative models:

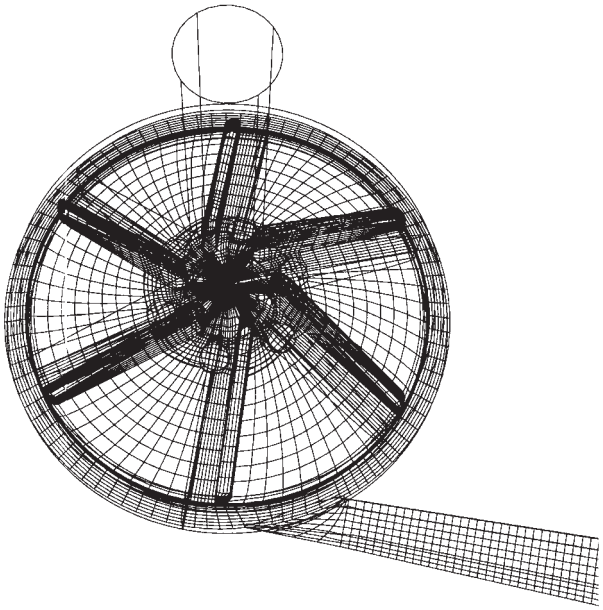

Figure 1. Computational grid.

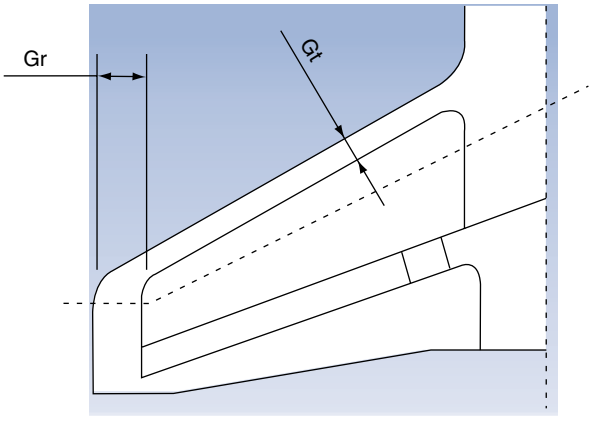

Figure 2. Cross-section of Model 2. The dotted line is starting from the center of outlet diameter to the mid-point between front casing and impeller hub.

1. The standard model similar to Nikkiso HPM–15 as a base
2. A model with a smaller diameter
3. A model with a larger diameter
4. A model with an outer pitch circle diameter (PCD).

Table 2 shows the diameter and location of wash-out holes. The numerical conditions on CFD in studies of flow stagnation have a common flow rate of 5 L min^{-1}, 3100 rpm, which reaches approximately 300 mmHg of differential pressure.

Results

Figure 4 shows velocity vector profiles obtained by CFD. The dotted line in Figure 2 shows the position of a cross-section through the center of the outlet diffuser, and in between the front casing and impeller hub. In Figure 4, there is flow turbulence at the tongue of the outlet diffuser in Models 2 and 3. Model 3 is observed to have a smoother flow along the flow path than Model 2.

Figure 5 shows the shear stress distribution of CFD as shown in the section in Fig. 4. Velocity gradients are calculated for three vectors in each node, and this is defined as dividing turbulent shear stress by the turbulent viscosity. The turbulent shear stress is defined as follows:

$$\text{Turbulent shear stress} = (s12^2+s23^2+s13^2)^{0.5}$$

Sij : Reynolds stress

The total shear is defined as follows:

$$\text{The total shear stress} = \text{Laminar shear stress} + \text{Turbulent shear stress}$$

$$= (\mu\text{molecular} + \mu\text{turbulent}) \times (\text{velocity gradient})$$

$$= (\mu\text{molecular} + \mu\text{turbulent}) \times ((s12^2+s23^2+s13^2)^{0.5}/\mu\text{turbulent})$$

Table 1. Configuration of models to find the influence of radial gap and outlet location change

Model No.	Gr (mm)	Gr (mm)	rpm	Outlet diffuser
1	3	1.5	3128	Standard
2	0.5	1.5	3426	Standard
3	0.5	1.5	3100	Tangential

Table 2. Size and location of wash-out holes. Variations of CFD models enables us to research good configuration of wash-out holes

Factor	Diameter	Location
Standard	ϕ3.5	PCD17
Outer PCD*	ϕ3.5	PCD25
Smaller diameter	ϕ2	PCD17
Larger diameter	ϕ4.4	PCD17

*PCD stands for pitch circle diameter.

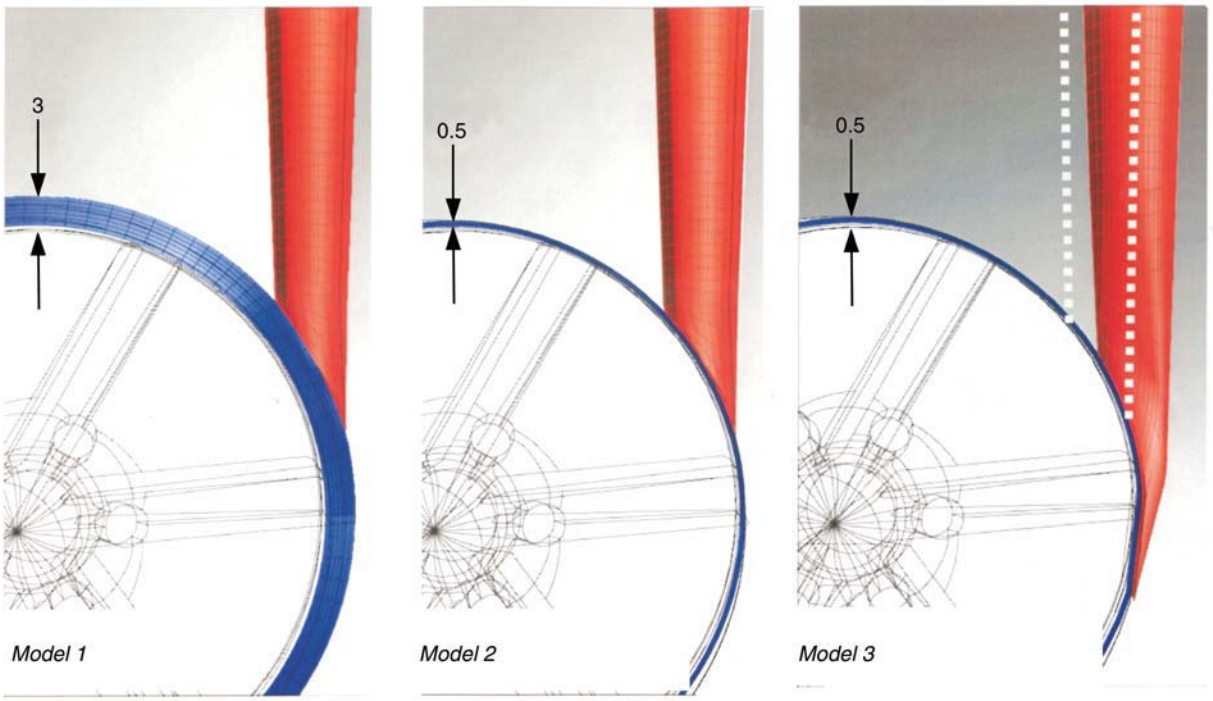

Figure 3. Comparison of three models. Blue: volute, Red: outlet diffuser.

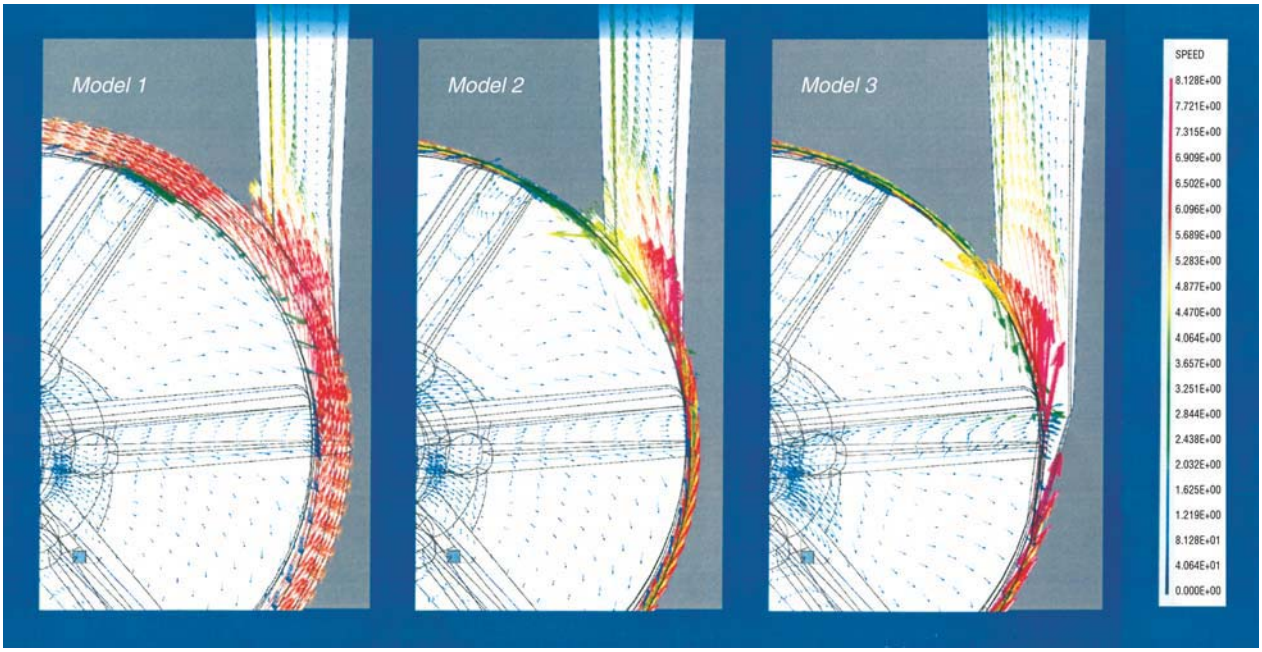

Figure 4. Velocity vector plots.

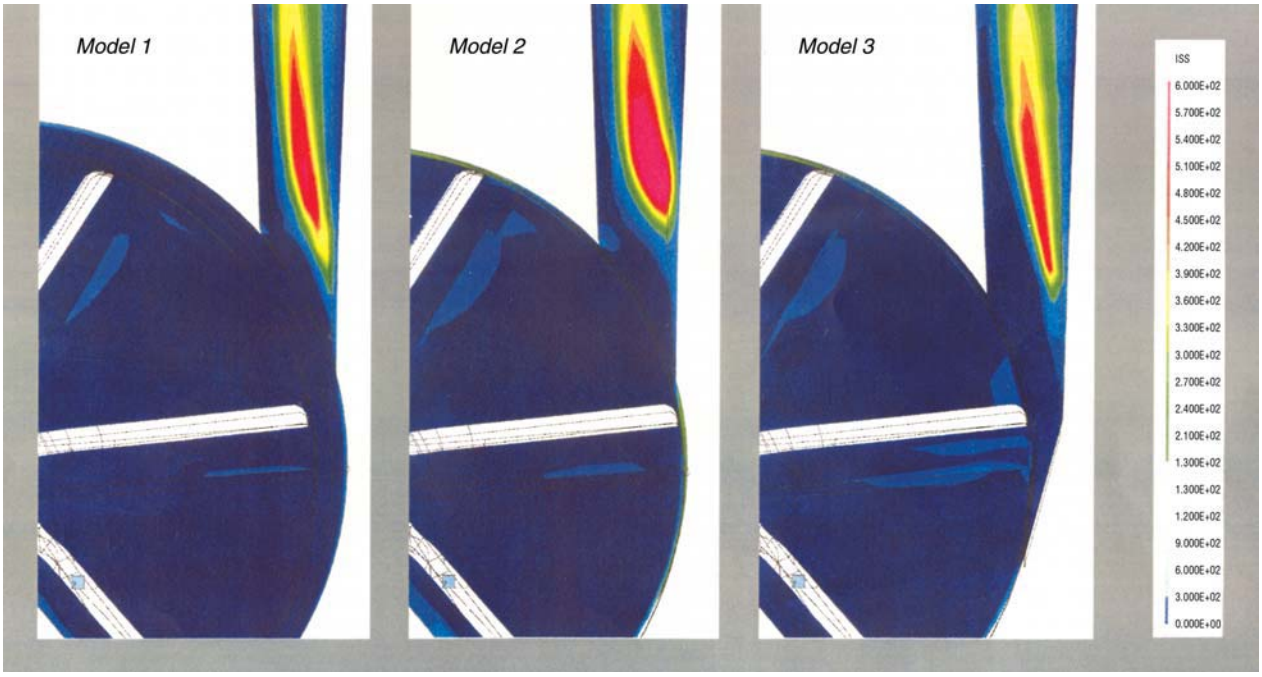

Figure 5. Shear stress distribution.

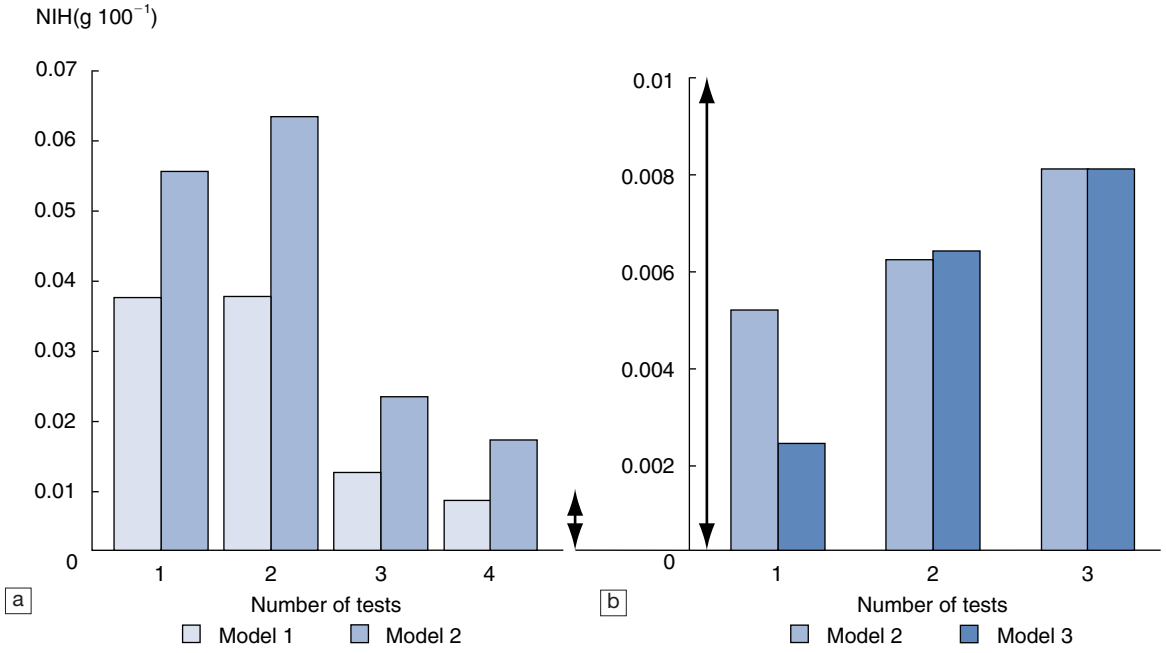

Figure 6. Hemolysis result: (a) radial gap change and (b) diffuser location change.

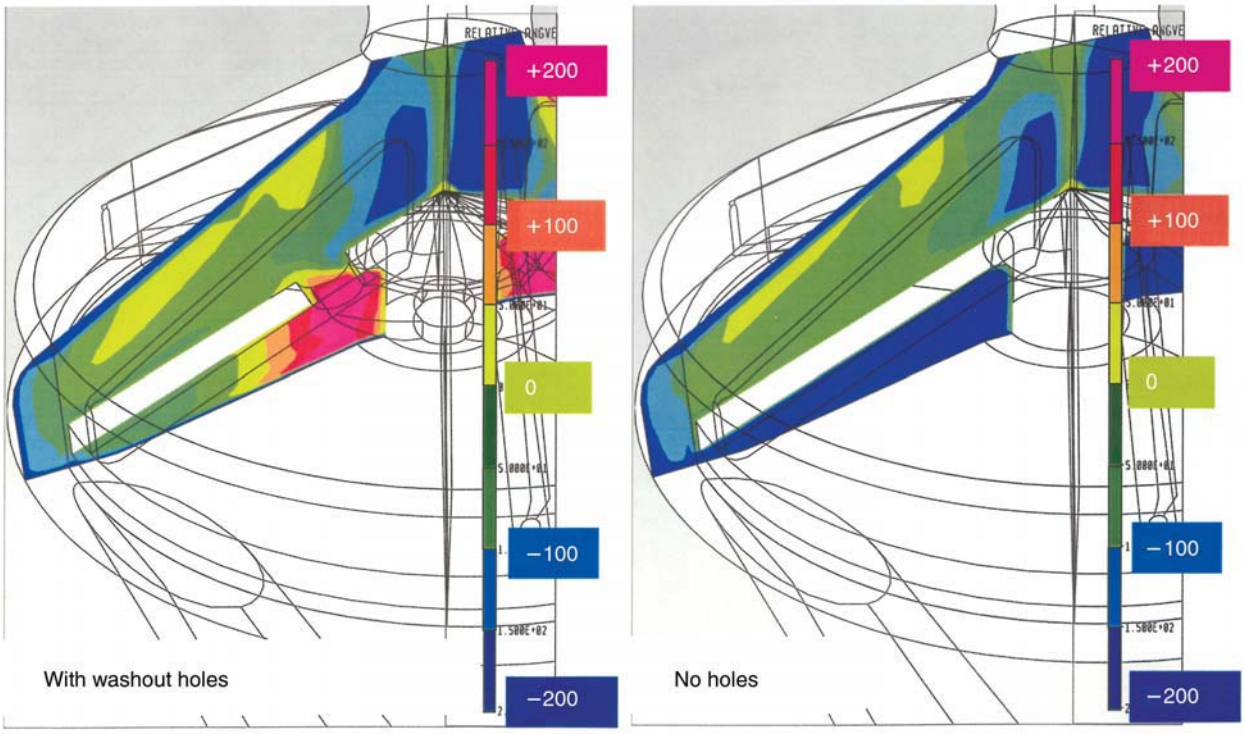

Figure 7. CFD result: relative angular velocity.

Model 2 shows a high shear stress region is expanding at the outlet diffuser that is wider than that in Model 1. Model 3 indicates that the high shear stress region is getting smaller than in Model 2.

Figure 6 shows the results of the hemolysis study, which was conducted using adult goat blood at a national cardiovascular center in Japan. The graph on the left indicated that Model 2 obtained more hemolysis Model 1. When comparing the hemolysis of Model 2 with Model 3, the level of three experiments was so small that a significant difference between the two models could not be found.

Figure 7 shows relative angular velocity toward the impeller with CFD compared to the models with and without wash-out holes. The unit is rad s^{-1}. Zero represents angular velocity of the impeller and the fluid is same. On the left, the area near the shaft behind the impeller with wash-out holes is in red. This means the fluid in that area rotates faster than the impeller. On the contrary, the right side of the figure shows that the whole area behind the impeller is rotating slower than the impeller. The wash-out holes affect the rotation of the fluid behind the impeller.

Figure 8 shows the comparison between CFD results and the flow visualization study. The left and right graphs are the results of the model with the wash-out holes. We selected three cross-sections at the lowest axial position of the impeller, the half position of the impeller, and 4.8 mm higher than the lowest axial position, respectively (see Figure 9).

The tangential velocity of the impeller is the straight line. When the fluid velocity gets higher than that of the impeller, it means that the fluid rotates faster than the impeller. We can see that the fluid behind the impeller around the shaft, in the model with the wash-out holes, rotates faster than the impeller with each radius.

Blue, green, red cross-sections revealed that CFD results and the data of the flow visualization study showed close tendency and we could obtain verification of the CFD analysis on the area behind the impeller.

Figure 10 shows velocity vector plots at various diameters and radial locations. When comparing the standard model, the model with smaller holes shows that the velocity passing through the hole becomes higher, but we found out by calculation that the total flow rate passing through the holes is reduced. The model with larger holes shows a flow pattern passing through the wash-out holes from the front to the rear and total flow rate passing through the holes does not vary significantly. The outer location of the model indicates that the flow rate passing through the holes is increasing, but the fluid behind the impeller, around the shaft, rotated slower than in the standard model.

These observations indicate that holes closer to the shaft enable a wash-out effect around the shaft, and enlarging the hole's diameter does not affect the flow rate passing through the holes.

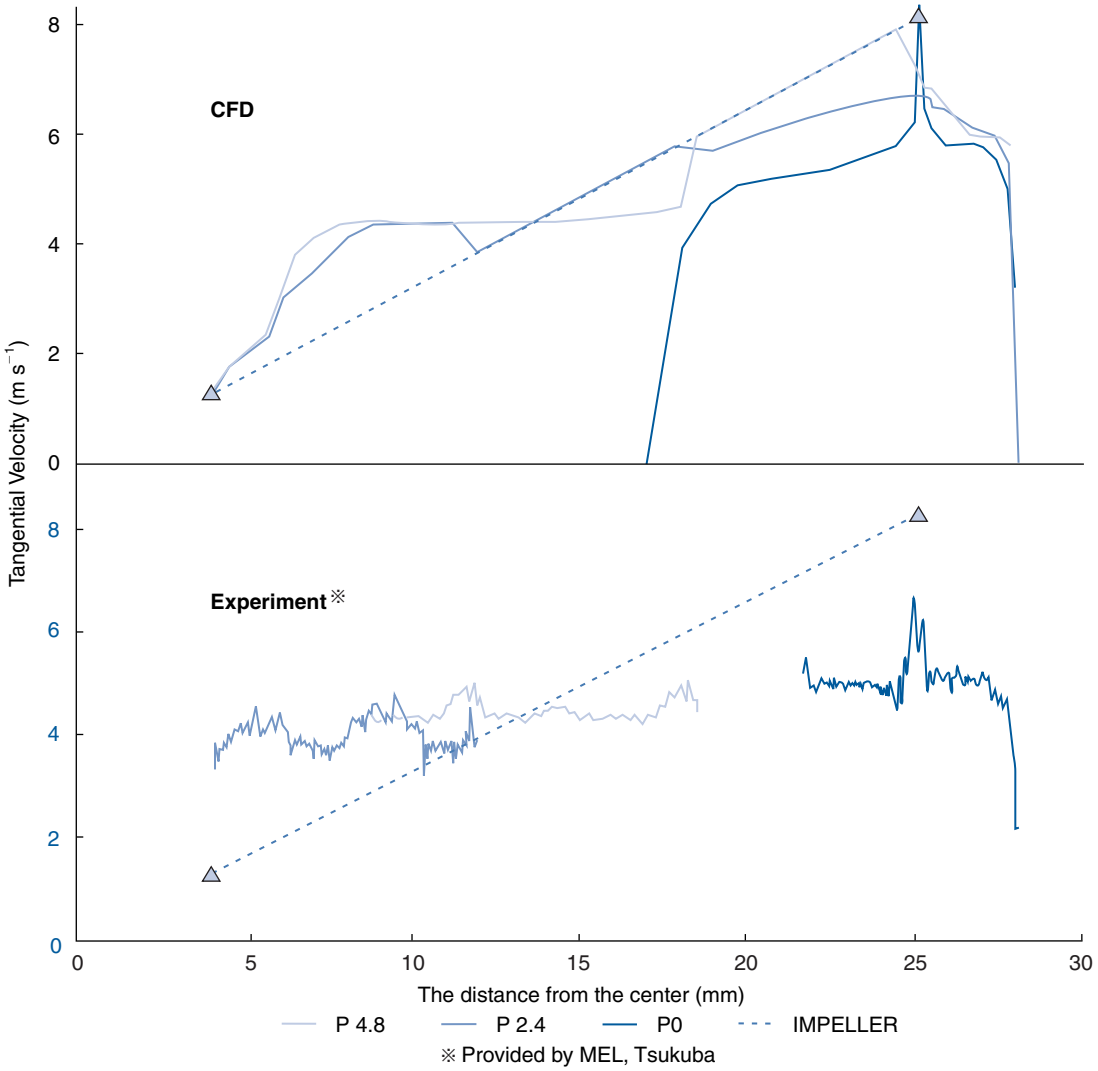

Figure 8. Comparison of CFD and flow visualization study.

Discussion

In order to observe the flow pattern behind the impeller, a relative angular velocity toward the impeller is applied. However, angular velocity itself is constant at each radius, so an absolute angular velocity can be obtained by adding relative angular velocity into one of the impellers. It is also important to consider relative motion between the stationary wall, such as between the rear casing and the fluid, because adhesion of the platelets to the stationary wall causes fluid stagnation. The larger the angular velocity of the fluid, the less likely flow stagnation becomes. The CFD result indicated that changing the location of the hole to a more outward position increases the flow rate passing through the holes, but a wash-out effect around the shaft cannot be expected. The CFD result also indicated that increasing the diameter of the hole does not lead to an increase in flow rate pass-

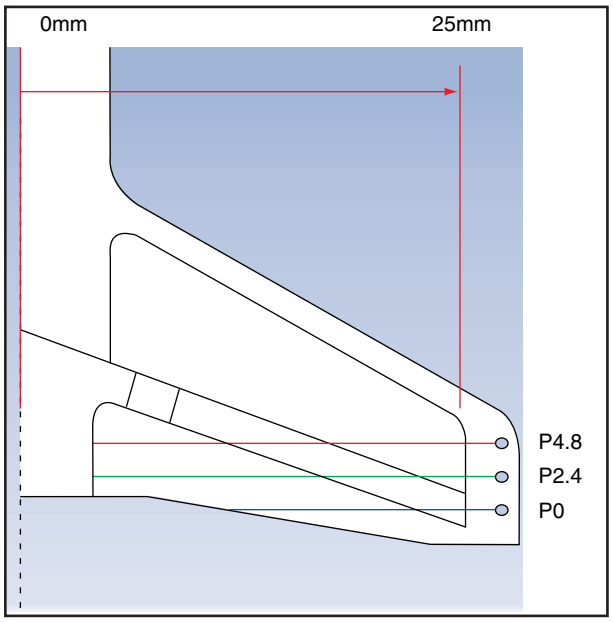

Figure 9. Three cross-sections: blue, green, red.

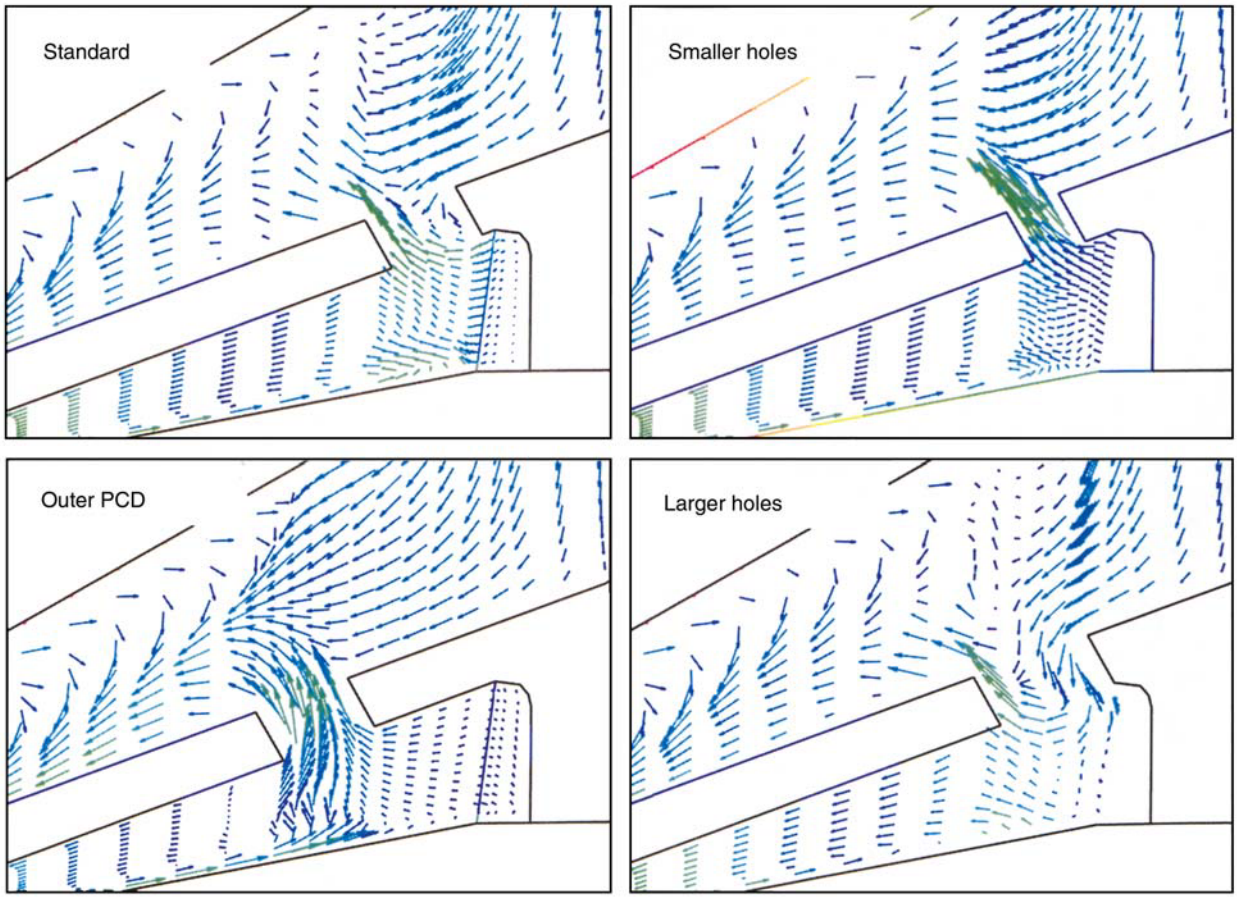

Figure 10. CFD result: comparison of the hole size and location are shown by velocity vector profiles.

ing through the holes, nor a wash-out effect around the shaft.

Conclusion

The change in radial gap largely affects the shear stress and hemolysis.

Wash-out holes effectively reduce flow stagnation behind the impeller and the size and location of the wash-out holes are very important and largely affects the flow pattern behind the impeller. CFD analysis is crucial to establishing a design for centrifugal blood pumps. CFD can further be used to investigate the blood pump characteristics.

Acknowledgements

The authors wish to thank Dr Yoichi Yokoyama from AEA Hyprotech KK, Yokohama, Japan for his technical support on CFD.

References

1. Orime Y, Takatani S, Sasaki T *et al.* Cardiopulmonary bypass with Nikkiso and BioMedicus centrifugal pumps. *Artif Organs* 1994;18:11–16.
2. Onoda K, Kondo C, Mizumoto T *et al.* Clinical experience with Nikkiso centrifugal pumps for extracorporeal circulation. *Artif Organs* 1994;18:706–10.
3. Shimono T, Makinouchi K, Nosé Y. Total erythrocyte destruction time: The new index for the hemolytic performance of rotary blood pumps. *Artif Organs* 1995;19:571–5.
4. Ohtsubo S, Naito K, Matsuura M *et al*. Initial clinical experience with the Baylor–Nikkiso centrifugal pump. *Artif Organs* 1995;19:769–73.
5. Naito K, Suenaga E, Cao ZL, Suda H, Ueno T, Natsuaki M, Itoh T. Comparative hemolysis study of clinically available centrifugal pumps. *Artif Organs* 1996;20:560–3.
6. Miyazoe Y, Toshio S, Ito K *et al.* Computational fluid dynamic analysis to establish design process of centrifugal blood pumps. *Artif Organs* 1998;22:381–5.
7. Yamane T, Asztalos B, Nishida M *et al.* Flow visualization for saving the number of hemolysis tests in the development of centrifugal blood pump. *Artif Organs* 1998;22:375–80.
8. Takiura K, Masuzawa T, Endo S *et al.* Development of design methods of a centrifugal blood pump with *in vitro* tests, flow visualization and computational fluid dynamics: Results in hemolysis tests. *Artif Organs* 1998;22:393–398.
9. Nishida M, Asztalos B, Yamane T *et al.* Flow visualization study to improve Hemocompatibility of a centrifugal blood pump. *Artif Organs* 1999;23:697–703.
10. Masuzawa T, Tsukiya T, Endo S *et al.* Development of design methods for a centrifugal blood pump with a fluid dynamic approach: Results in Hemolysis Tests. *Artif Organs* 1999;23:757–761.

Journal of Congestive Heart Failure and Circulatory Support (2001) Vol 1, No 4, 345–349

Computer simulation of the entire heart pump with application to IVAS centrifugal pump

S. Nakamura PhD
Department of Mechanical Engineering, Ohio State University, Columbus OH, USA

Abstract This paper reviews the current status and goals of developing computer simulation software with application to the Innovative Ventricular Assist System (IVAS) centrifugal heart pump which was developed by the Cleveland Clinic Foundation, Cleveland, OH, USA. The basic concept of selecting the mathematical models is discussed along with needs of further developments and milestones of experimental verification. The most updated version of the code being developed will be applicable to both centrifugal and axial heart pumps.

Need of fluid flow simulation codes

The objective of the present work is to develop computer codes that simulate the flows in the entire heart pump and accurately predict various quantities; this will eliminate many costly experimental efforts currently performed with prototypes to find out the effects of design parameters. The codes would produce, for a given design and operating conditions, the following quantities:

1. Time-dependent and time-averaged velocity and pressure fields
2. Shear stress distribution
3. Real-time history of particle trajectory
4. Estimate for blood cell damage
5. Energy consumption
6. Pump head.

Although blood is a non-Newtonian fluid, our view is that the flows in the artificial heart pump can well be simulated with the Newtonian assumption. The non-Newtonian aspects of the blood become important when the flow channel width is comparable to that of the blood cells, as well as when details of the flows in the boundary layer are of interest. If non-Newtonian features turn out to be important in the computer simulation, they can be implemented in the future once the numerical simulation for the entire pump with the Newtonian assumption is well established. We emphasize, however, the importance of research to investigate quantitatively the effect of non-Newtonian aspects on the blood flows at a fundamental level.

The flow equations for an incompressible Newtonian fluid is represented by the time-dependent Navier–Stokes equations. However, solving the Navier–Stokes equations is still a very challenging task, even with today's computers. Basically three solution methods are available:

1. Reynolds-averaged Navier–Stokes method (RANS)
2. Direct numerical simulation (DNS)
3. Large eddy simulation (LES) method.

With the RANS method, the time-averaged Navier–Stokes equations are solved. The RANS equations contain the Reynolds stress terms that are the time-averaged products of velocity fluctuations about the time-averaged velocities. The turbulence models deal with the transport of Reynolds stress and their closure. The RANS approach is currently the industry standard. For one reason, it is computationally fast and economical. The RANS approach however, requires, many empirical constants that are very difficult to determine.

The DNS on the other hand solves the Navier–Stokes equations with no modeling for the turbulent effects. All turbulent effects are captured by the computations if the grid is fine enough. The technical difficulty with DNS is that a sufficient number of grid points cannot be afforded except for low Reynolds number flows.

The LES has been offered as a remedy to the difficulties in both RANS and DNS. The core of the concept of LES lies in separation of the flow fields into two parts: (1) spatially filtered (or averaged) velocity distributions, and (2) the balance that is the exact solution minus the filtered distributions. Part 1 covers the flow fields that can be well represented with a coarse grid, while 2 includes all the fluid velocity components that are too small in scale to be captured by the grid. The momentum equations for the filtered velocities may be obtained by applying the filtering process to the unsteady Navier–Stokes equations. The filtered equations are almost the same as the original Navier–Stokes equations except they include the Reynolds stress terms that are very similar to those in the RANS equations. However, there is one significant

Correspondence to: S. Nakamura, Department of Mechanical Engineering, Ohio State University, 206 West 18th Avenue, Columbus, OH 43210, USA.

difference to be noted. The filtered momentum equations in LES are not time-averaged, so they are unsteady.

The LES is not free from difficulties, however. It needs a closure model for the Reynolds stress term, which normally requires at least one empirical constant. Another difficulty is that the LES cannot automatically recognize the difference between the laminar flow and turbulent flows – instead, it always assumes that the flow is turbulent. Therefore, it is dangerous to use LES when the flow can be laminar, at least partially.

Yet there is another approach – that is to use DNS with a coarse grid which is not sufficiently fine to capture fine-scale motions of turbulence. With this approach, the subgrid scale motions are simply truncated and ignored, but laminar flows are well captured. Interestingly, however, there are many works showing that the DNS with a coarse grid captures the large-scale motions of turbulent flows well, at least qualitatively.

The blood flows in centrifugal pumps are not purely turbulent nor purely laminar, which makes the selection difficult. We are not in a position to argue which method is superior to others from the purely theoretical point of view. We regard all as available options. Only verification with experiments can tell which one should be used in the future. In the past, we used the DNS approach with a coarse grid, but we have made the LES scheme also available in our current codes.

Current status of code development and overview of applications

The codes developed in the past as well as those under current development that contributed to the design study of IVAS[1] are listed in Table 1. The basic algorithms of numerical solutions are documented[2].

The two-dimensional (2D) single passage code was used for a large number of parametric studies for IVAS[3]. The 2D whole pump code was written for the parallel computer Cray T3E, which demonstrated the feasibility of developing 3D whole pump codes[4–6]. Figure 1 illustrates a velocity plot of the 2D whole pump computation. The success of this 2D whole pump code was important because it confirmed that the following techniques can be used for whole pump simulation:

1. Interpolative exchange of the iterative quantities between the moving and stationary grids
2. Parallel computing applied to the whole pump
3. Feasibility of the present numerical method to the whole pump.

Without these confirmations, we would not have ventured the development of the 3D whole pump codes.

The 3D single passage code was successfully used to investigate the flow fields and in the primary impeller as well as the secondary impellers[7–9]. Figures 2 and 3 illustrate the velocity vector plots of a 3D single passage computation. The 3D whole pump code Version A was completed. This code has been extensively applied to chemical mixing vessel analyses[10–12]. For the heart pump application, however, a major modification regarding the geometry definitions was felt necessary, which led to the development of Version B.

The last pump, the 3D whole pump Version B, is still being developed. A perspective view of the grid used for an entire heart pump is illustrated in Figure 4. Figure 5 illus-

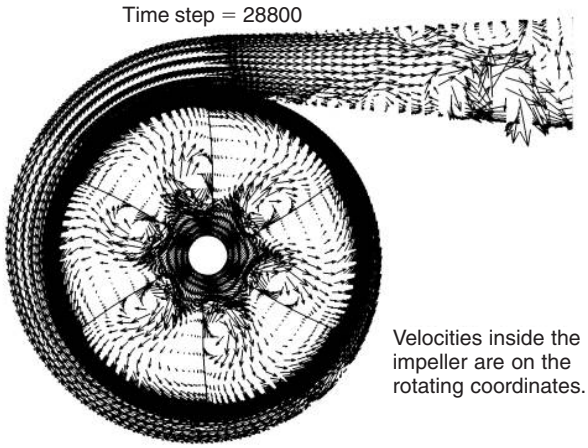

Figure 1. Velocity vector computed by the 2D whole pump code.

Table 1. Codes developed for flow simulation of IVAS

Name of code (with remarks)	Applications
2D single passage	IVAS parametric studies[3]
2D whole pump (Cray T3E, parallel computer)	IVAS parametric studies[4–6], Figure 1
3D single passage	IVAS primary pump[7–8], Figures 2 and 3 IVAS secondary pump[12]
3D whole pump version A	IVAS with no net flow; Hurricane lamp flow analysis[9]; Chemical mixers with a rotor impeller[10]; Counter jet chemical mixer[11]
3D whole pump version B (DNS, LES, hemolysis)	Under development; Figures 4 and 5; future comparisons with chemical reactors, Figures 9 and 10

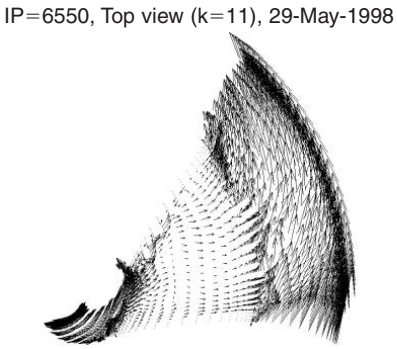

Figure 2. Top view of the velocity vectors computed by the 3D single passage code.

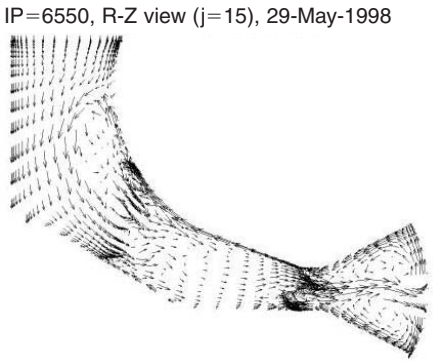

Figure 3. Side view of the velocity vectors computed by the 3D single passage code.

trates velocity vectors for a test run. The 3D whole pump Version B is essentially the same as Version A, but has been entirely rewritten in order to make definitions of the solid wall boundaries in the code automatic. Unfortunately, the code is not yet fully operable at the time of writing. When completed, Version B will be applicable to both centrifugal and axial heart pumps.

Experimental verification

Experimental verification is an important part of our effort in development of the computational tool. It is being worked in multiple paths.

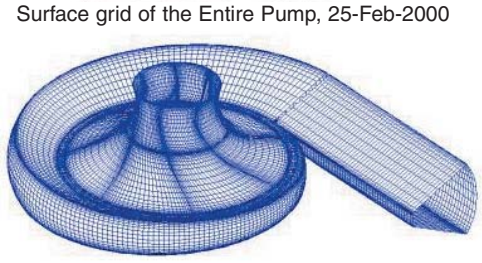

Figure 4. Perspective view of the grid used in the 3D whole pump code.

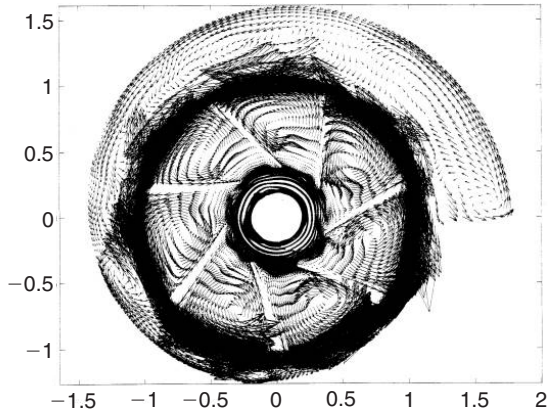

Figure 5. A velocity vector plot from a test run of the 3D whole pump code.

The first path is the development of the IVAS project of a scaled-up model of the centrifugal pump for experimental measurements, as illustrated in Figure 6[13,14]. With this device, the pump characteristics were extensively measured, which will be used to evaluate the results of Version B when it is completed. A few plots of the measured data are illustrated in Figures 7 and 8.

The second area of effort in experimental verification is in conjunction with the application of Version A to chemical mixing devices. This is possible because the geometrical model of the code can be modified easily to a chemical mixing vessel with or without a impeller rotor. This effort will provide important information regarding the accuracy of the computational method for the chemical mixer, but the same information will be applicable also to the artificial heart pump simulations. This effort is a multiyear collaborative effort with experimentalists in chemical engineering. Comparison of computations and flow visualization was performed for the three devices: (1) hurricane lamp[10], (2) counter jet mixing[11], and (3) mixing with rotor impeller and baffles[12]. The comparisons have only been qualitative so far to determine if further quantitative velocity field measurements would be

Figure 6. Photograph showing the scaled IVAS model[13].

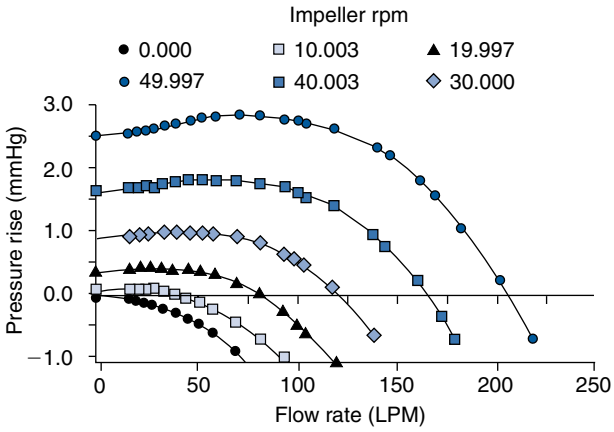

Figure 7. Pressure versus low rate[13].

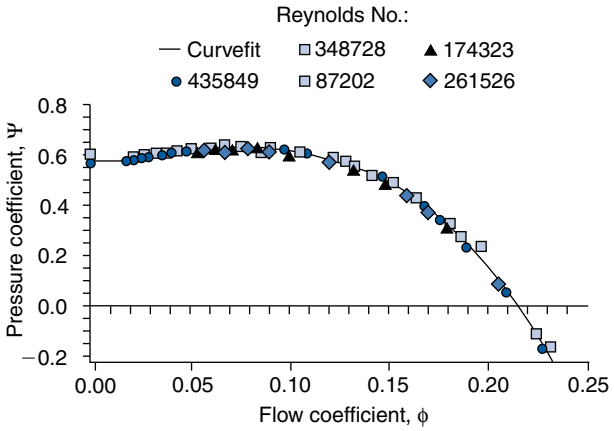

Figure 8. Pressure coefficient versus flow coefficient[13].

Figure 9. Jet mixing vessel for quantative measurements.

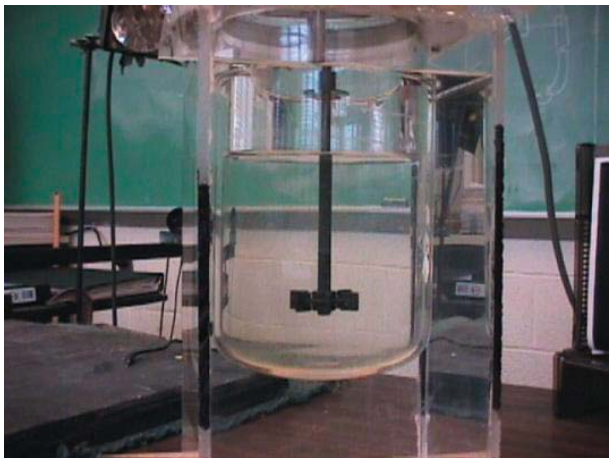

Figure 10. Biochemical mixer.

worthwhile. Fortunately, the qualitative comparisons have all been positive. The quantitative measurements for the counter jet mixer (Figure 9) and a biochemical mixer (Figure 10) have been initiated using the particle tracking velocimeter.

Although the configurations of the chemical mixers are different from the heart pumps, a significant amount of information gained from trials on chemical mixers is expected to be applicable to the heart pump. This is because the same codes are used and there is a significant similarity between the chemical mixers and heart pumps.

Further work required

There is an immediate problem in making the newest version of the whole pump code workable. The code has been cleared for possible human errors in programming. To confirm the integrity of the code, a number of tests were performed with simple test flow configurations; these tests have all been positive.

The core of the problem is that the pressure equation solved for each time step in the current codes is a singular problem, in which the summations of the unknown side and source side must both vanish. On the computer, however, the condition of zero total of the sources is not achievable in an absolute sense because of the round-off errors. When the number of grid points is not large, the flow solution is stable and the effects of solving a singular Poisson equations can be easily overcome. However, as the number of grid points becomes large, and particularly with the nonuniform grid intervals, a small amount of round-off errors in the source term can distort the pressure solution and cause significant feedback effects to the velocity field. Another problem with the singular Poisson equations is that the convergence rate is extremely slow particularly with a large number of grid points. Indeed, iterative convergence of the pressure correction equation is slow until a few thousand time steps are passed. After that stage, the iteration time decreases to a small number.

Therefore, the remedy of the current problem relies on implementation of a significantly more efficient iterative convergence scheme along with reduction of round-off errors. The round-off errors are expected to decrease by altering the grid point distribution in the vicinity of the watercut.

Conclusion

We have described our current attempts to develop a computer code to simulate the flows in an entire heart pump. The newest version of the code is expected to reduce experimental works on the prototypes of the heart pump. This code, when completed, will be applicable to both centrifugal and axial pumps. To achieve the goal, two things must be achieved. One is to resolve the current setback due to the singular Poisson equations. Another is the experimental verification and calibration that have been initiated. The former should be achieved shortly with the development of a new numerical algorithm. The experimental verifications will take much longer.

References

1. Golding LA, Medvedev A, Massiello A, Smith WA, Horvath D, Kasper R. Cleveland clinic continuous flow blood pump: Progress in development. *Artif Organs* 1998;22(6):447–50.
2. Nakamura S. *Options and Selection of Numerical Algorithms for Incompressible Navier-Stokes Equations.* FEDSM97–3666. Proceedings of ASME Fluids Engineering Division Summer Meeting, June 22–26, 1997, Vancouver, Canada.
3. Nakamura S, Ding W, Yano K, Veres JP. *A 2.5D Single Passage CFD Model for Centrifugal Pumps*. FEDSM98–4858. Proceedings of ASME Fluids Engineering Division Summer Meeting, June 21–25, 1998, Washington, DC.
4. Nakamura S, Yano K. Computational simulation of flows in an entire centrifugal heart pump. *Artif Organs* 1999;23(6):572–5.
5. Yano K, Nakamura S. *Flow Simulation of the IVAS Heart Pump Using a Parallel Computer, T3D.* FEDSM97–3439. Proceedings of ASME Fluids Engineering Division Summer Meeting, June 22–26, 1997, Vancouver, Canada.
6. Yano K, Nakamura S. *Computational Flow Simulation of an Entire Centrifugal Heart Pump using the Parallel Computer CRAY T3D.* 15th IMACS World Congreess, August 24–29, 1997, Berlin, Germany.
7. Ding W, Nakamura S. *Three-Dimensional Single Passage Simulation for the IVAS Centrifugal Pump.* FEDSM98–4989. Proceedings of ASME Fluids Engineering Division Summer Meeting, June 21–25, 1998, Washington, DC.
8. Nakamura S, Ding W. Computer simulation of blood flows in a rotary heart pump. *Artif Organs* (in press)
9. Nakamura S, Ding W, Smith WA, Golding LAR. Numerical flow simulation for the IVAS secondary impeller. *ASAIO J* 1999;45(1).
10. Nakamura S, Brodkey RS. *Computational and Experimental Study of the Fluid Flow in a Cylindrical Cavity with an Impeller Rotor at an Eccentric Location.* FEDS99–7193, Proceedings of 3rd ASME/JSME Joint Fluids Engineering Conference, July 18–23, 1999, San Francisco, CA.
11. Nakamura S, Bodkey RS. *Direct and Large Eddy Simulation of the Three-dimensional Unsteady Flows in the Counter-jet Mixing Vessel*. FEDS2000–11007, Proc. ASME Fluid Engineering Summer Conference, Boston, MA, 2000.
12. Nakamura S, Bodkey RS. *Computational Flow Analysis for the Chemical Mixing Vessel with Impeller and Baffles*. FEDS2000–11207. Proceedings of ASME Fluid Engineering Summer Conference, Boston, MA, 2000.
13. Miklosovic DS. *An Experimental Evaluation of the Non-Newtonian Scaling Effects in a Rotodynamic Left Ventricular Assist Device*. PhD Dissertation, The Ohio State University, 1999.
14. Miklosovic DS, Gregorek GM, Smith WA. *An Experimental Evaluation of the Non-Newtonian Scaling Effects in a Rotodynamic Left Ventricular Assist Device*. AIAA Fluid Dynamics Symposium, FLUIDS 2000, June 19–22, 2000, Denver.

Journal of Congestive Heart Failure and Circulatory Support (2001) Vol 1, No 4, 351–353

Development of the crank-motor vibrating flow pump for the left ventricular assist system

S. Kobayashi MD PhD[1], K. Imachi MD PhD[1], Y. Abe MD PhD[1], T. Isoyama MD PhD[1], S. Nitta MD PhD[2] and T. Yambe MD PhD[2]

[1]*Department of Biomedical Engineering Graduate School of Medicine, The University of Tokyo, Tokyo, Japan; and* [2]*Department of Medical Engineering and Cardiology, IDAC, Tohuku University, Sendai, Japan*

Abstract A new type of crank-motor actuator was used to improve the vibrating flow pump (VFP). The linear-motor actuator has the advantage of a flexible driving frequency and driving stroke, but it makes the total system heavy due to its low driving force within the target frequency (~10–40 Hz). The crank-motor structure has an advantage in that it enables an effective driving force within the target frequency, but it has a linear relationship between driving frequency and pumping output because of the fixed stroke of the crank. This linear relationship restricts the driving conditions. The newly designed crank-motor VFP is developed as a left ventricular assist system. It's driving condition was scheduled as 100 mm Hg/5 L min^{-1}/ ~20–25 Hz. A study determined that a driving stroke of 5 mm and a diameter of 10 mm were needed to drive the vibrating central tube. The trial crank-motor VFP was made to these specifications. The new VFP is 100 × 50 × 72 mm (L × W × H) and weighs 320 g. This pump almost satisfied the required pumping performance for left ventricular assistance. The new type crank-motor VFP may become a good pump with careful revision of its design and may be used in experiments for the studies of oscillated blood flow and impedance of the circulatory system.

Keywords vibrating flow pump, crank-motor actuator, oscillated blood flow, left ventricular assistance.

Introduction

High-frequency oscillated blood flow is generated by the vibrating flow pump (VFP). It has an oscillating effect on the arterial blood flow. The pumping performance of the steady flow (centrifugal) pump is excellent, in terms of its design, specifically its small size and high flow rate. However, an imbalance in blood circulation for each organ may be caused by its monotonic blood flow pattern.

Pulsatile blood flow may have some physiological advantages for organ blood circulation. The action of the 'pulse' to the blood vessels is still unclear, but blood flow allocation at the point of vascular branching may be influenced by pulsation. The elasticity of the vascular walls and the viscosity of blood may have an effect on pulsatile blood flow perfusion.

The mechanism for controlling oscillating blood flow is a recent development in artificial blood flow assistance. Oscillated blood flow consists of continuous flow and oscillation, as shown in Figure 1. The frequency of oscillation is ~10–40 Hz and the pressure width is approximately 30–40 mmHg. The oscillated blood flow feature may offer advantages in terms of high-flow efficiency and the possible effects of pulsation.

Background

The VFP has been developed as a left ventricular assist system (LVAS). It can generate a unique waving blood flow called 'oscillated blood flow'. High-frequency oscillated blood flow is now recommended for use in left ventricular assistance. Oscillation may change the flow pattern and distribution of blood to the arterial branches of each organ[1–3]. The driving frequency of the oscillated blood flow can be controlled by the motion of the central tube of the VFP.

Figure 2 shows the driving mechanism of the VFP. A jellyfish valve is mounted on the outlet side of the central tube. The piston motion and viscosity of the blood facilitate the segmental oscillated blood flow. The driving frequency of the central tube is equal to the frequency of the blood flow. The inline forward and backward motion of the central tube is the most important factor in the generation of oscillated blood flow. Figure 3 is a schematic illustration of the VFP. The previous pump used an electromagnetic linear actuator, which surrounded the central tube. The electromagnetic actuator can efficiently control driving frequency and moving stroke. The linear-motor VFP can easily control its driving frequency and pump output independently, but the electromagnetic actuator has a problem in terms of its weight, power and heat generation. In this study, the crank-motor structure is used in the new VFP to make the LVAS small and efficiently powered. The short-stroke and high-frequency driving, made possible by the crank-motor design, may allow for the development of a smaller-sized LVAS. Furthermore, if its driving frequency were carefully

Correspondence to: Shinichi Kobayashi, Department of Biomedical Engineering, Graduate School of Medicine, The University of Tokyo, 7–3–1 Hongo Bunkyo-ku, Tokyo 113-0033, Japan

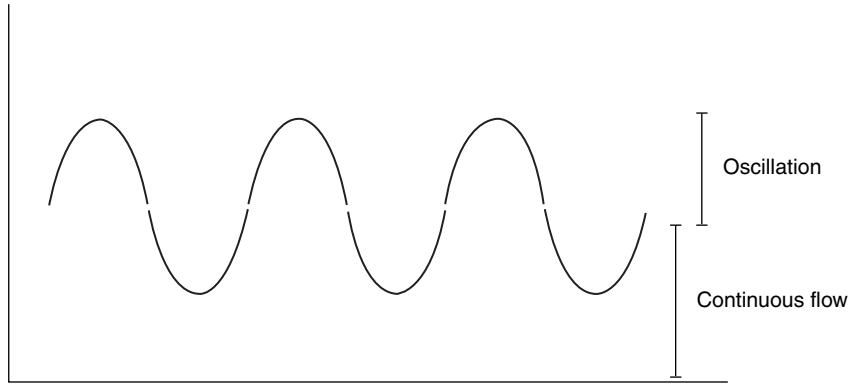

Figure 1. The oscillated flow of the VFP. The oscillated flow consists of two elements: continuous flow and oscillation. The continuous flow element creates an integrated flow rate. The oscillating element confers the benefits of pulsation.

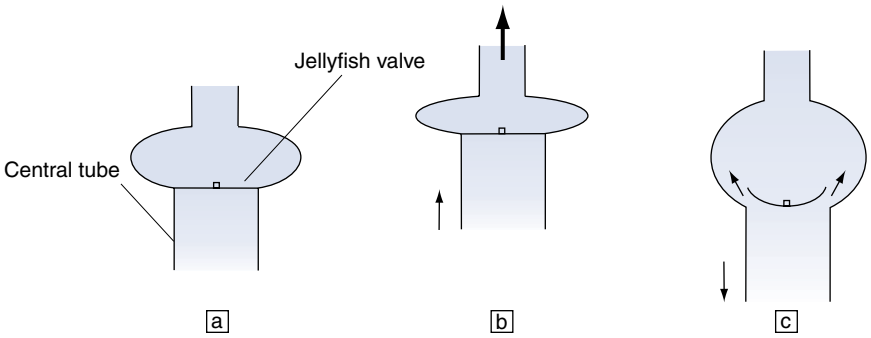

Figure 2. (a) The driving mechanism of the VFP. The oscillated flow is generated by the forward and backward motion of the central tube. (b) The piston motion facilitates the segmental blood flow. (c) The viscosity of the blood produces the continuous-flow portion of the process.

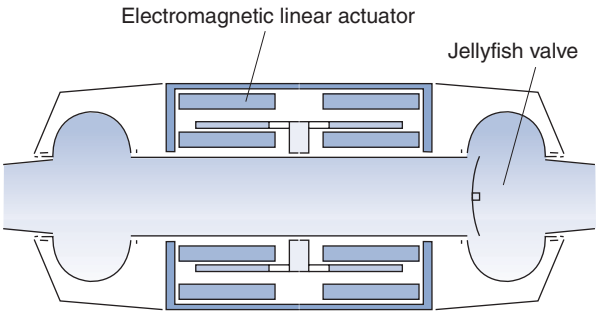

Figure 3. The electromagnetic actuator was used in the old type VFP. The electromagnetic linear motor was good for control of the driving frequency and moving stroke, but has some problems with its weight, power and heat generation.

considered, the artificial high-frequency oscillated blood flow may have the same advantageous effects for the arterial system as natural pulsatile blood flow circulation[4,5].

Results

The prototype crank-motor VFP was made for the mock circulation study (Figure 4). The diameter of the central tube is approximately 1.5 cm. A jellyfish valve (0.3 mm) is mounted on the outlet side of the central tube. The new VFP is 100 × 50 × 72 mm (L × W × H) and weighs 320 g. To create the inline forward and backward motion of the central tube, a straight slider is used to support the structure.

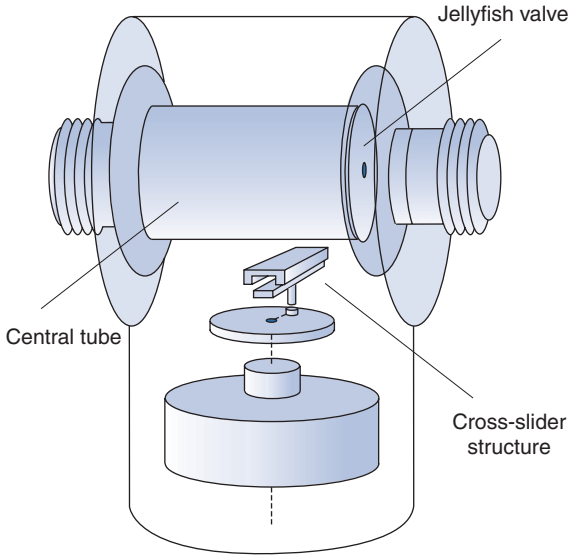

Figure 4. The new-type VFP is driven by the crank-motor actuator. The small LVAS may benefit from use of this new VFP system.

The crank system transforms the round motion to the forward and backward motion. In this study, a cross-slider structure is used in this new VFP system. Figure 5 shows the structure of the cross-slider. The supporting straight slider and moving slider are mounted between the central tube and the motor. The eccentric pivot connects the moving slider to the wheel of the motor. Effective actuation is

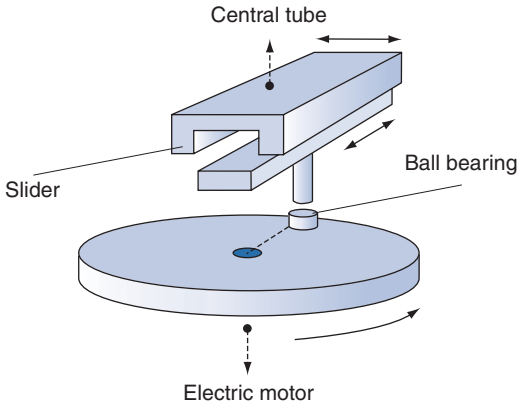

Figure 5. The cross-slider structure transforms the round motion of the electric motor into the linear forward and backward motion. The stroke of the crank motion depends on the eccentric pivot using a ball bearing.

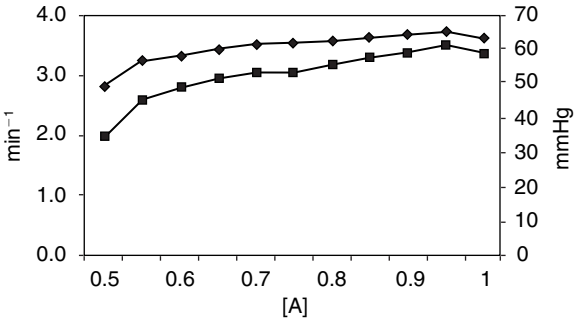

Figure 6. The pump performance of the new VFP. Appropriate pumping performance may be achieved with the suitable adjustment of the driving frequency and driving stroke. (■) press; (◆) flow.

facilitated by this cross-slider mechanism. Figure 6 shows the pumping performance of the new VFP in the mock circulation study. Pump output does not parallel changes in the driving frequency.

Discussion

Oscillated blood flow created by the VFP consists of two elements: continuous flow and oscillation. Short-stroke volume and high-frequency driving may be features that can facilitate development of a small pump system. A cross-slider structure can effectively transform the round motion of a crank motor into a forward and backward motion. The stroke of the central tube motion is decided by the eccentricity of the pivot of the cross-slider. In theory pump output is controlled by driving frequency; this means that output control should be equal to the change of the flow frequency. But actually, the frequency increment is not equal to the output increment (Figure 6). Due to the viscosity of the blood, it does not catch up with the acceleration of the fixed stroke motion of the central tube. The diameter of the central tube and moving stroke of the crank may be important to ensure good pump performance.

Driving frequency is an important factor in ensuring that the output control of the new-type VFP is within a suitable range. Suitable values of these factors may exist for the use of the left ventricular assistance. The crank-motor VFP may become a small and useful device for high-frequency oscillated blood flow driving[6,7]. Short-stroke and high-frequency driving may be good for the small implantable artificial heart device and the oscillatory effects may benefit organ blood circulation in a manner similar to natural pulsatile blood flow.

References

1. Yambe T, Nitta S, Sonobe T *et al*. Effect of left ventricular assistance on sympathetic tone. *Artif Organs* 1990;13:681–6.
2. Yambe T, Nitta S, Katahira Y *et al*. Postganglionic sympathetic nerve activity with correlation to heart rhythm during left ventricular assistance. *Artif Organs* 1991;15:212–7.
3. Yambe T, Nitta S, Katahira Y *et al*. Fundamental rhythm of sympathetic nerve discharges in animal with total artificial hearts. *ASAIO J* 1992;38:91–5.
4. Yambe T, Nitta S, Sonobe T *et al*. Chaotic hemodynamics during oscillated blood flow. *Artif Organs* 1994;18:633–7.
5. Yambe T, Sonobe T, Naganuma S *et al*. Fractal dimension analysis of the oscillated blood flow with a vibrating flow pump. *Artif Organs* 1995;19:729–33.
6. Kobayashi S, Nitta S, Yambe T *et al*. Experimental study of physiological advantages of assist circulation using oscillated blood flow. *Artif Organs* 1995;19:704–7.
7. Kobayashi S, Nitta S, Yambe T *et al*. Carotid arterial impedance during oscillated blood flow. *Artif Organs* 1994;18:627–32.

Session 8

Ventricular Assist Devices

Journal of Congestive Heart Failure and Circulatory Support (2001) Vol 1, No 4, 357–360

Assessment of sympathetic nerve activity in patients with long-term mechanical support

G. Matsumiya MD, S. Ohtake MD, M. Nishimura MD, Y. Sawa MD, N. Fukushima MD, S. Taketani MD, K. Horiguchi MD, S. Miyagawa MD and H. Matsuda MD

Department of Surgery, Course of Interventional Medicine, Division of Cardiovascular Surgery, Osaka University Graduate School of Medicine, Osaka, Japan

Background Myocardial recovery by ventricular unloading with mechanical circulatory support is reported to occur in some patients. However, the underlying mechanism is largely unknown. We analyzed changes in myocardial structure and sympathetic nerve activity during left ventricular assist system (LVAS) support using ^{123}I-metaiodobenzylguanidine (MIBG) cardiac imaging.

Methods Four nonischemic cardiomyopathy patients who underwent LVAS support over 6 months were analyzed with MIBG imaging. The ages ranged from 43–54 (mean 47.2) and all subjects were male. Two patients were diagnosed as having dilated cardiomyopathy and two as having the dilated phase of hypertrophic cardiomyopathy; one is waiting for heart transplantation and the other three patients have died. Myocardial structure was evaluated at the time of the LVAS implantation and at postmortem examination.

Results The heart:mediastinum ratio of MIBG uptake remained low and the wash-out rate was high; these did not show any improvement over time during the LVAS support. Through histological analyses, it was found that the area of fibrosis and cell diameter increased in all patients.

Discussion Despite the improvement of hemodynamic status, sympathetic nerve function assessed by MIBG imaging and histological recovery of myocardial structure was not observed. These results warrant further investigation on the utilization of MIBG imaging as a tool for evaluating myocardial recovery during LVAS support.

Keywords left ventricular assist device (LVAS), cardiomyopathy, MIBG imaging, sympathetic nerve activity.

Introduction

The increasing number of patients waiting for heart transplantation has stimulated investigation into the concept of myocardial recovery by ventricular unloading with assist devices. The successful explantation of the left ventricular assist device (LVAS) has been reported recently from several centers[1–3]. These reports demonstrated that sufficient recovery of the native heart function to allow the removal of LVAS does occur after a certain period of ventricular unloading in some patients, although the persistence of improved cardiac function is still unpredictable[1,2]. The mechanism of this phenomenon is largely unknown. However, improvements in hemodynamic status and unloading of the left ventricle with LVAS may facilitate the reversal of the overactivation of neurohormonal systems[4,5]. This may include the improvement of the sympathetic nerve function, up-regulation of α-receptor density, and reduction of adverse effects of cytokines and neurohormones. We investigated changes in the sympathetic nerve activity in cardiomyopathy patients who were supported with LVAS and evaluated the correlation between those changes and histological improvements.

Materials and methods

Four patients who underwent LVAS implantation and were supported over 6 months were included in this study. All patients were male and their ages ranged from 43–54 (mean 47.2 years). Two patients were diagnosed as having dilated cardiomyopathy (DCM), and two were in the dilated phase of hypertrophic cardiomyopathy (dHCM). At the time of LVAS implantation, all patients were at New York Heart Association class IV and required inotropic supports. Three patients were receiving intraaortic balloon pumping (IABP), one was receiving mechanical ventilation, and one percutaneous cardiopulmonary support. Two patients underwent Novacor LVAS (Baxter Co, Oakland, CA, USA) implantation and two had the National Cardiovascular Center (NCVC) TOYOBO LVAS (TOYOBO Co, Osaka, Japan). In the latter patient group, a left atrium (LA) inflow cannula was utilized. The two patients with NCVC-LA LVAS were switched to an implantable LVAS (one Novacor and one pneumatic HeartMate [Thermo Cardiosystems Inc, Woburn, MA, USA]) after 66 and 463 days of support respectively because of repeated thromboembolic events.

Correspondence to: Hikaru Matsuda, Professor and Chairman, Department of Surgery, Course of Interventional Medicine, Osaka University Graduate School of Medicine, 2–2 Yamadaoka, Suita, Osaka 565–0871, Japan.

^{123}I-metaiodobenzylguanidine (MIBG) imaging was obtained and analyzed as follows. An intravenous dose of 111 Mbq of commercially available MIBG (Daiichi Radioisotopes Laboratories, Tokyo, Japan) was given. Anterior planar images were obtained at 15 min (early) and 4 h (delayed) after the tracer injection. Average counts in the region around the left ventricle (H) and the upper mediastinum (M) were obtained. The H:M ratio was calculated to compare MIBG uptake by the heart in each individual. The wash-out rate (WR) was calculated using the following formula:

$$(H)_{early} - (H)_{delay} / (H)_{early}$$

A myocardial specimen was obtained, either from the apical cannulation site or endocardium during the LVAS implantation, and at the postmortem examination. Eight serial sections were obtained from each specimen, embedded in paraffin and stained with hematoxylin and eosin. The myocardial cell diameter was determined from 100 measurements of cross-sectioned myocyte at the level of the nucleus. The percentage of fibrosis (% fibrosis) was determined as the average of the ratio of the fibrosis area in the eight sections using an image-analyzing system.

Results

Three patients died after 195–548 (mean 329) days of LVAS support. The causes of death were cerebral accident in one patient and multiple organ failure (MOF) in the other two patients. The fourth patient has been waiting for cardiac transplantation on the LVAS support for 749 days.

MIBG uptake remained low after the initiation of the LVAS support. In the patient who was supported with the TOYOBO–LA drainage LVAS, MIBG distribution was assessed serially at months 4 and 8 after the implantation (Figure 1). The H:M ratio at the delayed phase remained below 1.5 (normal range 2.71–3.78) and the WR was above 45% (normal range 28.5 ± 7.8%). There was no improvement between these two time points. Figure 2 shows the serial MIBG imaging at the delayed phase in a patient supported with a Novacor device over 2 years. The H:M ratio got worse after 16 months of support compared to the preoperative value, and further decreased in the next 6 months. The WR did not improve in the 2 years of support. The changes in the H:M ratio and WR are plotted in Figure 3. In the other two patients evaluated at the second month after the LVAS implantation, the H:M ratio at the delayed phase was low compared to the normal range.

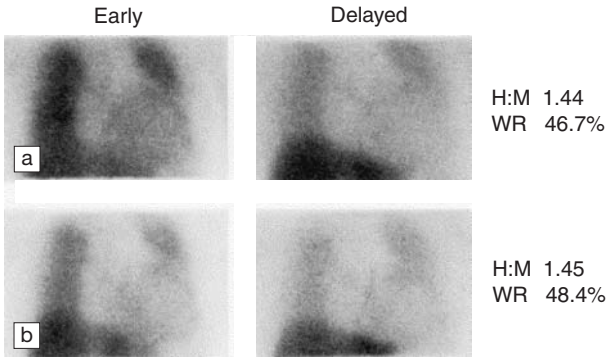

Figure 1. ^{123}I-MIBG imaging was assessed in a patient supported with the NCVC-TOYOBO LVAS with left atrial drainage. MIBG planar view at early (15 min after tracer injection) and delayed (4 h after tracer injection) phases at (a) 4 months and (b) 8 months after the LVAS implantation. The images show a low H:M ratio and increased wash-out rate at each point, which did not improve with LVAS support.

Both % fibrosis and cell diameter increased significantly at the time of transplantation or autopsy compared to preoperative values in all three patients evaluated at postmortem examination (Figure 4).

Discussion

There have been conflicting reports regarding myocardial recovery by ventricular unloading with LVAS[1–3,6,7]. Early reports on successful removal of LVAS recognized this as an extremely rare phenomenon that may occur in hearts affected with severe inflammatory damage or temporary normalization of systolic function that eventually fail with natural disease processes[6,7]. However, a recent series of patients reported by Hetzer *et al.*[1], demonstrated that this phenomenon can be observed even in patients with idiopathic cardiomyopathy and some patients maintain the recovered cardiac function for a long time. However, the parameters to predict the persistence of sustained

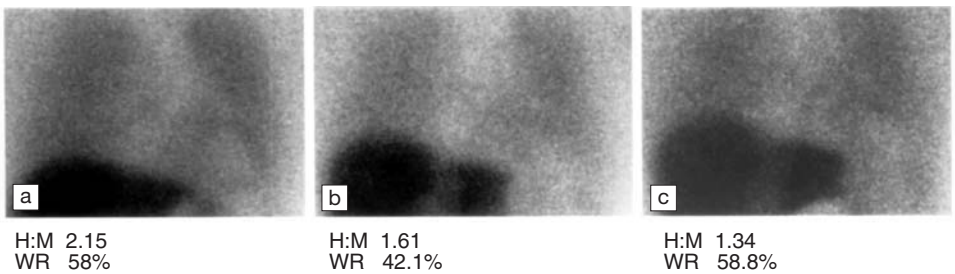

Figure 2. ^{123}I-MIBG planar view imaging at delayed phase (4 h after the tracer injection) in a patient who has been supported with Novacor LVAS for 2 years (a) before the LVAS implantation, at (b) 16 months after the LVAS implantation and (c) 22 months after the LVAS implantation is shown. The H:M ratio decreased and the wash-out rate did not improve during the LVAS support.

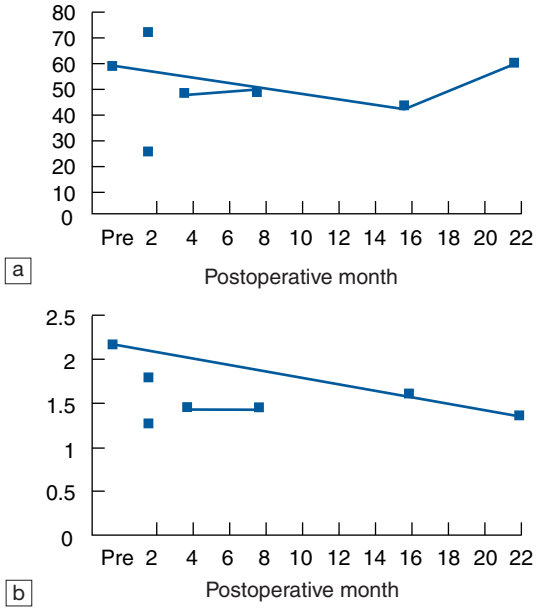

Figure 3. The changes in (a) wash-out rate and (b) H:M ratio in four patients are plotted.

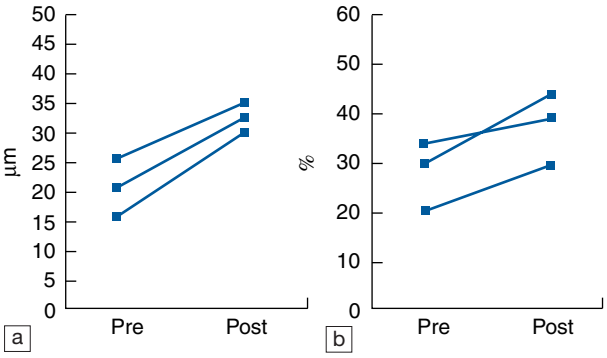

Figure 4. The changes in cell diameter (a) and % fibrosis (b) at the time of LVAS implantation and at the postmortem examination over 6 months of LVAS support.

recovery of cardiac function after LVAS removal are not available. In Japan it is difficult to successfully treat patients with a failed LVAS removal because there are very few available heart donors. This situation precludes the application of this strategy in clinical practice. Therefore, a clinical test designed to evaluate myocardial structure and support sustained recovered cardiac function is mandatory.

^{123}I-MIBG imaging has been utilized to evaluate sympathetic nerve activity. ^{123}I-MIBG is a radio-labeled norepinephrine (NE) analogue that, like NE, is taken up into the sympathetic nerve terminals, stored in the vesicles and released into the synaptic cleft. Therefore, this method has enabled the assessment of NE uptake and storage *in vivo*. In cardiomyopathy patients, diminished MIBG uptake and an increased MIBG WR secondary to sympathetic nerve overactivation has been reported[9,10]. The degree of these impairments has been reported to be well correlated with the prognosis of patients with congestive heart failure. A low H:M ratio at the delayed phase reflects impaired uptake into the vesicles and increased wash out from the synaptic cleft. Merlet *et al*. reported that ischemic and idiopathic cardiomyopathy patients with H:M ratios below 1.2 have poorer prognoses compared to patients with H:M ratios above 1.2[9]. Suwa *et al.* demonstrated that an H:M ratio of 1.7 on the delayed image provides a useful indicator to select the DCM patients who will respond well to β-blocker therapy and recover cardiac function[10]. Except for one patient, the H:M ratio remained or decreased below 1.7 in our patient group. Whether WR is the other index predicting poor prognosis of DCM patients is still controversial. However, WR in our patient group remained above 45%, which is the reported range associated with poor response to β-blocker therapy[10]. Therefore, our results suggest that despite unloading of the ventricle, sympathetic nerve activity does not improve and even deteriorates during LVAS support in the present patient group.

Histological evaluation of % fibrosis and cell diameter also worsened with time during LVAS support in our patients. This is consistent with the findings McCarthy *et al*. have previously reported[6]. They demonstrated the improvement of acute myocyte damage including a number of wavy fibers and contraction band necrosis, but also showed an increase of fibrosis and cell diameter during LVAS support. On the contrary, Mueller *et al*. reported the improvement of fibrosis in patients recovered cardiac function and were successfully removed from LVAS[2]. Further studies are needed to analyze the factors that promote this difference, but several possibilities exist. First, the number of patients in this study might be too small to include a patient who has myocardial recovery, which is considered a relatively rare phenomenon. Secondly, this study includes two patients in the dilated phase of hypertrophic cardiomyopathy, which is known to have a poorer prognosis compared to DCM[11]. The timing of the evaluation may be another issue. A recent report suggests that there is an optimal timing of recovery in each patient[1], which may be later or even earlier than when our patients underwent evaluation. The last point may indicate the most important direction for future investigation. If recovery does occur, there may exist specific treatments that facilitate that process. β-blocker therapy or gradual ventricular loading with weaning protocol[1,2] were not utilized in this study but could be the potential modality for this goal.

In summary, sympathetic nerve function assessed by MIBG imaging and histological recovery of myocardial structure were not observed in our patients with long-time mechanical left ventricular support. These results warrant further investigation on the utilization of MIBG imaging as

a tool for evaluating myocardial recovery during LVAS support.

References

1. Hetzer R, Muller J, Weng Y *et al.* Cardiac recovery in dilated cardiomyopathy by unloading with a left ventricular assist device. *Ann Thorac Surg* 1999;68:742–9.
2. Mueller J, Wallukat G, Weng Y *et al*. Weaning from mechanical cardiac support in patients with idiopathic dilated cardiomyopathy. *Circulation* 1997;96:542–9.
3. Frazier OH, Myers TJ. Left ventricular assist system as a bridge to myocardial recovery. *Ann Thorac Surg* 1999; 68:734–41.
4. James KB, McCarthy PM, Thomas JD *et al.* Effect of the implantable left ventricular assist device on neuroendocrine activation in heart failure. *Circulation* 1995;92(Suppl II):II-191–5.
5. Estrada-Quintero T, Uretsky BF, Murali S *et al.* Neurohormonal activation and exercise function in patients with severe heart failure and patients with left ventricular assist system. A comparative study. *Chest* 1995;107:1499–503.
6. McCarthy PM, Nakatani S, Vargo R *et al.* Structural and left ventricular histologic changes after implantable LVAD insertion. *Ann Thorac Surg* 1995;59:609–13.
7. Levin HR, Oz MC, Catanese KA *et al.* Transient normalization of systolic and diastolic function after support with a left ventricular assist device in a patient with dilated cardiomyopathy. *J Heart Lung Transplant* 1996;15:840–2.
8. Westaby S, Jin XY, Katsumata T *et al.* Mechanical support in dilated cardiomyopathy: signs of early left ventricular recovery. *Ann Thorac Surg* 1997;64:1303–8.
9. Merlet P, Valette H, Dubois Rande JL *et al.* Prognostic value of cardiac MIBG imaging in patients with congestive heart failure. *J Nucl Med* 1992;33:471–7.
10. Suwa M, Otake Y, Moriguchi A *et al.* Iodine-123 metaiodobenzylguanidine myocardial scintigraphy for prediction of response to β-blocker therapy in patients with dilated cardiomyopathy. *Am Heart J* 1997;133:353–8.
11. Fukushima N, Ohtake S, Sawa Y *et al.* Predicting outcomes and management of candidates for heart transplantation. *Transplant Proc* 1999;31:1961–2.

Journal of Congestive Heart Failure and Circulatory Support (2001) Vol 1, No 4, 361–370

Home discharge of patients with a modified HeartMate IP LVAD: a feasibility study

T.B. Icenogle MD, D. Sandler, D.J. Sato, S.C. Himley and M.P. Puhlman
Inland Northwest Thoracic Organ Transplant Program, Heart Institute of Spokane and Sacred Heart Medical Center, Spokane, WA, USA

Background The purpose of this study was to investigate the feasibility of patients with left ventricular assist device (LVAD) implants living outside the hospital.

Methods One female and six male patients were discharged home on the HeartMate IP LVAD, six with a modified hospital console and one with the HeartPak portable driver. The LVAD was modified in five patients and the surgical procedure changed to decrease complications and facilitate recovery. Protocols were developed for routine care and emergencies in the community. A second drive console and hand pump were available in case of failure.

Results The average implant duration was 173 days (range 73–284 days) (n=7). The average time from implantation to discharge was 63 days (range 29–128 days). The patients expressed an increase in perceived quality of life over living in the hospital. The average cost savings was $66 720 per patient.

Discussion Seven patients were bridged to transplant and are alive as of this writing. The conclusion of this small feasibility study was that patients could safely be discharged home with the HeartMate IP LVAD. From this experience a 50-patient, nonrandomized, single center (The Heart Institute of Spokane, WA, USA) safety study entitled Pneumatic HeartMate Assist as Destination Evaluation (PHADE) has begun to study the HeartMate IP and the HeartPak, a 20 lb portable driver, as a destination therapy for non-transplant candidates.

Keywords left ventricular assist device (LVAD), permanent, artificial heart, PHADE, HeartMate, HeartPak.

Introduction

Annually, 40 000 people in the USA could benefit from a heart transplant[1] but only 2400 donors are available. Today, increasing numbers of people wait on the transplant list in the USA[2], and more patients receive a left ventricular assist device (LVAD) as a bridge to transplant[3]. As transplant waiting times stretch from months to years[2], it is essential that LVAD patients wait at home for improved quality of life and cost savings. Since most people with end-stage heart disease will not get a transplant, the need for an assist device for destination therapy is also clear.

The ideal LVAD must be simple enough for a trained layperson to operate and portable enough that the patient can move about the community and enjoy a reasonable quality of life. Back-up systems must be available for failures. Freedom from stroke and long-term durability are imperative for patient peace of mind. The HeartMate IP has a favorable history when used in the hospital as a bridge to transplant. The *in vitro* life test data of the HeartMate IP suggest that the device could provide excellent long-term support and might be superior to the HeartMate VE (Figure 1). Our team, responding to the demands of patients waiting in house on the HeartMate IP, sought to develop a system to discharge patients to home for both a bridge to transplant and for destination therapy.

Methods

The protocols and procedures were developed to discharge HeartMate IP LVAD patients from the hospital. Consent forms, operative and postoperative protocols, patient checklists and educational materials were developed. Local Institutional Review Board (IRB) approval was received.

Ten patients were implanted with HeartMate IP LVADs between October 1994 and June 1999 at Sacred Heart Medical Center, Spokane WA, USA. Of these ten patients, one was confined to the intensive care unit (ICU) until death, one was transplanted within 41 days of implantation, and one had no caregiver assistance (required under the home discharge protocol). The remaining seven patients (one female and six males) together with their caregivers were asked to participate in this study.

The operative technique was developed over the course of the study. Extensive consultation between the team engineers and the surgeons facilitated the changes. Prior to this study, the driveline exit in the left lower quadrant was problematic. Patients complained that the stiff hose caused pressure while sitting. The subcutaneous tunnel was short in smaller patients, increasing the chance of a driveline and pocket infection. All patients in this study had the percutaneous driveline exit on the right abdomen, providing a long

Correspondence to: Timothy B. Icenogle, Suite 532, 105 West 8th Avenue, Spokane, WA 99204–2236, USA.

subcutaneous driveline and improving patient comfort. Experience revealed that the driveline could kink if it was brought out in the right lower quadrant (Figure 2). To decrease strain on the driveline, team engineers modified the HeartMate IP percutaneous driveline in the operating room on the last five patients. One patient weighing 44.7 kg (1.46 m^2 BSA) was under the body surface area criterion for implantation of the HeartMate IP. To facilitate fit, the valves were reversed, the device was implanted upside down, and the driveline was rotated (Figure 3). Without the rotation, the unmodified driveline would have exited in the groin. In the last four patients the driveline was rotated from its 180° position to 235° (Figure 4).

All operating team members with proximity to the HeartMate wore sterile hood systems to decrease the chance of a device infection. The use of the full-body isolation gowns was prompted by the high infection rates reported in the literature. The orthopedic literature has documented the efficacy of using these systems when implanting large orthopedic prostheses[4].

The prolonged operative time and excessive bleeding[5] associated with HeartMate implantation prompted changes in the implant procedure. The preperitoneal pocket dissection can lead to diffuse bleeding and a peritoneal placement can lead to bowel erosion[6] and other complications. In the last four patients, a 26 × 34 cm sheet of Gore-Tex Dual Mesh Plus Biomaterial with Holes (Item # 1DLMPH08, WL Gore & Associates Inc., Flagstaff, AZ, USA) was used as a 'pseudoperitoneum' to separate the HeartMate IP from the abdominal contents using the peritoneal location. This hernia repair fabric has a smooth side that faces the bowel to reduce adhesions. The mesh biomaterial was used to prevent bowel complications, reduce intraoperative bleeding, decrease the duration of the operation, and prevent hernia complications (Figures 5 and 6). The mesh biomaterial was secured using an Auto Suture ProTack (Item # 174006, Auto

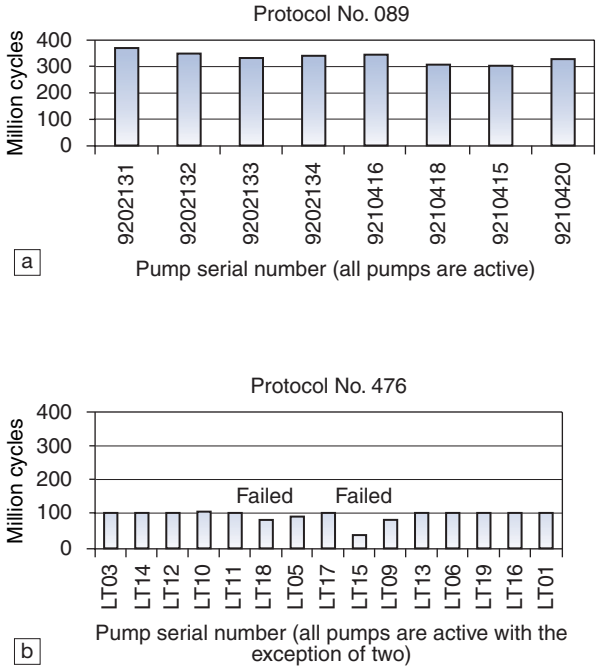

Figure 1. A comparison of the life test data of the HeartMate IP (a) and the HeartMate VE (b) shows that the HeartMate IP performed longer. As of January 26, 2000, there had been no failures in the HeartMate IP group (n=8) while there had been two failures in the HeartMate VE group (n=15). Data from ThermoCardiosystems Inc.

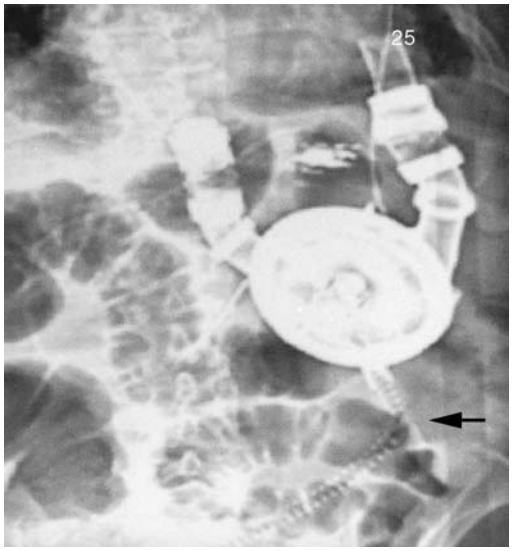

Figure 2. This abdominal X-ray of a HeartMate IP patient without driveline rotation shows a kink (arrow) in the driveline with a right lower quadrant exit site.

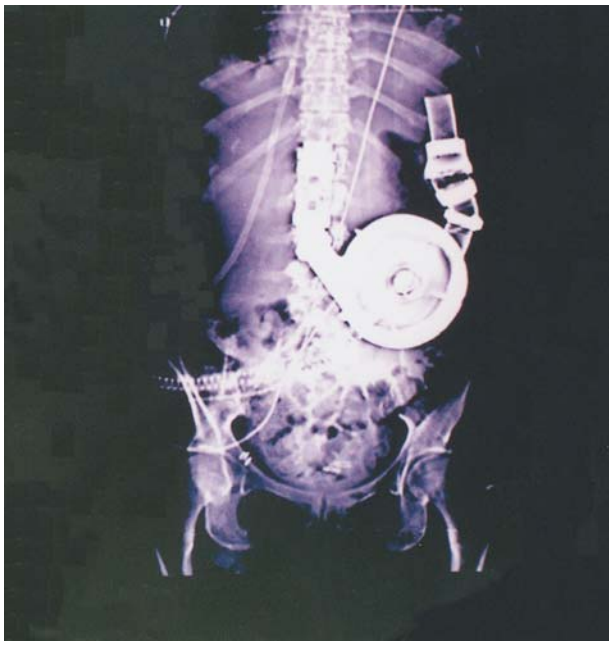

Figure 3. CT scan abdominal X-ray of patient weighing 44.7 kg. (1.46 m^2 BSA) shows the HeartMate IP implanted upside down with valves reversed and driveline rotated to facilitate fit.

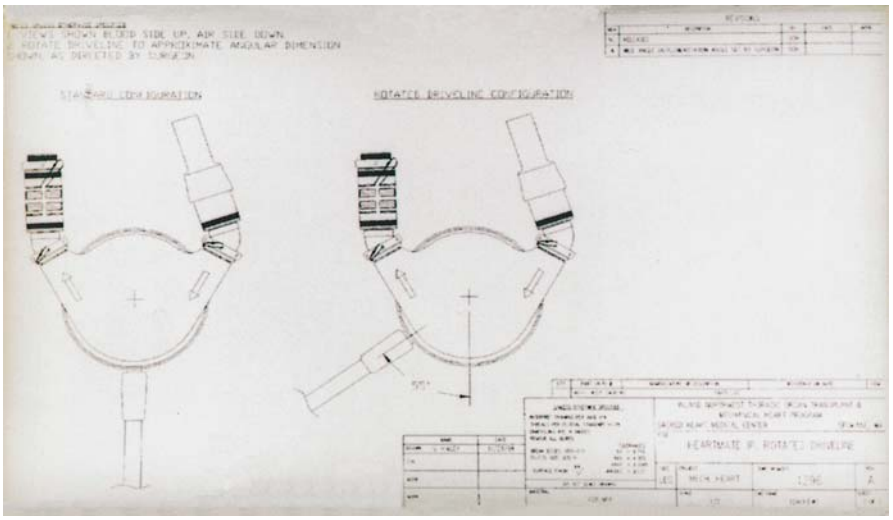

Figure 4. Driveline rotation of the HeartMate IP from 180° to 235° with a 55° rotation of the driveline clockwise.

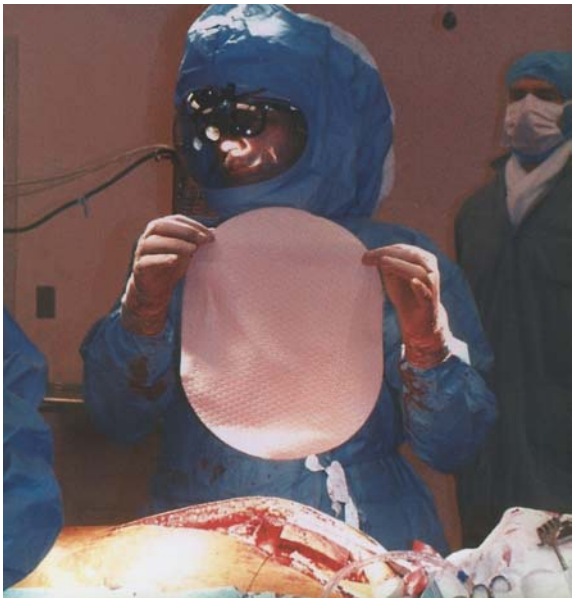

Figure 5. The implanting surgeon in an isolation hood system holds the Gore-Tex Dual Mesh Biomaterial with Holes prior to implantation in the peritoneal cavity.

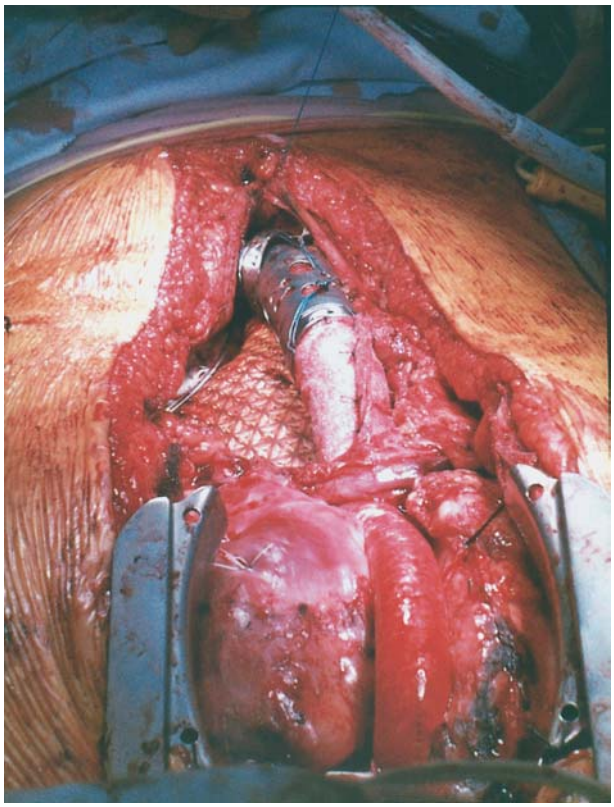

Figure 6. The HeartMate IP lies in the peritoneal cavity anterior to the Gore-Tex Dual Mesh Biomaterial, which separates it from the bowel.

Suture Inc., Norwalk, CT, USA) and interrupted 3-0 Prolene suture. A pursestring stitch of 3-0 Prolene was placed around the driveline exit site on the peritoneum to decrease peritoneal fluid from draining along the driveline. A 31 mm Auto Suture Premium Plus CEEA Stapler (Auto Suture Inc., Norwalk CT, USA) was used to cut a round hemostatic hole through the diaphragm for device inflow. The lie of the HeartMate IP in the abdomen can be changed prior to closure by adjusting the driveline to find the best fit for the patient.

Postoperatively, all patients and caregivers were given extensive training about the HeartMate IP LVAD. Emergency procedures were reviewed as well as the routine care of the system and driveline site. A checklist was used to assure that all information was reviewed with each patient and companion. All patients and companions were required to demonstrate the critical skills needed to care for the system.

Six patients went home on a modified hospital drive console called the 'Montana Driver' (Figure 7). Team engineers developed a console cart with a low center of gravity (to minimize the chance of overturning) and a lift point for easy hoisting. Team engineers built a lifting hoist for patients'

Figure 7. The patient (woman) adjusts the lift system on her minivan in preparation to load her Montana driver with assistance from her husband.

vehicles. Since the HeartMate drive console only has 45 min of battery life, a gel cell battery together with a battery charger and inverter were attached to the console to provide 6 h of battery life before recharging. A power supply was integrated into the electrical system of the vehicle to power the console while in transit, giving unlimited range. The entire modified console/cart battery system weighed 165 lb (75 kg).

The seventh patient was discharged on the HeartPak Portable Pneumatic Driver (Figure 8). This driver weighs 20 lb (9.3 kg) and measures 14 × 9 × 6 in (36 × 23 × 15 cm). It can be carried by handle, pulled on a trolley or carried in a backpack for maneuvering over rough terrain. Four rechargeable sealed lead acid batteries provide 4–6 h of power. The batteries are recharged in the power base unit (PBU). AC household current through the PBU can also power the HeartPak. DC power from an automobile cigarette lighter can run an inexpensive inverter to create AC power to run the PBU, giving an unlimited range for automobile travel.

The patients were discharged to their homes in Spokane, WA, USA. Each patient was seen in clinic once a week until it was felt that they were comfortable in the community and no adverse events were occurring. They were then assessed every second week. Each patient carried a hand pump in the event of catastrophic driver failure. They also carried an extra set of batteries for the HeartPak in case of battery depletion, and each patient had a back-up driver at home.

The number of days outside of the hospital while on LVAD support was calculated and multiplied by the average charge per day for an LVAD patient to stay in the hospital while awaiting transplant. The charge per day for an LVAD patient to stay in hospital was calculated from hospital charge sheets minus pharmacy, laboratory and radiology charges.

Quality of life was measured retrospectively using a time trade-off questionnaire (Appendix). Assuming a life expectancy of 5 years on the LVAD, patients were asked to trade-off life expectancy for perfect health. The perceived quality of life with an LVAD for 5 years was compared to perfect health for shorter periods of time. Perceived quality of life with an LVAD outside the hospital for 5 years was compared to that with an LVAD inside the hospital.

Results

Seven HeartMate IP LVAD patients were discharged to home between February 1995 and June 1999 (Table 1). These seven patients accumulated a total of 1214 days on the device. Of these, 708 days (57% of the total implant time) were spent at home, away from the hospital. The average time from implant to discharge was 62 days; the average time at home was 101 days. Examining the last five implants enrolled in the study, after the 'learning curve' had flattened, the average time from implant to discharge was 39 days.

Of the seven patients, four had re-admissions to the hospital, resulting in a total of 63 hospital days. These rehospitalizations were for a recurrent ileus (7, 2, and 1 days), a respite from self-care due to depression (10 days), a VAD pocket infection requiring i.v. antibiotics (25 days), hypovolemia (1 day), gout of the knee leaving the patient unable to walk (3 days), and a full cardiac arrest due to Torsades de Pointes (14 days).

The patient who arrested at home with ventricular arrhythmias had previously been implanted with an AICD. On the morning of his arrest, the AICD defibrillated the patient six times without converting. The LVAD maintained a flow of 3 L min^{-1} until the patient could be transported to the emergency room for definitive care.

One patient experienced a leak in the drive console diaphragm. This resulted in an increase in the venting frequency required by the console. The patient called the mechanical heart specialist, who directed the patient to change to the back-up console, which was done without problem. The patient using the HeartPak driver has had numerous nuisance problems and has changed drivers many times. Changing drivers has been well tolerated in this patient, who has severe biventricular failure.

The quality of life improved with discharge from the hospital. The quality of life average index improved from 0.60 to 0.77 (where 0 is death and 1 is perfect health). Patients were able to travel, fish, hike, shop, dine out and go to the theater. Two patients admitted that they drove vehicles

Table 1. Patient characteristics

Patient no.	Age	Sex	Weight (kg)	BSA	Etiology of myopathy	Total implant days	Implant to initial discharge	Total days at home	No. re-admissions	Total re-admission days	Causes of re-admissions
1	42	M	70	1.88	Ischemic	236	117	109	3	10	Recurrent ileus
2	51	M	100	2.27	Viral	203	128	75	0		
3	41	F	45	1.46	Idiopathic	223	59	154	1	10	Respite from self-care
4	57	M	66	1.77	Ischemic	60	39	21	0		
5	52	M	84	2.0	Ischemic	134	38	96	0		
6	62	M	93	2.1	Ischemic	74	29	20	1	25	VAD pocket infection
7	54	M	71	1.85	Idiopathic	284	31	233	3	18	● Hypovolemia ● Gout flair with inability to walk ● Ventricular fibrilation arrest

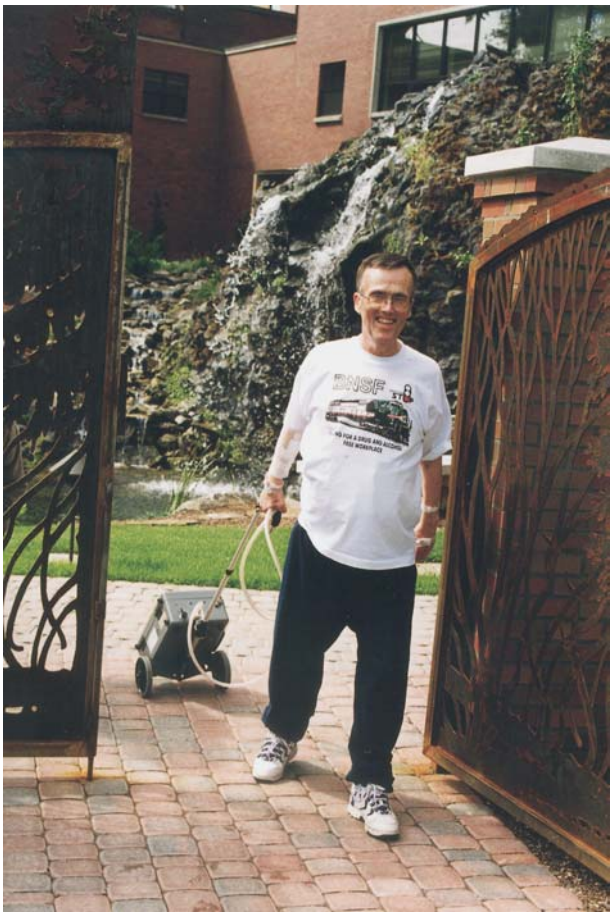

Figure 8. Patient walks with the HeartPak portable driver outside the hospital.

despite instructions to the contrary. They participated in a rehabilitation program and were able to interact with family members in their homes. All seven patients were bridged to transplant and are alive as of this writing.

The cost savings from hospital discharge were $467 099 or $66 720 per patient.

Discussion

The HeartMate IP LVAD was designed initially for in-hospital use as a bridge to transplant. The original hospital console was not designed for home use. The present configuration of the HeartMate IP with the driveline at 180° and skin exit in the left lower quadrant makes the device uncomfortable and unsuitable for long-term support, and it was difficult to implant in smaller patients.

Exiting the driveline on the right abdomen, rotating the driveline, and modifying the hospital console enabled HeartMate IP LVAD patients to be discharged from the hospital.

Use of the Gore-Tex biomaterial obviates the need for a preperitoneal pocket, a site for diffuse bleeding in the patient who is frequently debilitated and has hepatic congestion. It also prevents the problems with the peritoneal placement, such as bowel erosion and adhesion, and enabled easy device removal at transplant. This could be beneficial if device replacement became necessary in a destination therapy patient.

The value of the quality of life data is limited by the small sample size, the retrospective accumulation of the data, and the fact that patients were on two different drive systems. However, all patients expressed appreciation for discharge from the hospital, and thus the opportunity to live life on their terms. The use of electrical power from their vehicle to run the hospital driver and the HeartPak increased the patients' freedom to travel. The HeartPak portable driver

significantly improved the mobility of the most recent patient as compared to the modified hospital console.

Considerable cost savings can be realized by discharge from the hospital. In this preliminary study, nearly $67 000 was saved per patient. This savings would have been more if the first two patients, who were included early in our learning curve, had been discharged earlier. Aggressive efforts to minimize costs will open this therapy to broader segments of the population.

No failures of the HeartMate IP occurred in the seven patients in the study. This system appears to be durable and reliable, such that it enables patients to function well in the community. One patient, in consultation with the mechanical heart specialist, easily managed a drive console failure. The problems with the HeartPak driver appear to be related to its analog circuitry and will be addressed in the soon to be released HeartPak II driver with digital circuitry. All rehospitalizations in the study, except for the LVAD pocket infection, were due to the patients' underlying disease processes and not to the device.

The patients and their caregivers demonstrated through the use of testing, checklists and return demonstrations, an understanding of the device and its care. The HeartMate IP LVAD appears simple enough for the average individual to learn. The high survival rate in this small series may be a result of better conditioning of LVAD patients before transplant.

Based on this feasibility study, we hypothesize that the HeartMate IP LVAD could be used for destination therapy.

A 50-patient, nonrandomized, single-center safety study entitled Pneumatic HeartMate Assist as Destination Evaluation (PHADE) was initiated to study the HeartMate IP and HeartPak portable driver for destination therapy for nontransplant candidates. Patients may come from anywhere in the world. This FDA-approved clinical trial is available at The Heart Institute of Spokane, Spokane, WA, USA (www.this.org).

References

1. Torre-Amione G, Kapadia S, Short D, Young JB. Evolving concepts regarding selection of patients for cardiac transplantation. *Chest* 1996;109:223–32.
2. 1998 Annual Report of the US Scientific Registry for Transplant Recipients and the Organ Procurement and Transplantation Network: Transplant Data: 1988–1997. US Department of Health and Human Services, Health Resources and Services Administration, Office of Special Programs, Division of Transplantation, Rockville, MD; UNOS, Richmond, VA, USA.
3. Personal Communication: Tim Krauskopf, Vice President for Regulatory Affairs, Thermo Cardiosystems Inc., Woburn, MA, USA. Data from voluntary registry February 29, 2000.
4. An YH, Friedman RJ. Prevention of sepsis in total joint arthroplasty. *J Hosp Infect* 1996;33:93–108.
5. Frazier OH, Rose EA, Macmanus Q *et al*. Multicenter evaluation of the HeartMate 1000 IP left ventricular assist device. *Ann Thorac Surg* 1992;53:1080–90.
6. Philips WS, Burton NA, Macmanus Q, Lefrak EA. Surgical complications in bridging to transplantation: The Thermo Cardiosystems LVAD. *Ann Thorac Surg* 1992; 53:482–6.

Appendix

Inland Northwest Thoracic Organ Transplant and
Mechanical Heart Program at February 21, 2000
The Heart Institute of Spokane and
Sacred Heart Medical Center

Patient Name _____ Date _____

The following is a tool to assess your quality of life under two conditions in your past experience.

Hospitalized on IP LVAD

Remember what your experience was like while implanted with the HeartMate IP LVAD before going home. Imagine that you were back in the hospital on the IP Console and could not be transplanted. Imagine that you would remain there for 5 years and then die.

Suppose a simple new treatment became available that would relieve you of the need for the HeartMate IP LVAD and its care. This new treatment would be free, painless and have no risks. You would feel in perfect health and be free of the hospital and any health care needs.

Now imagine you have a choice. You could spend your remaining life (5 years) on the HeartMate IP Console in the hospital, or you could have perfect health but live fewer years.

Which do you prefer?

Directions:
1. Put an 'X' in the box next to the choice you prefer.
2. Please choose 1 answer for *every* question, until you choose B.
3. Once you choose B, you may stop.

Choice A		Choice B
1. Living in the hospital on the HeartMate IP Console for 5 years, then die	☐ or ☐	Painless death today (give up 5 years)
2. Living in the hospital on the HeartMate IP Console for 5 years, then die	☐ or ☐	Perfect health for 3 months, then die (give up 4 years, 9 months)
3. Living in the hospital on the HeartMate IP Console for 5 years, then die	☐ or ☐	Perfect health for 6 months, then die (give up 4 years, 6 months)
4. Living in the hospital on the HeartMate IP Console for 5 years, then die	☐ or ☐	Perfect health for 9 months, then die (give up 4 years, 3 months)
5. Living in the hospital on the HeartMate IP Console for 5 years, then die	☐ or ☐	Perfect health for 1 year, then die (give up 4 years)
6. Living in the hospital on the HeartMate IP Console for 5 years, then die	☐ or ☐	Perfect health for 1 year 3 months, then die (give up 3 years, 9 months)
7. Living in the hospital on the HeartMate IP Console for 5 years, then die	☐ or ☐	Perfect health for 1 year 6 months, then die (give up 3 years, 6 months)
8. Living in the hospital on the HeartMate IP Console for 5 years, then die	☐ or ☐	Perfect health for 1 year 9 months, then die (give up 3 years, 3 months)

Figure 9. Time trade-off questionnaire: IP LVAD, hospitalized and home.

Choice A		Choice B
9. Living in the hospital on the HeartMate IP Console for 5 years, then die	☐ or ☐	Perfect health for 2 years, then die (give up 3 years)
10. Living in the hospital on the HeartMate IP Console for 5 years, then die	☐ or ☐	Perfect health for 2 years 3 months, then die (give up 2 years, 9 months)
11. Living in the hospital on the HeartMate IP Console for 5 years, then die	☐ or ☐	Perfect health for 2 years 6 months, then die (give up 2 years, 6 months)
12. Living in the hospital on the HeartMate IP Console for 5 years, then die	☐ or ☐	Perfect health for 2 years 9 months, then die (give up 2 years, 3 months)
13. Living in the hospital on the HeartMate IP Console for 5 years, then die	☐ or ☐	Perfect health for 3 years, then die (give up 2 years)
14. Living in the hospital on the HeartMate IP Console for 5 years, then die	☐ or ☐	Perfect health for 3 years 3 months, then die (give up 1 year, 9 months)
15. Living in the hospital on the HeartMate IP Console for 5 years, then die	☐ or ☐	Perfect health for 3 years 6 months, then die (give up 1 year, 6 months)
16. Living in the hospital on the HeartMate IP Console for 5 years, then die	☐ or ☐	Perfect health for 3 years 9 months, then die (give up 1 year, 3 months)
17. Living in the hospital on the HeartMate IP Console for 5 years, then die	☐ or ☐	Perfect health for 4 years, then die (give up 1 year)
18. Living in the hospital on the HeartMate IP Console for 5 years, then die	☐ or ☐	Perfect health for 4 years 3 months, then die (give up 9 months)
19. Living in the hospital on the HeartMate IP Console for 5 years, then die	☐ or ☐	Perfect health for 4 years 6 months, then die (give up 6 months)
20. Living in the hospital on the HeartMate IP Console for 5 years, then die	☐ or ☐	Perfect health for 4 years 9 months, then die (give up 3 months)
21. Living in the hospital on the HeartMate IP Console for 5 years, then die	☐ or ☐	Perfect health for 4 years 10 months, then die (give up 2 months)
22. Living in the hospital on the HeartMate IP Console for 5 years, then die	☐ or ☐	Perfect health for 4 years 11 months, then die (give up 1 month)
23. Living in the hospital on the HeartMate IP Console for 5 years, then die	☐ or ☐	Perfect health for 5 years, then die (give up no time)

Figure 9. (Continued)

At Home on the IP LVAD

Remember what your experience was like while implanted with the HeartMate IP LVAD and discharged from the hospital. Imagine yourself on the HeartMate IP LVAD, living in the Spokane community, but without the possibility of transplantation. Imagine you would be in this situation for 5 years and then die.

Suppose a simple new treatment became available that would relieve you of the need for the HeartMate IP LVAD and its care. This new treatment would be free, painless and have no risks. You would feel in perfect health and be free of the HeartMate IP LVAD and any health care needs.

Now imagine you have a choice. You could spend your remaining life (5 years) on the HeartMate IP LVAD living in the Spokane community, or you could have perfect health but live fewer years.

Which do you prefer?

Directions:

1. Put an 'X' in the box next to the choice you prefer.
2. Please choose 1 answer for every question, until you choose B.
3. Once you choose B, you may stop.

Choice A		Choice B
1. Living in the Spokane community on the HeartMate IP LVAD for 5 years, then die	☐ or ☐	Painless death today (give up 5 years)
2. Living in the Spokane community on the HeartMate IP LVAD for 5 years, then die	☐ or ☐	Perfect health for 3 months, then die (give up 4 years, 9 months)
3. Living in the Spokane community on the HeartMate IP LVAD for 5 years, then die	☐ or ☐	Perfect health for 6 months, then die (give up 4 years, 6 months)
4. Living in the Spokane community on the HeartMate IP LVAD for 5 years, then die	☐ or ☐	Perfect health for 9 months, then die (give up 4 years, 3 months)
5. Living in the Spokane community on the HeartMate IP LVAD for 5 years, then die	☐ or ☐	Perfect health for 1 year, then die (give up 4 years)
6. Living in the Spokane community on the HeartMate IP LVAD for 5 years, then die	☐ or ☐	Perfect health for 1 year 3 months, then die (give up 3 years, 9 months)
7. Living in the Spokane community on the HeartMate IP LVAD for 5 years, then die	☐ or ☐	Perfect health for 1 year 6 months, then die (give up 3 years, 6 months)
8. Living in the Spokane community on the HeartMate IP LVAD for 5 years, then die	☐ or ☐	Perfect health for 1 year 9 months, then die (give up 3 years, 3 months)
9. Living in the Spokane community on the HeartMate IP LVAD for 5 years, then die	☐ or ☐	Perfect health for 2 years, then die (give up 3 years)
10. Living in the Spokane community on the HeartMate IP LVAD for 5 years, then die	☐ or ☐	Perfect health for 2 years 3 months, then die (give up 2 years, 9 months)
11. Living in the Spokane community on the HeartMate IP LVAD for 5 years, then die	☐ or ☐	Perfect health for 2 years 6 months, then die (give up 2 years, 6 months)

Figure 9. (Continued)

Choice A		Choice B
12. Living in the Spokane community on the HeartMate IP LVAD for 5 years, then die	☐ or ☐	Perfect health for 2 years 9 months, then die (give up 2 years, 3 months)
13. Living in the Spokane community on the HeartMate IP LVAD for 5 years, then die	☐ or ☐	Perfect health for 3 years, then die (give up 2 years)
14. Living in the Spokane community on the HeartMate IP LVAD for 5 years, then die	☐ or ☐	Perfect health for 3 years 3 months, then die (give up 1 year, 9 months)
15. Living in the Spokane community on the HeartMate IP LVAD for 5 years, then die	☐ or ☐	Perfect health for 3 years 6 months, then die (give up 1 year, 6 months)
16. Living in the Spokane community on the HeartMate IP LVAD for 5 years, then die	☐ or ☐	Perfect health for 3 years 9 months, then die (give up 1 year, 3 months)
17. Living in the Spokane community on the HeartMate IP LVAD for 5 years, then die	☐ or ☐	Perfect health for 4 years, then die (give up 1 year)
18. Living in the Spokane community on the HeartMate IP LVAD for 5 years, then die	☐ or ☐	Perfect health for 4 years 3 months, then die (give up 9 months)
19. Living in the Spokane community on the HeartMate IP LVAD for 5 years, then die	☐ or ☐	Perfect health for 4 years 6 months, then die (give up 6 months)
20. Living in the Spokane community on the HeartMate IP LVAD for 5 years, then die	☐ or ☐	Perfect health for 4 years 9 months, then die (give up 3 months)
21. Living in the Spokane community on the HeartMate IP LVAD for 5 years, then die	☐ or ☐	Perfect health for 4 years 10 months, then die (give up 2 months)
22. Living in the Spokane community on the HeartMate IP LVAD for 5 years, then die	☐ or ☐	Perfect health for 4 years 11 months, then die (give up 1 month)
23. Living in the Spokane community on the HeartMate IP LVAD for 5 years, then die	☐ or ☐	Perfect health for 5 years, then die (give up no time)

Figure 9. (Continued)

Journal of Congestive Heart Failure and Circulatory Support (2001) Vol 1, No 4, 371–377

A totally implantable VAD with remote patient monitoring and control

T. Mussivand PhD, D Eng, FRCS, P. J. Hendry MD, R. G. Masters MD and W. J. Keon MD
Cardiovascular Devices Division, University of Ottawa Heart Institute, Ottawa, Ontario, Canada

Purpose Ventricular assist devices (VADs) are increasingly being utilized outside the hospital setting, allowing patients greater mobility and autonomy. In order to meet the demand for these devices, the design of a fully implantable pulsatile VAD (i.e. one that functions without the need for percutaneous leads and vents) which also offers remote patient monitoring and control capabilities is needed.

Methods Two major issues concerning long-term use of VADs outside of the hospital setting are patient acceptance of the device and quality of life. To address these issues, the HeartSaver VAD development program focused on two areas of major improvement: (1) implantability of the device, and (2) recipient quality of life post-implant. In order to improve implantability, the device is designed to be implanted into the thoracic cavity (via median sternotomy). The device utilizes remote power transfer, requires no percutaneous connections and allows the recipient to indulge in a wide range of normal lifestyle activities (bathing, swimming, showering, changing clothes, etc.), unencumbered by external components. In order to improve the quality of life for the recipient the device can be remotely monitored and controlled via a remote patient monitoring system, thus freeing the patient from the need to frequently visit the hospital and allowing greater peace of mind for the recipient.

Results The first prototype of the device has been operating on the bench for over 7.5 years failure free. Three series of *in vivo* studies (n=45) in bovine, for up to 30 days of support, have been conducted, demonstrating: (1) device implantability, (2) performance and ability to sustain circulation, and (3) remote monitoring and control capabilities. The Remote Patient Monitoring System has been successfully demonstrated in Canada, Japan, USA, and Europe, allowing clinicians in one country the ability to monitor and control a device located in another country.

Conclusions Studies to date have demonstrated acceptable implantability and performance of the developed device. By utilizing the Remote Patient Monitoring System, it is now possible to provide patient access to health care professionals, without the need to have the patient physically visit the hospital. This capability could play an important role in reducing health care costs and improving the health care delivery system.

Introduction

The use of mechanical circulatory support has evolved over the last 3 decades, from experimental use as a last hope for patients with end-stage heart failure, to a viable clinical tool for providing both short-term postcardiotomy support as well as longer-term support as a bridge to cardiac transplantation[1]. The next step in the evolution of circulatory support is toward use of mechanical circulatory support as a long-term solution and alternative to transplantation or 'destination therapy'. This application requires devices that are capable of providing long-term support outside of the hospital setting, with a special emphasis on patient acceptance of the device and quality of life.

While the currently available devices have clearly established clinical effectiveness by substantially improving both the functional and physiological condition of patients with end-stage heart failure[2,3], their design and technical attributes make these devices less than ideal for use as a destination therapy. The most widely utilized devices fall into two major categories: (1) extracorporeal devices, such as the Thoratec Bi-VAD and Abiomed BVS–5000, and (2) implantable systems such as the Novacor LVAS and TCI HeartMate. Extracorporeal devices, while ideal for short-term use, are less suitable for long-term use due to their lack of portability. These systems utilize large external operating consoles, typically restricting them to in-hospital use. While some advancements have been made, most notably the new portable console for the Thoratec device, these devices lack the acceptance oif the device by the patient and provision of a sufficient quality of life that is required for a destination therapy device.

Implantable devices therefore offer the best hope as a long-term device due to their portability. In fact, implantable devices have been used quite successfully outside of the hospital setting for extended durations of months and even years[4–6]. Existing implantable devices are not without their problems in long-term use, most notably the use of percutaneous connections for powering, monitoring and venting these devices. While these percutaneous connections have been implicated in a high incidence of infection (25–45%),

Correspondence to: Tofy Mussivand, Director, Cardiovascular Devices Division, University of Ottawa Heart Institute, 40 Ruskin Street, Rm. H560B, Ottawa, Ontario, Canada KIY 4W7.

they also make the devices less acceptable to patients and limit their quality of life. In addition, there is evidence to suggest that the high rate of infections may play a role in thromboembolic events that are a major concern with circulatory support devices. An additional complication with existing implantable devices is the intra-abdominal implantation site. This implant site results in lengthy cannulation to the natural heart, which may also play a major role in both the high rate of incidence of both infectious complications and thromboembolic complications. The intra-abdominal implant site has also led to gastrointestinal complications in some patients and requires the extension of the standard median sternotomy to the umbilicus for device implantation, resulting in substantial surgical manipulation in the intra-abdominal area and perforation of the recipient's diaphragm for cannulation to the natural heart.

Based on these and other complications experienced with existing circulatory support devices, the Cardiovascular Devices Division of the University of Ottawa Heart Institute (Ottawa, Canada) established a research and development (R&D) program for a device specifically designed for long-term use outside of the hospital setting. The overall design goals called for a pulsatile left ventricular assist device (LVAD), capable of being implanted in the thoracic cavity, which would require no percutaneous connections, and would be capable of being monitored and controlled remotely. This program, which began in 1988, has resulted in the development of the HeartSaver VAD[7–10], which is currently undergoing pre-clinical evaluation in preparation for upcoming clinical trials (pending regulatory approval).

Methods and materials

Device description

The HeartSaver VAD system is shown schematically in Figure 1. The system consists of three implanted components: (1) the HeartSaver VAD unit, (2) the internal battery, and (3) the implanted transcutaneous energy and information transfer coil, and three external components: (1) the remote biotelemetry monitor, (2) the external battery, and (3) the external energy and information transfer coil.

The implantable VAD unit (Figure 2) utilizes electrohydraulic actuation and combines the blood chamber, volume displacement chamber, electrohydraulic axial flow pump, and control electronics into a single unit capable of being implanted into the thoracic cavity. The geometric design and configuration of the implantable unit was based on a series of cadaver and intraoperative fit trials[11] as well as extensive fluid dynamics studies[12]. The intrathoracic implant site offers several distinct advantages over intra-abdominal implantation, namely;

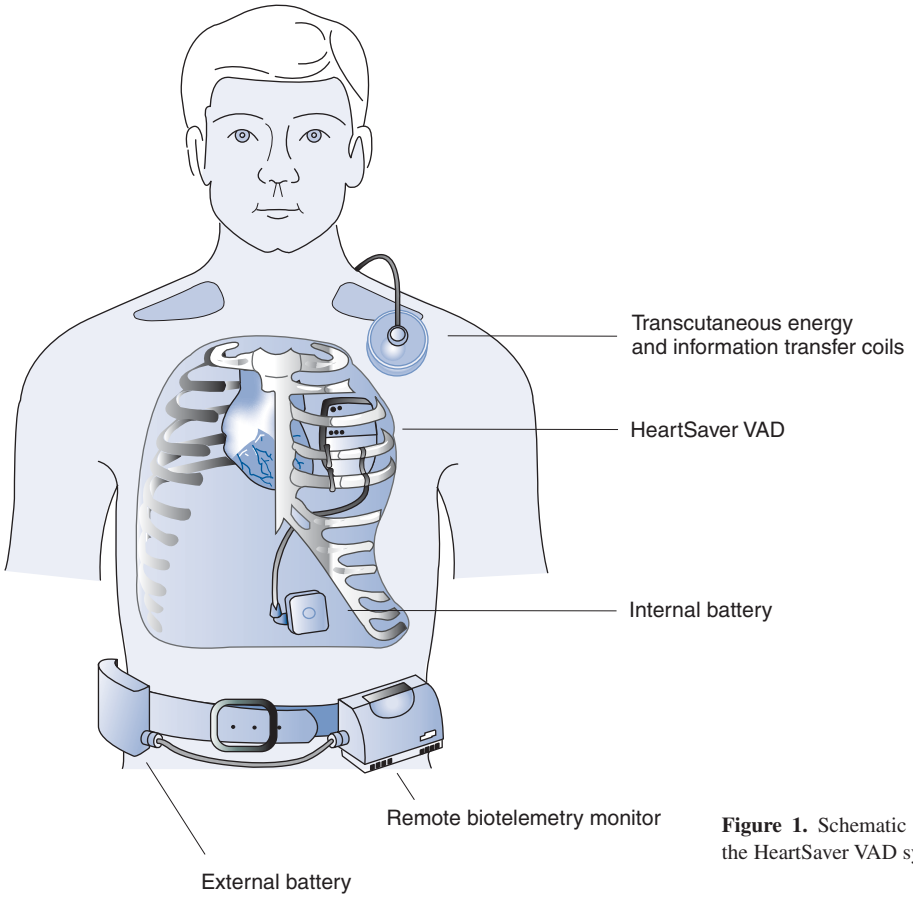

Figure 1. Schematic representation of the HeartSaver VAD system.

1. The device can be implanted via median sternotomy, eliminating the need for surgical manipulation of the abdominal area.
2. The diaphragm does not need to be perforated for cannulation to the natural heart.
3. The cannulation can be extremely short and direct (Figure 3).
4. The device can be anchored to the rib cage to prevent device migration.
5. A volume displacement chamber situated adjacent to the lung, allowing the pressure of the system to equalize with atmospheric pressures, can be integrated into the VAD unit, eliminating the need for percutaneous venting of the device.

Figure 2. The intrathoracically implantable HeartSaver VAD unit.

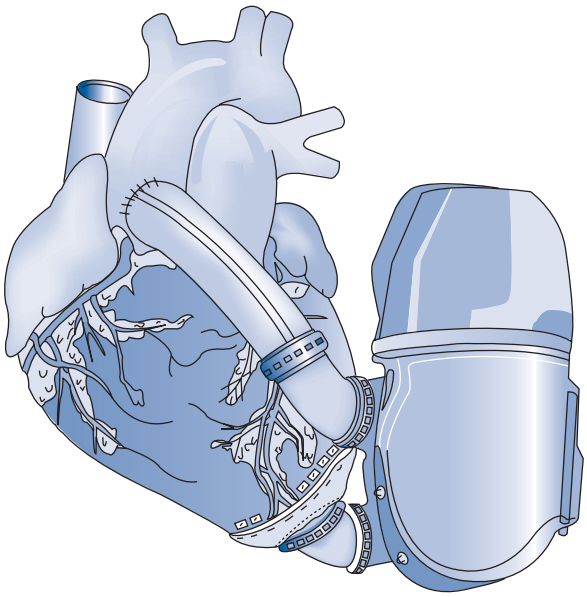

Figure 3. Cannulation of the HeartSaver VAD to the natural heart.

To eliminate the need for percutaneous connections to monitor, control and power the implantable VAD unit, a transcutaneous energy and information transfer system was developed. This system allows energy and information to be transferred through intact skin and tissue[13–17] via the two coils shown in Figure 4. One coil is implanted subcutaneously and connected via a cable to the implantable VAD unit, and the other coil rests on the outside of the body directly over the implanted coil and is connected via a cable to the remote biotelemetry monitor (Figure 5).

Energy to power the device comes from one of three possible sources:

1. The rechargeable implanted battery connected via cable to the implantable VAD unit

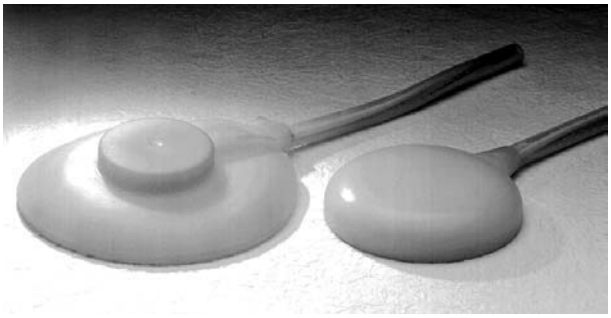

Figure 4. The transcutaneous energy and information transfer coils.

Figure 5. The wearable remote biotelemetry monitor.

2. An external wearable battery connected via cable to the remote biotelemetry monitor and transferred through the skin and tissue via the energy transfer system
3. From another external source (automobile cigarette lighter, household AC outlet, etc.) connected via cable to the remote biotelemetry monitor and transferred through the skin and tissue via the energy transfer system.

Both the external and internal batteries utilize rechargeable lithium ion battery cells. The internal battery provides up to 1 h of operating time, during which the patient requires no external components. This allows the patient total freedom of movement and the ability to partake in a wide variety of activities such as bathing, showering, swimming etc..

The implanted VAD unit is monitored and controlled via the information transfer system. This system utilizes transcutaneous infrared data communications between the implanted VAD unit and the wearable remote biotelemetry monitor via the coil system. The remote biotelemetry monitor provides device status displays and warning alarms to the patient. The monitor also offers the clinician the capability to perform routine device monitoring from a remote location, using phone lines or the Internet; this allows patients the convenience of having routine or emergency device assessment performed while at home, further enhancing their quality of life and acceptance of the technology.

During implantation of the device and patient recovery in the hospital, as well as for remote device monitoring after patient discharge, the clinician utilizes the Clinical User Interface (Figure 6). This system provides all the monitoring and control functions for the device, including real-time monitoring of device output and residual volume calculations. To provide ease of use, the Clinical User Interface is equipped with an RF modem to allow wireless communication with the device via the Remote Biotelemetry Monitor. This feature is especially useful during device implantation as it eliminates the need to drag cables into the sterile field. Furthermore, during the in-hospital recovery phase, it allows the patient to move around freely while maintaining continuous monitoring of device function.

Figure 6. The Clinical User Interface.

After discharge from the hospital, the clinician can also utilize this device to perform periodic remote monitoring of the patient using a standard phone line. This is accomplished using the Home User Interface, which is connected to the patient's phone line and communicates with the device via the RF modem in the Remote Biotelemetry Monitor. The clinician simply connects the Clinical User Interface to a phone line, sets the software option to 'telephone communications' and enters the patient's phone number (Figure 7). The Clinical User Interface then automatically calls the Home User Interface and establishes wireless communications with the device via the Remote Biotelemetry Monitor. Once communication has been established with the device, the clinician has access to all the monitoring and control functions of the device. Use of the Remote Monitoring and Control capability is also possible using the Internet (Figure 8).

Results

Throughout the R&D program the various components of the HeartSaver system have undergone extensive *in vitro* and *in vivo* testing. A summary of this testing is provided as follows.

In vitro studies

Testing of the individual components and the entire system is ongoing. Various versions of the device have been tested on mock circulatory loops, uninterrupted for extended time periods. One early prototype has now run for over 7.5 years – failure free. Several more recent prototypes have functioned for over 2 years, also failure free.

The Remote Patient Monitoring System has been tested under a variety of conditions, from across the lab to around the globe. The system allows monitoring and control functions to be accomplished remotely using standard phone lines and Internet connections. This system was demonstrated during the 7th International Symposium on Artificial Heart and Assist Devices in Tokyo, Japan on March 10–11, 2000. The system allowed personnel located in Japan to remotely monitor and control over standard phone lines the operating parameters (beat rate, operating mode, etc.) of the HeartSaver VAD located on a simulated patient in Ottawa, Canada. Utilizing the Clinical User Interface in Japan, the HeartSaver VAD located in Canada was monitored, operating parameters were modified, and confirmation that modifications were implemented were received in real-time. Patient data stored within the device could also be transferred from Canada to Japan using the system.

In vivo studies

Three series of *in vivo* experiments (n=45) have been conducted with the device to date[18–21]. The purpose of these studies was to assess the implantability of the developed device and to obtain design input for device optimization.

During the first series of experiments (n=12), the goal was to achieve success of an implant for 5 days to prove the overall concept of the design. During these experiments the animals were supported for periods up to 5 days (mean duration 16.5 h, range 1.5 h to 5 days). This series demonstrated the feasibility of the totally implanted system (without percutaneous connections), and provided vital input for the ongoing development of the device. Based on this series of implants, the device design was reiterated and optimized. The second series of implants (n=13) was then conducted, which focused on performance of the implanted VAD unit, specifically the inflow and outflow cannulae, the blood chamber fluid dynamics, and device positioning in the calf model. In this series of experiments the animals were supported for periods up to 30 days (mean duration 3.5 days, range 1 h to 30 days). A calf implanted with the HeartSaver VAD system is shown in Figure 9. This series of experiments successfully demonstrated the ability of the device to support a dysfunctional heart (during ventricular fibrillation), and allowed detailed assessment of device modifications implemented as a result of the series 1 implants. The third series of implants (n=20) is currently ongoing and is designed to assess the pre-clinical version of the device in preparation for a formal multi-centre animal trial. This series has concentrated on optimizing the implant procedure and assessing implantability/ease of use of individual components in their pre-clinical form, as they become available from the pilot manufacturing facility. Based on this series of implants, minor changes to the device design and manufacturing processes are being implemented in preparation of formal *in vitro* and *in vivo* studies to be conducted for regulatory approval purposes.

Figure 7. Clinical User Interface option to enable remote monitoring and control via telephone lines.

Figure 8. Clinical User Interface option to enable remote monitoring and control via the Internet.

Formal studies

Preparations for the formal *in vitro* and *in vivo* studies of the pre-clinical device are nearing completion. These studies are based on the guidelines[22] established by the National Institutes of Health (NIH), Food and Drug Administration (FDA), Society of Thoracic Surgeons (STS) and the American Society for Artificial Internal Organs (ASAIO). The studies will consist of a long-term multiple system *in vitro* study to determine overall system reliability and performance, and a multi-centre *in vivo* study focused on achieving eight long-term (90-day) survivors. The latter will assess hemodynamics at 30 and 90 days, monitor continuous device performance, and track all adverse events (including hemolysis, infection, thromboembolism, and end-organ damage). Data from these studies will be utilized to obtain regulatory approval for an initial clinical trial focused on the safety and efficacy of the device.

Figure 9. Calf with implanted HeartSaver VAD system.

Discussion and conclusions

The HeartSaver VAD R&D program started over 10 years ago, with the overall goal of developing a totally implantable VAD for long-term or chronic use. The approach utilized was to assess the limitations of existing technology and begin to address the issues related to patient acceptance and quality of life for future device recipients. These issues were considered vital for a device intended for long-term or 'destination therapy'.

The results of the R&D program are summarized as follows:

1. A totally implantable VAD that requires no percutaneous connections has been developed.
2. The VAD is expected to significantly reduce the incidence of infection and provide a better quality of life and be more acceptable to future recipients.
3. The implanted internal battery provides for the patient the ability to partake in a wide variety of activities, without the need for any external components whatsoever, thereby offering complete mobility and freedom of movement.

The Remote Patient Monitoring System allows for remote monitoring and, if required, remote control of operating parameters, eliminating the need for patients to visit the hospital for routine device assessment. This remote monitoring and control function is expected to provide patients with increased peace of mind after discharge from the hospital, as help will simply be a phone call away.

The device size and geometry allows intrathoracic implantation, eliminating the need for externalized venting (by utilizing an integrated volume displacement chamber). This device also allows implantation via a median sternotomy, reducing the overall invasiveness of the implantation procedure.

Each aspect of the device mentioned above enhances the potential of this device to be used for long-term support as a treatment for end-stage heart failure, and will offer patients an improved quality of life in comparison to existing technologies. Based on the ongoing experimental studies (both *in vitro* and *in vivo*), the HeartSaver VAD can function effectively as a totally implantable intrathoracic VAD. Formal evaluation of the pre-clinical device intended for use in the initial clinical trials, is now beginning and clinical utilization in humans will follow (pending regulatory approval).

Acknowledgements

This work was supported in part by the University of Ottawa Heart Institute and World Heart Corporation, Ottawa, Ontario, Canada.

References

1. Goldstein DJ, Oz MC, Rose EA. Implantable left ventricular assist devices. *N Engl J Med* 1998;339:1522–33.
2. Kormos RL, Murali S, Dew MA *et al.* Chronic mechanical circulatory support: rehabilitation, low morbidity, and superior survival. *Ann Thorac Surg* 1994;57:51–8.
3. Miller PJ, Billich TJ, LaForge DH *et al.* Initial clinical experience with a wearable controller for the Novacor left ventricular assist system. *ASAIO J* 1994;40:M465–70.
4. Catanese KA, Goldstein DJ, Williams DL *et al.* Outpatient left ventricular assist device support: A destination rather than a bridge. *Ann Thorac Surg* 1996;62:646–53.
5. Myers TJ, Catanese KA, Vargo RL, Dresslers DK. Extended cardiac support with a portable left ventricular assist system in the home. *ASAIO J* 1996;42:M576–9.
6. Oz MC, Argenziano M, Catanese KA *et al.* Bridge experience with long-term implantable left ventricular assist devices: Are they an alternative to transplantation? *Circulation* 1997;95:1844–52.
7. Musivand T, Hendry JP, Masters RG *et al.* A remotely controlled and powered artificial heart pump. *Artif Organs 1996;20:1314*–19.
8. Mussivand TV, Hendry PJ, Masters RG, Keon WJ. Multi-purpose mechanical circulatory device. *Int J Artif Organs* 1997;20:217–21.
9. Mussivand TV, Hendry PJ, Masters RG, Keon WJ. Evaluation of a totally implantable intrathoracic ventricular assist device. *Cor Europaeum* 1997;6:110–14.
10. Mussivand TV, Hendry PJ, Masters RG, Keon WJ. Development of a totally implantable intrathoracic ventricular assist device. In: Akutsu T, Koyangi H, editors. *Heart Replacement – Artificial Heart 6.* Tokyo: Springer-Verlag, 1998:15–20.
11. Mussivand TV, Masters RG, Hendry PJ *et al*. Critical anatomic dimensions for intrathoracic circulatory assist devices. *Artif Organs* 1992;16:281–5.
12. Mussivand TV, Day KD, Naber BD. Fluid dynamic optimization of a ventricular assist device using particle image velocimentry. *ASAIO J* 1999;45:25–31.
13. Mussivand TV, Miller JA, Santerre PJ *et al.* Transcutaneous energy transfer system performance evaluation. *Artif Organs* 1993;17:940–7.
14. Mussivand TV, Hum A, Holmes KS. Remote energy transmission for powering artificial hearts and assist devices. In: Akatsu T, Koyangi H, editors. *Heart Replacement – Artificial Heart 6.* Tokyo: Springer-Verlag, 1998:344–7.
15. Mussivand TV, Hum A, Diguer M *et al.* A transcutaneous energy and information transfer system for implanted medical devices. *ASAIO J*. 1995;41:M253–8.
16. Mussivand TV, Hum A, Holmes KS *et al.* Remote monitoring & control of artificial hearts and assist devices. In: Akutsu T, Koyangi H, editors. *Heart Replacement – Artificial Heart 6.* Tokyo: Springer-Verlag, 1998:370–3.
17. Mussivand TV, Hum A, Holmes KS, Keon WJ. Wireless monitoring and control for implantable rotary blood pumps. *Artif Organs* 1998;21:661–4.
18. Hendry P, Masters RG, Ibrahim M *et al.* In vivo evaluation of an intrathoracic ventricular assist device. *ASAIO J* 1999;45:123–6.
19. Hendry PJ, Masters RG, Keaney M, Bourke M, Mussivand TV, Keon WJ, The EVAD Team. Evolution of an electrohydraulic ventricular assist device through *in vivo* testing. *ASAIO J* 1996;42:M350–4.

20. Mussivand TV, Hendry PJ, Masters RG, Keon WJ. Evaluation of a totally implantable intrathoracic ventricular assist device. *Cor Europaeum* 1997;6:110–4.
21. Mussivand T, Masters RG, Hendry PJ, Keon WJ. Totally implantable intrathoracic ventricular assist device. *Ann Thorac Surg* 1996;61:444–7.
22. Pantalos GM, Altieri F, Berson A *et al.* Long-term mechanical circulatory support system reliability recommendation: American Society for Artificial Internal Organs and The Society of Thoracic Surgeons: long-term mechanical circulatory support system reliability recommendation. *Ann Thorac Surg* 1998;66:1852–9.

Session 9

Ventricular Assist Devices

Journal of Congestive Heart Failure and Circulatory Support (2001) Vol 1, No 4, 381–385

Evaluation of pump performances of Heart Ranger using heart failure model

K. Imanishi MD PhD[1], K. Imachi MD PhD[2], Y. Abe MD PhD[2], T. Chinzei MD PhD[3], T. Isoyama MD PhD[3], S. Mochizuki MD PhD[3], I. Saito PhD[2], M. Ishimaru MD[1], T. Ono BE[2], A. Kouno[2] and Y. Matuura[1]

[1]1st Department of Surgery, Hiroshima University School of Medicine , Hiroshima, Japan; [2]Department of Biomedical Engineering, Graduate School of Medicine, University of Tokyo, Tokyo, Japan; [3]Research Center of Advanced Science of Technology, University of Tokyo, Tokyo, Japan; and [4]Department of Cardiovascular Surgery, Dohi Hospital, Hirohsima, Japan

Abstract A new type of left ventricular assist device named Heart Ranger for use in postcardiotomy cardiogenic shock patients was developed. Heart Ranger was composed of a diaphragm-type blood pump and cannula in which inflow and outflow valves were installed. Heart Ranger was inserted from the ascending aorta into the left ventricle. Maximum pump flows of 3.1 L min^{-1} with an IABP driver and 3.7 L min^{-1} with an AH driver were obtained with the pumping rate of 60 bpm. In the animal experiment using the goat, more than 2 L min^{-1} of assisted flow by Heart Ranger was maintained throughout the 13 pumping days. As for the assist rate by Heart Ranger compared with cardiac output, 41–69% of assist rates were recorded with an increase in systolic pressure. In conclusion, Heart Ranger was thought to provide the effective circulatory assist in postcardiotomy cardiogenic shock patients.

Keywords left ventricular assist device (LVAD), postcardiotomy cardiogenic shock, jellyfish valve, pulsatile flow.

Background

A new type of left ventricular assist device (LVAD) named Heart Ranger (H-Ra) for use in postcardiotomy cardiogenic shock patients has been developed. In this study, pump performances were evaluated in in vitro and in vivo experiments.

Materials and methods

H-Ra was comprised of an air-driven blood pump and cannula. A single-port valveless diaphragm-type blood pump with a stroke volume of 40 mL was made of polyvinylchloride paste. In H-Ra, the length of the cannula was 30 cm and four types of cannulae with outer diameters of 7.0, 9.0, 11.0, 13.0 mm were designed. Any type of air-driven drivers (IABP or artificial heart) could be connected to the air driveline. Heart Ranger was inserted from the ascending aorta. The tip of the cannula was sent through the aortic valve into the left ventricle; therefore the outflow valve was located in the ascending aorta near the coronary orifice. The blood pump was therefore placed outside of the body (Figure 1). Systolic unloading and diastolic augmentation were obtained triggered with R-wave of an electrocardiogram (ECG). A spiral of stainless steel was installed into the wall of the cannula. For insertion and fixation of the cannula, the insertion port was newly designed. The insertion port was composed of an artificial graft and valve to prevent bleeding from the insertion port.

All animals received humane care according to the *Guidelines for the Care and Use of Laboratory Animals*. In

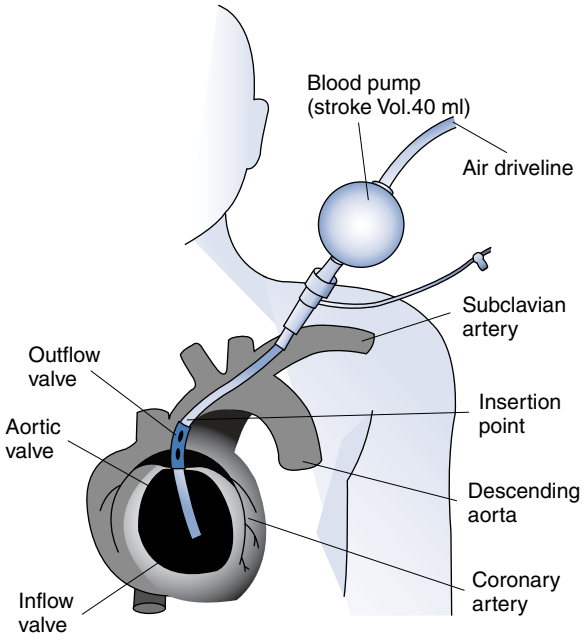

Figure 1. Clinical setting of H-Ra.

Correspondence to: Kaoru Imanishi, 1st Department of Surgery, Hiroshima University School of Medicine, Kasumi 1–2–3, Minamiku, Hiroshima 734-0037, Japan.

the animal experiment using the goat, a left thoracotomy was performed and an insertion port was anastomosed to the descending aorta. In order to make a heart failure model, chordae of the anterior papillary muscle was cut before insertion of the cannula. The cannula was then inserted through the insertion port into the left ventricle on the guidewire.

After fixation of the cannula, the blood pump was connected to the cannula and evacuation of the air was performed. Pumping was then started using an artificial heart (AH) driver (AISIN CORAT). The relationships between the cannula and left ventricle was observed using an echocardiogram (ECHO).

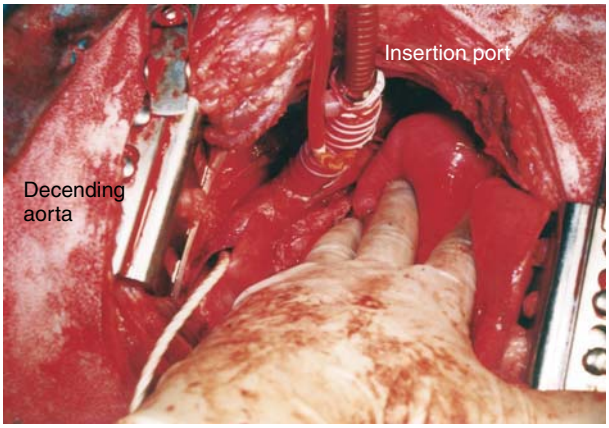

Figure 2. Cannulae of H-Ra inserted through insertion port and fixed.

ECG, aortic pressure, cardiac output, pump flow of to and fro, assist flow of actual forward flow by H-Ra were recorded.

Results

The cannula was smoothly inserted through the insertion port into the left ventricle on the guidewire (Figure 2). The inflow and outflow valves were inserted in the proper position in the left ventricle and ascending aorta, aided by ECHO (Figure 3). The cannula was then fixed at the insertion port.

The healthy goat stood up 1 h after the operation. Hemodynamics were stable during 13 pumping days postoperatively; stable assisted flow by H-Ra was observed on the seventh postoperative day. More than 2 L min^{-1} of assisted flow by H-Ra was maintained throughout the pumping days. As for the assist rate by H-Ra compared with cardiac output, 41–69% of assist rate were recorded while keeping the left ventricle in the resting state (Figure 4).

After causing heart failure by cutting the chordae of the anterior papillary muscle, cardiac output decreased from 5 L min^{-1} to 3.7 L min^{-1} and aortic pressure decreased from 100 mmHg to 60 mmHg. After starting the pumping, the assist rate was 65–86% with the assisted flow of 2.2–2.5 L min^{-1} by changing parameters of systolic pressure (Figures 4 and 5). When cardiac output and aortic pressure increased by catecholamine assist in the heart failure model, the assisted flow by H-Ra decreased relatively.

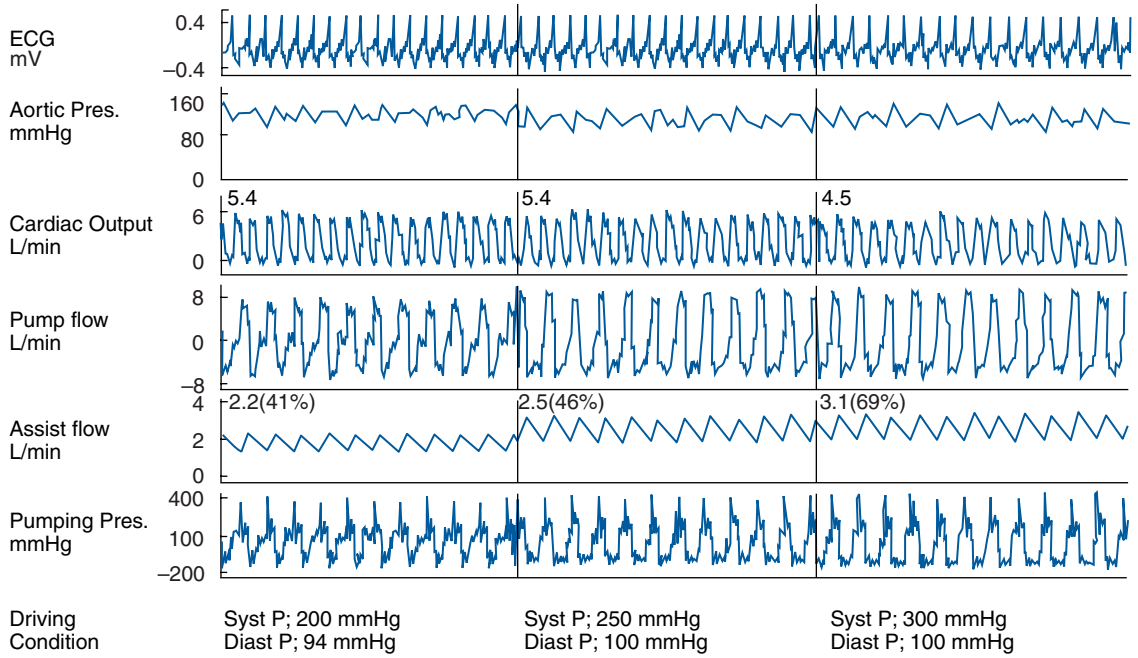

Figure 3. Chronic study on the healthy goat. Stable pumping at postoperative day 7 was observed. This assist rate was 41–69% in the healthy goat model.

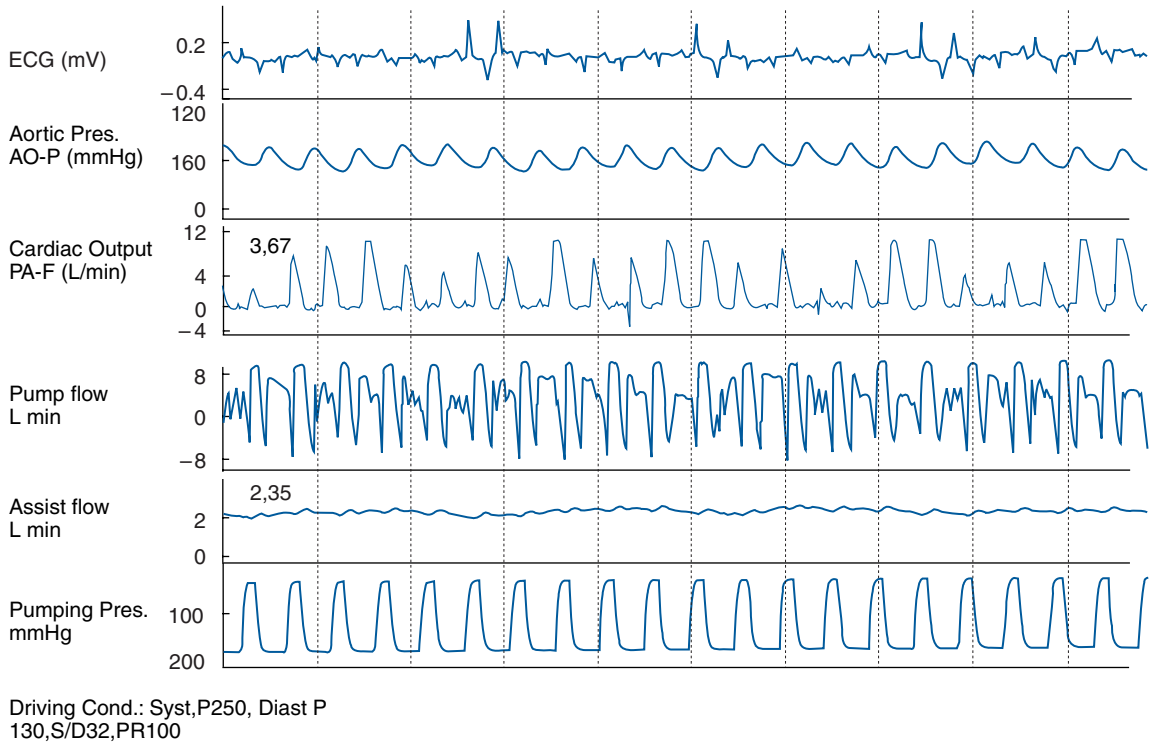

Figure 4. In the heart failure model, more than 2.0 L min^{-1} of assisted flow was observed, while cardiac output was 3.7 L min^{-1} and mean blood pressure was 60 mmHg.

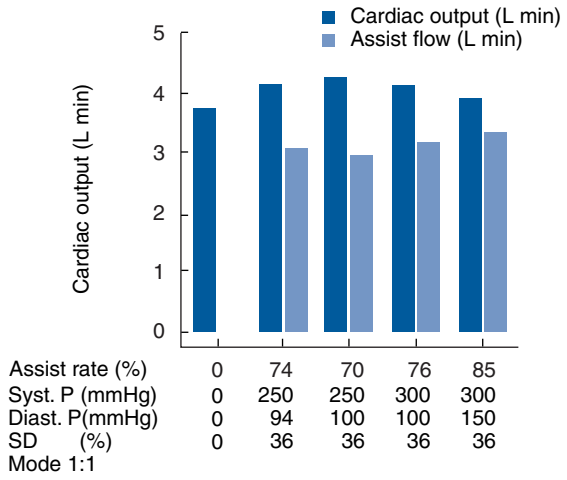

Figure 5. The assist rate compared with cardiac output in the healthy goat model was increased from 74–85% with an increase of systolic pumping pressure.

During ventricular fibrillation, cardiac output was almost zero. However, more than 2 L min^{-1} of systemic flow was maintained by H-Ra assist (Figure 6).

After termination of the animal experiment for 13 days in the healthy cases, pathological examinations were performed. No dislocation of inflow and outflow valves was observed. Almost no thrombus formation was observed in attachment of the valve membrane of the lantern valve and quick connector. There was no deterioration of the aortic valve or the constructions of the left ventricle. At autopsy in the heart failure model after pumping for 7 h, the chordae of the anterior papillary muscle were cut and no thrombus formation or dislocation of inflow and outflow valves was observed (Figures 7 and 8).

Discussion

We have been developing a percutaneously accessible left ventricular assist device to evaluate the device[1–3]. In the newest model, a maximum flow of 3.7 L min^{-1} was obtained and effective left ventricular circulatory assist was obtained in the animal experiment using mongrel dogs[4–6]. In order to evaluate the effectiveness of H-Ra, a chronic animal study was performed. In a healthy goat model,

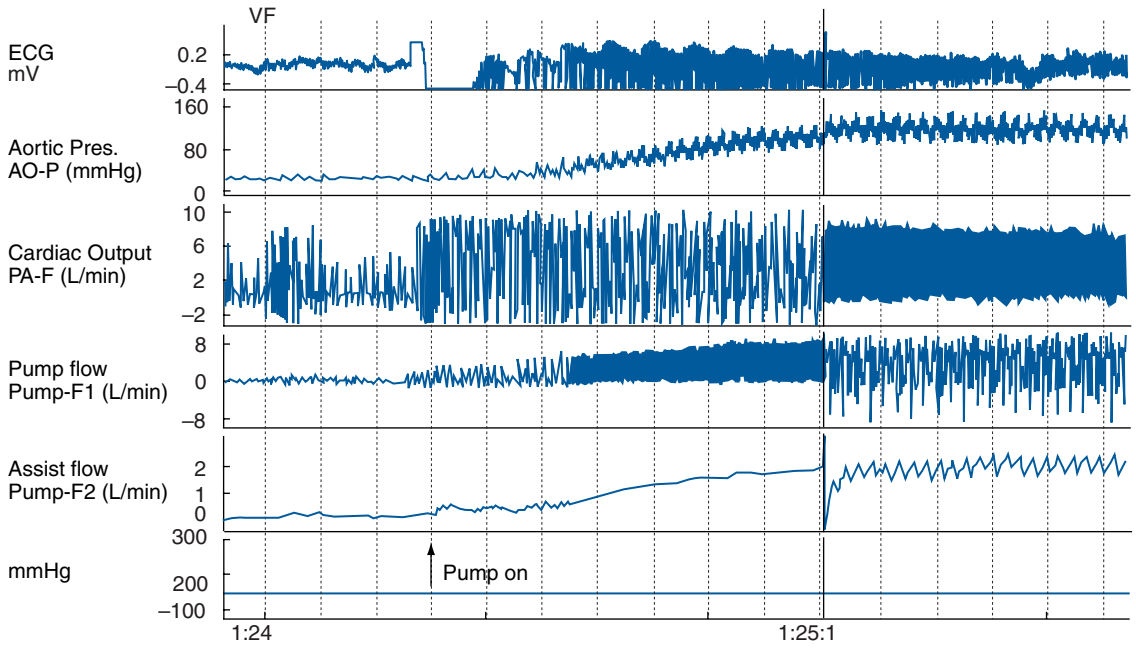

Figure 6. During ventricular fibrillation, more than 2 L min^{-1} was observed after starting of pumping.

stable assist was observed with a mean flow of 2.0–2.5 L min^{-1}. In the heart failure model, stable assist was also obtained with the left ventricle kept in the resting state. Several types of mechanical circulatory support devices have been developed and used clinically[7–9]. However, for application of those systems, general anesthesia and thoracotomy were necessary to provide circulatory assistance. Moreover, during prolonged assistance, the probability of complications such as bleeding, infection and thromboembolism increase [9]. Therefore, there is a need for a circulatory assist device that is easily accessible and reliable. Among the various types of circulatory assist devices, the Hemopump performed excellent circulatory support in clinical application[7]. On the other hand, Hemopump could not produce pulsatile flow. Moreover, there exists the limitation of perfusion time for application of PCPS because of the limitated duration of the artificial lung and centrifugal pump.

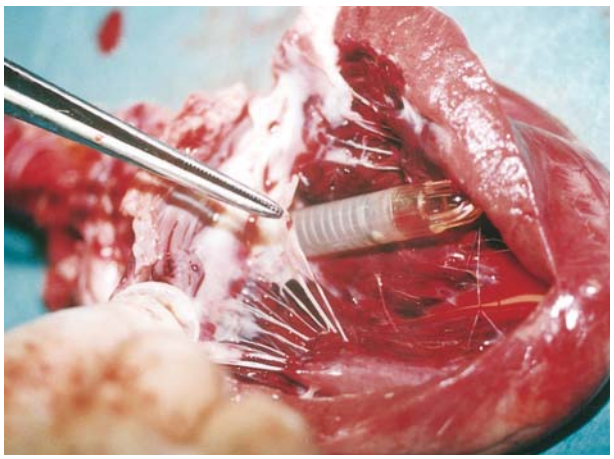

Figure 7. At autopsy, mitral valve regurgitation was created by cutting the chordae.

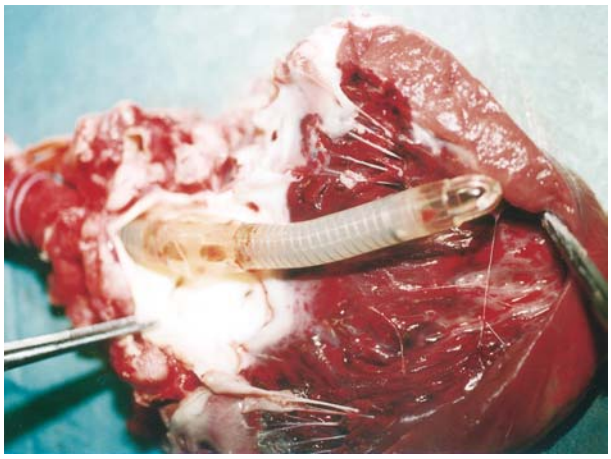

Figure 8. Blood pump and cannula after pumping 7 h in the heart failure model. No thrombus formation was observed in the inflow or outflow valves, and in the cannula.

To solve these problems, we developed a new LVAD called H-Ra. If we compare H-Ra with the centrifugal pump and PCPS from various viewpoints, the specificity of H-Ra will be demonstrated. The assist type of H-Ra was a pneumatically driven LVAD.

A maximum flow of 3.7 L min^{-1} with the AH driver was obtained in the mock circulatory study. The approach of H-Ra in its clinical application will be from the ascending aorta with a median sternotomy or MICS approach. Moreover, cost of H-Ra will be the lowest (Table 1).

As for hemodynamics, from our results obtained in the animal experiment using big animals (weighing 50–60 kg), the specificity of H-Ra which maintains cardiac output while maintaining the left ventricle in the resting state will be induced. Even during ventricular fibrillation, the systemic flow was maintained at higher than 2 L min^{-1}. At this time during the test, the test animal opened her eyes. This result showed that even during ventricular fibrillation, H-Ra maintained minimal flow to protect the function of the vital organs.

H-Ra is designed to perform short-term left ventricular circulatory support. Therefore, the insertion procedure is cannulation. Because the insertion point is in the ascending aorta, there is a small possibility of complications such as bleeding.

From the viewpoint of anatomical fit, there was no deterioration of the structure of the left ventricle observed at autopsy. These results indicated the H-Ra device was suitable for long-term circulatory assist in the left ventricular failure model. H-Ra was easily accessible and had less likelihood of causing complications such as bleeding.

Conclusions

1.H-Ra provided 2.2–2.5 L min^{-1} of pumping flow with 41–69% of assist in the healthy model and 65–86% of assist in the heart failure model.

2. H-Ra was found to be suitable for short-term circulatory assist in patients with profound left ventricular failure.

Table 1. Pre- and postoperative evaluation of device recipients.

	Centrifugal pump	PCPS	Heart Ranger
Assist type	L or R VAD	VA bypass	LVAD
Pulsatility	−	−	+
Pump flow (L min^{-1})	4–5	4–5	3.7 (AH driver) 3.1 (IABP)
Artifical lung	−	+	−
Approach	Thoracotomy	Percutaneous	Thoracotomy or MICS
Insertion point	LA-Aorta or RA-PA	Femoral A and V	Asc. Aorta
Cost			Lowest

References

1. Imachi K, Mabuchi K, Chinzei T *et al*. *In vitro* and *in vivo* evaluation of a jellyfish valve for practical use. ASAIO Trans 1989;35:298–301.
2. Imachi K, Mabuchi K, Chinzei T *et al*. Blood Compatibility of the jellyfish valve without anticoagulant. ASAIO Trans 1991;37(3):220–2.
3. Imanishi K, Imachi K, Abe Y *et al*. Development of a new circulatory assist method with the combined effects of intra-aortic balloon pumping and counter-pulsation: first report. *ASAIO Trans* 1989;35(3):715–17.
4. Imanishi K, Imachi K, Yoshito H *et al*. A percutaneously accessible pulsatile left ventricular assist device: modified assist device type–5. *Heart Replacement—Artificial Heart*, Springer Verlag
5. Imanishi K, Imachi K, Isoyama T *et al*. A percutaneously accessible pulsatile left ventricular assist device. *Artif Organs* 1996;20(2):147–151.
6. Imanishi K, Imachi K, Yshito H *et al*. Evaluation of pump performance of a percutaneous-type pulsatile left ventricular assist device (MAD Type–5 and Type 6). *Heart Replacement —Artificial Heart 6*. Springer Verlag: 453–8.
7. Richard K; Wampler JC, Moise O, Frazier OH. *In vivo* evaluation of a peripheral vascular access axial flow blood pump. *ASAIO Trans* 1988;34:450–4.
8. Whalen RL, Hurford WE, Skoskiewicz M *et al*. A new right ventrilular assist device: The extracorporeal pulsatile assist device (EPAD). *ASAIO Trans* 1987;33:223–6.
9. Ruzevich SA, Pennington DG, Kanter KR *et al*. Long-term follow-up study of survivors of postcardiotomy circulatory support. *ASAIO Trans* 1987;33:177–81.

Journal of Congestive Heart Failure and Circulatory Support (2001) Vol 1, No 4, 387–390

Anticoagulants reduced high intensity transient signals (HITS) during LVAD use

K. Hanzawa MD, M. Kitamura MD, H. Ohzeki MD and J.-I. Hayashi MD
Department of Cardiothoracic and Vascular Surgery, Niigata University School of Medicine, Niigata City, Japan

Background High intensity transient signals (HITS) by transcranial Doppler (TCD) have been reported to reflect microemboli in the cerebral artery. HITS are frequently detected in patients with left ventricular assist devices (LVADs). However, the significance of HITS in patients with LVADs is still unclear. We attempted to elucidate whether HITS during LVAD use were reduced by anticoagulants.

Methods A total of 11 pigs were divided into two groups. In the no-heparin group, heparin was used only at cannulation and the activated clotting time (ACT) was maintained for more than 150 s. HITS were detected by TC2020 with 2.0 MHz pulsed Doppler at the middle cerebral artery. Heparin or argatroban were used as anticoagulants.

Results HITS were frequently detected in the no-heparin group. HITS were reduced by additional heparin from 8.2±3.3 h^{-1} to 1.0±0.7h^{-1} (P<0.005). HITS were significantly reduced by argatroban from 9.8±3.9 h^{-1} to 1.0±1.4 h^{-1} (P<0.005). After a rapid increase of HITS, thromboembolism was occured in four animals.

Discussion HITS may reflect microthrombi during LVAD use. Detection of HITS is useful for monitoring of thrombus formation and may indicate a risk of cerebral embolism during LVAD use.

Keywords high intensity transient signals, transcranial Doppler, left ventricular assist device (LVAD), anticoagulants, cerebral embolism.

Background

The formation of thrombi is commonly seen in left ventricular assist devices (LVADs) even if patients have an adequate anticoagulation. The thromboembolic complication rate with the use of an LVAD has been reported to be above 30% and the rate of cerebral embolism has been reported to be above 10% or higher[1,2]. Recently, high intensity transient signals (HITS) by transcranial Doppler (TCD) have been reported to reflect microemboli in the cerebral artery. HITS were defined as having the following characteristics:

1. Short duration of time (<300 ms)
2. Higher intensity (>3 dB) than background that reflected erythrocytes
3. Unidirectional signals
4. Characteristic sound, similar to chirping.

This definition was approved by the Stroke meeting 1995[3]. HITS were frequently detected in studies of patients with symptomatic carotid stenosis or acute cerebral infarction. HITS seemed to indicate a risk of cerebral infarction. Although many HITS have been reported to detect during use of an LVAD, their clinical significance is still unclear. We attempted to elucidate whether HITS by TCD can indicate a risk of thromboembolism during use of an LVAD using an animal model.

Materials and methods

This study was performed according to the Niigata University Animal Care guidelines. A total of 11 female pigs weighing 25–27 kg were used. All the animals were anesthetized with ketaral and halothane. After intubation, arterial oxygen pressure was maintained at over 200 mmHg. Animals were divided into the following two groups: the heparin group (n=3) and the no-heparin group (n=8). In the heparin group, the activated clotting time was maintained for more than 180 s by heparin injection during LVAD use. In the no-heparin group, only 1000 u heparin was used at the insertion of the inflow cannula into the left ventricular apex.

Additional anticoagulation

When HITS exceeded 1/10 min or intradevice thrombus was observed, 2000 u heparin or 20 mg argatroban (specific thrombin inhibitor, Novastan, Tokyo Mitsubishi, Tokyo, Japan) was injected.

Left ventricular assist device

We used XEMEX (Nippon Zeon, Tokyo, Japan). The stroke volume was 60 ml, two Bjork–Sheily valves were attached in the device. After midline sternotomy, an end-to-side anastomosis of Goretex graft of the outflow cannula to the ascending aorta was performed while the heart was beating. An inflow cannula was inserted into the left ventricular apex. Both cannulae were attached to XEMEX and tightly

Correspondence to: Kazuhiko Hanzawa, Department of Cardiothoracic and Vascular Surgery, Niigata University School of Medicine, 1–757 Asahimachi-dori, Niigata City 951–8510, Japan.

secured by tie band. The pump flow was maintained at 1.5–3.0 L min^{-1}. The activated clotting time (ACT) (Hemocron, International Technidyne Corporation, New York, NY, USA) was measured during LVAD use.

HITS detection

HITS were detected by TC2020, PIONEER (Nicolet/EME) with 2.0 MHz pulsed Doppler. A TCD probe was placed on the eye. The sample volume was set at the middle cerebral artery, which was 50–65 mm in depth from the surface of the eye.

HITS were detected automatically with dual sample volume methods. The parameters of HITS detection were as follows:

1. Sample volume length of pulsed Doppler was set at 10 mm.
2. Threshold between background and HITS was set at 9 dB.
3. Length between sample volumes was more than 6 mm.
4. Time overlap window was more than 75%.

The data were recorded on hard disk and an off-line analysis was performed. HITS were recognized as having both a wave-form and a chirping sound.

Results

HITS were frequently detected in the no-heparin group, but rarely in heparin group (Figure 1). The total HITS count for 14 h in the heparin group and in the no-heparin group was 7.3±4.9 and 62.0±6.8, respectively. HITS count in the heparin group was significantly lower than that in the no-heparin group ($P<0.01$). In the no-heparin group, HITS were significantly reduced by anticoagulants (Figure 2). The HITS count before and after additional heparin injection was 8.2±3.3 h^{-1} and 1.0±0.7 h^{-1} ($P<0.01$), respectively. The HITS count before and after argatroban injection was 9.8±3.9 h^{-1} and 1.0±1.4 h^{-1} ($P<0.005$), respectively. Activated clotting time (ACT) before and after additional heparin injection was 100±19.5 s and 267.2±172.4 s ($P<0.01$), respectively. ACT before and after additional argatroban injection was 126.7±18.9 s and 211±16.3 s ($P<0.01$), respectively. Middle cerebral artery occlusion or myocardial infarction occurred immediately after rapid increase of HITS (Figure 4). Intradevice thrombi were observed in animals with many HITS, but were never observed in those without HITS.

Discussion

HITS were frequently detected during LVAD use without anticoagulants, and they were significantly reduced by anticoagulants. Cerebral embolism or myocardial infarction due to thromboemboli occurred after rapid increase of HITS during LVAD use. The present results may suggest that HITS correlate with the formation of thrombus during LVAD use. Detection of HITS is useful for brain protection or monitoring the thrombus formation during LVAD use.

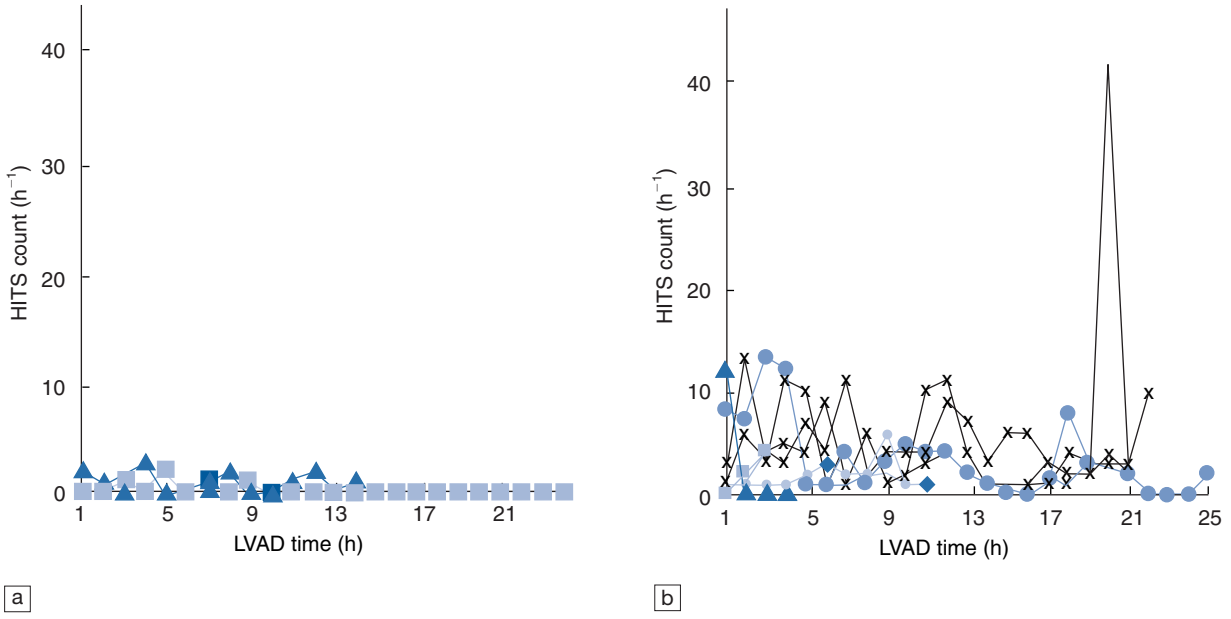

Figure 1. (a) Heparin group. (b) No-heparin group. In the no-heparin group, Doppler-detected microembolic signals (HITS) were frequently detected. In the heparin group, HITS were rarely detected.

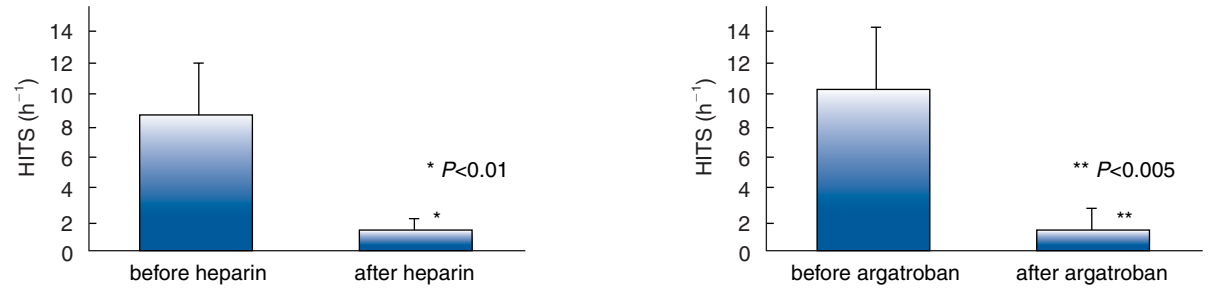

Figure 2. Doppler-detected microembolic signals (HITS) were significantly reduced by anticoagulants during porcine LVAD.

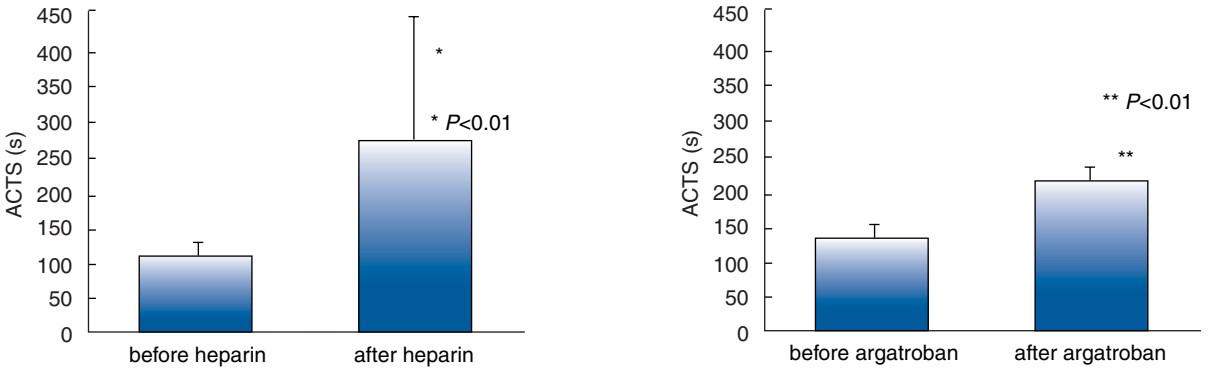

Figure 3. Activated clotting time (ACT) was significantly increased by anticoagulants during porcine LVAD.

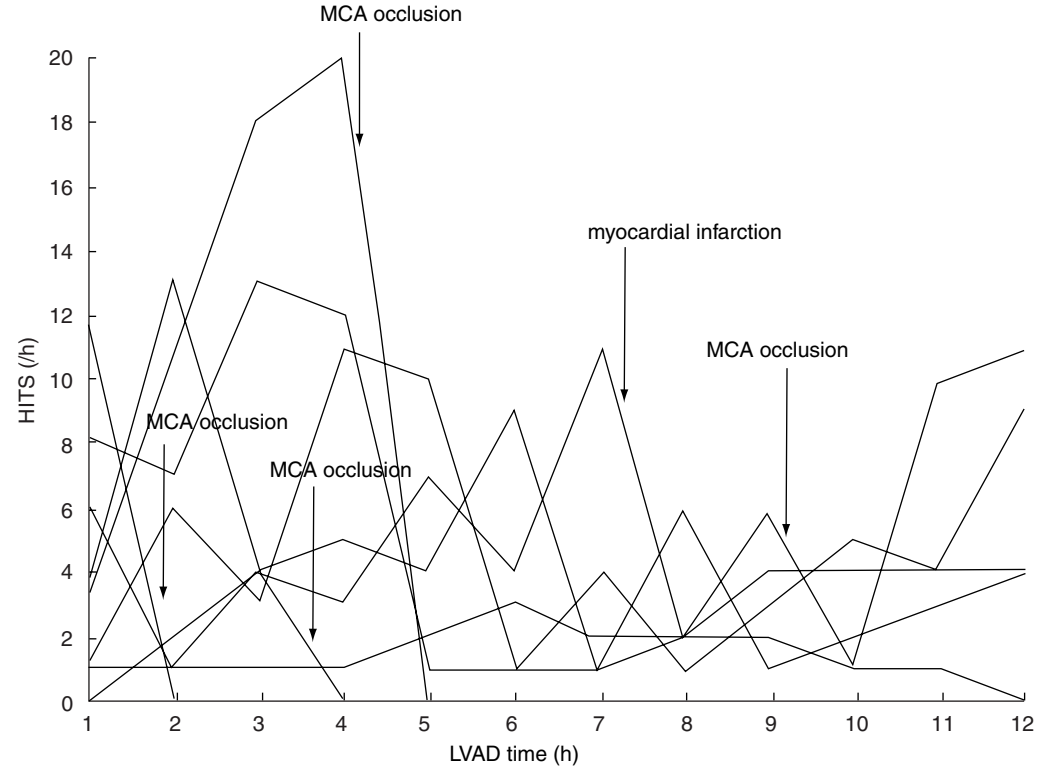

Figure 4. Chronograph of HITS in the no-heparin group. Immediately after rapid increase of HITS, embolic events occurred.

Recent reports have indicated that an increase of HITS may bring about cerebrovascular events[3,4] and an enhancement of anticoagulation reduces such a risk.[5] The present results support these reports. All HITS during LVAD use may not indicate microemboli, because they may include cavitation bubbles deriving from prosthetic cardiac valves[7]. Oxygen inhalation has been reported to reduce HITS in patients with prosthetic valves[6]. However, in the present study, cavitation bubbles decreased due to high arterial oxygen pressure, therefore HITS in the present study reflected microthrombus, and are clearly reduced by anticoagulants.

References

1. Kormos RL, Murali S, Dew MA *et al*. Chronic mechanical circulatory support, rehabilitation, low morbidity and superior survival. Ann Thorac *Surg* 1994;57:51–8.
2. Schmid C, Weymand M, Nabavi DG *et al*. Cerebral and systemic embolisation during left ventricular support with Novacor N100 device. *Ann Thorac Surg* 1998;65:1703–10.
3. Nabavi DG, Georgiadis D, Mumme T, *et al*. Clinical relevance of intracranial microembolic signals in patients with left ventricular assist devices. *Stroke* 1996;27:891–6.
4. Consensus Commitee of the Ninth International Cerebral Hemodynamics Symposium; Basic identification criteria of Doppler microembolic signals. *Stroke* 1995;26:1123.
5. Knepper LE, Eidelman BH, Wagner WR. Transcranial Doppler detection of emboli in patients with left ventricular assist devices. *Stroke* 1996;27:180.
6. Knepper LE, Benjamin BH, Eidelman BH. Transcranial Doppler monitoring of patients with left ventricular assist devices. *Abstract 7th International Symposium on cerebral Haemodynamics*. 1997;509
7. Kaps M, Hansen J, Weher M, Tiffert K, Kayser I, Droste W. Clinically silent microemboli in patients with artificial prosthetic aortic valves are predominantly gaseous and not solid. *Stroke* 1997;28:322–5.

Journal of Congestive Heart Failure and Circulatory Support (2001) Vol 1, No 4, 391–398

FEM and CAD/CAM technology applied for the implantable LVAD

E. Okamoto PhD[1], S.-I. Fukuoka[1], M. Momoi[1], E. Iwasawa[1], K. Watanabe[1] and Y. Mitamura PhD[2]
[1]Department of Information Systems, School of Engineering, Hokkaido Tokai University, Sapporo, Japan; and [2]Department of System Information Engineering, Graduate School of Engineering, Hokkaido University, Sapporo, Japan

Background Thrombus formation is a critical issue when designing a long-term implantable left ventricular assist device (LVAD). Fluid dynamic characteristics of the blood flow are one of the main factors that cause thrombus formation. In this study, we optimized blood chamber geometry, port design, and fluid dynamics in our implantable LVAD to ensure minimization of shear stress-related blood damage that could lead to thrombus formation.

Method A blood pump chamber (stroke volume: 65 mL, stroke 12 mm) and inflow and outflow port were designed with three-dimensional computer-aided design (CAD) software (ProENGINEERING ver. 20, Ansys Inc. Canonsburg, PA, USA) and estimated by finite element method (FEM) computational fluid dynamic (CFD) analysis (Ansys/Flotran ver. 5.4, Ansys Inc., Canonsburg, PA, USA). Shear stress and normalized index of hemolysis (NIH) were obtained from calculating distribution of turbulent kinetic energy.

Result Using the above-mentioned design method, the blood pump geometry was optimized to the maximum sheer stress during the pump ejecting phase. With the second model, sheer stress decreased to 50.3 Pa from 261.6 Pa with the first model. Theoretical NIH also decreased to 0.098 g/100 L in the second model, from 2.72 g/100 L with the first model. Areas of flow stagnation that were observed with the first model disappeared with the second model.

Discussion The stasis and turbulence areas in the blood chamber can be predicted by the results of distribution of the flow velocity. Also areas of high sheer stress can be predicted by the results of the distribution of turbulent kinetic energy. The quantitative evaluation method for calculating NIH from CFD analysis is easy to use for estimating the pump geometry.

The results given above, demonstrate that the CAD of the blood pump contributes to optimizing a blood pump chamber for the purpose of reducing thrombus formation.

Keywords artificial heart, ventricular assist device (VAD), implantable, computer-aided design (CAD) computer-aided manufacturing, computational fluidynamic (CFD) analysis. normalized index of hemolysis (NIH), fine element method (FEM).

Introduction

We have been developing a totally implantable left ventricular assist system (LVAS) for use as a bridge to heart transplantation and more for long-term use as an alternate therapy for patients with end-stage heart failure. The totally implantable LVAS mainly consists of a motor-driven pulsatile assist pump and its controller, a transcutaneous energy transmission system[1], and a transcutaneous data transmission[2] (Figure 1). The motor-driven assist pump consists of a brushless DC-motor and a ball-screw (Figure 2). The ball-screw converts the rotational motion of a rotor to the rectilinear motion of a pusher-plate.

Although the implantable LVAS employs high electronic and information technology, the success of the implantable LVAS depends on the performance of the blood pump. One of the main aims when designing a blood pump is to ensure either elimination or minimization of thrombosis. The degree of thrombosis formation depends on the following three factors:

1. Physiological condition of the patient
2. Biocompatibility of the blood-contacted surface material
3. Fluid dynamic characteristics of blood flow in the blood pump.

Severe activation of the blood, which in turn leads to thrombosis, can be caused by a number of adverse flow characteristics including: (1) turbulence, (2) recirculation stasis, and (3) high shear stresses.

Flow visualization and particle image velocimetry are used to determine flow conditions within total artificial heart (TAHs) and VADs[3–5]. Because this technique needs flow visualization apparatuses, and can only be used after pump manufacture, flow visualization studies need many trials over a long period of time before a suitable pump geometry is obtained.

Correspondence to: Eiji Okamoto, Department of Information Systems, School of Engineering, Hokkaido Tokai University, Minami-sawa 5–1–1–1, Minami-ku, Sapporo 005–8601, Japan.

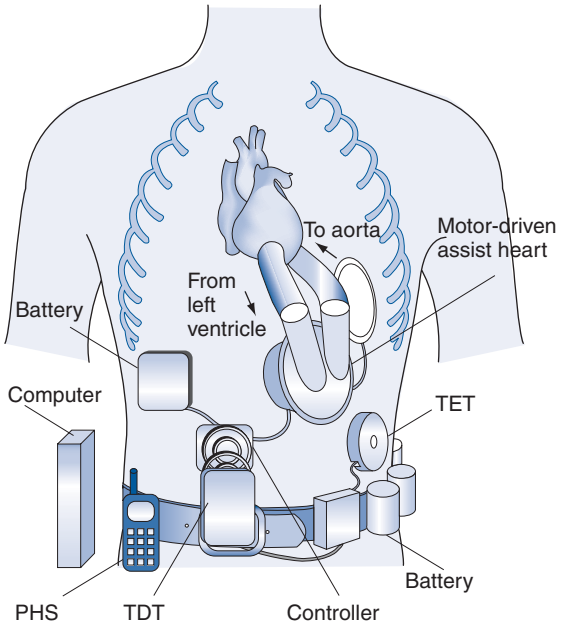

Figure 1. Totally implantable LVAS. PHS: personal handy-phone system; TDT: transcutaneous digital-data transmission; TET: transcutaneous energy transmission.

In this study we have designed and manufactured a blood pump based on the optimization of the characteristics of fluid dynamics related to blood flow in the pump using finite element method (FEM) computational fluid dynamics (CFD) analysis and Computer-aided design and manufacturing (CAD/CAM) technology. If the geometry of the blood pump can be evaluated before the pump is manufactured, and if an optimized pump geometry can be drawn on the computer, cost and time savings can be realized in developing a good blood pump.

Method

Figure 3 shows our design and manufacture process for blood pump development. The geometry of the blood pump was designed by CAD software (ProENGINEERING ver.20, Ansys Inc., Canonsburg, PA, USA). FEM software (Ansys/Flotran ver.5.4, Ansys Inc., Canonsburg, PA, USA) reads the pump geometry data, calculates the distribution of blood flow velocity in the pump, and calculates the distribution of the turbulent kinetic energy of the blood flow in the pump. The geometry of the pump was re-designed with consulting calculation results of CFD analysis. The optimized blood pump geometry data as translated to CAM software (Modela Player, Roland DG Corporation, Japan), and a three-axis computer-controlled machine tool (CAMM–3, Roland DG Corporation, Japan) pragmatized the pump geometry data in the computer.

Figure 4 shows the boundary conditions for CFD analysis of the blood pump at a pump outflow of 5 L min^{-1} against a pump after-load of 100 mmHg. During the filling phase, a pre-load of 10 mmHg was applied on the inflow port while the outflow port was occluded. The pusher-plate was moved to an end-diastolic position at a velocity of 27 mm/s. During the ejection phase, an after-load of 100 mmHg was applied on the outflow port while the inflow port was occluded. The

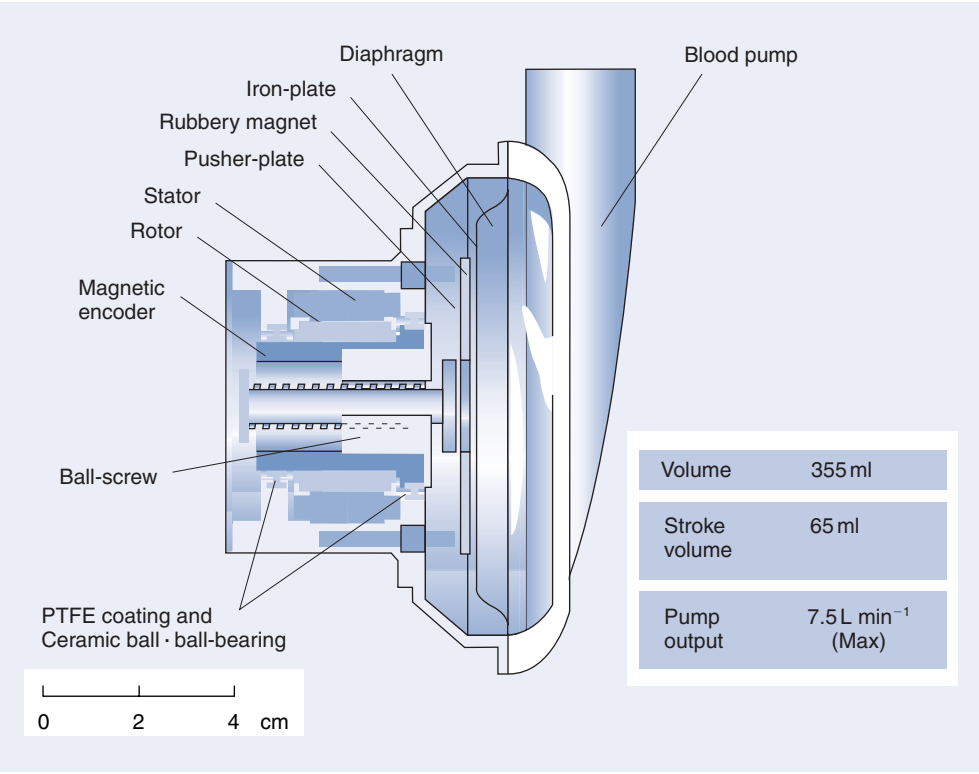

Figure 2. Cross-sectional drawing of motor-driven assist pump.

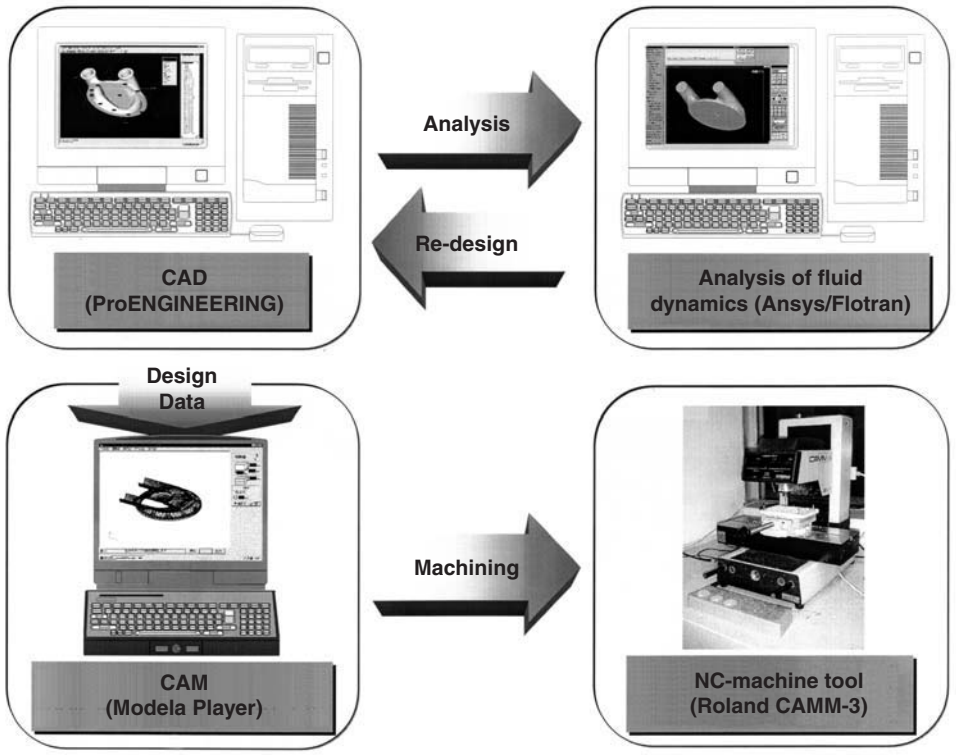

Figure 3. Design and manufacturing process of the blood pump.

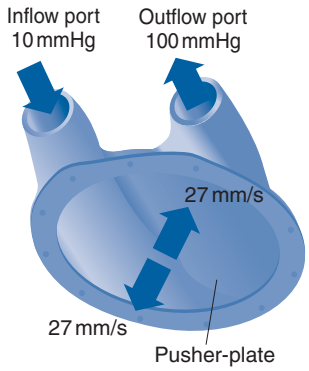

Filling phase

Inflow port: 10 mmHg
Outflow port: occlusion
Pusher-plate velocity: 27 mm/s

Ejection phase

Inflow port: Occlusion
Outflow port: 100 mmHg
Pusher-plate velocity: 27 mm s^{-1}

Blood condition

Density: 1.06×10^{-3} g/mm^3
Viscosity: 6×10^{-3} g/mm · s

Figure 4. Boundary conditions for CFD analysis. Pump outflow: 5 L min^{-1}; aortic pressure: 100 mmHg.

pusher-plate was moved to an end-systolic position at a velocity of 27 mm/s. A blood density of 1.06×10^{-3} g/mm^3 and a blood viscosity of 6×10^{-3} g/mm^3·s were used for calculation.

In this study, we calculated the normalized index of hemolysis (NIH) using the results of a CFD analysis for quantitative evaluation of the pump geometry.

In turbulent flow, Reynolds stress $\vec{\tau}$ is given by:

$$(1) \qquad \vec{\tau} = \rho \begin{pmatrix} \overline{v_x' v_x'} & \overline{v_x' v_y'} & \overline{v_x' v_z'} \\ \overline{v_x' v_y'} & \overline{v_y' v_y'} & \overline{v_y' v_z'} \\ \overline{v_x' v_z'} & \overline{v_y' v_z'} & \overline{v_z' v_z'} \end{pmatrix}$$

where v_x',v_y',v_z' are fluctuated flow velocity components of each direction, and ρ is density of blood[6]. Reynolds stress τ can be considered a flow-induced shear stress force in turbulent flow.

Turbulent kinetic energy k is given by:

$$(2) \qquad k = \frac{1}{2}\left(\overline{v_x' v_x'} + \overline{v_y' v_y'} + \overline{v_z' v_z'}\right)$$

Approximately, the magnitude of Reynolds stress τ and turbulent kinetic energy k has the following relation:

$$(3) \qquad \tau \cong \rho\left(\overline{v_x' v_x'} + \overline{v_y' v_y'} + \overline{v_z' v_z'}\right) = 2\rho k$$

Blood damage by shear stress is a function of the magnitude of shear stress τ acting on blood corpuscles and exposure time t_{exp} to the shear stress fields. Lysis rate of red blood cells L_{RBC} (%) can be estimated using the following mathematical correlation that was verified experimentally[7]:

$$(4) \qquad L_{RBC} = \frac{\Delta Hb}{Hb}(\%) = 3.62 \times 10^{-5} \times t_{exp}^{0.785} \times \tau^{2.416}$$

Free hemoglobin volume (f-Hb) can be estimated using the following equation:

$$(5) \qquad \text{f-Hb(Time)} = \text{TBV} \times \text{Ht}\left\{1-\left(1-\frac{L_{RBC-f}}{100}\right)^{\frac{FR\times Time}{TBV}}\left(1-\frac{L_{RBC-e}}{100}\right)^{\frac{FR\times Time}{TBV}}\right\}$$

where TBV is total blood volume (ml), Ht is hematocrit (%), FR is flow rate (L min^{-1}), and Time is a sampling interval

(min). L_{RBC-f} and L_{RBC-e} reveal lysis rate of red blood cells during the filling and ejection phases, respectively.

From above equations 1–5, we can obtain NIH using the following equation[8]:

$$(6)\ \text{NIH} = \Delta\text{freeHb} \times \frac{100 - \text{Ht}}{100} \times \text{TBV} \times \frac{100}{\text{FR} \times \text{Time}}$$

where Δ free Hb is the increase of plasma free hemoglobin concentration during sampling period (g/L), FR is flow rate (L min^{-1}).

ΔfreeHb (g/L) is given by:

$$(7)\qquad \Delta\text{freeHb} = \frac{\text{f} - \text{Hb(t)} \times \sigma}{\text{TBV}}$$

where σ is density of hemoglobin in a red blood cell.

Results

Figure 5 shows the geometry of blood chambers. The geometry of both pumps was designed with a pump stroke volume of 65 mL and a pump stroke of 12 mm. The diameters of the inflow and outflow ports were fixed to 18 mm, corresponding to diameter of valve used. The diameter of the bottom was also fixed to 90 mm, in order to attach an artificial heart actuator.

Figure 6 shows a distribution of flow velocity in the pump during the filling phase. Blood was flowing more uniformly in the whole of the pump with the second model than in the first model. Areas of flow stagnation were observed with the first model; this problem disappeared with the second model.

Figure 7 shows the distribution of flow velocity in the pump during the ejection phase. With the second model, an improvement in flow velocity distribution could be obtained as the result of CFD analysis during the filling phase.

Figure 8 shows the distribution of Reynolds stress during the filling phase. The distribution of Reynolds stress was obtained from the results of the distribution of turbulent kinetic energy k with equation 3. The lower figures on each result show a cross-section at the dotted line level on each of the figures above. The highest Reynolds stress was observed at the base of the inflow cannula in both models (dotted line level). But the maximum turbulent kinetic energy decreased from 357.4 Pa with the first model to 157 Pa with the second model.

Figure 9 shows the distribution of Reynolds stress during the ejection phase in both models. The maximum Reynolds stress decreased from 261.6 Pa with the first model to 50.3 Pa with the second model; this decrease was due to the improved geometry of the pump.

For a quantitative evaluation of pump geometry related to fluid dynamic performance, we calculated NIH using equations given earlier. Table 1 shows the calculated results of NIH under the conditions of a mean aortic pressure of 100 mmHg, a total blood volume of 4.55 L, a pump flow rate of 5 L min^{-1} and a hematocrit of 40%. The estimated NIH decreased from 2.72 g/100 L with the first model to 0.098 g/100 L with the second model. From these results we can observe quantitively changes to the pump geometry and the degree of fluid dynamic improvement.

Figure 10 shows the motor-driven assist pump with a blood pump we manufactured with CAD/CAM technology. The pump housing was made from epoxy resin and jellyfish valves are used on the inflow and outflow ports[9].

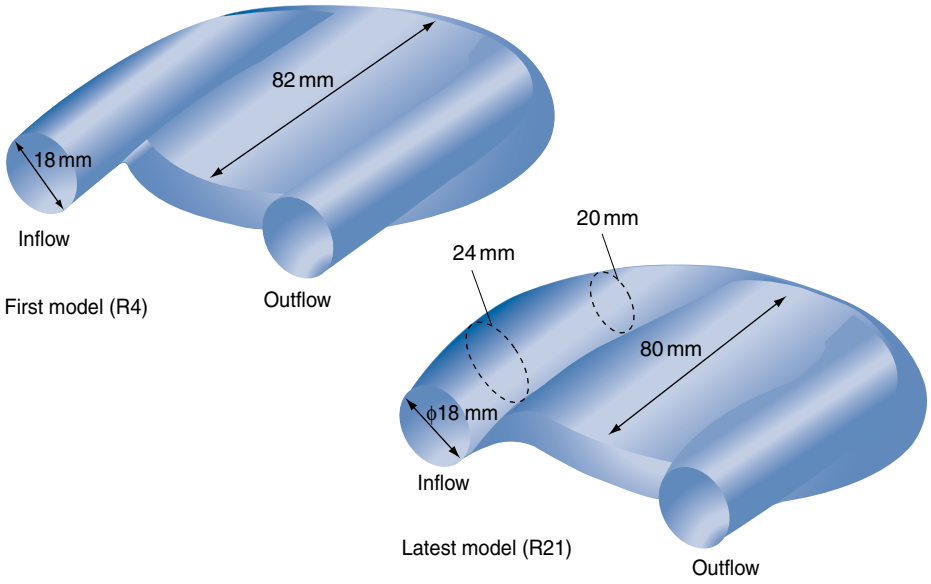

Figure 5. FEM analysis three-dimensional model.

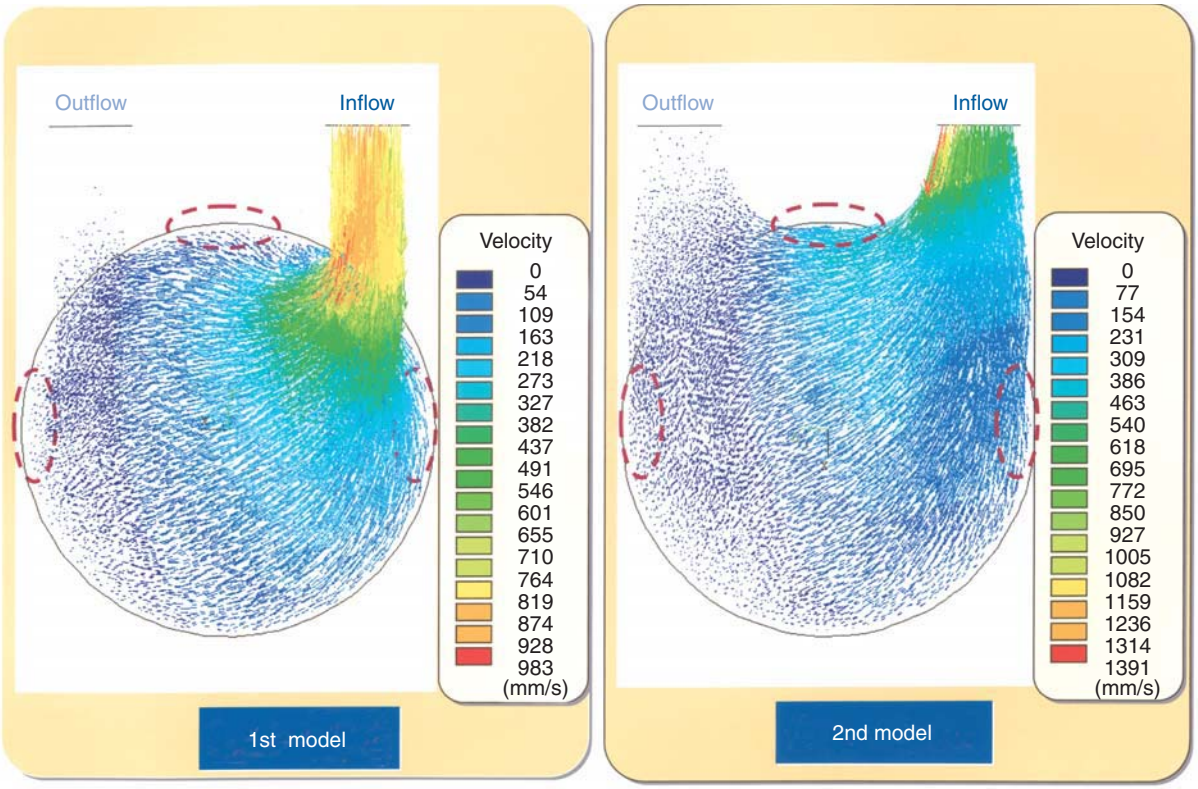

Figure 6. Distribution of flow velocity in the pump during filling phase.

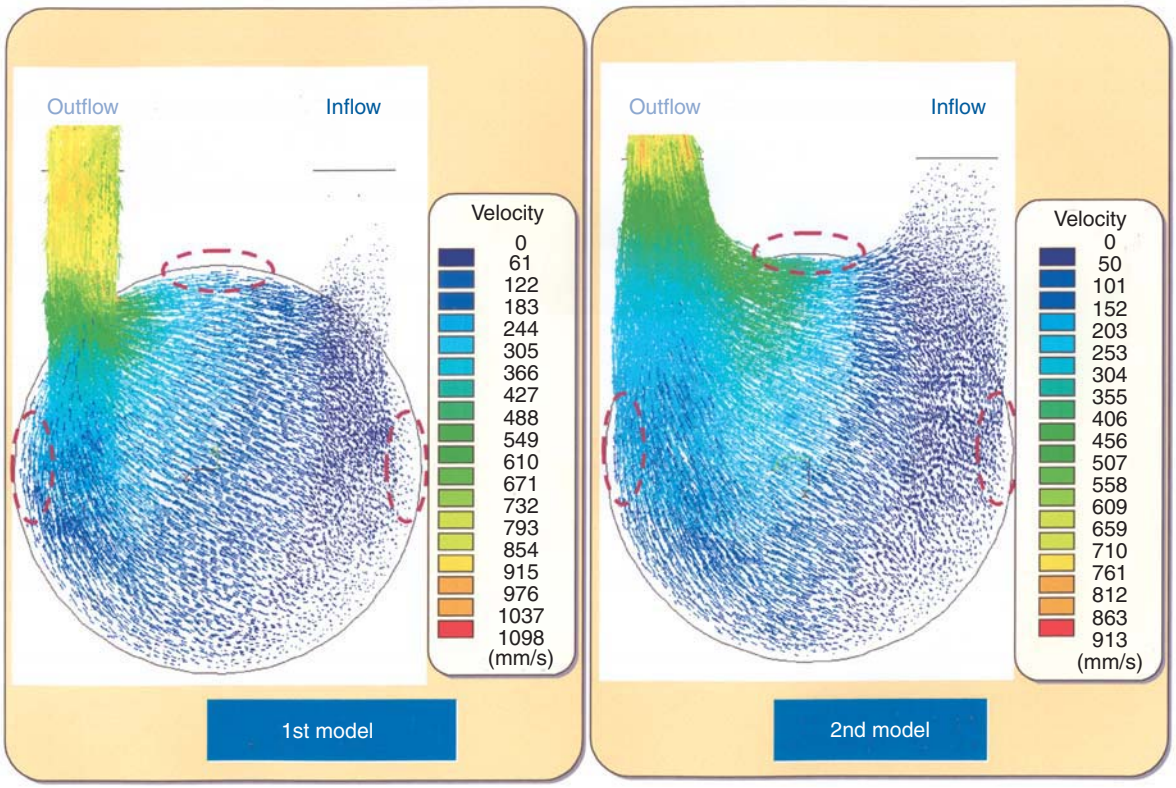

Figure 7. Distribution of flow velocity in the pump during ejection phase.

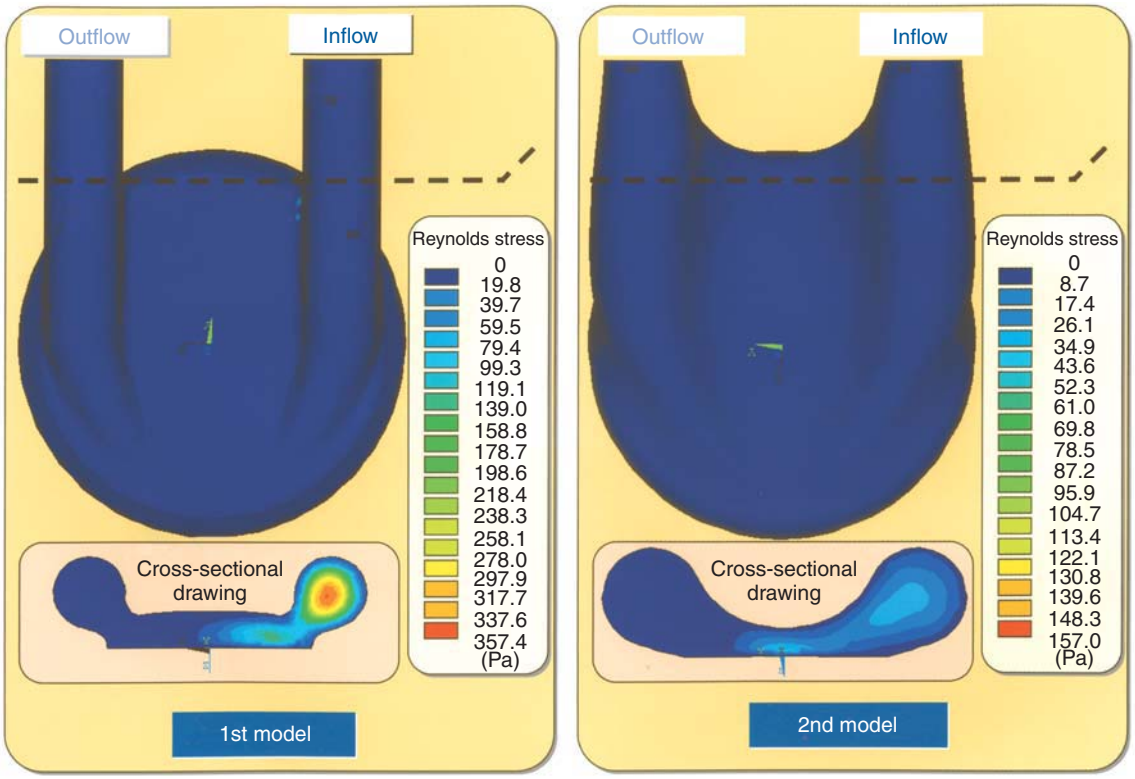

Figure 8. Distribution of turbulent kinetic energy in the pump during filling phase.

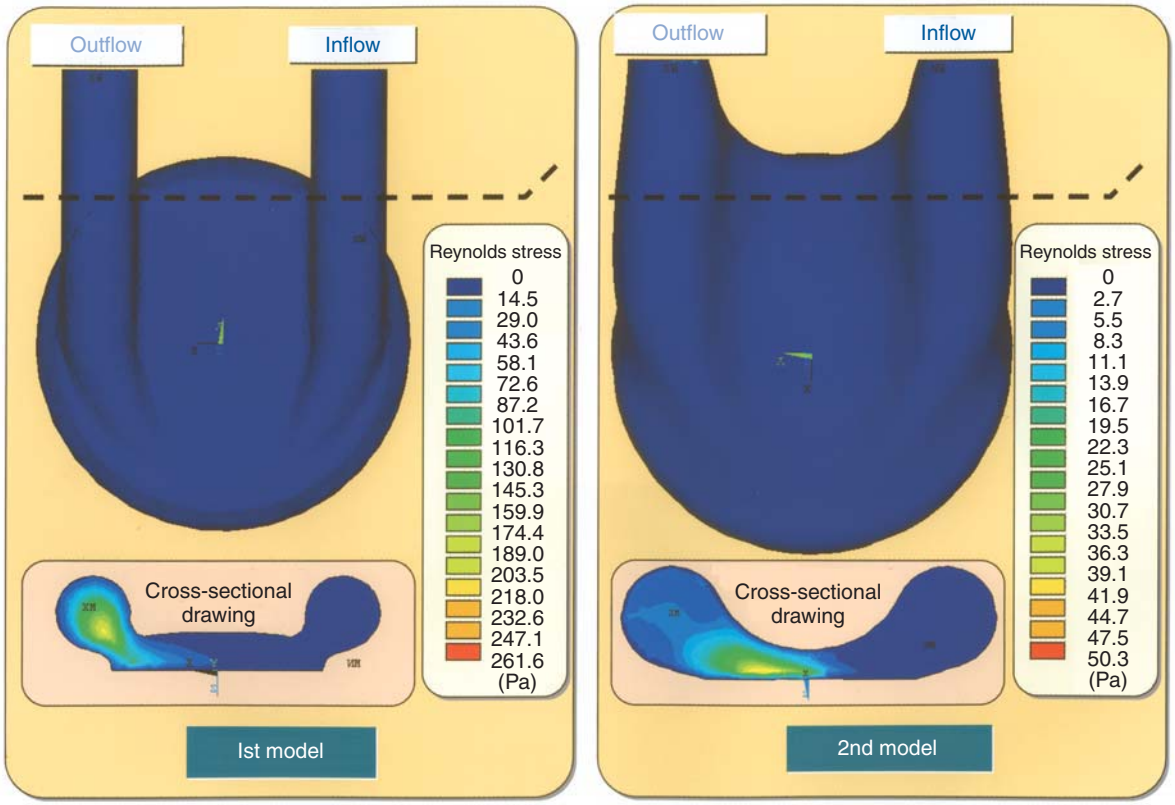

Figure 9. Distribution of turbulent kinetic energy in the pump during ejection phase.

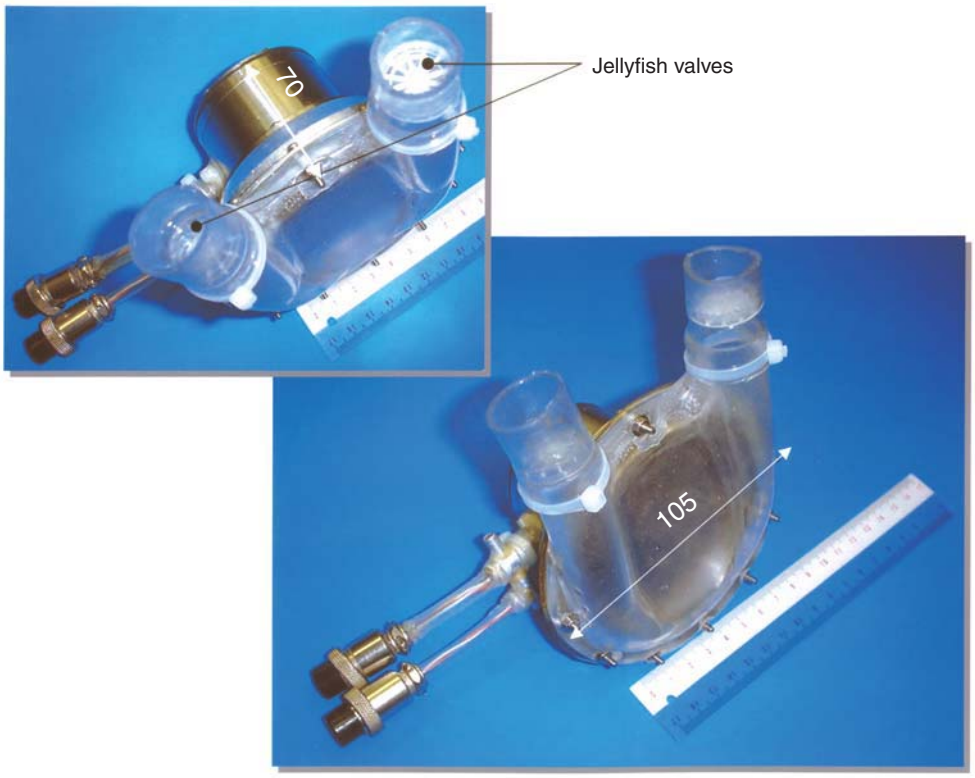

Figure 10. Motor-driven assist pump.

Table 1. Calculated results of NIH

Parameter	1st model	2nd model
$\bar{\tau}_{Filling}$	28.6 (Pa)	7.3 (Pa)
$\bar{\tau}_{Ejection}$	14.5 (Pa)	3.1 (Pa)
L_{RBC-f}	0.03311%	0.00122%
L_{RBC-e}	0.00642%	0.00015%
NIH	2.72 g/100 L	0.098 g/100 L

$\bar{\tau}$ Filling, Reynolds stress during filling phase;
$\bar{\tau}$ Ejection, Reynolds stress during ejection phase;
$L_{RBC-f,}$ lysis rate of red blood cells during filling phase;
$L_{RBC-e,}$ lysis rate of red blood cells during ejection phase;
NIH, normalized index of hemolysis

Discussion

We have developed the totally implantable LVAS for use on patients with end-stage heart failure. As the LVAS system needs various kinds of electronic sub-systems, many kinds of high electronic and information technology have already been applied to the LVAS. On the other hand, thrombus formation and resulting thromboemolism are major problems that have impeded the widespread use of ventricular assist devices. This issue is especially critical when designing long-term implantable LVASs. The three main factors that cause thrombus formation are: (1) coagulation systems, (2) material compatibility of the blood contacting surfaces, and (3) fluid dynamic characteristics of the blood flow. Severe activation of the blood, which in turns leads to thrombosis, can be caused by a number of adverse flow characteristics including turbulence, recirculation stasis, and high shear stresses. In this study, we designed and optimized the geometry of the blood chamber based on CFD analysis, and manufactured our system with CAD/CAM technology and a three-axis computer-controlled machine tool.

Stasis and turbulent areas in the blood chamber can be predicted with the first model by results of the distribution of the flow velocity. High-shear stress areas can also be predicted with the first model by the results of distribution of turbulent kinetic energy. From CFD analysis results, we redesigned the blood chamber and ports of the first model by reducing the flow velocity gradient between the blood chamber and each port in order to decrease shear stress. The second model improves fluid dynamic performance:

1. It decreases shear stress at the junction of both ports and the blood chamber
2. It diminishes the area of stasis corresponding to the D–H junction, where thrombi can easily form, by redesigning port geometry and port orientation.

In this study, we calculated NIH from CFD analysis results for the quantitative evaluation of the geometry of the blood chamber. The NIH reduced from 2.72 g/100 L with the first model to 0.098 g/100 L with the second model. As equation 4 was obtained from the measured results of

relatively higher-shear stress fields than in our blood pump, the value of lysis rate of red blood cells might be highly estimated. From the results discussed above, the value of calculated NIH is higher than that of an actual pulsatile blood pump. In order to evaluate the degree of hemolysis in the pump, we need to measure NIH in an *in vitro* experiment, but this quantitative evaluation method of calculating NIH makes it easy to optimize pump geometry.

In the current study, we demonstrate the process of design and manufacture of a blood pump using CAD/CAM and fluid dynamic analysis technology. A flow visualization study is required to optimize fluid dynamic characteristics of blood flow in the pump. The design process of this pump contributed to a reduction in cost and time in developing the blood pump, as design and evaluation can be carried out on the computer.

Conclusion

In this study, we demonstrate design and manufacture process of the blood pump using FEM CFD analysis and CAD/CAM technology. The results given suggest that the methods used to design the current pump improve the biocompatibility of the pump with blood and contribute to cost and time savings in developing the implantable LVAS.

Acknowledgement

This study was supported by the Program of Promotion of Fundamental Studies in Health Sciences of the Organization for Drug ADR Relief, R&D Promotion and Products Review of Japan.

References

1. Okamoto E, Tomoda K, Yamamoto K, Mitamura Y, Mikami T. Development of a compact, highly efficient totally implantable motor-driven assist pump system. *Artif Organs* 1994;18:911–17.
2. Okamoto E, Baba K, Nishibayashi K *et al*. Development of a transcutaneous digital-data transmission (TDT) system for an implantable artificial heart remote monitoring system. *ASAIO J* 1999;45:172.
3. Woodard JC, Shaffer FD, Schaub RD, Lund LW, Borovetz HS. Optimal management of a ventricular assist system–contribution of flow visualization studies. *ASAIO J* 1992; 38:216–19.
4. Meier D, Wernicke JT, Orime Y *et al*. Flow pattern analysis of the Baylor Total Artificial Heart. *Artif Organs* 1994;18: 923–32.
5. Mussivand T, Day KD, Naber BC. Fluid dynamic optimizations of a ventricular assist device using particle image velocimetry. *ASAIO J* 1999;45:25–31.
6. Okamoto S. *Fluid Dynamics*. Tokyo: Morikita Publisher, 1996 (in Japanese).
7. Gierseipen M, Wurzinger LJ, Optiz R, Reul H. Estimation of shear stress-related blood damage in heart valve prostheses - in vitro comparison of 25 aortic valves. *Int J Artif Organs* 1990;13:300–6.
8. Naito K, Mizuguchi K, Nose Y. The need for standardizing the index of hemolysis. *Artif Organs* 1994;18:7–10.
9. Imachi K, Mabuchi K, Chinzei T, Abe Y, Imanishi K, Yonezawa T. Fabrication of a jellyfish valve for use in an artificial heart. *ASAIO J* 1992;38:237–42.

Journal of Congestive Heart Failure and Circulatory Support (2001) Vol 1, No 4, 399–401

Ventricular assist device control with a biventricular potential trigger

M. Kitamura MD, K. Hanzawa MD, K. Aoki MD, M. Saitoh MD and J. Hayashi MD
Second Department of Surgery, Niigata University School of Medicine, Niigata, Japan

Background The counter-pulsation drive of the ventricular assist device (VAD) allows for maximum unloading of the ventricle and it would be ideal for myocardial recovery.

Methods As an electrocardiographic trigger for VAD control in various conditions of an experimental model, biventricular potential (BVP) was compared with a standard electrocardiogram (ECG) and right ventricular potential (RVP). A pneumatic VAD was implanted as a support bypass between the left ventricular apex and the ascending aorta in 11 adult pigs. Hemodynamic parameters and the pump output were monitored. Two tips of a bipolar electrode were set on the right ventricle (RV) (RVP group; *n*=5) or on the RV and left ventricle (LV) (BVP group; *n*=6) for recording direct cardiac potential. The counter-pulsation drive of the VAD was applied by using the R-wave in standard ECG or the direct cardiac potential (RVP or BVP) as an ECG trigger. Special conditions with various artifacts on an ECG (arrhythmia, electromusculogram, irregular ventilation and passive vibration (simulation of exercise) were set for assessing the ECG trigger modes.

Results Artifacts of irregular ventilation and passive vibration made the drive control poor under standard ECG triggers, and caused incomplete control in the case of the RVP trigger. In contrast, the BVP trigger maintained the counter-pulsation control of the VAD well in all conditions of this study.

Discussion The results of this study suggested that the biventricular potential trigger might be one of the control methods of choice for the stable drive of the VAD during patients' rehabilitation or exercise.

Keywords drive control, ventricular assist device (VAD), counter-pulsation, biventricular potential trigger, right ventricular potential trigger.

Introduction

An electrocardiogram (ECG) monitoring from temporary myocardial leads could be used for control of intra-aortic balloon pumping after cardiac operation. We surmised that direct cardiac potential trigger, by using a bipolar myocardial electrode, might be useful for stable control of the ventricular assist device (VAD), especially during patients' rehabilitation or exercise.[1–4]

This study was undertaken to evaluate the direct cardiac potential trigger for VAD control in various conditions of the experimental model and to compare biventricular potential (BVP) with right ventricular potential (RVP) as sensitive and stable ECG monitoring.

Methods

Under general anesthesia and mechanical ventilation, 11 adult pigs (body weight 25–53 kg) underwent implantation of a pneumatic VAD (sac-type blood pump; Nippon Zeon Co., Tokyo, Japan). An uptake cannula was inserted into the left ventricular apex and an outflow conduit connected to the ascending aorta through median sternotomy (Figure 1). Hemodynamic parameters and the pump flow were monitored. Two tips of a bipolar electrode were set on the right ventricle (RV) (RVP group; $n = 5$) or on the RV and left ventricle (LV) (BVP group; $n = 6$) for receiving the RVP or BVP, respectively. In cases of the RV and LV bipolar recording, one tip of the bipolar electrodes was fixed along the acute marginal branch of the right coronary artery and another tip was inserted along the obtuse marginal branch of the left coronary artery (Figure 1). Regarding a drive control mode of the VAD, the pump ejection in the diastolic phase (counter-pulsation) was applied by using the R-wave in standard ECG or the direct cardiac potential (RVP or BVP) as an ECG trigger. After evaluation of the baseline control at rest, assessment of drive control was performed in the conditions of arrhythmia, artifact (irregular ventilation and electromusculogram) and exercise (passive vibration of the animal). The status of the drive control was defined as complete, incomplete or poor.

Results

All animals successfully underwent implantation of the VAD and an entire assessment was performed in all cases. Counter-pulsation control of the VAD was well maintained at rest by adjustment of the pump ejection delay according to systolic length of the native heart on the ECG.

Correspondence to: Masaya Kitamura, Second Department of Surgery, Niigata University School of Medicine, 1–757 Asahimachi-dori, Niigata 951–8510, Japan.

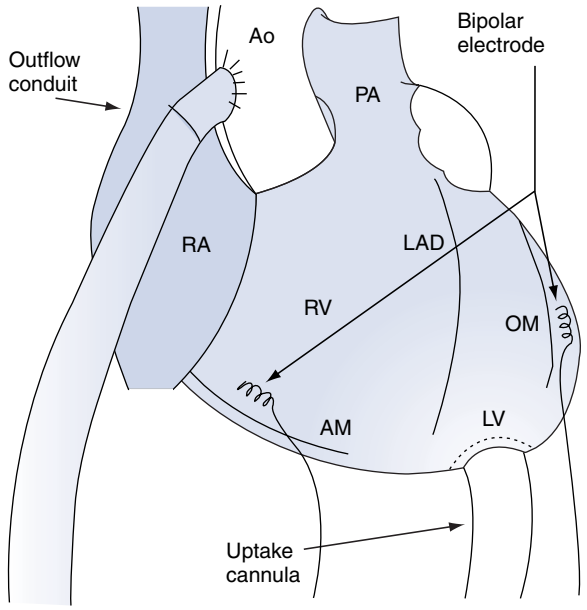

Figure 1. Schematic drawing of the biventricular bipolar electrode during the left ventricular support with an uptake cannula of the left ventricle and an outflow conduit of the ascending aorta. One tip of the bipolar electrode was fixed along the acute marginal branch of the right coronary artery and another tip was inserted along the obtuse marginal branch of the left coronary artery. AM = acute marginal branch, Ao = aorta, LAD = left anterior descending artery, LV = left ventricle, OM = obtuse marginal branch, PA = pulmonary artery, RA = right atrium, RV = right ventricle.

Figure 2 shows a monitoring record of the VAD drive control by using the BVP trigger. In the polygraphic recording of hemodynamic parameters and the pump flow, eminent diastolic aortic pressure is observed as a counter-pulsation. Some electromusculogram and irregular respiration are recognized in standard ECG, but no electromusculogram is noted in monitoring of the BVP.

Figure 3 demonstrates a polygraphic record of the VAD drive control by using the BVP trigger in the condition of passive vibration as a model of exercise. No QRS-wave was differentiated in standard ECG by artifact of the passive vibration. In contrast, a clear R-wave in each heartbeat is recognized in monitoring of the BVP, and complete counter-pulsation is maintained during the exercise-like condition.

Table 1 indicates assessment results of the counter-pulsation control in this investigation. All of the ECG triggers clearly established counter-pulsation control of the VAD while the animal was at rest. Some arrhythmias caused incomplete control in the case of the standard ECG trigger. Artifacts like irregular ventilation and exercise (passive vibration) made the drive control poor under the standard ECG trigger and caused incomplete control in case of the RVP trigger with use of the RV bipolar electrode. In contrast, the BVP trigger, by using the RV and LV bipolar electrode, completely maintained the counter-pulsation control of the VAD in all conditions of this investigation.

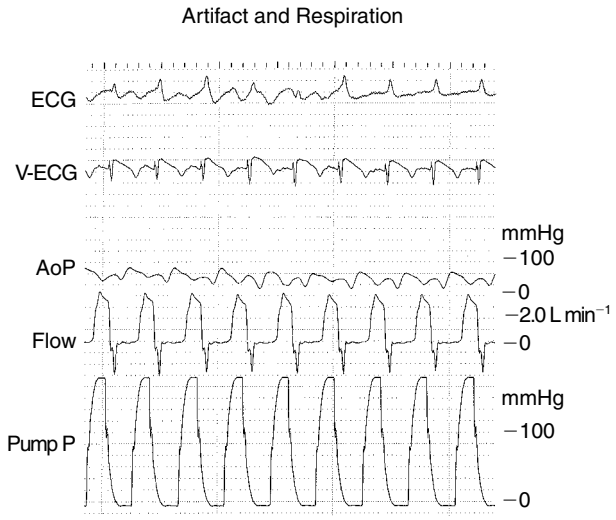

Figure 2. A polygraphic record of the counter-pulsation control of the VAD by using the biventricular potential trigger. Electromusculogram and irregular respiration are recognized in the standard electrocardiogram, but no artifact is noted in monitoring of the biventricular potential. ECG = electrocardiogram, V-ECG = ventricular electrocardiogram, AoP = aortic pressure, Flow = blood pump flow, Pump P = pump pressure.

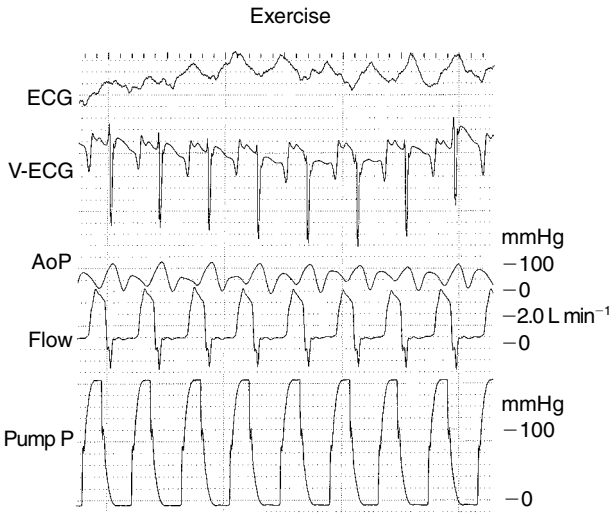

Figure 3. A polygraphic record of the counter-pulsation control of the VAD by using the biventricular potential trigger during exercise (passive vibration). No QRS-wave was differentiated in standard electrocardiogram by artifact of the passive vibration. In contrast, a clear R-wave in each heartbeat is recognized in monitoring of the biventricular potential, and complete counter-pulsation is maintained during the exercise-like condition. ECG = electrocardiogram, V-ECG = ventricular electrocardiogram, AoP = aortic pressure, Flow = blood pump flow, Pump P = pump pressure.

Discussion

The counter-pulsation drive of the VAD allows for maximum unloading of the ventricle[1,2] and it would be ideal for myocardial recovery. However, no drive control method except the fill-rate trigger of the Novacor system can maintain the counter-pulsation drive during patient exercise[1–7]. We developed a reliable drive control of the VAD with the BVP trigger by using the RV and LV bipolar electrode.

Table 1. Control status of counter-pulsation with electrocardiographic triggers for drive control of ventricular assist system

ECG trigger	Arrhythmia	Artifact	Exercise
Standard	Incomplete	Poor	Poor
RV bipolar	Complete	Incomplete	Incomplete
Biventricular	Complete	Complete	Complete

ECG = electrocardiogram, RV = right ventricle.

In clinical application of the next generation of the VAD, a drive control of the device, which allows sufficient systemic and pulmonary circulation, maximum unloading of the ventricle for myocardial recovery[1,2,8], no blood stagnation[2,9] thus preventing thromboembolism and so forth, is one of the essential factors for successful circulatory support in patients with severe heart failure. In addition to the above criteria, maintenance of the drive control during exercise[2,3] is very important because the duration of use of the VAD support is increasing as a bridge to transplantation,[2–4,10] bridge to recovery[8] or as long-term support.[11,12]

For effective myocardial recovery during rehabilitation of the patient, the counter-pulsation drive of the VAD is supposed to be ideal because maximum unloading of the ventricle is achieved. The ECG trigger drive of the VAD is one of the control methods that established counter-pulsation, but, standard ECG recording is impossible during exercise or rehabilitation. Therefore, we examined the possibility of the RVP or BVP trigger for maintaining the counter-pulsation control of the VAD.

From the results of this investigation, the direct cardiac potential trigger, especially the BVP trigger by using the RV and LV bipolar recording, could maintain the counter-pulsation control of the VAD during various conditions such as clinical conditions of the patient. Those results suggested that this counter-pulsation control with the BVP trigger might be one of the control methods of choice for various VADs of the next generation.

Conclusion

We conclude that the BVP trigger with the biventricular bipolar recording might be an adjunct drive control method for any VAD that could maintain a counter-pulsation-like flow during various conditions.

References

1. Kitamura M, Kawai A, Hachida M, Nishida H, Endo M, Koyanagi H. Clinical experience of left ventricular assist systems at The Heart Institute of Japan. *Artif Organs* 1999;23:286–9.
2. McCarthy PM, Portner PM, Tobler HG, Starnes VA, Ramasamy N, Oyer PE. Clinical experience with the Novacor ventricular assist system: bridge to transplantation and the transposition to permanent application. *J Thorac Cardiovasc Surg* 1991;102:578–87.
3. Poirier V, Dasse K. Clinical results of the HeartMate implantable blood pump. In Unger F, editor. *Assisted Circulation 4*. Berlin: Springer–Verlag, 1995:76–86.
4. Farrar DJ. Preoperative predictors of survival in patients with Thoratec ventricular assist devices as a bridge to heart transplantation. Thoratec ventricular assist device principal investigators. *J Heart Lung Transplant* 1994;13:93–101.
5. Nakatani T, Anai H, Eya K *et al*. Development and *in vivo* evaluation of an implantable left ventricular assist system with an impedance based monitoring and control system. *ASAIO J* 1995;41:M324–7.
6. Arai H, Fujiyoshi K, Sakamoto T, Suzuki A, Swartz MT. Optimal control algorithm for pneumatic ventricular assist devices: its application to automatic control and monitoring of ventricular assist device. *Artif Organs* 1996;20:1034–41.
7. Kitamura M, Morishita A, Kodera K, Endo M, Hashimoto A, Koyanagi H. *In vivo* assessment of optical fiber photoelectric switch system for implantable ventricular assist device. *ASAIO J* 1995;41:34.
8. Muller J, Wallukat G, Weng YG *et al.* Weaning from mechanical cardiac support in patients with idiopathic dilated cardiomyopathy. *Circulation* 1997;96:542–9.
9. Kitamura M, Akimoto T, Koyanagi H *et al.* Trans-mitral ventricular uptake for temporary left ventricular support without blood stagnation. In Akutsu T, Koyanagi H, editors. *Artificial Heart 4. Heart Replacement*. Tokyo: Springer–Verlag, 1993:339–41.
10. Vetter HO, Kaulbach HG, Haller M *et al.* Use of the Novacor left ventricular assist system as a bridge to cardiac transplantation: first experience with long-term patients on the wearable system. In Unger F, editor. *Assisted Circulation 4*. Berlin: Springer–Verlag, 1995:65–75.
11. Loebe M, Weng Y, Muller J *et al*. Successful mechanical circulatory support for more than two years with a left ventricular assist device in a patient with dilated cardiomyopathy. *J Heart Lung Transplant* 1997;16:1176–9.
12. DeRose JJ, Argenziano M, Sun BC, Reemtsma K, Oz MC, Rose EA. Implantable left ventricular assist devices: an evolving long-term cardiac replacement therapy. *Ann Surg* 1997;226:461–8.

Journal of Congestive Heart Failure and Circulatory Support (2001) Vol 1, No 4, 403–405

Smallest ventricular assist system by use of Peltier elements with shape memory alloy

T. Yambe MD[1], S. Maruyama[2], T. Takagi[2], M. Yoshizawa PhD[3], K.-I. Abe[3], K. Tabayashi[4], H. Takeda[5] and S. Nitta MD[1]

[1]Department of Medical Engineering and Cardiology, Institute of Development, Aging and Cancer, Tohoku University, Senday, Japan; [2]Institute of Fluid Science, Tohoku University, Sendai, Japan; [3]Graduate School of Engineering, Tohoku University, Sendai, Japan; [4]Department of Thoracic and Cardiovascular Surgery, Tohoku University School of Medicine, Sendai, Japan; and [5]Faculty of Engineering, Tohoku-gakuin University, Sendai, Japan

Abstract Further discussion may be necessary concerning the driving mechanisms of the totally implantable ventricular assist system (VAS). If consideration is given to the actuator with the shape memory alloys (SMAs), the system is simple enough for implantation. A simple system is, of course, desirable for the artificial heart, if durability, economy, reliability, and the implant are considered. When the actuator with the SMAs is considered, the problem of rate of reaction becomes important. With the SMAs, the reaction time is too slow for driving an artificial heart. One of the reasons for this slow reaction is the amount of time it takes to refrigerate. Heating can be done rapidly if the electric current is large enough, but because the process of refrigeration is slow, the function cycle becomes slow. The Peltier element was applied for the refrigeration process in this study. By application of the Peltier element, epoch-making improvement of the refrigeration speed is anticipated. An improvement in the rate of refrigeration will mean an improvement in the rate of reaction. An actuator driving frequency of around 1 Hz was possible with this design concept. This speed couldn't be anticipated in the previous reports of SMA. These results showed the possibility of application of the Peltier elements for use with the artificial heart system. We are now developing the artificial myocardium by using the SMA and Peltier elements. There are still problems with this system; however, it may be possible that this simple system may become the smallest VAS in future use.

Keywords ventricular assist device (VAD), Peltier element, shape memory alloy (SMA), artificial myocardium, moving patch.

Introduction

Heart transplantation has been resumed, even in Japan. The importance of mechanical circulatory assistance is being reconsidered due to an increase of patients awaiting transplantation[1–3]. Use of the ventricular assist system (VAS) as a bridge to heart transplantation may be necessary for a long time to come. Of course, the patient's quality of life (QOL) becomes important in such circumstances. Therefore, the totally implantable VAS system is desirable[2–6], especially if it is small enough to be implanted into the smaller physique of Japanese people[7–9].

At Tohoku University, we have devised a smaller sized ventricular assist device (VAD) for this purpose. As for the natural heart, the blood chamber is formed by heart muscle, therefore the chamber itself is a drive mechanism. This is unfortunately not so with the artificial heart (AH), so an alternative for the AH becomes necessary.

Artificial heart muscle

The constitution of an AH is not the final goal of this research. In this study, the goal is the development of an AH muscle. In other words, a natural heart was left in place and then the AH muscle sewn onto the wall of the ventricle. Our AH muscle supports the contraction of the natural heart ventricle.

Because a compact, lightweight actuator is needed, we paid particular attention to the use of shape memory alloy (SMA).

SMA actuator

The use of SMAs may make a high-efficiency drive possible, so the actuator of the SMA can be miniaturized. Furthermore, the drive mechanism of the SMA is simple, and its actuator may be of excellent durability.

We have carried out extensive research on the SMA for use with an AH actuator and have manufactured such a device as an experiment. The prototype SMA AH had a mechanism in which the coil of the SMA pushed an inner sac. It proved that it could be driven as an AH and its efficiency was good. Thrown energy becomes a drive in high efficiency. Heat increase can be set low. One important problem is the slow speed of cooling and this limiting factor

Correspondence to: Tomoyuki Yambe MD PhD, Department of Medical Engineering and Cardiology, Institute of Development, Aging and Cancer, Tohoku University, 4–1 Seiryo-machi, Aoba-ku, Sendai 980–8575, Japan.

was vitally important. In order to obtain the ideal conditions, we paid particular attention to Peltier elements.

SMA with Peltier elements

Electric energy becomes the movement of the heat in Peltier elements. In other words, heat is moved from one side to the other (Figure 1). One side is heated by electrical current and then the other side is cooled down rapidly. This device is the most suitable for rapid cooling.

In this study, we applied these characteristics. Figure 2 shows the concept of the SMA actuator with application of Peltier elements. Peltier elements were stuck onto SMA, and rapid cooling was achieved. First, an electrical current was added to the Peltier elements and one side was cooled down; then this procedure was reversed. Using this system, rapid heating and cooling became possible. A principle design of the moving patch by use of SMA and Peltier elements is shown in Figure 3. Some Peltier elements were stuck onto SMA. Fast operation becomes the embodiment of this device. The buffer of heat is applied to the opposite side. This device can facilitate the most suitable heat transfer.

Design concept of SMA Peltier actuator

The actuator can also be inserted between the ventricles and the driving of both ventricles becomes possible. It may be an ideal candidate as a drive mechanism for a TAH.

We are currently studying the application of this actuator to the right ventricle. Our institute is the designated facility for pulmonary transplants. Many patients have high blood pressure and right ventricular assistance is necessary for these patients. We are studying a device that would be sewn outside the right ventricle. An actuator for the right ventricular patch is presented in Figure 4.

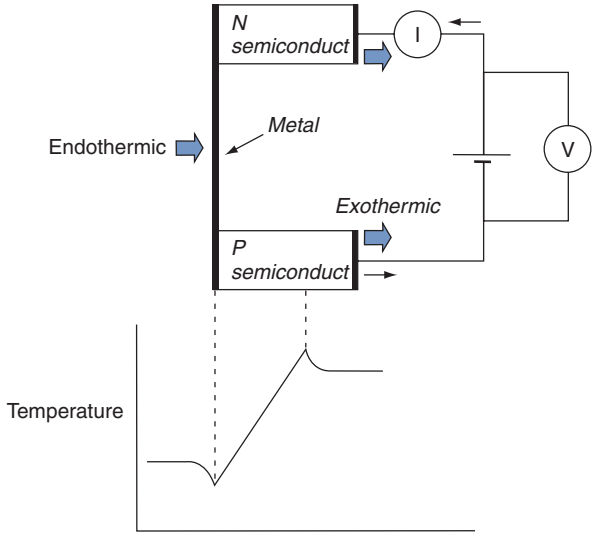

Figure 1. Schematic illustration of the Peltier elements. Electrical current was induced into the Peltier element; one side became endothermic and the another side became exothermic, so one side was cooled and the other side was heated.

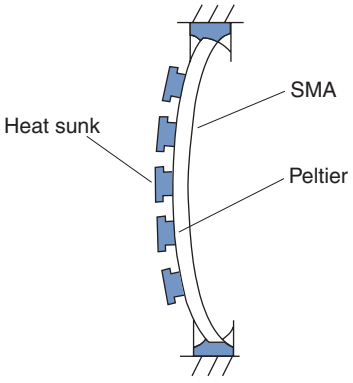

Figure 2. Schematic diagram of the moving patch for ventricular assistance.

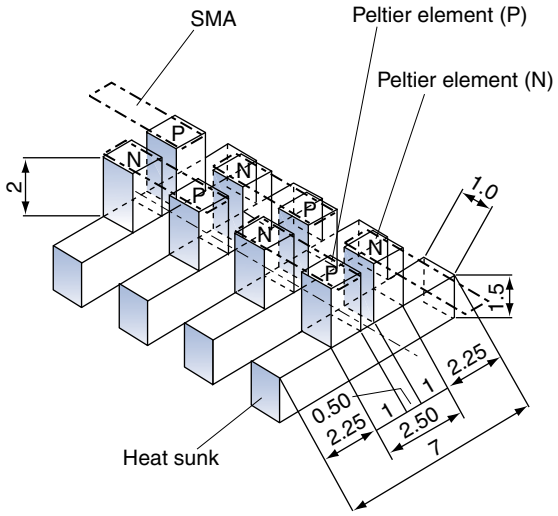

Figure 3 Blueprint of the moving patch by the use of SMAs and Peltier elements.

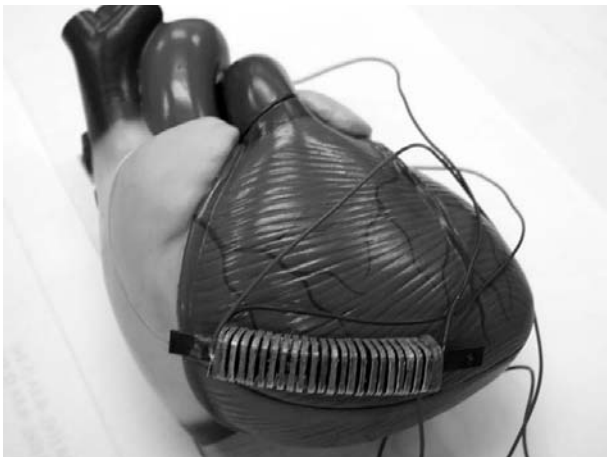

Figure 4. Photograph with SMA–Peltier actuator in a model heart.

In heat treatment outside SMA, an experiment of sewing the heat sunk on the right ventricle is being planned. The pressure has succeeded in this device with an operating time of almost 1; this speed cannot be achieved without Peltier elements.

The principle model of the SMA actuator with Peltier elements attached to the right ventricle of a heart is shown in Figure 4. The device, which pushes the wall of the right ventricle, works exactly like the massage of the heart.

There is one remaining problem in that the power may not appear when we give priority to a drive speed because the power is proportionate to the amount of the SMA. If we increase the amount of SMA, the speed of heat transfer will be limited, thus we must select the best design in the future. The actuator must be designed optimally.

In conclusion, the artificial heart muscle was manufactured as an experiment by use of the SMA with Peltier elements. Record-making high-speed cooling became the embodiment of use of the Peltier elements. Artificial myocardium was driven in the cycle for about 1 s. This speed cannot be reached if Peltier elements are not used. This may suggest the feasibility of the artificial heart muscle.

Acknowledgments

This paper was presented in part at the 7th International Symposium on Artificial Heart and Assist Devices held in March 10–11, 2000 at Tokyo, Japan. The authors thank Mr Kimio Kikuchi for experimental preparation and kind cooperation, Miss Rie Sakurai, Miss Takako Iijima, and Mrs Hisako Iijima for their excellent technical assistance and kind cooperation.

This work was partly supported by a Grant-in-aid for Scientific Research (No. 11480253), Research Grant for Cardiovascular Diseases from the Ministry of Health and Welfare and Program for Promotion of Fundamental Studies in Health Science of Organizing for Drug ADR Relief, R&D Promotion and Product Review of Japan.

References

1. Snyder AJ, Rosenberg G, Reibson J *et al.* An electrically powered total artificial heart: Over 1 year survival in the calf. *ASAIO J* 1992;38:M707–12.
2. Tatsumi E, Nakamura M, Masuzawa T *et al. In vitro* and *in vivo* evaluation of a left-right balancing chapacity of an interatrial shunt in an elctrohydraulic total artificial heart system. *ASAIO J* 1997;43:M619–25.
3. Yambe T, Owada N, Kobayashi S *et al.* Left heart bypass using the oscillated blood flow with totally implantable vibrating flow pump. *Artif Organs 1998;22:426–9.*
4. Kung RTV, Yu RS, Ochs BD, Parnis SM, Macris MP, Frazier OH. Progress in the development of the ABIOMED total artificial heart. *ASAIO J* 1995:41:M245–8.
5 Yambe T, Nitta S, Sonobe T *et al.* Chaotic hemodynamics during oscillated blood flow. *Artif Organs* 1994;18:633–7.
6. Nojiri C, Kijima T, Maekawa J *et al.* More than 1 year continuous operation of a centrifugal pump with a magnetically suspended impeller. *ASAIO J* 1997;43:M548–52.
7. Yambe T, Nitta S, Sonobe T, Naganuma S, Kobayashi S, Yoshizawa M, Fukutome A. Development of total artificial heart having advantages ineconomy and durability. *Int J Artif Organs* 1998;21:279–84.
8. Yambe T, Izutsu K, Hashimoto H *et al.* Control of the pulmonary arterial resistances by the use of the oscillated assist flow. *Artif Organs* 1998;22:430–3.
9. Yambe T, Abe Y, Yoshizawa M *et al.* Strange hemodynamic attractor parameter with 1/R total artificial heart automatic control algorithm. *Int J Artif Organs* 1996;19:302–6.

Journal of Congestive Heart Failure and Circulatory Support (2001) Vol 1, No 4, 407–412

Ultracompact, totally implantable, permanent, pulsatile VAD system

S. Takatani D Med PhD[1], K. Ouchi MS[1], M. Nakamura MD PhD[1] and T. Sakamoto MD PhD[2]
[1]Department of Artificial Organs, Institute of Biomaterials and Bioengineering; and [2]Department of Replacement Surgery, Tokyo Medical and Dental University, Tokyo, Japan

Abstract An ultracompact, totally implantable, permanent pulsatile ventricular assist device (VAD) intended for use in patients weighing 50–60 kg has been developed. It comprises a miniature electromechanical actuator and a pusher-plate-type blood pump. The external diameter is 90 mm with a thickness of 56 mm, yielding a total displacement volume of 285 cc. The pump housing was fabricated with a titanium alloy containing 6% aluminum and 7% niobium. The flexing diaphragm is made of polyurethane through a dip-coating technique. The total weight of the titanium VAD is 552 g. The electromechanical actuator consists of a miniature 14-pole, brush-less DC-motor and a planetary roller-screw. The motor speed, stroke length and rotational direction are all controlled by the commutation sensor signals. The VAD is operated in the passive fill/empty mode with the pusher-plate Hall effect position sensor signal. The design stroke volume is 55 cc with a 12 mm stroke length. The VAD can provide the maximum pump output of 8 L min^{-1} powered by 8 W. The maximum electrical-to-hydraulic efficiency is 24%. The VAD can be operated from re-chargeable nickel-metal-hydride (NiMH) batteries for over 2.5 h duration. This compact, implantable VAD is suitable for temporary, intermediate and permanent circulatory support of patients with end-stage cardiac failure.

Keywords ventricular assist device (VAD), bridge to transplantation, totally implantable VAD, bridge to recovery.

Introduction

Implantable ventricular assist devices (VADs) have become a powerful means to support circulation of patients with end-stage cardiac failure prior to heart transplantation[1,2]. Patients implanted with VADs can now be discharged from hospital while waiting for heart transplantation. It helps to improve general physical conditions of the patients as well as to reduce hospital expenses. For those patients who cannot be transplant recipients due to donor shortage, age limitation, immunological complications, cost and other social problems, destination therapy with the VAD has also taken place[3,4]. It is said that approximately 50 000 patients with end-stage cardiac failure could benefit annually from totally implantable VADs[5].

Both pulsatile and nonpulsatile implantable VAD systems have been investigated. To date, over 5000 patients have been implanted with pulsatile VADs; approximately half of these patients were successfully transplanted and discharged from the hospital[6]. Currently available implantable pulsatile VADs are intended for patients with a body weight of 80 kg or heavier. There is a difficulty in implanting the existing devices into patients weighing 50–60 kg, including women. Thus, there is a strong clinical need for development of a smaller sized, compact, high performance, totally implantable VAD system.

To meet the clinical need, continuous flow devices including centrifugal and axial flow pumps have been developed[7–10]. Because of their compact, easy-to-handle and valveless features, they have been gaining preference clinically as the implantable VAD. However, due to the pulseless feature, the physiological acceptability of nonpulsatile devices for prolonged or permanent support of circulation is questionable. Pulsatile devices are favored for long-term and/or permanent support.

This paper describes the current status of an ultracompact, high performance, totally implantable, permanent pulsatile VAD system that is under development at our institute. This VAD is intended as a bridge to transplant as well as for permanent support of patients' circulation. Genetic treatment to repair damaged cardiac tissue can be also conducted during VAD assistance. In this paper, design concept and performance of the VAD system *in vitro* will be explored.

Materials and methods

Design specifications of implantable VAD

The design specifications of the implantable VAD include:

1. VAD should be compact enough to fit into a patient of any size as permanent support of a failing heart.
2. Pump output during repose should be 4–5 L min^{-1} with the maximum output of 8–9 L min^{-1}.

Correspondence to: Professor Setsuo Takatani MD PhD, Department of Artificial Organs, Institute of Biomaterials and Bioengineering, Tokyo Medical and Dental University, 2-3-10 Surugadai, Kanda, Chiyoda-ku, Tokyo 101-0062, Japan.

3. Power requirement should be less than 10 W.
4. Durability should be 2–3 years.
5. For pump, diaphragm, and valve materials, titanium alloy and polyurethane will be used to enhance overall biocompatibility.
6. Cost should be affordable.

Concept of the totally implantable VAD

Figure 1 shows the anatomical configuration of the VAD and its components. The electrical energy is transmitted inside the body using a transcutaneous energy transmission (TET) concept. The electrical power from the external battery is first converted to an AC power using a switching circuit at around 100–200 kHz and then transmitted inside the body using a coupled coil system. The primary coil is placed outside the body over the secondary coil implanted in the subcutaneous space. The transmitted electrical energy is then used to power the implanted blood pump as well as to charge the internal battery. The internal battery can take over the function of powering the (VAD) for at least 30 min or longer in case the external coil of the TETS should be accidentally dislocated or the patient wishes to take a shower or bath. The run time of the external battery should be at least 7–8 h between initiating the re-charging process. A compliance chamber or variable volume device is implanted inside the chest cavity to compensate for volume changes that occur in the blood side of the pump chamber.

Components of the VAD[11–12]

A schematic diagram of the VAD is shown in Figure 2. The VAD was designed using the same basic components of the TAH that is also under development at our institute. The actuator comprises of a miniature, 14-pole Y-wound brushless DC-motor (Kollmorgen Inc., USA) and a planetary roller-screw (SKF, France). The rotational motion of the motor is converted to a recti-linear motion of the roller-screw to compress the diaphragm. The motor direction is reversed after completion of each ejection and retracted to allow passive filling of the blood chamber. The Hall effect sensor will be mounted and will continuously monitor the position of the pusher-plate. It will be used to run the pump in fill/empty mode and to derive beat-to-beat stroke volume, pump rate and minute pump output. The flexing diaphragm is made of polyurethane (Biospan SPU, Polymer Technology Inc, USA) through the dip-coating method. The external diameter of the VAD is 90 mm allowing an effective inner diameter of 84 mm. The thickness is 56 mm and this allows a stroke length of 12 mm. The designed stroke volume is 55 cc.

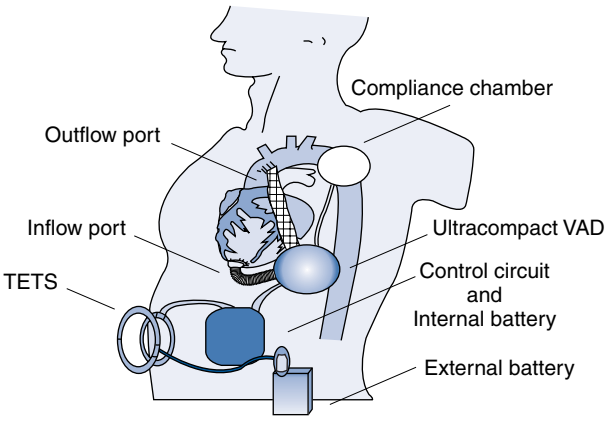

Figure 1. Anatomical placement of the totally implantable VAD and its components.

Fabrication of the VAD

The final goal is to fabricate the VAD housing as a one-piece unit out of a titanium alloy that contains 6% aluminum and 7% niobium (Ti-6Al-7Nb). The fabrication process of the VAD is shown in Figure 3. The computer-assisted design (CAD) system will be utilized to obtain three-dimensional images (3D) of the VAD. Based on the CAD data, a prototype VAD housing will be fabricated using the optically curable epoxy resin. Adjustments to various pump dimensions will be made to improve the profile of the VAD housing. By converting the 3D data to computer-assisted machining (CAM) data, the pump housing will be machined as a one-piece system out of titanium alloy (Ti-6Al-7Nb).

Results

Figure 4 shows images of the 3D VAD seen from various angles. Based on the data, epoxy pump housings were first fabricated using an optically curable epoxy resin. Its total volume and weight were 285 cc and 380 g, respectively. The titanium version was then fabricated. Figure 5 shows the VAD made of Ti-6Al-7Nb and its components. The volume and weight of the titanium version became 285 cc and 450 g, respectively. Figure 6 shows the pump output versus pump rate for various control voltage modes. They consisted of square wave (square), ramp mode during systolic phase (ramp [sys]), and ramp mode during diastolic phase (ramp [dia]). The highest pump output of 7 L min^{-1} was obtained at 140 bpm with the ramp (dia) mode. Figure 7 shows the input power required to generate a pump output of 3–7 L min^{-1}. The input power required was minimum with the ramp (dia) mode and less than 8 W to generate 7 L min^{-1} flow. Figure 8 shows the efficiency versus after-load for various heart valves used with the VAD. The maximum efficiency of 23% was obtained with polyurethane valves. Bjork–Shiley and St Jude valves resulted in lower efficiency due to higher regurgitation. Figure 9 shows the pump performance obtained at 100 bpm with re-chargeable nickel-metal-hydride (NiMH) batteries. It was possible to run the VAD with the re-chargeable NiMH batteries for over 2.5 h. Table 1 summarizes the pump characteristics of the current model in comparison to currently available implantable VADs. The pump size was considerably reduced, but the maximum pump flow remained approximately the same as with the previous design.

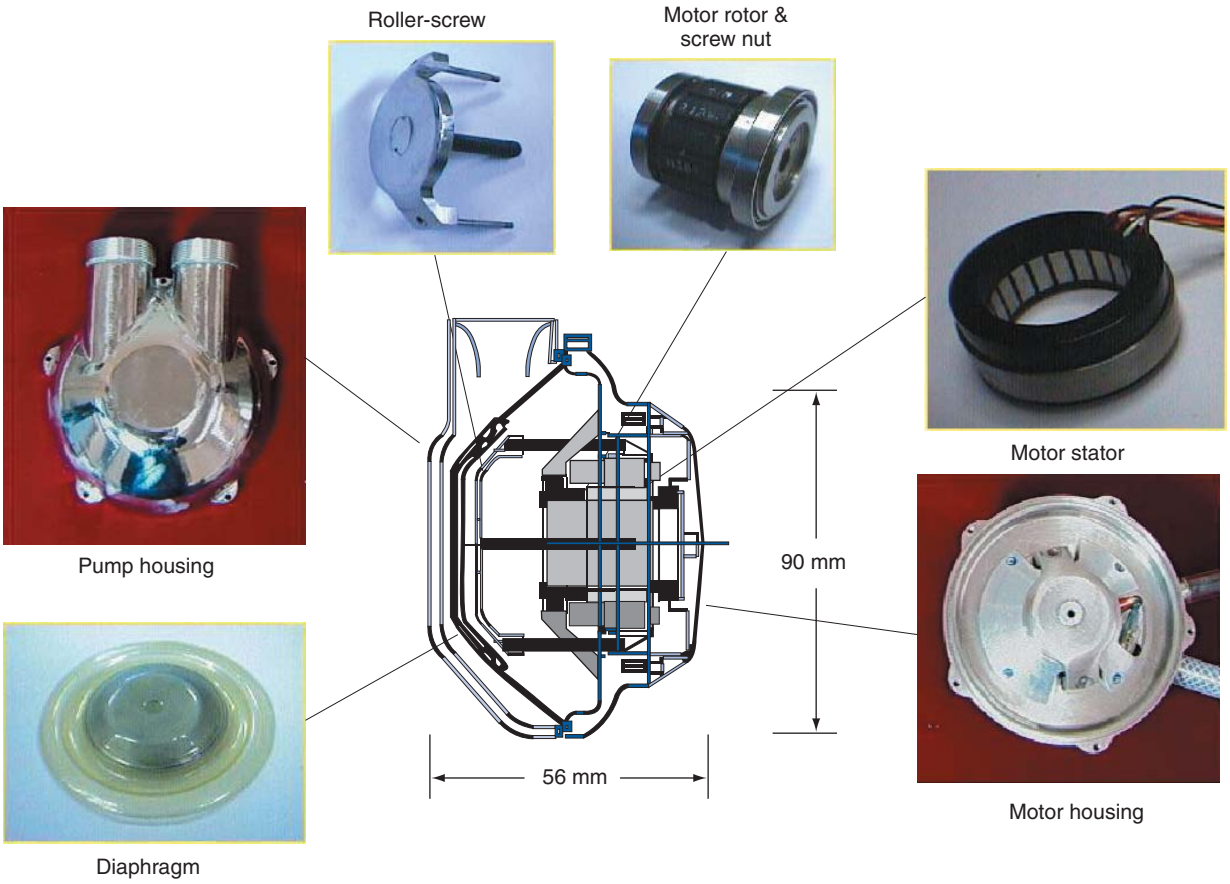

Figure 2. Schematic diagram of the totally implantable, electromechanical VAD system.

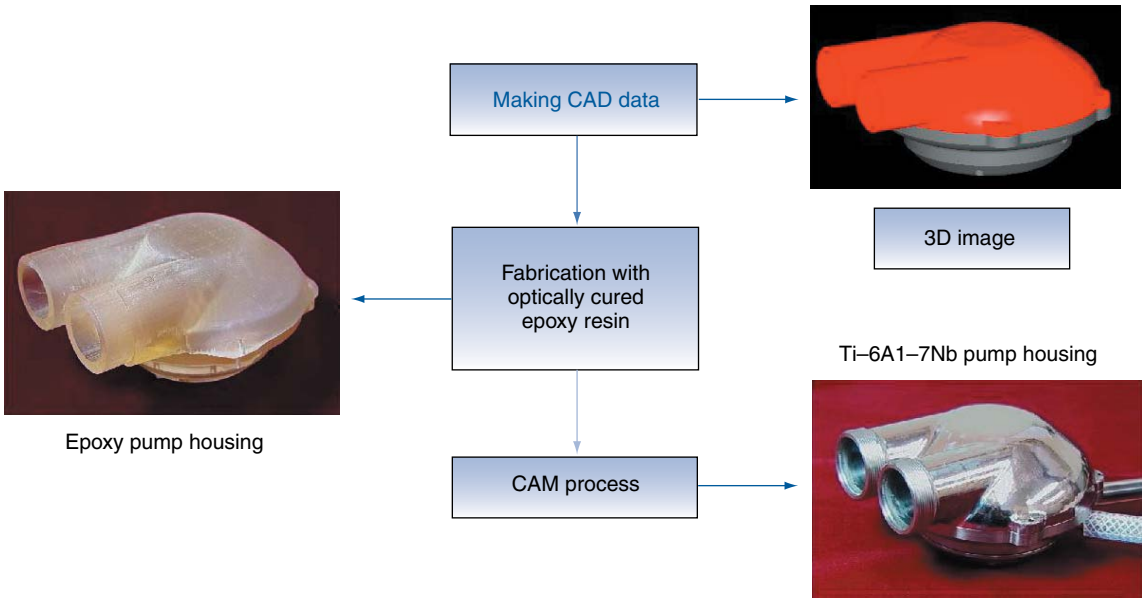

Figure 3. CAD/CAM fabrication process of the totally implantable VAD.

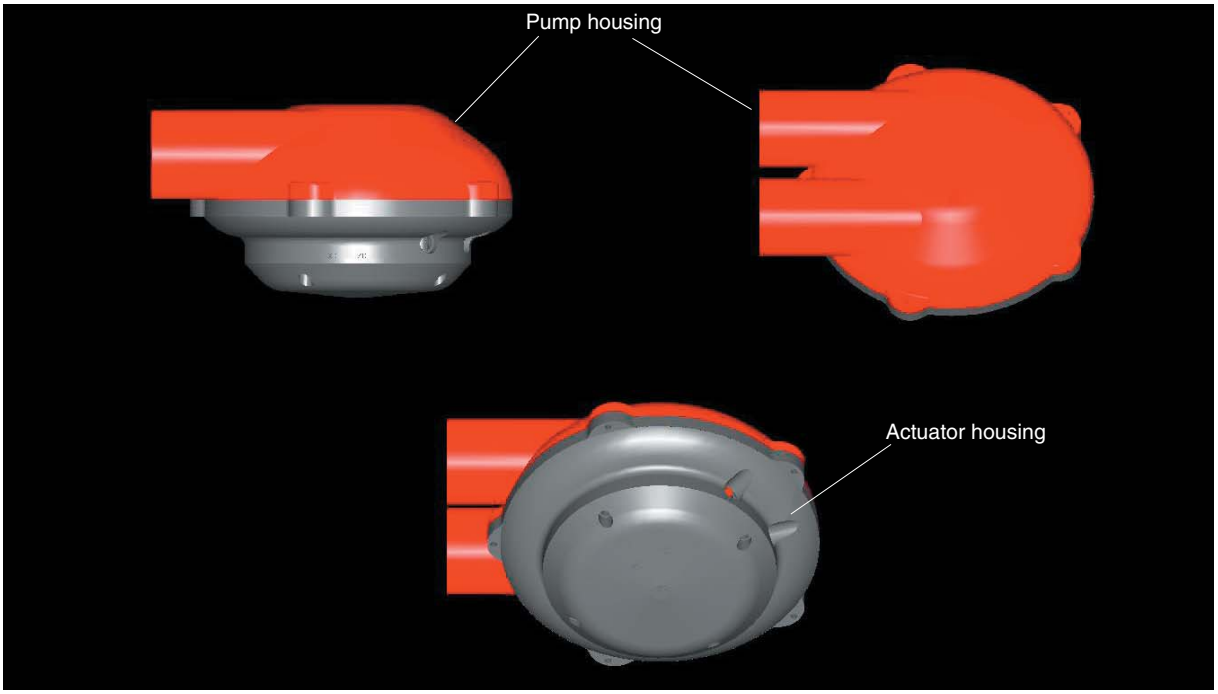

Figure 4. CAD images of the totally implantable, electromechanical VAD.

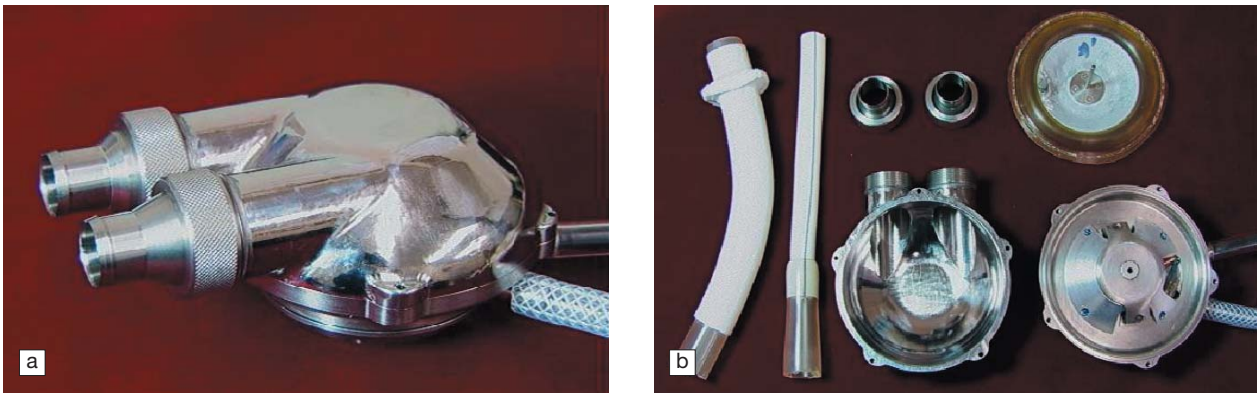

Figure 5. Totally implantable VAD (a) made of titanium alloy and (b) its components. Total volume: 285 cc; housing weight: 152 g; actuator weight: 400 g; valve housing: 50 g; diaphragm: 25 g.

Table 1. Comparison of pump size, weight, stroke volume, and pump flow of various VADs

	Diameter	Thickness	Volume	Weight	SV	Maximum flow
Yamagata VAD						
Epoxy	90 mm	56 mm	285 cc	380 g	53 ml	8 L min^{-1}
TMDU VAD						
Ti-6Al-7Nb	90 mm	56 mm	285 cc	552 g	53 ml	8 L min^{-1}
Baylor VAD*						
Carbon	98 mm	70 mm	360 cc	620 g	63 ml	10 L min^{-1}
Novacor			400 cc	690 g		
TCI			410 cc	870 g		

* Sasaki T, *et al*.: A biolized, compact, low noise . . .; *ASAIO Trans* 1991;37(3):M249–51.

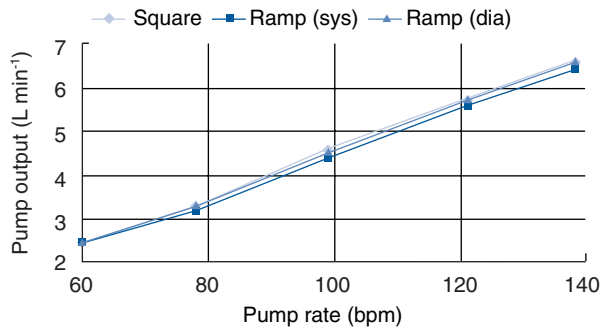

Figure 6. Pump output versus pump rate for various control modes.

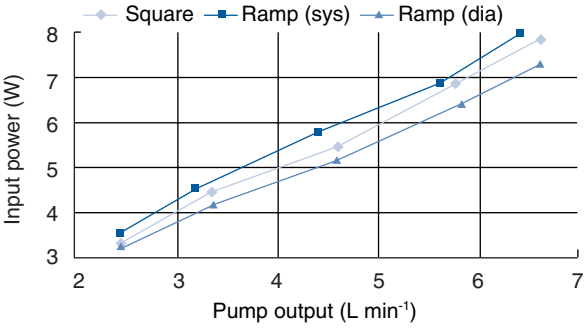

Figure 7. Input power versus pump rate.

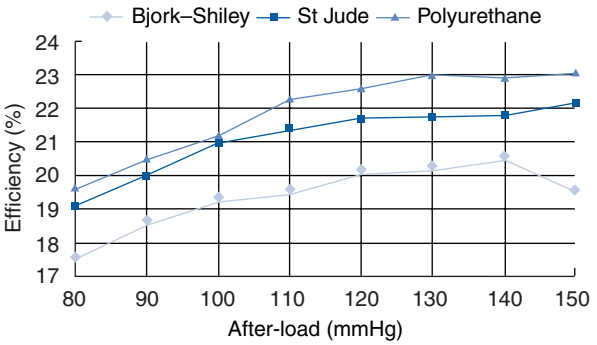

Figure 8. Efficiency versus after-load for various heart valves.

Discussion

An ultracompact, high performance, totally implantable VAD intended for use in patients weighing 50–60 kg (including women) has been developed and its performance was tested in a mock circulatory loop. In order to obtain a compact design, the actuator was down-sized to reduce the overall size of the pump system. Its outer diameter and thickness were 90 mm and 56 mm, respectively, yielding an overall volume of 285 cc. This volume is the smallest in comparison with the currently available clinical systems. The CAD pump data were generated to fabricate the pump housing using the CAM system. The experimental model was first fabricated with the optically curable epoxy resin to examine its basic performance. Then, the pump and motor housings were fabricated out of titanium alloy (Ti-6Al-7Nb). The epoxy pump had a volume and weight of 285 cc and 380 g, while the titanium pump had 285 cc and 450 g, respectively. The volume and weight of the titanium pump can be reduced further to probably half of the current value through an optimization process.

Although the pump size was reduced, the maximum pump output of 8 L min^{-1} was obtained at the pump rate of 150 bpm. The effective stroke volume was 53 cc. A maximum electrical-to-hydraulic efficiency of 24% was obtained with the required input power of less than 8 W. The efficiency improvement was due mainly to optimization of the hardware as well as the control algorithm. The selection of polyurethane valves in the inflow and outflow ports also helped to improve the volume efficiency of the pump. With this improvement, it was possible to operate the VAD from the re-chargeable NiMH batteries for over 2.5 h duration.

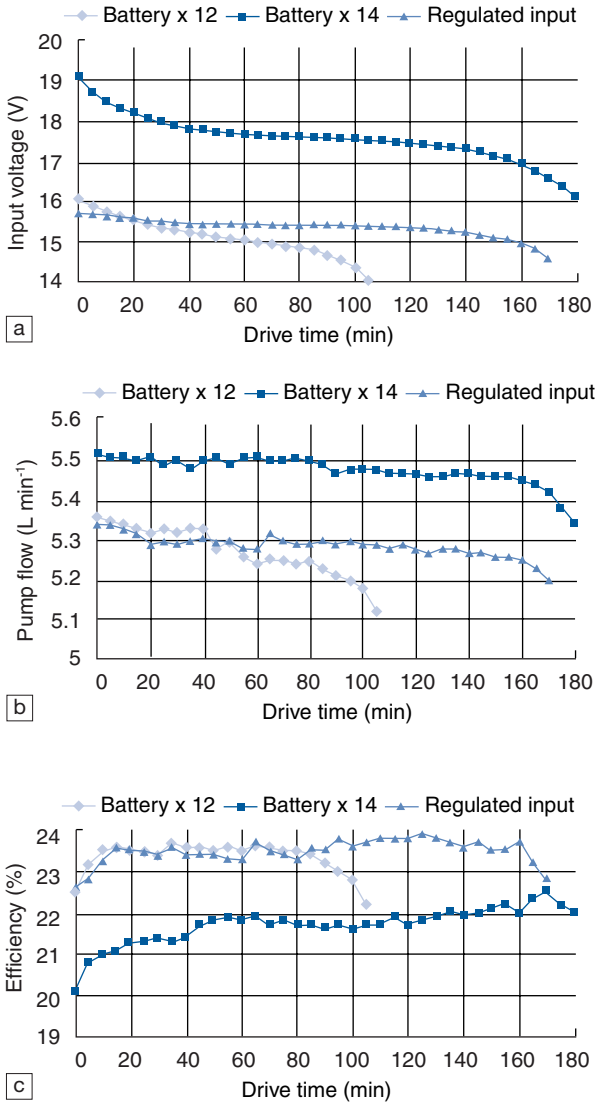

Figure 9. VAD performances obtained with the recargeable NiMH batteries.

The pump system was also evaluated in the mock circulatory loop with a compliance chamber. The compliance chamber, fabricated with an acrylic back plate with a flexing diaphragm made of latex rubber was connected to the vent port of the pump. The pump performance was little affected by the compliance chamber. We will implant the compliance chamber in the thoracic cavity. In order to reduce tissue adhesion and hence to prevent resistance for volume change, the flexing diaphragm will be covered with a textured surface[13]. A stable capsule formation should help operate the device for a prolonged period.

For pump material, titanium alloy (Ti-6Al-7Nb) was selected because of its stable, nontoxic performance in the biological environment over the commonly used Ti-6Al-4Va alloy[14]. Titanium forms an oxidized thin film, which provides a hydrophilic surface, and blood and tissue compatibility may be improved[15]. The titanium surface can also be polished to provide a mirror-like surface or textured to allow formation of a pseudo-neo-intimal surface. We intend to investigate the long-term blood-compatible performance of both surfaces in animal experiments.

As for inflow and outflow valves, polyurethane valves offered the best volume efficiency[16]. Both static and dynamic regurgitation through the valves was kept to a minimum to yield the best performance in comparison to the Bjork–Shiley and St Jude valves. However, the long-term stability and blood-compatible performance need to be tested in animal experiments as an integrated pump system.

As for the control aspect of the VAD system, the commutation pulse signals of the motor in combination with the Hall effect position signal can operate the pump in the fill/empty as well as fixed pulse rate mode. The pump rate and pump output can also be computed from the Hall effect pusher-plate position signal. A dedicated microprocessor control system is under development to replace the personal computer system and to evaluate the total system performance in the chronic animal experiment.

Summary

An ultracompact, totally implantable, permanent electromehanical VAD has been developed for use in patients weighing 50–60 kg. It can provide the maximum flow of 8 L min^{-1} at 150 bpm. The maximum electrical-to-hydraulic efficiency was 24% with the required power of less than 8 W. This VAD is ready for a biocompatibility as well as a durability study in chronic animal experiments.

Acknowledgement

This research was partially supported by grants-in-aid (Nos 11558102, 10044232) from the Ministry of Education.

References

1. Pristas JM, Winowich S, Nastala CJ *et al.* Protocol for releasing Novacor left ventricular assist system patients out-of-hospital. *ASAIO J* 1995;41:M539–43.
2. Arabia FA, Smith RG, Rose DS, Arzouman DA, Sethi GK, Copeland JG. Success rate of long-term circulatory assist device used currently for bridge to heart transplantation. *ASAIO J* 1996;42:M542–6.
3. Loisance D. Mechanical circulatory support toward permanent use. *Artif Organs* 1998;22(1):85–6.
4. Snyder AJ, Pae J, Bochmer J *et al.* First clinical trials of a completely implanted destination therapy ventricular assist system. *Heart Replacement Artif Heart* 2000;7000.
5. Hogness JR, VanAntwerp M. *The Artificial Heart; Prototypes, Policies, and Patients*. Washington, DC: National Academy Press, 1991.
6. Nosé Y. *Current status of cardiac prosthesis and future perspectives*. Special lecture at Tokyo Medical and Dental University, September 1, 1999.
7. Nojiri C, Kijima T, Maekawa J *et al.* More than 1 year continuous operation of a centrifugal pump with a magnetically suspended impeller. *ASAIO J* 1997;43(5):M548–52.
8. Thomas DC, Butler KC, Taylor LP *et al.* Continued development of the Nimbus/University of Pittsburgh (UOP) axial flow left ventricular assist system. *ASAIO J* 1997;43(5):M564–6.
9. Parnis SM, Conger JL, Fuqua JM *et al.* Progress in the development of a transcutaneously powered axial flow blood pump ventricular assist system. *ASAIO J* 1997;43(5):M576–9.
10. Tayama E, Olsen DB, Ohashi Y *et al.* The DeBakey ventricular assist device: Current status in 1997. *Artif Organs* 1999;23(12):1113–16.
11. Takatani S, Koyanagi H, Nogawa M, Inamoto T, Nishida H. Ultracompact, high performance, and completely implantable permanent electromechanical total artificial heart. *Heart Replacement Artif Heart* 1998;6:8–14.
12. Honda N, Inamoto T, Nogawa M, Takatani S. Ultracompact, completely implantable permanent use electromechanical ventricular assist device and total artificial heart. *Artif Organs* 1999;23(3):253–61.
13. Snow J, Harasaki H, Kasik J, Whalen R, Kiraly R, Nosé Y. Promising results with a new textured surface intrathoracic variable volume device for LVAS. *Trans Am Soc Artif Intern Organs* 1981;27:485.
14. Kobayashi E, Wang TJ, Doi H, Yoneyama T, Hamanaka H. Mechanical properties and corrosion resistance of Ti-6Al-7Nb alloy dental castings. *J Materials Science: Materials in Medicine* 1998;9:567–74.
15. Nosé Y. Blood contacting surface of titanium: Is it the metal or the water? *Artif Organs* 1998;22(12):1003–4.
16. Knierbein B, Rosaius N, Unger N, Reul H, Rau G. CAD-design, stress analysis and *in vitro* evaluation of three leaflet blood-pump valves. *J Biomed Eng* 275–283.

Journal of Congestive Heart Failure and Circulatory Support (2001) Vol 1, No 4, 413–417

Development of a compact, seal-less, tripod-supported centrifugal blood pump

K. Ouchi MS[1], A. Yuhki[3], M. Nakamura MD PhD[1], T. Sakamoto MD PhD[2] and S. Takatani D Med PhD[1]
[1]Department of Artificial Organs, Tokyo Medical and Dental University, Tokyo, Japan; [2]Department of Replacement Surgery, Tokyo Medical and Dental University, Tokyo, Japan; and [3]Department of Biomedical Engineering, Yamagata University, Yamagata, Japan

Abstract The pump performance of a newly designed, seal-less, tripod-supported centrifugal blood pump has been evaluated in a mock circulatory loop. The centrifugal blood pump developed in this study has an external diameter of 60 mm, and its total height including the motor driver is about 55 mm. This pump was made shaft- and seal-less by supporting an impeller with a tripod mechanism and driving it with a magnetic coupling force. The tripod, made of three ceramic balls 3 mm in diameter and mounted on the rear surface of the impeller, slides within a polyethylene groove mounted to the top surface of the bottom pump casing. The tripod mechanism allows elimination of the impeller's upper bearing system, which usually interferes with the flow stream inside the pump chamber. The magnetic coupling force generated between the follower permanent magnet mounted inside the impeller and the driver magnet mounted on the motor shaft external to the pump casing, allows a shaft-less and seal-less design of a compact centrifugal blood pump.

The pump performance was evaluated with both straight and curved vane impellers in the mock circulatory loop. The straight vane showed a slightly better performance than the curved vane. The tripod pump provided sufficient flows against physiological head pressures, and the results verified the basic pump characteristics to be acceptable as a left or right ventricular assist device. The hemolytic as well as anti-thrombogenic performances of the pump need to be examined prior to animal study.

Keywords seal-less centrifugal blood pump, tripod structure, implantable ventricular assist devices (VADs).

Introduction

The features of continuous flow devices such as centrifugal and axial pumps include compactness, ease of handling, and low cost, characteristics which make them suitable as implantable ventricular assist devices (VADs)[1,2]. Therefore, various designs of centrifugal as well as axial flow pumps are being investigated at many centers around the world[3–8].

In this research, we designed and evaluated a compact, seal-less, tripod-supported centrifugal blood pump for left or right heart support. The design concept of this pump is based on the free-impeller centrifugal blood pump system designed by Ohara and Nose[9]. In the free-impeller system, the impeller is supported by a tripod mechanism. Three ceramic balls mounted at the rear surface of the impeller support the impeller, which is magnetically coupled to the externally located drive magnet. One advantage of this design is elimination of the impeller's upper bearing system, but its stability, particularly at lower and higher rpms, is questionable. Although the feasibility of the tripod concept was proven in the *in vitro* study, problems such as the impeller's instability as well as its lift-off phenomenon at higher rpms were reported. In addition, hemolytic as well as thrombogenic properties have not been reported. In this research, we approached these problems through optimization of the impeller design, magnetic coupling forces between the follower and drive magnets and driver motor system through application of a computer-aided design (CAD) system. The CAD system was employed to design overall pump dimensions. As for a driver, a miniature, high-performance, DC brush-less motor was employed for optimization of the overall volume and better controllability of the device. We report the initial characterization of the prototype design in the mock circulatory loop.

Materials and methods

Tripod pump structure

A schematic diagram of the tripod-supported centrifugal blood pump system designed in this research is shown in Figure 1. The tripod-bearing system consists of three ceramic balls and a polyethylene groove. The configuration of the three ceramic balls is triangular in shape, and mounted on the rear surface of the impeller. The ceramic balls slide and rotate on the surface of a polyethylene groove mounted to the top surface of the bottom casing. The impeller's weight and the magnetic coupling force are entirely supported by the system. The pump is driven by a magnetic coupling force between a follower permanent magnet fixed inside the impeller and a driver magnet mounted to the shaft of a DC brush-less motor external to the pump head. For the driver and follower magnets, Neodium iron magnets were selected

Correspondence to: Katsuhiro Ohuchi, Department of Artificial Organs, Institute of Biomaterials and Bioengineering, Tokyo Medical and Dental University, Tokyo, Japan 2–3–10 Kanda Surugadai, Chiyoda-ku, Tokyo, 101-0062, Japan.

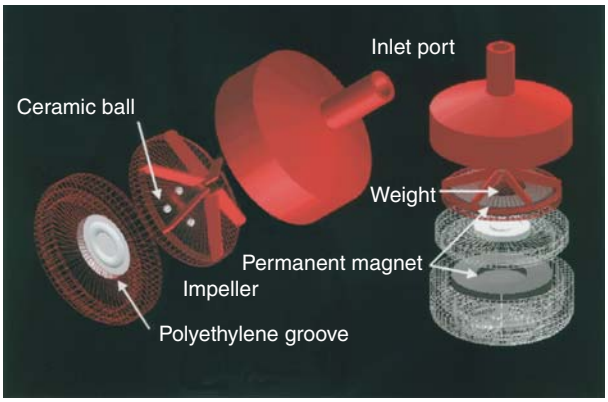

Figure 1. A schematic drawing of the tripod-supported, seal-less centrifugal blood pump.

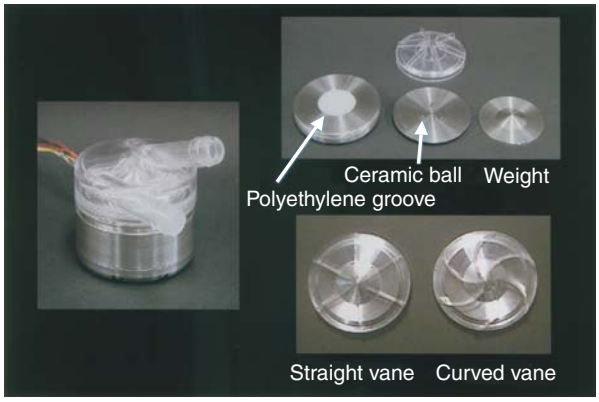

Figure 2. Assembled tripod-supported, seal-less centrifugal blood pump (left) and components and impeller (right).

because of their high magnetic strength. A balancing weight was placed inside the impeller toward its tip so that the center of the gravity will be at its tip allowing better stability of the impeller during rotation.

Prototype tripod pump system

Pump head

Figure 2 shows the assembled pump system and its components. The pump head consists of the top casing, impeller and bottom casing. The inflow and outflow ports are attached to the top pump casing to the eccentric location at its top and tangential to its periphery, respectively. The impeller is comprised of a top casing with six vanes, a bottom plate with three ceramic balls, a balancing weight and a follower permanent magnet. A polyethylene groove is mounted at the top surface of the impeller's bottom casing. The diameter of the impeller is 50 mm. The external diameter of the acrylic pump housing is 60 mm, allowing a gap distance between the impeller vane and pump casing of about 2 mm. The priming volume of the pump head is 25 ml (Table 1).

Impeller design

For evaluation of pump characteristics with different impeller designs, we tested both straight and curved vane impellers. The exit angle of the straight vane is 90 degrees but 30 degrees with the curved vane.

Table 1. The prototype tripod-supported, seal-less centrifugal blood pump assembled data

Tripod pump component	Pump head	Motor drive
Material	Acrylic	Stainless steel
Diameter (mm)	60	60
Height (mm)	26.4	28
Weight (g)	230	440
Volume (cm^3)	72	79.2
Priming volume (ml)	25	–

Pump driver

Figure 3 shows the schematic diagram of the drive system. A miniature, DC brush-less motor with a 14 pole, Y-wound, three-phase motor (Kollmorgen Inc., USA) is employed in this system. The motor rotor is supported with a set of radial bearings and a driver magnet is mounted to the rotor. The motor commutation is carried out using three Hall-effect position sensors and motor speed is controlled through a pulse width modulation technique.

Mock circulatory loop for static pump performance

Pump performances including flow pressure and system efficiency were measured using a mock circulatory loop as shown in Figure 4a. The inflow and outflow ports of the pump were connected to a reservoir using a set of 50 cm long, ^{3}Úinch Tygon tubes. Inflow and outflow pressures of the pump were measured using a mercury manometer while the pump flow (Q) was measured with an electromagnetic flowmeter. A clamp-type constrictor was applied to the outflow port of the pump to change pump flow, and resultant changes in the pump head pressure (P) were calculated as the difference between the outflow and inflow pressures. Motor current (I) and power supply voltage (V) were

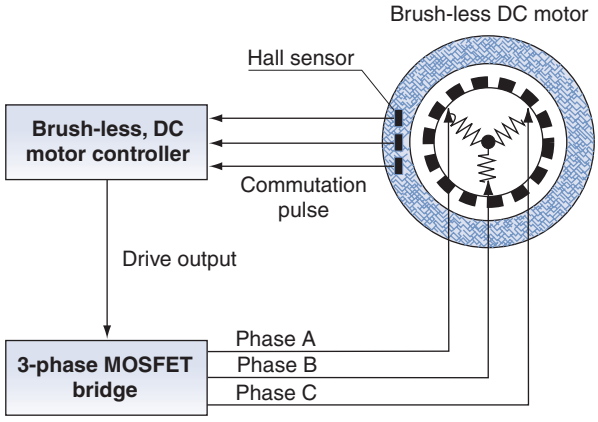

Figure 3. A block diagram for brush-less DC motor driving.

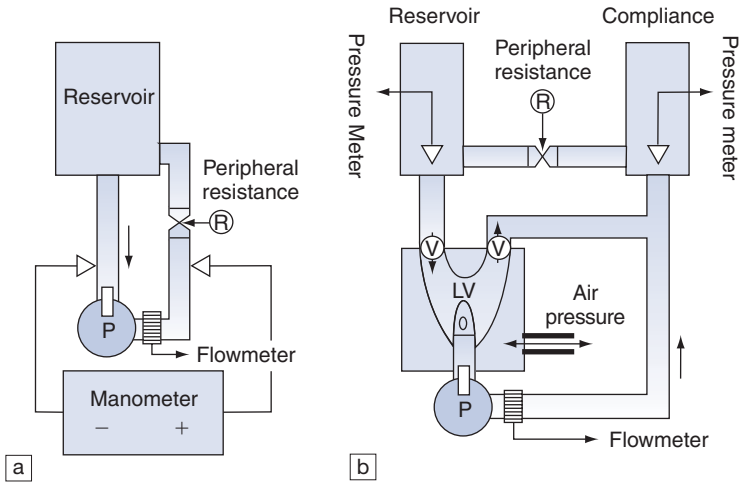

Figure 4. Mock circulatory loop for basic performance test (a) and for evaluation of physiological setup condition (b).

recorded on a digital oscilloscope to derive the input power of the pump driver. The input power (Pi) and externally delivered power (Po) as well as the system efficiency (E) were derived using following equations:

$$\text{Input power } Pi = V \times I,$$

$$\text{Output power } Po = P \times Q,$$

$$\text{Efficiency } E = Po / Pi$$

Left heart and right heart bypass study

The pulsatile mock circulatory system consisted of a pulsatile ventricle, an aortic compliance chamber, a peripheral resistance and an atrial reservoir which were connected in series as shown in Figure 4b**.** A pneumatic pulsatile blood pump made of Latex rubber was used to simulate the natural heart. The prototype centrifugal blood pump was connected from the apex of the simulated ventricle to the aorta using a 5 mm diameter tube. The pump flow through the tripod pump using an electromagnetic flowmeter, aortic pressure, motor current, and total flow were continuously monitored. The pulsatile ventricle was driven at a rate of 80 bpm, against a mean after-load of 100 mmHg with the pre-load of 10 mmHg. For right heart support, a mean after-load of 15 mmHg with a pre-load of 5 mmHg was used. The motor rotational speed of the tripod pump was gradually increased from 800 to 2400 rpm, while the hydrodynamic conditions were continuously monitored.

Results

Static pump performances

The relationships between head pressure and pump flow for various pump rpms for the straight vane and curved vane are shown in Figure 5 and 6, respectively. In order to obtain pump flow of 5 L min^{-1} against a head pressure of 100 mmHg, pump speeds were required ranging from 1800–2000 rpm for the straight vane and 2000–2200 rpm for the curved vane. The maximum pump flow at 2200 rpm for the straight vane was 8.5 L min^{-1} against a 110 mmHg head pressure, while for the curved vane it was 8.0 L min^{-1} against a 90 mmHg head pressure. When the pump rotational speed was increased to a level greater than 2400 rpm, the lift-off force exceeded the magnetic coupling force, and resulted in the pump floating free from the driver magnet.

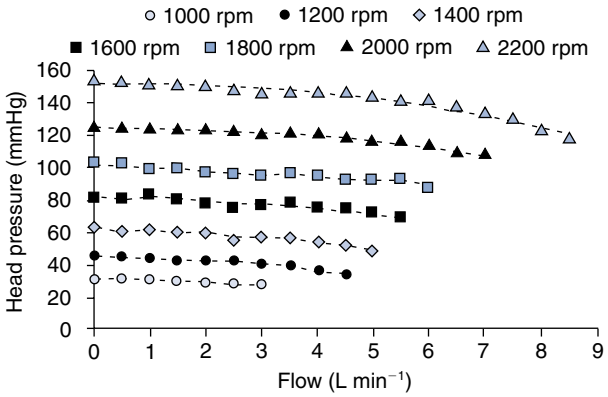

Figure 5. Flow–pressure curves of the prototype tripod supported, seal-less centrifugal blood pump with a straight vane-type impeller.

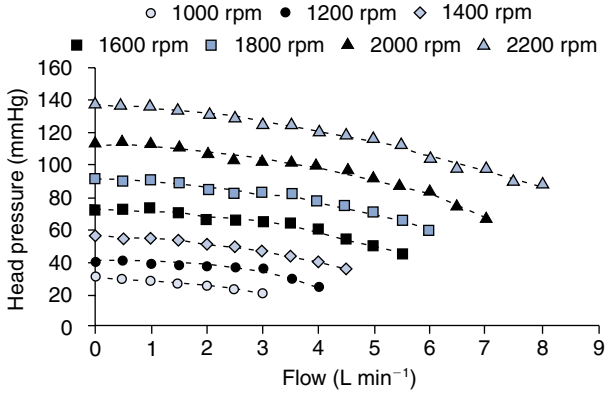

Figure 6. Flow–pressure curves of the prototype tripod supported, seal-less centrifugal blood pump with a curved vane-type impeller.

System efficiency

The system efficiencies of the tripod pump with straight vanes and curved vanes are shown in Figure 7 and 8, respectively. The system efficiency ranged from 9–10% for the pump speed from 1800–2000 rpm with straight vanes, and 2000–2200 rpm with curved vanes. The maximum system efficiency was about 12% with the straight vanes, and 11% with the curved vanes.

Dynamic pump performances

The system response in either the left heart or right heart bypass mode was tested. For this study, the straight-vane impeller was selected because of its superior performance. In the left heart bypass set-up with 100 mmHg after-load and 10 mmHg pre-load, a pump rpm of 1900–2400 rpm was required in order to obtain a bypass flow of 3–5 L min^{-1}. On the other hand, in the right heart mode with 15 mmHg after-load and 5 mmHg pre-load, a pump rpm of 1000–1400 rpm was sufficient to generate pump flow of 3–5 L min^{-1}. In both modes, appropriate unloading of the ventricles was observed.

Discussion

Both the straight and the curved vane satisfied the basic pump performance. However, the straight-vane impeller provided 10–30 mmHg higher head pressure than the curved-vane impeller at a given rpm. The straight-vane impeller can thus generate the required head pressure and flow at a lower rpm than the curved-vane impeller. The prototype pump satisfied the pressure flow performances in both left heart and right heart bypass set-ups. Overall performances of both impellers obtained in the mock loop agreed fairly well with the theoretically predicted results.

As for system efficiency, there was no significant difference between the two impellers. The effect of friction in the tripod mechanism seemed to be the main factor in determining overall system efficiency. This friction force between the ceramic balls and the polyethylene groove depends on the magnet coupling force. An appropriate adjustment of the coupling distance or selection of the magnet material may be needed to improve the efficiency of the system as well as its life expectancy.

The durability of the polyethylene material for a prolonged duration seems to be of great concern. We experienced constant wear in the polyethylene material. Appropriate adjustment of the magnetic coupling force is needed for prolonged life expectancy of this pump. Further study is needed to quantitate the wear characteristics of the polyethylene material as used in this type of application.

At an rpm greater than 2400, lift-off of the impeller was observed with either impeller type. This phenomenon was the outcome of the lift-off force generated at a higher rpm overcoming the fluid pressure of blood inflow, the gravitational force of the impeller and the magnetic coupling force between the driver and follower magnets (Figure 9). The same phenomenon was reported previously by Ohara and Nosé[9]. The continuous monitoring of impeller position and appropriate motor speed control is needed to prevent this

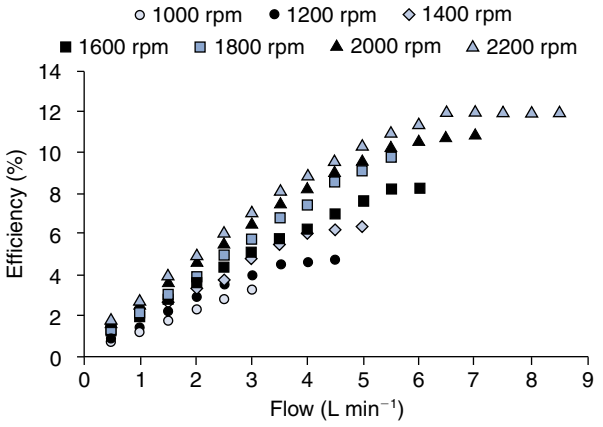

Figure 7. System efficiency versus pump flow of the prototype tripod supported, seal-less centrifugal blood pump with a straight vane-type impeller.

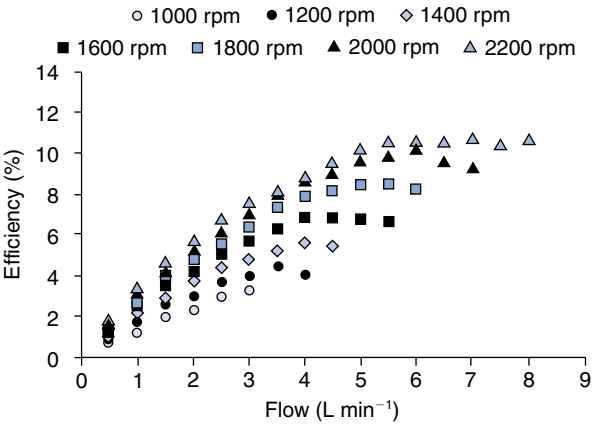

Figure 8. System efficiency versus pump flow of the prototype tripod supported, seal-less centrifugal blood pump with a curved vane-type impeller.

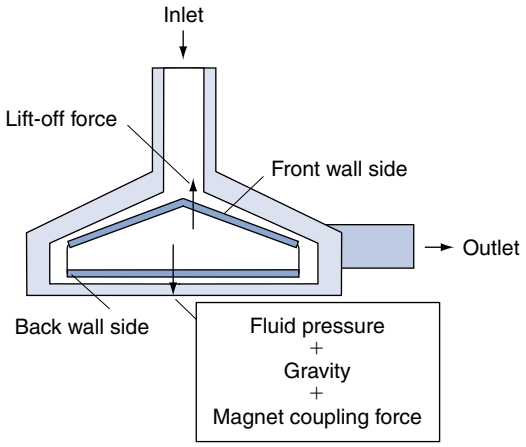

Figure 9. Lift-off phenomenon of the tripod-supported pump impeller.

phenomenon. Appropriate control of this phenomenon may result in realization of a condition similar to a magnetically suspended impeller pump.

Conclusion

In conclusion, the tripod centrifugal blood pump system was designed and its performance was evaluated in a mock circulatory loop. The static as well as dynamic performances as obtained in the simulated physiological conditions revealed that this device will meet basic requirements for either left or right heart bypass application. For a long stable performance of the tripod pump system, continuous monitoring of impeller position and appropriate motor speed control is required.

References

1. Nosé Y, Kawahito K, Nakazawa T. Can we develop a nonpulsatile permanent rotary blood pump? Yes, we can. *Artif Organs* 1996;20:467–74.
2. Macha M, Litwak P,Yamazaki K *et al*. Survival for up to six months in calves supported with an implantable axial flow ventricular assist device. *ASAIO J* 1997;43:311–5.
3. Taenaka Y, Wakisaka Y, Masuzawa T *et al.* Development of a centrifugal pump with improved antithrombogenicity and hemolytic property for chronic circulatory support. *Artif Organs* 1996;20:491–6.
4. Nakazawa T, Makinouchi K, Ohara Y *et al.* Development of a pivot bearing supported seal-less centrifugal pump for ventricular assist. *Artif Organs* 1996;20:485–90.
5. Nojiri C, Kijima T, Maekawa J *et al.* More than 1 year continuous operation of a centrifugal pump with a magnetically suspended impeller. *ASAIO J* 1997;43:M548–52.
6. Wampler R, Lancisi D, Indravudh V, Gauthier R, Fine R. A seal-less centrifugal blood pump with passive magnetic and hydrodynamic bearings. *Artif Organs* 1999;23:780–4.
7. Allaire PE, Wood HG, Awad RS, Olsen DB. Blood flow in a continuous flow ventricular assist device. *Artif Organs* 1999;23:769–73.
8. Hilton EF, Allaire PE, Wei N *et al.* Test controller design, implementation, and performance for a magnetic suspension continuous flow ventricular assist device. *Artif Organs* 1999;23:785–91.
9. Ohara Y, Nosé Y. The next generation Baylor C-Gyro pump: antithrombogenic 'free-impeller' design for long-term centrifugal VAD. *Artif Organs* 1994;18:238–43.

Journal of Congestive Heart Failure and Circulatory Support (2001) Vol 1, No 4, 419–429

The influence of the rotary blood pump on the natural heart

K.-I. Nakata MD PhD[1], M. Shiono MD PhD[1], Y. Orime MD PhD[1], S. Yagi MD PhD[1], T. Yamamoto MD PhD[1], H. Okumura MD PhD[1], S. Kimura MD[1], M. Hata MD PhD[1], H. Hirose MD[1], Y. Sezai MD PhD[1] and Y. Sankai PhD[2]

[1]The Second Department of Surgery, Nihon University School of Medicine, Tokyo, Japan; and [2]Control and Biomedical Engineering Mechanics, University of Tsukuba, Ibaraki, Japan

Abstract Rotary blood pumps are frequently used as left ventricular assist devices (LVADs). However, the influence of the rotary blood pump on the natural heart has not been elucidated. The natural heart is a pulsatile pump; however, the rotary blood pump is a nonpulsatile pump. In this study, the relationship between the rotary pump and the native heart was examined. Five pigs were the subjects of this acute study. The pump was implanted as an LVAD, in which the inlet cannula was inserted into the left ventricle and the outlet cannula was inserted into the ascending aorta. The ventricular assist ratio was changed from 30% to 95%. The relationship between the total flow rate (the ascending aortic flow rate + the pump flow rate), and the pump flow rate and the ascending aortic flow rate was examined. There was a high positive correlation between the total flow rate and the ascending aortic flow rate. However, the pump produced a characteristic flow loop between the pump flow rate and the total flow rate at the assisted ratio of 30–60%. There was a positive correlation between the total flow rate, ascending aortic flow rate and the pump flow rate in the assisted ratio of 80–95%. These results suggest that the rotary blood pump needs a high assisted ratio to regulate the total cardiac output.

Keywords rotary blood pump, nonpulsatile pump, left ventricular assist device.

Introduction

Rotary blood pumps can be used for long-term left ventricular assist devices (LVADs)[1,2].

These pumps have several advantages over conventional pulsatile pumps such as a smaller size, higher efficiency, and a simple design and construction[3,4]. However, one of the difficulties associated with the rotary blood pump is there is no proper control method to maintain an optimum flow rate in different physiological conditions[5–8].

The influence of the rotary blood pump on the natural heart is unclear, because the natural heart is a pulsatile pump, and the rotary blood pump is a nonpulsatile pump. In this study, the relationship between the rotary pump and native heart was examined.

Materials and methods

Five pigs (~40–45 kg) were the subjects of this study. Each animal was anesthetized with intravenous sodium pentobarbital (20 ml/kg) and ketamine choloride (1 mg/h). After a tracheotomy and intubation, controlled mechanical ventilation was established under a tidal volume of 10–15 ml/kg. After a median sternotomy, the inflow cannula of the LVAD was inserted into the left ventricle from the apex, and the outflow cannula was inserted into the ascending aorta.

A central venous line was introduced via the right internal jugular vein. Two fluid-filled arterial catheters were placed via the right and the left common carotid arteries to measure the blood pressure of the ascending aorta and left ventricle. An electromagnetic flow probe (FB type, Nihon Kohden, Tokyo, Japan) was placed in the ascending aorta to measure the native cardiac output.

The centrifugal pump (Gyro pump, Kyocera, Kyoto, Japan) was used as the LVAD. The pump flow rate was measured via an electromagnetic flowmeter (FB type, Nihon Kohden, Tokyo, Japan). Two disposable pressure transducers were placed proximally to the pump inflow and the pump outflow (Figure 1).

Experimental readings from the study were recorded on a Macintosh personal computer using Acknowledge III for the MP 1000 WS (Biopac System, Inc. CA, USA).

Results

Figure 2 shows the actual pump flow rate at the assisted ratios of 30% and 60%. There was a difference in the peak flow rate between the pump flow rate and the native cardiac output.

However, the phase of maximum pump flow rate corresponded with the maximum native cardiac output at the assisted ratio of 80%. There is no relationship between the pump flow rate and the native cardiac output at the assisted

Correspondence to: Kin-ichi Nakata MD PhD, The Second Department of Surgery, Nihon University School of Medicine, 30–1 Oyaguchi, Kami-machi, Itabashi-ku, Tokyo, Japan.

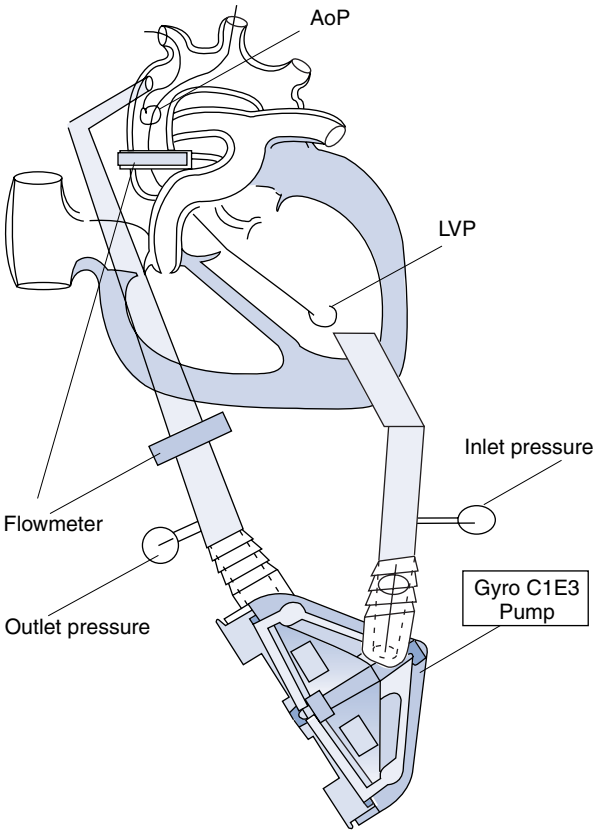

Figure 1. Schematic drawing of the experimental model. Animals: five pigs (~40–45 kg). Bypass type: left ventricular apex to ascending aorta. Pump: Gyro centrifugal pump. Data acquisition system: Acknowledge III MP 1000 WS; sampling time 200 Hz. Parameters: native heart cardiac output (ascending aorta flow rate), pump flow rate, aortic pressure (AoP), left ventricular pressure (LVP), pump inlet pressure, pump outlet pressure.

ratio of 95% (Figure 3). This is the relationship between the motor speed and the pump flow rate. This study was performed with a speed control actuator, therefore, the motor speeds were kept stable by the servo system under all conditions (Figure 4).

Figure 5 shows the aortic pressure and the pump flow rate at an assisted ratio of 30%. The pump produced a maximum flow rate at the diastolic phase. The maximum pump flow rate did not corresponded to the systolic phase. Figure 6 shows the total head pressure and the pump flow rate at the assisted ratio of 30%. The pump could not produce the maximum flow rate at the smallest total head pressure. The pump flow rate did not correspond to the total head pressure.

Figure 7 shows the aortic pressure and the pump flow rate at an assisted ratio of 60%.The pump produced a maximum flow rate at the beginning of the systolic phase. Figure 8

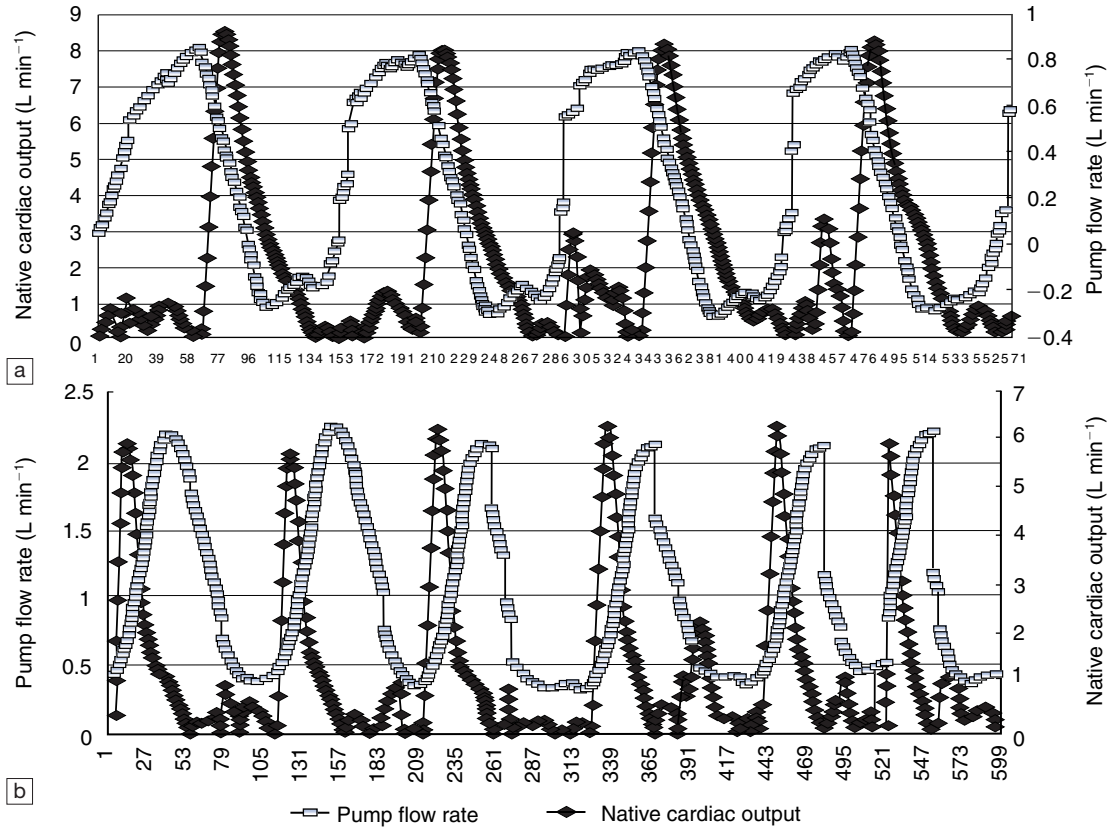

Figure 2. Relationship of the pump flow rate and the native cardiac output at the assisted ratios of (a) 30% and (b) 60%.

shows the total head pressure and the pump flow rate at the assisted ratio of 60%. The pump could not produce the maximum flow rate with the smallest total head pressure. The pump flow rate did not correspond to the total head pressure completely.

Figure 9 shows the aortic pressure and the pump flow rate at an assisted ratio of 80%. The pump produced a maximum flow rate at the systolic phase. Figure 10 shows the total head pressure and the pump flow rate at the assisted ratio of 80%. The pump could produce the maximum flow rate at the smallest total head pressure. The pump flow rate corresponded to the total head pressure.

The relationship between the pump flow rate and the total cardiac output (the sum of the pump flow rate and the native cardiac output is the total cardiac output) is shown in Figures 11 and 12. There was a characteristic flow loop between the pump flow rate and the total flow rate at the assisted ratio of 30–60% (Figure 11). These results suggest that the phase of the maximum pump flow rate did not correspond with the phase of the maximum total cardiac output at the assisted ratio of 30–60%. However, there was a positive correlation between the pump flow rate and the total flow rate at the high assisted ratio (Figure 12).

Figures 13 and 14 show the relationship between the total cardiac output and the native cardiac output; there was a high positive correlation between the pump flow rate and the total flow rate from the low assisted ratio to the high assisted ratio.

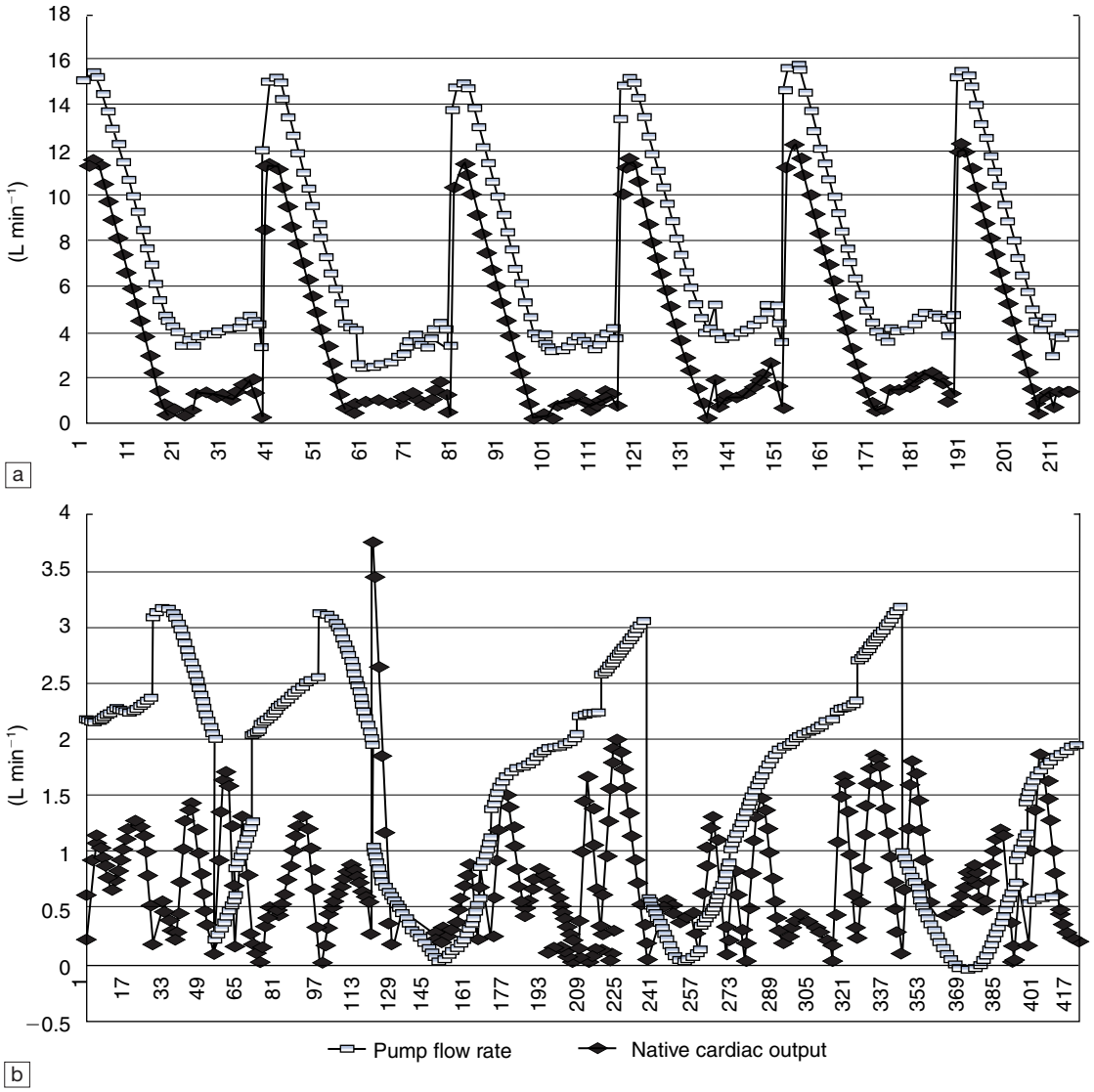

Figure 3. Relationship of the pump flow rate and the native cardiac output at the assisted ratios of (a) 80% and (b) 95%.

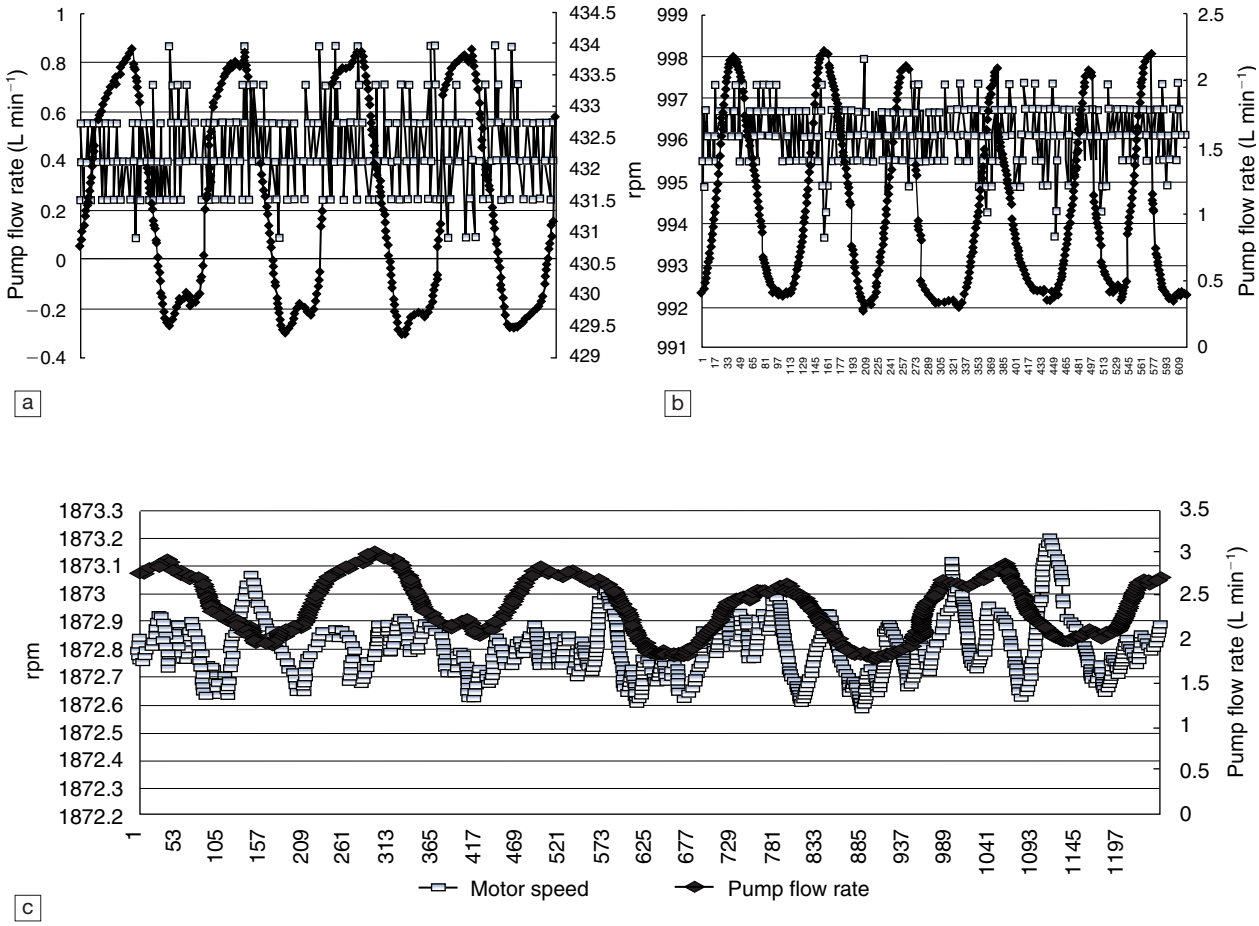

Figure 4. Relationship of the motor speed and the pump flow rate at the assisted ratios of (a) 30%, (b) 60% and (c) 80%.

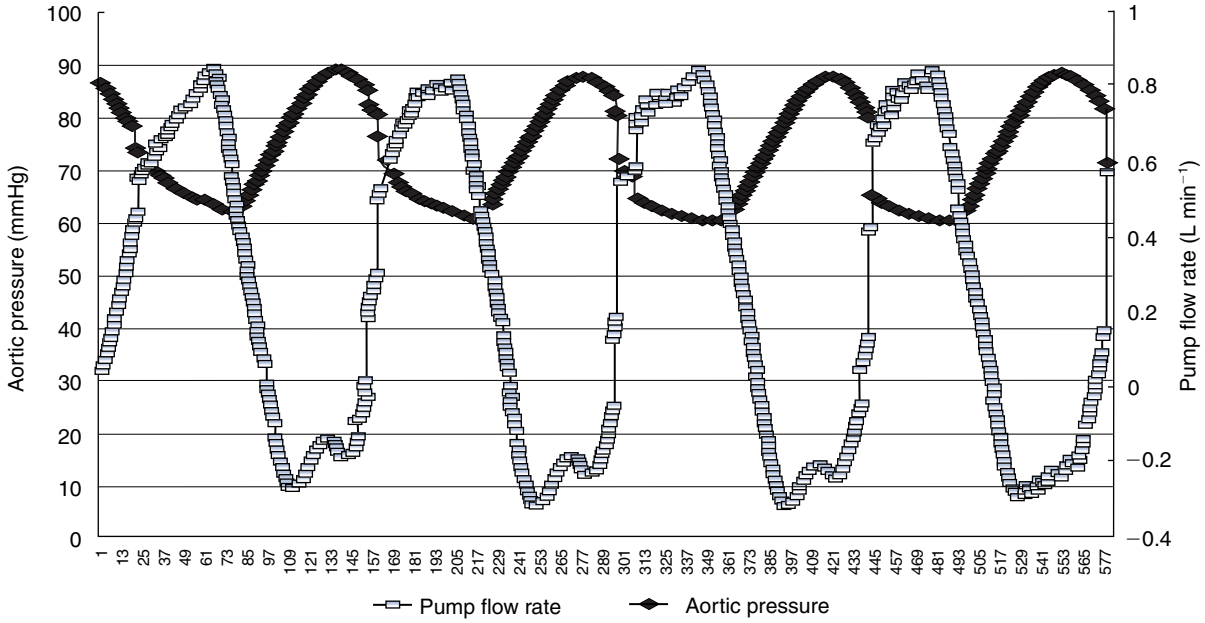

Figure 5. Relationship of the aortic pressure and the pump flow rate at the assisted ratio of 30%.

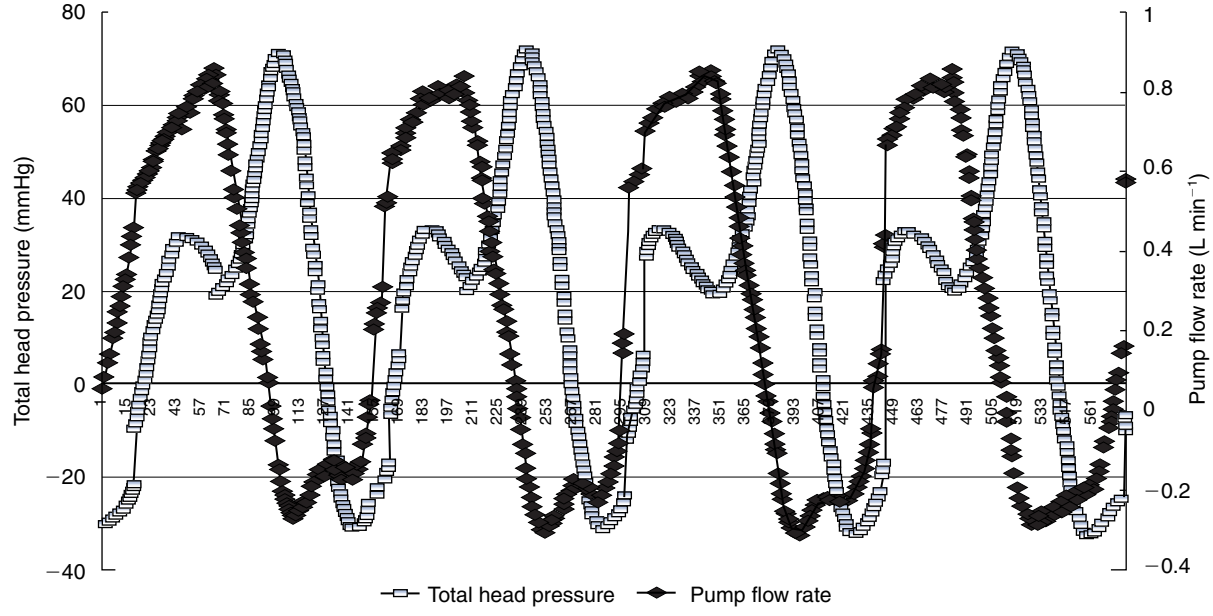

Figure 6. Relationship of the total head pressure and the pump flow rate at the assisted ratio of 30%.

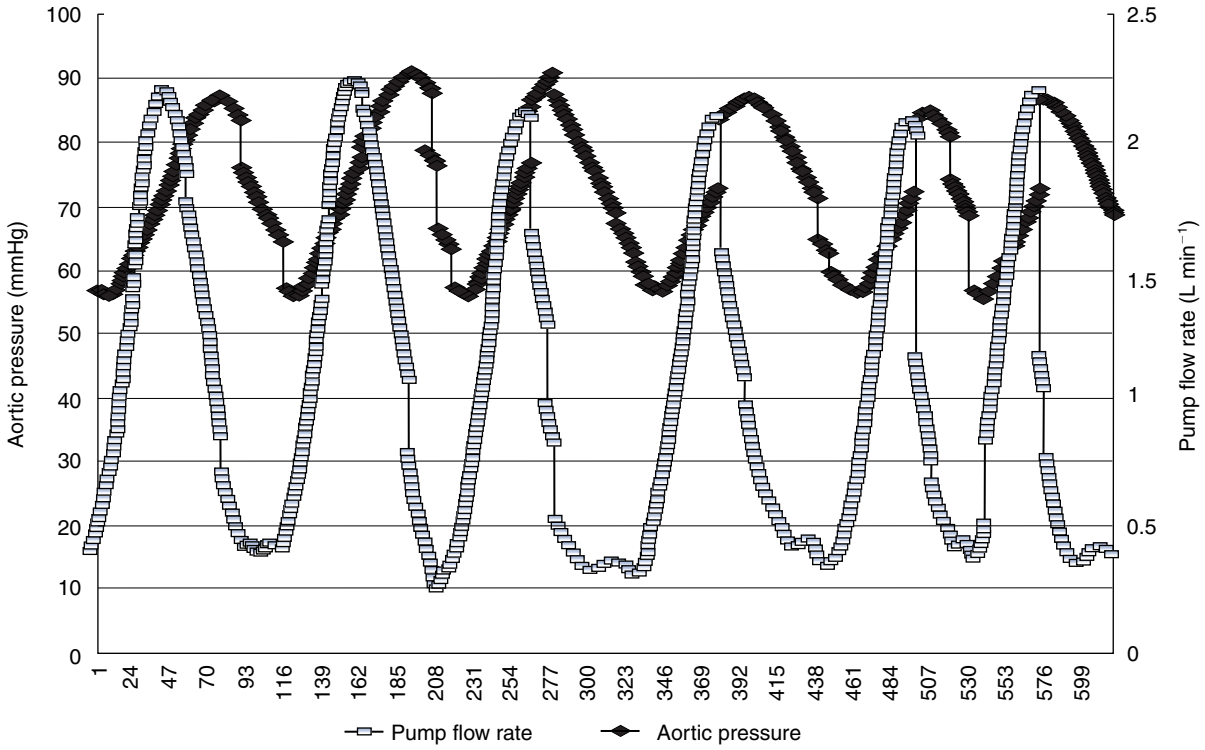

Figure 7. Relationship of the aortic pressure and the pump flow rate at the assisted ratio of 60%.

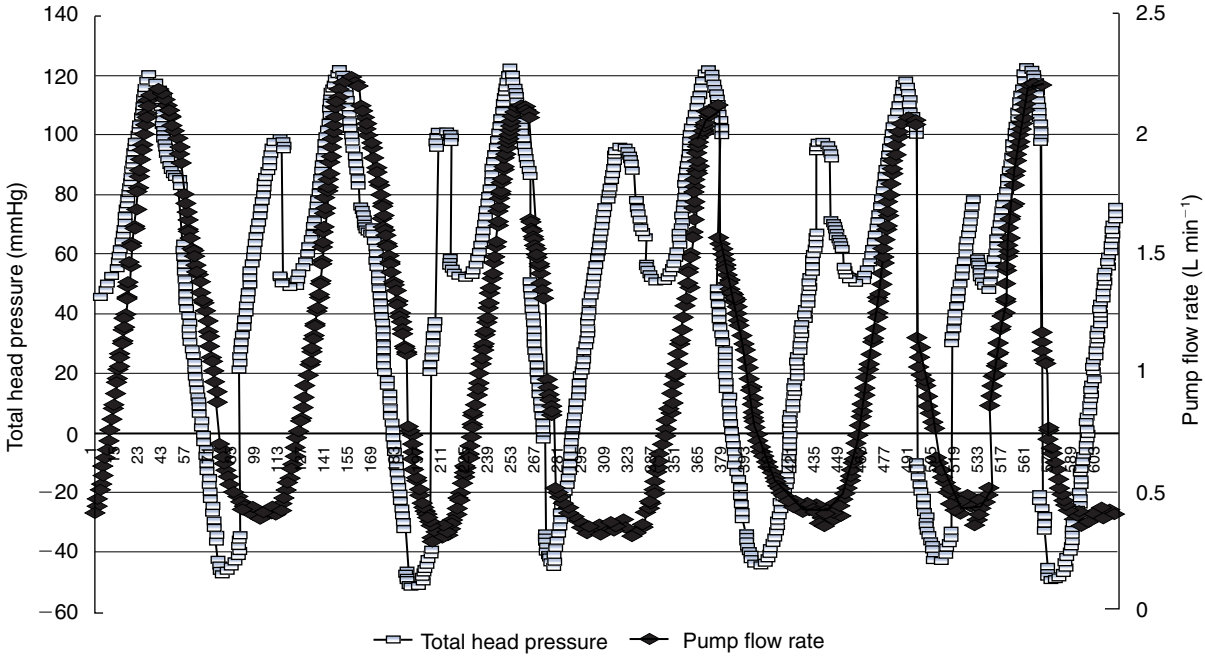

Figure 8. Relationship of the total head pressure and the pump flow rate at the assisted ratio of 60%.

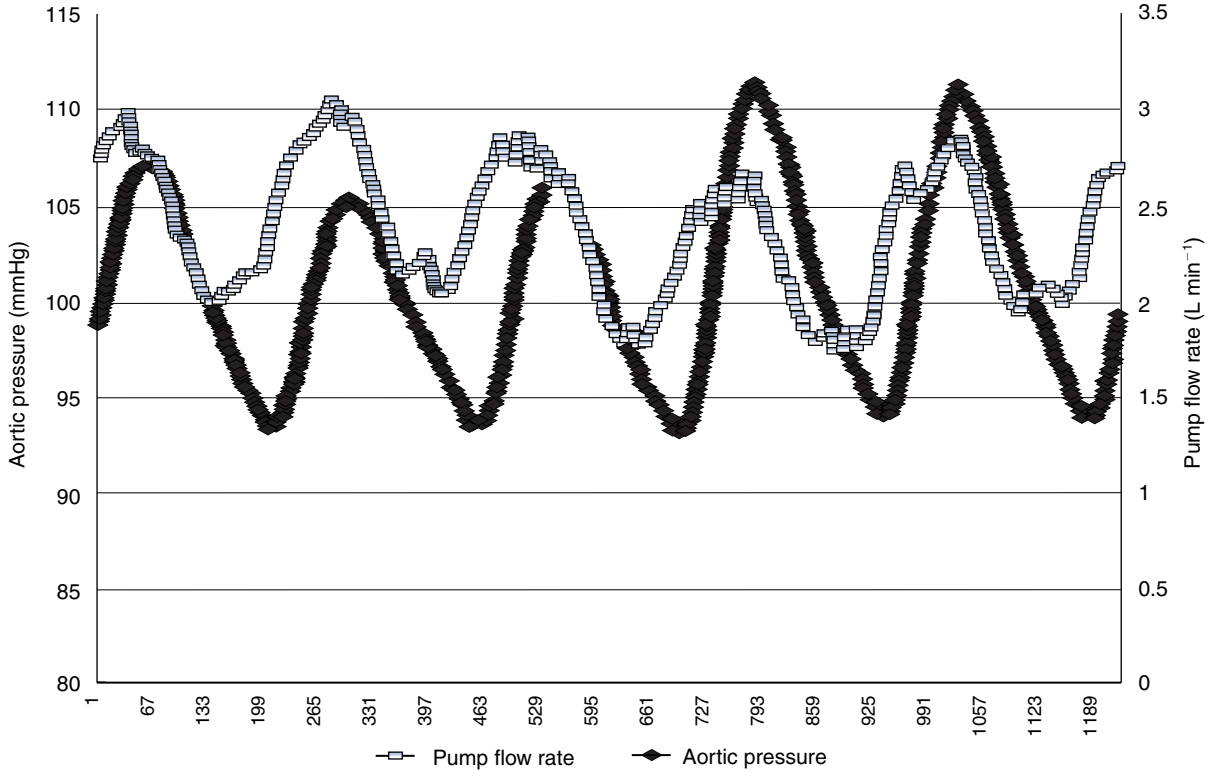

Figure 9. Relationship of the aortic pressure and the pump flow rate at the assisted ratio of 80%.

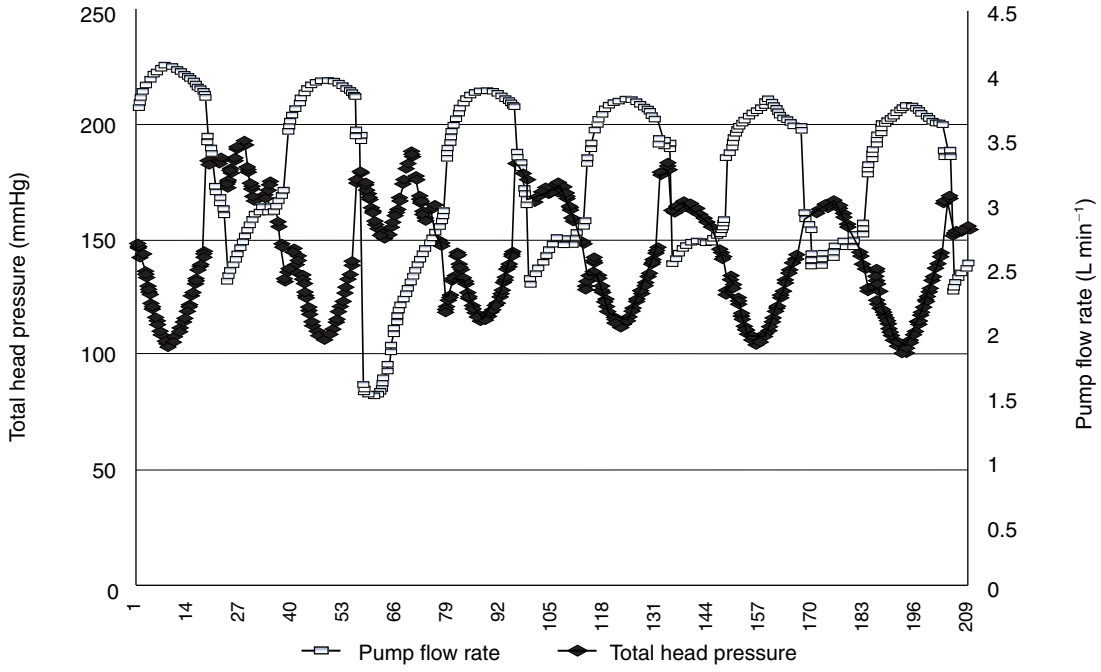

Figure 10. Relationship of the total head pressure and the pump flow rate at the assisted ratio of 80%.

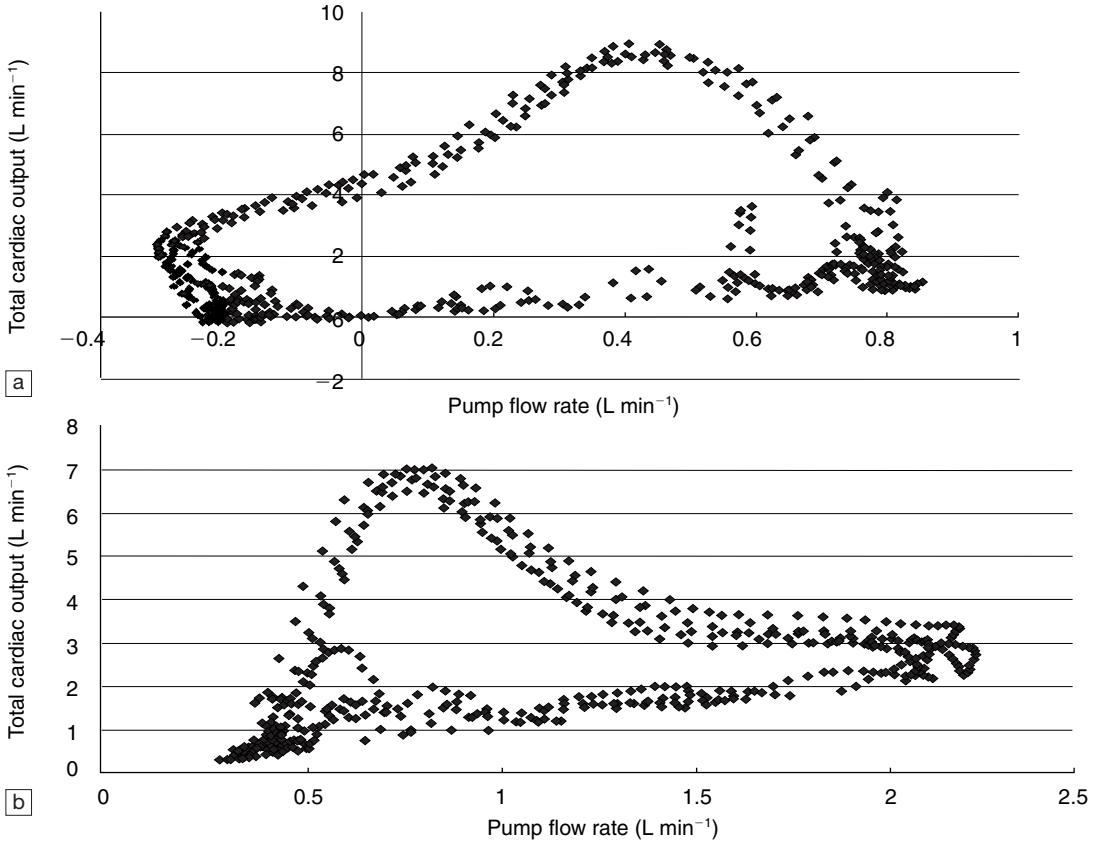

Figure 11. Relationship of the total cardiac output and the pump flow rate at the assisted ratios of (a) 30% and (b) 60%.

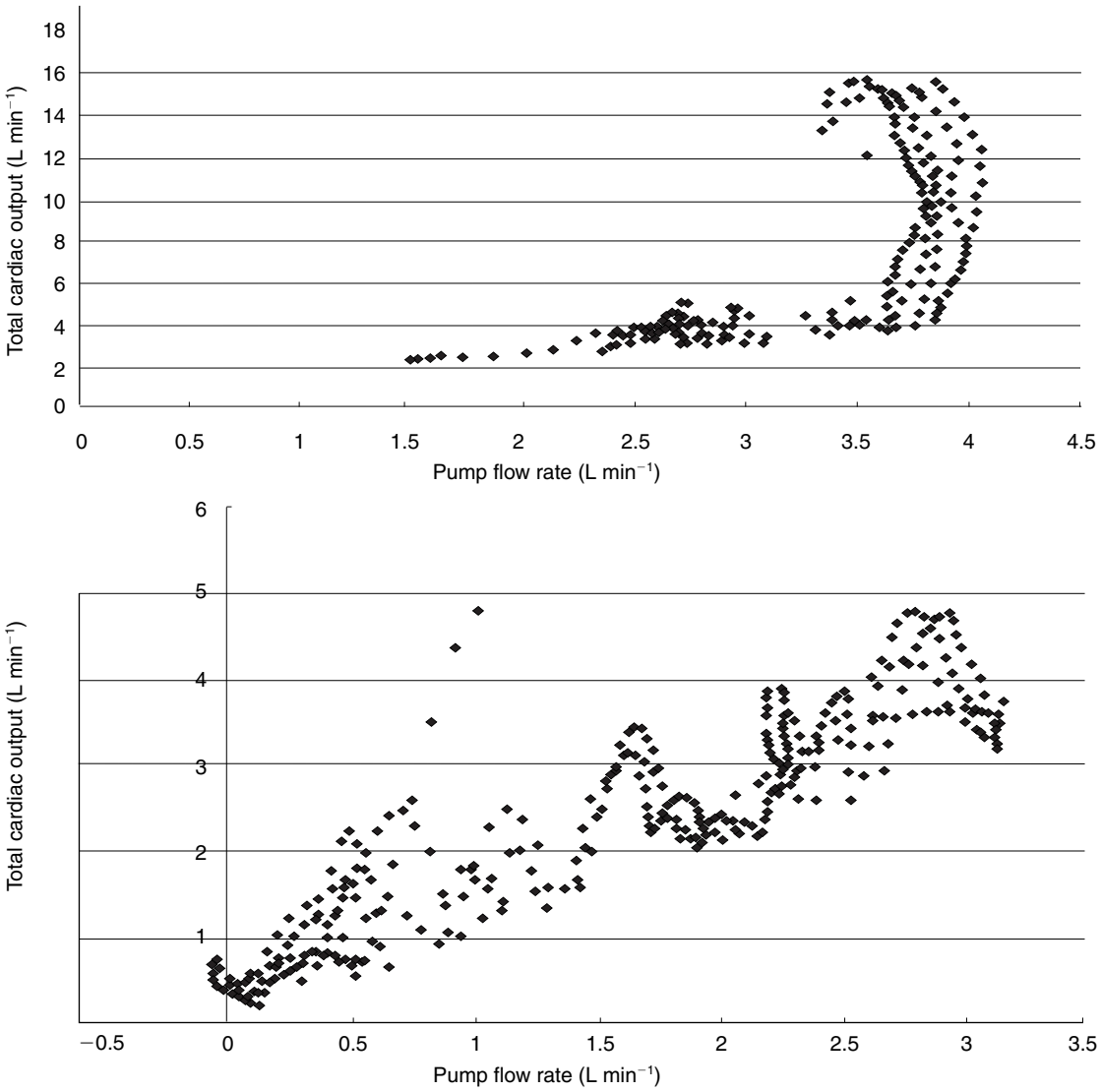

Figure 12. Relationship of the total cardiac output and the pump flow rate at the assisted ratios of (a) 80% and (b) 95%.

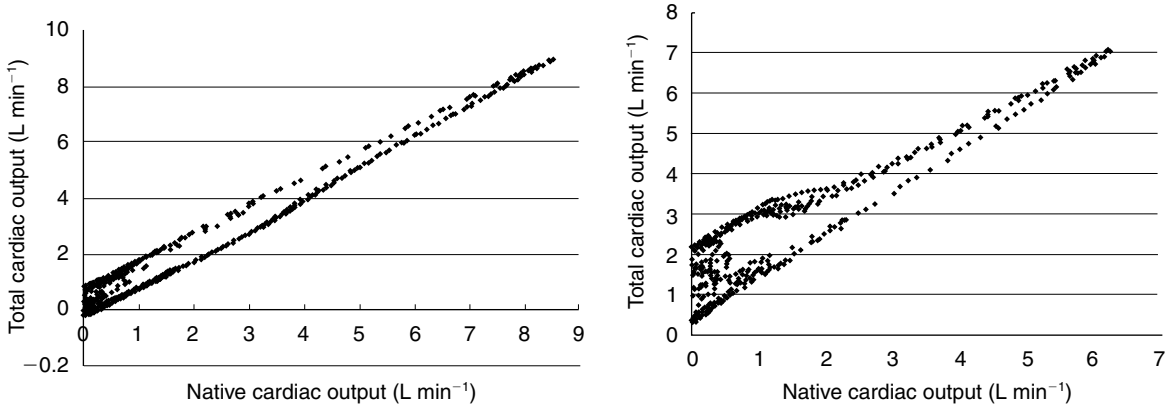

Figure 13. Relationship of the total cardiac output and the native cardiac output at the assisted ratios of (a) 30% and (b) 60%.

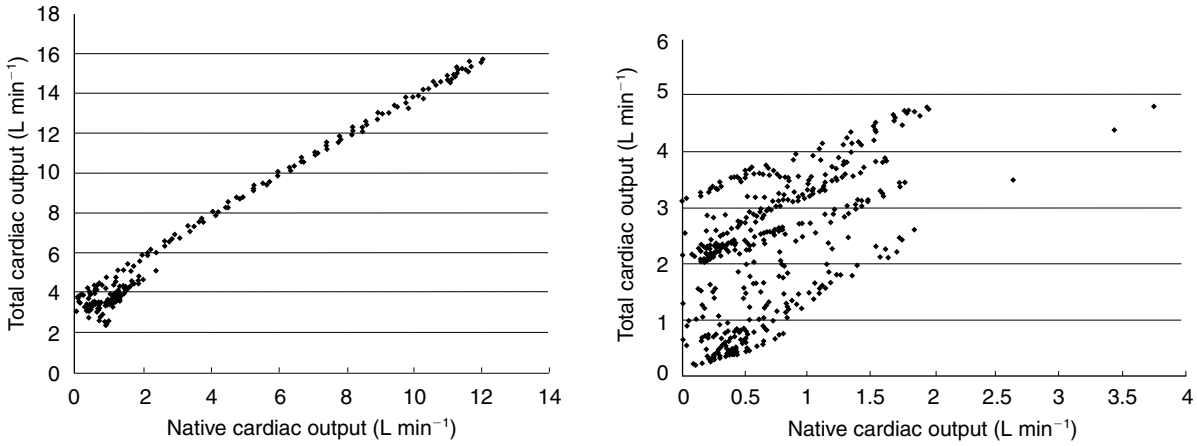

Figure 14. Relationship of the total cardiac output and the native cardiac output at the assisted ratios (a) 80% and (b) 95%.

Discussion

Generally, the rotary pump flow rate depends upon the motor speed and the total head pressure under static conditions. However, the rotary blood pump, which is implanted as the LVAD, is subjected to the pulsatile condition because the natural heart is a pulsatile pump. In this study the pump flow rate did not depend only on the total head pressure and the motor speed under dynamic conditions at the assisted ratio of 30–60%. The pump flow rate depends on the total head pressure and the motor speed under dynamic conditions at the assisted ratio from 80–95%. These results suggest that the pump flow rate is not only regulated by the driving condition of the motor but also the native heart function. If the pump flow rate is regulated by the pump only, the pump will need a high motor speed to negate the native heart function. In addition, the control system for the rotary blood pump will need the information of the natural heart function.

There was a characteristic flow loop between the pump flow rate and the total flow rate at the assisted ratio of 30–60%. However, there was a high positive correlation between the total cardiac output and native cardiac output.

These results suggested the natural heart and rotary blood pump have a different influence on total cardiac output. In addition, the rotary blood pump needs to have a high pump flow rate in order to have a positive correlation with the total cardiac output.

Conclusion

There is a difference in pump performance between the static condition and the implantable condition. Therefore, we believe that the rotary blood pump needs a control system that can reflect a natural heart function. The rotary blood pump needs a high assisted ratio to regulate the total cardiac output.

References

1. Nosé Y, Kawahito K, Nakazawa T. Can we develop a nonpulsatile permanent rotary blood pump? Yes, we can. *Artif Organs* 1996;20:464–74.
2. Westaby S, Katsumata T, Jarvik RK. The Jarvik 2000 system. Prospect for the future. In: Akutsu T, Koyanagi H, editors. *Heart Replacement: Artificial Heart 6*. Tokyo: Springer-Verlag 1996:172–8.
3. Butler K, Thomas D, Antaki J *et al.* Development of the Nimbus/Pittsburgh axial flow left ventricular assist system. *Artif Organs* 1997;21:602–10.
4. Nosé Y, Nakata K, Yoshikawa M *et al.* Development of a totally implantable biventricular bypass centrifugal pump system. *Ann Thorac Surg* 1999;68:775–9.
5. Nakata K, Ohtsuka G, Yoshikawa M *et al.* A new control method that estimates the backflow in a centrifugal pump. *Artif Organs* 1999;23:538–641.
6. Konishi H, Antaki JF, Amin DV *et al.* Controller for an axial flow blood pump. *Artif Organs* 1996;20:618–20.
7. Schima H, Trubel W, Moritz A *et al.* Noninvasive monitoring of rotary blood pumps: necessity, possibilities, and limitations. *Artif Organs* 1992;16:195–202.
8. Inamoto T, Iijima T, Nogawa M, Takatani S. Control of centrifugal blood pump on the motor current. *Jpn J Artif Organs* 1997;26:396–9.

Journal of Congestive Heart Failure and Circulatory Support (2001) Vol 1, No 4, 431–435

Automatic control of the implantable centrifugal blood pump based on analysis of the motor current waveform

K. Ouchi MS[1], E. Hatoh[3], A. Yuhki[3], M. Nakamura MD PhD[1], T. Sakamoto MD PhD[2] and S. Takatani DMed PhD[1]

[1]Department of Artificial Organs, Tokyo Medical and Dental University, Tokyo, Japan; [2]Department of Replacement Surgery, Tokyo Medical and Dental University, Tokyo, Japan; and [3]Yamagata University, Yamagata, Japan

Abstract In this study, a control method for the implantable centrifugal ventricular assist pump used from the left ventricular apex to the aorta has been developed without relying on external pressure or flow sensors; its performance was evaluated in a mock circulatory loop. The control algorithm consisted of two phases. In the initial phase, the pump rpm was adjusted to a theoretical level based on the native heart rate. This was established based on the relationship between the native heart rate and centrifugal pump flow that was obtained from the preliminary studies. In the second phase, abnormal circulatory conditions such as suction in the ventricle were examined through analysis of the motor current waveform. The waveform deformation index (WDI) was computed through Fast Fourier analysis of the motor current waveform. When the WDI value was greater than 0.2, an abnormal circulatory condition was assumed. Changes in the pump rpm were made to improve the situation. The system response was examined in the mock loop in which heart rate changes and the occurrence of suction were simulated. The control system functioned acceptably in the mock loop. System stability as well as its capability in optimizing the assist pump flow will be tested in chronic animal study.

Keywords implantable centrifugal blood pump, suction effect, Fast Fourier Transfer (FFT) method, motor current analysis, automatic rpm control.

Introduction

The progress of continuous flow pump technology has been increasing their clinical application from temporary to long-term support of patients' circulation[1–6]. Especially because of their compact, easy to handle and valve-less features, they have been considered as implantable ventricular support devices bridging to heart transplantation[7–10]. In order to meet the requirements for reliable implantable devices, in addition to long-term mechanical durability, appropriate rpm control is an important problem attracting immediate attention[11]. The device must work well with the pulsatile ventricle without causing deleterious effects to the host system. Since the use of flow and pressure sensors may invite a danger of clot and thromboemboli formation, they are not suitable for long-term implantable applications.

The automatic pump rpm control algorithm that we tested in this study was derived from motor current waveform analysis using the Fast Fourier Transform (FFT) method. This paper describes the automatic control system and its evaluation in a mock circulatory loop.

Materials and methods

Automatic pump rpm system

A schematic diagram of an automatic pump rpm control system is shown in Figure 1. The control-drive system consists of a personal computer (CPU), a digital signal processor (DSP), motor speed controller and motor driver. Inputs to the DSP are the commutation signals (21 pulses/revolution) and motor current waveform, which are processed to derive motor speed as well as waveform deformation index (WDI) value. Upon receiving this information, the CPU then determines if the pump rpm is too high or not and sends out the command signal to adjust the motor rpm. Based on the command signal from the DSP, the motor speed controller then varies the motor speed through a pulse width modulation technique.

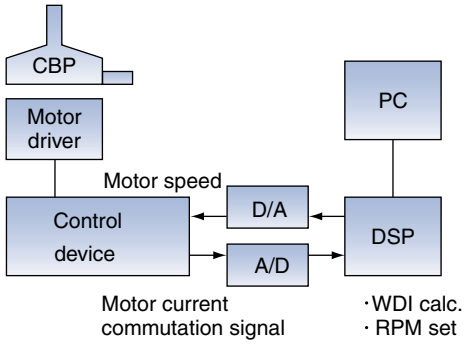

Figure 1. Automatic pump rpm control system.

Automatic pump rpm control algorithm

The proposed automatic pump rpm control algorithm consisted of two phases. In the initial phase, the pump rpm was adjusted to the theoretical level based on the native heart

Correspondence to: Katsuhiro Ohuchi, Department of Artificial Organs, Institute of Biomaterials and Bioengineering, Tokyo Medical and Dental University, Tokyo, 2–3–10, Kanda Surugadai, Chiyoda-ku, Tokyo, 101-0062 Japan.

rate. This was established utilizing the relations between (1) native heart rate versus its cardiac output, and (2) centrifugal pump flow versus pump rpm, which were available from the preliminary studies.

In the second phase, suction and regurgitation in the ventricle were examined through analysis of the motor current waveform. Previously, we reported that the deformation of the motor current waveform showed a strong correlation with the impaired flow[12]. From this viewpoint, the WDI was computed through the FFT analysis of the motor current waveform. Power spectral density (PSD) obtained from the fast FFT showed that the PSD component level changed with changes in the circulatory status, particularly with the occurrence of suction and regurgitation. The ratio of the sum of the PSD components higher than the fundamental frequency to the fundamental PSD, the latter corresponding to the heart rate frequency, was thus computed to quantify the level of waveform deformation. The WDI was calculated using the following equation:

$$\text{WDI} = (\text{higher order harmonics of PSD})/(\text{fundamental component})$$

Based on the theoretical study conducted earlier[12], it was revealed that significant waveform deformation existed when the WDI value was above 0.2. Therefore, the threshold level of 0.2 was used to determine the presence of waveform deformation based on the FFT analysis. When the WDI was less than 0.2, we assumed that the waveform was normal, and hence there was neither suction nor regurgitation. When the WDI value was greater than 0.2, a regurgitation at low rpm or the suction effect at higher rpm was assumed.

Mock circulatory loop

A schematic diagram of the mock circulatory loop used to evaluate the proposed automatic rpm control algorithm is shown in Figure 2. This mock loop simulates the left ventricular apex to descending aorta bypass using the pneumatically driven pulsatile ventricle. The pivot bearing supported the Kyocera centrifugal blood pump (Kyocera Corporation, Kyoto, Japan) was used as a left ventricular assist device. The circulatory system consisted of the aortic compliance, a constrictor as the peripheral resistance, and an atrial reservoir. Björk–Shiley tilting disk type valves (Shiley Inc., CA, USA) were used in the inflow and outflow positions of the mock ventricle.

Experimental setup and analysis

Preliminary setup

To obtain the target pump rpm in automatically controlling the centrifugal blood pump, we obtained the heart rate versus cardiac output characteristics of the pneumatically driven left ventricle of Figure 2 (Figure 3). Also, the pump flow versus pump rpm characteristics of the centrifugal blood pump were obtained and are shown in Figure 4.

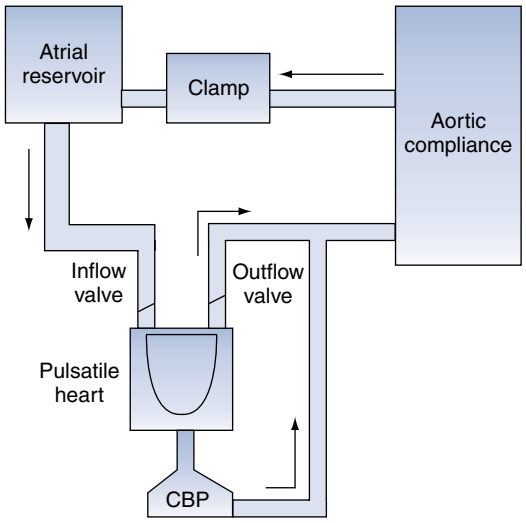

Figure 2. Mock circulatory loop for evaluation of automatic control of the centrifugal blood pump (CBP) based on the analysis of motor current waveform.

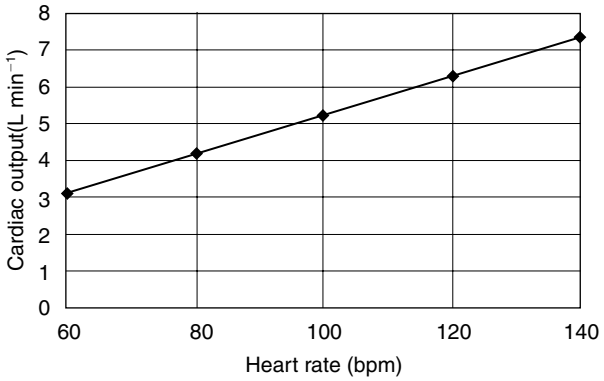

Figure 3. Relationship of heart rate versus cardiac output with mock circulatory loop simulated left ventricle.

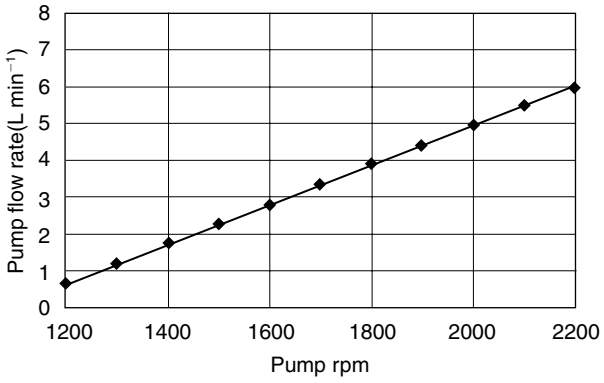

Figure 4. Pump flow versus pump rpm characteristics of the centrifugal blood pump.

System response evaluation for heart rate changes

The system's response speed and circulatory conditions in response to rapid changes in the native heart rate change from 60 to 80 and vice versa were tested. Motor current and bypass flow through the centrifugal pump were recorded with a sampling frequency of 50 Hz and 100 sampling number.

System response evaluation for suction occurrence

To test the system response for the occurrence of an abnormal circulatory condition, aortic pressure was suddenly dropped from 100 mmHg to 40 mmHg to cause a suction effect. Motor current, aortic pressure, and bypass flow through the centrifugal blood pump were recorded with a sampling frequency of 50 Hz and 250 sampling number.

Results

System response to heart rate change

Figure 5a shows the system response to the heart rate increasing from 60 bpm to 80 bpm. Pump rpm automatically increased from about 1600 rpm to 1800 rpm, followed by a pump flow change from 2.6 to 4.3 L min^{-1}. It took 2.3 s before the motor current change took place, and 3.5 s before completion of the rpm change. The system response to the heart rate decreasing from 80 bpm to 60 bpm is shown in Figure 5b. Pump rpm decreased from around 1800 rpm to

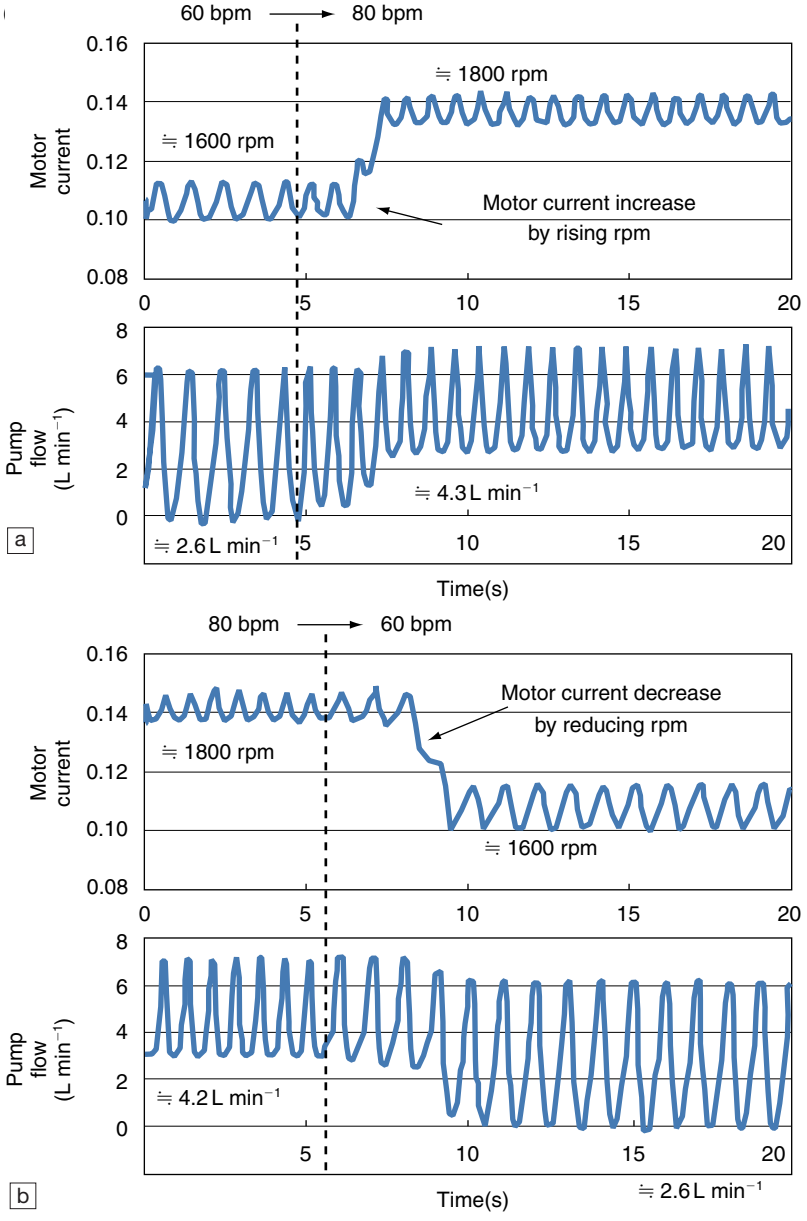

Figure 5. System response to the change of heart rate (a) increasing and (b) decreasing.

1600 rpm, causing a flow decrease from 4.2 to 2.6 L min^{-1}. It took 2.6 s for the system to respond to the heart rate decrease.

System response to suction occurrence

Figure 6 shows the system response to the occurrence of suction. When the aortic pressure was decreased suddenly from 100 mmHg to 40 mmHg, suction occurred immediately, followed by a motor current change in 9.8 s. The pump rpm decreased from 1500 rpm to 1200 rpm to minimize the suction. The total recovery time from suction was 12.2 s. The WDI value changed from 0.08 to 0.36 with the aortic pressure change, then settled at 0.14 as the system recovered from suction.

Discussion

In assisting the pulsatile ventricle with a continuous flow device, pump rpm determination requires careful attention. When the pump rpm is set at too high a level, suction occurs, while when it is set too low, regurgitation develops. In order to meet this difficult requirement, the automatic rpm control algorithm for an implantable centrifugal blood pump bypassing from the native left heart apex to the descending aorta proposed in this research consisted of two phases: the coarse rpm-adjusting phase, followed with the fine-tuning phase. In the initial phase, coarse tuning of the pump rpm was carried out based on the relationships between (1) the native heart rate and cardiac output, and (2) centrifugal pump rpm and pump flow. The control loop started with estimation of the native heart rates followed by the estimation of the pump output from the pre-determined relationship between heart rate and cardiac output. Then the controller determined the coarse pump rpm based on the pre-determined pump rpm flow characteristics.

In the second phase the rpm optimization was carried out by analysis of the motor current waveform by WDI computation. The pump rpm was gradually increased or decreased until the suction disappeared as evaluated from the recalculated WDI values. We used the threshold WDI value of 0.2. When WDI was greater than 0.2, we assumed suction was present, while when it was below 0.2, a normal condition was assumed. Although the threshold value of 0.2 was determined empirically, it seemed to have predicted both the suction and regurgitation well, and the deleterious conditions were successfully reversed when the WDI value was decreased to less than 0.2.

The performance of the control algorithm was acceptable in response to extreme changes in the circulatory conditions such as heart rate and after-load. The suction effect that developed in response to a sudden decrease in the pump after-load was reversed by a subsequent reduction in pump rpm. The WDI value usually settled at less than 0.2. The system response time was around 10 s.

We believe this two-phase control algorithm is suitable for the implantable centrifugal pump without relying on external flow or pressure sensors. The controller should respond to the cardiac output changes due to alterations in the heart rate, venous return, circulating blood volume, peripheral vascular resistance and oxygen consumption.

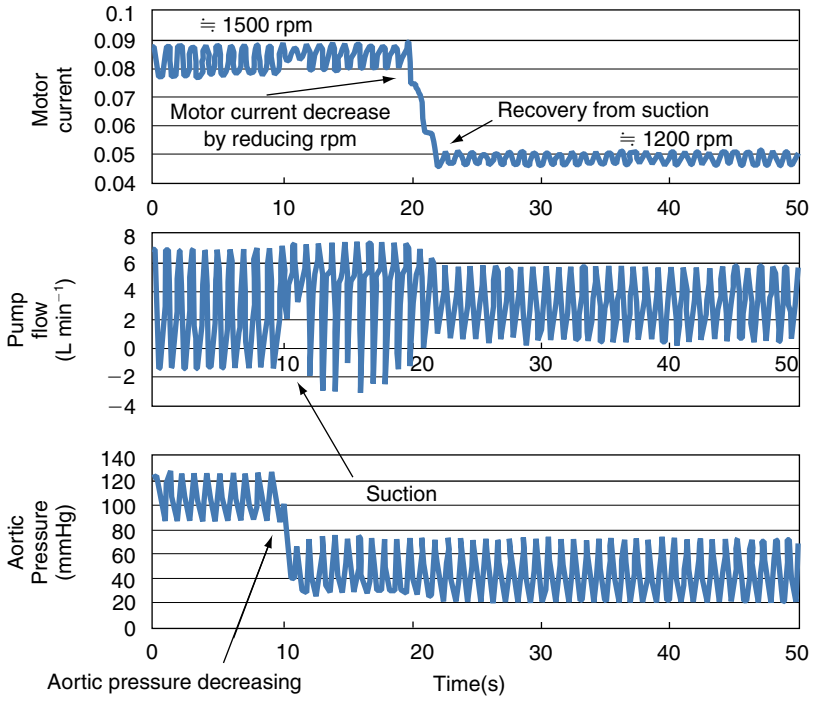

Figure 6. System response to the occurrence of suction.

Conclusion

In conclusion, the automatic pump rpm control system functioned acceptably concerning the target pump rpm determination and recovered from suction on the whole. The simulated system responses in the mock loop made it simple to follow changes in heart rate and simultaneously detect and compensate for abnormal circulation. For more evaluation of system stability as well as capability in optimizing the assist pump flow, more detailed analysis under various operating conditions and chronic animal study is needed.

References

1. Noon GP, Ball JW Jr, Papaconstantinou HT. Clinical experiments with BioMedicus centrifugal ventricular support in 172 patients. *Artif Organs* 1995;19:756–60.
2. Curtis JJ, Walls JT, Schmaltz RA *et al*. Improving clinical outcome with centrifugal mechanical assist for postcardiotomy ventricular failure. *Artif Organs* 1995;19:761–5.
3. Koyanagi H, Kitamura M, Nishida H, Hachida M, Endo M, Hashimoto A. Current strategy for severe heart failure with mechanical circulatory support. *Artif Organs* 1995;19: 766–8.
4. Ohtsubo S, Naito K, Matsuura M *et al.* Initial clinical experience with the Baylor–Nikkiso centrifugal pump. *Artif Organs* 1995;19:769–73.
5. Watson JT. Innovative ventricular assist systems. *ASAIO J* 1994;40:M902.
6. Akamatsu T, Tsukiya T, Nishimura K, Park CH, Nakazeki T. Recent studies of the centrifugal blood pump with a magnetically suspended impeller. *Artif Organs* 1995;19:631–4.
7. Nakazawa T, Makinouchi K, Ohara Y *et al.* Development of a pivot bearing supported sealless centrifugal pump for ventricular assist. *Artif Organs* 1996;20:485–90.
8. Taenaka Y, Wakisaka Y, Masuzawa T *et al.* Development of a centrifugal pump with improved antithrombogenicity and hemolytic property for chronic circulatory support. *Artif Organs* 1996;20:491–6.
9. Parnis SM, Macris MP, Jarvik R *et al.* Five month survival in a calf supported with an intraventricular axial flow blood pump. *ASAIO J* 1995; 41: M333–6.
10. Nakatani T, Sasako Y, Kumon K *et al.* Long-term circulatory support to promote recovery from profound heart failure. *ASAIO J* 1995;41:M526–30.
11. Konishi H, Antaki JF, Amin DV *et al.* Controller for an axial flow blood pump. *Artif Organs* 1996;20:618–20.
12. Iijima T, Inamoto T, Nogawa M, Takatani S. Control of centrifugal blood pump based on the motor current. *Artif Organs* 1997;21:655–60.

Journal of Congestive Heart Failure and Circulatory Support (2001) Vol 1, No 4, 437–442

Systems approach to mechanical support of the circulation

J. D. Hill MD
Department of Cardiac Surgery, California Pacific Medical Center, San Francisco, CA, USA

Introduction

In the USA, congestive heart failure affects 4.8 million people, with 400 000 new cases appearing each year. Because of more effective therapies to treat congenital, valvular, coronary and arrhythmic heart disorders, the myocardium and subsequent congestive heart failure (CHF) becomes the final common pathway. The morbidity and financial impact of treating patients with CHF are highly visible to health care providers and third-party payers. The increasing prevalence of CHF has created a need to develop therapies that are both beneficial to the patient and cost-effective.

Established therapies for CHF that have varying degrees of success include: (1) standard medical therapy (digoxin, diuretics, ACE inhibitors and β-blockers), (2) surgical intervention (revascularization, valve repair or replacement, aneurysmectomy), and (3) heart transplantation. The widespread use of medical management is the single most important current opportunity in which to make an impact on CHF. Unfortunately, most patients with CHF are managed by primary care and internal medicine physicians, the majority of whom are not knowledgeable or skilled in the current medical therapeutics of CHF. This is the domain of heart failure cardiologists. Heart transplantation has become an established and very successful option. However, due to the shortage of donor organs it is available to a very small number of patients. This is a universal problem; therefore, despite its clinical success, heart transplantation is a failure in public health both in terms of its cost and its impact on the lives of the millions of patients who suffer from CHF.

There are some other very attractive therapies on the horizon at varying stages of development. The most visible therapy is with mechanical support devices, which are the subject of this report. Devices used to support the heart and circulation are in their fifth decade of development, and offer the most immediate opportunity to change the natural history of heart failure and make a public health impact on CHF. In the USA, three devices have been approved by the FDA to treat CHF: the Novacor, HeartMate and Thoratec devices, used as a bridge to transplantation. Other new approaches must also be recognized, such as:

- Myocardial remodelling
- Ventricular restraining devices
- Biventricular pacing
- Muscle cell transplants
- Genetics
- Xenographs
- Cloning.

At this stage, most of these therapies are unproven but they are nonetheless important to explore. Investigations into therapies such as latissimus dorsi supported cardiomyoplasty and a host of drugs have come and gone over time.

Mechanical and circulatory support devices: A systems approach

It is not the purpose of this report to review all of the mechanical devices that are currently available, or in development, that will become part of the therapy for CHF and/or circulatory collapse. Rather, the purpose of this report is to recognize the degree of sophistication of the available devices, and to characterize their ability to provide treatment options for patients with heart failure.

This report presents a systems approach to mechanical support. The details are confined to using mechanical devices once a general strategy of care is chosen for the patient. Inherent in this approach is the characterization of a ventricular assist device (VAD) versus a ventricular assist system (VAS).

The physician caring for a patient with heart failure has a series of treatment choices to make. These choices are driven by clinical parameters, which will be referred to as decision drivers. Decision drivers include:

- Type of disease
- Clinical requirements
- Surgical methodology and surgical and/or medical constraints
- Patients' clinical status and process.

From the evaluation of the decision drivers will emerge the end strategy the physician believes is the best therapy for the patient (Figure 1). The decision on an end strategy is made early in the management plan.

Decision drivers

Decision drivers play an important role in the four end strategies. They are particularly dominant in the surgical and bridge therapy category. As clinical parameters (drivers) become known, the clinical options are either broad-

Correspondence to: J. Donald Hill, Department of Cardiac Surgery, California Pacific Medical Center, 2100 Webster Street, San Francisco, CA 94115, USA.

ened or narrowed for the physician managing the patient. There are four groups of decision drivers as shown in Figure 1. Most surgeons go through this process (algorithm) subconsciously. But as more devices become available with different capabilities, physicians have a menu of options to consider that demand careful characterization of the end therapy that is sought and the pathway(s) to follow.

The disease

The pathophysiology and natural history of a specific heart condition is probably the most important factor that will determine the pathway of care and outcome. These factors include the following general areas of pathology:

- Acute cardiomyopathy
- Chronic idiopathic cardiomyopathy
- Chronic ischemic cardiomyopathy
- Acute myocardial infarction
- Postcardiotomy failure
- Post-transplant failure
- Pre/postmyocardial reduction surgery
- Congenital heart disease.

Clinical requirements

There is a growing array of clinical requirements that must be met to allow different therapies to be part of the management plan. In standard of care terms these would be referred to as 'indications' and 'contraindications' to a particular therapy. Once again, the choices are becoming so numerous and varied, especially in the end strategy of surgery and bridge therapy, that what works for one approach will not necessarily work for another. The physician must fit the therapy with all its ramifications to the anatomy, pathology, setting and logistics that are attached to a specific patient. The clinical requirements that direct the patient management plan are detailed under three categories: (1) hemodynamics, (2) medical needs and (3) logistics.

Hemodynamics include the cardiac performance parameters with which the patient presents, and the benchmark goals the therapy must provide. They include: (1) cardiac index, (2) pulmonary artery pressures and wedge, (3) right atrial pressure, and (4) pulmonary and systemic vascular resistance.

Medical needs include information on:

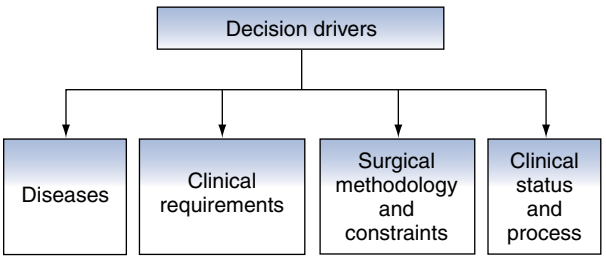

Figure 1. Decision drivers.

- Meeting transplant criteria
- Status of coagulation
- Any infection
- Nutrition
- Liver function
- Renal function
- CNS function.

Logistics consider the potential mobility of the patient and portability of the system. If the patient is bed ridden or hospital bound it will limit the choices. Compliance and emotional stability are important considerations in any patient being considered for a VAD. The needs and opportunities of ancillary support also must be assessed.

Surgical methodology and constraints

These are of immediate concern to the surgeon as he or she decides on the feasibility of VAD therapy and how to deploy it. Constraints that limit the surgical choices include:

- Overall surgical risk
- Patient size
- Incision choices
- Redos
- Coagulation status
- Infection
- Peripheral vascular disease
- Right ventricular function
- Presence of patent coronary artery bypass grafts
- Prosthetic valves
- Aortic insufficiency.

The successful deployment of a VAD via a minimally invasive approach, without sternotomy or a thoracotomy, has put the surgical constraints in an entirely new light. The methodology requires an assessement of how the VADs can be safely implanted, which includes:

- The need for cardiopulmonary bypass (CPB)
- CPB circuit
- Status of different cannulation sites
- Para- or intracorporeal pumps
- Presence of an atrial septal defect
- Need for follow-up operations
- Pump removal strategy
- Hemodynamic monitoring needs.

Clinical status and process

The patient can present in varying degrees of stability from an elective procedure to an emergency presentation that requires peripheral CPB to gain control of the circulation followed by VAD implants. It is not always possible to judge the status of other organ function (e.g. the brain) (Figure 2). Temporizing for 24–48 h utilizing peripheral CPB before making a definitive decision on the use of VAD therapy is an acceptable practice. Postcardiotomy

heart failure is often managed with centrifugal pumps as a temporizing maneuver. Only when other more sophisticated and durable pumps are not available is this an acceptable practice. The damage imposed by these devices outweighs any reason for using them in place of VAD devices that are designed for longer-term support. In the presence of centrifugal pumps, or other short-term pumps (CPB or extracorporeal membrane oxygenation [ECMO]) the best strategy is to convert the patient to a pumping system designed to support the patient over long periods of time with low morbidity.

End strategy

Based on the clinical parameters (decision drivers), the physician must formulate early on a treatment plan that is believed to offer the best possible outcome for the patient, from one of the six end strategies shown in Figure 3.

The six end strategies shown in Figure 4 can be compressed into four main areas for the purpose of formulating a treatment plan: (1) medical therapy, (2) transplantation, (3) surgical or bridge therapy, and (4) permanent cardiac support. In choosing a treatment plan, a balance must be reached between the best outcome versus the therapy with the lowest risk of morbidity and mortality that uses the least invasive approach. It must be noted that at this point in time, permanent cardiac support is not an established therapy. However, preliminary studies are ongoing and test protocols are being developed for its clinical use. Even at this stage, those involved should be thinking in terms of permanent support as an end strategy.

The end strategy characterizes the distinction between VADs and a VAS. A permanent cardiac support system will be a goal that most likely will be set at the front end of the clinical management plan. The system will include an implanted pump with an air venting chamber and an energy system as well as a back-up energy system. The device description 'permanent' connotes that this therapeutic cardiac support option will, in most cases, be a permanent, one-step, elective, end-therapy device implantation procedure. Current displacement pumps, or some of the axial flow pumps, are theoretically suited to be a VAS. A single, integrated, comprehensive design is the feature that characterizes a VAS from a VAD.

VADs are used in the surgical and bridge-to-transplant therapeutic strategies. The most important feature of VADs is their flexibility. The more seamless the process is, the better the device. VADs:

- Can be used in elective or urgent situations
- Can be used long term, but not necessarily permanently
- Are selectively modular
- Are para- or intracorporeal
- Are adaptive to more than a single stage management plan.

The most important feature of a VAD system is its ability to work seamlessly in a variety of patients and clinical situations.

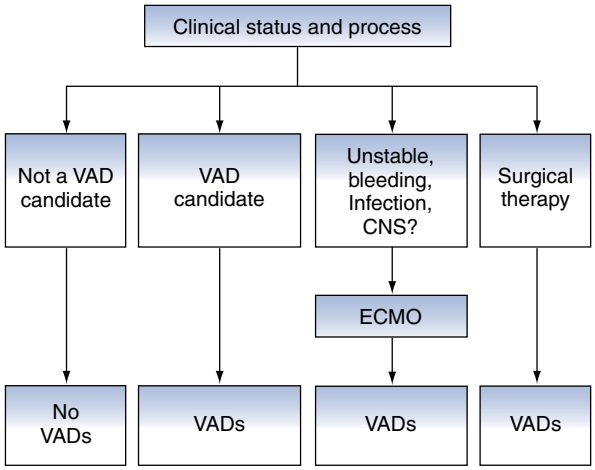

Figure 2. Decision process by clinical status.

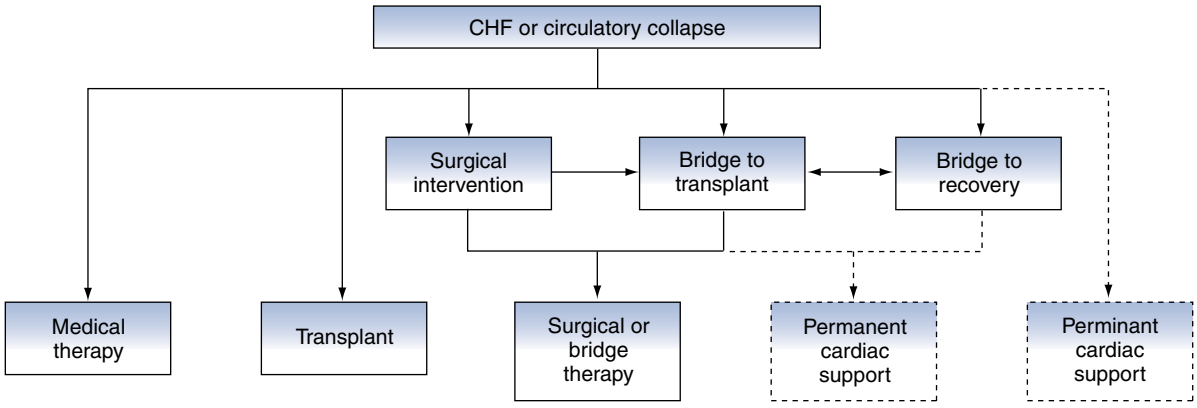

Figure 3. End strategies for treatment of cardiac or circulatory failure. --------- = Not a currently available therapeutic option.

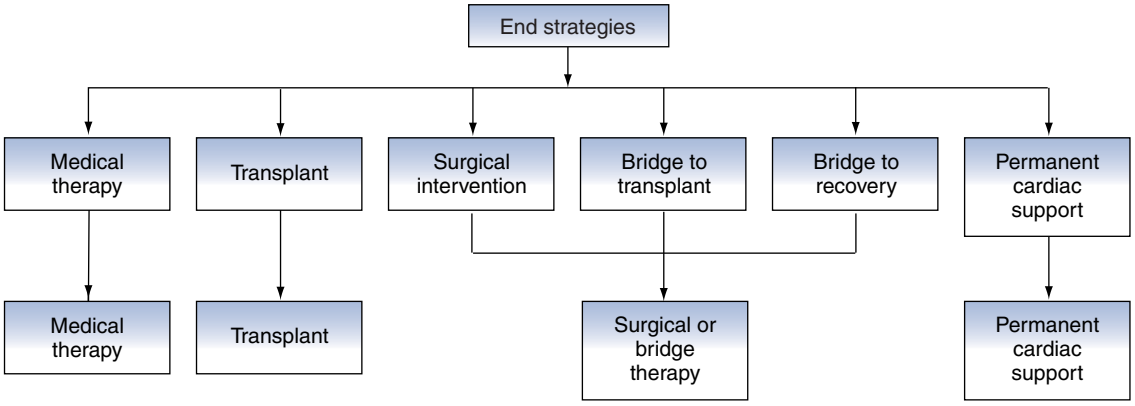

Figure 4. Compression of six end strategies into four.

If medical therapy or transplantation are not options in the management of congestive heart failure or circulatory collapse, the physician must find another option through either surgery or bridge-to-transplant therapy. This opens up many choices that are dictated by decision drivers but are also dependent upon the characteristics of the chosen support device. Therefore, the distinguishing feature of a VAD that separates it from a VAS is its seamless flexibility to move from one therapeutic destination to another as the course of the disease unfolds. The more developed this feature the better the physician can manage the patient.

Emergence of bridge-to-transplant patients experiencing myocardial recovery

The management pathways described earlier are used in varying frequencies depending on the case-mix of patients a medical centre attracts, and on the types of mechanical devices they use. One attractive unplanned pathway is beginning to appear in centres all around the world: bridge-to-transplant that becomes a bridge to recovery (Figure 5).

Bridge-to-transplant therapy has been available since 1984 and is a very successful therapy. This is especially true when the recipient is in a good general condition with isolated severe and life-threatening heart failure. In the past decade, and particularly during the last three years, patients with a support device and on a pathway to transplant have on some occasions recovered and had the device removed. There are now more than 50 published or recorded cases (Table 1).

Recovery has most frequently occurred in patients younger than 50 years of age who had a diagnosis of idiopathic cardiomyopathy. Recovery is occurring more often than can be attributed to chance alone. At this point there is very little evidence to say why this is occurring, and no apparent way to identify patients who may be candidates for recovery. Many centres are systemically studying these patients more carefully. Some of the areas being looked into are:

- Disease etiology of patients who recover
- Medical management during and after recovery
- Weaning protocols
- Reconditioning of the heart and circulation
- Optimum time needed for recovery
- Identifying the markers of recovery.

The time to recovery has ranged from 30 to 2000 days. The devices are being used in the standard protocol of bridge-to-transplant therapy. Since they are going to be possibly removed, paracoporeal devices are particularly suited to the therapy, although several different types of devices have been successfully used.

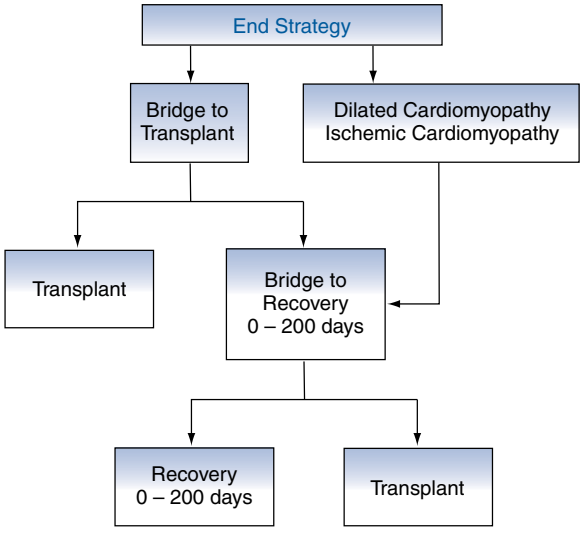

Figure 5. Clinical path showing the development from bridge-to-transplant therapy to bridge-to-recovery therapy.

Table 1. Reports of spontaneous recovery during use of a support device

Institution	Author	Year	N.	Etiology	Device	Outcome	Length of support (days)	Duration since explant (days unless otherwise stated)
University of Alabama, Birmingham	Holman	1991	1	Viral myocarditis	Thoratec	Alive	70	N/A
Berlin Heart Institute	Muller	1997	5	DCM	Novacor TCI	All alive NYHA IA	160–794	51–592
Columbia Presbyterian Medical Center	Mancini	1998	5	4–DCM ICM	TCI	2–Deaths (3months and 27 months post-op) 2– Required VADs 4– Recurrent heart failure	58–380	90–810
California Pacific Medical Center	Hill[1]	1999	1	Viral myocarditis	Thoratec–Biventricular VAD	Alive NYHA 1A	125	190
Texas Heart Institute	Frazier	1999	5	3–ICM 2–PCM	1–Thoratec 1–Novacor 3–TCI	1–Death (POD 10) 4– Alive	46–447	10–1050
Berlin Heart Institute	Hetzer	1999	19	DCM	2–TCI 1–Berlin Heart 16–Novacor	13– Alive, well 4– Recurrent failure 2–Heart Tx 2–died 1–LVAD to heart Tx	36–794	8–930
Multi-institutional (Thoratec Registry)	Farrar	1999	17	6–Myocarditis 4– Viral CM 2–PCM 5–IdCM	Thoratec	4–Death (< 7 months post-op) 13–Alive	11–97	4 months–8 years
Christ Hospital and Medical Center	Silver	2000	5	Moderate–severe MR DCM	Thoratec[2]	Alive NYHA I	30–118	11–119

[1] unpublished results, [2] patients had concomitant mitral valve repair and partial left ventriculectomy at explant, DCM = dilated cardiomyopathy, ICM = ischemic cardiomyopathy, PCM = postpartum cardiomyopathy, IdCM = idiopathic cardiomyopathy, MR = mitral regurgitation, VAD = ventricular assist device, LVAD = left ventricular assist device, POD = post-op days, NYHA = New York Heart Association, Tx = transplant.

Conclusion

More devices with different features are becoming available. Patients present with a wide spectrum of pathophysiologies. The device must fit the patient's condition. A method to follow that will establish an end strategy using decision drivers early in the patient's management will guide the physician to the best choice of a device or devices.

References

1. Frazier OH, Myers TJ. Left ventricular assist system as a bridge to myocardial recovery. *Ann Thorac Surg* 1999;68(2):734–41.
2. Muller J *et al*. Weaning from mechanical cardiac support in patients with idiopathic dilated cardiomyopathy. *Circulation* 1997;96(2):542–9.
3. Mancini DM, Baniaminovitz A, Levin H *et al*. Low incidence of myocardial recovery after left ventricular assist device implantation in patients with chronic heart failure. *Circulation* 1998;98(22):2367–9.
4. Hill JD, Farrar DJ, Hershon JJ *et al*. Use of a prosthetic ventricle as a bridge to cardiac transplantation for postinfarction cardiogenic shock. *N Engl J Med* 1986;314(10):626–8.

Session 10

Ventricular Assist Devices

Journal of Congestive Heart Failure and Circulatory Support (2001) Vol 1, No 4, 445–448

Mechanical circulatory support with Abiomed BVS 5000 and BioMedicus BP–80 for postcardiotomy cardiogenic shock

A. Sezai MD, K. Minami MD PhD, A. El-Banayosy MD, L. Arusoglu MD, P. Sarnowsky MD, L. Kizner MD, Y. Bonkohara MD and R. Koerfer MD PhD

Department of Thoracic and Cardiovascular Surgery, Heart Center North Rhine-Westphalia Bad Oeynhausen, Ruhr-University of Bochum, Germany

Abstract Recently, the survival rate for patients with severe cardiogenic shock was improved with the use of a mechanical device. However, many reports indicate that death can be caused by multiple organ failure, bleeding, infection and neurological accident. Between September 1989 and July 1999, 369 patients were supported by various mechanical circulatory support systems in our institute, and 89 patients were treated for postcardiotomy cardiogenic shock. Out of the 89 patients, BioMedicus BP-80 was used in 22, Abiomed BVS5000 in 45, Thoratec in seven, Novacor in two, Medos in one, BioMedicus + Thoratec in two, and a combination of others in four. In this study, we report the outcome of mechanical circulatory support with Abiomed and BioMedicus for postcardiotomy cardiogenic shock.

The mean duration of mechanical support was 5 days with BioMedicus and 5.3 days with Abiomed. The weaning and discharge rates of the patients by type of support were 68% and 45% with BioMedicus and 58% and 47% with Abiomed, respectively. As to complications, bleeding was recognized in 36% of patients using BioMedicus and 22% using Abiomed; neurologic disorders were reported in 5% using BioMedicus and 11% using Abiomed.

The complete results of this study were acceptable. Although increasing clinical experience with mechanical circulatory support appears to result in a clinically relevant decrease in morbidity, complications, such as bleeding, neurological accident, and multiple organ failure were recognized.

Keywords mechanical ventricular support, Abiomed BVS 5000, BioMedicus BP-80, postcardiotomy cardiogenic shock.

Introduction

Recently, the survival rate in patients with severe heart failure has been improved as a result of use of mechanical circulatory support[1,2]. Between September 1989 and July 1999, 369 patients were supported by various mechanical circulatory support systems in our institute[3]. Mechanical circulatory support can be used not only in patients with postcardiotomy cardiogenic shock, but also in patients with cardiogenic shock due to acute myocardial infarction or as a bridge to heart transplantation. However, complications such as multiple organ failure (MOF), infection, bleeding, and nervous disorders, have still been reported from many investigators[4,5].

In this study, we reported on use at our institute of Abiomed BVS5000 (Abiomed Cardiovascular, Inc., Danvers, MA, USA) and BioMedicus BP-80 (Medtronic, Inc., Minneapolis, MN, USA) for postcardiotomy cardiogenic shock.

Methods

Between September 1989 and July 1999, 89 patients were treated with various mechanical circulatory support devices for postcardiotomy cardiogenic shock. Abiomed was the device most often used (in 45 cases), and BioMedicus was used in the next largest number of cases (22) followed by Thoratec (Thoratec, Berkeley, CA, USA) in seven cases, Novacor (Baxter Healthcare Corporation, Novacor Division, Oakland, CA, USA) in two, and Medos, which was used for a child. Two cases first received a BioMedicus device and then a Thoratec device; four cases received other combinations of devices (Table 1). The type of support used in patients with Abiomed and BioMedicus is shown in Table 2. As a characteristic of our therapeutic strategies, a BioMedicus system was used for simple right heart failure, and a Abiomed for biventricular heart failure (Table 2). The ages of the subjects in the Abiomed group ranged 29–73 years with a mean age of 55 years and in the BioMedicus group ranged 35–82 years with a mean age of 58 years. The Abiomed group consisted of 30 male and 15 female

Correspondence to: Dr Akira Sezai, Georgstr. 11, 32545 Bad Oeynhausen, Germany, Department of Thoracic and Cardiovascular Surgery, Heart Center North Rhine-Westphalia Bad Oeynhausen, Ruhr-University of Bochum, Germany.

Table 1. Application of ventricular assist device for postcardiotomy cardiogenic shock

Device	Patients (No.)
Abiomed	45
BioMedicus	22
Thoratec	7
Novacor	2
Medos	1
BioMedicus/Thoratec	2
Combination of others	4

Table 2. Type of ventricular assist device for postcardiotomy cardiogenic shock

Type of device	Abiomed patients (No.)	BioMedicus patients (No.)
LVAD	37	18
RVAD	0	3
BVAD	8	1

patients, while 16 male and 6 female patients comprised the BioMedicus group. Among surgeries performed, coronary artery bypass grafting (CABG) was the most common procedure in both groups (Table 3). As for anticoagulation therapy, heparin is reversed with protamine and in the first 24 h postoperatively the patients were not given any such therapy. Thereafter, the therapy is begun with heparin to maintain the activated clotting time at 180 s. BioMedicus group have a Carmeda-coated circuit (Medtronic, Inc., Minneapolis, MN, USA). Our criteria for implantation of mechanical circulatory support in postcardiotomy cardiogenic shock were as follows[1,6]:

1. Technically satisfactory operation
2. Subsequent perfusion time of at least 60 min
3. Acceptable blood-gas analysis as well as acid–base and electrolyte balances
4. Body temperature greater above 35.5°C
5. Optimal cardiac rhythm and heart rate
6. Optimal pre-load and after-load (vasodilator, volume)
7. Optimal inotropic support:
   - Dopamine ≧ 10–12μg/kg/min
   - Phosphodiesterase III inhibitors ≧ 10 μg/kg/min
   - Adrenaline ≧ 0.1μg/kg/min (in valve patients)
8. Use of intraaortic balloon pumping (IABP) in CABG patients; the hemodynamic criteria include:
   - Cardiac index < 2.0 L/min/m^2
   - Systemic vascular resistance > 900 dyn.s/cm^{-5}
   - Central venous pressure > 20 mmHg
   - Left atrial/pulmonary capillary wedge pressure > 20 mmHg
   - Mean arterial pressure < 60 mmHg.

Table 3. Patient characteristics with Abiomed and BioMedicus

Characteristic		Abiomed patients (No.)	BioMedicus patients (No.)
Patient (No.)		45	22
Age (mean)		55 (29–73)	58 (35–82)
Gender (male:female)		30:15	16:6
Diagnosis	CABG	40	12
	Valve replacement	4	8
	Ebstein anomaly	0	1
	VAR	1	1

CABG: coronary artery bypass grafting; VAR: ventricular aneurysmal resection

Results

The patients were supported with a device for 5.3 days on average and 28 days for the longest time in a case in the Abiomed group, and for 5 days on average and 16 days for the longest time in a case in the BioMedicus group. The weaning rate was 58% in the Abiomed group and 68% in the BioMedicus group; the discharge rate was 47% in the Abiomed group and 45% in the BioMedicus group. There were no differences in these rates between the two types of devices. Heart transplantation was performed on four patients (9%) of the Abiomed group and on one patient (5%) of the BioMedicus group (Table 4).

As for complications, bleeding occurred most frequently in both groups, showing an incidence of 22% in the Abiomed group and 36% in the BioMedicus group. Nervous disorders occurred in 11% of the Abiomed group and 5% of the BioMedicus group. Renal dysfunction occurred in 6% of the Abiomed group and 5% of the BioMedicus group. Liver dysfunction occurred in 4% of the Abiomed group. Infection occurred in 2% of the Abiomed group. There was no infection or liver dysfunction in the BioMedicus group. MOF occurred in 4% of the Abiomed group and 5% of the BioMedicus group. Bleeding tended to occur more frequently in the BioMedicus group, while nervous disorders tended to occur more frequently in the Abiomed group (Table 5). As for causes of death, MOF accounted for 18% in the Abiomed

Table 4. Results comparing patient treatment and outcome with use of Abiomed and BioMedicus

Treatment/outcome	Abiomed patients ($n = 45$)	BioMedicus patients ($n = 22$)
Support days	5.3 (max:28)	5 (max:16)
Weaned	26 (58%)	15 (68%)
Discharged	21 (47%)	10 (45%)
On device	0	1
Transplanted	4 (9%)	1 (5%)

Table 5. Postoperative complications

Complication	Abiomed patients ($n = 45$)	BioMedicus patients ($n = 22$)
Bleeding	10 (22%)	8 (36%)
Neurology	5 (11%)	1 (5%)
Renal failure	3 (6%)	1 (5%)
Liver failure	2 (4%)	0
Pneumonia	2 (4%)	1 (5%)
Infection	1 (2%)	0
MOF	2 (4%)	1 (5%)
Hemolysis	0	1 (5%)

MOF: multiple organ failure

Table 6. Causes of death

Cause of death	Abiomed patients ($n = 45$)	BioMedicus patients ($n = 22$)
MOF	8 (18%)	3 (14%)
Sepsis	2 (4%)	2 (10%)
Cerebral	3 (6%)	0
Bleeding	0	0
Air embolism	1 (2%)	0
ARDS	1 (2%)	0

ARDS: adult respiratory distress syndrome; MOF: multiple organ failure

group and 14% in the BioMedicus group. Sepsis accounted for 4% in the Abiomed group and 10% in the BioMedicus group. Cerebral disorders were recognized in 6%, air embolism 2%, and adult respiratory distress syndrome (ARDS) 2% in the Abiomed group (Table 6).

Discussion

In recent years, various ventricular assist devices have been developed and used as mechanical support. Abiomed BVS 5000 and BioMedicus BP-80 have been widely used clinically for postcardiotomy cardiogenic shock. At our institute, the established treatment for postcardiotomy cardiogenic shock includes use of Abiomed or BioMedicus if sufficient hemodynamics are not obtained with drug therapy and IABP[7]. However, a Thoratec, Novacor, or HeartMate device may be selected if preoperative or intraoperative cardiac function suggests the need for long-term circulatory support. Thoratec is used especially as a biventricular assist device (Figure 1). In principle, Abiomed is used for early postcardiotomy cardiogenic shock, namely it is implanted during surgery in the operation room. BioMedicus is used for postcardiotomy cardiogenic shock occurring in the postoperative intensive care unit and used for single right heart failure. However, theses are just general rules, and Abiomed, which provides a pulsatile flow, is used if (1) renal dysfunction or another complication is detected before surgery, (2) preoperative cardiac function is poor, or (3) an IABP cannot be inserted because of peripheral vascular disease. One advantage of Abiomed is that it can provide a pulsatile flow. The advantages characteristic of BioMedicus are its easy and rapid insertion and that it is used in combination with IABP. The outcomes of mechanical circulatory support for postcardiotomy cardiogenic shock were previously reported from a single institute. In these reports, the weaning rate was 47%–62%, and the discharge rate was 17–50%[8–12]. Pae *et al.* evaluated 965 patients from a number of institutions and reported the weaning rate to be 45%, and the discharge rate 24.6%. We conclude that the complete results of this study are acceptable, and compared with the previous reports that, our cases had a better discharge rate[5]. This improvement is thought to be because we used either a Thoratec, Novacor, or HeartMate device, or performed heart transplantation in the cases that developed heart failure again after weaning. Additionally, a shorter cardiopulmonary bypass time and earlier implantation of a right ventricular assist device for right heart failure helped to prevent postoperative hepatic and renal dysfunction and MOF.

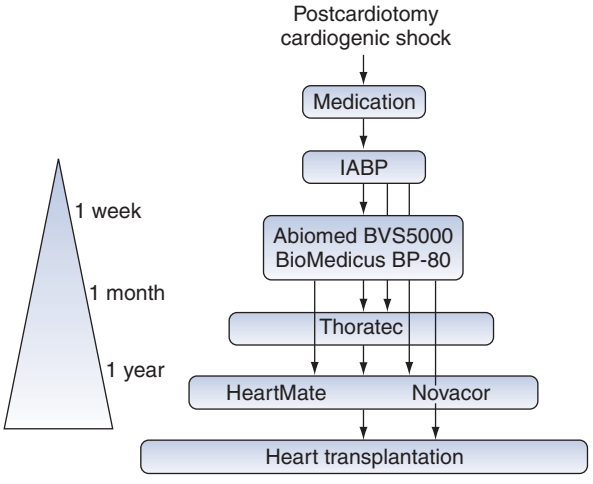

Figure 1. Strategy of ventricular assist device for postcardiotomy cardiogenic shock in our institute. IABP, intraaortic balloon pumping.

Many investigators have studied pulsatile and nonpulsatile flows from various viewpoints. Most of these studies have examined extracorporeal circulation, and even though other studies examined this issue from many different perspectives, no conclusive data are available[13,14]. In previous reports, authors examined two types of flow on left ventricular and biventricular assist devices after cardiogenic shock, and reported that even though there were no marked differences between nonpulsatile- and pulsatile-assisted circulation in terms of effect on the heart, pulsatile-assisted circulation seemed superior in terms of its effect on the peripheral organs and cellular metabolism[15,16]. Although there have been only a few clinical reports comparing the pulsatile flow pump of the Abiomed system with the

nonpulsatile flow pump of BioMedicus, Jett and his coworkers reported that Abiomed pumps provided better weaning and discharge rates, in addition to lower incidences of some complications, including bleeding and nervous disorders[12]. Minami *et al.* of our institute also reported that Abiomed pumps, which provide a pulsatile flow, are superior to BioMedicus pumps in organ perfusion and catecholamine reduction[17,18]. However, no apparent differences were observed between the two types of devices in the present study. Possible reasons for this are that Abiomed pumps are used if poor preoperative cardiac function or complication is detected, and that a pulsatile flow is obtained for BioMedicus pumps by the concomitant use of an IABP. However, these two devices cannot be compared directly because of the difference in pathological conditions between the two groups in this study. Further studies will be conducted to clarify this issue.

References

1. Koerfer R, El-Banayosy A, Posival H *et al.* Mechanical circulatory support. The Bad Oeynhausen experience. *Ann Thorac Surg* 1995;59:S56–63.
2. Frazier OH. New technologies in the treatment of severe cardiac failure: the Texas Heart Institute experience. *Ann Thorac Surg* 1995;59:S31–8.
3. Minami K, El-Banayosy A, Sezai A *et al.* Morbidity and outcome after mechanical ventricular support using Thoratec, Novacor, and HeartMate for bridging to heart transplantation. *Artif Organs* 2000;24:421–6.
4. Hunt SA, Frazier OH. Mechanical circulatory support and cardiac transplantation. *Circulation* 1998;97:2079–90.
5. Pae WE, Miller CA, Matthews Y, Pierce WS. Ventricular assist devices for postcardiotomy cardiogenic shock. *J Thorac Cardiovasc Surg* 1992;104:541–53.
6. El-Banayosy A, Posival H, Minami K *et al.* Mechanical circulatory support: lessons from a single center. *Perfusion* 1996;11:93–102.
7. Koerfer R, El-Banayosy A, Posival H *et al.* Mechanical circulatory support with Thoratec assist device in patients with postcardiotomy cardiogenic shock. *Ann Thorac Surg* 1996;61:314–16.
8. Golding LAR, Crouch RD, Stewart RW *et al*. Postcardiotomy centrifugal mechanical ventricular support. *Ann Thorac Surg* 1992;54:1059–64.
9. Noon GP, Lafuente JA, Irwin S. Acute and temporary ventricular support with BioMedicus centrifugal pump. *Ann Thorac Surg* 1999;68:650–4.
10. Magovern GJ. The Biopump and postoperative circulatory support. *Ann Thorac Surg* 1993;55:245–9.
11. Couper GS, Dekkers RJ, Adams DH. The logistics and cost-effectiveness of circulatory support: advantages of the Abiomed BVS 5000. *Ann Thorac Surg* 1999;68:646–9.
12. Jett GK. Abiomed BVS 5000: experience and potential advantage. *Ann Thorac Surg* 1996;61:301–4.
13. Hickey PR, Buckley MJ, Philbin DM. Pulsatile and nonpulsatile cardiopulmonary bypass review of a counterproductive controversy. *Ann Thorac Surg* 1983;36:720–37.
14. Minami K, Koerner MM, Vyska K, Kleesiek K, Knobl H, Koerfer R. Effects of pulsatile perfusion on plasma catecholamine levels and hemodynamics during and after cardiac operations with cardiopulmonary bypass. *J Thorac Cardiovasc Surg* 1990;99:82–91.
15. Sezai A. Major organ microcirculation during assisted circulation. Comparison studies of pulsatile and nonpulsatile assists. *Ann Thorac Cardiovasc Surg* 1996;2:215– 23.
16. Sezai A, Shiono M, Orime Y *et al.* Major organ function under mechanical support. Comparative studies of pulsatile and nonpulsatile circulations. *Artif Organs* 1999;3:280–5.
17. Minami K, El-Banayosy A, Posival H *et al.* Improvement of survival rate in patients with cardiogenic shock by using nonpulsatile and pulsatile ventricular assist device. *Int J Artif Organs* 1992;15:715–21.
18. Minami K, Posival H, El-Banayosy A *et al.* Mechanical ventricular support using pulsatile Abiomed BVS 5000 and centrifugal BioMedicus pump in postcardiotomy shock. *Int J Artif Organs* 1994;17:492–8.

Journal of Congestive Heart Failure and Circulatory Support (2001) Vol 1, No 4, 449–454

Prevention and treatment for hyperbilirubinemia after left ventricular assist device implantation

E. Tayama MD, PhD, H. Kashikie MD, PhD, N. Hayashida MD, PhD, S. Fukunaga MD, PhD, M. Nishimi MD, PhD, T. Kosuga MD, PhD, K. Akasu MD, PhD, H. Akashi MD, PhD, T. Kawara MD, PhD and S. Aoyogi MD, PhD

Department of Surgery, Kurume University School of Medicine, Kurume-city, Japan

Background After insertion of a left ventricular assist device (LVAD), some patients occasionally develop severe hyperbilirubinemia. We describe our two experiences with this syndrome: a successful treatment of hyperbilirubinemia by plasma exchange (PE) and a useful application of percutaneous cardiopulmonary support (PCPS) as right ventricular assist in LVAD recipients.

Case 1 A 49-year-old male with end-stage dilated cardiomyopathy underwent LVAD implantation. After LVAD insertion (left atrial drainage), hyperbilirubinemia developed; total bilirubin (TB) rose from 5.7 g dL^{-1} preoperatively to 33.6 g dL^{-1} on postoperative day 3. PE was repeated during postoperative days 4–10 (seven times), and the TB level decreased to 16.3 g dL^{-1} at postoperative day 11. The TB level declined to a normal range thereafter.

Case 2 A 75-year-old male with ischemic cardiomyopathy underwent coronary artery bypass grafting (three times), mitral valve plasty, and endoventricular circular patch plasty (Dor's procedure). For postcardiotomy assist, an LVAD was implanted on postoperative day 4 (left atrial drainage) following the insertion of an intra-aortic balloon pump and PCPS, which were employed immdiately after the initial surgery. To prevent right heart dysfunction, which is a possible cause of hyperbilirubinemia, the PCPS was continued for 3 more days after LVAD insertion. A PCPS flow of 0.8 L min^{-1} effectively reduced right ventricular pre-load and a stable LVAD of 3 L min^{-1} was also maintained. In this case, TB level was maintained within the normal range.

Discussion These experiences suggest that (1) early application of PE is an effective method of treating hyperbilirubinemia after LVAD implantation, and that (2) PCPS effectively supports right ventricle function and may help to prevent hyperbilirubinemia, though close attention is essential to maintain a right–left heart system flow balance.

Keywords left ventricular assist device (LVAD), hyperbilirubinemia, plasma exchange (PE), percutaneous cardiopulmonary support (PCPS).

Introduction

Hyperbilirubinemia is one of the major consequences of using left ventricular assist devices (LVADs)[1,2]; however, the mechanism for its occurrence is not well understood. Once hyperbilirubinemia develops, the prognosis is quite poor[1,3]. We report a case in which plasma exchange (PE) was effective in treating severe hyperbilirubinemia following LVAD implantation. Additionally, we report an experience of percutaneous cardiopulmonary support (PCPS) usage as right ventricular assist simultaneously with LVAD, which might be helpful in preventing hyperbilirubinemia.

Case 1

The patient was a 49-year-old man, who had been diagnosed with and treated for dilated cardiomyopathy since 1992. He had presented with New York Heart Association (NYHA) Class IV symptoms and suffered from sustained ventricle fibrillation on April 26, 1999. After that event, his congestive heart failure could not be controlled despite the use of inotropic drugs, respirator control, intra-aortic balloon pump (IABP), continuous hemodiafiltration, or PCPS. The patient's liver and renal function began to deteriorate

Table 1. Preoperative conditions of Case 1

Circulation	Bp 90/50 mmHg, HR 114 min^{-1} CVP 19 mmHG, mPA 42 mmHg, PCWP 38 mmHg CO 1.4 L min^{-1} with PCPS 1.7 L min^{-1} and IABP 1:1
Chest X-ray	CTR 65%
Echocardiography	MR IV, TR IV LAD 50 mm, LVDd/LVDs 72/66 mm IVST/PWT 5/8 mm, LVEF 22%
Blood analysis	GOT 119 IU L^{-1}, GPT 288 IU L^{-1}, LDH 531 IU L^{-1} TB 5.7 mg dL^{-1}, DB 2.4 mg dL^{-1}, PT 17%, HCV(+) BUN 44.6 mg dL^{-1}, Cr 2.1 mg dL^{-1}
Urine output	240 mL day^{-1}

Correspondence to: Eiki Tayama MD, PhD, Department of Surgery, Kurume University School of Medicine, 67 Asahi-machi, Kurume-city, 830-0011 Japan.

(Table 1). The liver was palpable five fingerbreadths beneath the right costal margin. Precise neurological assessment could not be made due to deep sedation. On April 28, 1999, the patient underwent implantation of an LVAD (Toyobo Co., Osaka, Japan), along with removal of the IABP and PCPS. Blood was drained from the right side of the left atrium and perfused to the ascending aorta.

Immediately after LVAD implantation, the mean pulmonary capillary wedge pressure (PCWP) and central venous pressure (CVP) were decreased from 38 mmHg to 15 mmHg, and 19 mmHg to 17 mmHg, respectively, with an LVAD flow of 3.2 L min^{-1} (Figure 1). Although the circulatory condition showed improvement, the volume load (PCWP >18 mmHg, CVP >15 mmHg) was still necessary to maintain a certain level of systemic circulation in the first week after surgery. With regard to hepatic function, the serum TB level rose as high as 33.6 mg dL^{-1} on postoperative day 3 while other transaminase levels and coagulability remained within the normal range (GOT 40 U L^{-1}, GPT 40 U L^{-1}, LDH 910 U L^{-1}, and prothrombin time (PT) 55%). No mechanical bile obstruction was found by abdominal echography.

To reduce the serum bilirubin level, PE was performed daily on postoperative days 4–10 (seven times). Fresh frozen plasma (3200 mL per section) was used as replacement plasma. Although the serum TB level was high even after repeated PEs (16.3 mg dL^{-1} on postoperative day 11), icterus gradually disappeared as the circulation condition

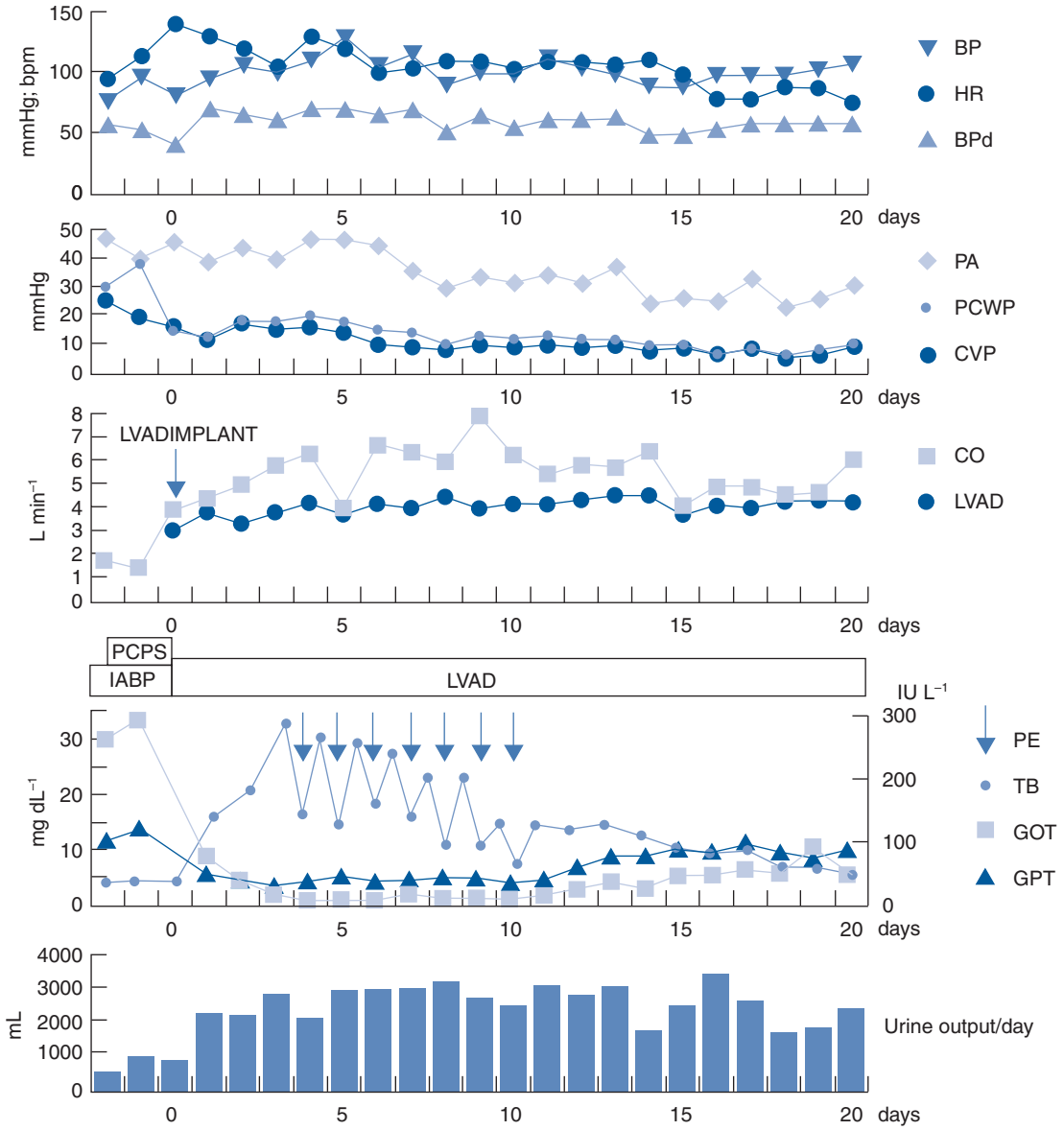

Figure 1. Time course of Case 1.

improved. Serum TB levels were 3.2 mg dL^{-1} on postoperative day 30 and 2.7 mg dL^{-1} on postoperative day 40. During this early postoperative period, renal function was maintained within the normal range, including a sufficient urine output (>2000 mL per day). Unfortunately, the level of consciousness did not improve after the surgery due to a midbrain infarction, which was diagnosed by brain CT on postoperative day 19. Since circulation status and liver function were stabilized, use of the LVAD was discontinued and replaced by IABP on postoperative day 41. The IABP was also removed seven days later, but the patient never recovered from the neurological complication and eventually died 83 days following LVAD implantation (42 days after the LVAD removal). No thrombus was discovered in the pump at postoperative inspection. The reason for cerebral infarction is unknown; it may have been due to thromboembolism or to brain damage from preoperative shock.

Case 2

The patient was a 75-year-old man who had been diagnosed with ischemic cardiomyopathy (left ventricular ejection farction [LVEF] <20%) and mitral regurgitation (Sellers II) and had a history of three myocardial infarctions since 1976. He underwent a coronary artery bypass graft three times, mitral annuloplasty using a Carpentier ring, and endoventricular circular patch plasty (Dor's procedure). Since he could not be weaned from the cardiopulmonary bypass, IABP (from the left femoral artery) and PCPS (blood drained through the right femoral vein and perfused to the right subclavian artery) were initiated. Despite employment of these assist devices for three days, neither the patient's circulatory status nor cardiac function was improved. He underwent implantation of an LVAD (Toyobo Co., Osaka, Japan) and removal of the IABP on postoperative day 4. The PCPS was continuously applied simultaneously with the LVAD to reduce right ventricular pre-load (Figures 2 and 3). Even with only 0.8 L min^{-1} of PCPS assist, CVP and PA declined significantly and systemic oxygenation was improved under an LVAD flow of 3.0 L min^{-1} as shown in Table 2. The patient was slowly weaned from the PCPS without difficulty three days after LVAD implantation. After LVAD initiation, the circulatory status was significantly improved and urine output was also increased. Serum TB levels did not rise beyond 4 mg dL^{-1} in the early postoperative period. After two weeks of LVAD assist, the LVAD was removed and converted to an IABP. For a few days following LVAD weaning, the circulatory status was stable. Unfortunately, the patient eventually died 45 days after the initial operation due to low output syndrome.

Discussion

The clinical role of LVADs has been increasing because it is acknowledged that LVADs can improve end-organ function and create a healthier heart transplantation recipient candidate[1,4,5]. However, hyperbilirubinemia is occasionally experienced in the early period on LVAD support[1,2,6]. Although the prognosis is poor when hyperbilirubinemia is present, the cause of hyperbilirubinemia is not well understood.

Several possible causes have been proposed. Two ways in which liver damage is caused by heart failure[7] are, firstly, hypoperfusion due to left-sided heart failure and

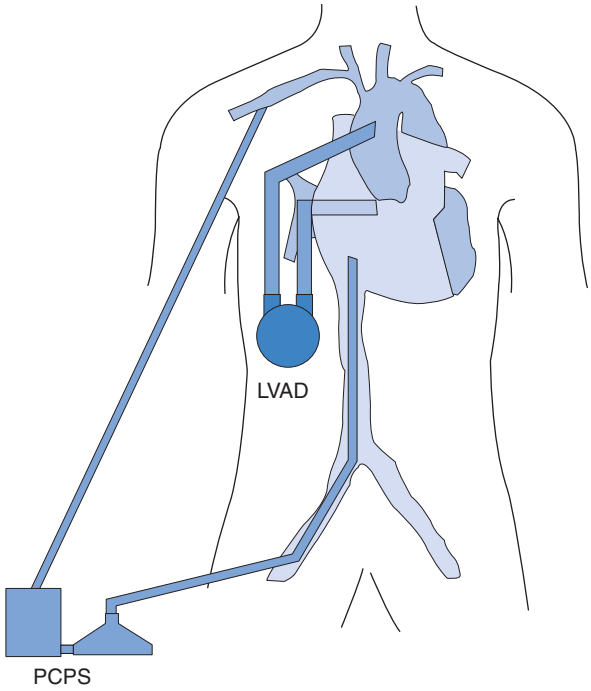

Figure 2. Schema of the LVAD and PCPS circuits.

Table 2. Hemodynamic parameters of Case 2

PCPS		Off	On (0.8 L min^{-1})
BP	(mmHg)	79/40	93/43
PA	(mmHg)	34/11	28/8
CVP	(mmHg)	11	8
PCWP	(mmHg)	12	11
HR	(bpm)	80	85
SvO2	(%)	51	67
CO	(L min^{-1})	3.9	3.8
LVAD flow	(L min^{-1})	3.2	3.0
Blood gas analysis			
	pH	7.48	7.49
	pCO_2	33.2	35.7
	pO_2	63.8	79.2
	BE	2.0	3.7
	SaO_2	92.8	95.9

A PCPS flow of only 0.8 L min^{-1} significantly reduced CVP and PA, and improved systemic oxygenation saturation. In this situation a substantial LVAD flow was maintained.

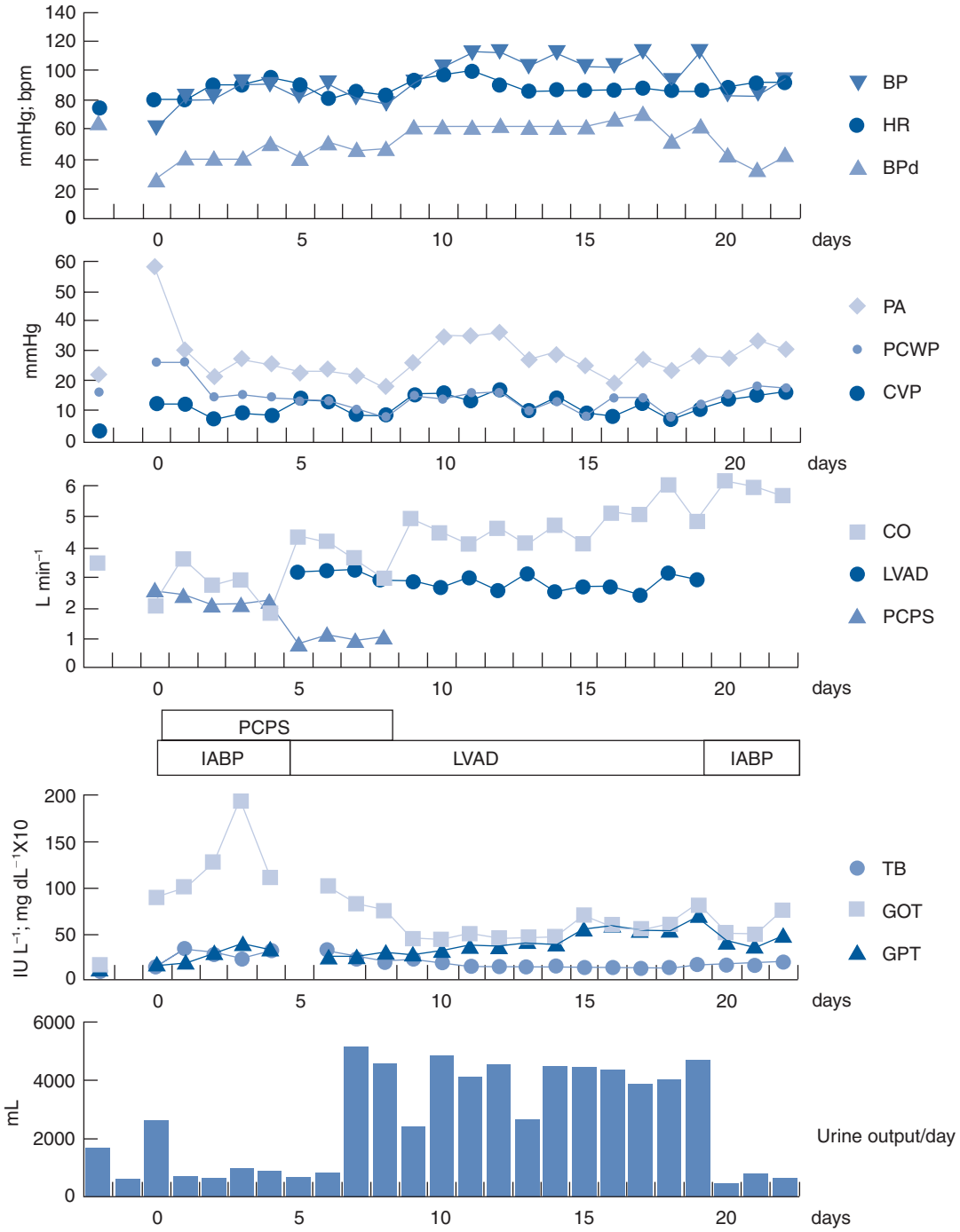

Figure 3. Time course of Case 2.

secondly, chronic passive congestion due to right-sided heart failure. Hyperbilirubinemia after LVAD implantation may be closely associated with right ventricular (RV) failure, because systemic hemodynamic condition is usually improved by use of the device. Furthermore, an LVAD occasionally impairs RV function due to an increased RV pre-load and leftward septal shift, though the LVAD commonly contributes to RV function by reducing RV after-load[8,9]. Depending on the pathophysiologic conditions, these effects by LVAD can either be detrimental or beneficial to the determinants of RV function. Another possible mechanism is so-called hepatic sinusoid endothelial dysfunction[6]. Once mitochondrial function is impaired, the energy production is lacking for

releasing bile into the bile canalicules, where the last and most energy-dependent phase of bile metobolism takes place. Therefore, soluble conjuncted bilirubin is readsorbed into the bloodstream, causing jaundice. Of course, preoperative liver dysfunction is also one of the major risk factors for hyperbilirubinemia. In summary, there are multiple potential causes of hyperbilirubinemia in LVAD patients.

In Case 1, the preoperative serum TB was already over 5 mg dL^{-1} and PT was lower than 20% due to liver cirrhosis and severe congestion. In such a situation, any number of small events has the potential to damage the liver fatally, for example surgical trauma, bleeding, blood transfusion, anesthesia, or hypoxia. Although CVP was decreased after LV assist, a high level of more than 15 mmHg had been sustained. This high CVP may also lead to development of hepatic malfunction due to significantly reduced portal flow and poor splanchnic circulation. Hemolysis is also a possible cause of hyperbilirubinemia, but it was excluded in our case because the LDH level was not extraordinarily high. Even though the serum TB level was over 30 mg dL^{-1}, we judged that the liver function was still recoverable because coagulability maintained a PT of over 50% and the circulatory condition had begun to improve. Fortunately, the renal function was not impaired, and hepato-renal syndrome was absent. We therefore performed PE to control the serum bilirubin level.

PE has been clinically performed as hepatic assist since 1967[10]; however, the prognosis of postoperative hyperbilirubinemia is still poor[11]. Kodama *et al.*[11] summarized the results of therapeutic plasmapheresis for treatment of postoperative hepatic failure, which included both cardiac and general surgery in 215 cases in Japan. They suggested that early application of PE is essential in order to improve its outcome. It is difficult to assess the recoverability of liver function and to determine the optimal timing for introduction of PE.

The recommended criteria for initiation of PE are: (1) coma grade (II–III), (2) TB >5 mg dL^{-1}, and (3) PT $<40\%$[11]. These criteria, particularly a TB of 5 mg dL^{-1}, seemed too early for LVAD recipients; however, it should be kept in mind that its earlier application is more effective and has a better prospect of success. We felt that urine output volume is a primitive but informative indicator for assessing the prognosis. Although not measured in our patients, arterial ketone body ratio and hyaluronic acid may be informative in assessing the prognosis of liver function[6]. It goes without saying that preventing infection is essential and therefore careful blood access maintenance and aggressive enteral nutrition are recommended. Problems with PE include the difficulty in obtaining a large amount of fresh frozen plasma and its high cost. Plasma adsorption and hemoadsorption may be alternative options[12]; however, the efficacy of removal of serous bilirubin is relatively lower and coagulation factors cannot be supplied as they can in PE. Deciding when to cease treatment is also a difficult issue. In most cases, the physician is able to judge the effectiveness of PE with less than five treatments[11].

It is obvious that prevention of hyperbilirubinemia is the most important way to obtain a better outcome. Early LVAD application prior to damage of end organs is essential. Concerning hepatic function, serum TB should not be over 2.5 mg dL^{-1}. Moreover, aggressive application of RVADs along with LVADs, namely the application of biventricular assist devices (BiVADs), is recommended to prevent potentially irreversible end-organ injury[13,14]. If we had applied the BiVAD in Case 1, we might have been able to prevent the hyperbilirubinemia. However, at the time point where the TB was over 30 mg dL^{-1}, it would probably have been too late for RVAD application to be effective.

Unfortunately there is no reliable predictor for evaluating the consequences of RV failure[15–17]. Kormos *et al.*[16] reported that there are no differences in preimplantation hemodynamics between patients who exhibit RV failure during LV assist. They concluded that the need for a BiVAD depends more on the patient's clinical status than on hemodynamic parameters. Some groups therefore aggressively use BiVADs to simplify medical management[17]. However, a substantial number of patients using BiVADs need the RVAD only in the early postoperative period, because perioperative RV failure is often due to increased pulmonary artery resistance associated with blood transfusion and cardiopulmonary bypass.

If a peripherally accessible RVAD becomes clinically available, it would be quite useful. Since this is not the case at present, we utilized the PCPS as an RVAD. Although PCPS has been widely used in cardiogenic shock patients[18,19], it has not been commonly employed during LVAD application. Wudel *et al.*[20] described 12 cases of extracorporeal life support as a supplement for RV failure, respiratory insufficiency or both after LVAD implantation. However, in only one case they used a peripheral veno-arterial bypass circuit such as we used in our patient. They used veno-pulmonary artery bypass or veno-veno bypass with an oxygenator in their other 11 cases. PCPS is generally contraindicated in LVAD recipients, because PCPS uses a veno-arterial bypass circuit, which means blood does not go through the LA or the LV chamber. Consequently, sufficient LVAD flow from the LA or LV cannot be maintained if a high-flow PCPS is applied. However, if the PCPS and LVAD flows are well balanced, the PCPS application may not only reduce RV pre-load, but also provide high systemic oxygenation. Concerning cerebral and cardiac metabolism, the subclavian artery is preferable to the femoral artery for PCPS perfusion. Additionally, because this blood access is peripheral, no additional major surgery is necessary upon PCPS termination.

Inhaled nitric oxide, an endothlium-derived relaxing fac-

tor and selective pulmonary vasodilator, has been available for clinical use for some time. This option should be effective to some extent, because it can reduce RV after-load without systemic deterioration of circulation[21].

Conclusion

The experiences detailed earlier suggest that (1) early application of PE is an effective method of treating hyperbilirubinemia after LVAD implantation, and that (2) PCPS effectively supports RV function and may help to prevent hyperbilirubinemia, though close attention is essential to maintain the right–left heart system flow balance.

References

1. Frazier OH, Rose EA, Macmanus Q *et al.* Multicenter clinical evaluation of the HeartMate 1000 IP left ventricular assist device. *Ann Thorac Surg* 1992;53:1080–90.
2. Kaplan RJ, Cillinov AM, Smedira NG *et al. J Heart Lung Transplant* 1999;18:346–50.
3. McCarthy PM, Savage RM, Fraser CD *et al.* Hemodynamic and physiologic changes during support with an implantable left ventricular assist device. *J Thorac Cardiovasc Surg* 1995;109:409–18.
4. Burnett CM, Duncan JM, Frazier OH, Sweeney MS, Vega JD, Radovancevic B. *Ann Thorac Surg* 1993;55:65–71.
5. Wang I, Kotte-Marchant K, Vargo R, McCarthy PM. Hemostatic profiles of HeartMate ventricular assist device recipients. *ASAIO J* 1995;41:M782–7.
6. Yamaguchi T, Sawa Y, Masai T *et al.* Hepatic sinusoid endothelial dysfunction plays a role in hyperbilirubinemia in patients following implantation of an LVAD. *ASAIO J* 1997;43:M449–52.
7. Arcidi JM, Moore GW, Hutchins GM. Hepatic morphology in cardiac dysfunction. *Am J Pathol* 1981;104:159–66.
8. Farrar DJ, Compton PG, Hershon JJ, Fonger JD, Hill JD. Right heart interaction with mechanically assisted left heart. *World J Surg* 1985;9:89–102.
9. Hendry PJ, Ascah KJ, Rajagopalan K, Calvin KE. Does septal position affect right ventricular function during left ventricular assist in an experimental porcine model? *Circulation* 1994;90(5Pt2):353–8.
10. Lepore MJ, Martel A. Plasmapheresis in hepatic coma. *Lancet* 1967;II:771–2.
11. Kodama M, Tani T, Inoue N. Therapeutic plasmatheresis to treat postoperative hepatic failure clinical course and therapeutic outcome in Japan. *J Jpn Surg Soc* 1993;94:707–13.
12. Soeda K, Odaka M, Isono K. Diversified hemopeurification in the treatment for hepatic failure; from hemoadsorption and plasma exchange to plasma adsorption. *Jpn J Artif Organs* 1992;21:1318–23.
13. Chen JM, Levin HR, Rose EA *et al.* Experience with right ventricular assist devices for postoperative right-sided circulatory failure. *Ann Thorac Surg* 1996;61:305–10.
14. Farrar DJ, Hill JD. Univentricular and biventricular Thoratec VAD support as a bridge to transplantation. *Ann Thorac Surg* 1993;55:276–82.
15. Hetzer R, Hennig E, Schiessler A, Friedel N, Warnecke H, Adt M. Mechanical circulatory support and heart transplantation. *J Heart Lung Transplant* 1992;11:S175–81.
16. Kormos RL, Gasior TA, Kawai A *et al.* Transplant candidate's clinical status rather than right ventricular function defines need for univentricular versus biventricular support. *J Thorac Cardiovasc Surg* 1996;111:773–83.
17. Farrar DJ, Hill JD, Pennington DG *et al.* Preoperative and postoperative comparison of patients with univentricular and biventricular support with the Thoratec ventricular assist device as a bridge to cardiac transplantation. *J Thorac Cardiovasc Surg* 1997;113:202–9.
18. Philips SJ, Ballentine B, Slonine D *et al.* Percutaneous initiation of cardiopulmonary bypass. *Ann Thorac Surg* 1982;36:223–5.
19. Anderson H, Steimle C, Shapiro M *et al.* Extracorporeal life support for adult cardiopulmonary failure. *Surgery* 1993;114:161–73.
20. Wudel JH, Hlozek CC, Smedira NG, McCarthy PM. Extracorporeal life support as a post left ventricular assist device implant supplement. *ASAIO J* 1997;43:M441–3.
21. Chang JC, Sawa Y, Ohtake S *et al.* Hemodynamic effect of inhalated nitric oxide in dilated cardiomyopathy patients on LVAD support. *ASAIO J* 1997; 43:M418–21.

Journal of Congestive Heart Failure and Circulatory Support (2001) Vol 1, No 4, 455–457

Catheter ablation of incessant arrhythmia for LVAD implantation

A. Kawai MD[1], S. I. Kihara MD[1], T. Jikuya MD[2], T. Tsutsui MD[2] and H. Koyanagi[1]
[1]The Heart Institute of Japan, Tokyo Women's Medical University; [2]Tsukuba University, Ten-Noudai, Tsukuba, Japan

Background Arrhythmia is one of the common but unpredictable complications for patients with end-stage heart failure. We studied clinical impact and management of incessant arrhythmia in patients who required left ventricular assist device (LVAD) implantation.

Methods and patients Two patients had incessant arrhythmia with end-stage heart failure, requiring LVAD implantation. Aggressive treatment for the arrhythmia was performed with electrical ablation (EA). LVAD implantation was performed successively with stable cardiac rhythm.

Conclusion Aggressive treatment with EA for patients who were candidates for LVAD implantation was proven safe and effective.

Keywords left ventricular assist device (LVAD), arrhythmia, electrical ablation (EA).

Introduction

The use of left ventricular assist devices (LVADs) is becoming very popular in treatment of patients with end-stage heart failure. A recent report showed that 76% of patients were successfully bridged to heart transplantation[1]. These promising outcomes have moved physicians to use LVADs for long-term support without the goal of transplantation[2]. In general, the indication for LVAD implantation is determined by the circumstances of hemodynamic and end-organ function. Arrhythmia is one common but often unpredictable complication for the patients with end-stage heart failure. The existence of incessant ventricular arrhythmia is a clear indication for LVAD implantation. It is not uncommon that atrial arrhythmia aggravates marginal patients' hemodynamic condition, resulting in LVAD implantation, therefore arrhythmic control is essential in the effective treatment of patients with end-stage heart failure.

There are other important clinical implications concerning arrhythmia in patients using LVADs. After LVAD implantation, systemic circulation is supported by the LVAD; however, pulmonary circulation is regulated by the native right ventricle. Post-LVAD implant arrhythmias can cause hemodynamic derangement by right ventricular dysfunction. Patients with post-LVAD incessant arrhythmia may need to use a biventricular assist device (BiVAD). If the patient requires biventricular support, an extracorporeal BiVAD or total artificial heart (TAH) must be used. The clinical result and quality of life for patients using these devices is much worse than those using the portable LVAD.

Electrical ablation (EA) with a catheter is also gaining popularity in treatment of resistant arrhythmia. AV-nodal ablation and pacemaker implantation can control atrial tachycardia and atrial fibrillation. EA is also a possible method of treatment for ventricular arrhythmia; however, generally it is not practical for marginal patients due to clinical risks involved.

We report two patients who underwent LVAD implantation combined with EA as treatment for incessant arrhythmia.

Case 1

The patient was a 45-year-old female with end-stage heart failure due to dilated cardiomyopathy (DCM). She had been suffering from congestive heart failure (CHF) for 4 years with a dilated left ventricle and a left ventricular ejection fraction (LVEF) of 21%. She had been taking carvedilol and her symptoms were been relatively stable for 3 years. She developed dyspnea on exertion and required admission in December 1998. She was placed on diuretics and i.v. inotropic support. Although she was successfully weaned from inotropics within 7 days, her clinical course was complicated by ventricular tachycardia (VT), which required direct current shock and intratracheal intubation. Amiodarone was initiated with a loading dose, which caused up to a 5-second sinus arrest; thereafter the dosage was reduced to 100 mg day^{-1}. It was not sufficient to suppress her arrhythmogenic activity and she suffered from frequent paroxysmal ventricular tachycardia (PSVT) attacks. These recurrent PSVT episodes apparently aggravated her cardiac function and she fell into low output syndrome and was back on intravenous inotropic support and intra-aortic balloon pumping. Clinically, her VT arrest episodes were always preceded by low blood pressure due to PSVT. Since medication seemed ineffective in controlling

Correspondence to Akihiko Kawai MD, The Heart Institute of Japan, Tokyo Women's Medical University, 8–1 Kawada, Shinjyuku-ku Tokyo 162–8666 Japan.

her PSVT, AV block creation by AV node ablation with a pacemaker implantation was performed. After EA treatment, she was kept on DDD pacemaker rhythm without an episode of VT arrest. On day 51 after EA treatment she underwent LVAD implantation because of worsening CHF and multiple organ failure (MOF).

After LVAD implantation, although she required high dose inotropic support for right ventricular failure, she could keep regular pacemaker rhythm.

Case 2

The patient was a 14-year-old boy with familial dilated cardiomyopathy. He had cardiomegaly and arrhythmia at birth. He developed palpitations and was admitted to our hospital at the age of 3. ECG showed pacemaker shift, rate-dependent CRBBB, and PSVT. At the age of 6, he complained of frequent palpitation and he was hospitalized again. EPS showed wide QRS atrial tachycardia and HV block, but his pump function was almost normal. At the age of 14, he developed fatigue and vomiting and was admitted to our hospital with the diagnosis of CHF. A chest X-ray showed cardiomegaly with a cardiothoracic ratio of 73%. Two-dimensional echocardiography presented an LVDd of 69 mm, LVDs of 66 mm, and LVFS of 0.05. Despite the aggressive treatment for CHF, his clinical condition deteriorated and required intubation and high-dose inotropic support. His condition was complicated by wide QRS tachycardia (Figure 1), which was resistant to medication. Eventually, wide QRS tachycardia induced ventricular fibrillation and cardiopulmonary resuscitation (CPR) was carried out. He was placed on a percutaneous cardiopulmonary bypass system (PCPS, V-A ECMO). Although he was supported with 3–4 L min^{-1} of PCPS flow without inotropic support, multiple VT caused complications. The EPS showed bundle branch re-entrant VT, which was resistant to medication, and low-dose catecholamine aggravated it.

Since it was impossible to support him with an LVAD due to multiple VT, we decided to use EA to halt bundle branch re-entrance and successive DDD pacemaker implantation (Figure 2). LVAD implantation was successfully performed one day after EA and the patient functioned well on LVAD support without arrhythmia.

Conclusion

We report two cases of LVAD recipients who had complications of incessant arrhythmia before LVAD implantation. Their arrhythmia was successfully treated with EA and pacemaker implantation. This combined therapy seems to expand the indication of the LVAD to include patients with malignant arrhythmia.

Cardiac arrhythmia is one common complication for patients with end-stage heart failure. Ventricular arrhythmia is a major cause of death for these patients. Atrial arrhythmia is also a worrying complication that can cause hemodynamic deterioration or lead to ventricular arrhythmia. The incidence of ventricular arrhythmia was studied in 40 LVAD recipients. Non-sustained VT was the most common type of arrhythmia and 80% of LVAD recipients experienced it before LVAD implantation. The incidence of sustained VT and ventricular fibrillation before implantation were 25% and 13%, respectively[3]. These end-stage heart failure patients suffer from hypotension, low cardiac output,

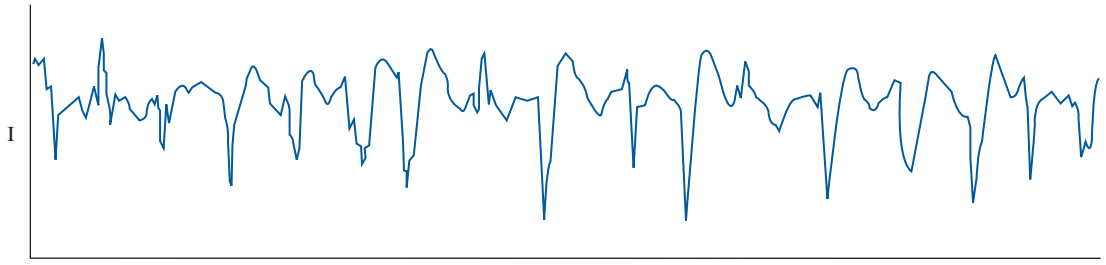

Figure 1. Pre-EA ECG for the patient in Case 1 with multiple VT.

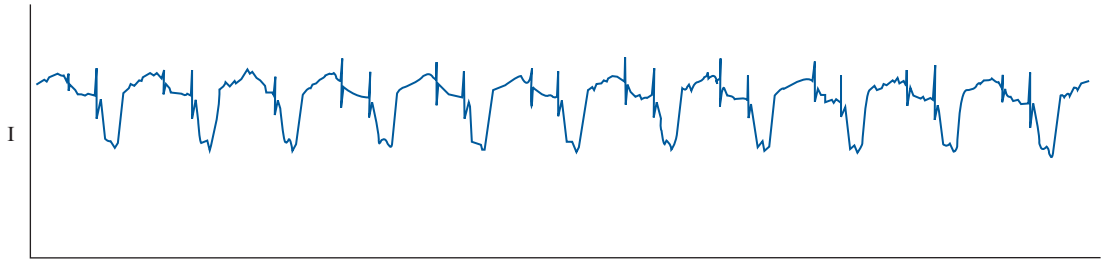

Figure 2. Post EA ECG for the patient in Case 1 using DDD pacemaker rhythm.

and elevated pre-load pressures, resulting in myocardial hypoperfusion. This hemodynamic derangement is the major cause of arrhythmia. The other aggravating factor for arrhythmia is the need for high-dose inotropic support. In general, after LVAD implantation, ventricular arrhythmia becomes less malignant due to improved hemodynamics. However, the patients who developed right ventricular failure after LVAD implantation were still at risk of ventricular arrhythmia because of poor hemodynamic and high-dose inotropic support.

The conditions of our patients were complicated by incessant arrhythmia without or with low dose of inotropic support and their arrhythmias were resistant to medical treatment. For the first patient, arrhythmic control was essential in order to stop progression of heart failure. Successful EA and pacemaker implantation eventually pushed back LVAD implantation to 51 days. After LVAD implantation, the two patients had complications of right ventricular dysfunction, and required high-dose inotropic support. These patients were still at risk of arrhythmia after surgery; however, aggressive treatment with EA completely controlled their arrhythmias. Implantable cardiac defibrillation may be another option for these patients and a further study on this method of treatment is required.

References

1. McCarthy PM, Smedira NG, Vargo RL *et al*. One hundred HeartMate LVAD patients: evolving concepts and technology. *J Thorac Cardiovasc Surg* 1998;115:904–12.
2. McCarthy PM, Young JB, Smedira NG *et al*. Permanent mechanical circulatory support with an implantable left ventricular assist device. *Ann Thorac Surg* 1997;63:1458–61.
3. Kawai A, Kormos RL, Pham SM, Griffith BP Impact of arrhythmia for patients on left ventricular assist devices *J Heart Lung Transplant* 1996;15:S88.

Author Index

Subject Index

Abbreviations:

LVAD	left ventricular assist device
LVAS	left ventricular assist system
RVAD	right ventricular assist device
TAH	total artificial heart
VAD	ventricular assist device
VAS	ventricular assist system